INAUGURAL-DISSERTATION

zur
Erlangung der Doktorwürde
der
Naturwissenschaftlich-Mathematischen
Gesamtfakultät
der
Universität Heidelberg

Vorgelegt von
Diplom-Geologe Gregor Austermann
aus Berlin

2016

Tag der mündlichen Prüfung: 29.04.2016

Sedimentology and depositional environment of the middle Cambrian Manuels River Formation in the type locality at Conception Bay South, Newfoundland, Canada

Gutachter: Prof. Dr. Peter Bengtson
PD Dr. Christina Ifrim

Eidesstattliche Versicherung gemäß § 8 der Promotionsordnung der Naturwissenschaftlich-Mathematischen Gesamtfakultät der Universität Heidelberg

1. Bei der eingereichten Dissertation zu dem Thema

SEDIMENTOLOGY AND DEPOSITIONAL ENVIRONMENT OF THE MIDDLE CAMBRIAN MANUELS RIVER FORMATION IN THE TYPE LOCALITY AT CONCEPTION BAY SOUTH, NEWFOUNDLAND, CANADA

handelt es sich um meine eigenständig erbrachte Leistung.

2. Ich habe nur die angegebenen Quellen und Hilfsmittel benutzt und mich keiner unzulässigen Hilfe Dritter bedient. Insbesondere habe ich wörtlich oder sinngemäß aus anderen Werken übernommene Inhalte als solche kenntlich gemacht.

3. Die Arbeit oder Teile davon habe ich bislang nicht an einer Hochschule des In- oder Auslands als Bestandteil einer Prüfungs- oder Qualifikationsleistung vorgelegt.

4. Die Richtigkeit der vorstehenden Erklärungen bestätige ich.

5. Die Bedeutung der eidesstattlichen Versicherung und die strafrechtlichen Folgen einer unrichtigen oder unvollständigen eidesstattlichen Versicherung sind mir bekannt.

Ich versichere an Eides statt, dass ich nach bestem Wissen die reine Wahrheit erklärt und nichts verschwiegen habe.

Ort und Datum Unterschrift

“A dream you dream alone is only a dream.
A dream you dream together is reality.”
- John Lennon

“The only true wisdom is in knowing you know nothing.”
- Socrates

“Any fool can know. The point is to understand.”
- Albert Einstein

Abstract

A detailed bed-by-bed study of fossiliferous, marine, grey to black shales of the middle Cambrian (Drumian, Cambrian Series 3) Manuels River Formation along its type locality in Newfoundland, Canada, was carried out and provides insight into the sedimentology, depositional environment, palaeogeography and climatology of the area. The formation was deposited on the microcontinent Avalonia, the largest terrane of the peri-Gondwanan realm situated in temperate latitudes. The partly organic-rich (up to 3.36 % TOC) shales of the succession were deposited mainly conformably under dysoxic conditions. Deposition was controlled by two shallowing trends and occurred below, near and above mean storm-wave base. The contact of the top of the first shallowing-upward trend in the succession is conformably, whereas the second shallowing-upward trend is truncated by an erosional unconformity, forming the top of the formation. An average sedimentation rate of c. 3.8 m/Ma is estimated. The clay-mineral composition and illite crystallinity suggest a subsidence of approximately 5.7–6.3 km and a burial temperature of c. 280 °C. The low chlorite/kaolinite ratios indicate a mainly warm semi-humid climate setting at 35°–65° S, with sudden changes to a semi-arid setting. The subsidence, sedimentation rate and depositional environment suggest an Early Ordovician Avalonia-Gondwana separation.

Keywords: Black shales, clay mineralogy, palaeogeography, middle Cambrian, Series 3, Drumian, Avalonia, Newfoundland, Manuels River Formation.

Kurzfassung

Eine detaillierte Schicht-für-Schicht-Aufnahme von fossilreichen, marinen, grauen bis schwarzen Tonsteinen der mittelkambrischen (Drumium, Kambrium Serie 3) Manuels-River-Formation an ihrer Typuslokalität in Neufundland, Kanada, liefert Einblicke in die Sedimentologie, den Ablagerungsraum, die Paläogeographie und das Paläoklima dieser Region. Die Ablagerung erfolgte auf Avalonia, dem größten Gondwana vorgelagerten Mikrokontinent, in gemäßigten Breiten. Die Tonsedimente wurden hauptsächlich ungestört unter dysoxischen Bedingungen abgelagert und sind teilweise reich an organischem Kohlenstoff (bis zu 3,36% C_{org}). Die Ablagerung erfolgte unter dem Einfluss zweier Verflachungstrende im Bereich der Sturmwellenbasis (darunter und darüber). Das Top des ersten Trends ist konkordant, während der Zweite durch eine Erosionsdiskordanz beendet wurde, die das Top der Formation bildet. Die durchschnittliche Sedimentationsrate wird auf ca. 3,8 m/Ma abgeschätzt. Aus der Tonmineralzusammensetzung und der Illit-Kristallinität kann auf eine Subsidenz von ca. 5.7–6.3 km geschlossen werden. Die Schiefer waren einer Temperatur von ca. 280 °C ausgesetzt. Geringe Chlorit/Kaolinit-Verhältnisse deuten auf ein warmes semi-humides Klima mit plötzlichen Wechseln in semi-arides Klima in Breiten von ca. 35°–60° S hin. Die Subsidenz, die Sedimentationsrate und die Ablagerungsverhältnisse legen eine Abtrennung Avalonias von Gondwana während des frühen Ordoviziums nahe.

Schlüsselwörter: Schwarzschiefer, Tonmineralogie, Paläogeographie, Mittelkambrium, Serie 3, Drumium, Avalonia, Neufundland, Manuels-River-Formation.

Contents

1. Introduction

The Avalon Peninsula in eastern Newfoundland, Canada, was part of the former micro-continent Avalonia, which is believed to have been located near the supercontinent Gondwana in high southern latitudes throughout the Cambrian Period. Other well-known parts of Avalonia are nowadays scattered on both sides of the Atlantic Ocean (e.g., Nova Scotia and New Brunswick, and southeast Ireland and Wales). Thus Avalonia is geographically subdivided in West and East Avalonia, depending on the side of the ocean (e.g., Williams, 1979; Trench *et al.*, 1992; O'Brien *et al.*, 1996; Cocks and Torsvik, 2002; Pollock *et al.*, 2012). The Avalon Zone comprises the parts of the Appalachians and Newfoundland considered to belong to Avalonia.

Cambrian sedimentary rocks are exposed along Manuels River, on the south-east coast of Conception Bay on the Avalon Peninsula, which is the site of the type locality of the middle Cambrian (Drumian, Series 3) Manuels River Formation. Because of the abundance of fossils and their extraordinary preservation, this locality is of particular interest. Although there is a long history of palaeontological studies of the succession (e.g., Whiteaves, 1878; Howell, 1925; Hutchinson, 1962; Bergström and Levi-Setti, 1978; Poulsen and Anderson, 1975; Martin and Dean, 1988; Hildenbrand, 2012; Hildenbrand, 2016), only a few authors have discussed the sedimentology and depositional environment of the formation (Howell, 1925; Bergström and Levi-Setti, 1978; Landing and Westrop, 1998a). The succession consists mainly of shales, with interbedded volcanic ash layers and carbonate concretions.

Shales are the most abundant sedimentary rock types on earth, comprising approximately two-thirds of the sedimentary rock record (Schieber, 1998; Potter *et al.*, 2005). Despite their abundance, shales remain relatively poorly understood in comparison with other sedimentary rocks. They commonly lack macroscopic characteristics of high-energy environments; therefore, the depositional environment was for decades over-simplified as of low energy environments. However, recent progress in sedimentology has shown that detailed, high-resolution, bed-by-bed studies lead to a better understanding of the deposition of shales (Plint, 2014; Schieber and Bennet, 2013; Wilson and Schieber, 2015).

Based on a detailed bed-by-bed examination of the succession exposed along Manuels River (June–September 2012, July–August 2013 and July–August 2014), the present study provides detailed information about the sedimentology and the depositional environment of the Manuels River Formation. The results give new insights into the geographic position and the climate of Avalonia during the middle Cambrian.

1.1. Historical review

The type locality of the Manuels River Formation and the entire Cambrian section in the area of Conception Bay South have been the subject of several studies over the past decades and a number of different names and classifications have been introduced. To illustrate how the nomenclature and classifications have changed over time, chrono- and lithostratigraphic names in the present chapter are given as originally published. The nomenclature and classifications used in this work are listed in Chapter 2.

The first mention of sedimentary rocks in the Conception Bay area surrounding Manuels River was by Jukes (1842, 1843). He referred the shales exposed in the area to the "Upper Slate Formation" (Jukes, 1842: pp. 249, 329), without any mention of fossils from this area. Later, in 1868, Murray was the first one to give an overview on the sediments at Manuels River valley. In his report of the Geological Survey of Newfoundland for 1868 he described a Lower Silurian conglomerate, which is today referred to the lower Cambrian Brigus Formation, overlying the "syenitic gneiss" (Murray, 1869: pp. 23–24). Furthermore he mentioned "dark brown or blackish shales, with a very fine lamination coinciding with the bedding", conformably overlying the conglomerate (Murray, 1869: p. 24). A ca. 30.48 m thick bed of "Topsail limestone", overlying the shales, was reported. The succession continues with brown, black, red and green slates with beds of limestone. Murray (1869: p. 27) suggested to refer "the slates" (probably the "Upper Slate Formation"), reported by (Jukes, 1842, 1843), to these beds. As horizon of the upper part of these beds he suggested the *Paradoxides* beds of Branch, St. Mary's Bay. A total thickness of ca. 383 m was measured for the section at Manuels River by him (Murray, 1869: p. 27).

Twelve years later Whiteaves (1878) reported trilobites from Manuels River, found during field work in summer 1874 by T. C. Weston. He commented on the similarity of the trilobite fauna at Manuels River to that the slates of St. John, New Brunswick: *Agnosus acadicus* Hartt in Dawson, 1886, *Eodiscus punctatus* (Salter, 1864), named in Whiteaves (1878) *Microdiscus punctatus* Salter, 1864, *Dawsonia dawsoni* (Hartt in Dawson, 1868) named in Whiteaves (1878) *Microdiscus dawsoni* Hartt in Dawson, 1868, *Badulesia tenera* (Hartt in Dawson, 1868) named in Whiteaves (1878) *Conocephalites tener* Hartt in Dawson, 1868 and *Bailiella baileyi* (Hartt in Dawson, 1868), named in Whiteaves (1878) *Conocephalites baileyi* Hartt in Dawson, 1868 were labelled common in the slates of St. John, N.B., whereas *Conocephalites orestes*? Hartt in Dawson, 1868 was referred to as "possibly common". It was also mentioned by him, that "Mr. Murray and others" supposed the idea of a similar age of the rocks at Manuels River and St. John, N. B., prior to any palaeontological evidence (Whiteaves, 1878: p. 225). This may likely have been a note on personal communication.

Series (2004)	**Middle Cambrian**				**Upper Cambrian**
Series (2015)	**Series 3**				**Furongian**
Jukes (1842), Jukes (1843)	Upper Slate Formation				
Murray (1869)	Brown, black, red and green slate/shale with beds of limestone / Paradoxides Beds at Branch in the upper part				Kelly's Island sandstones and shales
Murray and Howley (1881: 237)	Red, green and black shales and gray limestones, containing *Paradoxides bennetti*				Kelly's Island sandstones and shales
Matthew (1886)	Horizon of the Conocoryphinae	Horizon of *Paradoxides spinosus*	Horizon of *Paradoxides tessini*	Horizon of *Paradoxides davidis*	Fauna of the *Olenus* division
Walcott (1888a)	Newfoundland, Lower Cambrian with *Paradoxides*				
Walcott (1888b), Walcott (1889), Walcott (1891)	Avalon, Middle Cambrian (*Paradoxides*)				Belle Isle, Upper Cambrian, (*Olenus*)
Marcou (1890)	Bohemian, or *Paradoxides* Zone, late Middle Taconic				
Matthew (1896)	Subzone of *Paradoxides etemenicus*	Subzone of *Paradoxides abenacus*	Subzone of *Paradoxides davidis*		
Matthew (1899)	Paradoxidian				Olenian
Walcott (1900)	*Paradoxides* Zone (Avalon, Acadian, Middle Cambrian)				*Olenus* Zone
van Ingen (1914)	Manuels Formation / Manuels Series				Elliot Cove Formation
Howell (1925)	Chamberlin's Brook Formation Beds 1–35	Long Pond formation Beds 36–92	Kelligrew Brook formation Beds 93–125		Elliot Cove Formation
Hutchinson (1962)	Chamberlain's Brook Formation	Manuels River Formation			Elliot Cove Group
Poulsen and Anderson (1975)		Manuels River Formation			Elliot Cove Group
Martin and Dean (1988)	Chamberlain's Brook Formation	Manuels River Formation			Elliot Cove Formation
Landing and Westrop (1998a)	Chamberlain's Brook Formation	Manuels River Formation			MacLean Brook Group
Malang (2015), Wetzel (2015)	Chamberlain's Brook Formation	Manuels River Formation			Elliot Cove Formation

Fig. 1: Different classifications and nomenclature of the Cambrian sediment layers in the area of Manuels River and Conception Bay from 1842–2015.

In the years 1881 to 1900 several studies were carried out focusing on the palaeontology, classification and dating of rocks in North America and Atlantic Canada in general and thus touching Manuels River area (Murray and Howley, 1881; Matthew, 1886, 1896, 1899; Walcott, 1888a, 1888b, 1889, 1891, 1900; Marcou, 1890; Weston, 1896). The fast improvement in the knowledge of the fauna and rocks, which resulted in broad variety of different classifications

and names, is illustrated in Fig. 1. The names “Manuels Formation”, “Manuels Series” and “Elliot Cove” were introduced in van Ingen’s (1914) “Table of the Geological Formations of the Cambrian and Ordovician Systems about Conception and Trinity Bays, Newfoundland and their Northeastern-American and Western-European Equivalents, based upon the 1912-1913 field work”.

The first detailed account of the sedimentary succession exposed along Manuels River was by Howell (1925). In his PhD thesis, focusing mainly on palaeontology, he proposed the name Chamberlain’s Brook Formation for the lower part of the succession, beds 1–35, based on lithological differences Howell (1925). For the upper part of the succession he defined the Long Pond and Kelligrew Brook formations (beds 36–92 and 93–125, respectively) on the basis of two biozones, *Paradoxides hicksi* and *Paradoxides davidis*, respectively, and lithological differences at the Manuels River locality, comprising a succession of 20.7 m of grey to black mudstones. Howell rejected the name “Manuels Formation”, which had been introduced by van Ingen (1914) for the entire Middle Cambrian succession. He noted that the *Paradoxides* beds at Manuels “appear to be divisible into at least three formations” and suggested that the term “Manuels” should be retained only in its wider sense van Ingen (1914) and used “Manuels” for “the *Paradoxides* beds of the Conception Bay region, where the lithology appears to be approximately the same as that of the type locality at Manuels” (Howell, 1925: p. 57).

Decades later, (Hutchinson, 1962) proposed the name Manuels River Formation for a combination of Howell’s (1925) Long Pond and Kelligrew Brook formations. Hutchinson accepted Howell’s (1925) division of the succession into two subunits, which he designated as members only recognizable at the type locality, whereas in other parts of Newfoundland the formation showed a more homogeneous lithology. As type locality of the Manuels River Formation, Hutchinson designated the west bank of the river, being the best-exposed, accessible and known locality of the formation at that time (Hutchinson, 1962).

The term “Elliot Cove” was accepted by him as a group name for all “Upper Cambrian rocks of south-eastern Newfoundland, except those north of Fortune Bay” (Hutchinson, 1962: p. 25). The section at Manuels River comprises of 32 beds of mainly grey to black shale with nodules and rare limestone with a total thickness of 188.06 m. As indicated, this publication was more focused on the general deposition of Cambrian rocks on Newfoundland, so other sections of Chamberlain’s Brook Formation, Manuels River Formation and Elliot Cove Group were presented too.

Poulsen and Anderson (1975) presented a study on the biostratigraphy and a conclusion on the palaeoenvironment in the upper part of Manuels River Formation and the transition into Elliot Cove Group. Study areas were Manuels River and Highland Cove on Random Island. They proposed a Middle Cambrian age for the lower part of Elliot Cove Group

supported by their biostratigraphy of agnostides.

Subsequent research published by Bergström and Levi-Setti (1978) brought a more detailed insight into the upper part of Manuels River Formation on the east side of Manuels River. They applied powder x-ray analysis, thin sectioning and palaeontological techniques to their samples and provided detailed information on the Paradoxides fauna, lithology and finally the palaeoenvironment of the upper 7.5 m of the formation. They proposed a coincidence of depositional discontinuities and "boundaries between subspecies ranges" (Bergström and Levi-Setti, 1978: p. 16).

Another biostratigraphic work at the type locality and surrounding areas was carried out by Martin and Dean (1988). They presented a trilobite and acritarch zonation at Manuels and Random Island for Middle and Upper Cambrian age in particular for the Chamberlain's Brook, Manuels River and Elliot Cove formations and subdivided the Manuels River Formation in the biozones of *Tomagnostus fissus* and *Ptychagnostus atavus*, *?Hypagnostus parvifrons* and *Ptychagnosus punctuosus*.

In this context the recent diploma thesis of Hildenbrand (2012) and the B.Sc. thesis of Vetter (2012) are also worth mentioning. Hildenbrand (2012) dealt with the limestone concretions occurring in the Manuels River Formation at its type locality and the small shelly fossils inside, whereas Vetter (2012) provided information about the composition of the volcanic ash layers included in the Manuels River Formation and marked the designation of the ash-layers as "Metabentonite" (see Fletcher, 1972, 2006; Landing and Westrop, 1998a) as doubtful.

Malang (2015) and Wetzel (2015) focused in their most recent M.Sc. thesis on a mapping of both, crystalline basement and sediments on either side of Manuels River. The study evidenced a strike-slip fault in the river valley. Current research is carried out by Hildenbrand (2016). Her thesis gives detailed insight into the palaeontology of the succession and lead to a revision of the taxonomy of agnostoid trilobites at the type locality. Furthermore she subdivides the Manuels River Formation in five local biozones, (1) *Peronopsis scutalis*, (2) *Tomagnostus fissus*, (3) *Ptychagnostus atavus*, (4) *Ptychagnostus affinis* and (5) *Ptychagnostus punctuosus* Zone. In addition her thesis supports the relative geographic proximity of Baltica and Avalonia during the middle Cambrian (Drumian, Series 3) on the basis of agnostoid trilobite distribution.

Beside this research, several field-trip guides, field books, conference contributions and unpublished theses outlined at least parts of the type locality (e.g., Nautiyal, 1966; King *et al.*, 1974; Brückner, 1978; Anderson, 1987; Boyce, 1988, 2001, 2006; Landing and Benus, 1988; Landing *et al.*, 1988; Landing and Westrop, 1998a, b; Austermann *et al.*, 2012; Hildenbrand *et al.*, 2012). Detailed photographic work about the trilobites occurring in the Manuels River sediments was done by Levi-Setti (1993, 2014).

1.2. Palaeogeographic overview of Avalonia

The microcontinent Avalonia is considered the largest terrane of the peri-Gondwanan realm, and is today, as a result of the opening of the Atlantic Ocean, divided into East and West Avalonia (Pollock *et al.*, 2012). East Avalonia extends across Europe, from the Bohemian massif in the east over Brunia, the West-Sudets, the Rheno Hercynian Zone in central Europe to southern England, Wales and southeast Ireland in western Europe (Trench *et al.*, 1992; Friedl *et al.*, 2000; Kröner *et al.*, 2000; Kröner *et al.*, 2001; Cocks and Torsvik, 2002; Nance *et al.*, 2002). West Avalonia (Fig. 2) consists of the Avalon and Burin peninsulas in southeastern Newfoundland, Cape Breton Island, northern Nova Scotia, eastern New Brunswick, Cnnecticut, New Hampshire, Maine, Rhode Island and eastern Massachusetts (e.g., Williams, 1979; Barr and Raeside, 1989; Barr and White, 1996; O'Brien *et al.*, 1996; Rabu *et al.*, 1996; Hibbard *et al.*, 2007).

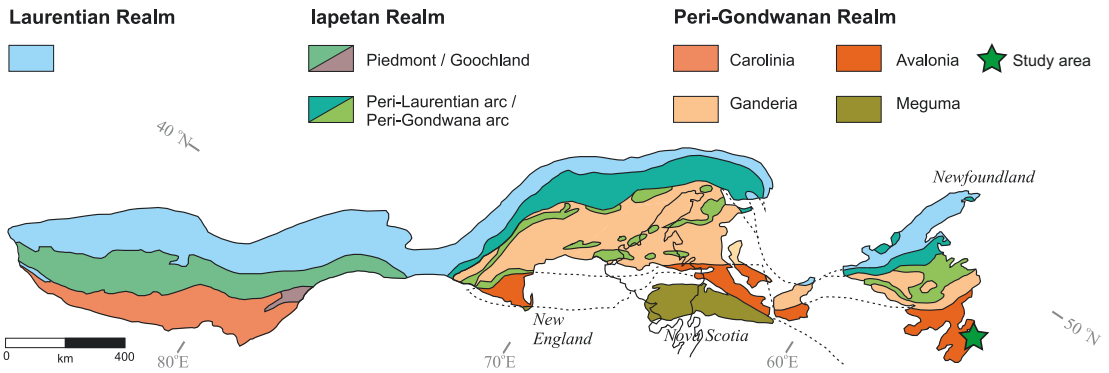

Fig. 2: Setting of West Avalonia in relation to the Appalachian peri-Gondwanan realm (modified after Pollock *et al.*, 2012).

1.2.1. Neoproterozoic (1.1 Ga–541 Ma)

In the Neoproterozoic and Cambrian the supercontinent Gondwana was located at high latitudes near the South Pole (Cocks and Torsvik, 2006). U-Pb ages for Neoproterozoic volcanic rocks (Barr *et al.*, 2003; Murphy *et al.*, 2004; Pollock *et al.*, 2009) suggest proximity of Avalonia either to West Africa or Amazonia at the margin of Gondwana. Because of the lack of the characteristic Pan-African magmatism (660–680 Ma) and tectonothermal events (0.7–2.0 Ga) in West Africa (Rocci *et al.*, 1991), Avalonia is considered to have been positioned near to Amazonia at that time (Fig. 3) (McKerrow *et al.*, 1992; Keppie, 1993; Pollock *et al.*, 2012).

The formation of the Avalonian arc started with Proto-Avalonia 0.8–1.1 Ga ago. (Nance

et al., 2002; Murphy, 2000). Its Neoproterozoic evolution is characterised by three different stages of volcanic-arc and rift development.

The first stage (1.1 Ga–635 Ma) is represented by arc- and rift-related plutonic rocks, for example the Burin Group on Burin Peninsula (Nance *et al.*, 2002), the Hawkes Hill Tuffs or the Tickle Point Formation (Swinden and Hunt, 1991).

The second stage (635–570 Ma) is characterised by volcanic sediments, deposited in inter-, intra- and back-arc basins, linked with both plutonic and volcanic rocks (Murphy and Nance, 1989). On the Avalon Peninsula this stage is represented for instance by the Harbour Main Group or the Conception Group (King, 1990).

The third stage (570–541 Ma) is characterised by volcanic and sedimentary rocks, deposited in conjunction with the rifting of Avalonia and the termination of active arc volcanism (Murphy and Nance, 1989; O'Brien *et al.*, 1996; Murphy *et al.*, 1999; Keppie *et al.*, 2003; Pollock *et al.*, 2012). Though Avalonia moved towards Gondwana since 665 Ma there is no evidence of orogenic collision (Murphy and Nance, 1989). A model by Murphy and Nance (1989) later expanded by Murphy *et al.* (1999) suggests a ridge-trench collision and a progressive development of a dextral continental transform fault (Fig. 4). This resulted in the diachronous termination of the subduction and inversion of the arc basins with new pull-apart basins opening up.

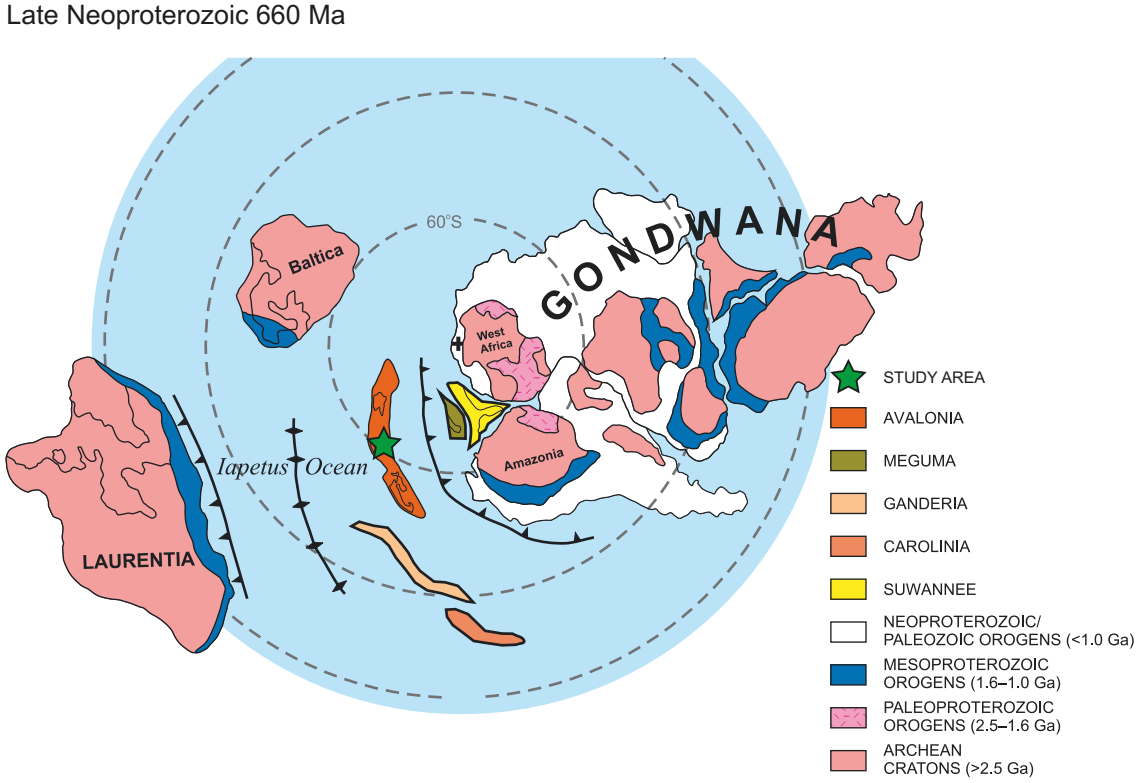

Fig. 3: Proposed late Neoproterozoic palaeogeography (based on Cambrian reconstruction by Pollock *et al.*, 2012).

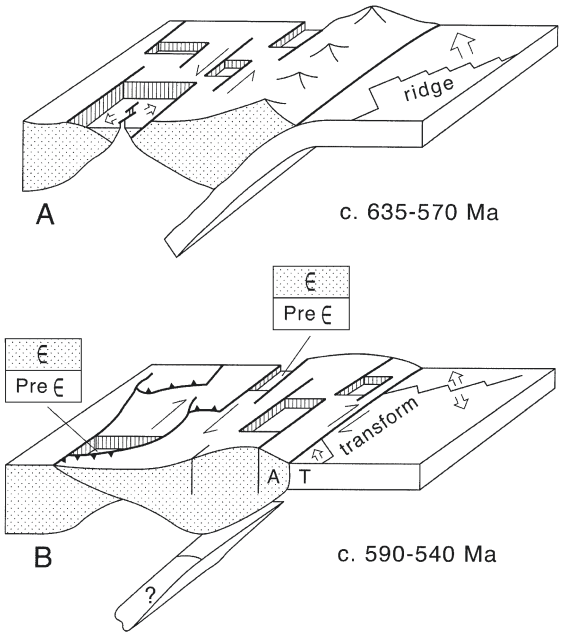

Fig. 4: General model of the late Neoproterozoic evolution of Avalonia (modified after Nance *et al.* 2002). (A) Oblique subduction at ca. 635–570 Ma producing the main arc phase of Avalonian magmatism and opening a variety of volcanic-arc basins in response to sinistral motion on basin-bounding faults. (B) Ridge–trench collision resulting in the structural inversion of the volcanic arc basins, opening of new pull-apart basins and diachronous termination of subduction at ca. 590–540 Ma in response to the progressive development of a dextral continental transform fault (after Murphy *et al.*, 1999).

1.2.2. Cambrian (541–485 Ma)

Throughout the Cambrian Avalonia appears to have continued its lateral movement along the margins of Gondwana (Fig. 5), which was caused by the development of the dextral fault in the Neoproterozoic (Nance *et al.*, 2002; Keppie *et al.*, 2003; Satkoski *et al.*, 2010). Although Landing and MacGabhann (2010) found evidence for an early Cambrian glaciation on Avalonia in southern New Brunswick and thus proposed the separation of Avalonia from Gondwana in the early Cambrian, palaeomagnetic data (e.g., van Staal *et al.*, 1998) suggests a continued connection with Gondwana during the Cambrian. Also in contrast to palaeomagnetic data, Landing *et al.* (2013a, b) suggested an equatorial setting of Gondwana, Laurentia, Siberia and South China and a high southern latitude position of Baltica and Avalonia during the early Cambrian.

1.2.3. Ordovician (485–419 Ma)

The separation of Avalonia from Gondwana started with the opening of the Rheic Ocean and closure of the Iapetus Ocean in the early Ordovician (Fig. 1). The timing is supported by the change the cold-water and low-diverse Gondwanan similar faunas of the Cambrian and earliest Ordovician (Landing, 2005; Fletcher *et al.*, 2005) to more mixed Laurentia-Avalonian faunas of the Ordovician (Lees *et al.*, 2002). Avalonia moved northwards, towards Laurentia. At the end of the Cambrian, prior to the separation from Gondwana, it was located at ca. 65–62°S (Trench *et al.*, 1992) and moved to ca. 44–41°S during the Ordovician (Trench

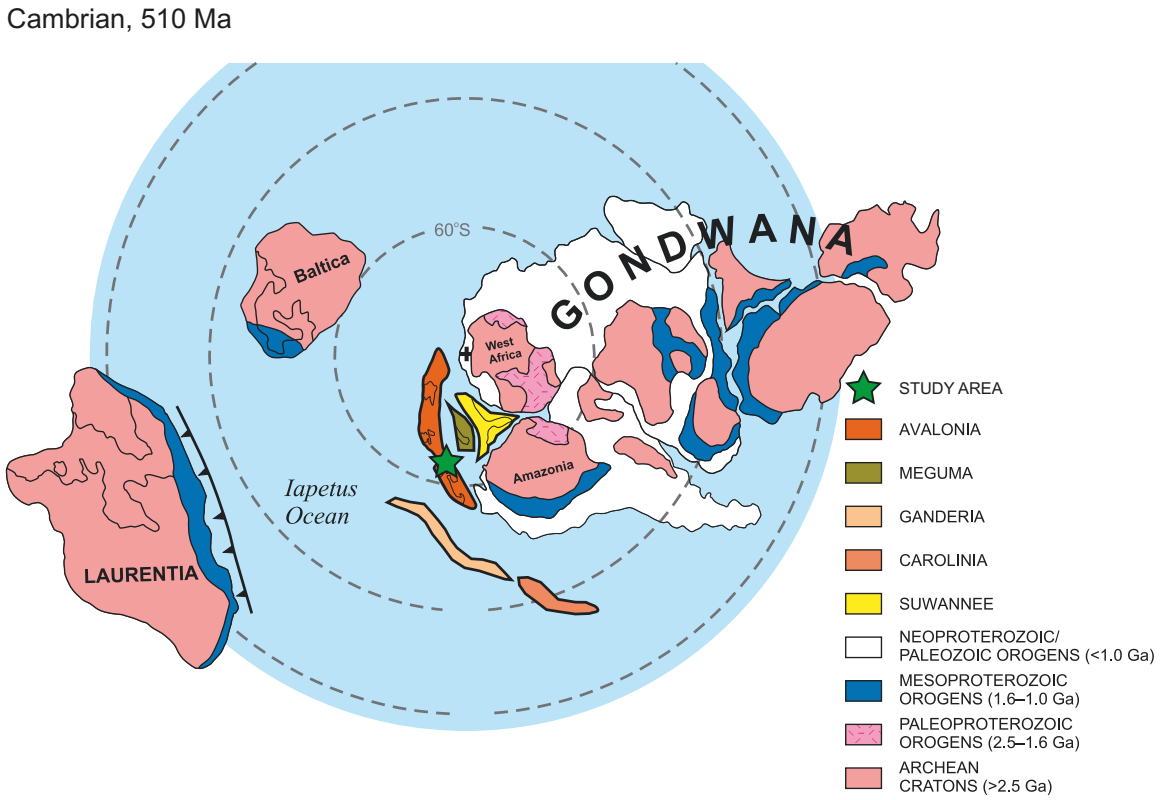

Fig. 5: Cambrian palaeogeography (modified from Pollock *et al.*, 2012).

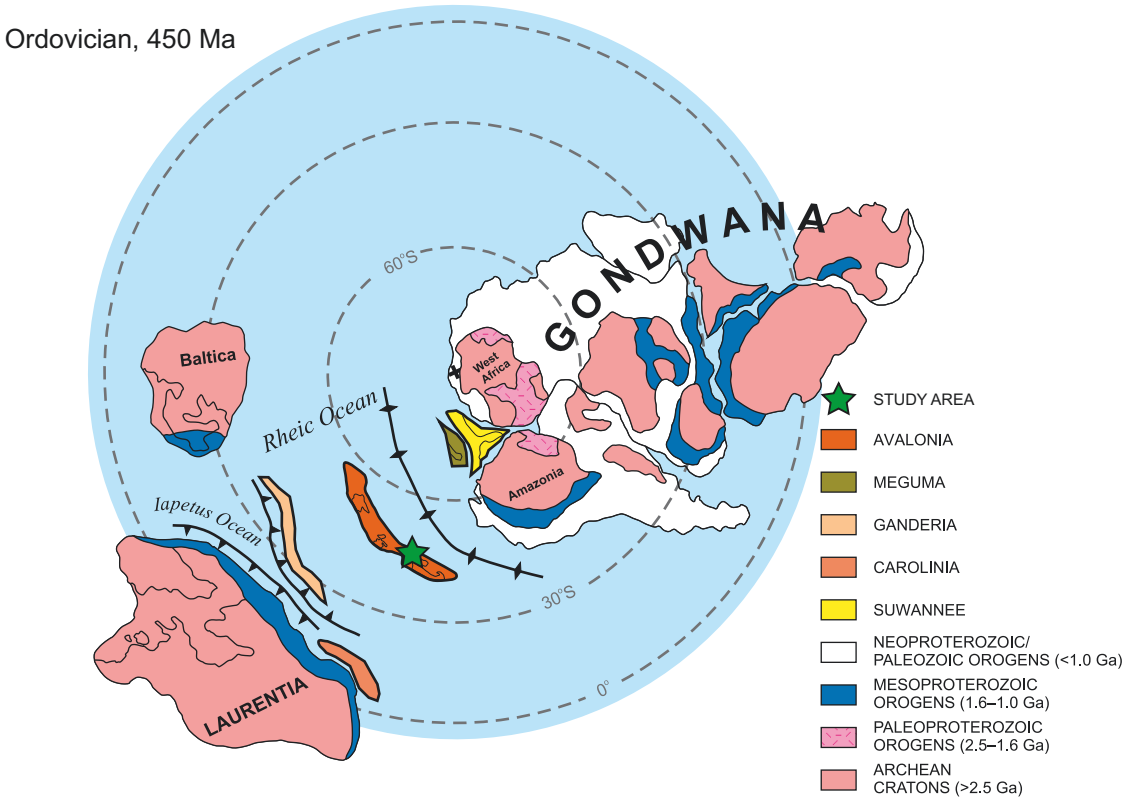

Fig. 6: Ordovician palaeogeography (modified from Pollock *et al.*, 2012).

et al., 1991).

1.2.4. Silurian–Neogene (419 Ma–today)

The movement of Avalonia towards Laurentia continued during the Silurian (Fig. 8). The Iapetus Ocean was closed (Pollock *et al.*, 2012). The fauna of Avalonia still differed from the Laurentian fauna. Faunal differences between Gondwana and Avalonia suggest the existence of a dispersal barrier, probably the Rheic Ocean (Cocks *et al.*, 1997; Pollock *et al.*, 2012). In the latest Silurian, accretion of Avalonia to Laurentia started and caused the Acadian orogenesis, which led to faulting of the rocks on the Avalon Peninsula (King, 1990). Because of the high stability of the rocks forming the Holyrood Horst, these tectonic movements had only a minor effect on the overlying Cambrian–Ordovician succession.

Avalonia finally docked to Laurentia in the early Devonian (Pollock *et al.*, 2012). During the late Devonian and the Carboniferous, Laurentia collided with Gondwana to form the supercontinent Pangaea (Figs. 8–9). During the Carboniferous–Jurassic, Avalonia was part of Pangaea. In the Cretaceous, the opening of the Atlantic Ocean caused the split up of Avalonia into the present east and west parts.

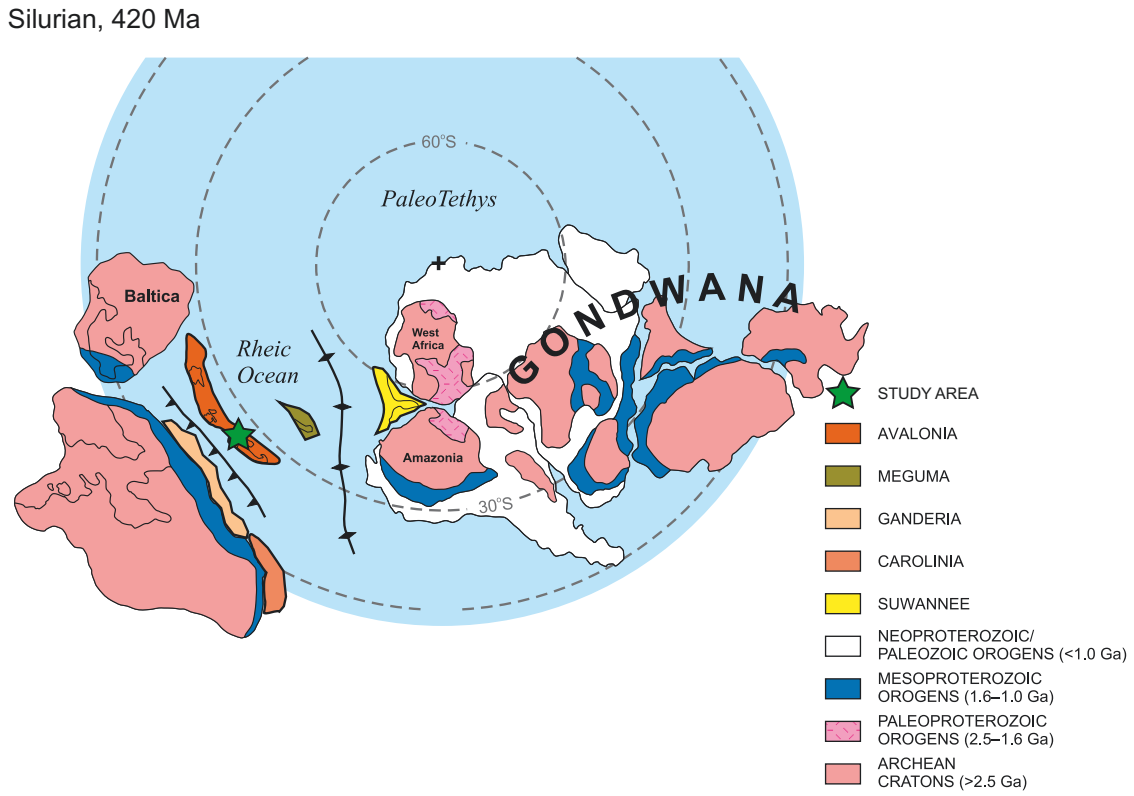

Fig. 7: Silurian palaeogeography (modified from Pollock *et al.*, 2012).

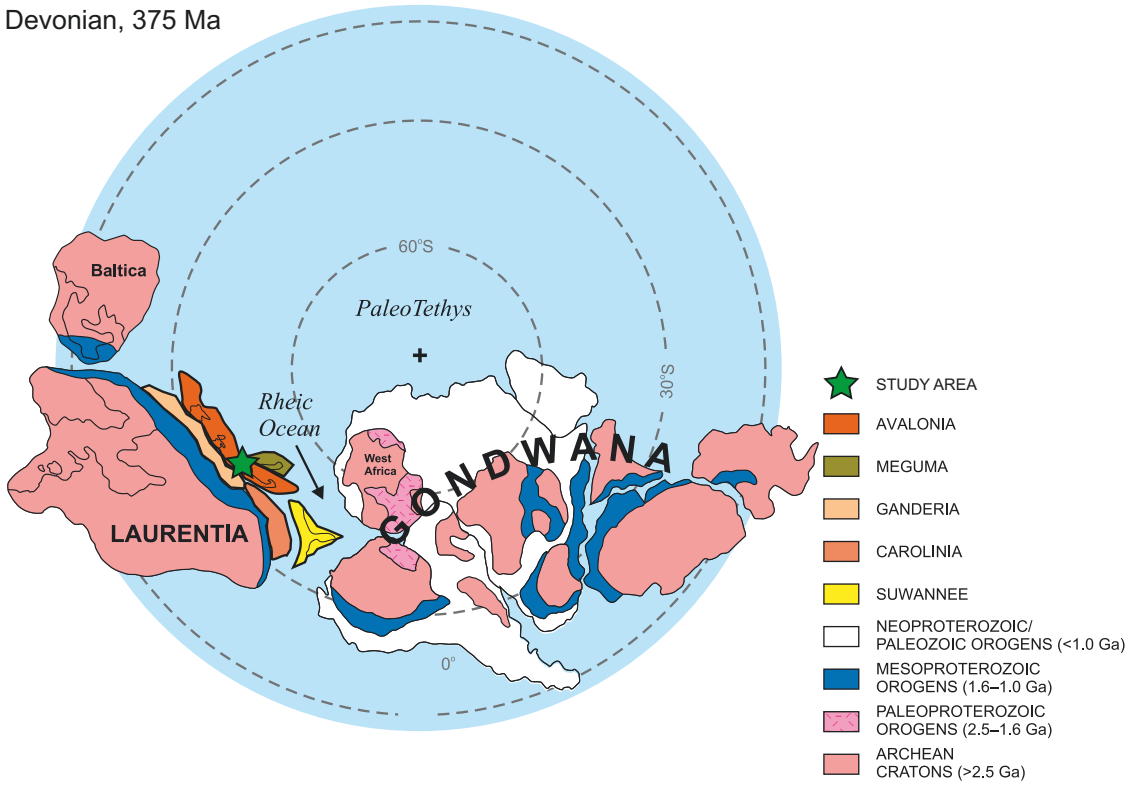

Fig. 8: Devonian palaeogeography (modified from Pollock *et al.*, 2012).

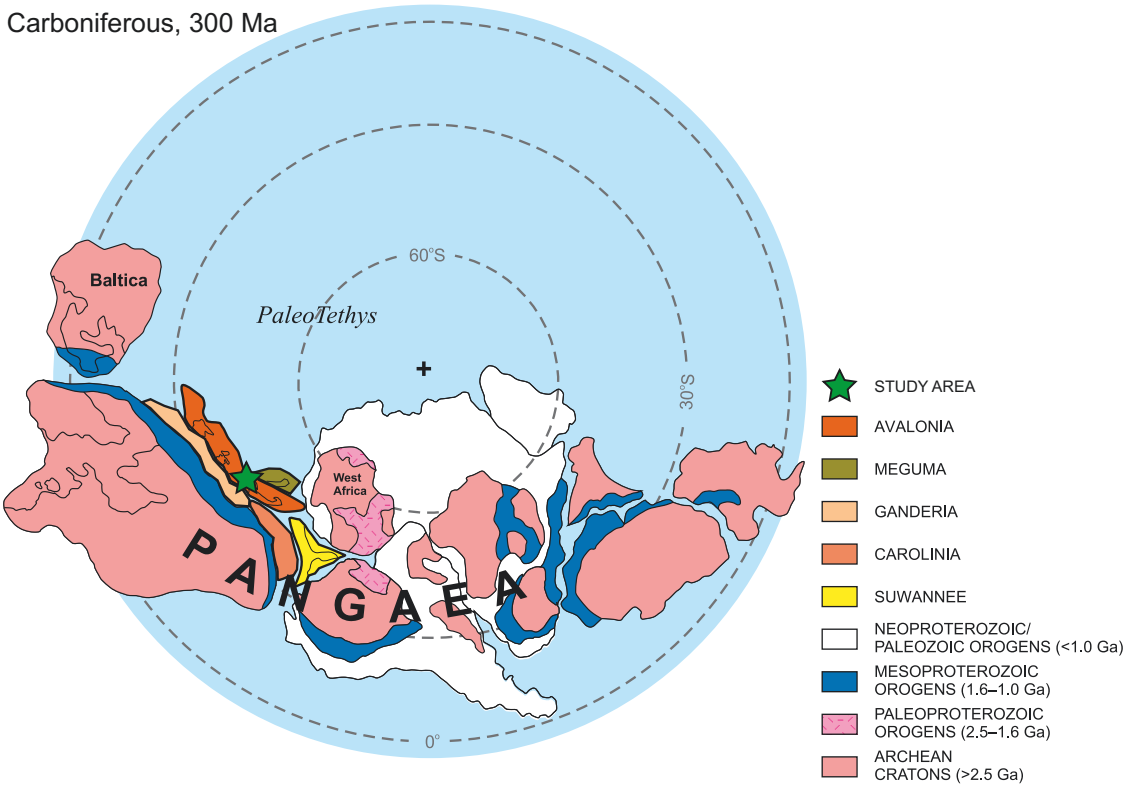

Fig. 9: Carboniferous palaeogeography (modified from Pollock *et al.*, 2012).

1.3. Regional geology of the Avalon Peninsula

1.3.1. Neoproterozoic (729–541 Ma)

The oldest rocks on the Avalon Peninsula are the ca. 729 Ma old Hawkes Hill Tuffs (O'Brien *et al.*, 2001), unconformably overlain by the volcanoclastic and turbiditic sediments of the ca. 635–570 Ma old Conception Group (Fig. 8). The sediments of Conception Group are exposed widely over the eastern Avalon Peninsula and are considered to represent a base-of-slope to toe-of-slope environment (Fig. 10 A) (Eyles and Eyles, 1989; Wood *et al.*, 2003; Ichaso *et al.*, 2007; Carto and Eyles, 2012; Liu *et al.*, 2012). The conformably overlying St. John's Group consists of silt- and sandstones. Shales occur scattered as well as tuffaceous sandstones (King, 1988, 1990). The St. John's Group (Fig. 8) has likely been deposited in a prograding slope environment (Fig. 10 B) and occurs at the eastern margin of Avalon Peninsula as well as on the western side of Conception Bay (King, 1988, 1990). An upheaval of todays Avalon Peninsula during 650–560 Ma, probably related to the movement of the microcontinent Avalonia towards Gondwana, resulted in the development of an alluvial plain on the margins of the Avalon Peninsula and the deposition of the conformably overlying Signal Hill Group (King *et al.*, 1974; King, 1990; O'Brien *et al.*, 1996). The base of Signal Hill Group consists mainly of greenish grey sand- and siltstones or conglomerates. A nonconformity between greenish-grey sand- and siltstones and thick bedded red arkosic sandstones marks the beginning of molasses-type fluvial and alluvial redbeds . The Signal Hill Group is the youngest Neoproterozoic strata on the Avalon Peninsula and occurs in the most easterly part of it (King, 1988, 1990).

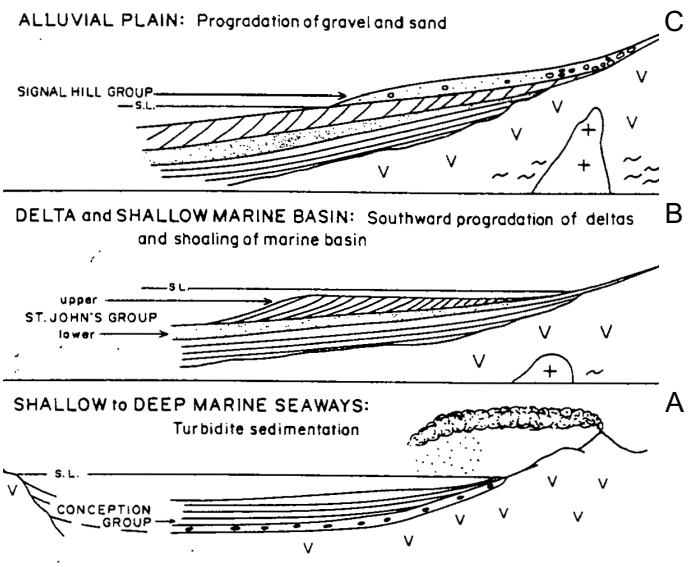

Fig. 10: The three different stages of Neoproterozoic sedimentation on the Avalon Peninsula (modified from O'Brien *et al.*, 1983). **A**: Oldest sequence of sedimentation: Turbidites and volcanic sediments derived from the arc. **B**: Progradation of the basin resulting in shallowing-upward and deposition of delta and shallow-marine sediments. **C**: Upheaval of the Avalon Peninsula resulting in the formation of an alluvial plain and deposition of redbeds.

The Neoproterozoic basement of the area surrounding the Manuels River differs from the whole other Avalon Peninsula of today. Bounded by two main faults of Neoproterozoic age in the east and west, Topsail fault and Brigus Fault respectively (Fig. 6), the magmatic rocks of Harbour Main Group build a solid basement, called Holyrood Horst, for the overlying Cambrian–Ordovician succession (Rose, 1952; King, 1988, 1990). A sketched cross section of the Holyrood Horst and surrounding strata is given in Fig. 9.

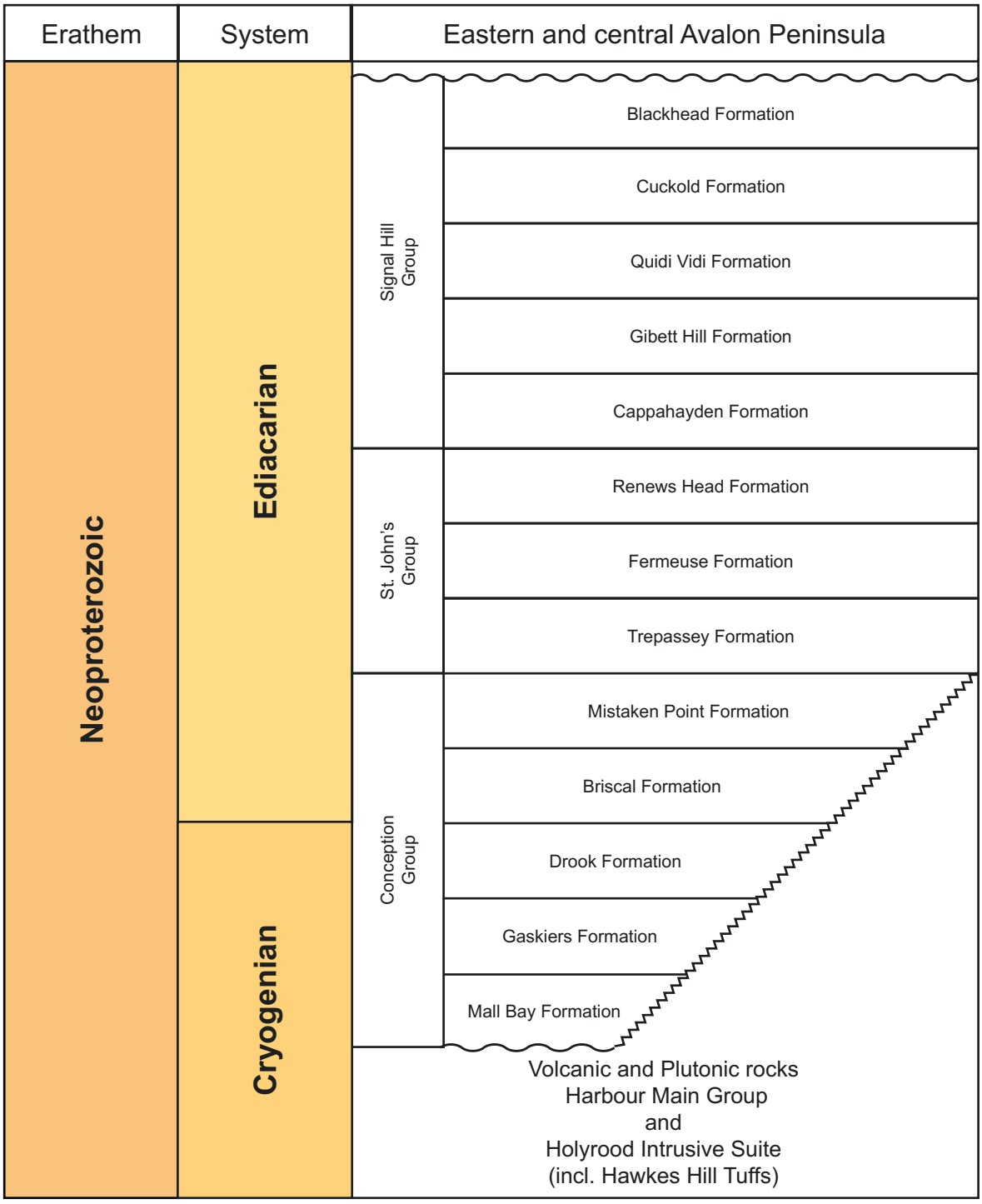

Fig. 11: Simplified chronostratigraphic table for the Neoproterozoic on the eastern and central Avalon Peninsula (based on Narbonne *et al.,* 1987; King 1988, 1990).

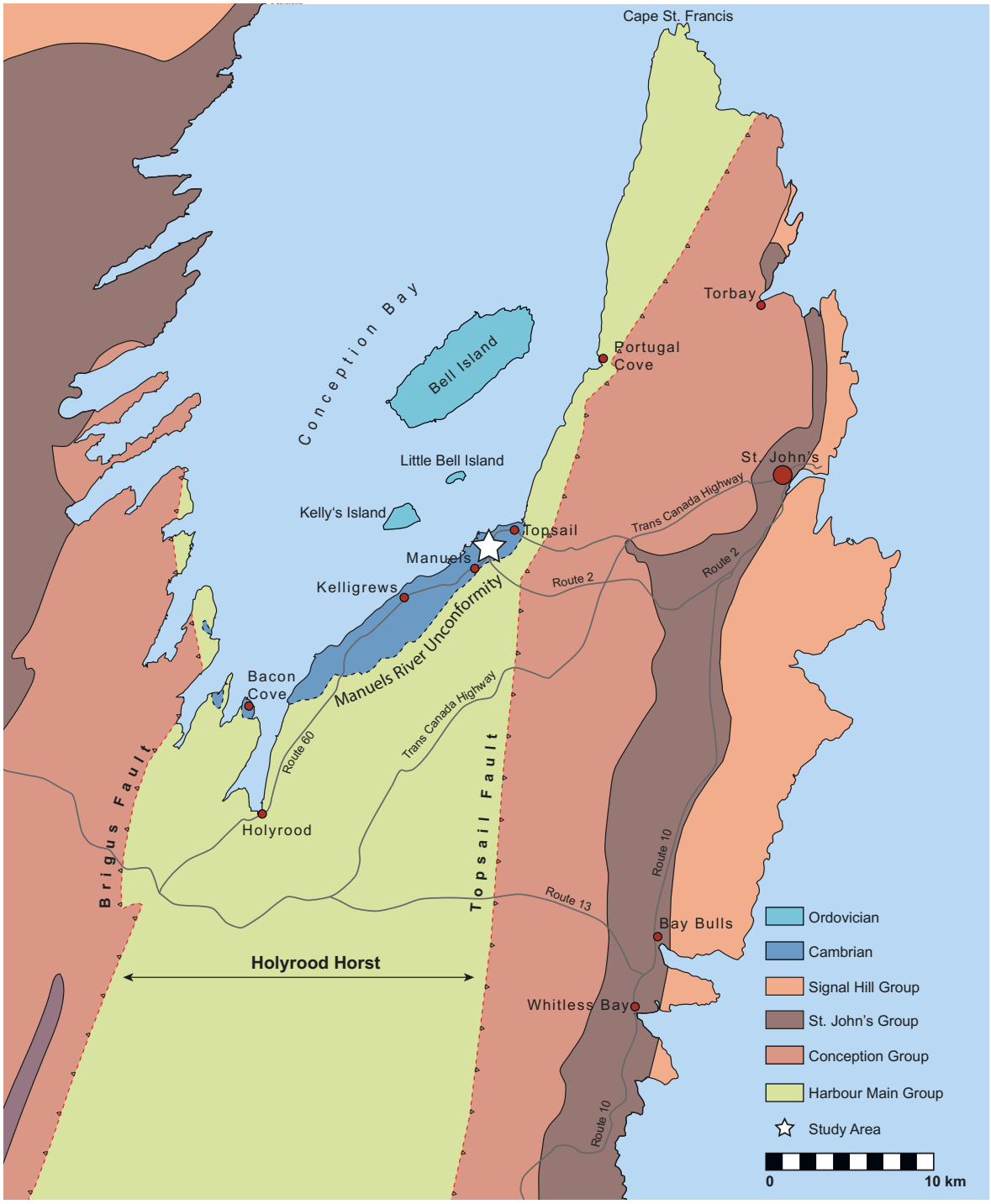

Fig. 12: Simplified geological Map of the Conception Bay area, northeastern Avalon Peninsula, Newfoundland (based on King, 1988).

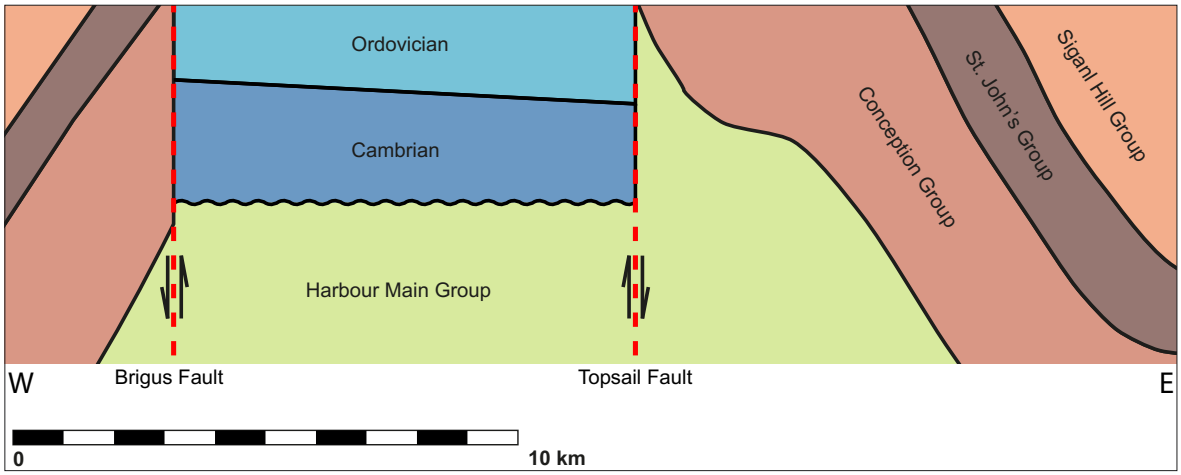

Fig. 13: Simplified sketch of a west–east cross section of the Conception Bay area, northeastern Avalon Peninsula, Newfoundland (based on King, 1988).

1.3.2. Cambrian (541–488 Ma)

The Neoproterozoic alluvial plain on the Avalon Peninsula was eroded in part and then flooded during the early Cambrian. Thus the Neoproterozoic–Cambrian boundary on the Avalon Peninsula is unconformably. At Manuels River an angular disconformity separates the magmatic rocks of the Harbour Main Group from the lower Cambrian conglomerate of the Brigus Formation (Anderson, 1987; Hutchinson, 1962). Throughout the Cambrian a continuous succession of shallow-marine to deep-marine sediments was deposited with only minor hiatuses, on the Avalon Peninsula (Hutchinson, 1953, 1962; Fletcher, 1972, 2006; Landing, 2004; Landing *et al.*, 2008). On the southern Burin Peninsula in contrast a continuous succession of shallow-marine sediments was deposited during the latest Neoproterozoic and the early Cambrian (Narbonne *et al.*, 1987; Landing *et al.*, 1988).

On the Avalon Peninsula the Cambrian mainly consists of grey, black or green mudstones and silt- to sandstones. Minor volcanic sediments occur in the succession. The lower Cambrian Smith Point Formation consists of 3–5 m thick, reef-like limestones. At Manuels River the Brigus, Chamberlain's Brook, Manuels River and Elliot Cove formations form the Cambrian succession (Fig. 5). The basal conglomerate of the lower Cambrian Brigus Formation is interpreted to represent a former coastline, for example a beach (Anderson, 1987). The Mudstones and intercalated thin-bedded limestones of the Brigus Formation represent a beginning transgression on the Avalon Peninsula (Landing and Westrop, 1998a; Wetzel, 2015). The nonconformably overlying manganese-rich sedimentary rocks at the base of the middle Cambrian Chamberlain's Brook Formation represent a temporary early middle Cambrian regression followed by a new transgression forming the mudstones and intercalated thin-bedded limestones of middle Cambrian Chamberlain's Brook Formation (Hutchinson, 1962; Wetzel, 2015). The mudstones of the Manuels River and the upper Cambrian Elliot

Cove formations are interpreted as shelf deposits (Hutchinson, 1962; Bergström and Levi-Setti, 1978). Wetzel (2015) found evidence for a shallowing-upward trend in the Elliot Cove Formation.

1.3.3. Ordovician (485–477 Ma)

On todays Avalon Peninsula Ordovician rocks are only exposed on three Islands in Conception Bay: Kelly's Island, Little Bell Island and Bell Island (Fig. 6). The rocks of the Bell Island and Wabana groups are characterised by cycles of shallow marine and terrestrial deposits and represent the youngest strata in Conception Bay Area. The beds consist mainly of siltstones and sandstones (Ranger *et al.*, 1984; King, 1988).

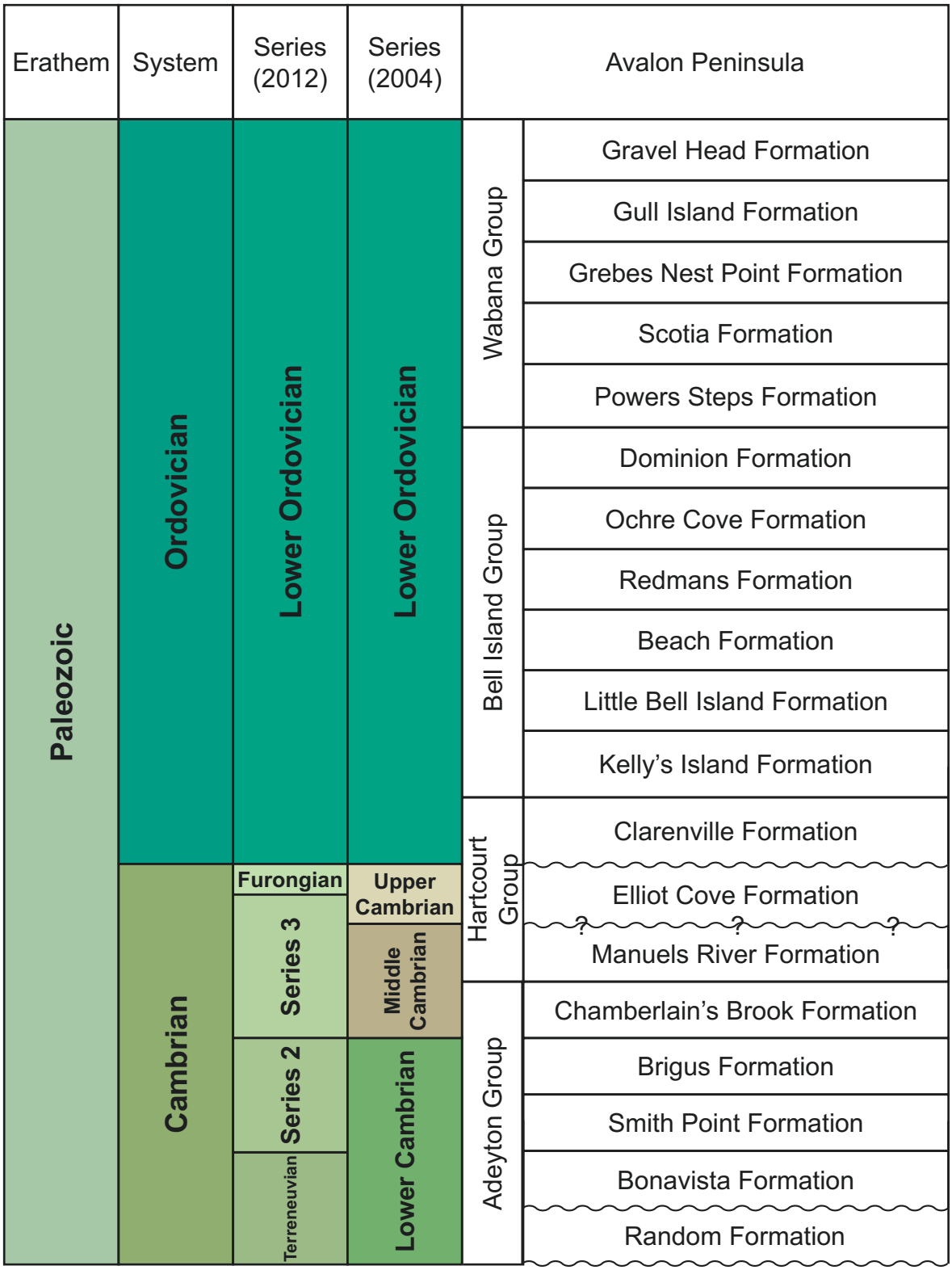

Fig. 14: Simplified chronostratigraphic table for the Palaeozoic on the Avalon Peninsula (based on Narbonne *et al.,* 1987; King 1988, 1990).

1.4. Study area

The valley of Manuels River is located on the south-eastern side of Conception Bay, on Newfoundland's Avalon Peninsula in the community of Manuels, Conception Bay South, Canada (Fig. 6). The capital city of Newfoundland, St. John's, is approximately 21 km east of the valley. The drainage basin of the 10 km long Manuels River is south of Newfoundland's Route 60. The river flows to the north-west with a weak current.

Access to the valley is on foot via trail from the Manuels River Hibernia Interpretation Centre, which is situated next to Newfoundland's Route 60. The type locality of Manuels River Formation, described in this study, is located on the west side of the river valley north of the Centre and south of the estuary of Manuels River (Fig. 1). Here the base of the Manuels River Formation is exposed at approximately 4 m above mean sea level (ASML) and is on coordinates 47.52512° N, -52.95119° E. The Manuels River valley is protected under Newfoundland and Labrador Regulation 67/11 "Palaeontological Resource Regulations under the Historic Resources Act".

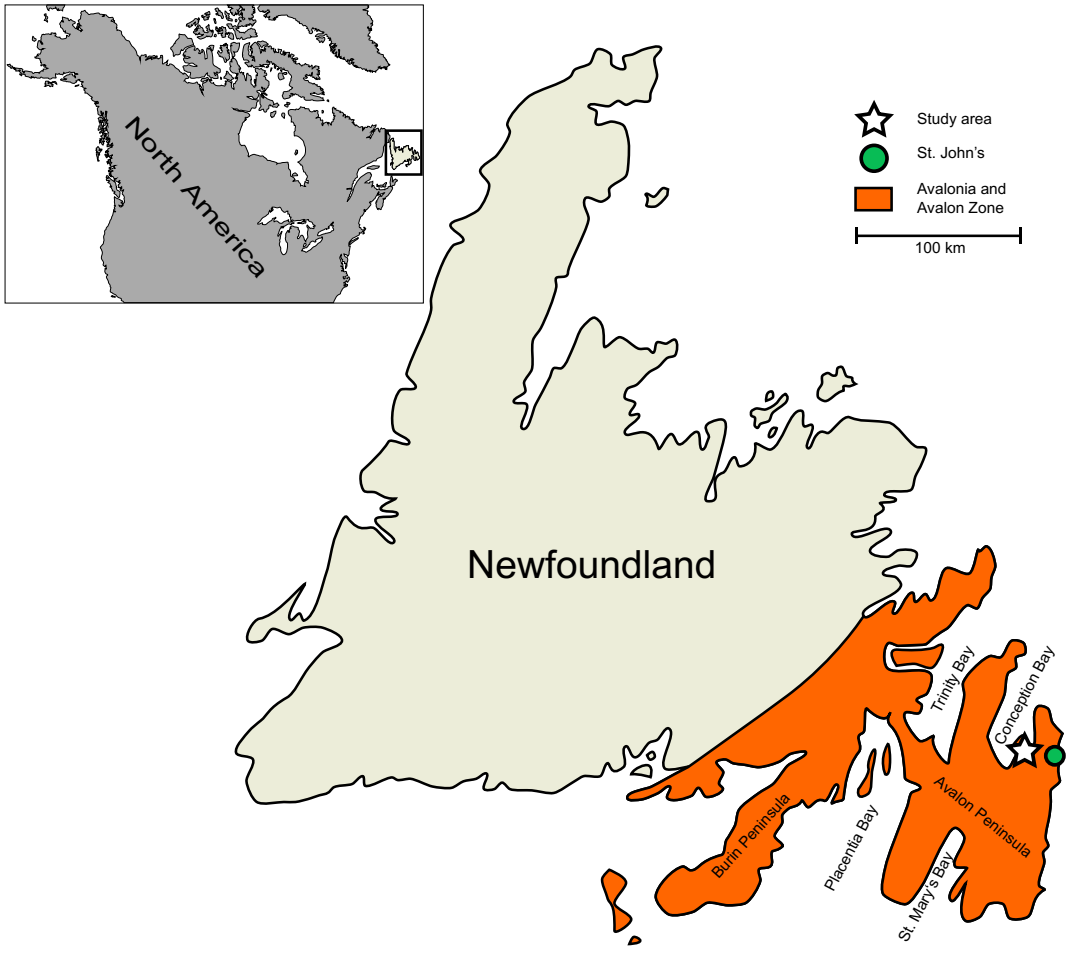

Fig. 15: Map of Newfoundland. The green dot marks its capital city St. John's, the white star the location of Manuels River valley.

Fig. 16: Map of the northern part of Manuels River. The black dashed line marks the trail to the type locality of Manuels River Formation. The star marks the type locality.

1.5. The Manuels River Formation

1.5.1. Definition

The Manuels River Formation was first formally defined by Hutchinson (1962) on the base of Howell's (1925) Long Pond and Kelligrew Brook formations (beds 36–125 incl.). It represents a late Middle Cambrian succession of mainly grey to black mudstones conformably overlying the greenish mudstones of the Chamberlain's Brook Formation. Its base consists of 5–13 cm thick soft white bentonite bed, considered by Fletcher (1972) as a "Metabentonite". This marker bed was also observed at other exposures like in Smith Sound, Trinity Bay or Deep Cove, St. Mary's Bay (Hutchinson, 1962; Fletcher, 1972, 2006).

The contact between Manuels River Formation and the overlying "Elliot Cove Group" was described by Hutchinson (1962) as a transitional zone from thick bedded shale with grey nodules to a mainly silty shale with black nodules. In addition he observed a faunal break in the Manuels River Formation in this interval. Thus he defined the bed with the apparent palaeontological break as the top of the Formation, bed 125 of Howell (1925). However, in 1975 the bed was proven not to represent a faunal break, as also proposed by Walcott (1900), but a break in sedimentation (Poulsen and Anderson, 1975), resulting from a regression. Howell's (1925) Long Pond and Kelligrew Brook formations were considered as local members of the Manuels River Formation by Hutchinson (1962), as they could not have been distinguished elsewhere on Avalon Peninsula. The type section at the west bank of the Manuels River is 20.76 m (68 ft.) thick (Howell, 1925; Hutchinson, 1962).

Fletcher (2006) proposed a reference section in Deep Cove, St. Mary's Bay with a thickness of 42.5 m and distinguished it in 4 Members, A–D. The base of the section is the previously mentioned Metabentonite and as of the top Fletcher (2006) suggested "the top of the highest limestone that forms a raised feature at the northern end of the Deep Cove beach" (Fletcher, 2006: 83).

1.5.2. Distribution and Thickness

The Manuels River Formation is exposed widespread over eastern Newfoundland, although most of it might have been removed by erosion (Hutchinson, 1962). Known exposures are in the region east of the Conception Bay, in St. Mary's Bay, Placentia Bay, Trinity Bay, on Red Island and on the southern Burin Peninsula, as well as on St. Pierre and Michelon and Cape Breton Island. Though the formation was found in many areas, complete sections are rare, as it is often faulted, closely folded and metamorphosed (Hutchinson, 1962). Thickness

varies from ca. 20 m at the Manuels River to ca. 42 m at St. Mary's Bay. The sections at Highland Cove, Trinity Bay and Fosters Point on Random Island comprise of ca. 33 m and 29 m respectively.

1.5.3. Lithology

The Manuels River Formation comprises of a succession of fine-clastic grey to black fossiliferous sedimentary rocks, mainly shales, with intercalated minor limestones or calcareous concretions (Howell, 1925; Hutchinson, 1962; Fletcher, 1972, 2006; Normore, 2012). Hutchinson (1962) reported more limestone in the upper half of the formation than in the lower half, especially for the areas of Conception Bay, Trinity Bay and Clarenville, whereas Fletcher (2006) reported a contrary proportion for Deep Cove St. Mary's. In most areas the mudstones have been metamorphosed to slate. The thin limestone beds and the limy lenses are commonly fossiliferous and remain even in regions affected by metamorphosis unmetamorphosed (Hutchinson, 1952, 1953). In St. Mary's Bay major volcanic sediments (basaltic flows, tuffs, etc.) were deposited in the upper portion of the formation (Fletcher, 2006, 1972).

1.5.4. Age and Correlation

The Manuels River Formation represents late Middle Cambrian strata, ranging from medial Middle Cambrian to late Middle Cambrian (Hutchinson, 1962; Fletcher, 1972, 2006). As Hutchinson (1962) marked, the formation is abundantly fossiliferous and several biostratigraphic arrangements and correlations were proposed. Howell (1925) distinguished his bed 35–125 into two biozones, the *Paradoxides hicksi* and the *Paradoxides davidis* zones (Fig. 1). Although the two upper zones have been marked by him as questionable, he stated, that the "*Paradoxides* faunas at Manuels may be closely related with those of Massachusetts, New Brunswick, and northwestern Europe" (Howell, 1925: 133). The lower zone (beds 36–92), the *Paradoxides (P.) hicksi* Zone, was correlated with New Brunswick's *P. abenacus* Zone, Great Britain's *P. hicksi* Zone and the *P. hicksi* Zone of Scandinavia. The upper *P. davidis* Zone (beds 93–125) was correlated with both Great Britain's and Scandinavia's *P. davidis* Zone. A new Brunswick analogue was not proven. This arrangement of the type section of the Manuels River Formation was adopted by (Hutchinson, 1962). He added a correlation of the *P. hicksi* Zone with the central part of the Trout Brook formation of Cape Breton Island and the Porter Road formation of New Brunswick. For the *P. davidis* Zone, he proposed a correlation with the upper part of the Trout Brook formation of Cape Breton Island, with the Hastings Cove formation of New Brunswick and with the *P. davidis* beds

	Newfoundland (Manuels River and Highland Cove)		New Brunswick		Cape Breton Island	Great Britain		Scandinavia	
Regional Unit	Howell (1925)	Hutchinson (1962)	Howell (1925)	Hutchinson (1962)	Hutchinson (1962)	Howell (1925)	Hutchinson (1962)	Howell (1925)	Hutchinson (1962)
Acadian		*Paradoxides forchhammeri* (present only in Highland Cove)			Mac Lean Brook formation				*Paradoxides forchhammeri*
	Paradoxides davidis (beds 92–125)	*Paradoxides davidis*		Hastings Cove formation	Trout Brook formation (upper part)	*Paradoxides davidis*	*Paradoxides davidis*	*Paradoxides davidis*	*Paradoxides davidis*
	Paradoxides hicksi (beds 36–91)	*Paradoxides hicksi*	*Paradoxides abenacus*	Porter Road formation	Trout Brook formation (central part)	*Paradoxides hicksi*	*Paradoxides hicksi*	*Paradoxides hicksi*	*Paradoxides hicksi*

Fig. 17: Chart showing the correlation of the Manuels River Formation by Howell (1925) and Hutchinson (1962).

of Great Britain. The *P. forchhammeri* Zone, only exposed in Highland Cove, Trinity Bay, has been correlated with the Mac Lean Brook formation of Cape Breton Island and the *P. forchhammeri* Zone of Scandinavia. The *Lejopyge laevigata* Zone, common in many late Middle Cambrian exposures of Europe, wasn't found in Newfoundland by Hutchinson (1962: 24). As previously mentioned, Hutchinson observed a faunal break at the contact of the Manuels River Formation and the "Elliot Cove Group", with missing *Lejopyge laevigata* Zone in the disconformity. Thus he proposed the contact of the two formations to represent the Middle–Upper Cambrian transition. Poulsen and Anderson (1975) proposed the existence of the *Lejopyge laevigata* Zone directly above the contact of the Manuels River Formation and the overlying "Elliot Cove Group", but there is evidence for a misassignment of the *Lejopyge laevigata* specimens (Rushton, 1978; Landing and Westrop, 1998a). However, *Andrarina costata* (Angelin), found in the same interval in Newfoundland and Sweden, suggests the existence of the *Lejopyge laevigata* Zone at the base of "Elliot Cove Group" (Landing and Westrop, 1998a). Thus the contact is considered to represent a late–latest Middle Cambrian transition.

For the section at Deep Cove, St. Mary's Bay, Fletcher (2006) presented two biozones, the lower *P. hicksii* Zone and the upper *P. davidis* Zone (Fig. 2.16). The lower one was correlated with *P. paradoxissimus* stage of Sweden including the top part of the *Ptychagnostus gibbus* Zone, the *Tomagnostus fissus–Acidusus atavus* zones, the *Hypagnostus parvifrons* Zone and the lowest part of the *Ptychagnostus punctuosus* Zone. Also it was correlated with sequences containing these zones in England, Siberia, Australia, USA (New York State, Utah and Alaska) and Denmark (Greenland). The upper one was correlated with the upper part of the *P. davidis* Zone of Great Britain, the upper part of *Ptychagnostus punctuosus* Zone of Scandinavia, the high Menevian beds of Wales and Australia, the Piso de *Solenopleuropsis* of Spain and the Ferrals-Les-Montagnes of France and southern Turkey.

2. Definitions

2.1. Chronostratigraphy

The subdivision of the Cambrian System has been the subject of discussion for fifteen decades. Brief overviews of the history of the debate were given for example by Peng and Babcock (2011) and Peng *et al.* (2012). Sedgwick (1852) divided the Cambrian System into three series: lower, middle and upper Cambrian. The base of the Cambrian System was traditionally characterised by the first appearance of trilobites. This concept was revoked recently by the International Subcommission on Cambrian Stratigraphy (ISCS) in 2004 (Peng, 2004; Peng and Babcock, 2011; Peng *et al.*, 2012). Now the basal Cambrian is characterised

<table>
<tr><th colspan="3">International Stratigraphic Chart 2015/01</th><th>Regional units</th><th>GSSPs and provisional stratigraphic tie points (after Peng et al., 2012)</th></tr>
<tr><th>System</th><th>Series</th><th>Stages</th><th>West Avalonia</th><td rowspan="15"></td></tr>
<tr><td>Ordovician</td><td>Lower</td><td>Tremadocian</td><td>Tremadocian</td></tr>
<tr><td rowspan="13">Cambrian</td><td rowspan="3">Furongian</td><td>Stage 10</td><td rowspan="4">Merionethian</td></tr>
<tr><td>Jiangshanian</td></tr>
<tr><td>Paibian</td></tr>
<tr><td rowspan="3">Series 3</td><td>Guzhangian</td></tr>
<tr><td>Drumian</td><td rowspan="3">Acadian</td></tr>
<tr><td>Stage 5</td></tr>
<tr><td rowspan="2">Series 2</td><td>Stage 4</td><td rowspan="2">Branchian</td></tr>
<tr><td>Stage 3</td></tr>
<tr><td rowspan="3">Terreneuvian</td><td>Stage 2</td><td rowspan="3">Placentian</td></tr>
<tr><td rowspan="2">Fortunian</td></tr>
<tr><td colspan="2">Ediacarian</td></tr>
</table>

⊥ *Iapetognathus fluctivagus* (GSSP)

⊥ *Lotagnostus americanus*

⊥ *Agnostotes orientalis* (GSSP)

⊥ *Glyptagnostus reticulatus* (GSSP)

⊥ *Lejopyge laevigata* (GSSP)

⊥ *Ptychagnostus atavus* (GSSP)

⊥ *Oryctocephalus indicus* / *Ovatoryctocara granulata*

? *Olenellus*, *Redlichia*, *Judomia*, or *Bergeroniellus*

? Trilobites

? *Watsonella crosbyi* or *Aldanella attleborensis*

⊥ *Trichophycus pedum* (GSSP)

Fig. 18: Chronostratigraphic subdivison and regional correlation of the Cambrian System for West Avalonia (composed and modified from Babcock *et al.*, 2005; Peng *et al.*, 2012; Cohen *et al.*, 2013).

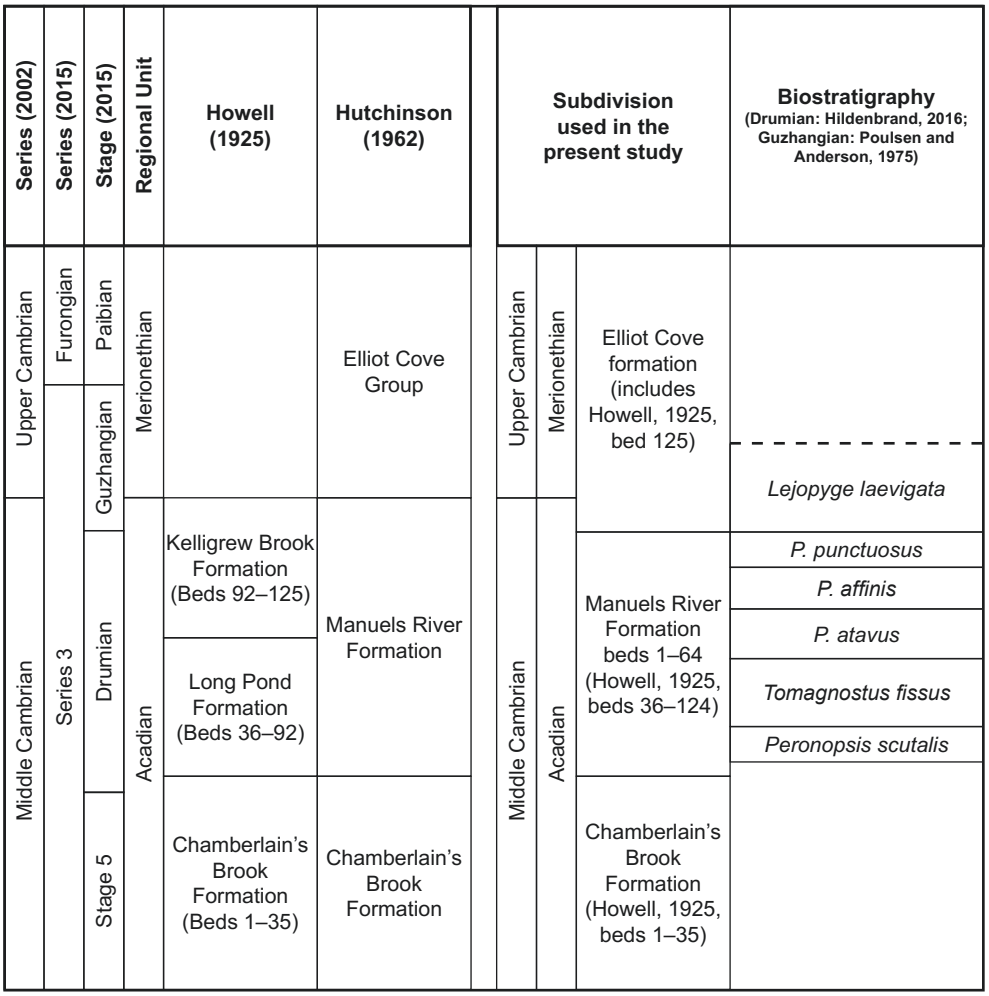

Fig. 19: Correlation of previous works with the subdivision used in the present study (composed and enhanced from Howell, 1925; Hutchinson,1962; Poulsen and Anderson, 1975; Landing and Westrop, 1998a; Cohen *et al.*, 2013; Hildenbrand, 2016). *P.*: *Ptychagnostus*.

by a significant change in trace-fossil associations and the first appearance datum (FAD) of the trace fossil *Trichophycus pedum*. The global stratotype section and point (GSSP) for the Precambrian-Cambrian boundary succession is located at Fortune Head, Newfoundland and was ratified in 1994 (Brasier *et al.*, 1994). No trilobites occur in the newly defined lowermost Cambrian layers, so the ISCS suggested a new four series concept. The basal series is devoid of trilobites, overlain by three series with trilobite zonation (Babcock *et al.*, 2005; Peng and Babcock, 2005). As shown in Fig. 18 the most recent stratigraphic chart (2015/01) of the International Commission on Stratigraphy (ICS) shows four series, subdivided into ten stages for the Cambrian System (Cohen *et al.*, 2013). The Cambrian System of Avalonia is subdivided into four regional units, Placentian, Branchian, Acadian and Merionethian. The here examined Acadian ranges from the basal Series 3 to upper but not topmost Series 3, more precisely from the base of Stage 5 to the middle Guzhangian (Fig. 18) (Peng *et al.*, 2012).

Most studies of the Cambrian in Avalonia and especially in the area of the Conception Bay, Newfoundland, were carried out before the new concept was established. The traditional three-series concept was considered to be very useful in the Avalonian terms, so some recent studies still use it (e.g. Fletcher, 2006; Landing *et al.*, 2006, 2013a). To simplify correlations with previous works, the traditional terms (e.g. middle Cambrian) are used in the present study. The classification and correlation with previous works, with the 2002 concept and with the 2015 concept respectively is shown in Fig. 19.

As top of the Manuels River Formation bed 124 of Howell (1925) is selected. This definition disagrees with Hutchinson (1962) and is discussed in the Chapter 5.1. The base of the Elliot Cove formation is bed 125 of Howell (1925). As a result of the inconsistency of the top of the Manuels River Formation with Hutchinson (1962), the overlying Elliot Cove formation is in need of a redefinition. Thus, this formation is herein treated as unformal.

2.2. Lithology

2.2.1. Carbonates

For the classification of carbonate rocks the nomenclature of Dunham (1962) is used. A summary is given in Fig. 20.

<table>
<tr><td colspan="5">Depositional texture recognizable</td><td rowspan="2">Depositional texture not recognizable</td></tr>
<tr><td colspan="4">Original components not bound together during deposition</td><td rowspan="3">Original components bound together during deposition</td></tr>
<tr><td colspan="3">Contains mud (particles of clay and fine silt size)</td><td rowspan="3">Lacks mud, grain-supported</td></tr>
<tr><td colspan="2">Mud-supported</td><td rowspan="2">Grain-supported</td></tr>
<tr><td>Less than 10% grains</td><td>More than 10% grains</td><td></td><td></td><td rowspan="2">Crystalline carbonate</td></tr>
<tr><td>Mudstone</td><td>Wackestone</td><td>Packstone</td><td>Grainstone</td><td>Boundstone</td></tr>
</table>

Fig. 20: Classification of Carbonate rocks (from Dunham, 1962).

2.2.2. Conglomerates and Breccias (more than 50% clasts > 2 mm)

Pettijohn (1975) basically distinguished three main types of conglomerates/breccias, Orthoconglomerates (matrix <15%), Paraconglomerates (matrix >15%) and intraformational conglomerates or breccias. The classification used in the present study is shown in Fig. 21.

Extraformational	Orthoconglomerates and breccias (matrix < 15 %)
	Paraconglomerates and breccias (matrix > 15 %)
Intraformational	Intraformational conglomerates and breccias

Fig. 21: Classification of conglomerates and breccias (modified after Pettijohn, 1975).

2.2.3. Sandstones (0.063–2 mm)

For the (sub-) determination of sandstones the classification of Dott (1964) is used in this study. An overview is given in Fig. 22.

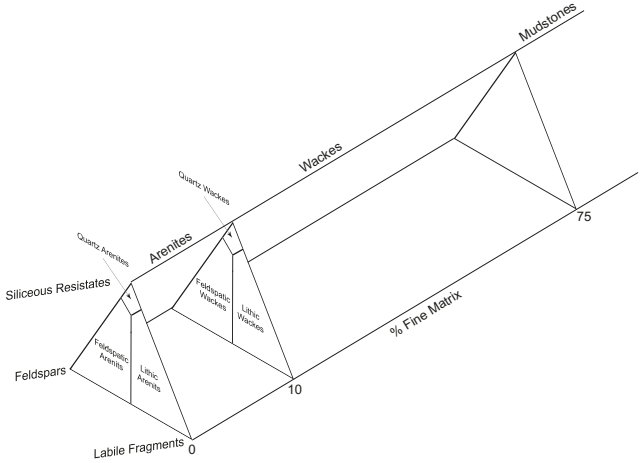

Fig. 22: Classification of sandstones (modified after Dott, 1964).

2.2.4. Shales (0.002–0.0625 mm)

According to Dott (1964) a fine-clastic rock with more than 75% matrix is referred to as a mudstone. By contrast, Blatt *et al.* (1972) defined fine-clastic rocks with a grain size less than 0.0625 mm as shales. Several recent studies account on the discussion of the terms "mudstone", "claystone", "siltstone" and "shale" (e.g., Potter *et al.*, 2005; Schieber, 1998; Boggs, 2009; Ulmer-Scholle *et al.*, 2015). Regardless of their texture and the sedimentary structures, Ulmer-Scholle *et al.* (2015) referred to siltstones and mudstones as shales, with a sub-classification of shale based on chemical composition. This classification is used for all chemical analyses in this study (Fig. 23). This classification is not useful in the field, so the term shale is used for all fine-clastic rocks with a grain size less than 0.0625

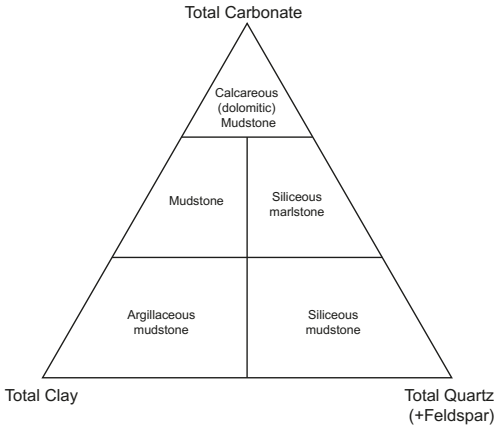

Fig. 23: Classification of shales (modified after Ulmer-Scholle *et al.*, 2015).

mm in all non chemical analyses and results, such as thin sections or description of the section in this study.

3. Methodology

3.1. Sampling

The material described in this study was sampled by the present author together with A. Hildenbrand (see Hildenbrand, 2016). The section was taken by a bed by bed measurement. Before the analyses, all samples have been randomised, in order of avoiding methodical errors (e.g. as a result of an increase of experience level).

3.2. Sample preparation and analyses

In order to obtain detailed information e.g. on the mineralogy and the chemical composition of the rocks at the type locality of the Manuels River Formation, several analyses were applied to the samples during this study. An overview is given in Fig. 24.

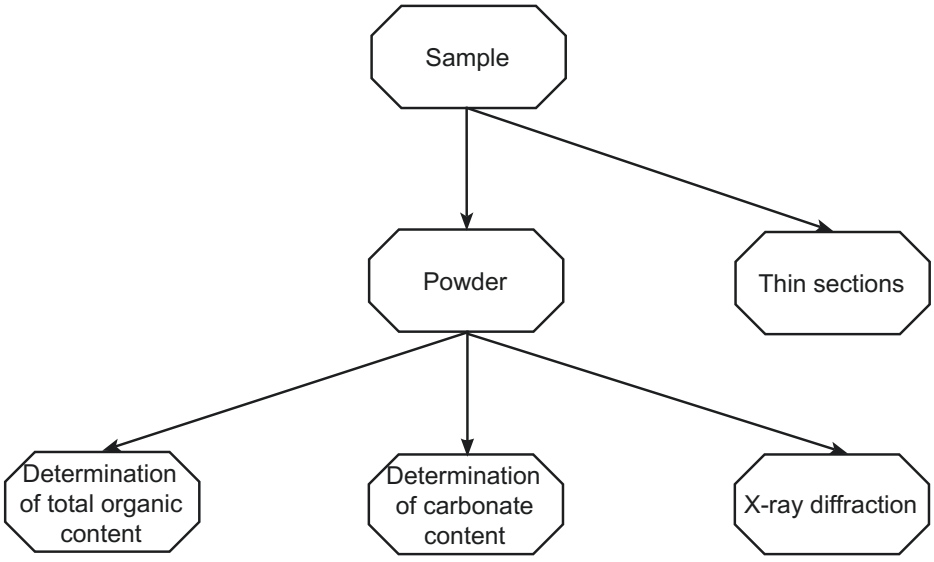

Fig. 24: Scheme of the physical and chemical analyses used in this study.

3.2.1. Thin sections

For the optical analysis of the samples under a stereo-microscope thin sections were fabricated. The thin sections were polished to an average thickness of 30 µm.

3.2.2. Grinding

All chemical and physical analyses, e.g. the determination of total organic content (TOC) or the X-ray diffraction (XRD), require a powder derived from the original material as base materials. Before the grinding, all samples were desiccated for 24 h at 45° C.

A key factor in obtaining a good powder sample for the XRD is the grain size (x) of the powder. Too coarse (x>40 µm) powder, may lead to unusual sharp peaks or intensities (Bish and Reynolds, 1989). Although longer grinding leads to a more homogeneous powder, too much grinding (e.g. x<0.1 µm) causes weakening or disappearing of reflexes (Reay, 1981; Bish and Reynolds, 1989; Milosevic *et al.*, 1992). The effect of the grinding time on the intensity of the peaks, as studied by Milosevic *et al.* (1992), is shown in Fig. 25. With too fine material (x<0.1 µm), one will also obtain unusual broad peaks (Bish and Reynolds, 1989). Moore and Reynolds (1997) recommended a grain size of 5–10 µm. Soft material, e.g. calcite, will be ground faster than harder material, e.g. quartz, which leads to a differentiation of the grain sizes dependent on the degree of hardness of the grains. With respect to these issues, a grinding time of 15 min. at 400 rpm in a Fritsch Pulverisette 5 vario-planetary agate mill was chosen as treatment.

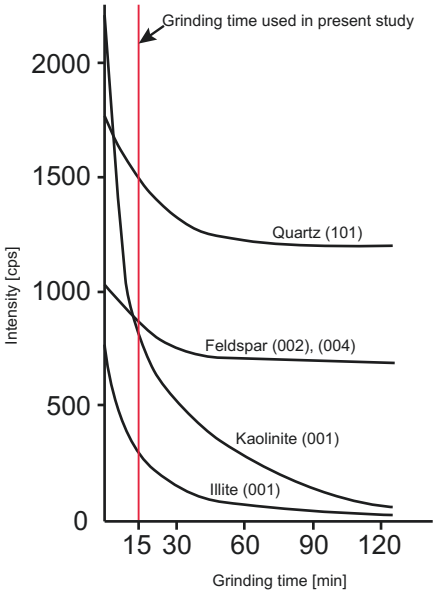

Fig. 25: Effect of the grinding time on the reflex intensity of different clay minerals (Milosevic *et al.*, 1992). Red line shows the grinding time used in this study (cps: counts per second).

3.2.3. Determination of total carbonate content

The total carbonate content was measured with a “Karbonate-Bombe”. The measurement was conducted after the method of Müller and Gastner (1971). For lowering the limit of detection, the quantity of material was increased significantly in most samples.

3.2.4. Determination of total organic content

The total organic content was measured indirectly, with the measurement of total carbon content. This was conducted with 1–2mg of the powder in a SC-analyzer (Model: Leco SC144Dr). Standardization was reached by measuring a calibration curve with pure $CaCo_3$. The previously measured total carbon content (anorganic) was subtracted from the measurement, to identify the total organic content.

3.2.5. X-ray diffraction

The analysis and interpretation of X-ray diffraction patterns or lines (diffractogram) is a common tool for the determination of the mineral phases of a sample. This method operates on the principle, that the different atom layers of a mineral diffract an incident X-ray beam (Fig. 26). With the distinctive wavelength (λ) and the angle (θ) of the beam, one can calculate the distance (d) of the different atom layers with Bragg's law (Bragg, 1913):

$$2 \cdot d \cdot \sin \theta = n \cdot \lambda, (n=1,2,3\ldots).$$

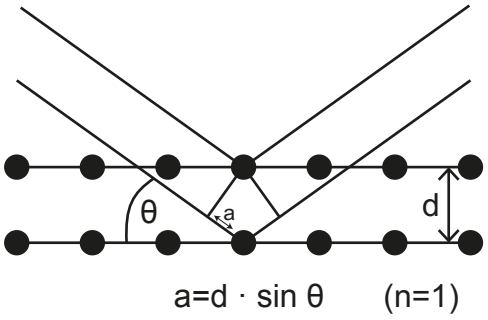

Fig. 26: Illustration of Bragg's law. The distance of the different layers can be calculated with $d = \lambda / (2 \sin \theta)$.

3.2.5.1. Sample preparation and measurement

The sample preparation user for the XRD carried out in this study mainly followed the description of Moore and Reynolds (1997) and is illustrated in Fig. 27. A Bruker D8 ADVANCE ECO Bragg-Brentano-diffractometer with a CuKα source was used for all measurements, with the diffraction angle (2θ) ranging from 0°–70°. The parameters used herein are given in (Table 1).

The powder, derived from the previously described grinding, was prepared separately for the quantitative analysis ("bulk rock") and the qualitative analysis and the identification of the carbonate-free clay minerals respectively.

Deionised water (2 ml) was mixed and shaken for approximately 15 sec with 4.5 mg of the powder for the bulk rock analysis. After pipetting the water-powder-mixture onto a 26 mm · 26 mm · 1 mm sized glass slide, it was desiccated for 24 h at 21° C under an extractor hood (see also "Glass Slide Method", Moore and Reynolds, 1997: 214).

Table 1: Measurement parameter of the diffractometer.

X-ray tube		**Detector**	
Power:	1.0 kW	Type:	Silicon strip detector
Amperage:	25 mA	Channels:	160
Acceleration voltage:	40 kV	Kβ-filter:	Nickel
Radiation:	$CuK\alpha_1$ (λ=1.540598 Å)		
	$CuK\alpha_2$ (λ=1.544426 Å)	**Aperture**	
Goniometer		Aperture diaphragm:	2.0 mm
Measurement range:	0°–70° [2θ]	Axial soller	2.5 °

One measurement with 2θ=0°–70° and one measurement with 2θ=0°–22° was taken. For the identification of the swell-able minerals a saturation with ethylene-glycol was ensured by exposing the samples to the vapour of the reagent in an desiccator for approximately 12 hrs, followed by a measurement with 2θ=0°–22°. Identification of water saturated minerals was ensured by heating the samples for 1 hr at 550° C in an oven, followed by a measurement with 2θ=0°–22°.

The identification of the clay minerals required a separation of the grain sizes x<2 µm, 2 µm < x <16 µm and x >16 µm. All separations of the different fractions were done by hydro-extraction in a Heraeus Megafuge 2.0r. The spinning times for the centrifuge were calculated under the usage of Stokes's law with the equation of Hathaway (1956) and the simplification of Rügner (2000):

$$T = \frac{9\mu \cdot \ln(R2 / R1)}{8\pi^2 \cdot N^2 \cdot r^2 (p - p_0)} + \frac{2(ta + td)}{3}$$

T = Runtime [sec]
μ = Viscosity
R1 = Inner distance to midpoint of rotor
R2 = Outer distance to midpoint of rotor
ta = Acceleration time [sec]
td = Slow-down time [sec]
N = Angular velocity
r = average particle size [cm]
p = Average density of particles [g/cm³]
p_0 = Density of the medium [g/cm³]

All parameters for the separation and concentration of the different fractions are given in Table 2.

For the separation 6 mg of the powder and approximately 50 ml of deionised water were mixed in a centrifuge tube. After approximately 15 sec of shaking, the samples were dispersed for 5 min. in an ultrasonic bath. Hydro-extraction for 2 min. at 700 rpm separated the x<2 µm and the x>2 µm fraction. After pipetting the upper portion (x<2 µm) into a new 50 ml tube (T1), the tube with the lower portion (x>2 µm) was filled up to 50 ml with deionised water (T2). Both tubes were dispersed 5 min. in an ultrasonic bath. For a higher concentration of the particle <2 µm T1 was hydro-extracted for 20.5 min. at 4000 rpm and

Table 2: Parameters for the differentition of the grain fractions using hydro-extraction

Grain size (x) [µm]	Temperature [° C]	Spinning velocity [rpm]	Spinning time [min]
2<x<16	20	300	2
<2	20	700	2

then pipetted on a glass slide. T2 was hydro-extracted for 1.75 min. at 100 rpm to separate the fraction x>16 µm from 2<x<16 µm. The upper portion (2<x<16 µm) was pipetted in a new tube (T2), whereas the lower portion (x>16 µm) was dismissed. For a higher concentration of the particle 2<x<16 µm T2 was hydro-extracted for 20.5 min. at 4000 rpm and then pipetted (approximately 4 ml) on a 26 mm x 26 mm x 1 mm sized glass slide. All glass slides were desiccated for 24 h at 21° C under an extractor hood.

One measurement with 2θ=0°–70° and one measurement with 2θ=0°–22° was taken. For the identification of the swell-able minerals a saturation with ethylene-glycol was ensured by exposing the samples to the vapour of the reagent in an desiccator for approximately 12 hrs., followed by a measurement with 2θ=0°–22°. Identification of water saturated minerals was ensured by heating the samples for 1 hr. at 550° C in an oven, followed by a measurement with 2θ=0°–22°.

For the qualitative detection of kaolinite random samples of the x<2 µm and 2<x<16 µm fractions were chosen. The samples were exposed to a formamide-containing atmosphere in an desiccator for 21 days (Churchman *et al.*, 1984). The samples were measured with 2θ=0°–22° before and after the treatment with formamide.

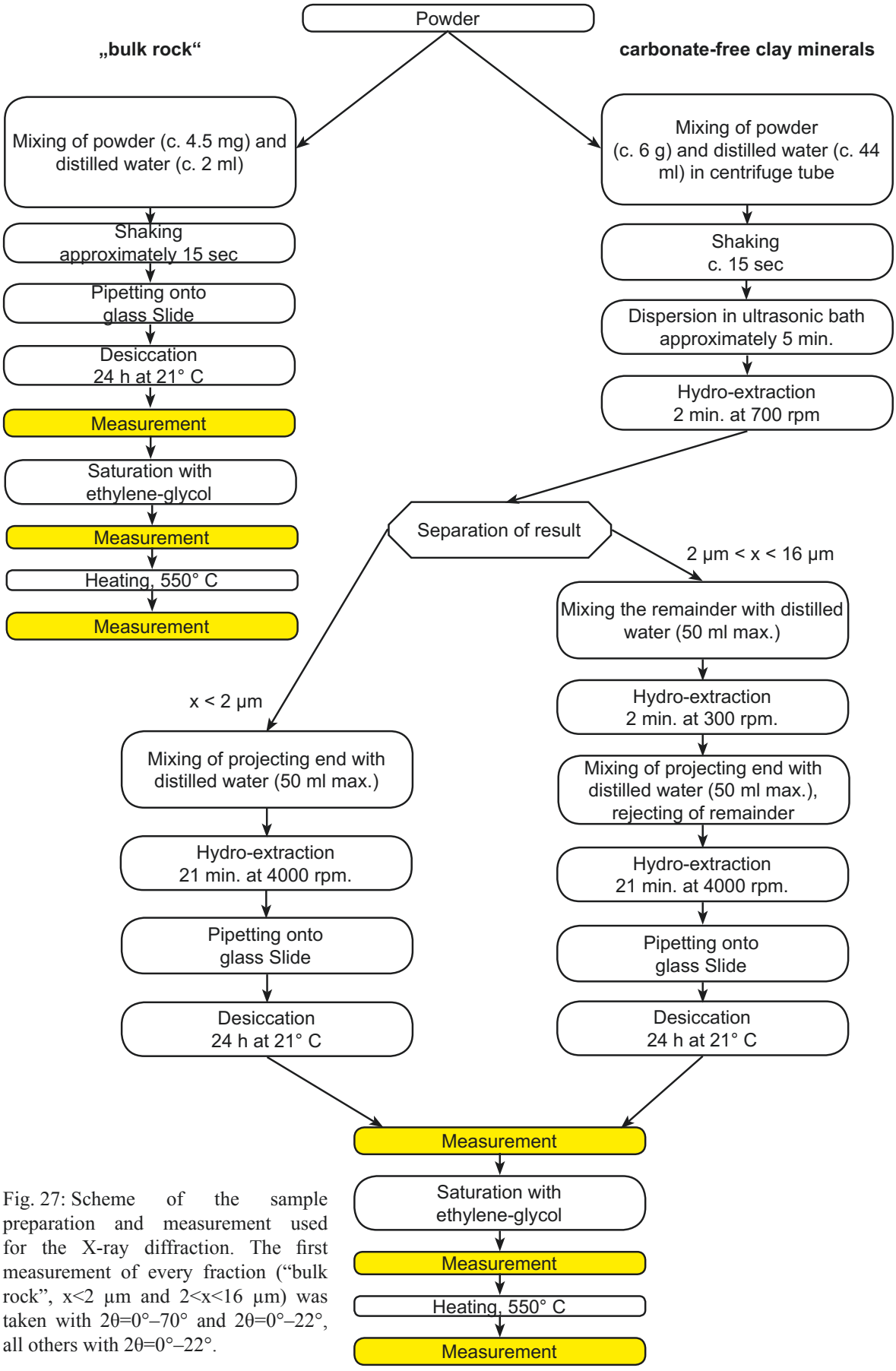

Fig. 27: Scheme of the sample preparation and measurement used for the X-ray diffraction. The first measurement of every fraction (“bulk rock”, x<2 µm and 2<x<16 µm) was taken with 2θ=0°–70° and 2θ=0°–22°, all others with 2θ=0°–22°.

3.2.5.2. Evaluation

For the computer-based evaluation of the results the software suites of Bruker DIFFRAC.EVA 3.1, Bruker DIFFRAC.TOPAS, Fityk 1.2.0 (Wojdyr, 2010) and R 3.2.2 (R Core Team, 2016) were used. XRD mineral data was provided by the ICDD PDF2 1999 database.

3.2.5.3. Illite crystallinity

A common tool for the determination of the degree of diagenesis is the calculation of the illite crystallinity (Kübler Index) as shown by Kübler (1967). According to Eberl and Velde (1989) a more accurate measurement and calculation of the illite crystallinity is obtained by the usage of the Środoń intensity ratio Ir (Środoń, 1984):

$$Ir = [001/003]_{air\text{-}dried} / [001/003]_{glycolated}$$

As the obtained peak data is commonly compound from overlaps of different reflexes (Klug and Alexander, 1974), a mathematical model (peak fitting) for the description of the mineral peaks was applied. After eliminating the background of the measurement (Fig. 28 A) the model was fitted to the obtained data in an iterative process under the usage of the Split-Pseudo-Voigt-Function (Fig. 28 B). Afterwards the maximum, the position and the full width at half maximum (FWHM) of the illite reflexes were calculated. The FWHM of the [001] $_{air\text{-}dried}$ reflex of the Illite was plotted against *Ir*. The modelling and FWHM calculation was carried out with the computer program Fityk 1.2.0 (Wojdyr, 2010), the statistical analysis of the data with R 3.2.2 (R Core Team, 2016).

3.2.5.4. Systematic aberrations

The measurement accuracy of XRD-analysis is influenced by systematic aberrations, deriving from the sample preparation and handling and the measurement instrument itself. As the inaccuracies were already discussed in detail in a couple of studies (e.g. Bish and Reynolds, 1989; Moore and Reynolds, 1997), a brief overview of the most important ones is given in the following paragraphs (after Bish and Reynolds, 1989):

Flat specimen: In a Bragg-Brentano diffractometer the sample surface is not co-concentric

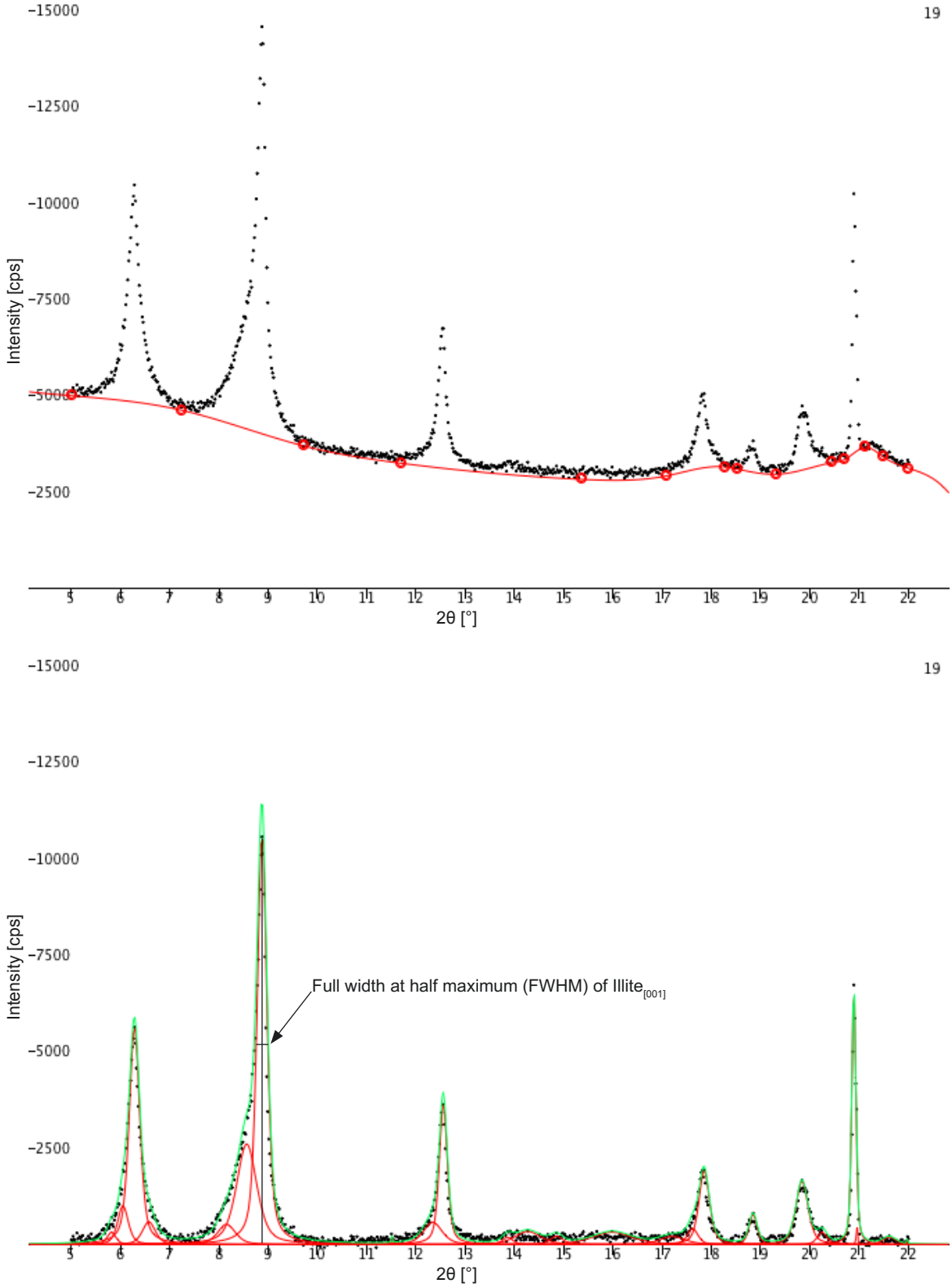

Fig. 28: A) Example XRD data. The area below the red graph marks the background, which must be subtracted to calculate any crystallinity. B) Same example data as A with subtracted background. The red graphs represent the calculated peaks (Split-Pseudo-Voigt fitted). The green graph marks the result of the iterative fitting process.

with the goniometer, but tangentially aligned with the circle of focus of the goniometer. This configuration "causes an asymmetric broadening of the diffracted line profile towards low 2θ angles" (Bish and Reynolds, 1989: 26):

$$\Delta 2\theta = - 1/6 \cdot \delta 2 \cdot \cot \theta$$

δ angular aperture of the divergence slit

The aberration is increasing with increasing 2θ, as the circle of focus is decreasing with increasing 2θ.

Displacement error: This aberration is caused by misplacing the sample on the focusing circle of the goniometer. One will obtain an asymmetric broadening of the diffracted line profile, towards low 2θ angles. Bish and Reynolds (1989) marked on a total shift of peak 2θ positions of about 0.01° 2θ per 15 μm of displacement. It is given by:

$$\Delta 2\theta = - 2s \cdot (\cos \theta / R)$$

s displacement of the sample
R Radius of the goniometer

Kα_2-aberration: Braggs's Law requires a distinct wavelength of the used radiation for an accurate determination of the peak position. As the used CuKα radiation source is composed of a Kα_1 and a Kα_2 portion, it is not a strict monochromatic radiation and thus does not have a distinct wavelength. This causes a dispersion of the ray, causing an asymmetric broadening of the peaks, that increasing towards higher 2θ angles. The intensities of the peaks decrease towards higher 2θ angles (Moore and Reynolds, 1997).

4. Results

4.1. Fieldwork

The detailed bed-by-bed macroscopic description of the middle Cambrian succession along the west bank of Manuels River is given in Table 3 and is drawn as section in Fig. 30. The succession comprises the Manuels River Formation at its type locality as defined by Hutchinson (1962).

The succession consists of 19.07 m of mainly grey to black shale. The basal bed consists of a 2-cm-thick soft volcanic ash layer (bentonite), overlying the lower middle Cambrian Chamberlain's Brook Formation (Fig. 29). The top consists of a 7-cm-thick layer of coarse sandstone to conglomerate, unconformably overlying the shale. Besides this unconformity, the whole succession appears to be conformable.

Scattered thin layers of volcanic ashes are interbedded (beds 1, 16, 33, 52, 55 and 57). Also beds with thin limy or siliciclastic concretions occur, especially in the lower half of the succession (beds 3, 5, 7, 9, 11, 13, 18, 20, 25, 29, 31, 35, 39, 43 and 48). The shales are highly fossiliferous. The fossil content is discussed in detail by Hildenbrand (2016). The lower half of the succession is characterised by mainly grey to dark grey shale, whereas the upper half is characterised by mainly dark grey to black shale, locally with abundant bioturbation. The burrows and holes are often filled with pyrite. The number of fissile shales increases towards the top of the formation.

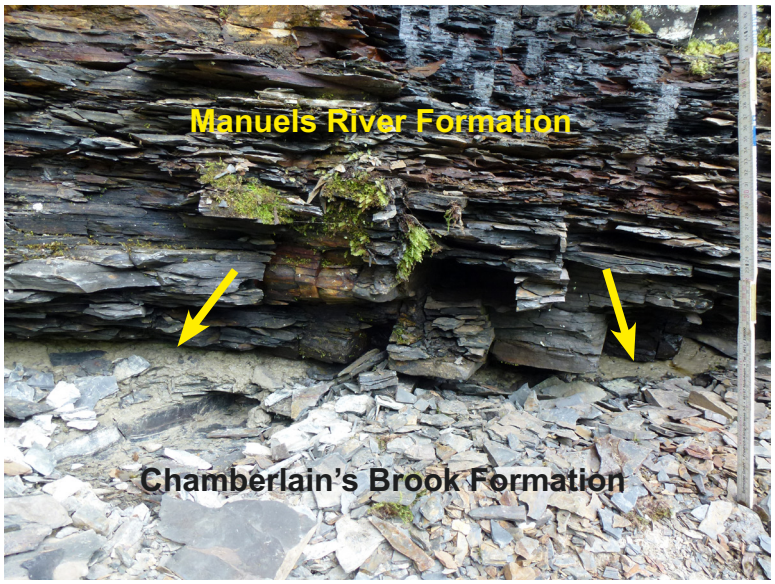

Fig. 29: Basal bentonite (bed 1, arrows) of the Manuels River Formation.

Fig. 30: (next page) Measured section along the west bank of Manuels River. Two shallowing upward trends are interpreted from the thin sections. No macroscopic sedimentary structures are observed.


Formation
Biozone (Hildenbrand 2016)
Bed
Thickness [m]
Lithology
Key
Conglomeratic sandstone
Calcareous concretions
Shale
Bentonite
Shallowing upward
ECf
Elliot Cove formation
ECf
Manuels River Formation
Ptychagnostus punctuosus
Ptychagnostus affinis
Ptychagnostus atavus
Tomagnostus fissus
Peronopsis scutalis

Table 3: Macroscopic description of the succession at the type locality of the Manuels River Formation. The base is at bed 92 and the top at bed 125 of Howell (1925).

Bed	Thickness [cm]	Description	Overall thickness [m]	Bed (Howell, 1925)
1	2	White soft volcanic ash, irregular bedding at base	0.02	36
2	22	Grey shale, very compact, sub-cm-bedded with fragments of brachiopods	0.24	37–38
3	7	Grey calcareous concretions	0.31	
4	40	Grey shale, very compact at the base softer to the top, sub-cm-bedded with fragments of brachiopods	0.71	
5	0.5	Grey calcareous concretions	0.715	
6	15	Grey shale, very compact, sub-cm-bedded with fossil fragments	0.865	39
7	0.5	Grey calcareous concretions	0.87	
8	29	Grey shale, very compact, sub-cm-bedded with fragments of brachiopods and trilobites	1.16	
9	2	Grey calcareous concretions	1.18	
10	10	Grey shale, very compact, sub-cm-bedded	1.28	40
11	2	Grey calcareous concretions, bluish colour at the top	1.3	
12	23	Dark grey to black shale, very compact, sub-cm-bedded with brown to orange weathering fragments of brachiopods and trilobites, fossil abundancy is decreasing to the top	1.53	
13	1	Grey calcareous concretions	1.54	

14	22	Dark grey to black shale, very compact, sub-cm-bedded with brown to orange weathering fragments of brachiopods and trilobites,fossil abundancy is decreasing to the top	1.76	40
15	16	Grey shale with irregular bedding, containing scattered calcareous concretions, fragments of brachiopods and trilobites	1.92	41
16	2	White soft volcanic ash	1.94	42
17	42	Light grey hard shale, cm bedded with irregular bedding, containing well preserved trilobites, some layers contain well-assortet fragments of trilobites	2.36	43–44
18	2	Grey calcareous concretions	2.38	
19	47	Grey shale, compact, irregular mm bedded, some layers thin weathered and very fragile, brown to reddish lens shaped weathering, scattered layers containing huge amounts of small fossil fragments	2.85	45–49
20	2	Grey calcareous concretions	2.87	
21	17	Grey shale, compact, irregular mm bedded, some layers thin weathered and very fragile, brown to reddish lens shaped weathering, scattered layers containing huge amounts of small fossil fragments and scattered layers contain thin concretions	3.04	50–52

22	30	Light grey hard shale, cm bedded with irregular bedding, containing well preserved trilobites, some layers contain well-assortet fragments of trilobites	3.34	
23	22	Grey to brown hard shale, cm bedded, brown to reddish weathering, isolated poorly preserved fossil fragments	3.56	50–52
24	23	Grey shale, compact, brown to reddish weathering, fragments of trilobites	3.79	
25	10	Grey calcareous concretions	3.89	
26	26	Grey shale with irregular bedding, containing scattered calcareous concretions, fragments of trilobites	4.15	
27	2	Grey calcareous concretions	4.17	
28	54	Dark grey to black shale, very compact, sub-cm-bedded, to the top cm bedded, with brown to orange weathering fragments of trilobites, isolated layers contain well-assorted fragments	4.71	53–57
29	3	Grey calcareous concretions	4.74	
30	35	Dark grey to black shale, very compact, sub-cm-bedded, to the top cm bedded, with brown to orange weathering fragments of trilobites, isolated layers contain well-assorted fragments	5.09	
31	2	Grey calcareous concretions	5.11	
32	15	Dark grey to black, bluish shale, hard, sub-cm-bedded, to the top cm bedded, with brown to orange weathering fragments of trilobites, isolated layers contain well-assorted fragments	5.26	58–59

33	4	Bright grey soft volcanic ash, irregular bedding at base	5.3	60
34	11	Light grey hard shale, sub-cm-bedded with irregular bedding, isolated layers contain fragments of trilobites	5.41	61–63
35	1	Grey calcareous concretions	5.42	
36	10	Light grey hard shale, sub-cm-bedded with irregular bedding, isolated layers contain fragments of trilobites	5.52	64–73
37	25	Dark grey to black shale, very compact, sub-cm-bedded, reddish to brown weathering, top with wavy bedding	5.77	
38	49	Dark grey to bluish shale, sub-cm-bedded	6.26	
39	1	Grey calcareous concretions	6.27	74
40	13	Grey to greenish shale, sub-cm-bedded	6.4	75–80
41	18	Dark grey shale, mm bedded, fissile, isolated fragments of fossils	6.58	
42	73	Grey shale, very compact, sub-cm-bedded, scattered reddish weathering	7.31	
43	4	Grey calcareous concretions	7.35	81–88
44	36	Grey to greenish shale, sub-cm-bedded	7.71	
45	32	Grey shale, hard, cm bedded	8.03	
46	43	Dark grey shale, mm bedded, fissile, isolated fragments of fossils	8.46	
47	22	Grey shale, irregular sub-cm-bedded, brown to reddish weathering	8.68	
48	12	Grey calcareous concretions	8.80	89–92

49	73	Grey hard shale, sub-cm-bedded, layers in the middle part contain very well preserved yellow weathering trilobite specimens	9.53	89–92
50	3	Dark grey shale, very fissile	9.56	
51	107	Dark grey to black pyritiferous shale, very compact, sub-cm to cm bedded, middle part contains isolated thin (sub-mm) layers of soft volcanic ash, brown to reddish weathering, fragments of trilobites common	10.63	93–98
52	13	Grey soft volcanic ash, orange to brown weathering	10.76	
53	62	Dark grey to black soft pyritiferous shale, sub-cm-bedded, fragments of trilobites and bioturbation common	11.38	99–100
54	127	Grey to dark grey compact pyritiferous shale, cm to sub-cm-bedded, middle part contains some thin (sub-mm) layers of soft volcanic ash, reddish weathering, fragments of trilobites common	12.65	101–103
55	6	Grey soft volcanic ash, orange to brown weathering	12.71	
56	120	Grey pyritiferous shale, irregular sub-cm-bedded, brown to reddish weathering, to the increasing amount of fossil fragments	13.91	104–107
57	2	Grey soft volcanic ash, orange to brown weathering	13.93	
58	183	Dark grey pyritiferous shale, sub-cm-bedded, thinner-bedded at the base, isolated concretions, fragments of fossils common	15.76	108–113

59	43	Dark grey shale, very fissile	16.19	114–115
60	46	Light grey to greenish shale, irregular cm bedded, isolated concretions	16.65	
61	19	Dark grey pyritiferous compact shale, cm bedded, trilobite fragments common	16.84	
62	3	Black shale, mm bedded, containing huge amount of fossil fragments	16.87	
63	110	Dark grey pyritiferous weakly compacted shale, mm bedded, very fissile, orange to brown weathering, trilobite fragments and bioturbation common	17.97	116–124
64	103	Dark grey pyritiferous shale, sub-cm-bedded, fragments of fossils and bioturbation common	19	
65	7	Coarse sandstone to conglomerate with clasts of shale, marly matrix, base is erosional	19.07	125

4.2. Thin Sections

For the detailed optical analysis of the rock samples and beds, thin sections from selected beds were made. The stratigraphic levels given for each sample refer to the base of the Manuels River Formation.

Bed 2 (Table 3 A) consists of a massive, unsorted shale. A lamination is not visible. Scattered organic matter in dark lenses or flattened seams occurs. The thin section shows some bedding-parallel fractures, which are possibly a result of the grinding and polishing process.

Bed 3 (Table 3 B) is composed of calcareous concretions. Shell fragments, possibly of trilobites and brachiopods are abundant. The concretions contain a significant amount of mud (>10%) and are classified as wackestone.

Bed 4 (Table 3 C–D) shows similar characteristics to bed 2. The shale is massive and has no visible lamination. Dark seams of organic matter are abundant. In Table 3 D a larger (c. 1 mm long) sub-rectangular shaped fragment, possibly of an acritarch, is visible.

Bed 8 (Table 3 E) shows a massive, unsorted shale of bed 8. Compared to beds 2 and 4 the matrix appears to be coarser. The shale contains some sub-rounded fragments of organic matter, possibly of acritarchs. The fragments were in part or completely washed out, possibly during the grinding and polishing process.

Bed 12 (Table 3 F) shows similar features to bed 8. The diagonal lines visible in the thin section were caused by the grinding process. Typical for this bed are the relatively large shell fragments of trilobites. Organic matter, as visible in bed 4 is almost absent.

Bed 14 (Table 3 G–H) is composed of weakly laminated shale. Organic matter occurs in lenses and dark seams. The apparent cross-bedding in the upper part of the thin section is an artefact caused by the grinding and polishing.

Bed 15 (Fig. 30) is a massive shale. Abundant brown to black organic matter is formed in lenses and seams. In the lower part a larger hole is visible. The shape of the hole suggests a washed out trilobite shell.

Bed 17 (Fig. 30 B) consists of a massive shale with concentrated organic matter in dark seams. A lamination is not visible, but appears traceable by the dark seams. The sample also shows bedding-parallel fractures, possibly caused by the grinding and polishing process.

Bed 19 (Fig. 30 C–D) is a massive, unsorted shale. No lamination is visible, but appears to be traceable by dark seams (concentrated organic matter). Shell fragments, possibly of trilobites are abundant. The fragments are unsorted and seem to float in the sediment. Some fragments are covered in part or completely by a black mineral, possibly haematite or the original shell material may be altered. Also scattered sub-rounded organic matter occurs, possibly fragments of acritarchs.

Bed 21 (Fig. 30 E–F) consists of thin calcareous concretions bedded in shales. The lamination of the shale, traceable by dark organic-rich seams, flows around the light grey concretion in the middle of the figure. There occur shell fragments, in part or completely altered or covered by haematite. The concretion contains a significant amount of mud (>10%) and is therefore classified as a wackestone. Unsorted shell fragments, possibly of trilobites and brachiopods are abundant, except in the centre of the concretion. The concretion seems to develop from the border to the centre, followed by a shell-rich zone, to the centre-zone, where the recrystallisation is complete and shells are not visible anymore.

Bed 22 (Fig. 30 G) is a laminated shale. Concentrated organic matter occurs in the pores and as lenses in the laminae or flattened in seams. The organic matter appears only in distinct layers, rather then in the entire bed.

Bed 23 (Fig. 30 H) consists of laminated shale resembling bed 22. The uppermost part of the thin section consists of coarser material. Concentrated organic matter occurs in the pores and as lenses in the laminae or flattened in seams. The sample also shows bedding-parallel fractures, possibly caused by the grinding and polishing process.

Bed 26 (Fig. 29 A) is a laminated shale. Abundant organic matter occurs in dark seams, especially in the lower part of the thin section. Scattered shell fragments occur, in part or completely altered and covered by haematite.

Bed 28 (Fig. 29 B) is very similar to bed 26. Concentrated organic matter in dark seams is abundant. Shells or fragments of shells are not visible in the thin section.

Bed 30 (Fig. 29 C) consists of laminated shale. Concentrated organic matter occurs in the pores and as lenses in the laminae or flattened in seams. The thin section also shows bedding-parallel fractures, possibly caused by the grinding and polishing process.

Bed 37 (Fig. 29 D) is a fine laminated shale. Organic matter occurs in dark lenses or short seams. The thin section also shows bedding-parallel fractures, possibly caused by the grinding and polishing process.

Bed 38 (Fig. 29 E) consists of massive, unsorted shale with concentrated organic matter in dark seams. No lamination is visible, but it appears to be traceable by the dark seams. Scattered shell fragments possibly of trilobites, covered and altered by haematite occur. The hatch covering the whole thin section was caused by the grinding and polishing process.

Bed 40 (Fig. 29 F) consists of laminated shale. In the middle part, finer and darker material is interbedded. Concentrated organic matter occurs in the pores and as lenses in the laminae or flattened in seams. A large orange to brown prismatic crystal is visible near the right margin of the thin section. The organic matter and also the lamination flow around the crystal. The crystal appears to be altered and covered by organic material.

Bed 42 (Fig. 29 G) consists of laminated shale. Concentrated organic matter occurs in

the pores and as lenses in the laminae or flattened in seams. A shell fragment occurs, possibly of a trilobite, covered and altered by haematite. Below the shell fragment compaction is visible.

Bed 44 consists of laminated shale (Fig. 29 H). Concentrated organic matter occurs in the pores and as lenses in the laminae or flattened in seams. In the lower part of the thin section, lenticular bedding is faintly visible. Scattered, large opaque crystals (0.5 mm in diameter) with the habitus of pyrite occur.

Bed 46 (Fig. 34 A) is a massive, unsorted shale. No lamination is visible. Scattered opaque minerals occur, possibly pyrite and haematite.

Bed 47 (Fig. 34 B–D). The lower part of B (detailed in C) consists of a chaotic accumulation of shell fragments (e.g., trilobites, brachiopods, echinoderms). The shell material is relatively unaltered and not covered by haematite or other material. The upper part of the thin section consists of laminated shale with scattered shell fragments. As shown in D, compacted organic matter in seams follows the shape of the shell fragments. The fractures, visible in the figure are possibly a result of the grinding process.

Bed 49 (Fig. 34 E–G). The lower part of the bed consists of a shale with a high amount of shell fragments. The lower part of the thin section consists of coarser, partly sandy material with "floating" shells. The lower third appears to be somewhat chaotic. The upper half of the thin section is composed by a lens-shaped accumulation of shell fragments with calcite cement. Some of the fragments are trilobite shells, but most are of doubtful origin.

The upper part of the bed (Fig. 34 H) is a laminated shale. Concentrated organic matter occurs in the pores and as lenses in the laminae or flattened in seams.

Bed 51 (Fig. 35 A–C). The lower part of the bed 51 consists of massive to laminated shale with synsedimentary soft-sediment deformation. Scattered altered shell fragments occur, possibly of trilobites (Fig. 35 B). The fragments do not appear to "float" in the sediment, rather then have been curled or twisted. Concentrated organic matter occurs in the pores and as lenses in the laminae or flattened in seams.

The upper part of the bed (Fig. 35 C) is a laminated shale. In the lower half of the thin section abundant concentrated organic matter occurs in the pores and as lenses in the laminae or flattened in seams. Finer and coarser material alternate. The upper half is laminated and homogeneous. Organic matter is concentrated in lenses and pores. The amount of organic matter decreases towards the top of the thin section.

Bed 54 (Fig. 35 D–G). The lower part of the bed (Fig. 35 D) is a laminated shale with interbedded lenticular fabric. Scattered, relatively large (approx. 0.5 mm in diameter) ,sub-rounded holes in which clasts appear to have been seated are visible. Abundant concentrated organic matter occurs in the pores and as lenses in the laminae or flattened in seams. The thin section also shows bedding-parallel fractures, possibly caused by the grinding and polishing

process.

The middle part of the bed (Fig. 35 E–F) consists of a massive to laminated shale. Some large (up to 3 mm in diameter) opaque crystals occur, possibly pyrite or haematite (Fig. 35 E). The lamination "flows" around the minerals. Compaction is visible below the crystals. Abundant relatively large (approx. 0.2 mm in diameter) sub-rounded holes in which clasts appear to have been seated are visible (Fig. 35 F). Concentrated organic matter occurs in the pores and as lenses in the laminae or flattened in seams. Some fractures, partly diagonal to the bedding, occur.

The upper part of the bed (Fig. 5.48 G) consists of a laminated shale. Abundant concentrated organic matter occurs in the pores and as lenses in the laminae or flattened in seams. Some opaque crystals occur, possibly pyrite or haematite.

Bed 56 (Fig. 5.49 H) consists of laminated shale, with interbedded lenticular fabric. Scattered sub-rounded holes in which clasts appear to have been seated are visible. Abundant concentrated organic matter occurs in the pores and as lenses in the laminae or flattened in seams. The thin section also shows bedding-parallel fractures, possibly caused by the grinding and polishing process.

Bed 58 (Fig. 36 A–E). The lower part of the bed (Fig. 36 A) is a laminated shale interbedded with lenticular fabric. Some opaque crystals occur, possibly pyrite or haematite. Scattered sub-rounded holes in which clasts appear to have been seated are visible. Concentrated organic matter occurs in the pores and as lenses in the laminae or flattened in seams. Some fractures occur, partly diagonal to the bedding.

The second quarter of the bed (Fig. 36 B–C) is a laminated shale, interbedded with lenticular fabric. The lower third (B) of the thin section is dominated by coarse material with lamination. The middle third consists of shale with lenticular fabric and abundant concentrated organic matter, flattened in seams. In this part, fractures occur, diagonal to the bedding, partly filled with goethite (red) or covered by haematite. Also other opaque crystals are visible, possibly pyrite. The border to the overlying fine laminated shale in the upper third is very distinctive (C). At the base of the laminated shale, organic matter is concentrated in a dark seam.

The third quarter of the bed (Fig. 36 D) consists of a laminated shale. Darker and finer material is interbedded with brighter and coarser material. In part altered shells are visible, possibly of trilobites. Concentrated organic matter occurs in the pores and as lenses in the laminae or flattened in seams. In the lower part scattered sub-rounded holes in which clasts appear to have been seated are visible. In the upper part lenticular holes occur, possibly of washed-out lenticular fabric. The thin section also shows bedding-parallel fractures, possibly caused by the grinding and polishing process.

The fourth quarter of the bed (Fig. 36 E) consists of a massive to laminated shale.

Concentrated organic matter occurs in the pores and as lenses in the laminae or flattened in seams. The lower part is more or less massive, whereas the upper half shows lamination. The amount of organic matter is decreasing from the middle towards both ends of the thin section. A relatively large altered sub-rounded clast occurs, covered by possibly haematite. The sample also shows bedding-parallel or diagonal fractures, possibly caused by the grinding and polishing process.

Bed 60 (Fig. 36 F) is a massive laminated shale. Concentrated organic matter occurs in the pores and as lenses in the laminae or flattened in seams. In part, the lamination is traceable by the organic matter.

Bed 61 (Fig. 36 G–H) consists of a laminated shale with organic matter in seams or in the pores (G). Scattered shell fragments occur, possibly of trilobites (H). The shells are altered and the margins of the shells are thus not always distinctive.

Bed 64 (Fig. 37 A–B) consists of interbedded coarser (silty) and finer (muddy) shales. The shale is wavy bedded (B). Organic matter is concentrated at the base of silty layers. Scattered sub-rounded holes in which clasts appear to have been seated are visible.

Bed 65 (Fig. 37 C–E) is a coarse sandstone to conglomerate. Fig. 37 C shows the relatively high quartz amount and the sandy matrix. Fig. 37 D shows a small volcanic clast with intraclasts of opaque material. Fig. 37 E shows a clay clast, possibly resulting from recycled underlying material.

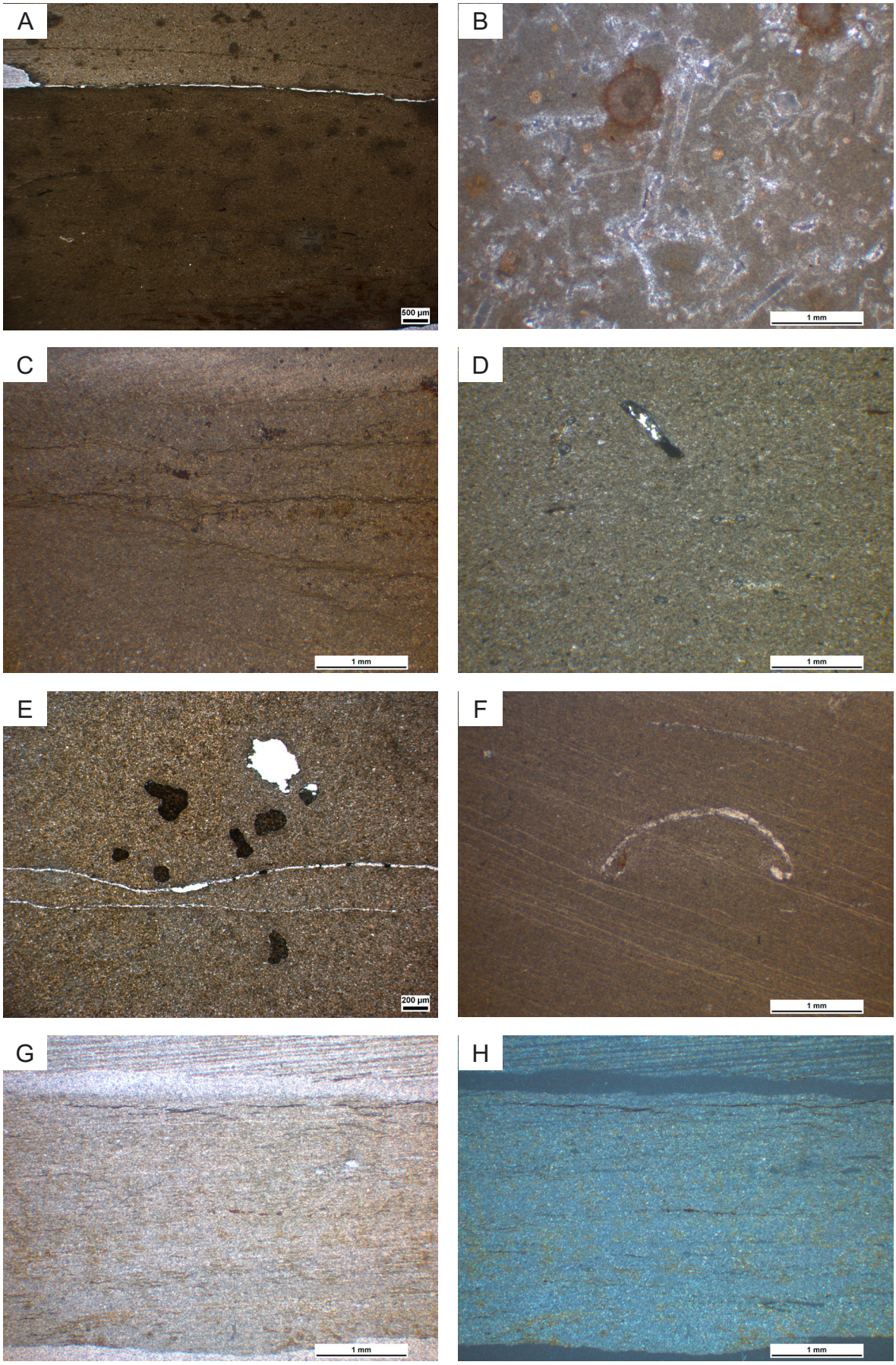
A
500 µm
B
1 mm
C
1 mm
D
1 mm
E
200 µm
F
1 mm
G
1 mm
H
1 mm

Fig. 31: Thin sections of the succession. A) Sample from bed 2, stratigraphic level: 0.06 m. B) Sample from bed 3, stratigraphic level: 24 cm. C–D) Sample from bed 4, stratigraphic level: 0.42 m. E) Sample from bed 8, stratigraphic level: 1.08 m. F) Sample from bed 12, stratigraphic level: 1.34 m. G–H) Sample from bed 14, stratigraphic level: 1.76 m. The appearing cross stratiphication in the upper part of G is a residual of the grinding process, as shown in H (H is under crossed nichols).

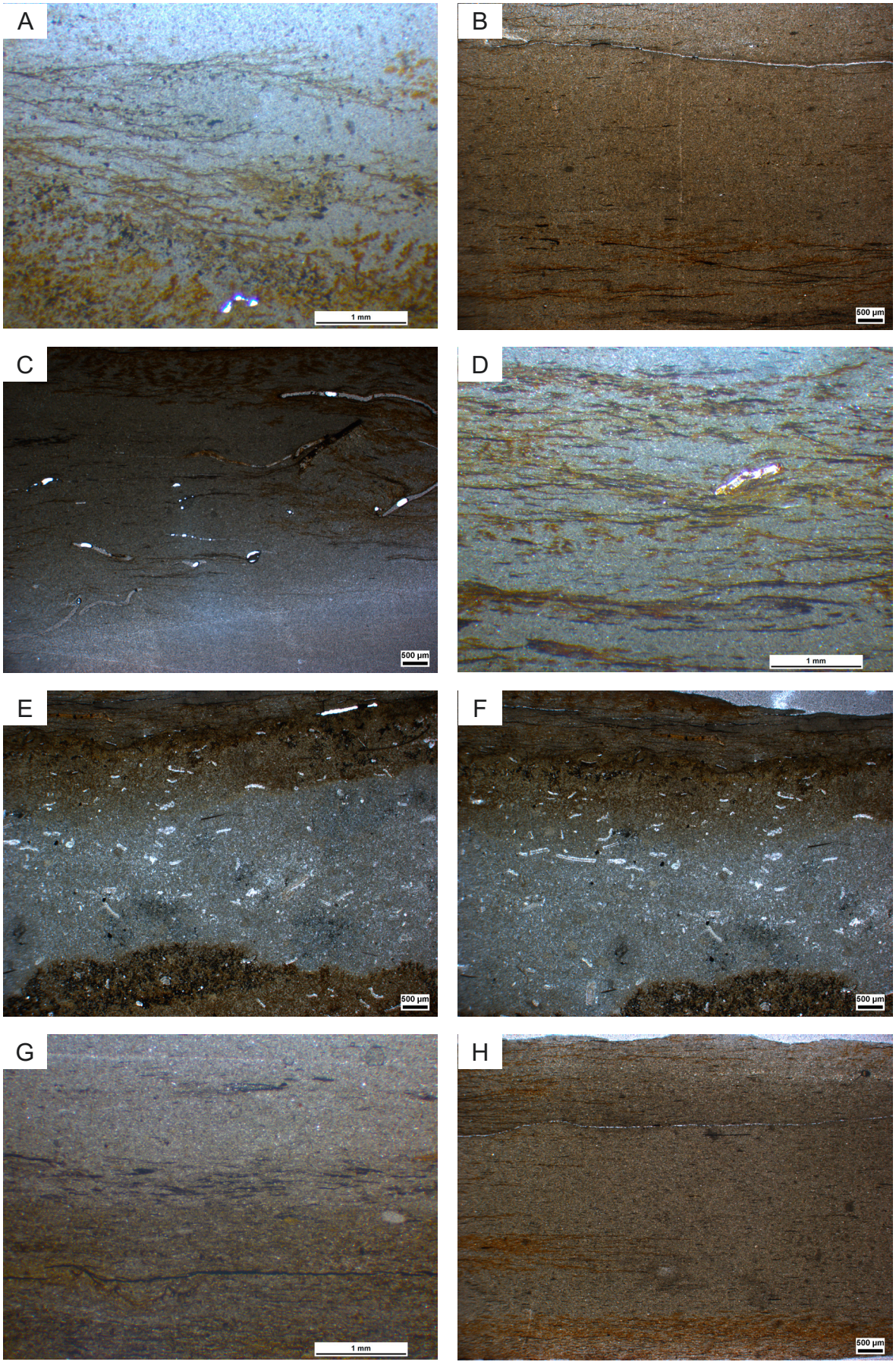
A
1 mm
B
500 µm
C
500 µm
D
1 mm
E
500 µm
F
500 µm
G
1 mm
H
500 µm

Fig. 32: Thin sections of the succession. A) Sample from bed 15, stratigraphic level: 1.92 m. B) Sample from bed 17, stratigraphic level: 1.95 m. C–D) Sample from bed 19, stratigraphic level: 2.51 m. E–F) Sample from bed 21, stratigraphic level: 3.02 cm. G) Sample from bed 22, stratigraphic level: 3.10 H) Sample from bed 23, stratigraphic level: 3.50 m.

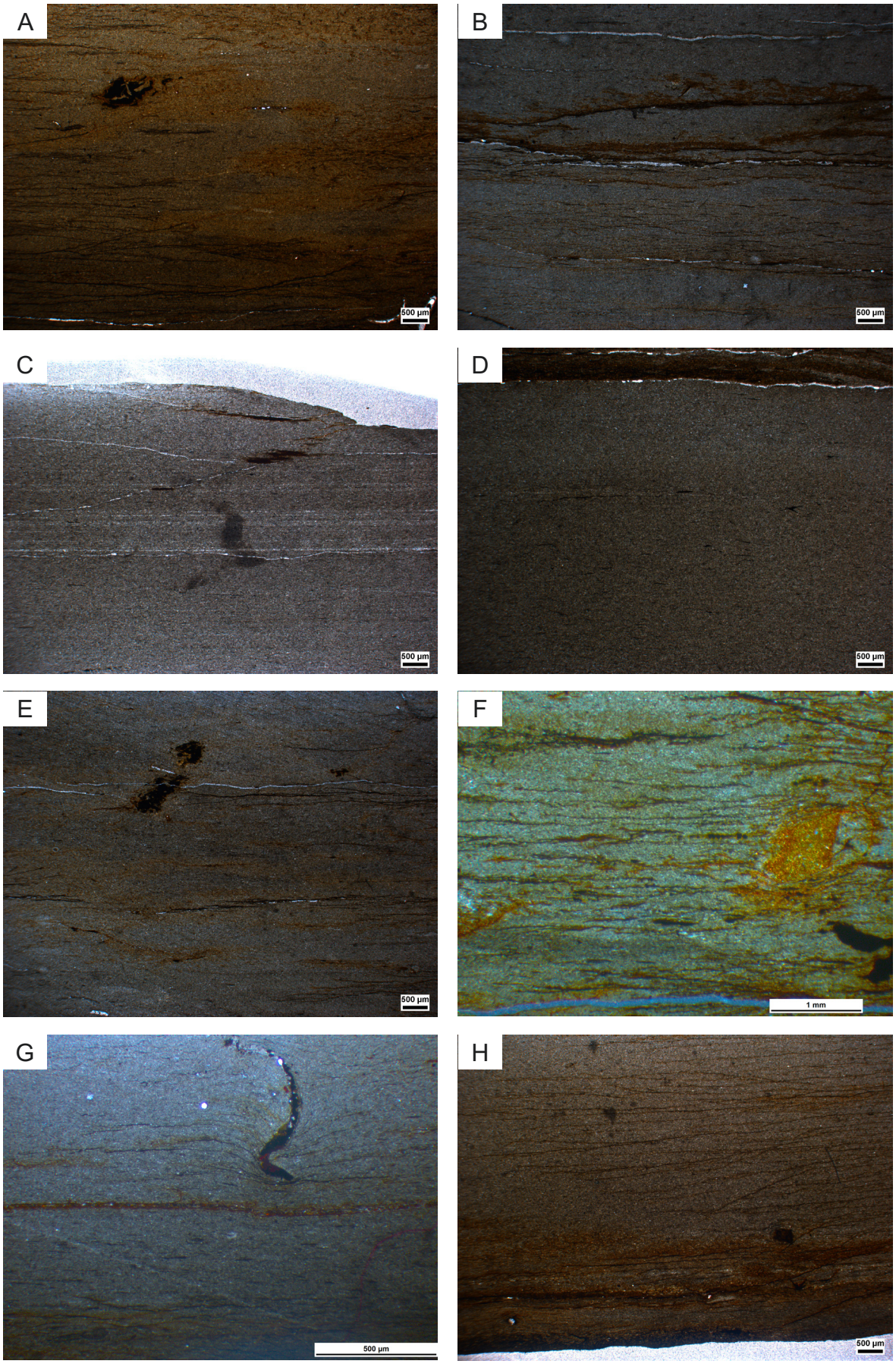
A
500 µm
B
500 µm
C
500 µm
D
500 µm
E
500 µm
F
1 mm
G
500 µm
H
500 µm

Fig. 33: Thin sections of the succession. A–B) Sample from bed 26, stratigraphic level: 4.00 m. B) Sample from bed 28, stratigraphic level: 4.50 m. C) Sample from bed 30, stratigraphic level: 5.02 m. D) Sample from bed 37, stratigraphic level: 5.65 cm. E) Sample from bed 38, stratigraphic level: 6.07 m. F) Sample from bed 40, stratigraphic level: 6.31 cm. (crossed nichols) G) Sample from bed 42, stratigraphic level: 7.05 m. H) Sample from bed 44, stratigraphic level: 7.54 m.

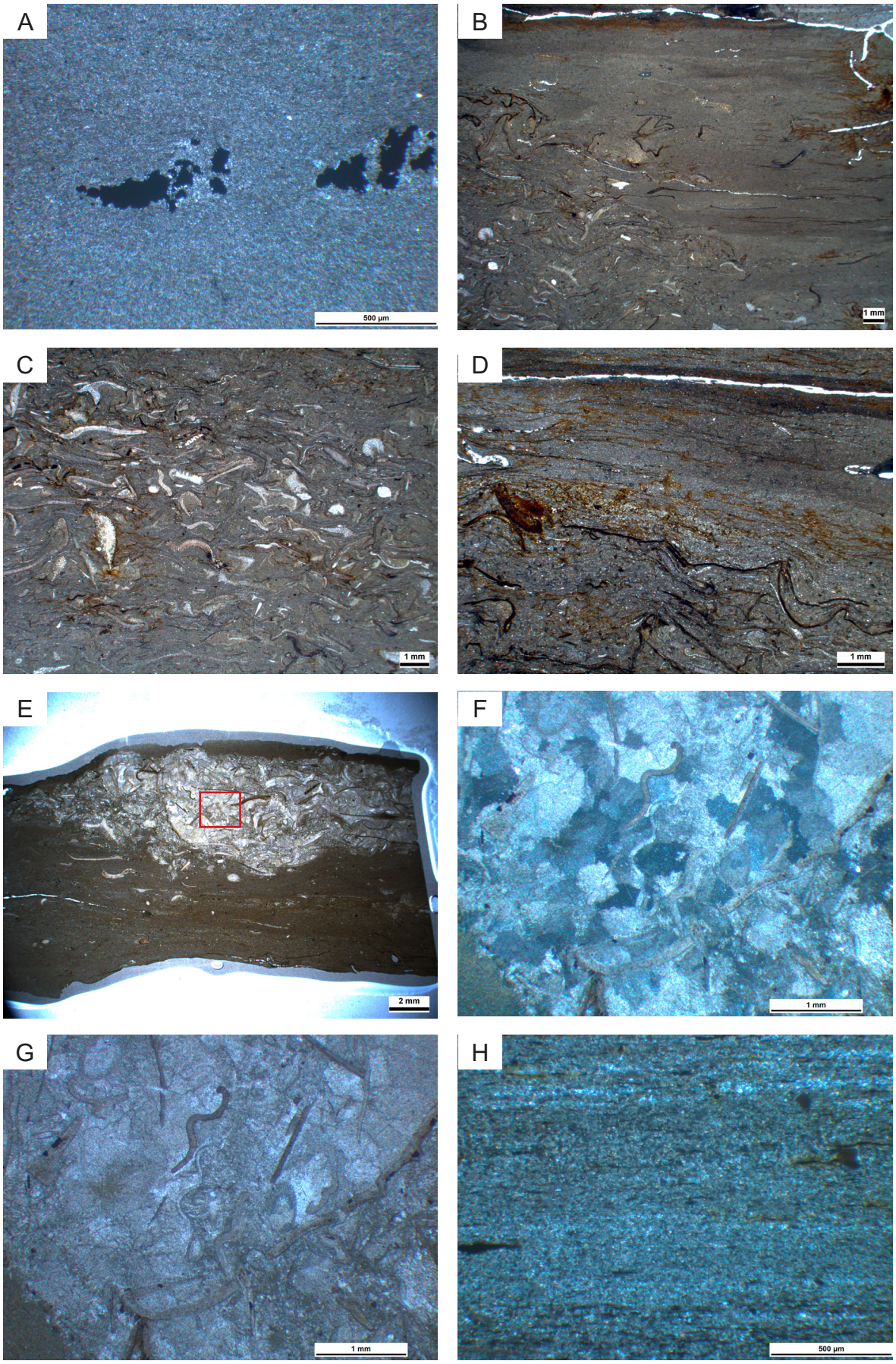
A
500 µm
B
1 mm
C
1 mm
D
1 mm
E
2 mm
F
1 mm
G
1 mm
H
500 µm

Fig. 34: Thin sections of the succession. A) Sample from bed 46, stratigraphic level: 8.25 m. B–D) Sample from bed 47, stratigraphic level: 8.50 m. E–G) Sample from bed 49, lower part, stratigraphic level: 8.95 m. F–G are zoomed in the red box of E (F: crossed nichols). H) Sample from bed 49, upper part, stratigraphic level: 9.53 m.

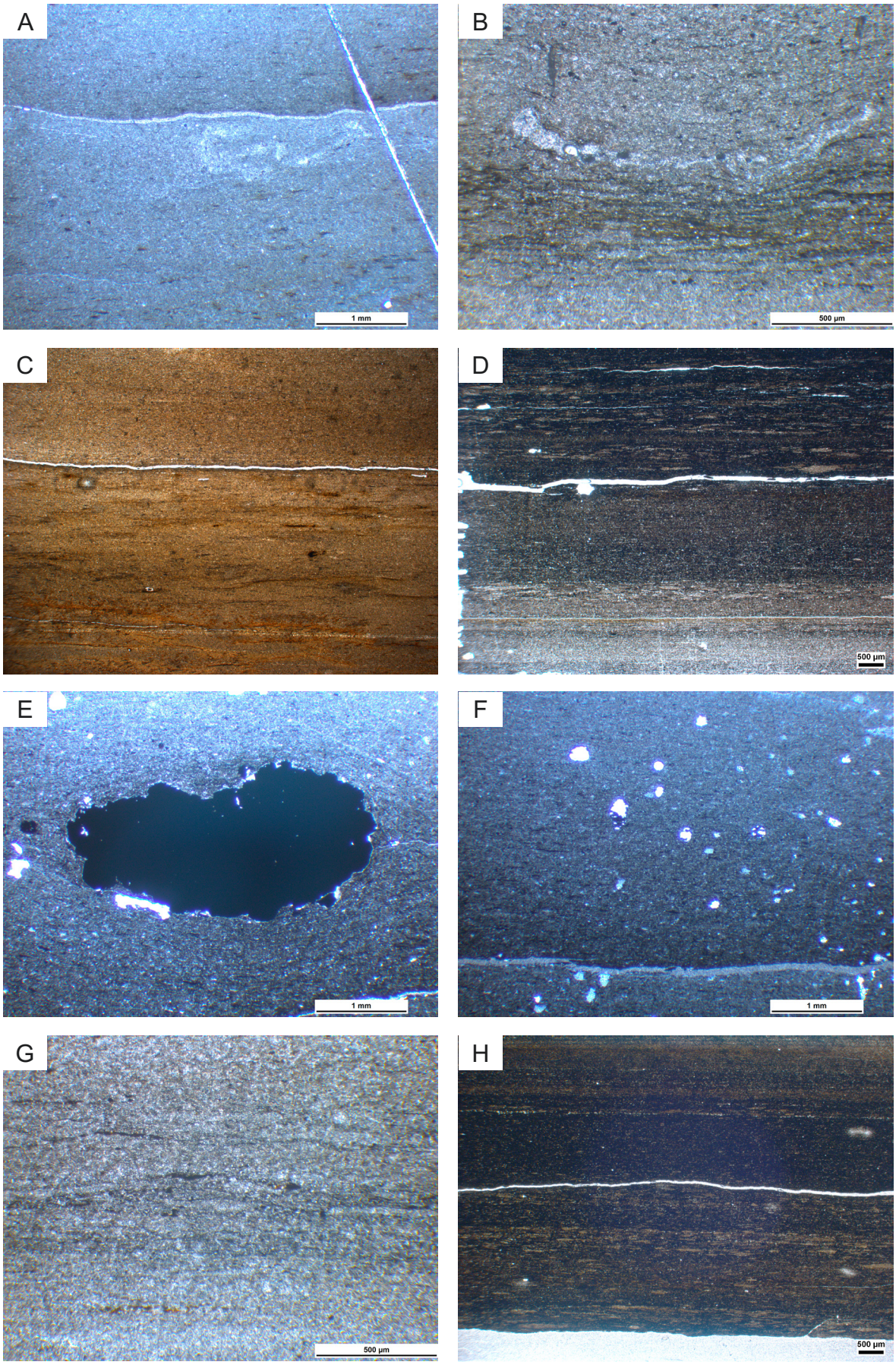
A
1 mm
B
500 µm
C
D
500 µm
E
1 mm
F
1 mm
G
500 µm
H
500 µm

Fig. 35: Thin sections of the succession. A–B) Sample from bed 51, lower part, stratigraphic level: 9.95 m. C) Sample from bed 51, upper part, stratigraphic level: 10.52 m. D) Sample from bed 54, lower part, stratigraphic level: 11.50 m. E–F) Sample from bed 54, middle part, stratigraphic level: 12.05 m. G) Sample from bed 54, upper part, stratigraphic level: 12.65 m. H) Sample from bed 56, stratigraphic level: 13.50 m.

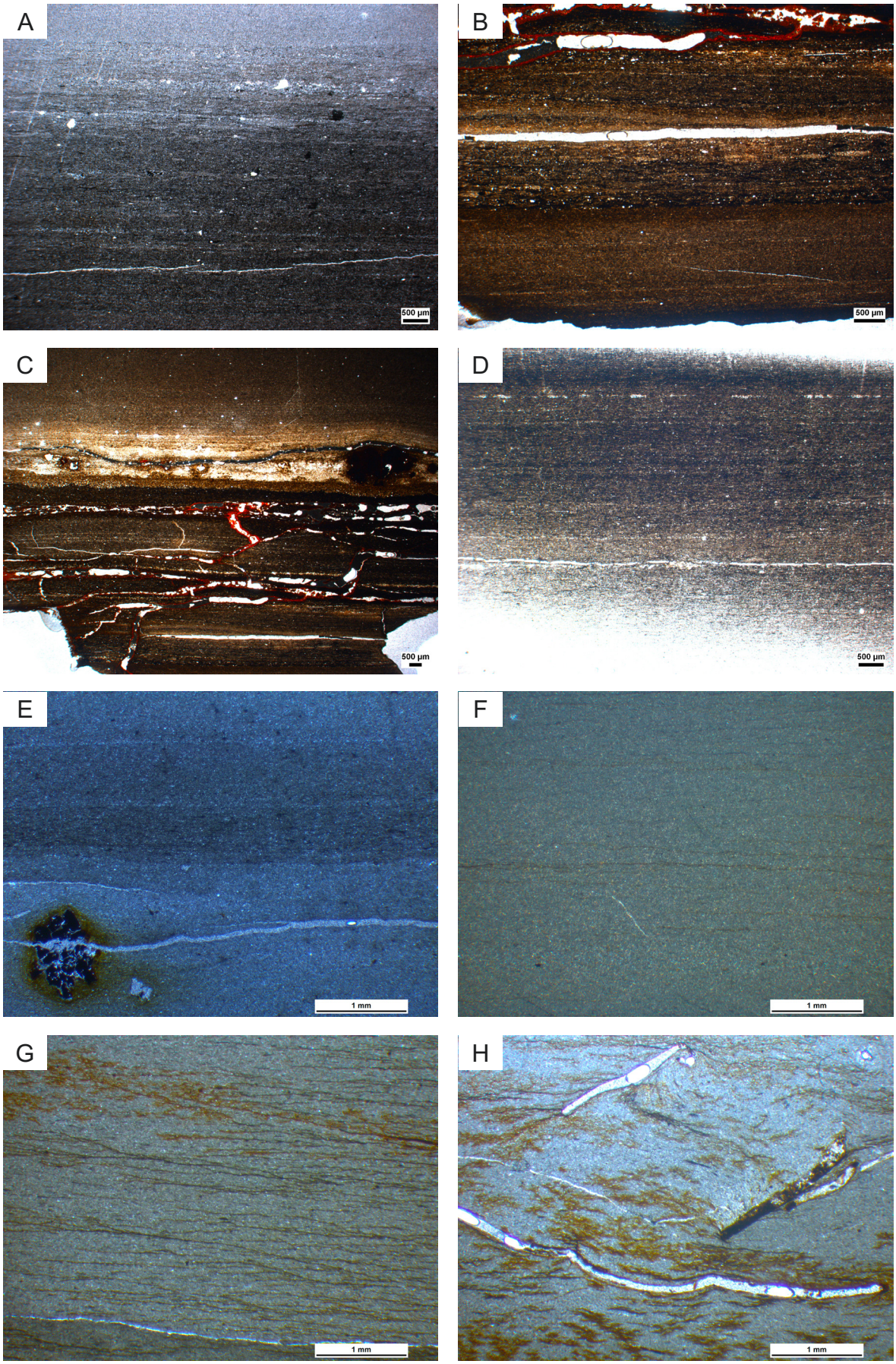
A
500 µm
B
500 µm
C
500 µm
D
500 µm
E
1 mm
F
1 mm
G
1 mm
H
1 mm

Fig. 36: Thin sections of the succession. A) Sample from bed 58, first quarter, stratigraphic level: 14.57 m. B–C) Sample from bed 58, second quarter, stratigraphic level: 14.98 m. D) Sample from bed 58, third quarter, stratigraphic level: 15.30 m. E) Sample from bed 58, fourth quarter, stratigraphic level: 15.57 m. F) Sample from bed 60, middle part, stratigraphic level: 16.45 m. G–H) Sample from bed 61, stratigraphic level: 16.68 m.

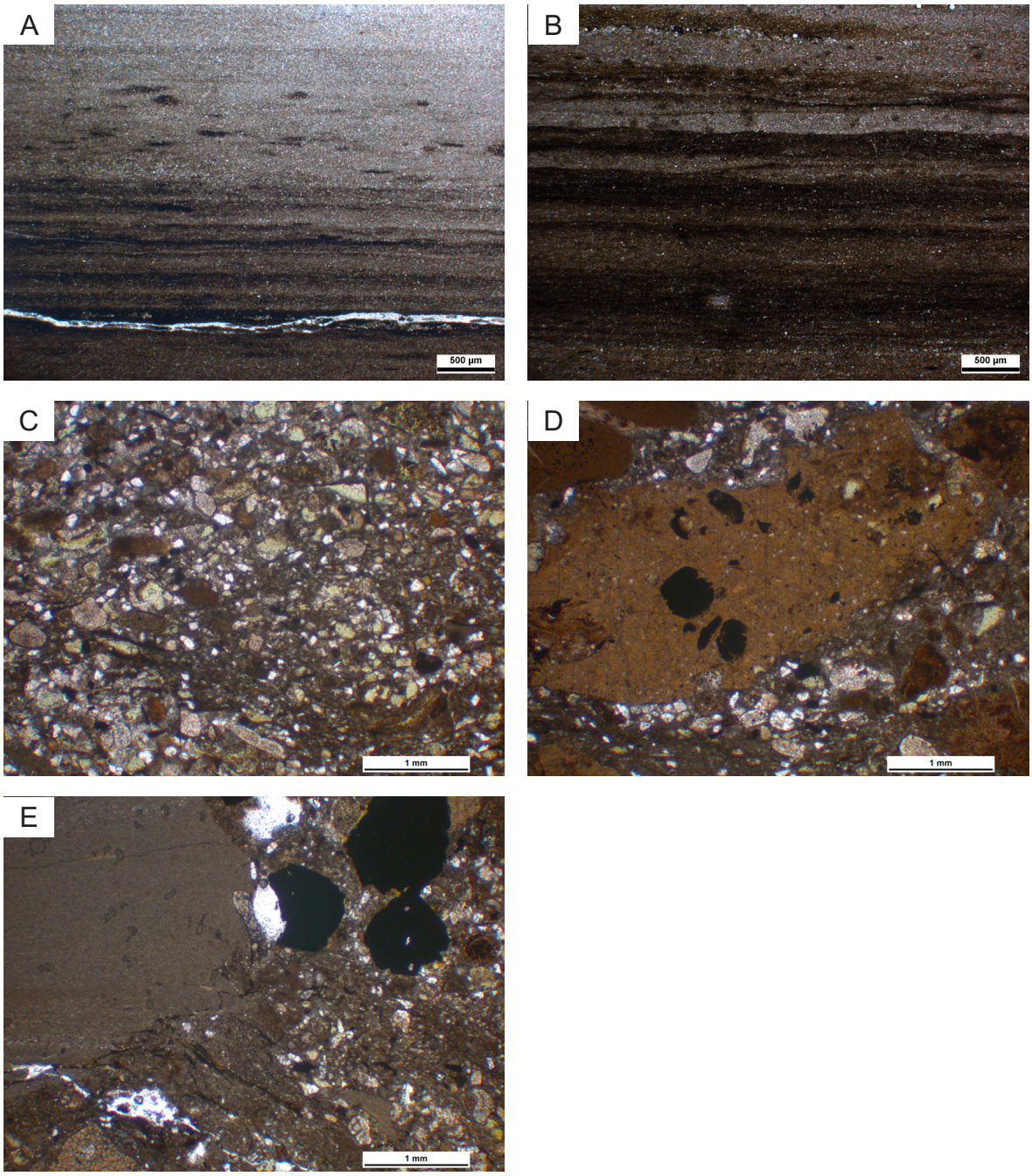
A
500 µm
B
500 µm
C
1 mm
D
1 mm
E
1 mm

Fig. 37: Thin sections of the succession. A–B) Sample from bed 64, stratigraphic level: 18.95 m. C–E) Sample from bed 65, third quarter, stratigraphic level: 19.02 m.

4.3. Total organic carbon

For the determination of the total organic carbon (TOC) in the shales, 36 samples were analysed in a LECO SC144Dr SC ANALYZER. Common TOC-analysis methods, such as SC-analysing, include both, the organic and the inorganic carbon. The predominant inorganic carbon derives from carbonate phases, so the total carbonate content (TCC, see Chapter 4.4) must be subtracted from the results of the TOC measurements, in order to get the organic carbon. As all samples contain very low carbonate contents, the inorganic portion of the TOC-measurements is ignored (see Chapter 4.4). The TOC of the samples from different stratigraphic levels is given in Table 3. The TOC varies throughout the succession from 0.24% to 3.36%. In the lower half of the succession the TOC generally varies between 0.24% and 0.71%. A jump to significantly higher TOC values at approximately half-way up of the section is seen. In the upper part of the succession the TOC also increases to its maximum value, but it varies significantly between <1% and >2%. The statistical values of the TOC analyses are given in Fig. 29.

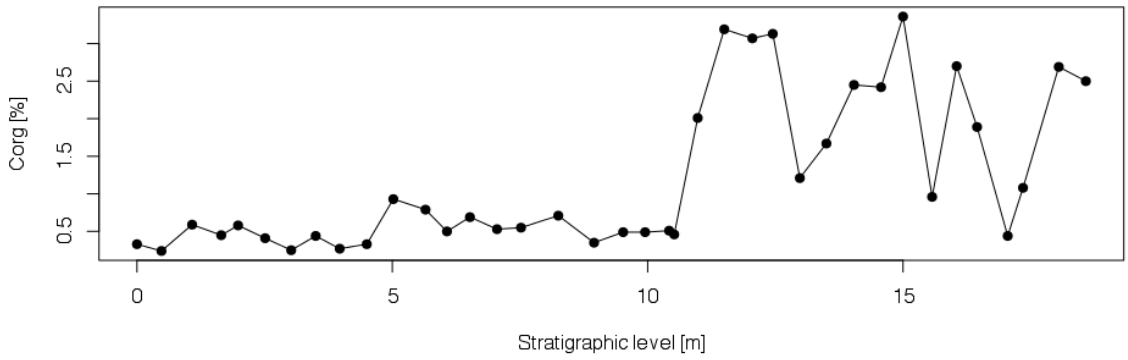

Fig. 38: TOC data related to the stratigraphic level. The TOC increases significantly in the upper half of the succession.

Table 4: Statistical values of the TOC analyses.

Minimum	1st Quarter	Median	Mean	3rd Quarter	Maximum
0.2400	0.4525	0.6400	1.2020	1.9800	3.3600

4.4. Total carbonate content

The total carbonate content (TCC) is of particular interest for the determination of TOC, as the common measurement method for TOC includes both, organic and inorganic carbon (see Chapter 4.3). In addition, the X-ray diffraction (XRD) measurements require the separation of the carbonate minerals prior measurement. For determination of the TCC in the shales, 36 samples were analysed. The TCC was in all samples below the limit of detection (<5%). With the addition of more material, the limit of detection decreased to a minimum of 2.53%. The TCC of all samples was below this minimum (Fig. 30). In some samples even lower limit of detection was reached (lowest: 0.38%). Because of the low TCC in all samples, the inorganic portion of the TOC-measurement is ignored and the carbonate is not separated prior the XRD-analysis.

Table 5: Measurements of the TCC.

Stratigraphic level [m]	Limit of detection [%]	Stratigraphic level [m]	Limit of detection [%]
0.06	1.66	10.42	1.67
0.49	1.66	10.52	1.66
1.07	1.66	10.98	1.66
1.65	1.66	11.5	1.66
1.98	1.66	12.05	1.66
2.51	1.67	12.45	1.66
3.5	1.66	12.98	1.66
4	1.66	13.5	1.67
4.5	1.66	14.04	2.49
5.02	1.25	14.57	1.67
5.65	1.66	15	1.66
6.26	1.66	15.57	1.66
6.52	1.66	16.05	1.66
7.05	0.83	16.45	1.66
7.52	1.66	17.05	1.66
8.95	1.66	17.35	1.66
9.52	1.66	18.05	1.66
9.95	1.66	18.58	2.53

4.5. Minerals

For determination of the minerals, 36 samples were analysed with x-ray diffraction technique (XRD). In the following paragraphs the results of the mineral determinations, the quantitative analyses and the illite crystallinity calculations are briefly described and a correlation of the minerals, the TOC and the stratigraphic level are given. The mineral phases that were only identified in thin sections or macroscopically (pyrite, haematite and goethite) are not included in the quantitative analyses. Fig. 33 A shows a representative sample with the full XRD determination. A stacked-to-100% plot of the content of all determined phases against the stratigraphic level is given in Fig. 33 B.

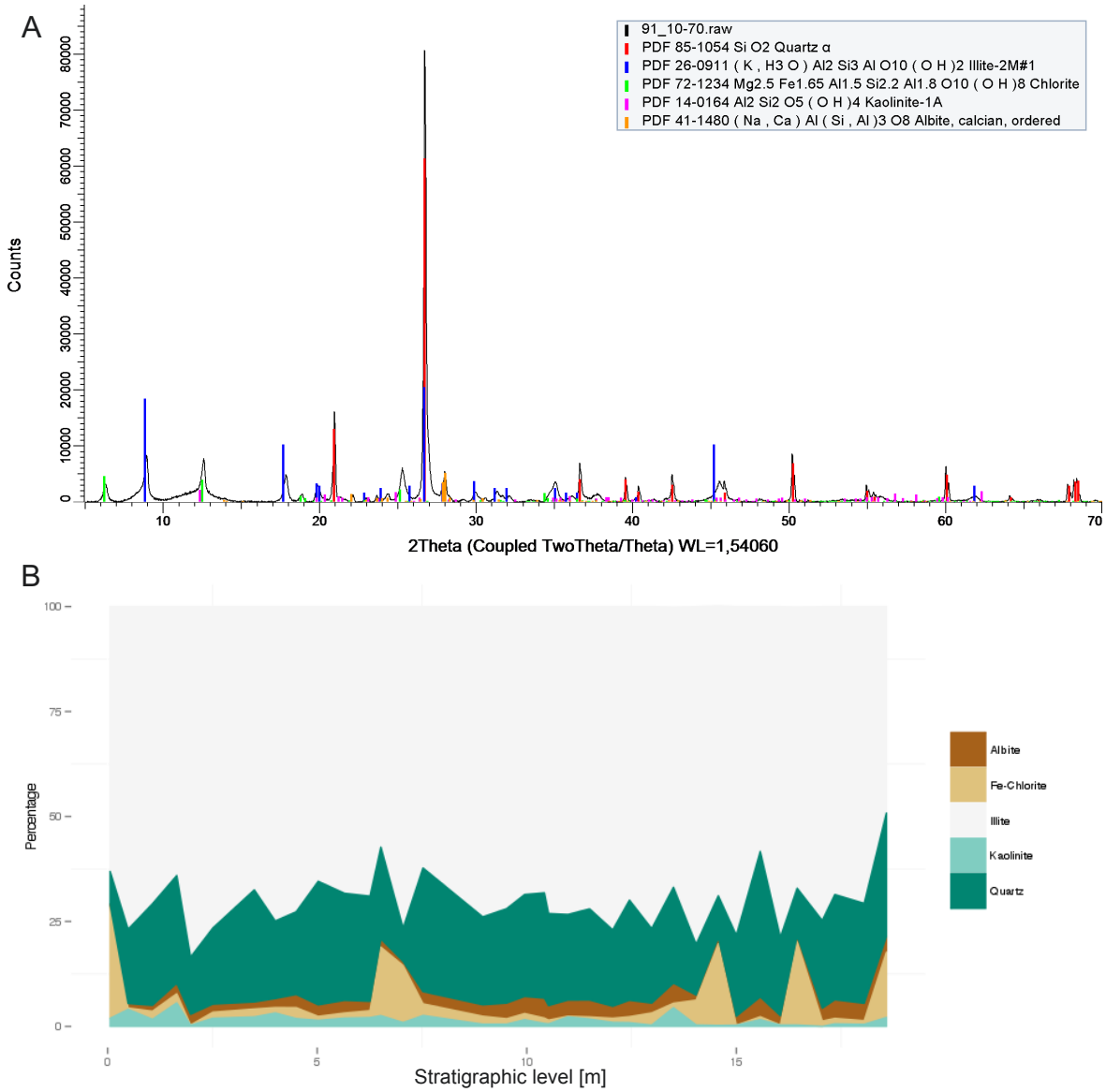

Fig. 39: A) Mineral determination from the diffractogram for one representative sample. B) A 100%-stacked-plot of the mineral content, calculated from the XRD measurement.

4.5.1. Albite ((Na, Ca)Al(Si, Al)$_3$O$_8$)

Albite was detected in all samples. Fig. 34 shows its characteristic reflexes in the diffractogram. The amount of albite is plotted against the stratigraphic level of the sample in Fig. 46 A. The minimum is 0.78% and the maximum is 4.8%. All statistical values are given in Fig. 29. The amount fluctuates between c. 1% and c. 3–4% across the whole succession, with minima at the base, at c. 7.05 m, c. 14.04 m and c. 16.45 m.

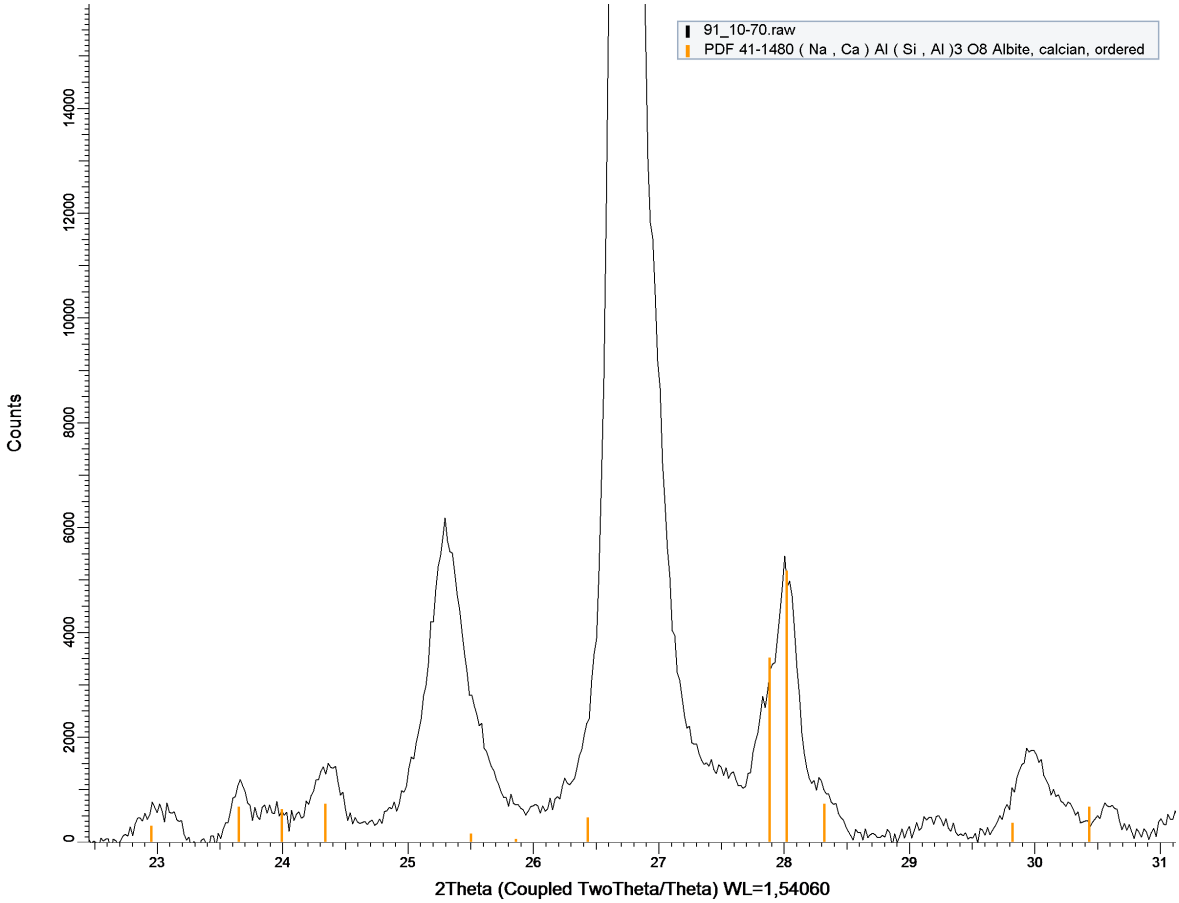

Fig. 40: Characteristic reflexes for albite ((Na, Ca)Al(Si, Al)$_3$O$_8$). For a better representation, the axes are zoomed to a part of the measurement range.

Table 6: Statistical values of the quantitative analysis of albite.

Minimum	1st Quarter	Median	Mean	3rd Quarter	Maximum
0.780	1.958	2.745	2.790	3.782	4.800

4.5.2. Fe-chlorite ($Mg_{2.5}Fe_{1.65}Al_{1.5}Si_{2.2}Al_{1.8}O_{10}(OH)_8$)

Fe-chlorite was detected in most samples, except from the stratigraphic levels 15.00 m and 16.05 m. Fig. 35 shows the characteristic reflexes for chlorite in the diffractogram. Fe-chlorite is distinguished from other chlorites by the characteristics of the reflex at c. 6.0° 2θ. After one hour heating at 550° C, this reflex changes its position to c. 6.4° C in Fe-rich chlorites (4.3). This was observed in all samples containing chlorite. The amount of Fe-chlorite is plotted against the stratigraphic level of the sample in Fig. 46 B. The amount fluctuates around 2% across the whole succession but shows five peaks close to or higher than 15% (at the base of the succession, in the range of c. 6.52–7.05 m, at c. 14.57 m, at 16.45 m and at the top of the succession). All statistical values are given in (Fig. 36).

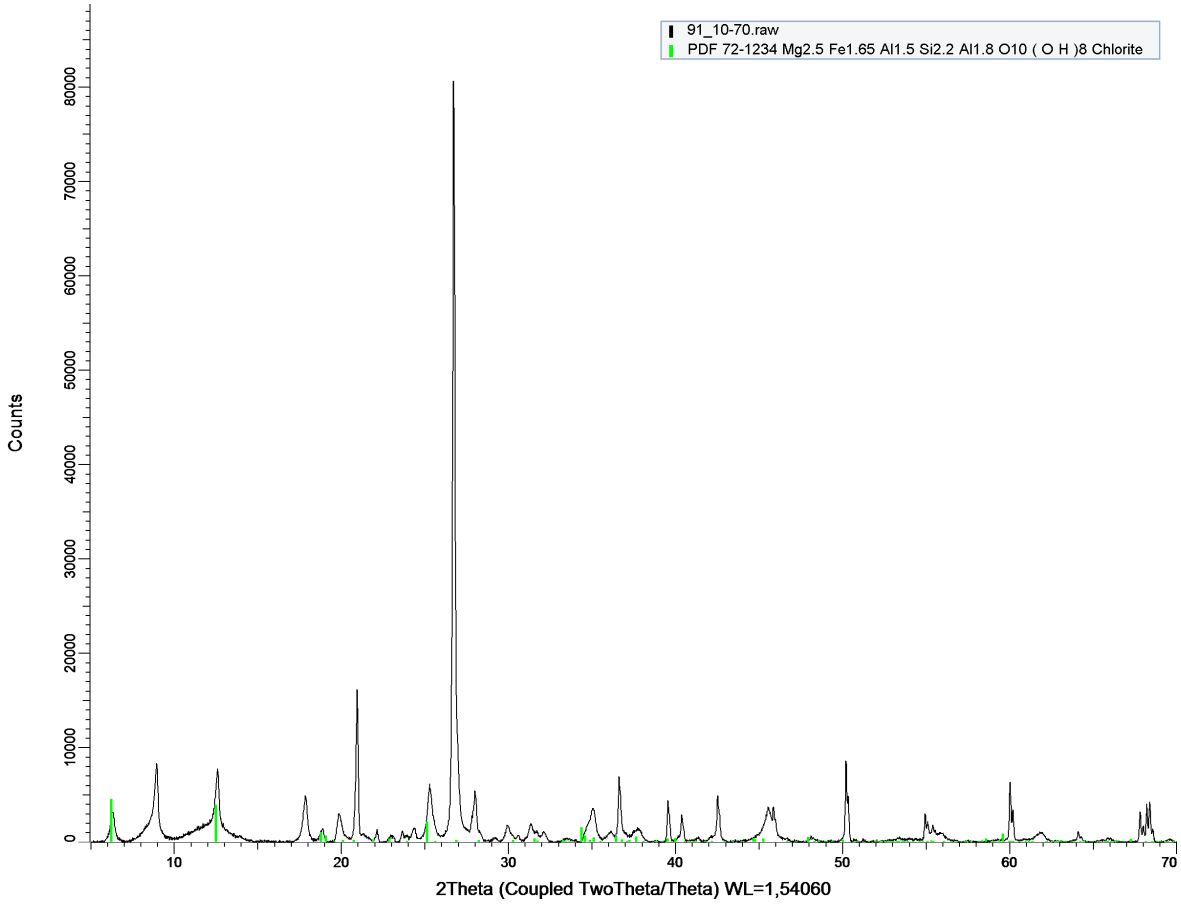

Fig. 41: Characteristic reflexes for Fe-chlorite ($Mg_{2.5}Fe_{1.65}Al_{1.5}Si_{2.2}Al_{1.8}O_{10}(OH)_8$).

Table 7: Statistical values of the quantitative analysis of Fe-chlorite.

Minimum	1st Quarter	Median	Mean	3rd Quarter	Maximum
0	0.9275	1.3550	4.2610	2.6520	26.4600

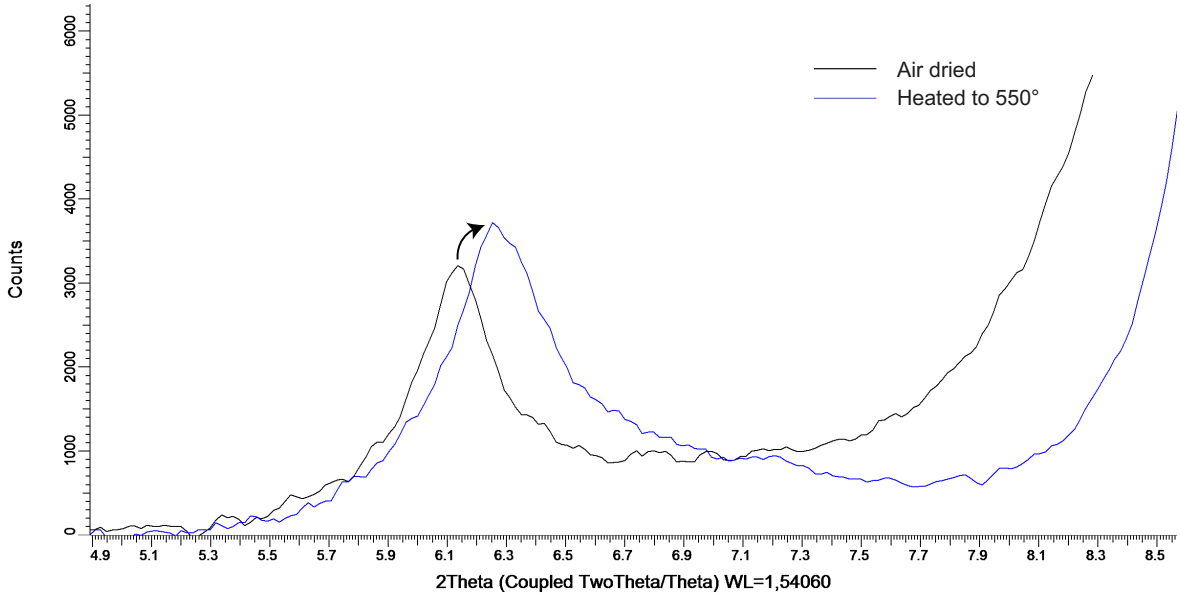

Fig. 42: Characteristic movement (arrow) of the Fe-rich-chlorite reflex at c. 6.0 °2θ to c. 6.4 °2θ, with the sample heated to 550° for approximately 1 hr.

4.5.3. Illite ($(K, H_3O)Al_2Si_3AlO_{10}(OH)_2$)

The clay mineral illite was detected in all samples. The illite is in 2M1 configuration. 4.4 shows its characteristic reflexes in the diffractogram. The amount of illite is plotted against the stratigraphic level of the sample in Fig. 46 C. The amount fluctuates between 65 and 78% across the whole succession, with a minimum of 49.18% and a maximum of 83.51%. All statistical values are given in Table 5. Illite is the predominant mineral in all samples. Nevertheless, the fluctuation is very high across the succession, with a large drop to 49.18% towards the top. The absence of smectite or mixed layered smectite/illite was proven, as the reflexes didn't show any reaction on ethylene-glycol.

Table 8: Statistical values of the quantitative analysis of illite.

Minimum	1st Quarter	Median	Mean	3rd Quarter	Maximum
49.18	67.36	70.74	70.43	75.30	83.51

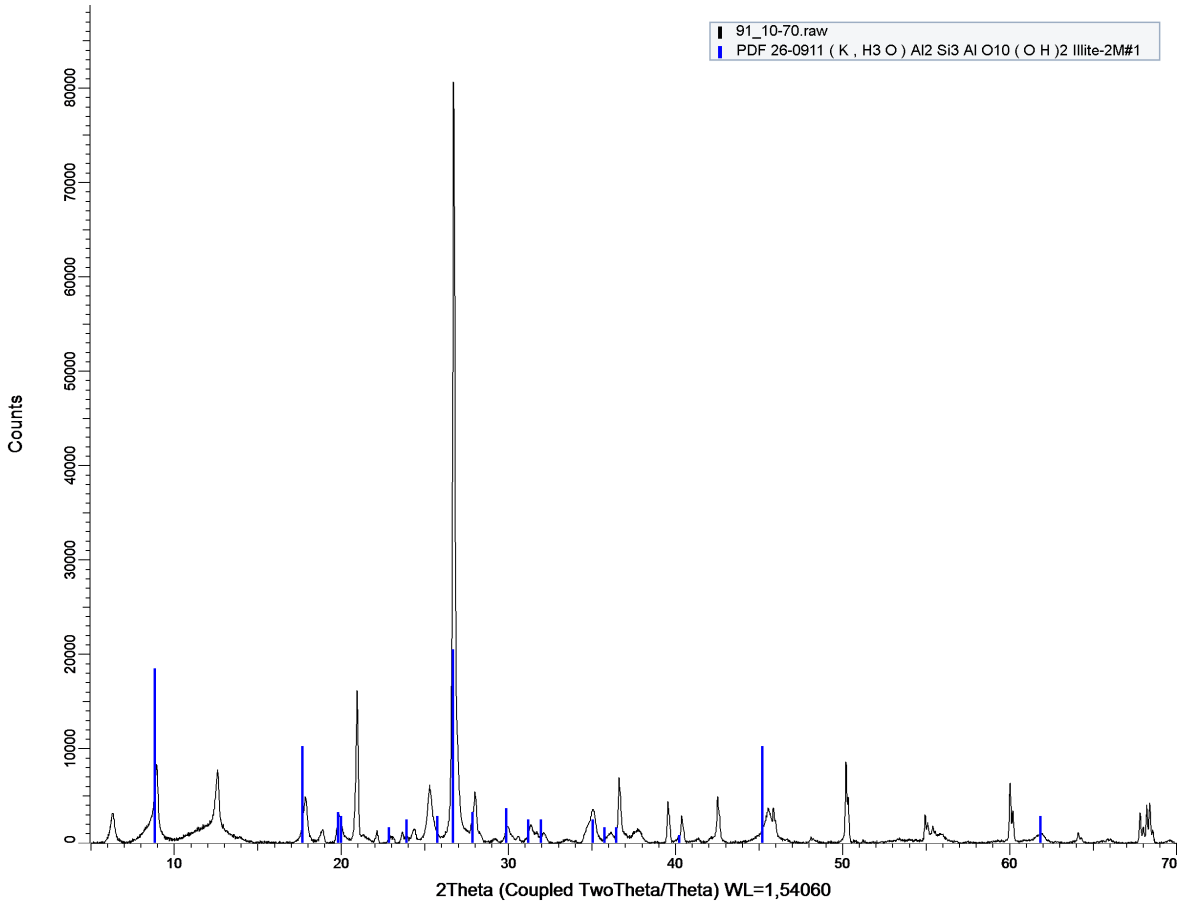

Fig. 43: Characteristic reflexes for 2M1 Illite (K, H_3O)$Al_2Si_3AlO_{10}(OH)_2$).

4.5.4. Kaolinite ($Al_2Si_2O_5(OH)_4$)

Kaolinite was detected in most samples. The amount of kaolinite is plotted against the stratigraphic level of the sample in Fig. 41 D. The sample from c. 17.05 m contains only 0.01% of kaolinite, which is here assigned to a zero value. The samples from c. 1.98 m and c. 14.57 m contain less than 0.30% kaolinite, which is here suggested to be the limit of detection for kaolinite. The maximum is 5.60%. The statistical values are shown in 4.3. The amount of kaolinite decreases over the succession from the base to the top. In the lower part it mainly fluctuates between c. 2% and 3% and in the upper part it mainly fluctuates between c. 1% and 2% (with some higher peaks). The maximum is located in the lowermost part of the succession. 4.4 A shows the characteristic reflexes of kaolinite in the diffractogram. The kaolinite is in 1A configuration. Kaolinite is distinguished from chlorite by the usage of formamide, as the characteristic peak at c. 12.4° 2θ changes to 8.8° 2θ after the long-term treatment with formamide (4.4 B). The diffractogram shows two new reflexes, so it is assumed that the intercalation of the formamide was not fully finished in all crystals.

Table 9: Statistical values of the quantitative analysis of kaolinite.

Minimum	1st Quarter	Median	Mean	3rd Quarter	Maximum
0.010	0.9275	1.3550	1.536	2.095	5.600

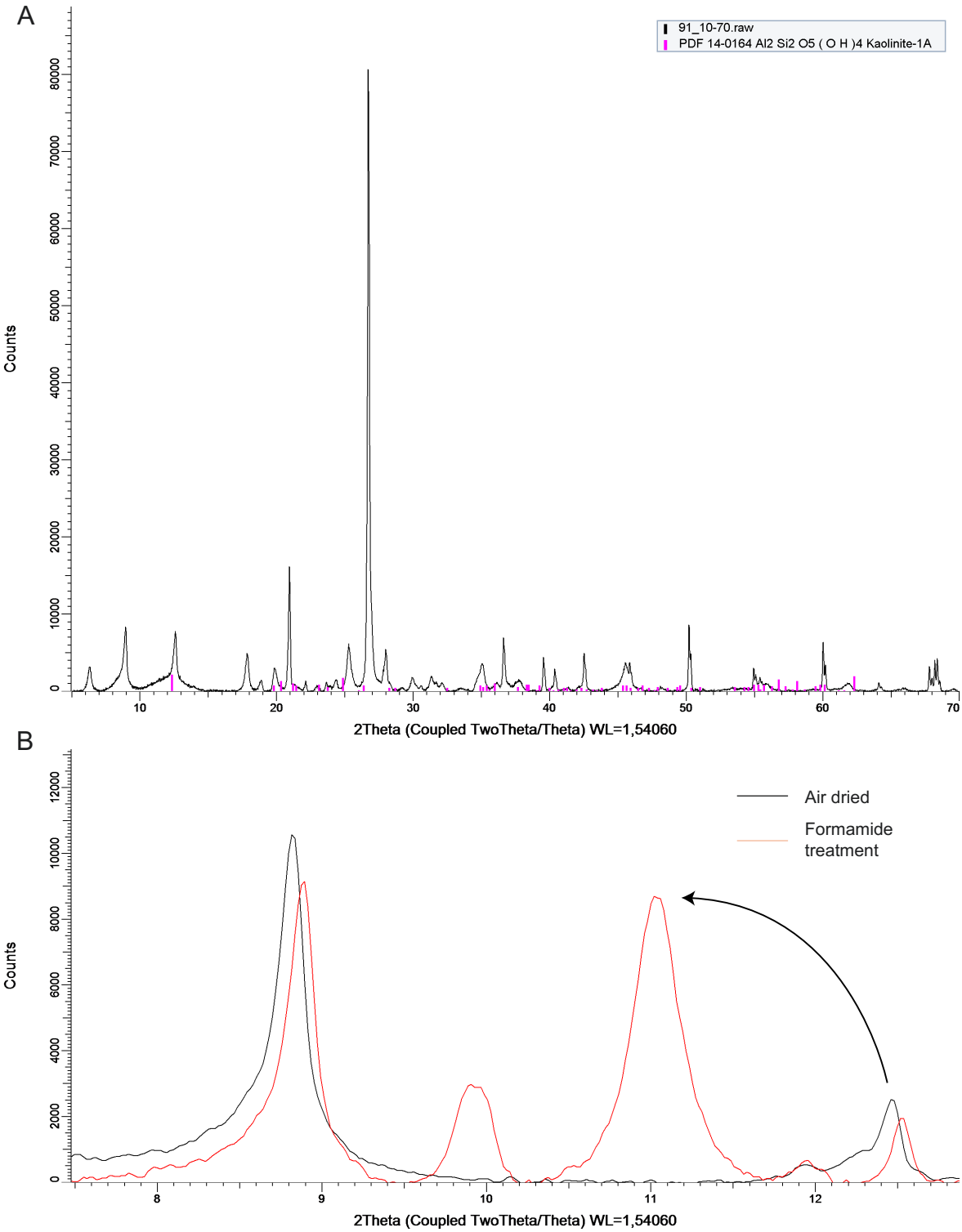

Fig. 44: A) Characteristic reflexes for kaolinite ($Al_2Si_2O(OH)_4$). B) Characteristic movement (arrow) of the kaolinite reflex if formamide is intercalated. As two reflexes are shown, a non-finished reaction with the formamide is assumed.

4.5.5. Quartz (SiO_2)

Quartz was detected in all samples. Fig. 39 shows its characteristic reflexes in the diffractogram. The amount of quartz is plotted against the stratigraphic level of the sample in Fig. 41 E. The minimum is 7.75% and the maximum is 34.65%. All statistical values are given in Fig. 40. Quartz has the second highest amount in all samples and is a main phase in the system. The fluctuation is high in the lower third and the upper third of the succession. In the middle part the amount of quartz is almost stable at c. 23%. The amount of quartz increases strongly in the first 1.5 m, from c. 1.75% to c. 25.67%. At c. 6.5 m the amount drops from c. 21.86% to low 7.93% and increases at c. 7.05 m to c. 29.46%. The maximum is reached at c. 15.57 m. Towards the top, the amount is increasing from c. 11.34% to c. 29.36%.

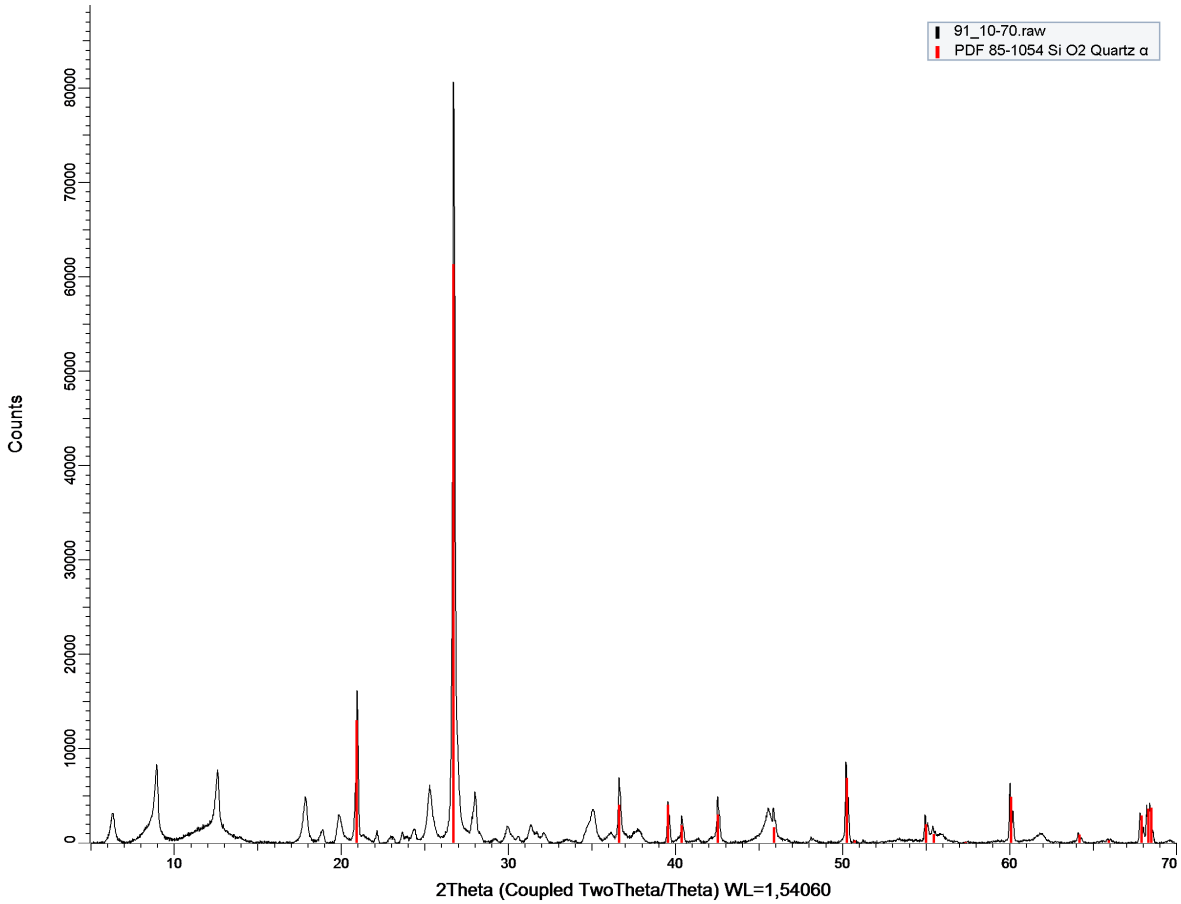

Fig. 45: The characteristic reflexes for quartz (SiO_2).

Table 10: Statistical values of the quantitative analysis of quartz.

Minimum	1st Quarter	Median	Mean	3rd Quarter	Maximum
7.75	18.16	21.78	20.98	25.04	34.65

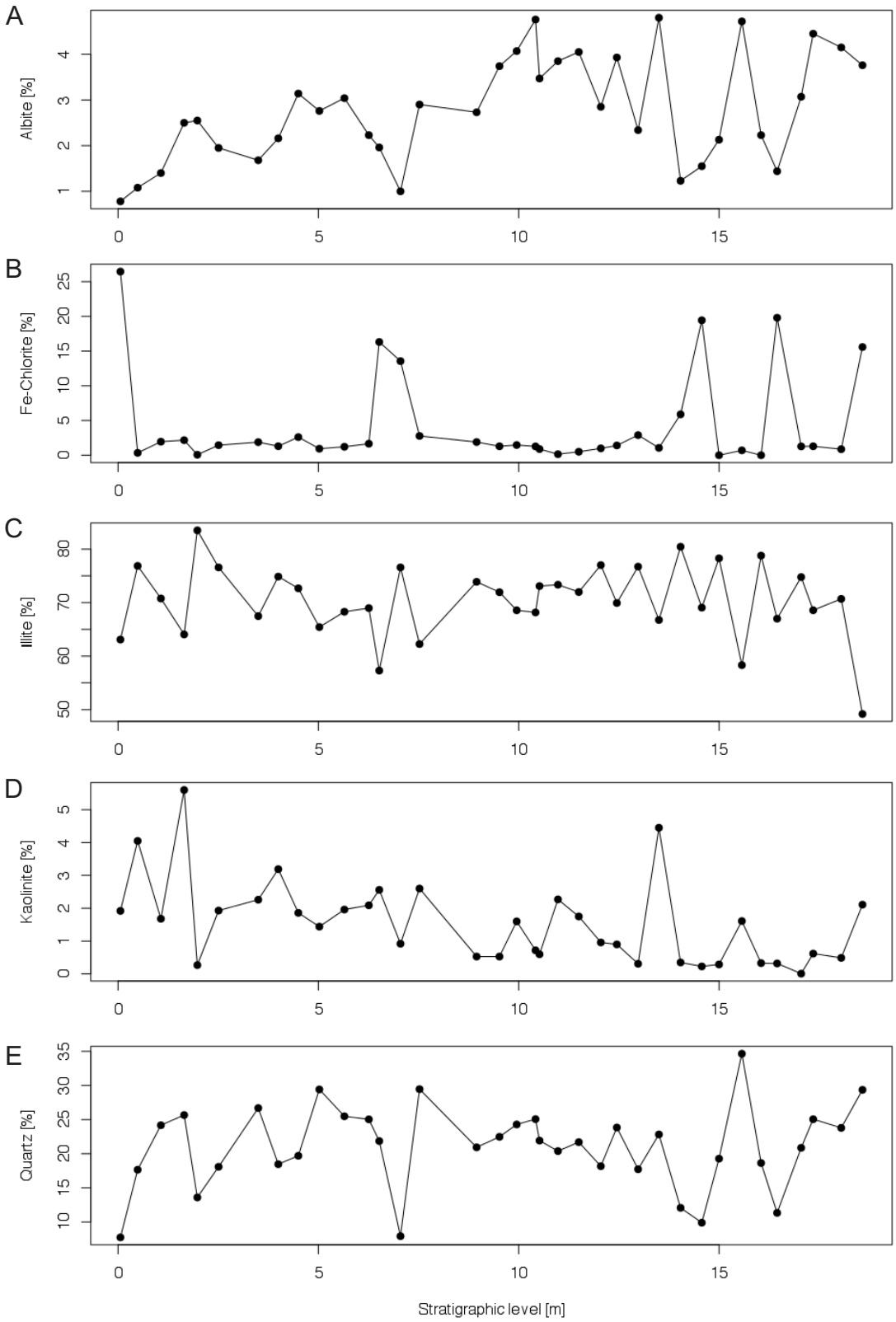

Fig. 46: The different mineral content relating to the stratigraphic level in the succession. A) Albite. B) Fe-chlorite. C) Illite. D) Kaolinite. E) Quartz.

4.5.6. Classification of the samples based on chemical composition

All samples are classified as shale (see Chapter 2.2.4). Nevertheless, a sub-classification based on the chemical composition of the samples, is possible (Table 6). As shown in Chapter 4.4, the total carbonate content of the samples never reached the limit of detection. In Table 6 the highest limit of detection therefore is shown as horizontal line, but all data points are plotted with their limits of detection, standardised on 100% in this plot. Due to this and to the high amount of clay minerals (>50% in all samples), all samples are classified as argillaceous mudstone.

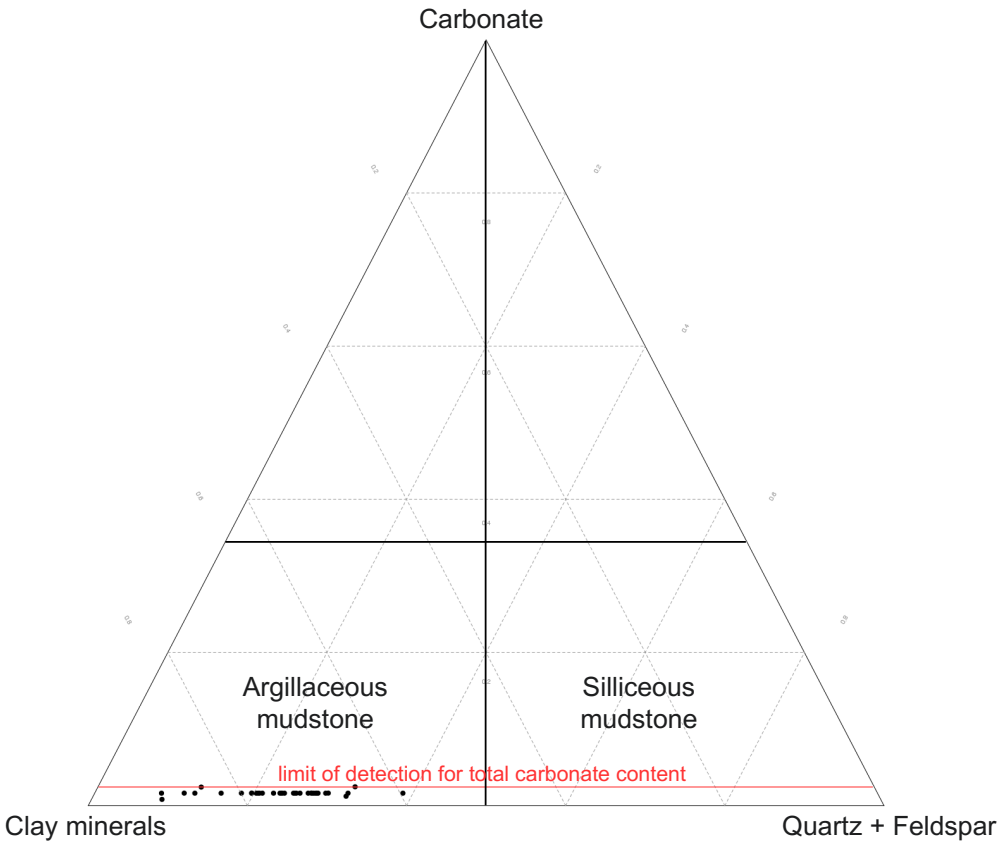

Fig. 47: Ternary diagram for the classification of the samples, based on the chemical composition. All data points are in the field of argillaceous mudstone.

4.5.7. Illite crystallinity

The illite crystallinity was calculated on the basis 69 measurements. Table 3 shows the full width at half length (FWHM) of the reflex intensity of illite$_{[001]}$ against the Środoń intensity ratio Ir (Środoń, 1984). The statistical values of Ir and the FWHM are given in Table 7.

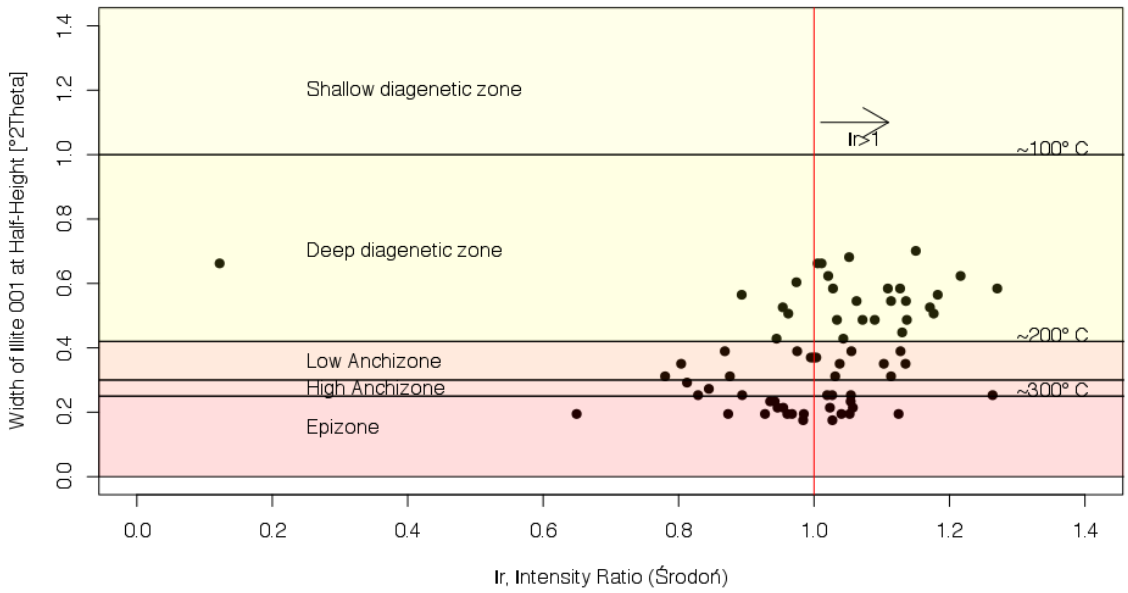

Fig. 48: FWHM of the reflex intensity of illite[001] against the Środoń intensity ratio Ir. The red line marks Ir=1.

Most of the data points are distributed in the FWHM area of 0.3–0.6. Fig. 31 shows box-plots of the FWHM of the reflex intensity of illite$_{[001]}$. The box-plot for all data points shows significantly lower FWHM values than the box-plot for data points with Ir>1. Data points with Ir>1 also show a higher distribution than those with Ir<1. The statistical values for the data points with Ir>1 are also given in Table 7.

Fig. 32 shows the FWHM of the reflex intensity of illite$_{[001]}$ against the stratigraphic level. Overall, the FWHM decreases relatively moderate from around 0.4° 2θ to 0.6° 2θ at the base of the succession to around 0.2° 2θ to 0.3° 2θ at its top. The minimum is at 17.35 m with 0.1753° 2θ and the maximum is at 3.02 m with 0.701° 2θ. At the base a short increase from c. 0.40 to c. 0.55° 2θ is shown, followed by an almost sinusoidal decrease of the FWHM to c. 0.2° 2θ in the area of 2.5 m to 10 m thickness. The FWHM is relatively constant from 10 m to approximately 15 m at c. 0.2° 2θ to 0.25° 2θ. An increase of the FWHM to c. 0.4° 2θ is following at approximately 16 m, with a subsequently decrease to c. 0.2° 2θ close to the top of the succession.

Table 11: Statistical values of the illite crystallinity.

	Minimum	1st quarter	Median	Mean	3rd quarter	Maximum
Ir	0.1222	0.9538	1.0270	1.0050	1.1030	1.2710
FWHM illite$_{[001]}$	0.1735	0.2337	0.3701	0.3870	0.5259	0.7012
FWHM illite$_{[001]}$ (Ir>1)	0.1735	0.2532	0.4480	0.4295	0.5649	0.7012

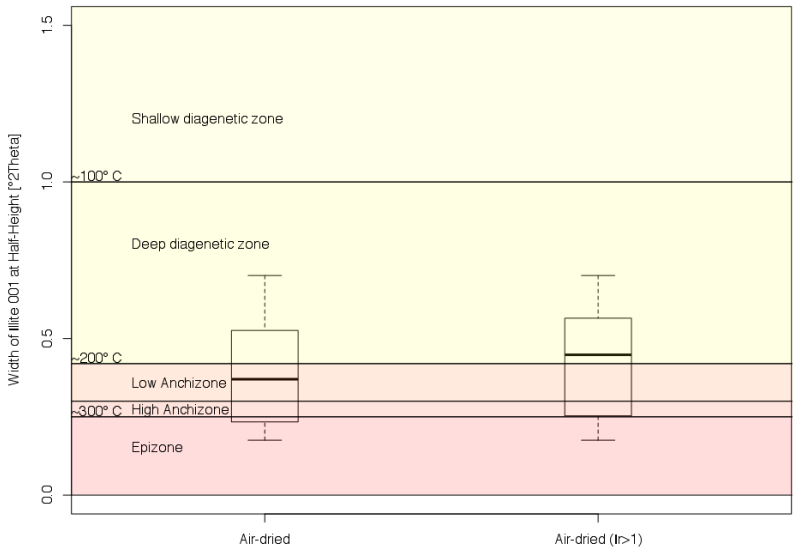

Fig. 49: Box-plots of the FWHM of the reflex intensity of the illite[001]. Left box-plot is composed by all data points shown in Fig. 48. The right box-plots shows data points from Fig. 48 with Ir>1.

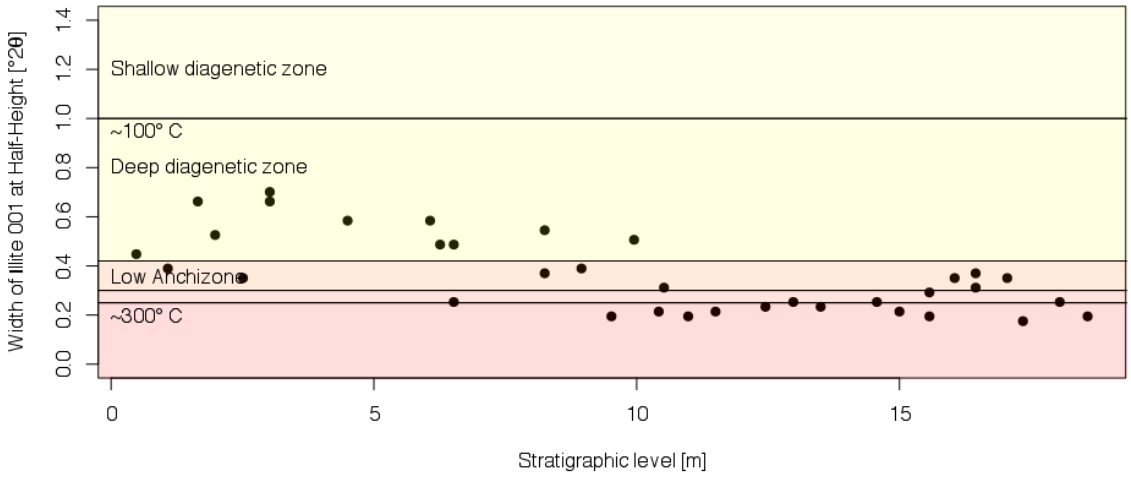

Fig. 50: The FWHM of the reflex intensity of illite[001] against the stratigraphic level.

4.5.8. Correlation

For the correlation of the quantitative XRD, TOC and illite crystallinity analyses, a cross plot with the stratigraphic level is shown in Fig. 42. The determination of total carbon content is excluded, as this content is always below the limit of detection. The statistical data for the correlation are given in Table 8.

The content of albite correlates linearly positively with the stratigraphic level and the quartz content. It correlates linearly negatively with the illite content and slightly negatively with the kaolinite content. A logarithmic correlation is suggested for kaolinite with Fe-chlorite. For Fe-chlorite, a logarithmic correlation with quartz is suggested. The illite content shows a negative linear correlation with the quartz content. The cross plot of kaolinite against the stratigraphic level suggests a negative linear correlation. Positive linear positive correlations can be seen for the kaolinite content with the quartz content and the illite crystallinity. Kaolinite and TOC are proposed to show a logarithmic correlation. TOC shows a negative linear correlation with the illite crystallinity. The cross plot of TOC against the stratigraphic level shows the previously mentioned jump to dominantly higher TOC values at approximately half-way up of the succession. The illite crystallinity decreases almost linearly with the stratigraphic level.

Table 4 shows a ternary diagram of the clay-mineral content of the samples, standardised to 100%. The predominance of illite, compared to the other clay minerals is clearly visible. Also, the previously mentioned peaks of the Fe-chlorite are easily identified. The highest amounts of Fe-chlorite reach 35% of the total clay-mineral content. The diagram also shows that high Fe-chlorite values coincide with low kaolinite values. In sumary these samples are mainly composed of illite and Fe-chlorite.

Table 12: Correlation coefficient of the different factors. Calculated with cross correlation of vectors (e.g., Crawley, 2010; R Core Team, 2016). The coefficient indicates the level of correlation (1: perfect linear correlation, 0: no correlation). The algebraic sign indicates the direction of the correlation (negative or positive). Reliable values are >|0.4|.

	Stratigraphic level	Albite	Fe-chlorite	Illite	Kaolinite	Quartz	TOC	FWHM illite$_{[001]}$
Stratigraphic level	1	0.471	0.018	-0.096	-0.503	0.106	0.655	-0.503
Albite	0.471	1	-0.470	-0.271	-0.009	0.639	0.172	-0.174
Fe-chlorite	0.018	-0.470	1	-0.423	-0.067	-0.521	0.026	-0.288
Illite	-0.096	-0.271	-0.423	1	-0.373	-0.536	0.086	-0.006
Kaolinite	-0.503	-0.009	-0.067	-0.373	1	0.287	-0.305	0.419
Quartz	0.106	0.639	-0.521	-0.536	0.287	1	-0.094	0.268
TOC	0.655	0.172	0.026	0.086	-0.305	-0.094	1	-0.471
FWHM illite$_{[001]}$	-0.503	-0.174	-0.288	-0.006	0.419	0.268	-0.471	1

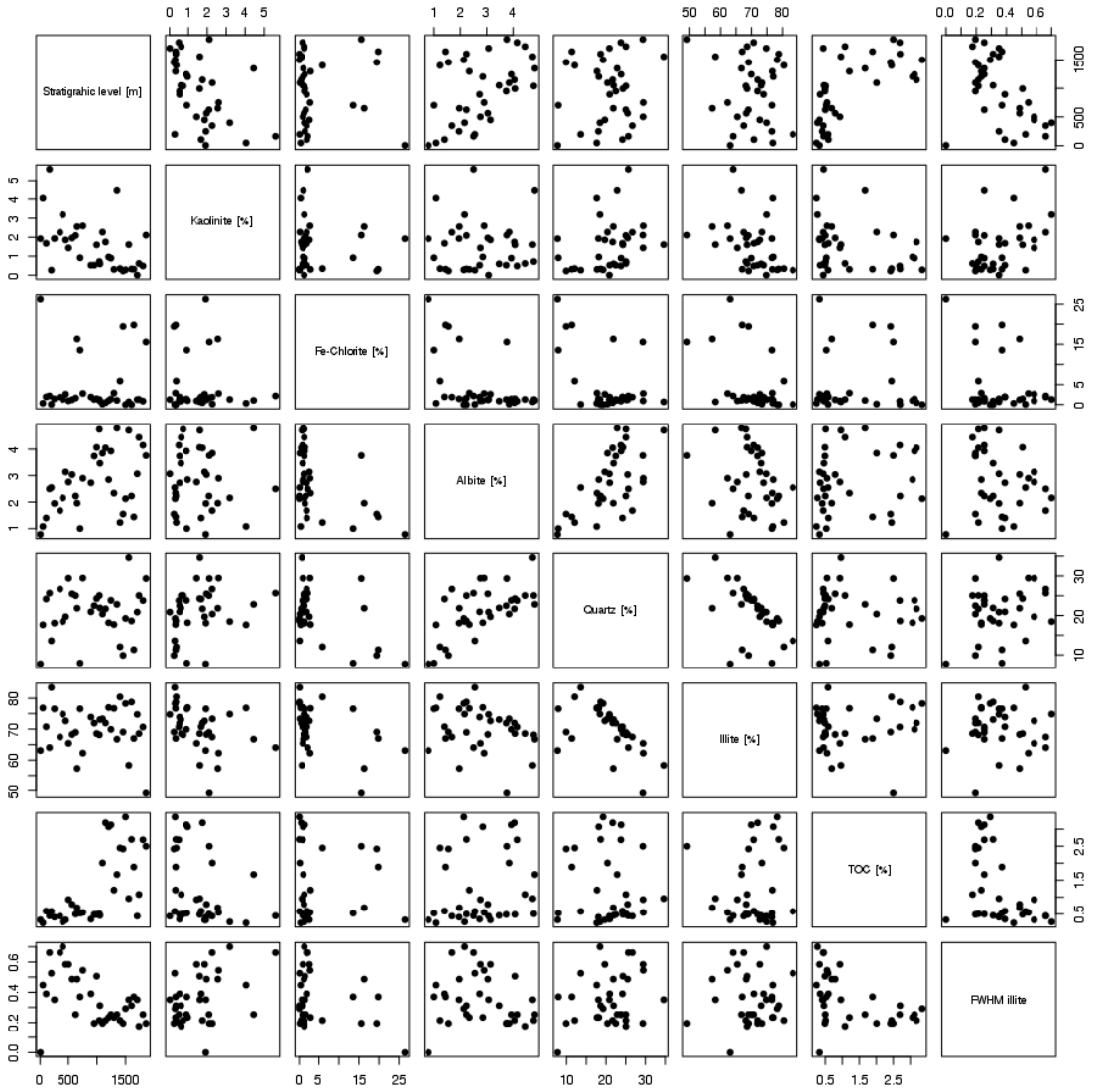

Fig. 51: Cross-plot of the different factors, showing their correlations.

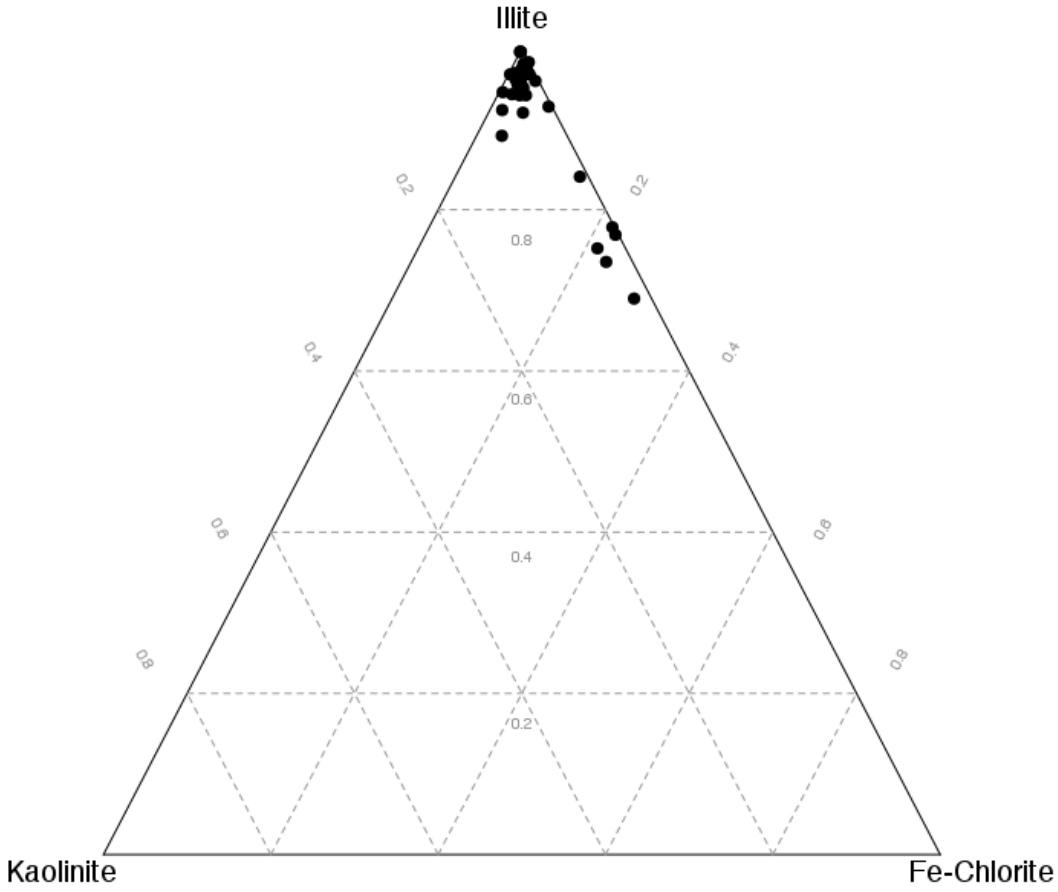

Fig. 52: Ternary diagram of the clay-minerals.

5. Interpretation and discussion

5.1. Definition and subdivision of the Manuels River Formation

The exposed succession consists of 19.07 m of dominantly shales with interbedded volcanic ashes and carbonate concretions. The volcanic ash layer forming the base of the succession (bed 1, Fig. 29) can be easily followed throughout the Avalon Peninsula (Hutchinson, 1962; Fletcher, 1972, 2006; Normore, 2012). It is a significant mappable marker bed and seperates Manuels River Formation from the underlying shales of the Chamberlain's Brook Formation. The top of the succession consists of a coarse sandstone to conglomeratic layer (bed 65, Fig. 37 C–E). Howell (1925) designated this bed as the top of his Kelligrew Brook Formation and Hutchinson (1962) as the top of the Manuels River Formation. Bed 65 is here interpreted as a basal conglomerate of the overlying Elliot Cove formation, as the top of bed 64 is erosional (see Hutchinson, 1962). Following Martin and Dean (1988) the bed immediately below the conglomeratic layer is here taken as the top of the Manuels River Formation. This agrees also with Fletcher's (2006) suggestion, where he interpreted the contact of the Manuels River Formation with the overlying Beckford Head Formation in the St. Mary's area as erosional and thus selected the uppermost bed below the unconformity as the top of the formation. He excluded Howell's (1925) bed 125 from the correlation with his reference section.

The Manuels River Formation is here subdivided in 64 beds. The slight difference in thickness from Howell's (1925) 20.71 m for his beds 36–124 are explained by measurement and rounding errors. Howell (1925), and implicit by Hutchinson (1962), used an inch resolution for the section at Manuels River, whereas the present study was carried out at a centimetre resolution, which is a c. 2.5× higher accuracy.

The results of the present study agree well with those of Howell (1925) with only minor differences in the subdivision of the beds. When Howell examined the succession in the early 1900s, the exposures might have been slightly different Also the formation is known to vary throughout the Avalon Peninsula (Hutchinson, 1962; Fletcher, 1972, 2006), as a result of facies fluctuations.

Landing and Westrop (1998a) presented a three-member subdivison of the Manuels River Formation at its type locality, based on colour and very slight lithological differences. Although there might be evidence for different coloured zones in the succession, the changes found in the present study are subtle. Also, whether existing or not, these colour changes happen in zones and intervals and never at distinct bases or tops of beds. As a result of covered beds, the boundary between members 2 and 3 was marked as doubtful (Landing and Westrop, 1998a). Dring the present field work all beds were uncovered without revealing

any kind of lithological boundary in that interval. Beside the volcanic ashes and concretions, the lithological changes are minor; a subdivision of the formation is therefore not justified. This also prevented the application of Fletcher's (2006) subdivision of the reference section at Deep Cove, St. Mary's Bay in four members.

Hutchinson (1962) collected material from the type locality along the west bank of the Manuels River. One sample (GSC 13048) can only be assigned from the type section with doubts (see Hildenbrand, 2016). As stated in Hutchinson's field book for his 1962's study (the field book is housed together with his collection and available from the Geological Survey of Canada, Ottawa, Canada), this sample derives from the east bank of the river. The studies of Malang (2015) and Wetzel (2015) have shown clear evidence of a strike-slip fault in the riverbed, which caused a displacement of the east bank of the river c. 67 m towards the coastline. If Hutchinson indeed collected this sample at the point indicated by Howell (1925), Hutchinson may not even have sampled the Manuels River Formation, which would explain the difference in lithology.

5.2. Sedimentation rate

The time-span for the sedimentation of the formation is estimated to 5 Ma, so the average sedimentation rate can be estimated at c. 3.8 m/Ma (Fig. 53). The sedimentation rate is assumed to vary, as a result of changing depositional environments. Low-energy environments have lower sedimentation rates, whereas in high-energy environments sedimentation is generally higher.

Using data from Hutchinson (1962) it is possible to estimate the sedimentation rate of the late Cambrian Elliot Cove formation in the Conception Bay region at c. 7.8 m/Ma (Fig. 53). This data should only be used as an initial evidence, as the exact correlation and dating of the Elliot Cove formation remains doubtful. The top of the formation in the area of Manuels River is erosional, as the formation is exposed and subject to weathering at the mouth of the river (Hutchinson, 1962).

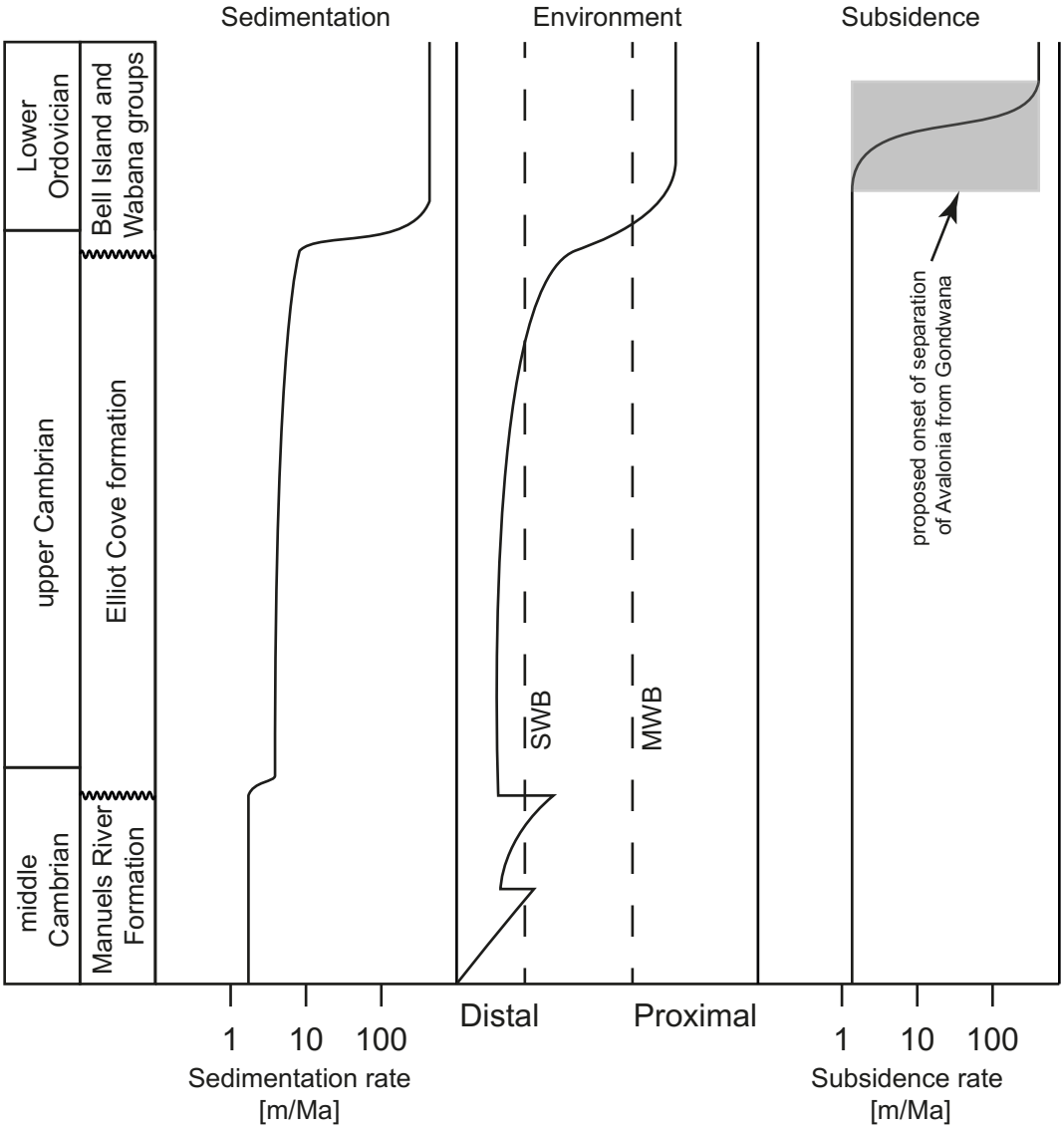

Fig. 53: Interpretation of the middle Cambrian to Early Ordovician sedimentation, palaeoenvironment and subsidence in the area of Conception Bay. The high subsidence in the Ordovician is suggested to result from the beginning separation of Avalonia from Gondwana. SWB: Mean storm wave base, MWB: mean fairweather wave base. Upper Cambrian data composed from and proposed by Hutchinson (1962) and Malang (2015), Ordovician data from Ranger *et al.* (1984).

5.3. Degree of diagenesis

The degree of diagenesis and its change throughout the succession is shown in Fig. 50, based on the FWHM of illite$_{[001]}$ as a proxy. The FWHM of illite$_{[001]}$ decreases almost linearly, so a linear increase of the degree of diagenesis towards the top of the succession is assumed. Nevertheless, a peak is observed at the stratiraphic level of c. 10 m. Below this level, most of the samples are in the deep-diagenetic zone, whereas the ones above are mainly in the anchi- or epizone. This suggests that the upper part of the succession was exposed to higher

temperatures, up to c. 350° C, whereas the lower part was only exposed to a maximum of c. 190° C. This curve progress is unusual, as the degree of diagenesis is expected to be stable throughout such a relatively thin succession or be slightly decreasing towards the top (Kübler, 1967). Apparently the upper part of the succession was exposed to a higher, secondary metamorphic event during or after its burial. There is no evidence of magmatic intrusions in the overlying beds of the Cambrian–Ordovician succession (Hutchinson, 1962; Ranger *et al.*, 1984), which might have caused higher temperatures or pressure. Thus local fluids or pore water heated during burial might have caused the second metamorphic event (Bucher and Frey, 2002). The lower part of the succession was apparently unaffected, as a result of the presence of bentonite layers in the interval of c. 10 m. These layers might have served as aquicludes and thus prevented the fluids from affecting the underlying beds.

The rocks of the Avalon Peninsula, except the Holyrood Horst were intensively faulted by the Acadian Orogeny (Rose 1952; Hutchinson, 1953, 1962; Fletcher, 1972, 2006; King, 1988, 1990), so the relatively low metamorphic grade in the area of Conception Bay is unexpected. The crystalline rocks forming the basement of the Holyrood Horst (mainly granites and rhyolites (King, 1988, 1990)) may have prevented the overlying beds from being affected by the orogeny.

5.3.1. Subsidence, uplift and erosion

Presuming an average primary exposure of the beds to c. 170°–190°, an average thermal gradient of 30° K/km and only a slight increase in pressure, a subsidence of approximately 5.7–6.3 km can be estimated.

The Cambrian and Ordovician beds in the area of Conception Bay dip mainly conformably approximately 10° north–north-west. With the assumed subsidence of c. 5.7–6.3 km it is possible to estimate the area where the primary sedimentary cover would be now exposed, in approximately 32.8–36.3 km north-north-west of the type locality. Fig. 12 shows that this area is now covered by the ocean. Nevertheless, the Holyrood Horst and the faults bounding it might be extended to that area, as the exposures of both end not far away in the south and Ordovician beds are exposed on Bell Island. This suggests that the middle Cambrian beds of Conception Bay were only covered by a more or less conformable succession of upper Cambrian to Ordovician, possibly Silurian beds. As nearly a third of the original sedimentary cover (c. 2000 m) is still exposed (upper Cambrian and Ordovician), it can be assumed that uplift and the onset of erosion of the Cambrian and Ordovician beds are significantly younger than Silurian. A possible subsidence path for the Manuels River Formation is shown in Fig. 54.

However, a subsidence of 5.7–6.3 km only can be assumed, if the exposure of the

samples to 170°–190° is primary. Fluids and pore water possibly affected all parts of the Manuels River Formation and obscured the primary temperatures (Bucher and Frey, 2002). The timing of the subsidence later than lower Ordovician can also only be assumed. It is possible that a younger subsidence happened later than Silurian, what caused this illite crystallinity.

An upper Tremadocian to lower Floian age for the uppermost beds exposed on Bell Island is assumed (Ranger *et al.*, 1984), so approximately 25 Ma of sedimentation can be estimated for the upper Cambrian to middle Tremadocian succession (c. 2 km). This leads to an average subsidence rate of c. 80 m/Ma for the still exposed coverage. In terms of the complete suggested coverage (upper Cambrian to possibly Silurian) a somewhat higher average subsidence rate of approximately 95–105 m/Ma can be estimated. Data of Hutchinson (1962) and Malang (2015) suggest a slightly shallowing upward trend for the upper Cambrian Elliot Cove formation. With respect to the estimated sedimentation rate, it can be assumed that the subsidence rate was very low to zero throughout the deposition of this formation. So it is here suggested that the main subsidence happened in the Early Ordovician (Fig. 53), maybe also in the Middle or Late Ordovician. This subsidence rate can be estimated to a minimum of c. 130 m/Ma.

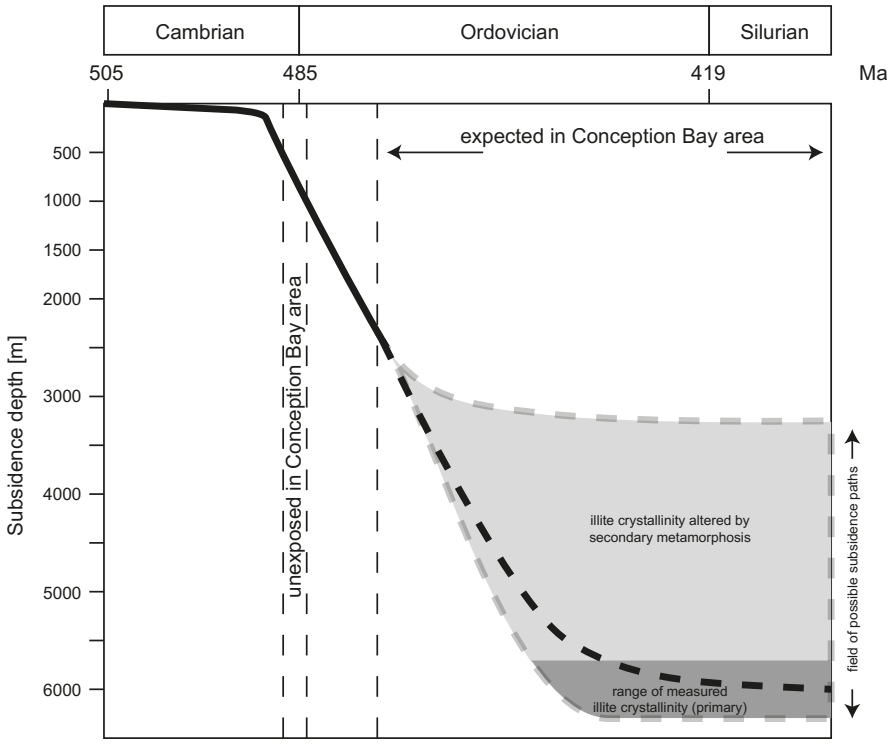

Fig. 54: A proposed subsidence path for the Manuels River Formation in the Conception Bay area. The omset of the uplift is questionable, so there is no uplift path in this figure. Nevertheless, the uplift timing must have been significantly later than Silurian.

5.4. Organic matter and minerals

5.4.1. Organic matter

The amount of total organic carbon changes significantly from c. 0.5–1% to c. 2.5–3% at approximately the half stratigraphic height of the succession. This was also qualitatively observed in the field with pyrite as a proxy. The higher amount of organic carbon in the upper part of the succession in conjunction with pyrite may have led to the black shales exposed in that part, whereas the shales in the lower part of the succession are bright grey, rather than dark. The thin sections show a similar trend. Figs. 33 D–H and 34 A–D from the upper part of the succession show a very high amount of organic carbon in the beds. Assuming a stable metamorphic grade, this suggests a higher organic productivity or a higher preservation of organic material. The metamorphic grade increases upwards. Keeping in mind that organic matter is highly affected even by low-grade metamorphism, this trend suggests that the amount of original organic carbon in the upper half of the succession was significantly higher than the one observed.

In general two different scenarios for the interaction of oxygen-depleted shales and organic matter have been proposed: the productivity model and the preservation model. The former model explains the formation of black shales as a result of high organic productivity at the surface-water level (Morris, 1987; Calvert, 1987). The productivity model usually requires high accumulation rates (Wignall, 1994). In contrast, the preservation model explains the preservation of organic matter as result of anoxic environments (Woolnough, 1937; Wignall, 1991; Paropkari *et al.*, 1992). This model usually requires low sediment accumulation rates (Wignall, 1994). Because of the low sedimentation rate observed in the succession, it is assumed that the oxygen-depleted environment caused the preservation of the organic carbon.

5.4.2. Minerals

Albite. The amount of albite increases almost linearly towards the top of the succession. Simultaneously, no correlation with the degree of diagenesis was observed, which suggests a detrital origin for the albite. However, studies of the Oligocene Frio Formation shales and sandstones from the Gulf of Mexico observed a decrease of K-feldspar in conjunction with a simultaneous increase in albite during burial (Freed, 1982; Loucks *et al.*, 1984; Milliken, 1989; Lynch, 1997). It is shown in Fig. 55 A, that the K-feldspar would be absent in the metamorphic field of the present study, but a portion of K-feldspar (<3% in average) and less albite (<4% in average) in the original composition can be assumed. Kirsimäe *et al.* (1999b) proposed a complete loss of the K-feldspar, with a simultaneous increase in albite during

burial.

Fe-chlorite and **kaolinite**. The relatively stable low Fe-chlorite content throughout the succession, shows five major peaks. As the Fe-chlorite shows no correlation with the degree of diagenesis, it is herein suggested that the curve is externally influenced, possibly by the environmental factors. However, Pirrus (1973) showed an increase in Fe-chlorite with a simultaneous decrease in kaolinite in Neoproterozoic sediments of the Baltic Basin. The high iron amount is typical of diagenetic chlorites (Curtis *et al.*, 1985). Lynch (1997) showed that the chlorite content increases towards higher burial depths. Fig. 55 B suggests a decrease to almost zero for chlorite contents below approximately 7% for the given metamorphic grade. According to Bjørlykke (1998), kaolinite in homogenous shales is believed to be detrital.
As shown in Chapter 4.5.4, the kaolinite content decreases towards the top of the succession. This correlates with the increase in the degree of diagenesis. This curve can be explained by the stability of kaolinite. Towards higher metamorphic grades, kaolinite becomes unstable and decreases. The upper boundary of the stability field of the paragenesis kaolinite and quartz is in the range of 250–280° C (Bucher and Frey, 2002) (Fig. 56). This was most probably reached during the secondary metamorphic event (see Chapter 5.3), so only a fraction of the original amount of kaolinite is preserved in the upper part of the succession. It can be assumed, that the original amount of kaolinite was around 2–3% higher than observed in the upper part of the succession. In addition, the study of Lynch (1997) suggests a loss of approximately 20% of the kaolinite during burial to 6 km (Fig. 55 C). This leads to a c. 20% higher amount of kaolinite in the present study.

With the exception of the five major peaks of chlorite, the entire succession is characterised by low chlorite/kaolinite (C/K) ratios. The chlorite peaks lead to high C/K ratios for these samples. Low C/K ratios are well known from the middle Cambrian of Baltica (Kirsimäe *et al.*, 1999b; Raidla *et al.*, 2010). By contrast, samples from the Iberian Range show relatively high C/K ratios (Bauluz *et al.*, 1998).

Pyrite. The pyrite content was determined qualitatively in the field and in thin sections. It corresponds well with the observation of the organic carbon, despite the fact that pyrite shows a higher stability in higher metamorphic grades. Thus a linear correlation of the stratigraphic height and the pyrite content is assumed.

Quartz and illite. Neither the quartz nor the illite contents show any correlation with the stratigraphic height or the metamorphic grade. Nevertheless the two phases show a negative correlation. The absence of the mixed-layer clay mineral illite/smectite in the succession is

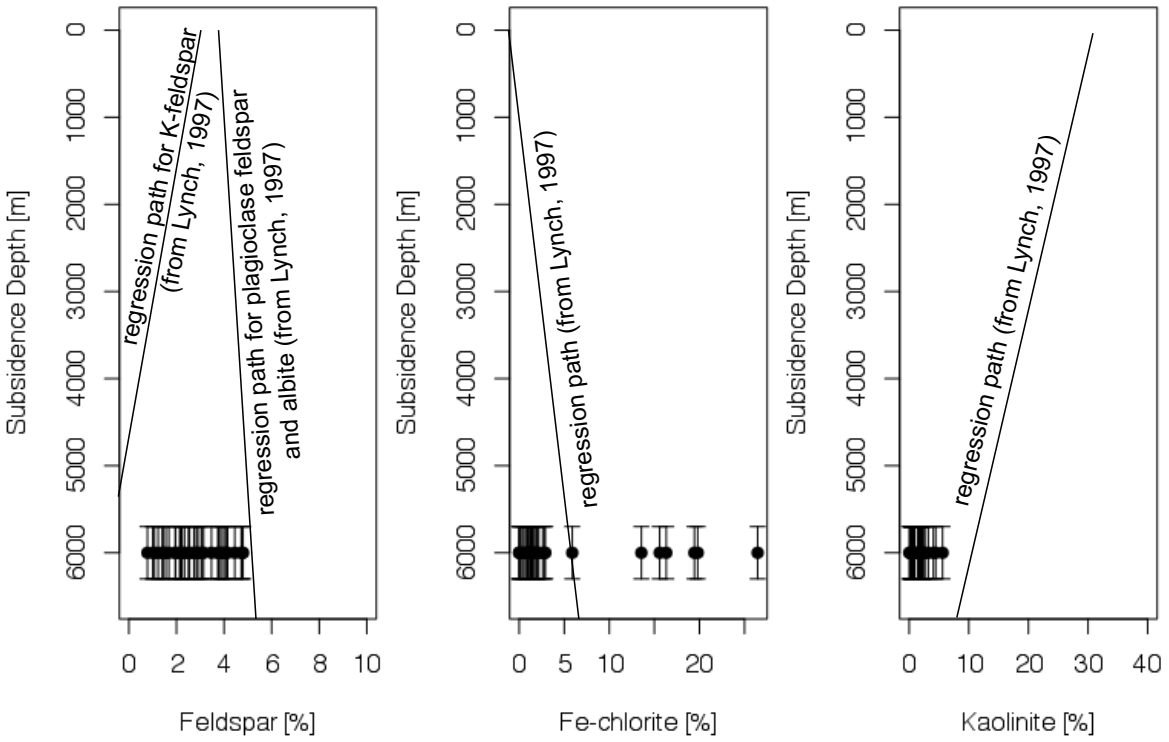

Fig. 55: Mineral abundances in %. The regression paths show the proposed original composition as suggested by Lynch (1997). Redrawn after Lynch (1997).

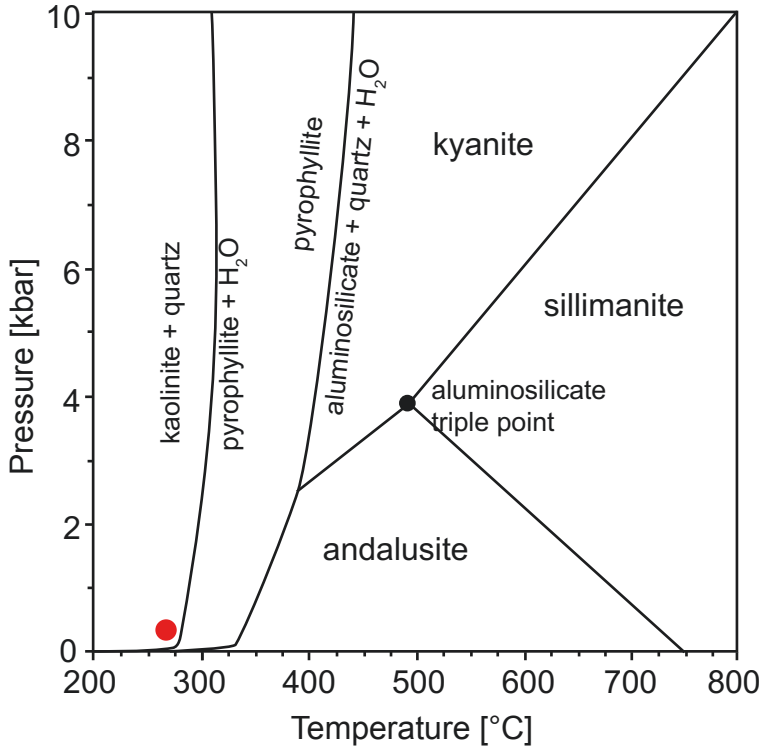

Fig. 56: Stability field of the paragenesis kaolinite and quartz (Bucher and Frey, 2002). Red dot marks the present study.

remarkable. It is assumed that the smectite was completely altered and recrystallised to illite and quartz, with less formation of chlorite during burial, as also suggested by Lynch (1997). Boles and Frank (1979) proposed the following reaction for burial of smectite:

$$\text{smectite} + K^+ \rightarrow \text{Illite} + \text{chlorite} + \text{quartz} + H^+.$$

The mineral composition of the shales represents a typical shale composition (Fig. 57). High amounts of illite, quartz, kaolinite and chlorite are characteristic of pelagic or shelf clays (Bucher and Frey, 2002). The paragenesis albite and kaolinite is unusual, but the whole-rock composition can be explained on the basis of the reaction of Kirsimäe *et al.* (1999a):

$$\text{smectite (illite/smectite mixed layer)} + \text{K-feldspar} + (\text{mica}) \rightarrow \text{illite} + \text{quartz} + \text{chlorite} + \text{albite}$$

Bergström and Levi-Setti (1978) used the semi-quantitative XRD method of Brindley (in Brown, 1961). Since this method was state of the art, XRD analysis in general and the factors influencing the measurement were intensively studied and were repeatedly improved (e.g. Bish and Reynolds, 1989; Moore and Reynolds, 1997). Thus the mineral composition presented in the present study differs from the one of the earlier study of Bergström and

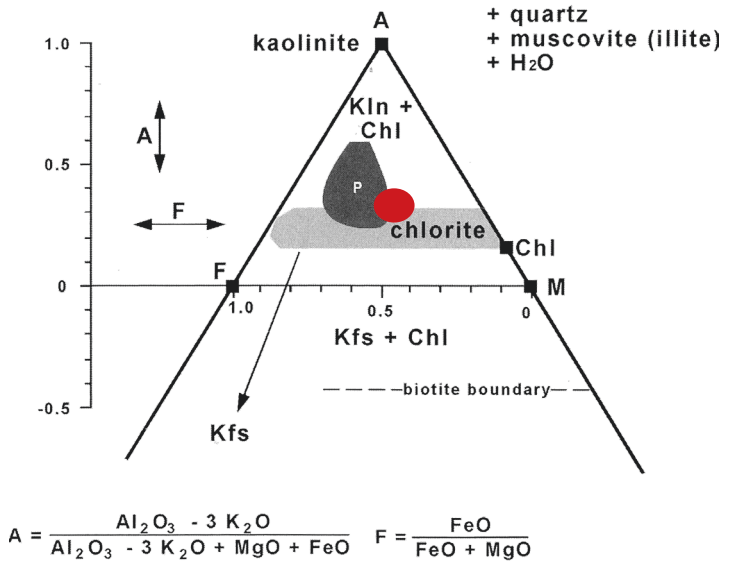

Fig. 57: AFM diagram for low-metamorphic shales. An average pelagic or shelf clay is marked by P. AFM coordinates of minerals and rocks can be calculated from the equations given at the bottom of the figure (Bucher and Frey, 2002). Red field: Current study.

Levi-Setti (1978).

5.5. Depositional environment

The basal bentonite and the different subsequent volcanic ash layers in the lower part of the succession are evidence of volcanic activity in Avalonia. These layers have been also reported from other exposures of the Manuels River Formation across the Avalon Peninsula (e.g. Hutchinson, 1962; Fletcher, 1972, 2006).

The succession along the west bank of the Manuels River can be subdivided into two parts. The shale beds of the lower half of the succession (stratigraphic level < c. 10 m) show features of a low-energy shelf environment (Fig. 53). Mainly laminated shales with scattered or abundant fossils and less than one percent TOC occur in this part. Inter-bedded concretions are assumed to be the result of diagenesis. Most concretions show no concentric structure, so growth according to the pervasive model proposed by Raiswell and Fisher (2000) is suggested.

According to Wignall (1994) and Ullmer-Scholle *et al.*, (2015) the commonly found irregular bedding is suggested to originate from the diagenetic compaction of the mineral grains and the fossil and organic carbon. Towards the top of the lower half of the succession the shales show higher-energy environment features, with abundant thin-layered tempestites filled with shell fragments (Fig. 34 B–G). The tempestites include fragments of shells (e.g., echinoderms), that were transported from shallower areas of the basin. Following Wignall (1994) this part of the succession is interpreted to have been deposited at the level of mean storm wave base (Fig. 53). The higher energy level and the more fissile beds suggest a shallowing-upward trend, as a result of a regression, from the base of the succession to the top of bed 51. Several thin bentonite layers suggest volcanic activity during deposition of bed 51. This activity shows a peak at bed 52 with a 13-cm-thick bentonite layer. Above this layer, the shales are characterised by relatively high organic (1.5–3%) and pyrite contents. Bed 53 shows features of a low-energy environment, indicating a transgression. There is no evidence of a nonconformity at the base of bed 53, although any evidence might be obscured by the soft bentonite. The lenticular fabric shown in some samples (Fig. 35 D, H) is suggested to result from redeposited and compacted current ripples of sea-floor muds (see Schieber *et al.*, 2010; Ullmer-Scholle *et al.*, 2015). This suggests a somewhat higher energy level than expected in a usual shelf clay (see Wignall, 1994). Similar evidence may be given by the intra-bed changes of coarser and finer clay material shown in the same samples (see Ullmer-Scholle, 2015). These features suggest that the upper part of the succession was influenced by changes in energy level, which agrees with the conclusions of Bergström and Levi-Setti

(1978). Bergström and Levi-Setti (1978) found only evidence of relative bathymetric shifts, not of absolute ones in the uppermost 7.4 m of the succession. Changes in water level occurred during deposition, possibly as a result of sea-level changes. Towards bed 64, clear evidence of a higher-energy environment is given by wavy bedding (Fig. 37 A–B) and interbedded coarser material (Fig. 37 B). Similar results were proposed by Ullmer-Scholle *et al.*, (2015). Thus a shallowing-upward trend, resulting from a regression is here proposed. This part of the succession is interpreted to have been deposited at or above mean storm-wave base level (Fig. 53). Evidence of the trend might also be given by the overall increase of albite and especially by the sudden increase in quartz towards bed 64. This interpretation is supported by the cross stratification observed by Malang (2015). The black shales of the succession are suggested to have been deposited in a dysoxic environment (see Wignall, 1994; Arthur and Sageman, 1994). Bed 65 shows a different lithology than the rest of the succession. Its base is erosional and is therefore interpreted as an unconformity. On account of its conglomeratic character, with recycled material from the underlying layers, it is here interpreted as a basal conglomerate, deposited during a transgression.

Shales are widely known to be deposited in relatively low-energy environments, such as deep ocean basins or distal shelfs. Thus, the present interpretation of the depositional facies appears somewhat surprising. However, some recent studies on mud-dominated material suggest high-energy and shallow depositional environment, respectively (Rine and Ginsburg, 1985; Schieber, 1998; Plint, 2014). Schieber and Yawar (2009) and Schieber *et al.* (2010) proved the transport of water-rich mud and muddy current ripples as clasts over tens of km. The muddy material might be deposited through flocculation and/or deposition through gravity. Also redeposition by currents and waves on basin floors is possible (Schieber, 2011). Another option is the weathering and erosion of other shale material as shown by Plint *et al.* (2012) and Plint (2014) and Schieber and Bennett (2013).

In accordance with Arthur and Sageman (1994) the development of marine oxygen -depleted shales can be attributed to five well-known major environment models: (1) deep, enclosed basins with a positive water balance (e.g. Black Sea), (2) a deep borderland basin with a O2 minimum zone (e.g. South California), (3) coastal upwelling on continental slopes (e.g. Peru), (4) shallow stratified basins (e.g. Baltic Sea) and (5) coastal zones with organic-rich sediments. Howell (1925), Hildenbrand (2012), Hildenbrand *et al.*, (2012) and Hildenbrand (2016) proved the occurrence of a benthic macrofauna (e.g., trilobites, brachiopods) in the shales of the Manuels River Formation, which excludes a Black-Sea-situation for the succession. The palaeoenvironment (close to mean storm-wave base and relatively low relief) and the highly fossiliferous shales make the deep borderland basin and coastal upwelling situations unlikely, although coastal upwelling is the only model, that does not require an enclosed basin (Arthur and Sageman, 1994). The existence of organic-

rich sediments (high-productivity model) is a prerequisite for the coastal model, so this is unlikely here. A shallow stratified basin, such as a fjord or an estuary, appears the only possibility. The main issue of the application of this model to the Manuels River Formation is the unproven existence of an opposite barrier of the basin. Another issue might be salinity, as it is expected to be lower in fjords and estuaries than in the open ocean. The fauna (see Howell, 1925; Hutchinson 1962; Fletcher, 1972, 2006; Hildenbrand, 2012; Hildenbrand *et al.*, 2012; Hildenbrand, 2016) does not reflect the existence of a lower salinity, rather one of an open ocean. Nevertheless it is possible that the salinity was not decreased in the basin. Also an adaptation of the fauna to changes in salinity is feasible.

The widespread, although low, presence of kaolinite (Fig. 46 D) and the almost complete absence of chlorite in the samples (Fig. 46 B) suggest a mainly warm, semi-arid to semi-humid environment of deposition for the Manuels River Formation, as kaolinite (and smectite) are formed during stages with higher weathering rates (Weaver, 1989). The predominance of illite in the samples is proposed to result from detrital illite and from recrystallised smectite. The possible, significant amount of smectite in the original clay composition would also suggest a semi-humid to semi-arid environment (Ruffel *et al.*, 2002). Fig. 39 B shows a decrease in the kaolinite content for every significant peak in the Fe-chlorite graph. This might suggest sudden changes from warm to cold climate and vice versa, although clear evidence is lacking.

A mainly warm climate during deposition of the Manuels River Formation is also supported by Landing (2012), who proposed nine global hyperwarming stages for the Early Palaeozoic on the basis of black shale dysoxic/anoxic (d/a) intervals found in Laurentia. The deposition of the Manuels River Formation is coevally with his Hatch Hill d/a interval. The global hyperwarming caused an extreme eustatic highstand, which may have led to the deposition of oxygen depleted shales (Landing, 2012).

5.6. Palaeogeography

It is considered that Avalonia was positioned at high latitudes of around 70–80° S throughout the middle Cambrian (e.g. Cocks and Torsvik, 2002, 2006; Pollock *et al.*, 2009, 2012). Even with a relatively warm global climate with ice-free poles, this would result in a cool climate setting for Avalonia. A number of authors accounted on the cool-water fauna of Avalonia (e.g., Robison, 1994; Pollock *et al.*, 2012, Landing *et al.*, 2013b). Results of the present study of the Manuels River Formation challenge this interpretation. The clay-mineral composition of the present study agree with the results of Dera *et al.* (2009) from very low latitudes (20° N) in the Early Jurassic. Assuming an increase of kaolinite (up to 25%) in conjunction with a decrease of illite in the original composition the results are comparable with those of Dera *et al.* (2009) of 35–40° N. In view of the global hyperwarming during the middle Cambrian (Landing, 2012), this suggests a position of Avalonia at lower latitudes (30°–65° S) than previously thought (Fig. 58). The range indicated is also supported by palaeomagnetic studies (Trench *et al.*, 1992; McNamara *et al.*, 2001; Hamilton and Murphy, 2004; Thompson *et al.*, 2010) in conjunction with trilobite faunal proximities and endemisms (Keppie and Keppie, 2014). Hildenbrand (2016) showed a relative proximity of Avalonia Baltica and Greenland.

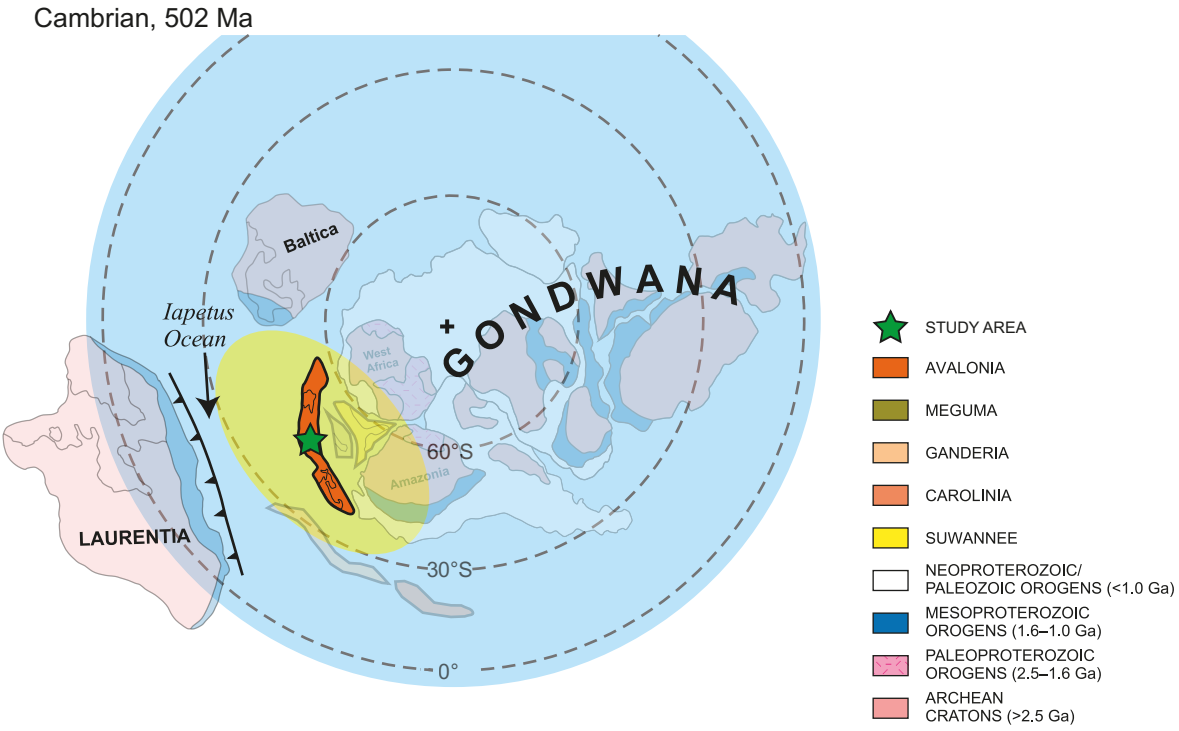

Fig. 58: Proposed position of Avalonia at lower latitudes during deposition of the Manuels River Formation. The yellow field marks the range of possible positions. The other continents are faded out, as they have not been the subject of the present study. Data for Baltica, Laurentia, the proximity of Avalonia and Gondwana and the graphic layout are from Pollock *et al.* (2012).

This is also supported by similar C/K ratios of Avalonia and Baltica (see Chapter 5.5.2). However, a connection of these areas during the Cambrian can be excluded (e.g., Cocks and Thorsvick, 2006; Pollock *et al.*, 2009; Pollock *et al.*, 2012; Landing *et al.*, 2013a, b).
Further it is proposed that the overlying beds were deposited at an average subsidence rate of c. 100 m/Ma (see Chapter 5.4). The Ordovician beds were previously shown to have been deposited in a mainly proximal marine environment (Ranger *et al.*, 1984), as also shown in Fig. 53, so an equilibrium between subsidence and sedimentation rate can be assumed. The subsidence rate indicates that a continuous extension of the accommodation space took place, proposed here to result from the separation of Avalonia from Gondwana. The exact timing of the onset of the extension remains questionable for the Conception Bay area. Nevertheless, an early Ordovician beginning is likely, as a coarsening- and shallowing-upward trend and thus a higher sedimentation rate with a lesser subsidence rate for the upper Cambrian shales of the Elliot Cove formation was observed by Malang (2015). The lowest Ordovician beds exposed indicate a proximal marine setting, which leads to the suggestion that the previously assumed steady state of subsidence and sedimentation rate was reached at that time (Fig. 53).

On the basis of the development of rise prisms and continental slopes Landing (2005) proposed an early Cambrian separation of Avalonia and Gondwana. Keppie *et al.* (2003) proposed on the basis of Landing's (1996) study, a barrier to faunal migration between Avalonia and Gondwana during the Cambrian. Landing and MacGabhann (2010) supported an early Cambrian separation based on the occurrence of dropstone deposits in New Brunswick. Landing *et al.* (2013b) postulate on the basis of earlier studies (Landing, 1996, 2005) a consistent disconnection between Avalonia and Gondwana during the Cambrian.

However, the results of the present study for timing of the separation fit well with the zircon detrital data of Pollock *et al.* (2009) from the Lower Ordovician of Bell Island, although the present study suggests a somewhat earlier separation. The difference possibly results from the resolution of Pollock *et al.* (2009), as they only measured samples from lower Cambrian and Lower Ordovician. A higher resolution in zircon sampling may lead to better results and a more accurate timing. Willner *et al.* (2013) suggested an Early Ordovician separation for Avalonia based on zircon provenance data from east and west Avalonia. Linnemann *et al.* (2012) dated the separation for the eastern Avalonian Brabant Massiv (France) at 485 Ma, i.e. earliest Ordovician. On the basis of subsidence analysis in eastern Avalonia, Prigmore *et al.*, (1997) proposed a separation either in the late Cambrian to early Tremadocian or in the Arenigian to Llanvirnian. The results of the present study agree with the former suggestion, whereas the latter appears unlikely.

6. Conclusions and outlook

The shales of the Manuels River Formation at its type locality were formed from organic-rich muds that were deposited mainly conformably in relatively shallow water. The energetic level fluctuated from relatively low to very high. Laminated beds are evidence of a deposition below the mean storm wave base, and tempestites, cross stratification and other sedimentary structures indicate deposition close to and above mean storm-wave base at some levels. This indicates two shallowing-upward trends, divided by a drop in water level at c. 10.76 m. There is no indication for a nonconformity at this level, but any evidence might have been obscured the relatively rapid transgression. By contrast the upper shallowing-upward trend is truncated by an erosional unconformity, overlain by the basal conglomerate of the Elliot Cove formation. Both trends are interpreted as results of relatively slow regressions followed by transgressions. The calcareous concretions, that occur scattered in the lower half of the succession show features of pervasive, rather than concentric growth. Interbedded bentonite layers indicate volcanic activity in the area, with a peak at the level of 10.63–10.76 m. The sedimentation rate was estimated at a relatively low average value of approximately 3.8 m/Ma, compared to the assumed depositional environment. Most probably, the sedimentation rate was significantly higher in the higher-energetic environments.

The organic-rich muds were deposited in a dysoxic environment. The depositional environment, the faunal content and the low sedimentation rate suggest an estuary or a fjord with stratified water. The precise coastal environment remains uncertain.

The organic matter preserved in the shales is proposed to have been preserved as a result of the oxygen-depleted environment (preservation model), not to be the cause of it (productivity model). In the lower half of the succession, total organic carbon is relatively low (<1.5%), increases suddenly after a transgression and varies strongly in the upper half of the succession. In general, the amount of organic matter was significantly higher in the original sediment than today.

The shales are mainly characterised by the minerals illite, quartz, kaolinite, albite, Fe-chlorite and pyrite. The mineral composition varies only slightly. The predominance of illite possibly results the palaeoclimate and/or from the diagenetic alteration of smectite during burial. Kaolinite is shown to be abundant, but low on average, as a result of diagenetic impact. Additionally kaolinite is shown to decrease towards the top of the formation, as a result of the secondary metamorphic event. The degree of diagnesis suggests a higher original detrital kaolinite content. The albite and the Fe-chlorite are shown to result mainly from alteration of K-feldspar and smectite. Only the five major peaks of Fe-chlorite indicate a detrital provenance. The possibly original content of K-feldspar and smectite is completely lost, as a result of diagenetic alteration.

The mineral composition of the shales suggests a mainly warm, semi-arid to semi-humid palaeoenvironment. The five major peaks of the Fe-chlorite may indicate sudden changes in the climate to cold stages. These results indicate that during the late middle Cambrian Avalonia was located not in high latitudes, as previously asumed, but in temperate latitudes, more specifically within the range of 30°–65° S, near Amazonia.

The results of the illite-crystallinity analysis indicate a relatively low diagenetic impact in the shales, compared to adjacent areas. The basement of the Holyrood Horst probably prevented the Manuels River succession from being strongly affected by any orogeny. However, the results suggest a higher metamorphic grade for the upper part of the succession than for the lower part and imply a second metamorphic event resulting from hot fluids or heated pore waters. The succession was subjected to a subsidence of approximately 5.7–6 km. Presumingly, the main subsidence occurred during the Early Ordovician, which led to high subsidence and sedimentation rates during that time interval and indicates a rapid extension of the accumulation space. This process is proposed to result from the separation of Avalonia from Gondwana, which started in the Early Ordovician.

Although the present study gives insights into the depositional environment of the Manuels River Formation along its type locality, detailed study is needed of the formation in other areas, such as other exposures in Newfoundland, St. Pierre and Miquelon, Nova Scotia, New Brunswick and New England. Also the overlying Elliot Cove formation is in need of a revision, as the base and the top remain undefined. The sedimentology and the depositional environment of the Cambrian–Lower Ordovician succession of West Avalonia is of particular interest to provide insights into the Cambrian Avalonian basins, facies, palaeogeography and climate of Avalonia in this time interval. The results of the clay-mineralogy of the Upper Cambrian–Lower Ordovician succession will enhance the knowledge of subsidence paths and diagenesis.

Throughout the Cambrian, several Burgess Shale-type deposits bearing soft tissue fauna were formed, such as Burgess Shale, Chengjiang, Kinzers Formation, Emu Bay Shale, Spence Shale or Wheeler Formation (e.g., Briggs, 1978; Glaessner, 1979; Robison, 1985; Hou, 1987; Conway Morris and Robison, 1988). Despite the extraordinary fossil preservation, the abundant organic carbon and the low metamorphic grade of the Manuels River Formation, it is remarkable that no soft tissue preservation in the clastic sediments of the succession is reported. Also, Hildenbrand (2012) did not report any soft tissue from the carbonate concretions intercalated in the succession. However, the concretions are still promising, as the method Hildenbrand (2012) used, possibly destroyed any soft tissue. The general mechanism of the preservation of non-mineralising tissue in fine-clastic sediments is relatively poorly understood. Gaines *et al.* (2005) marked on the importance of abundant carbonate in clay-rich sediments for the preservation of non-mineralising tissue in the

Wheeler Formation. The lack in carbonate input into the Manuels River Formation might have prevented the preservation. Nevertheless, future findings will possibly reveal soft tissues preserved in clastic sediments of the succession, especially from the concretions.

These research topics will be part of a postdoc project by the present author and co-worker Anne Hildenbrand, focussing on the palaeontology and sedimentology of the Cambrian basins of West Avalonia and adjacent areas. The project will be fully funded by the Klaus Tschira Foundation (KTS 00.272.2015).

7. Acknowledgements

First of all I want to thank the Klaus Tschira Foundation for funding the current project (KTS 00.195.2011) and their continuous support, especially Gerda and Klaus Tschira, Beate Spiegel and Claudia Spahn. Without the effort and support of all foundation members, this project would not have been possible.

I thank very much my supervisor Peter Bengtson for very helpful discussions, for carefully reading my manuscript, for having endless patience with me and providing me with the possibility to do research for a PhD at the University of Heidelberg.

My sincere thank to Christina Ifrim for reading the manuscript, for countless helpful discussions, the “always-open” door and her support for the current study.

I gratefully acknowledge the province of Newfoundland and Labrador, especially the Provincial Archaeology Office of the Department of Business, Tourism, Culture and Rural Development for supporting the project and providing the permits for the fieldwork and export. I would like to mention here Martha Drake, Delphina Mercer and Doug Boyce.

I thank very much all the former and actual board members of the Manuels River Natural Heritage Society and the management of The Manuels River Experience for supporting the project in any possible way. On behalf of all of them I would like to mention Gary Gallagher, Don Sword, Michael Mooney, Shannon Maguire Harding, Jeremy Hall, Keith Christopher Moore, Corinne LeDrew, Barbara FitzGerald, Karen Rodden and Pat Sword.

The town of Conception Bay South is thanked for providing a storage room during fieldwork, for help with the permits and the support of the project.

I thank very much Wolfgang Stinnesbeck for helpful advices and his continuous support for this and the following project.

For providing their help in different analyses and sharing their knowledge, I owe a huge thanks to Michael Burchard, Ilse Glass, Margit Brückner and Stefan Rheinberger.

In particular I want to thank Francisco Cueto for numerous helpful discussions regarding computer sciences and geology and his help in any kind of (IT-)emergency.

I thank the entire staff of the Institute of Earth Sciences for sharing their knowledge and help, especially Torsten Hoffmann, Hans Ebert, Michael Bühler and Elfriede Grohmann.

Special thanks to Manuela Böhm, Natalie Schröter, Sven Wetzel, Melanie Kling and Lukas Klose, who contributed as student workers to the project.

I will never forget anyone of the staff members of The Manuels River Experience giving a hand and great advices during the last four years, in particular Sydney, Emily, Millie, Evan, Nathaniel and Matthew. The chalet had the spirit!

I thank very much Gerda and Klaus Tschira and their families for giving me the chance to visit one of the most beautiful places on earth, for sharing their enthusiasm in Geology and Newfoundland with me, for great dinners and for the continuous support and personal commitment for the project.

Last but not least I am very grateful to my parents. This study would not exist without their continuous support, patience and believe in me.

To my co-worker and friend Anne Hildenbrand for all the help, discussions, support, patience and anything else she contributed to this study and my life my sincere thank.

To all others, colleagues, friends and companions,

THANK YOU!

8. References

ANDERSON, M. M. 1987. Stratigraphy of Cambrian rocks at Bacon Cove, Duffs, and Manuels River, Conception Bay, Avalon Peninsula, eastern Newfoundland. Geological Society of America Centennial Field Guide - Northeastern Section, 5(1):467–472.

ARTHUR, M. A., and B. B. SAGEMAN. 1994. Marine black shales: Depositional Environments of Ancient Deposits. Annual review of earth and planetary sciences, 22(1):499–551.

AUSTERMANN, G., A. HILDENBRAND, A., F. J. CUETO BERCIANO, and P. BENGTSON. 2012. Growth-line analysis of the Middle Cambrian brachiopod Vandalotreta djagoran (Kruse (1990)) from the manuels River Formation, Conception Bay South, Newfoundland, Canada, using ImageJ and R. In: F. Witzmann & M. Aberhan (eds): Centenary Meeting of the Paläontologische Gesellschaft, Programme, Abstracts and Field Guides, Terra Nostra 2012(3), p. 242.

BABCOCK, L. E., S. PENG, G. GEYER, and J. H. SHERGOLD. 2005. Changing perspectives on Cambrian chronostratigraphy and progress toward subdivision of the Cambrian System. Geosciences Journal, 9(2):101–106.

BARR, S. M., and R. P. RAESIDE. 1989. Tectono-stratigraphic terranes in Cape Breton Island, Nova Scotia: Implications for the configuration of the northern Appalachian orogen. Geology, 17(9):822–825.

BARR, S. M., and C. E. WHITE. 1996. Contrasts in late Precambrian-early Paleozoic tectonothermal history between Avalon composite terrane sensu stricto and other possible peri-Gondwanan terranes in southern New Brunswick and Cape Breton Island, Canada. Geological Society of America Special Papers, 304:95–108.

BARR, S. M., C. E. WHITE, and B. V. MILLER. 2003. Age and geochemistry of Late Neoproterozoic and Early Cambrian igneous rocks in southern New Brunswick: similarities and contrasts. 2003:55–73.

BAULUZ, B., C. FERNÁNDEZ-NIETO, and J. LOPEZ. 1998. Diagenesis–very low-grade metamorphism of clastic Cambrian and Ordovician sedimentary rocks in the Iberian Range (Spain). Clay Minerals, 33(3):373–393.

BERGSTRÖM, J., and R. LEVI-SETTI. 1978. Phenotypic variation in the Middle Cambrian trilobite *Paradoxides davidis* Salter at Manuels, SE Newfoundland. Geologica et Palaeontologica, 12(1):1–40.

BISH, D. L., and R. C. REYNOLDS JR. 1989. Sample preparation for X-ray diffraction. In:

D. L. Bish and J. E. Post (eds.), Modern Powder Diffraction.Volume 20. Mineralogical Society of America, Washington D.C, pp. 73–99.

BJØRLYKKE, K. 1998. Clay mineral diagenesis in sedimentary basins–a key to the prediction of rock properties. Examples from the North Sea Basin. Clay Minerals, 33(1):15–34.

BLATT, H., G. MIDDLETON, and R. C. MURRAY. 1972. Origin of Sedimentary Rocks. Prentice-Hall, Englewood Cliffs, N.J., 634 pp.

BOLES, J. R., and S. G. FRANKS. 1979. Clay diagenesis in Wilcox sandstones of southwest Texas: implications of smectite diagenesis on sandstone cementation. Journal of Sedimentary Petrology, 49(1):55–70.

BOGGS, S. 2009. Petrology of Sedimentary Rocks. Second edition, Cambridge University Press, 600 pp.

BOYCE, W. D. 1988. Field Trip Guidebook: Trip A8. Cambrian Trilobite Faunas on the Avalon Peninsula, Newfoundland, 79 pp.

BOYCE, W. D. 2001. Field Trip Guidebook, Trip A3: Classic Cambrian Trilobite Localities of the Conception Bay South Area, Avalon Peninsula, Eastern Newfoundland, 46 pp.

BOYCE, W. D. 2006. Fossils of Newfoundland and Labrador. URL http://www.nr.gov.nl.ca/mines&en/geosurvey/education/fossils.stm. Last access on 2016-01-11.

BRAGG, W. L. 1913. The diffraction of short electromagnetic waves by a crystal. Proceedings of the Cambridge Philosophical Scociety, 17(1):43–57.

BRASIER, M., J. COWIE, and M. TAYLOR. 1994. Decision on the Precambrian-Cambrian boundary stratotype. Episodes, 17(1–2):3–8.

BRIGGS, D. E. 1978. A new trilobite-like arthropod from the Lower Cambrian Kinzers Formation, Pennsylvania. Journal of Paleontology:132–140.

BROWN, G. 1961. The X-ray Identification and Crystal Structures of Clay Minerals. Mineralogical Society, London, 544 pp.

BRÜCKNER, W. D. 1978. Manuels River fossil locality. The Newfoundland Journal of Geological Education, 3(2):16–23.

BUCHER, K., and M. FREY. 2002. Petrogenesis of Metamorphic Rocks. Springer, Berlin, 341 pp.

CALVERT, S. E. 1987. Oceanographic controls on the accumulation of organic matter in marine sediments. Geological Society, London, Special Publications, 26(1):137–151.

CARTO, S. L., and N. EYLES. 2012. Identifying glacial influences on sedimentation

in tectonically-active, mass flow dominated arc basins with reference to the Neoproterozoic Gaskiers glaciation (c. 580 Ma) of the Avalonian-Cadomian Orogenic Belt. Sedimentary Geology, 261–262(1):1–14.

CHURCHMAN, G. J., J. S. WHITTON, and G. G. C. CLARIDGE. 1984. Intercalation methode using Formamide for differentiating Halloysite from Kaolinite. Clays and Clay Minerals, 32(4):241–248.

COCKS, L. R. M., and T. H. TORSVIK. 2002. Earth geography from 500 to 400 million years ago. A faunal and palaeomagnetic review. Journal of the Geological Society, 159(6):631–644.

COCKS, L. R. M., and T. H. TORSVIK. 2006. European geography in a global context from the Vendian to the end of the Palaeozoic. Memoirs of the Geolgical Society of London, 32:83–95.

COCKS, L. R. M., W. S. MCKERROW, and C. R. VAN STAAL. 1997. The margins of Avalonia. Geological Magazine, 134(5):627–636.

COHEN, K. M., S. FINNEY, and P. L. GIBBARD. 2013. The ICS International Chronostratigraphic Chart. Episodes, 36(1):199–204.

CONWAY MORRIS, S., and R. A. ROBISON. 1988. More soft-bodied animals and algae from the Middle Cambrian of Utah and British Columbia. The University of Kansas Paleontological Contributions, 122(1):1–48.

CRAWLEY, M. J. 2010. The R book. Wiley, Chichester, 942 pp.

CURTIS, C., C. HUGHES, J. WHITEMAN, and C. WHITTLE. 1985. Compositional variation within some sedimentary chlorites and some comments on their origin. Mineralogical Magazine, 49(1):375–386.

DAWSON, J. W. 1868. Acadian Geology. The geological structure, organic remains, and mineral resources of Nova Scotia. Second Edition. MacMillan and Company, London, 694 pp.

DERA, G., P. PELLENARD, P. NEIGE, J.-F. DECONINCK, E. PUCÉAT, and J.-L. DOMMERGUES. 2009. Distribution of clay minerals in Early Jurassic Peritethyan seas: Palaeoclimatic significance inferred from multiproxy comparisons. Palaeogeography, Palaeoclimatology, Palaeoecology, 271(1–2):39–51.

DOTT, R. H. J. 1964. Wacke, Graywacke and Matrix – What approach to immature sandstone classification. Journal of Sedimentary Petrology, 34(3):625–632.

DUNHAM, R. J. 1962. Classification of carbonate rocks according to depositional texture. AAPG Memoir, 1(1):108–121.

EBERL, D. D., and B. VELDE. 1989. Beyond the Kubler Index. Clay Minerals, 24(1):571–577.

EYLES, N., and C. EYLES, H. 1989. Glacially-influenced deep-marine sedimentation of the Late Precambrian Gaskiers Formation, Newfoundland, Canada. Sedimentology, 36(1):601–620.

FLETCHER, T. P. 1972. Geology and Lower to Middle Cambrian Trilobite Faunas of the Southwest Avalon, Newfoundland, Cambridge University, Cambridge, 558 pp. Unpublished PhD thesis.

FLETCHER, T. P. 2006. Bedrock geology of the Cape St. Mary's Peninsula, Southwest Avalon Peninsula, Newfoundland (includes parts of NTS sheets 1M/1, 1N/4, 1L/16 and 1K13). Government Newfoundland and Labrador, Geological Survey, Department of Natural Resources, St. John's, 06-02, 117 pp.

FLETCHER, T. P., G. THEOKRITOFF, G. S. LORD, and G. ZEOLI. 2005. The early Paradoxidid Harlani Trilobite fauna of Massachusetts and its correlatives in Newfoundland, Marocco, and Spain. Journal of Paleontology, 79(2):312–336.

FREED, R. L. 1982. Clay mineralogy and depositional history of the Frio Formation in two geopressured wells, Brazoria County, Texas. Transactions of the Gulf Coast Association of Geological Societies, 31(1):289–293.

FRIEDL, G., F. FINGER, N. J. MCNAUGHTON, and I. R. FLETCHER. 2000. Deducing the ancestry of terranes: SHRIMP evidence for South America–derived Gondwana fragments in central Europe Geology, 28(11):1035–1038.

GAINES, R. R., M. J. KENNEDY, and M. L. DROSER. 2005. A new hypothesis for organic preservation of Burgess Shale taxa in the middle Cambrian Wheeler Formation, House Range, Utah. Palaeogeography, Palaeoclimatology, Palaeoecology, 220(1–2):193–205.

GLAESSNER, M. F. 1979. Lower Cambrian Crustacea and annelid worms from Kangaroo Island, South Australia. Alcheringa: An Australasian Journal of Palaeontology, 3(1):21–31.

HAMILTON, M. A., and J. B. MURPHY. 2004. Tectonic significance of a Llanvirn age for the Dunn Point volcanic rocks, Avalon terrane, Nova Scotia, Canada: implications for the evolution of the Iapetus and Rheic Oceans. Tectonophysics, 379(1–4):199–209.

HATHAWAY, J. C. 1956. Procedure for clay mineral analysis used in the sedimentary petrology laboratory of the U.S. Geological Survey. Clay Minerals, 3(15):8–13.

HIBBARD, J. P., C. R. VAN STAAL, and B. V. MILLER. 2007. Links among Carolinia, Avalonia, and Ganderia in the Appalachian peri-Gondwanan realm. Geological Society

of America Special Papers, 433:291–311.

HILDENBRAND, A. 2012. “Small shelly fossils” der mittelkambrischen Manuels-River-Formation in Conception Bay South, Avalon-Halbinsel, Neufundland, Kanada. Universität Heidelberg, Heidelberg, 59 pp. Unpublished “Diplomarbeit”.

HILDENBRAND, A. 2016. Agnostoid trilobites and biostratigraphy of the middle Cambrian Manuels River Formation in the type locality at Conception Bay South, Newfoundland, Canada. Universität Heidelberg, Heidelberg, 111 pp. Unpublished PhD thesis.

HILDENBRAND, A., G. AUSTERMANN, and P. BENGTSON. 2012. “Small shelly fossils” of the Middle Cambrian Manuels River Formation at its type locality along Manuels River, Conception Bay South, Avalon Peninsula, Newfoundland, Canada. In: F. Witzmann & M. Aberhan (eds): Centenary Meeting of the Paläontologische Gesellschaft, Programme, Abstracts and Field Guides, Terra Nostra 2012(3), pp. 77–78.

HOU, X.-G. 1987. Two new arthropods from Lower Cambrian, Chengjiang, eastern Yunnan. Acta Palaeontologica Sinica, 26(3):236–256.

HOWELL, B. F. 1925. The faunas of the Cambrian *Paradoxides* Beds at Manuels, Newfoundland. Bulletins of American Paleontology, 11(43):1–140.

HUTCHINSON, R. D. 1952. The Stratigraphy and Trilobite Faunas of the Cambrian Sedimentary Rocks of Cape Breton Island, Nova Scotia. Geological Survey of Canada Memoir, 263:1–124.

HUTCHINSON, R. D. 1953. Geology of Harbour Grace Map-Area, Newfoundland. Geological Survey of Canada Memoir, 275(1):1–43.

HUTCHINSON, R. D. 1962. Cambrian stratigraphy and trilobite faunas of Southeastern Newfoundland. Geological Survey of Canada Bulletin, 88(1):1–156.

ICHASO, A. A., R. W. DALRYMPLE, and G. M. NARBONNE. 2007. Paleoenvironmental and basin analysis of the late Neoproterozoic (Ediacaran) upper Conception and St John’s groups, west Conception Bay, Newfoundland. Canadian Journal of Earth Sciences, 44(1):25–41.

JUKES, J. B. 1842. Excursions in and About Newfoundland; During the Years 1839 and 1840. John Murray, London, 2, 365 pp.

JUKES, J. B. 1843. General Report of the Geological Survey of Newfoundland: executed under the direction of the government and legislature of the colony during the years 1839 and 1840. John Murray, London, 160 pp.

KEPPIE, J. D. 1993. Synthesis of Palaeozoic deformational events and terrane accretion in

the Canadian Appalachians. Geologische Rundschau, 82(3):381–431.

KEPPIE, J. D., and D. F. KEPPIE. 2014. Ediacaran–Middle Paleozoic Oceanic Voyage of Avalonia from Baltica via Gondwana to Laurentia: Paleomagnetic, Faunal and Geological Constraints. Geoscience Canada, 41(1):5–18.

KEPPIE, J. D., R. D. NANCE, J. B. MURPHY, and J. DOSTAL. 2003. Tethyan, Mediterranean, and Pacific analogues for the Neoproterozoic–Paleozoic birth and development of peri-Gondwanan terranes and their transfer to Laurentia and Laurussia. Tectonophysics, 365(1–4):195–219.

KING, A. F. 1988. Geology of the Avalon Peninsula, Report 90–2, Newfoundland: Parts of 1K, 1M, 1N and 2C. Government of Newfoundland and Labrador, Geological Survey, Department of Mines and Energy, St. John's, 1 p.

KING, A. F. 1990. Geology of the St. John's area. Geological Survey Branch, St. John's, 93 pp.

KING, A. F., W. D. BRÜCKNER, M. M. ANDERSON, and T. P. FLETCHER. 1974. Late Precambrian and Cambrian Sedimentary Sequences of Southeaster Newfoundland; Field Trip B-6: Guidebook. Geological and Mineralogical Associations of Canada, 56 pp.

KIRSIMÄE, K., P. JØRGENSEN, and V. KALM. 1999a. Low-temperature diagenetic illite-smectite in Lower Cambrian clays in North Estonia. Clay Minerals, 34(1):151–163.

KIRSIMÄE, K., V. KALM, and P. JØRGENSEN. 1999b. Diagenetic transformation of clay minerals in Lower Cambrian argillaceous sediments of North Estonia. Proceedings of the Estonian Academy of Sciences, Geology, 48(1):15–34.

KLUG, H. P., and L. E. ALEXANDER. 1974. X-ray Diffraction Procedures: for Polycrystalline and Amorphous Materials. Wiley, New York, 966 pp.

KRÖNER, A., P. ŠTÍPSKÁ, K. SCHULMANN, and P. JAECKEL. 2000. Chronological constraints on the pre-Variscan evolution of the northeastern margin of the Bohemian Massif, Czech Republic. Geological Society, London, Special Publications, 179(1):175–197.

KRÖNER, A., P. JAECKEL, E. HEGNER, and M. OPLETAL. 2001. Single zircon ages and whole-rock Nd isotopic systematics of early Palaeozoic granitoid gneisses from the Czech and Polish Sudetes (Jizerské hory, Krkonoše Mountains and Orlice-Sněžník Complex). International Journal of Earth Sciences, 90(2):304–324.

KÜBLER, B. 1967. La cristallinité de l'illite et les zones tout a fait superieures du métamorphisme, Étages tectoniques, Colloque de Neuchâtel 1966, A La Baconniere,

Neuchâtel:105–121.

LANDING, E. 1996. Avalon: Insular continent by the latest Precambrian. Geological Society of America Special Papers, 304:29–63.

LANDING, E. 2004. Precambrian–Cambrian boundary interval deposition and the marginal platform of the Avalon microcontinent. Journal of Geodynamics, 37(3–5):411–435.

LANDING, E. 2005. Early Paleozoic Avalon–Gondwana unity: an obituary – response to "Palaeontological evidence bearing on global Ordovician–Silurian continental reconstructions" by R.A. Fortey and L.R.M. Cocks. Earth Science Reviews, 69:169–175.

LANDING, E. 2012. Time-specific black mudstones and global hyperwarming on the Cambrian–Ordovician slope and shelf of the Laurentia palaeocontinent. Palaeogeography, Palaeoclimatology, Palaeoecology, 367–368(2012):256–272.

LANDING, E., and A. P. BENUS. 1988. Field Trip Guidebook: Trip A3. Cambrian Depositional History and stratigraphy, Avalon-Bonavista Region, Southeastern Newfoundland, 50 pp.

LANDING, E., and B. A. MACGABHANN. 2010. First evidence for Cambrian glaciation provided by sections in Avalonian New Brunswick and Ireland: Additional data for Avalon–Gondwana separation by the earliest Palaeozoic. Palaeogeography, Palaeoclimatology, Palaeoecology, 285(3-4):174–185.

LANDING, E. and S. R. WESTROP. 1998a. Cambrian faunal sequence and depositional history of Avalonian Newfoundland and New Brunswick: field workshop. In: E. Landing and S. R. Westrop (eds.), Avalon 1997– The Cambrian standard. New York State Museum Bulletin 492, pp. 5–75.

LANDING, E. and S. R. WESTROP. 1998b. Revisions in stratigraphic nomenclature of the cambrian of Avalonian North America and comparisons with Avalonian Britain. In: E. Landing, and S. R. Westrop (eds.), Avalon 1997– The Cambrian standard. New York State Museum Bulletin 492, pp. 76–87.

LANDING, E., G. M. NARBONNE, P. MYROW, A. P. BENUS, and M. M. ANDERSON. 1988. Faunas and Depositional Environments of the upper Precambrian through Lower Cambrian, southeastern Newfoundland. In: E. Landing, G .M. Narbonne, and P. Myrow (eds.), Trace fossils, small shelly fossils and the Precambrian-Cambrian boundary. Proceedings. New York State Museum Bulletin 463, pp. 18–52.

LANDING, E., G. GEYER, and W. HELDMAIER. 2006. Distinguishing eustatic and epeirogenic controls on Lower – Middle Cambrian boundary successions in West

Gondwana (Morocco and Iberia). Sedimentology, 53(4):899–918.

LANDING, E., S. C. JOHNSON, and G. GEYER. 2008. Faunas and Cambrian Volcanism on the Avalonian Marginal Platform, Southern New Brunswick. Journal of Paleontology, 82(5):884–905.

LANDING, E., G. GEYER, M. D. BRASIER, and S. A. BOWRING. 2013a. Cambrian Evolutionary Radiation: Context, correlation, and chronostratigraphy—Overcoming deficiencies of the first appearance datum (FAD) concept. Earth-Science Reviews, 123:133–172.

LANDING, E. D., S. R. WESTROP, and S. A. BOWRING. 2013b. Reconstructing the Avalonia palaeocontinent in the Cambrian: A 519 Ma caliche in South Wales and transcontinental middle Terreneuvian sandstones. Geological Magazine, 150(06):1022–1046.

LEES, D. C., R. A. FORTEY, and L. R. M. COCKS. 2002. Quantifying paleogeography using biogeography: a test case for the Ordovician and Silurian of Avalonia based on brachiopods and trilobites. Paleobiology, 28(3):343–363.

LEVI-SETTI, R. 1993. Trilobites. The University of Chicago Press, Chicago, 103 pp.

LEVI-SETTI, R. 2014. The trilobite book: a visual journey. The University of Chicago Press, 273 pp.

LINNEMANN, U., A. HERBOSCH, J.-P. LIÉGEOIS, C. PIN, A. GÄRTNER, and M. HOFMANN. 2012. The Cambrian to Devonian odyssey of the Brabant Massif within Avalonia: a review with new zircon ages, geochemistry, Sm–Nd isotopes, stratigraphy and palaeogeography. Earth-Science Reviews, 112(3):126–154.

LIU, A. G., D. MCILLROY, J. J. MATTHEWS, and M. BRASIER. 2012. A new assemblage of juvenile Ediacaran fronds from the Drook Formation, Newfoundland. Journal of the Geological Society, London, 169(1):395–403.

LOUCKS, R. G., M. M. DODGE, and W. E. GALLOWAY. 1984. Regional controls on diagenesis and reservoir quality in lower Tertiary sandstones along the Texas Gulf Coast. AAPG Memoir, 37(1):15–46.

LYNCH, F. L. 1997. Frio shale mineralogy and the stoichiometry of the smectite-to-illite reaction: the most important reaction in clastic sedimentary diagenesis. Clays and Clay Minerals, 45(5):618–631.

MALANG, T. 2015. Detailkartierung der neoproterozoisch bis oberkambrischen Abfolge entlang des westlichen Ufers des Manuels River, Conception Bay South, Neufundland, Kanada. Universität Heidelberg, Heidelberg, 103 pp. Unpublished MSc thesis.

MARCOU, J. 1890. The Lower and Middle Taconic of Europe and North America, I.

American Geologist, 5(1):356–375.

MARTIN, F., and W. T. DEAN. 1988. Middle and Upper Cambrian acritarch and trilobite zonation at Manuels River and Random Island, Eastern Newfoundland. Geological Survey of Canada Bulletin, 381(1):1–91.

MATTHEW, G. F. 1886. Illustrations of the fauna of the St. John group continued, No. 3 – Descriptions of new genera and species (including a description of a new species of Solenopleura by J. F. Whiteaves). Proceedings and Transactions of the Royal Society of Canada, 1st ser., 3(4):29–84.

MATTHEW, G. F. 1896. Faunas of the *Paradoxides* beds in eastern North America, No. 1. Transactions of the New York Academy of Sciences, 15(1):192–247.

MATTHEW, G. F. 1899. A Palaeozoic terrane beneath the Cambrian. Annals of the New York Academy of Sciences, 12(2):41–56.

MCKERROW, W. S., C. R. SCOTESE, and M. D. BRASIER. 1992. Early Cambrian continental reconstructions. Journal of the Geological Society, 149(4):599–606.

MCNAMARA, A. K., C. MAC NIOCAILL, B. A. VAN DER PLUIJM, R. VAN DER VOO, and C. M. NIOCAILL. 2001. West African proximity of the Avalon terrane in the latest Precambrian. Geological Society of America Bulletin, 113(9):1161-1170.

MILLIKEN, K. 1989. Petrography and composition of authigenic feldspars, Oligocene Frio Formation, south Texas. Journal of Sedimentary Petrology, 59(3):361–374.

MILOSEVIC, S., M. TOMESEVIC-CANOVIC, R. DIMITRIJEVIC, M. PETROV, M. DJURICIC, and B. ZIVANIVIC. 1992. Amorphization of aluminosilicate mineral during micronization process. American Ceramic Society Bulletin, 71(5):771–775.

MOORE, D. M., and R. C. J. REYNOLDS. 1997. X-Ray Diffraction and the Identification and Analysis of Clay Minerals. Oxford University Press, Oxford, 378 pp.

MORRIS, R. J. 1987. The formation of organic-rich deposits in two deep-water marine environments. Geological Society, London, Special Publications, 26(1):153–166.

MÜLLER, G., and M. GASTNER. 1971. The'Karbonat-Bombe', a simple device for the determination of carbonate content in sediment, soils, and other materials. Neues Jahrbuch für Mineralogie-Monatshefte, 10:466–469.

MURPHY, J. B. 2000. Tectonic influence on sedimentation along the southern flank of the late Paleozoic Magdalen basin in the Canadian Appalachians: Geochemical and isotopic constraints on the Horton Group in the St. Marys basin, Nova Scotia. Geological Society of America Bulletin, 112(7):997–1011.

MURPHY, J. B., and R. D. NANCE. 1989. Model for the evolution of the Avalonian-Cadomian belt. Geology, 17(8):735–738.

MURPHY, J. B., J. D. KEPPIE, J. DOSTAL, and R. D. NANCE. 1999. Neoproterozoic-early Paleozoic evolution of Avalonia. Geological Society of America Special Papers, 336:253–266.

MURPHY, J. B., J. FERNÁNDEZ-SUÁREZ, T. JEFFRIES, and R. STRACHAN. 2004. U–Pb (LA–ICP-MS) dating of detrital zircons from Cambrian clastic rocks in Avalonia: erosion of a Neoproterozoic arc along the northern Gondwanan margin. Journal of the Geological Society, 161(2):243–254.

MURRAY, A. 1869. Report upon the Geological Survey of Newfoundland for the Year 1868. Honoury House of Assembly, St. John's, 68 pp.

MURRAY, A., and J. P. HOWLEY. 1881. Geological Survey of Newfoundland. Edward Stanford, London, 536 pp.

NANCE, R. D., J. B. MURPHY, and J. D. KEPPIE. 2002. A Cordilleran model for the evolution of Avalonia. Tectonophysics, 352(1–2):11–31.

NARBONNE, G. M., P. M. MYROW, E. LANDING, and M. M. ANDERSON. 1987. A candidate stratotype for the Precambrian–Cambrian boundary, Fortune Head, Burin Peninsula, southeastern Newfoundland. Canadian Journal of Earth Sciences, 24(7):1277–1293.

NAUTIYAL, A. C. 1966: The Cambro-Ordovician sequence in the southeastern part of of the Conception Bay area, eastern Newfoundland. Memorial University of Newfoundland, St. John's, 334 pp. Unpublished MSc thesis.

NORMORE, L. S. 2012. Geology of the Random Island Map Area (NTS 2C/04), Newfoundland. Current Research Newfoundland and Labrador Department of Natural Resources, Geological Survey, Report 12-1, 2012(1):121–145.

O'BRIEN, S. J., R. J. WARDLE, and A. F. KING. 1983. The Avalon Zone: A Pan-African terrane in the Appalachian Orogen of Canada. Geological Journal, 18:195–222.

O'BRIEN, S. J., B. H. O'BRIEN, G. R. DUNNING, and R. D. TUCKER. 1996. Late Neoproterozoic Avalonian and related peri-Gondwanan rocks of the Newfoundland Appalachians. Geological Society of America Special Papers, 304:9–28.

O'BRIEN, S. J., G. R. DUNNING, D. B., C. F. O'DRISCOLL, B. SPARKES, S. ISRAEL, and J. KETCHUM. 2001. New insights into the Neoproterozoic geology of the central Avalon Peninsula (Parts of NTS Map Areas 1N/6, 1N/7 and 1N/3), Eastern Newfoundland. Current Research Newfoundland and Labrador Department of Mines

and Energy, 2001(1):169–189.

PAROPKARI, A. L., C. PRAKASH BABU, and A. MASCARENHAS. 1992. A critical evaluation of depositional parameters controlling the variability of organic carbon in Arabian Sea sediments. Marine Geology, 107(3):213–226.

PENG, S. 2004. Suggested global subdivision of Cambrian System and two potential GSSPs in Hunan, China for defining Cambrian stages. In: D. K. Choi (ed.), IX International Conference of the Cambrian Stage Subdivision Working Group, Abstracts with Program. School of Earth and Environmental Sciences and Institute of Geology and Environmental Sciences, Seoul National University and Palaeontological Society of Korea, Taebaek, Korea, p. 25.

PENG, S., and L. E. BABCOCK. 2005. Towards a new global subdivision of the Cambrian System. Journal of Stratigraphy, 29(1):171–177.

PENG, S., and L. E. BABCOCK. 2011. Continuing progress on chronostratigraphic subdivision of the Cambrian System. Bulletin of Geosciences, 86(3):391–396.

PENG, S., L. E. BABCOCK, and R. A. COOPER. 2012. The Cambrian Period. In: F. M. Gradstein, J. G. Ogg, M. D. Schmitz, and G. Ogg (eds.), The Geologic Time Scale 2012.Volume 2. Elsevier, Oxford, pp. 437–488 .

PETTIJOHN, F. J. 1975. Sedimentary Rocks. Harper & Row, New York, 628 pp.

PIRRUS, E. 1973. Chamosite in Late-Vendian sediments of the Leningrad region. Proceedings of Estonian Academy of Sciences. Chemistry, Geology, 22(1):58–64.

PLINT, A. G. 2014. Mud dispersal across a Cretaceous prodelta: storm-generated, wave-enhanced sediment gravity flows inferred from mudstone microtexture and microfacies. Sedimentology, 61(3):609–647.

PLINT, A. G., J. H. MACQUAKER, and B. L. VARBAN. 2012. Bedload transport of mud across a wide, storm-influenced ramp: Cenomanian–Turonian Kaskapau Formation, Western Canada Foreland Basin. Journal of Sedimentary Research, 82(11):801–822.

POLLOCK, J. C., J. P. HIBBARD, and P. J. SYLVESTER. 2009. Early Ordovician rifting of Avalonia and birth of the Rheic Ocean: U–Pb detrital zircon constraints from Newfoundland. Journal of the Geological Society, 166(3):501–515.

POLLOCK, J. C., J. P. HIBBARD, C. R. VAN STAAL, and B. MURPHY. 2012. A paleogeographical review of the peri-Gondwanan realm of the Appalachian orogen. Canadian Journal of Earth Sciences, 49(1):259–288.

POTTER, P. E., J. B. MAYNARD, and P. J. DEPETRIS. 2005. Mud and mudstones: Introduction and overview. Springer Science & Business Media, 297 p.

POULSEN, V., and M. M. ANDERSON. 1975. The Middle-Upper Cambrian Transition in Southeastern Newfoundland, Canada. Canadian Journal of Earth Sciences, 12(1):2065–2079.

PRIGMORE, J. K., A. J. BUTLER, and N. H. WOODCOCK. 1997. Rifting during separation of Eastern Avalonia from Gondwana: Evidence from subsidence analysis. Geology, 25(3):203–206.

R CORE TEAM. 2016. R: A language and environment for statistical computing, Vienna, Austria. URL https://www.R-project.org/. Last access on 2016-01-11.

RABU, D., D. THIÉBLEMONT, M. TEGYEY, C. GUERROT, C. ALSAC, J.-J. CHAUVEL, J. B. MURPHY, and J. D. KEPPIE. 1996. Late Proterozoic to Paleozoic evolution of the St. Pierre and Miquelon islands: A new piece in the Avalonian puzzle of the Canadian Appalachians. Geological Society of America Special Papers, 304:65–94.

RAIDLA, V., K. KIRSIMÄE, L. BITYUKOVA, A. JOELEHT, A. SHOGENOVA, and S. SLIAUPA. 2010. Lithology and diagenesis of the poorly consolidated Cambrian siliciclastic sediments in the northern Baltic Sedimentary Basin. Geological Quarterly, 50(4):395–406.

RAISWELL, R., and Q. J. FISHER. 2000. Mudrock-hosted carbonate concretions: a review of growth mechanisms and their influence on chemical and isotopic composition. Journal of the Geological Society, London, 157(1):239–251.

RANGER, M. J., R. K. PICKERILL, and D. FILLION. 1984. Lithostratigraphy of the Cambrian? – Lower Ordovician Bell Island and Wabana groups of Bell, Little Bell, and Kellys islands, Conception Bay, eastern Newfoundland. Canadian Journal of Earth Sciences, 21(11):1245–1261.

REAY, A. 1981. The effect of disc mill grinding on some rock-forming minerals. Mineralogical Magazine, 44(334):179–182.

RINE, J. M., and R. N. GINSBURG. 1985. Depositional facies of a mud shoreface in Suriname, South America; a mud analogue to sandy, shallow-marine deposits. Journal of Sedimentary Research, 55(5):633–652.

ROBISON, R. A. 1985. Affinities of Aysheaia (Onychophora), with description of a new Cambrian species. Journal of Paleontology, 59(1):226–235.

ROBISON, R. A. 1994. Agnostoid trilobites from the Henson Gletscher and Kap Stanton formations (Middle Cambrian), North Greenland. Grønlands Geologiske Undersøgelse Bulletin, 169(1):25–77.

ROCCI, G., G. BRONNER, and M. DESCHAMPS. 1991. Crystalline Basement of the

West African Craton. In: R. D. Dallmeyer and J. P. Lécorché (ed.), The West African Orogens and Circum-Atlantic Correlatives. Springer Berlin Heidelberg, pp. 31–61.

ROSE, E. R. 1952. Torbay Map-Area. Geological Survey of Canada Memoir, 265(1):1–64.

RUFFELL, A., J. M. MCKINLEY, and R. H. WORDEN. 2002. Comparison of clay mineral stratigraphy to other proxy palaeoclimate indicators in the Mesozoic of NW Europe. Philosophical Transactions of the Royal Society of London A: Mathematical, Physical and Engineering Sciences, 360(1793):675–693.

RÜGNER, O. 2000. Tonmineral-Neubildung und Paläosalinität im Unteren Muschelkalk des südlichen Germanischen Beckens, Ruprecht-Karls-Universität, Heidelberg, 189 pp. Unpublished PhD thesis.

RUSHTON, A. W. A. 1978. Fossils from the Middel–Upper Cambrian transition in the Nuneaton District. Palaeontology, 21(2):245–283.

SALTER, J. W. 1864. On some New Fossils from the Lingula-flags of Wales. Quarterly Journal of the Geological Society, 20(1):233–241.

SATKOSKI, A. M., S. M. BARR, and S. D. SAMSON. 2010. Provenance of Late Neoproterozoic and Cambrian Sediments in Avalonia: Constraints from Detrital Zircon Ages and Sm-Nd Isotopic Compositions in Southern New Brunswick, Canada. The Journal of Geology, 118(2):187–200.

SCHIEBER, J. 1998. Deposition of mudstones and shales: Overview, problems, and challenges. In: J. Schieber, W. Zimmerle, and P. Sethi (eds.), Schales and Mudstones: Basin Studies, Sedimentology and Paleontology. Schweizerbart'sche Verlagsbuchhandlung, Stuttgart, pp. 131–146.

SCHIEBER, J. 2011. Reverse engineering mother nature—shale sedimentology from an experimental perspective. Sedimentary Geology, 238(1):1–22.

SCHIEBER, J., and R. BENNETT. 2013. Bedload transport of mud across a wide, storm-influenced ramp: Cenomanian–Turonian Kaskapau Formation, Western Canada Foreland Basin—discussion. Journal of Sedimentary Research, 83(12):1198–1199.

SCHIEBER, J., and Z. YAWAR. 2009. A new twist on mud deposition—mud ripples in experiment and rock record. The Sedimentary Record, 7(2):4–8.

SCHIEBER, J., J. SOUTHARD, and A. SCHIMMELMANN. 2010. Lenticular shale fabrics resulting from intermittent erosion of muddy sediments–comparing observations from flume experiments to the rock record. Journal of Sedimentary Research, 80(1):119–128.

SEDGWICK, A. 1852. On the classification and nomenclature of the Lower Palaeozoic rocks

of England and Wales. Quarterly Journal of the Geological Society, 8(1):136–168.

ŚRODOŃ, J. 1984. X-Ray powder diffraction identification of illitic materials. Clays and Clay Minerals, 32(5):337–349.

SWINDEN, H. S., and P. A. HUNT. 1991. A U-Pb zircon age from the Connaigre Bay Group, southwestern Avalon Zone, Newfoundland: implications for regional correlations and metallogenesis. Radiogenic age and isotopic studies: report 4; by Geological Survey Of Canada; Geological Survey of Canada, Paper, 90(2):3–10.

THOMPSON, M. D., A. M. GRUNOW, and J. RAMEZANI. 2010. Cambro-Ordovician paleogeography of the Southeastern New England Avalon Zone: Implications for Gondwana breakup. Geological Society of America Bulletin, 122(1–2):76–88.

TRENCH, A., T. H. TORSVIK, M. A. SMETHURST, N. H. WOODCOCK, and R. METCALFE. 1991. A palaeomagnetic study of the Builth Wells-Llandrindod Wells Ordovician Inlier, Wales: palaeogeographic and structural implications. Geophysical Journal International, 105(2):477–489.

TRENCH, A., T. H. TORSVIK, and W. S. MCKERROW. 1992. The palaeogeographic evolution of Southern Britain during early Palaeozoic times: a reconciliation of palaeomagnetic and biogeographic evidence. Tectonophysics, 201(1–2):75–82.

ULMER-SCHOLLE, D. S., P. A. SCHOLLE, J. SCHIEBER, and R. J. RAINE. 2015. A Color Guide to the Petrography of Sandstones, Siltstones, Shales and Associated Rocks. AAPG Memoir, 109: 1–526.

VAN INGEN, G. 1914. Table of the Geological Formations of the Cambrian and Ordovician Systems about Conception and Trinity Bays, Newfoundland, and their Northeastern-American and Western-European Equivalents, based upon the 1912–1913 field work. Princeton, 1 p.

VAN STAAL, C. R., J. F. DEWEY, C. M. NIOCAILL, and W. S. MCKERROW. 1998. The Cambrian-Silurian tectonic evolution of the northern Appalachians and British Caledonides: history of a complex, west and southwest Pacific-type segment of Iapetus. Geological Society, London, Special Publications, 143(1):199–242.

VETTER, S. 2012. Mineralogische und geochemische Untersuchung von Tonhorizonten in der mittelkambrischen Manuels-River-Formation, Conception Bay South, Neufundland, Kanada. Heidelberg University, Heidelberg, 38 pp. Unpublished BSc thesis.

WALCOTT, C. D. 1888a. The stratigraphical succession of the Cambrian faunas in North America. Nature, 38(1):551.

WALCOTT, C. D. 1888b. The Taconic system of Emmons and the use of the name Taconic in geologic nomenclature. American Journal of Science, 3rd ser, 35(1):229–242, 307–327, 394–401.

WALCOTT, C. D. 1889. Stratigraphic position of the *Olenellus* fauna in North America and Europe. American Journal of Science, 3rd ser(1):374–392.

WALCOTT, C. D. 1891. The fauna of the Lower Cambrian or *Olenellus* Zone. Extract from the Tenth Annual Report of the Director (1888–89), US Geological Survey 10th Annual Report:511–774.

WALCOTT, C. D. 1900. Lower Cambrian terrane in the Atlantic Province. Proceedings of the Washington Academy of Sciences, 1(1):301–339.

WEAVER, C. E. 1989. Clays, Muds, and Shales. Elsevier, Amsterdam, 819 pp.

WESTON, T. C. 1896. Notes on the geology of Newfoundland. Proceedings and Transactions of the Nova Scotia Institute of Science, 9(1):150–157.

WETZEL, S. 2015. Detailkartierung der neoproterozoischen bis oberkambrischen Abfolgen entlang des östlichen Ufers des Manuels River, Conception Bay South, Neufundland, Kanada. Universität Heidelberg, Heidelberg, 126 pp. Unpublished MSc thesis.

WHITEAVES, J. F. 1878. On some Primordial Fossils from Southeastern Newfoundland. American Journal of Science, 3rd ser, 16(1):224–226.

WIGNALL, P. B. 1991. Model for transgressive black shales? Geology, 19(2):167–170.

WIGNALL, P. B. 1994. Black Shales. Clarendon Press, Oxford, 127 pp.

WILLIAMS, H. 1979. Appalachian Orogen in Canada. Canadian Journal of Earth Sciences, 16(3):792–807.

WILLNER, A. P., S. M. BARR, A. GERDES, H.-J. MASSONNE, and C. E. WHITE. 2013. Origin and evolution of Avalonia: evidence from U–Pb and Lu–Hf isotopes in zircon from the Mira terrane, Canada, and the Stavelot–Venn Massif, Belgium. Journal of the Geological Society, 170(5):769–784.

WILSON, R. D., and J. SCHIEBER. 2015. Sedimentary Facies and Depositional Environment of the Middle Devonian Geneseo Formation of New York, U.S.A. Journal of Sedimentary Research, 85(11):1393–1415.

WOJDYR, M. 2010. Fityk: a general-purpose peak fitting program. Journal of Applied Crystallography, 43(1):1126–1128.

WOOD, D. A., R. W. DALRYMPLE, G. M. NARBONNE, J. G. GEHLING, and M. E. CLAPHAM. 2003. Paleoenvironmental analysis of the late Neoproterozoic Mistaken

Point and Trepassey formations, southeastern Newfoundland. Canadian Journal of Earth Sciences, 40(10):1375–1391.

WOOLNOUGH, W. G. 1937. Sedimentation in barred basins, and source rocks of oil. AAPG Bulletin, 21(9):1101–1157.

9. Appendix

9.1. XRD-data

9.1.1. Diffractograms

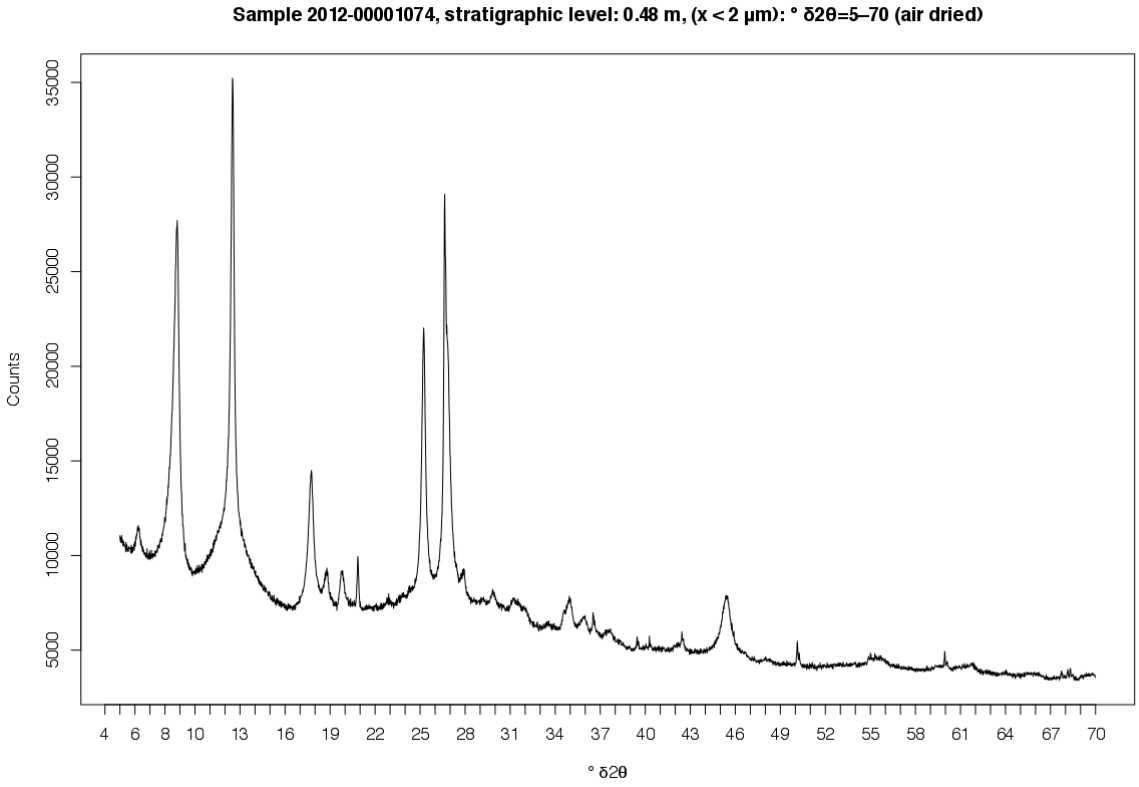
Sample 2012-00001074, stratigraphic level: 0.48 m, (x < 2 µm): ° δ2θ=5–70 (air dried)
Counts
5000
10000
15000
20000
25000
30000
35000
4 6 8 10 13 16 19 22 25 28 31 34 37 40 43 46 49 52 55 58 61 64 67 70
° δ2θ

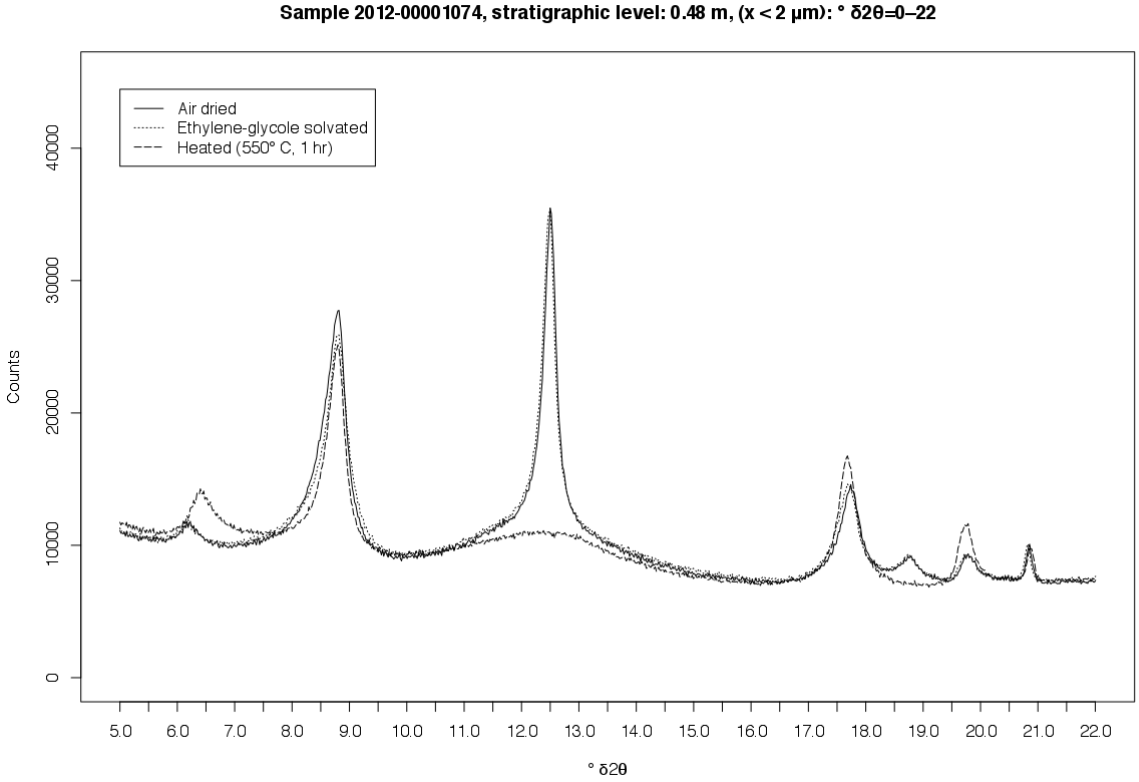
Sample 2012-00001074, stratigraphic level: 0.48 m, (x < 2 µm): ° δ2θ=0–22
Air dried
Ethylene-glycole solvated
Heated (550° C, 1 hr)
Counts
0
10000
20000
30000
40000
5.0 6.0 7.0 8.0 9.0 10.0 11.0 12.0 13.0 14.0 15.0 16.0 17.0 18.0 19.0 20.0 21.0 22.0
° δ2θ

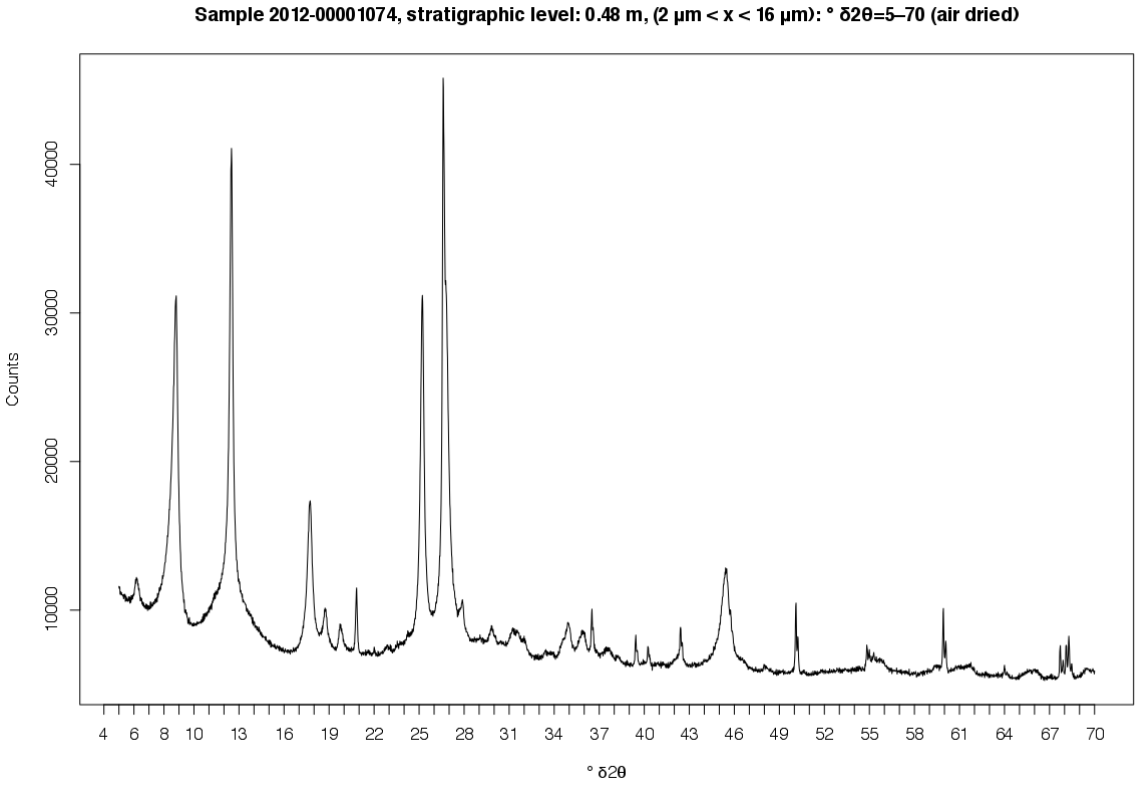
Sample 2012-00001074, stratigraphic level: 0.48 m, (2 µm < x < 16 µm): ° δ2θ=5–70 (air dried)
Counts
10000
20000
30000
40000
4 6 8 10 13 16 19 22 25 28 31 34 37 40 43 46 49 52 55 58 61 64 67 70
° δ2θ

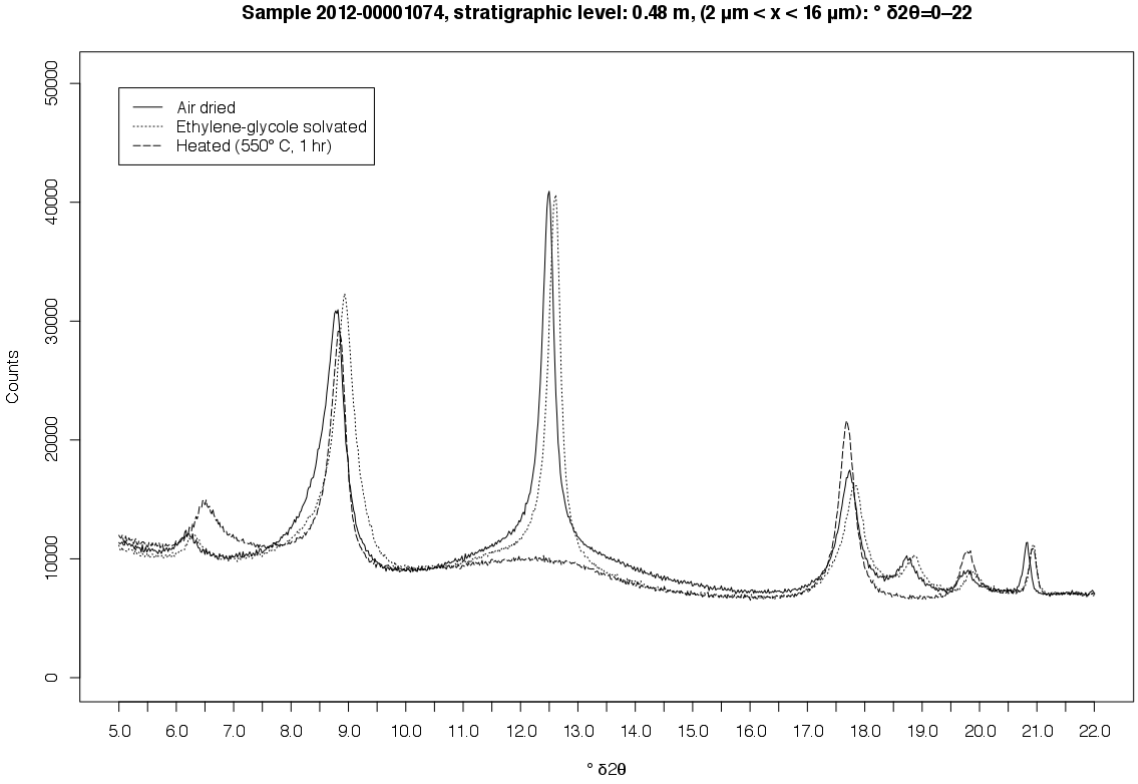
Sample 2012-00001074, stratigraphic level: 0.48 m, (2 µm < x < 16 µm): ° δ2θ=0–22
Air dried
Ethylene-glycole solvated
Heated (550° C, 1 hr)
Counts
0
10000
20000
30000
40000
50000
5.0 6.0 7.0 8.0 9.0 10.0 11.0 12.0 13.0 14.0 15.0 16.0 17.0 18.0 19.0 20.0 21.0 22.0
° δ2θ

Sample 2012-00001063, stratigraphic level: 1.08 m, (x < 2 µm): ° δ2θ=5–70 (air dried)

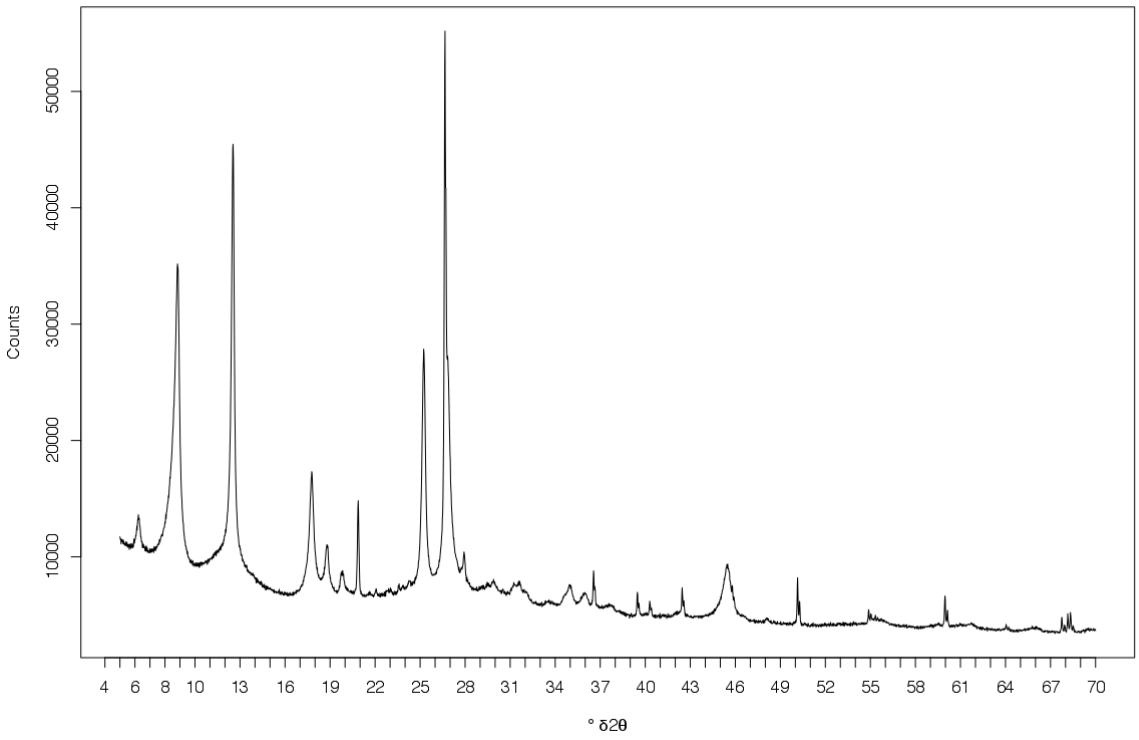

Sample 2012-00001063, stratigraphic level: 1.08 m, (x < 2 µm): ° δ2θ=0–22

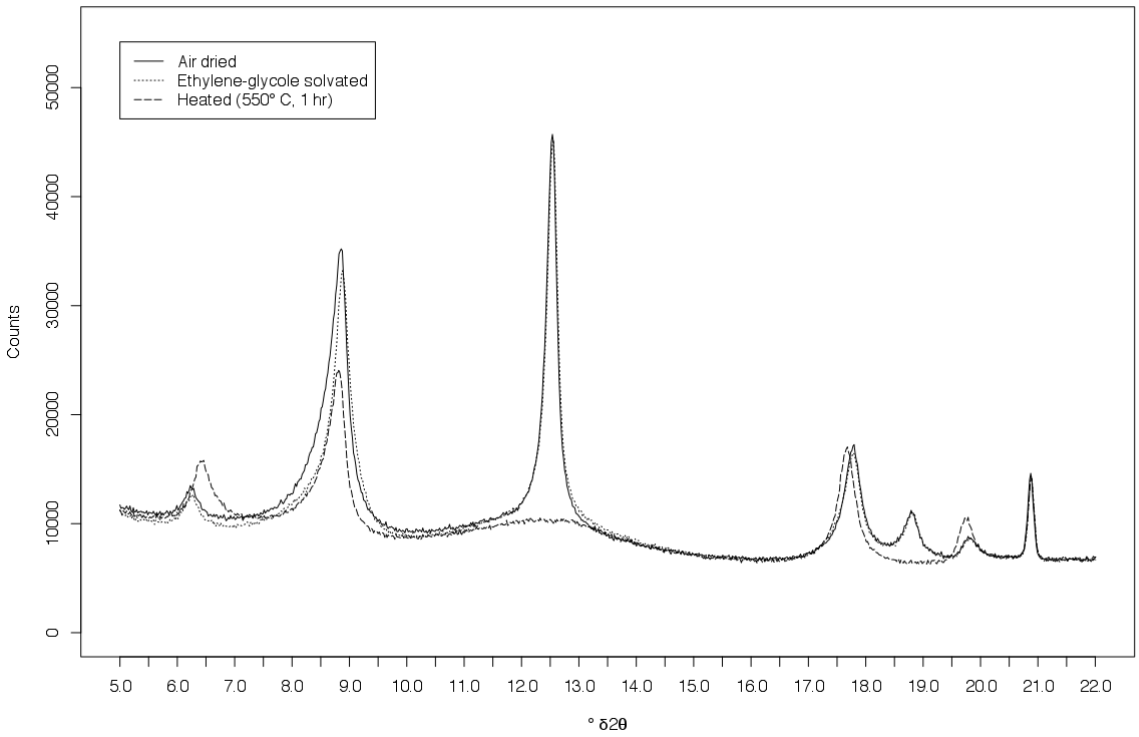

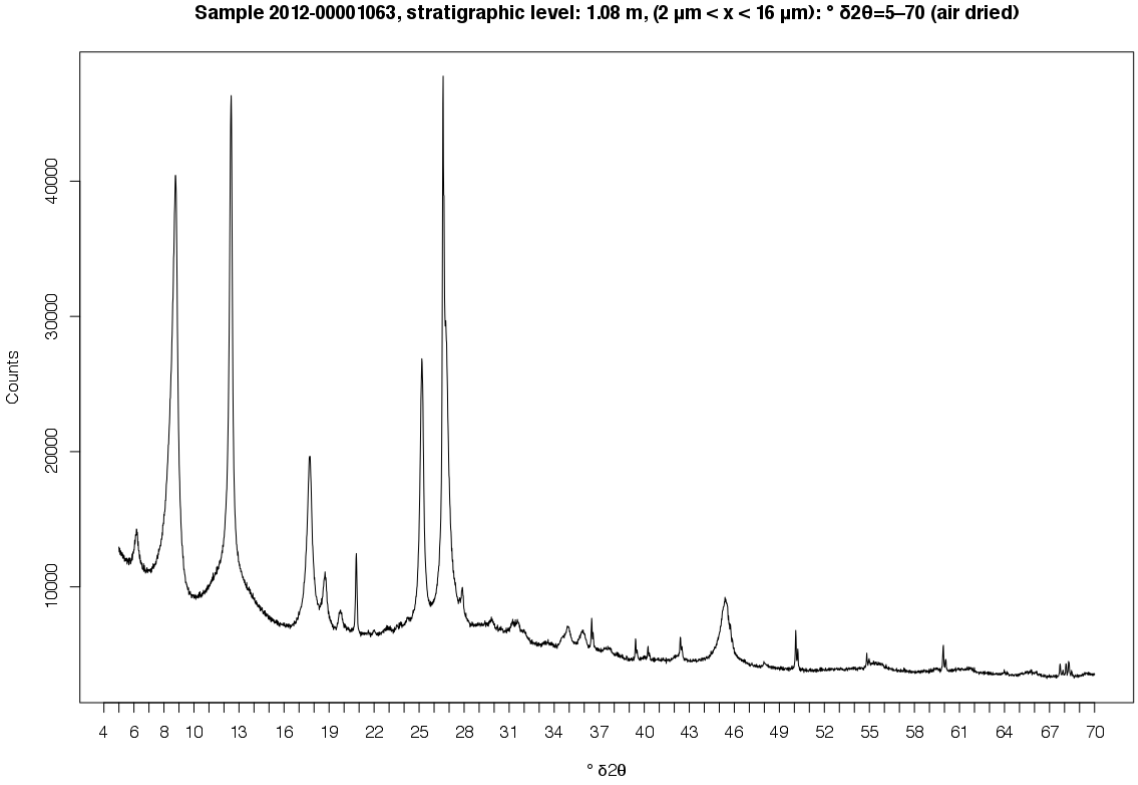
Sample 2012-00001063, stratigraphic level: 1.08 m, (2 µm < x < 16 µm): ° δ2θ=5–70 (air dried)
Counts
10000
20000
30000
40000
4 6 8 10 13 16 19 22 25 28 31 34 37 40 43 46 49 52 55 58 61 64 67 70
° δ2θ

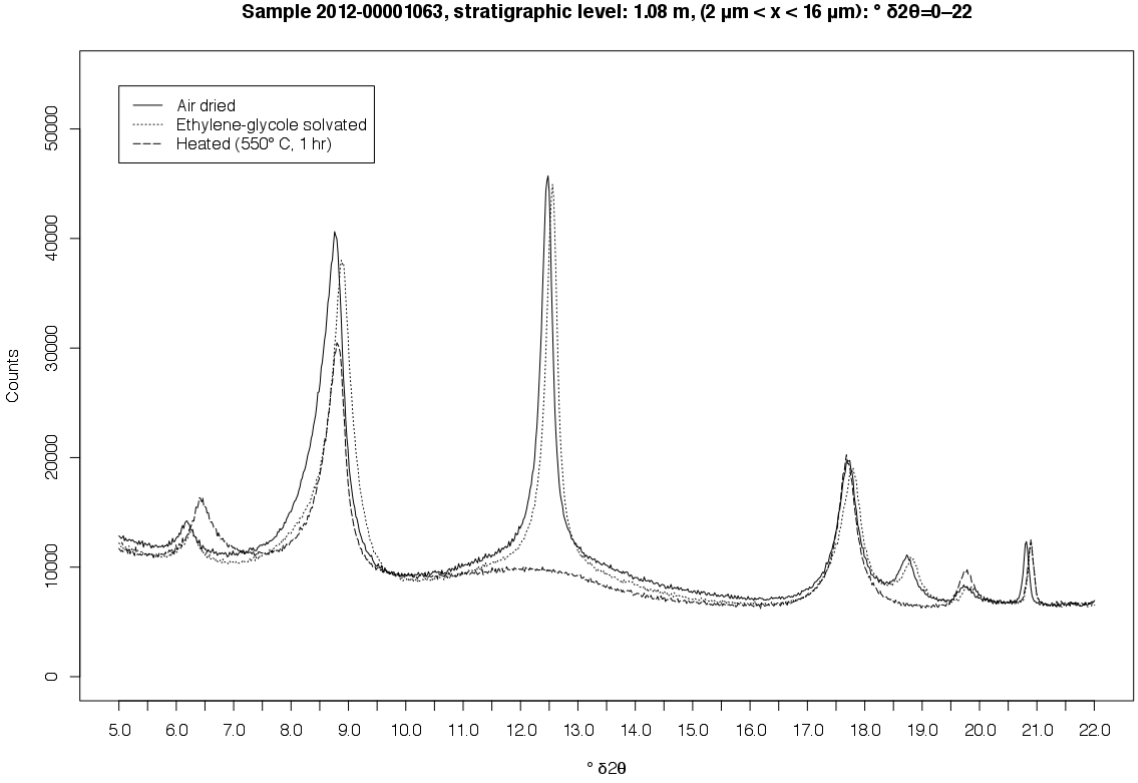
Sample 2012-00001063, stratigraphic level: 1.08 m, (2 µm < x < 16 µm): ° δ2θ=0–22
Air dried
Ethylene-glycole solvated
Heated (550° C, 1 hr)
Counts
0
10000
20000
30000
40000
50000
5.0 6.0 7.0 8.0 9.0 10.0 11.0 12.0 13.0 14.0 15.0 16.0 17.0 18.0 19.0 20.0 21.0 22.0
° δ2θ

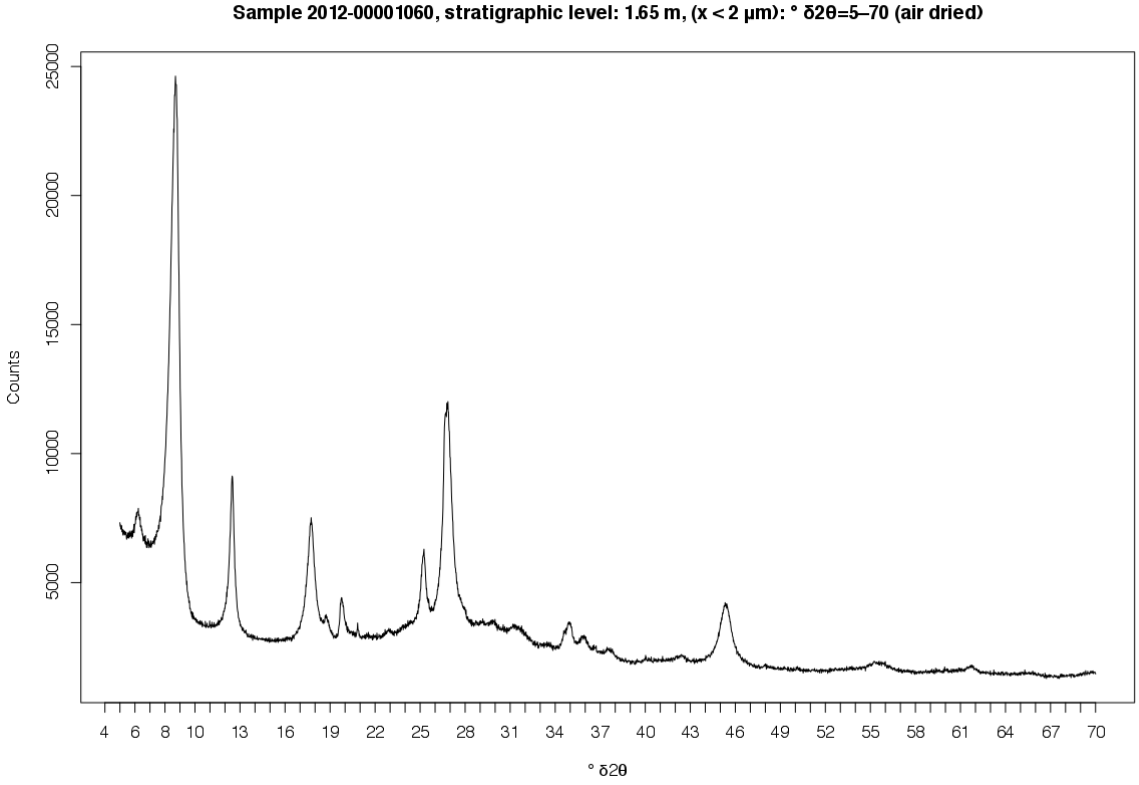
Sample 2012-00001060, stratigraphic level: 1.65 m, (x < 2 µm): ° δ2θ=5–70 (air dried)
Counts
5000
10000
15000
20000
25000
4 6 8 10 13 16 19 22 25 28 31 34 37 40 43 46 49 52 55 58 61 64 67 70
° δ2θ

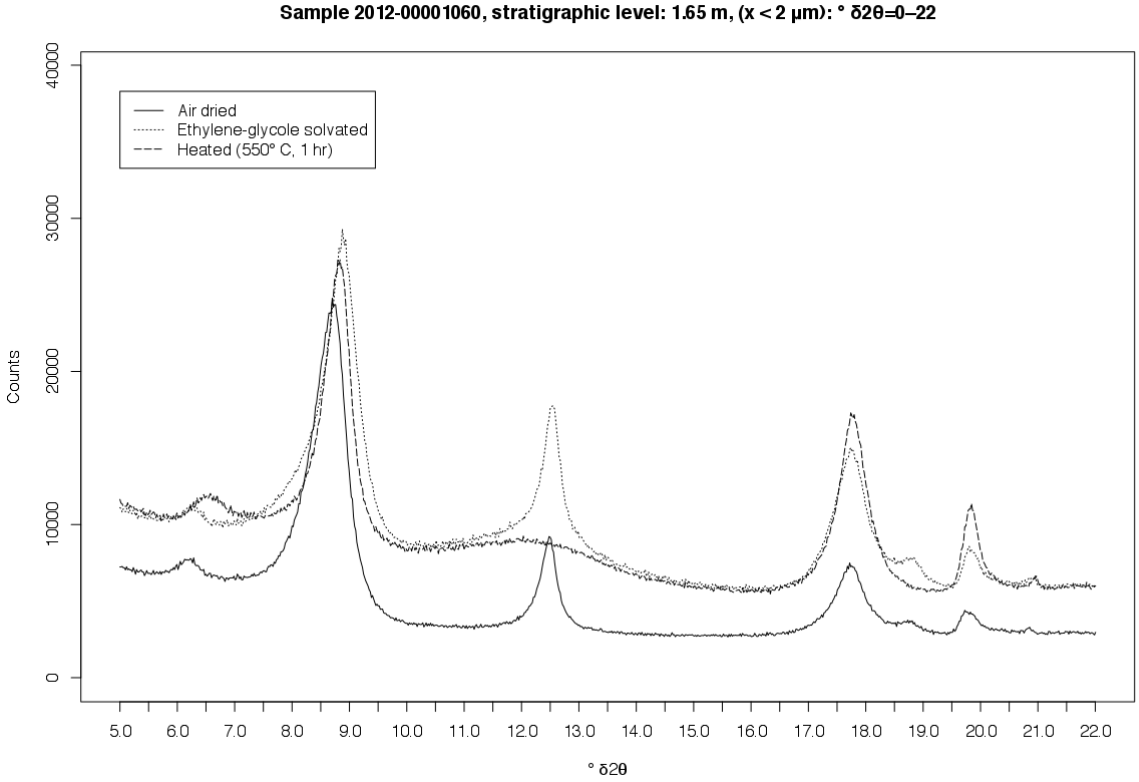
Sample 2012-00001060, stratigraphic level: 1.65 m, (x < 2 µm): ° δ2θ=0–22
Air dried
Ethylene-glycole solvated
Heated (550° C, 1 hr)
Counts
0
10000
20000
30000
40000
5.0 6.0 7.0 8.0 9.0 10.0 11.0 12.0 13.0 14.0 15.0 16.0 17.0 18.0 19.0 20.0 21.0 22.0
° δ2θ

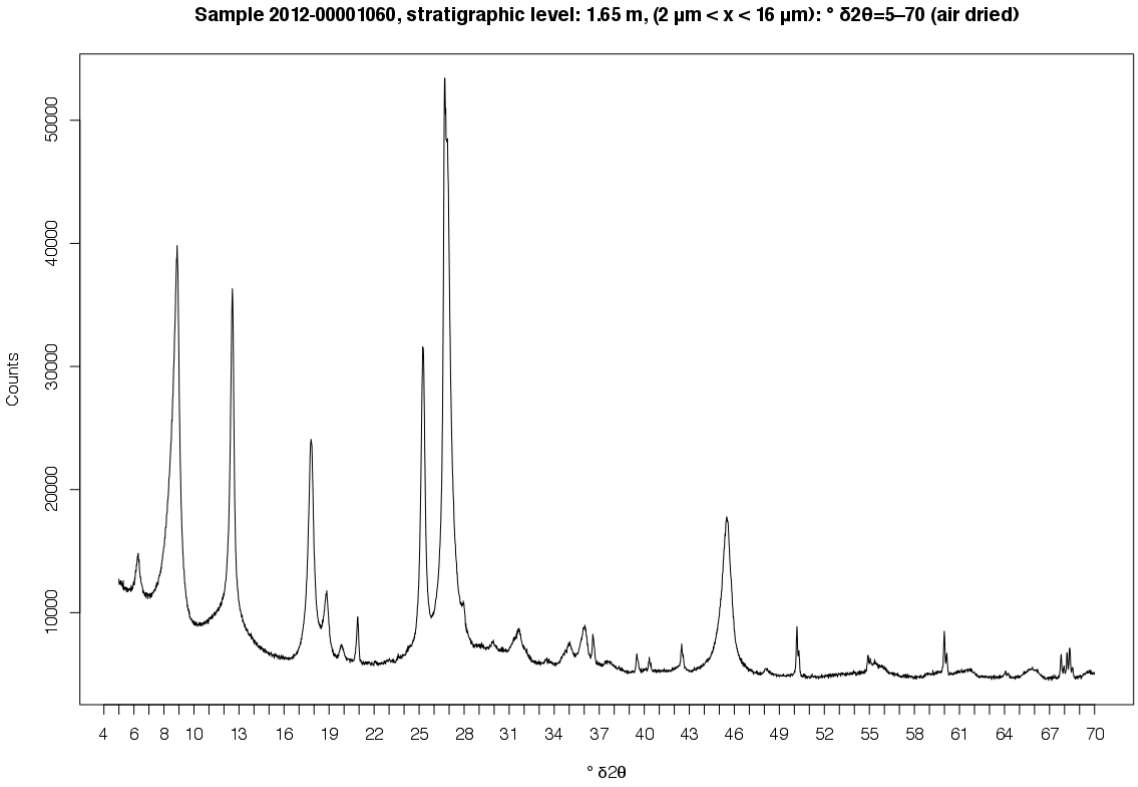
Sample 2012-00001060, stratigraphic level: 1.65 m, (2 µm < x < 16 µm): ° δ2θ=5–70 (air dried)
Counts
10000
20000
30000
40000
50000
4 6 8 10 13 16 19 22 25 28 31 34 37 40 43 46 49 52 55 58 61 64 67 70
° δ2θ

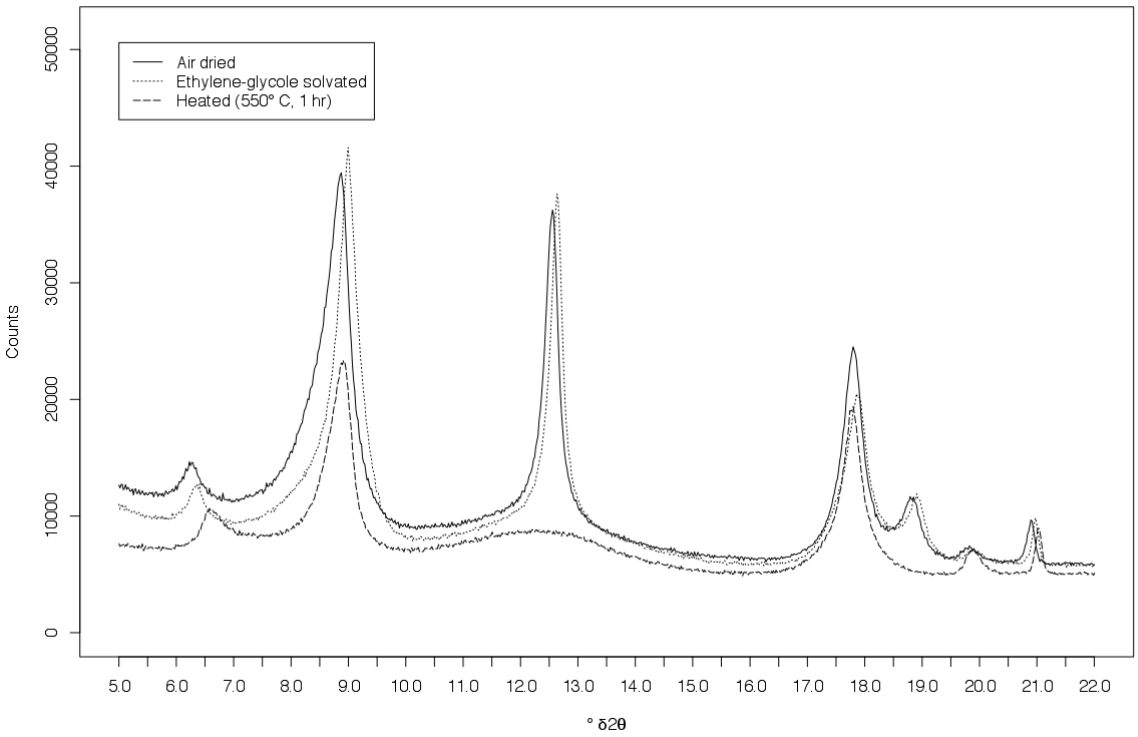
Sample 2012-00001060, stratigraphic level: 1.65 m, (2 µm < x < 16 µm): ° δ2θ=0–22
Air dried
Ethylene-glycole solvated
Heated (550° C, 1 hr)
Counts
0
10000
20000
30000
40000
50000
5.0 6.0 7.0 8.0 9.0 10.0 11.0 12.0 13.0 14.0 15.0 16.0 17.0 18.0 19.0 20.0 21.0 22.0
° δ2θ

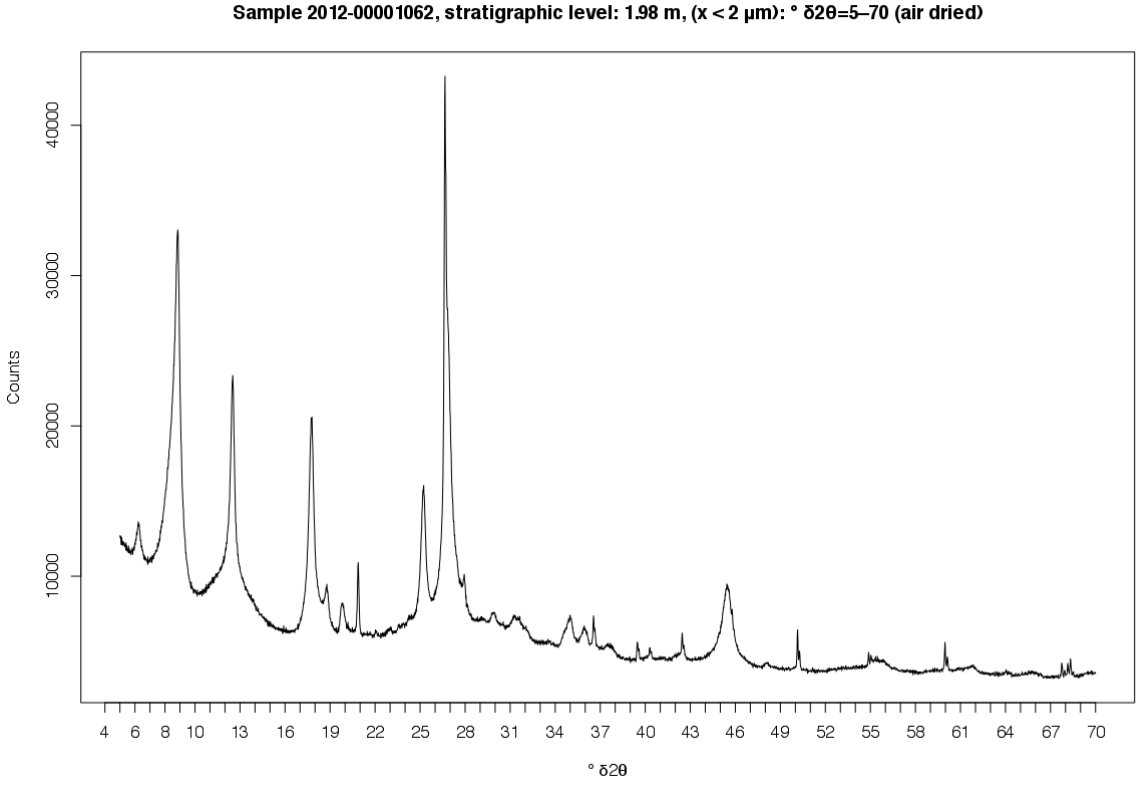
Sample 2012-00001062, stratigraphic level: 1.98 m, (x < 2 µm): ° δ2θ=5–70 (air dried)
Counts
10000
20000
30000
40000
4 6 8 10 13 16 19 22 25 28 31 34 37 40 43 46 49 52 55 58 61 64 67 70
° δ2θ

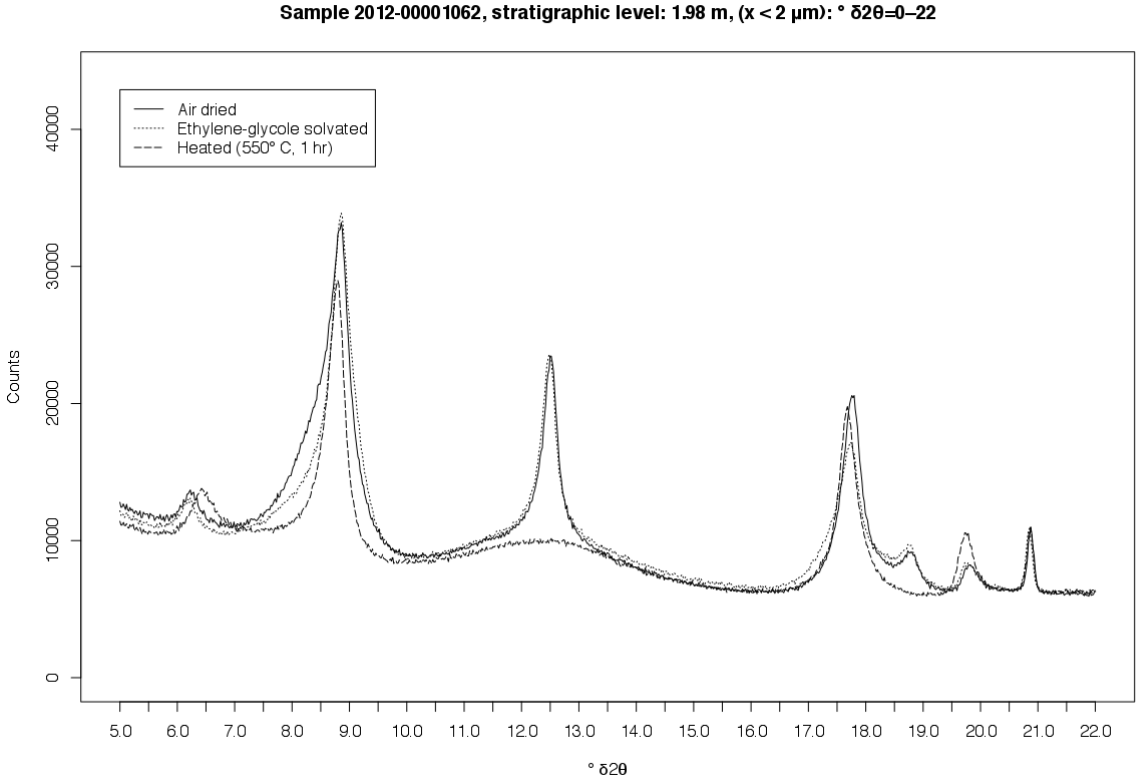
Sample 2012-00001062, stratigraphic level: 1.98 m, (x < 2 µm): ° δ2θ=0–22
Air dried
Ethylene-glycole solvated
Heated (550° C, 1 hr)
Counts
0
10000
20000
30000
40000
5.0 6.0 7.0 8.0 9.0 10.0 11.0 12.0 13.0 14.0 15.0 16.0 17.0 18.0 19.0 20.0 21.0 22.0
° δ2θ

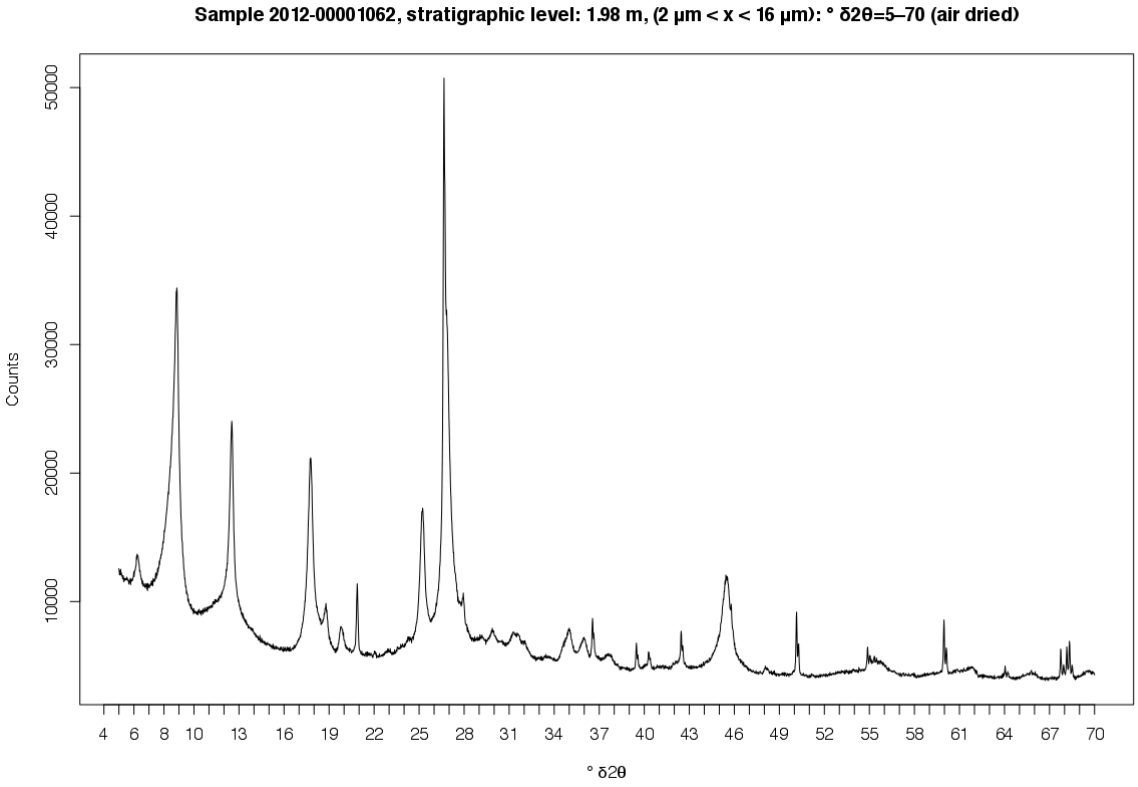
Sample 2012-00001062, stratigraphic level: 1.98 m, (2 µm < x < 16 µm): ° δ2θ=5–70 (air dried)
Counts
10000
20000
30000
40000
50000
4 6 8 10 13 16 19 22 25 28 31 34 37 40 43 46 49 52 55 58 61 64 67 70
° δ2θ

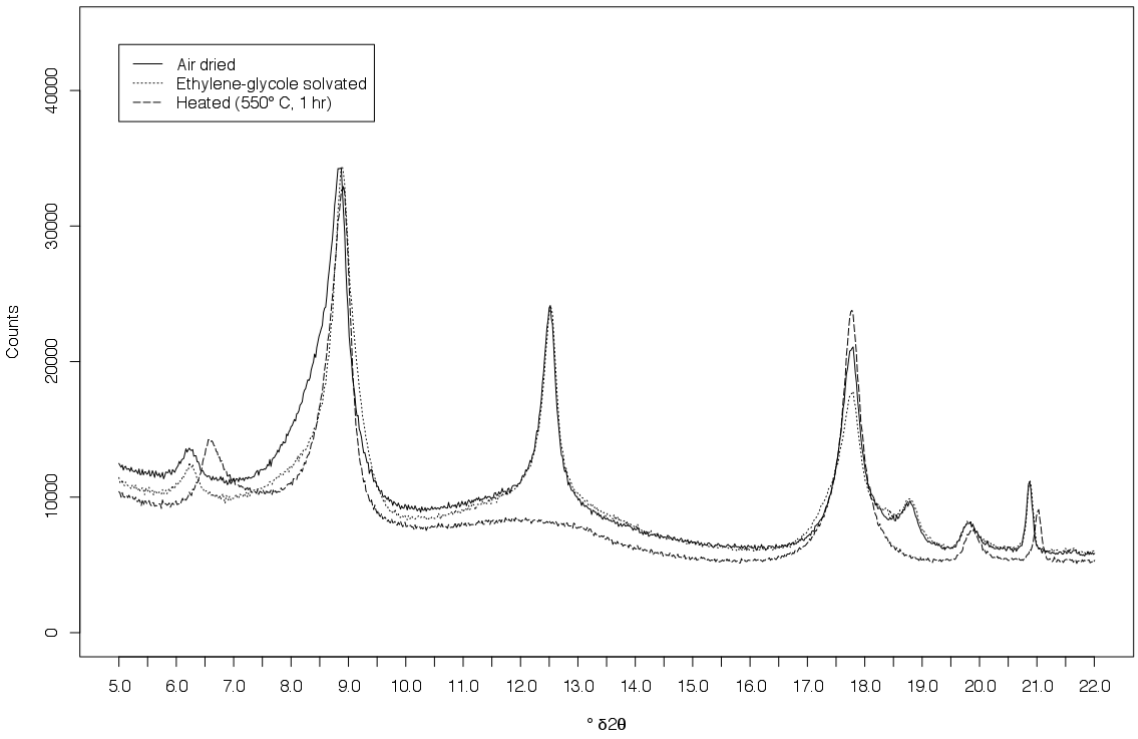
Sample 2012-00001062, stratigraphic level: 1.98 m, (2 µm < x < 16 µm): ° δ2θ=0–22
Air dried
Ethylene-glycole solvated
Heated (550° C, 1 hr)
Counts
0
10000
20000
30000
40000
5.0 6.0 7.0 8.0 9.0 10.0 11.0 12.0 13.0 14.0 15.0 16.0 17.0 18.0 19.0 20.0 21.0 22.0
° δ2θ

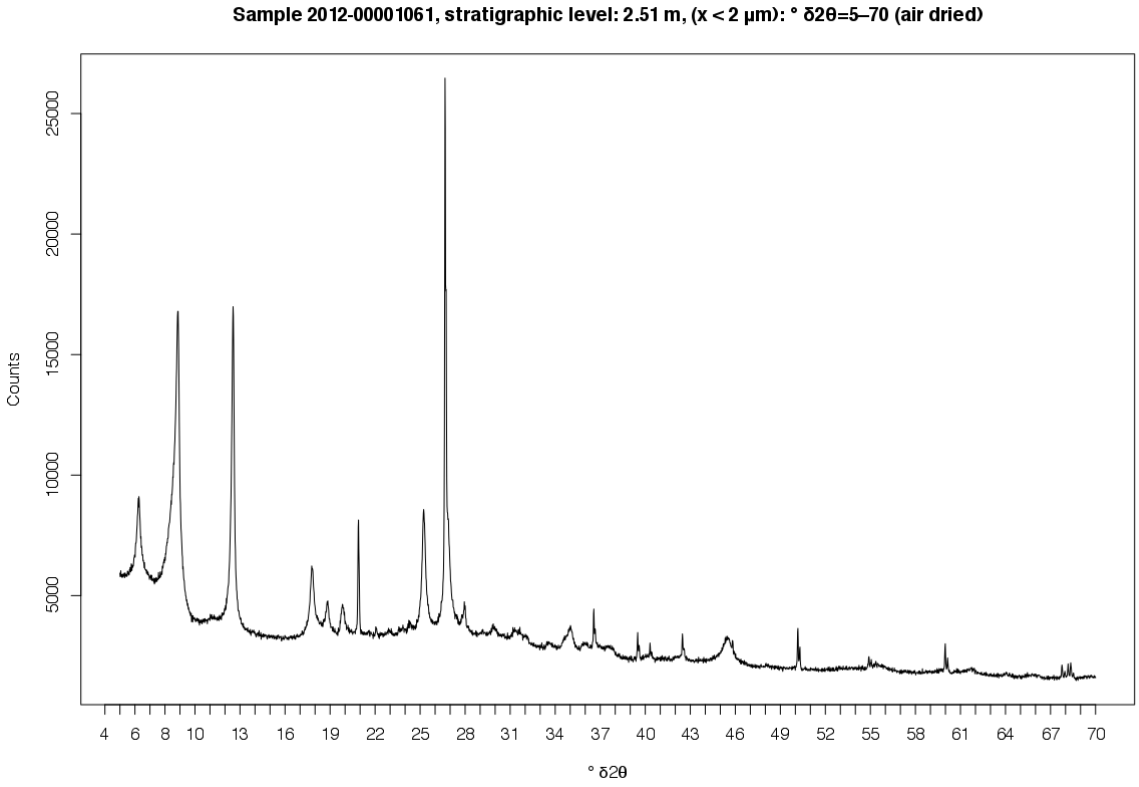
Sample 2012-00001061, stratigraphic level: 2.51 m, (x < 2 µm): ° δ2θ=5–70 (air dried)
Counts
5000
10000
15000
20000
25000
4 6 8 10 13 16 19 22 25 28 31 34 37 40 43 46 49 52 55 58 61 64 67 70
° δ2θ

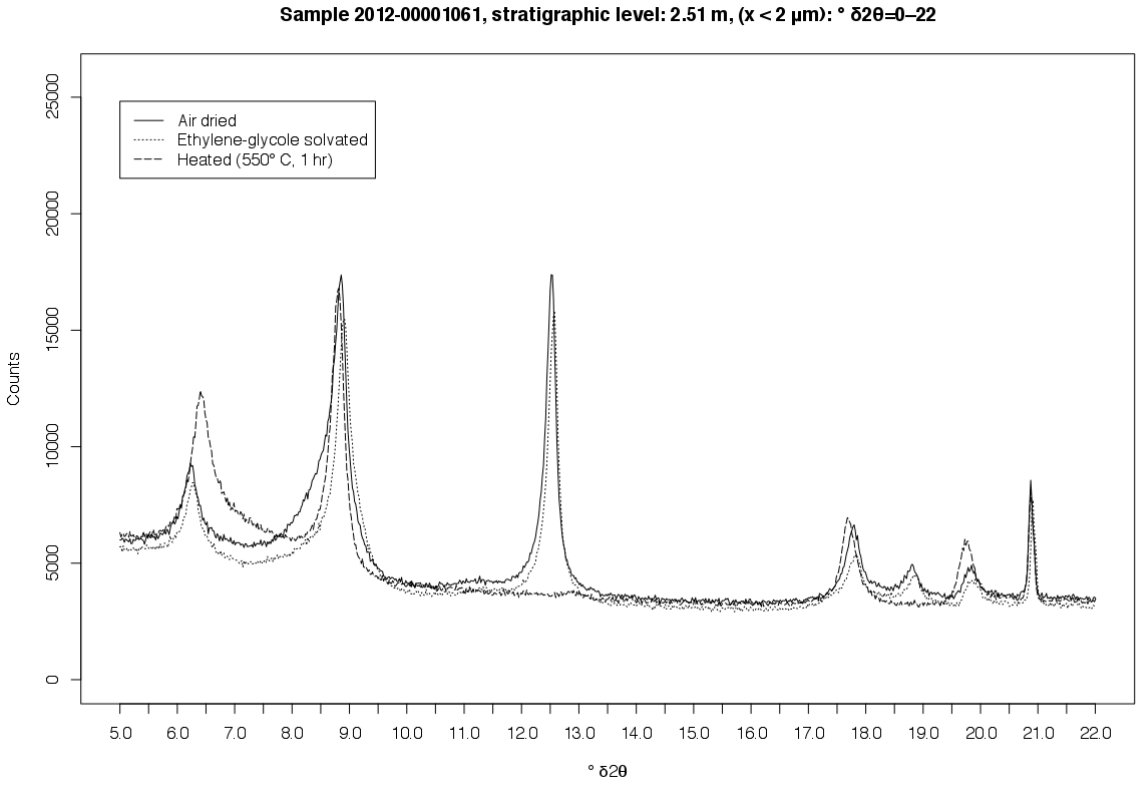
Sample 2012-00001061, stratigraphic level: 2.51 m, (x < 2 µm): ° δ2θ=0–22
Air dried
Ethylene-glycole solvated
Heated (550° C, 1 hr)
Counts
0
5000
10000
15000
20000
25000
5.0 6.0 7.0 8.0 9.0 10.0 11.0 12.0 13.0 14.0 15.0 16.0 17.0 18.0 19.0 20.0 21.0 22.0
° δ2θ

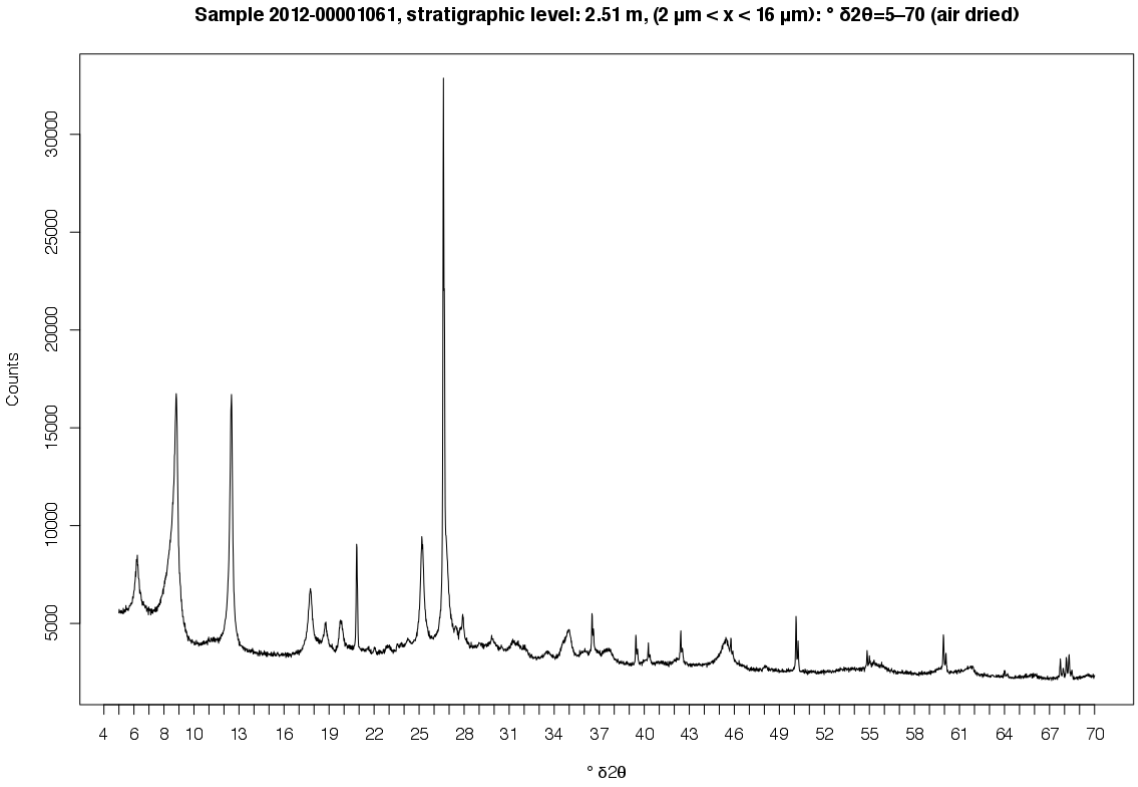
Sample 2012-00001061, stratigraphic level: 2.51 m, (2 µm < x < 16 µm): ° δ2θ=5–70 (air dried)
Counts
5000
10000
15000
20000
25000
30000
4 6 8 10 13 16 19 22 25 28 31 34 37 40 43 46 49 52 55 58 61 64 67 70
° δ2θ

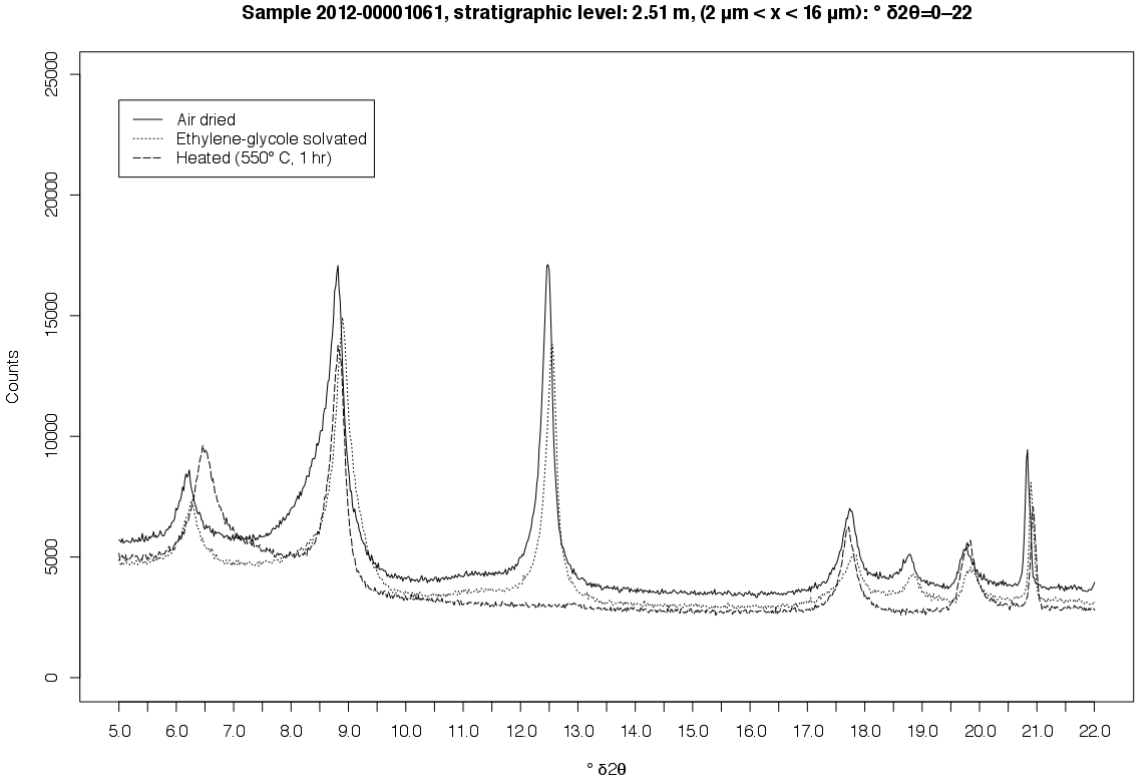
Sample 2012-00001061, stratigraphic level: 2.51 m, (2 µm < x < 16 µm): ° δ2θ=0–22
Air dried
Ethylene-glycole solvated
Heated (550° C, 1 hr)
Counts
0
5000
10000
15000
20000
25000
5.0 6.0 7.0 8.0 9.0 10.0 11.0 12.0 13.0 14.0 15.0 16.0 17.0 18.0 19.0 20.0 21.0 22.0
° δ2θ

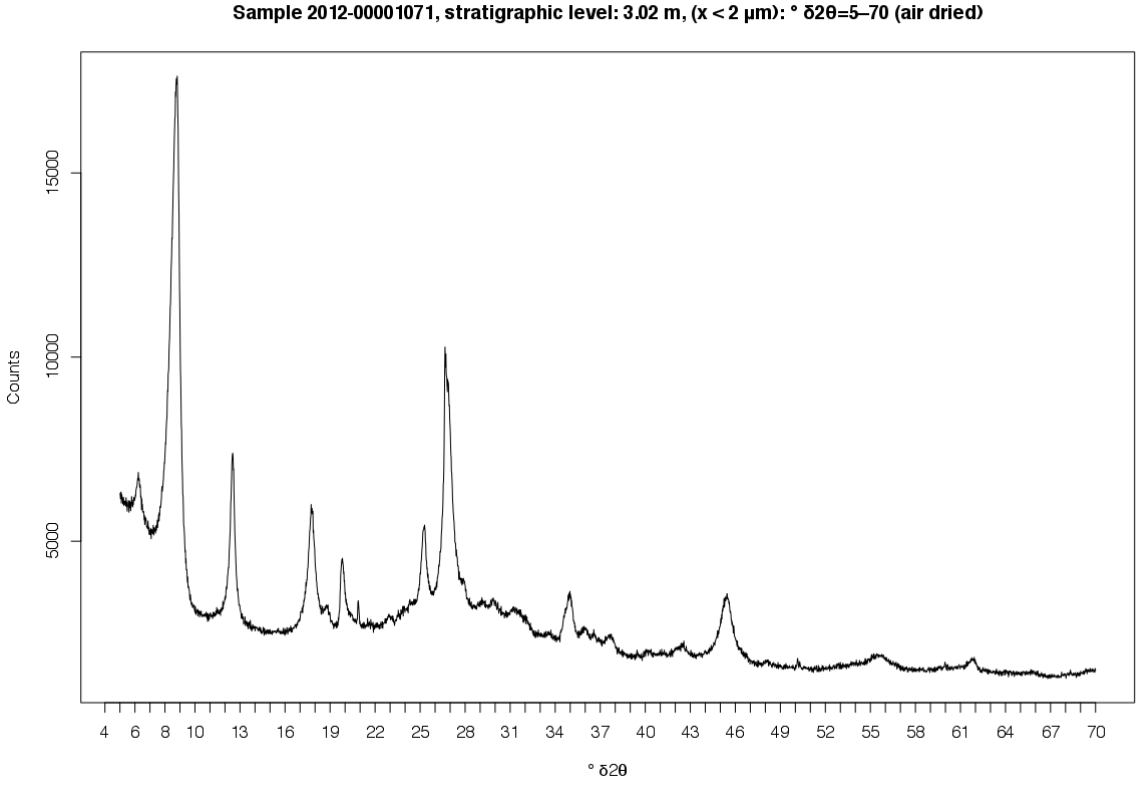
Sample 2012-00001071, stratigraphic level: 3.02 m, (x < 2 µm): ° δ2θ=5–70 (air dried)
Counts
5000
10000
15000
4 6 8 10 13 16 19 22 25 28 31 34 37 40 43 46 49 52 55 58 61 64 67 70
° δ2θ

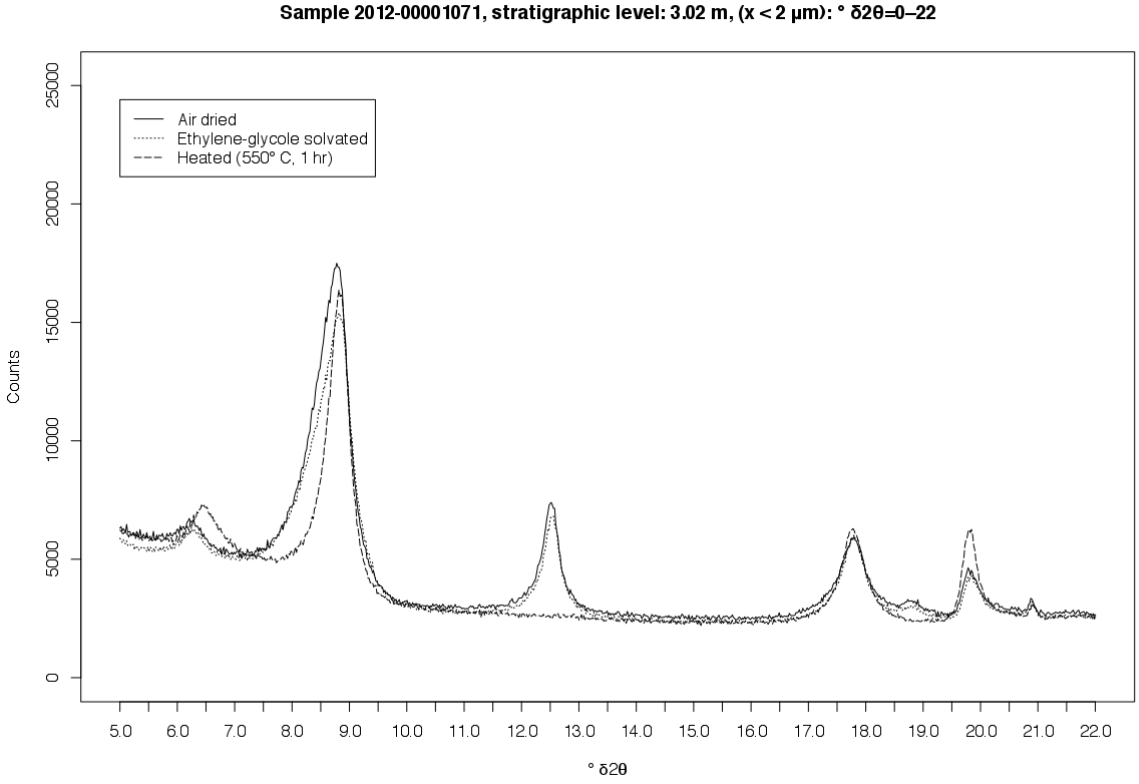
Sample 2012-00001071, stratigraphic level: 3.02 m, (x < 2 µm): ° δ2θ=0–22
Air dried
Ethylene-glycole solvated
Heated (550° C, 1 hr)
Counts
0
5000
10000
15000
20000
25000
5.0 6.0 7.0 8.0 9.0 10.0 11.0 12.0 13.0 14.0 15.0 16.0 17.0 18.0 19.0 20.0 21.0 22.0
° δ2θ

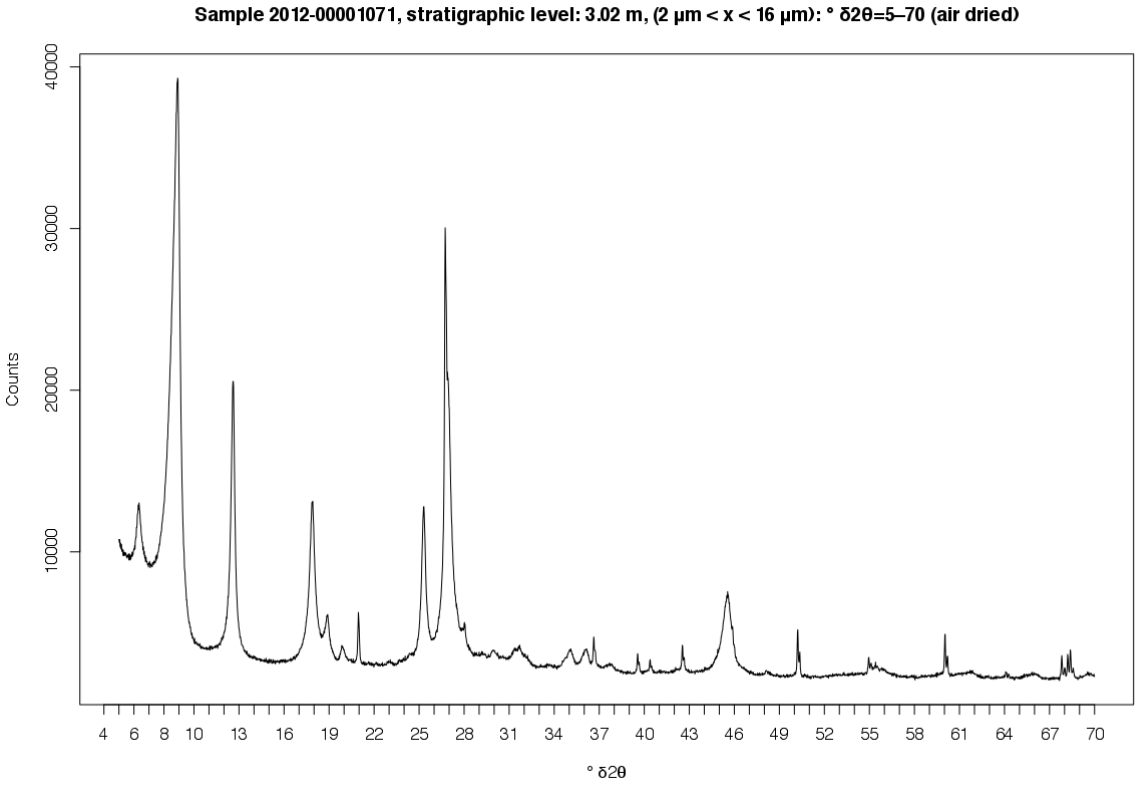
Sample 2012-00001071, stratigraphic level: 3.02 m, (2 µm < x < 16 µm): ° δ2θ=5–70 (air dried)
Counts
10000
20000
30000
40000
4 6 8 10 13 16 19 22 25 28 31 34 37 40 43 46 49 52 55 58 61 64 67 70
° δ2θ

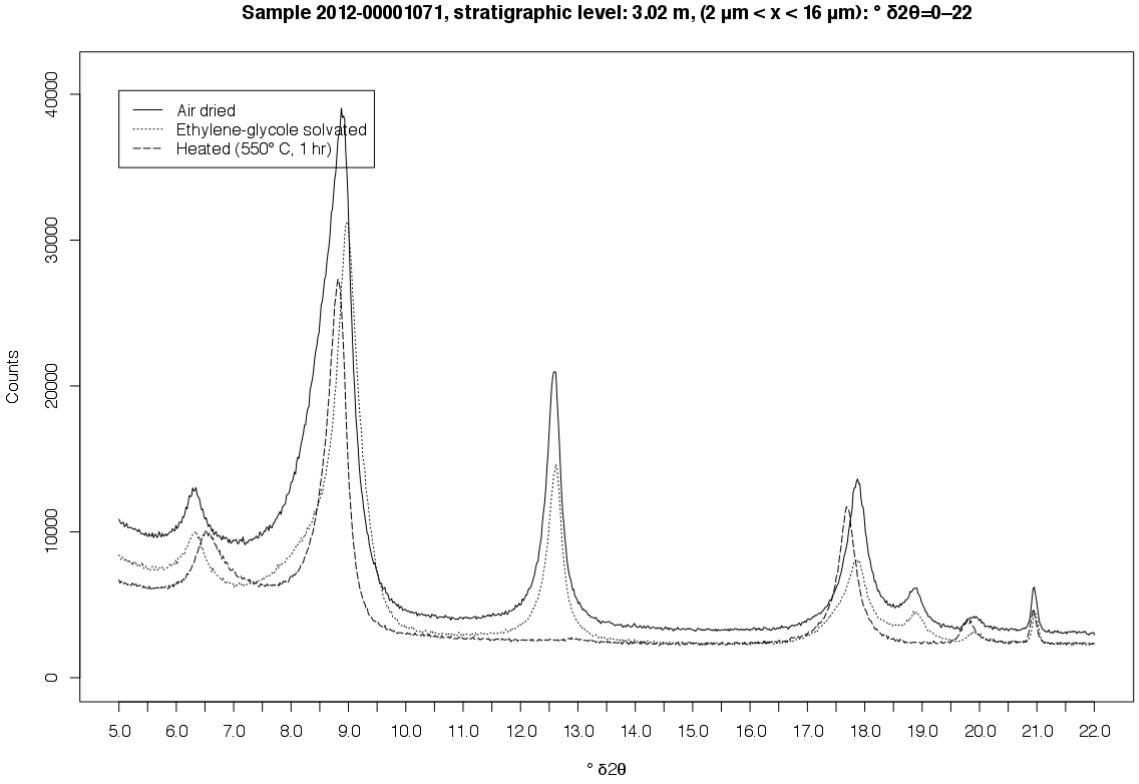
Sample 2012-00001071, stratigraphic level: 3.02 m, (2 µm < x < 16 µm): ° δ2θ=0–22
Air dried
Ethylene-glycole solvated
Heated (550° C, 1 hr)
Counts
0
10000
20000
30000
40000
5.0 6.0 7.0 8.0 9.0 10.0 11.0 12.0 13.0 14.0 15.0 16.0 17.0 18.0 19.0 20.0 21.0 22.0
° δ2θ

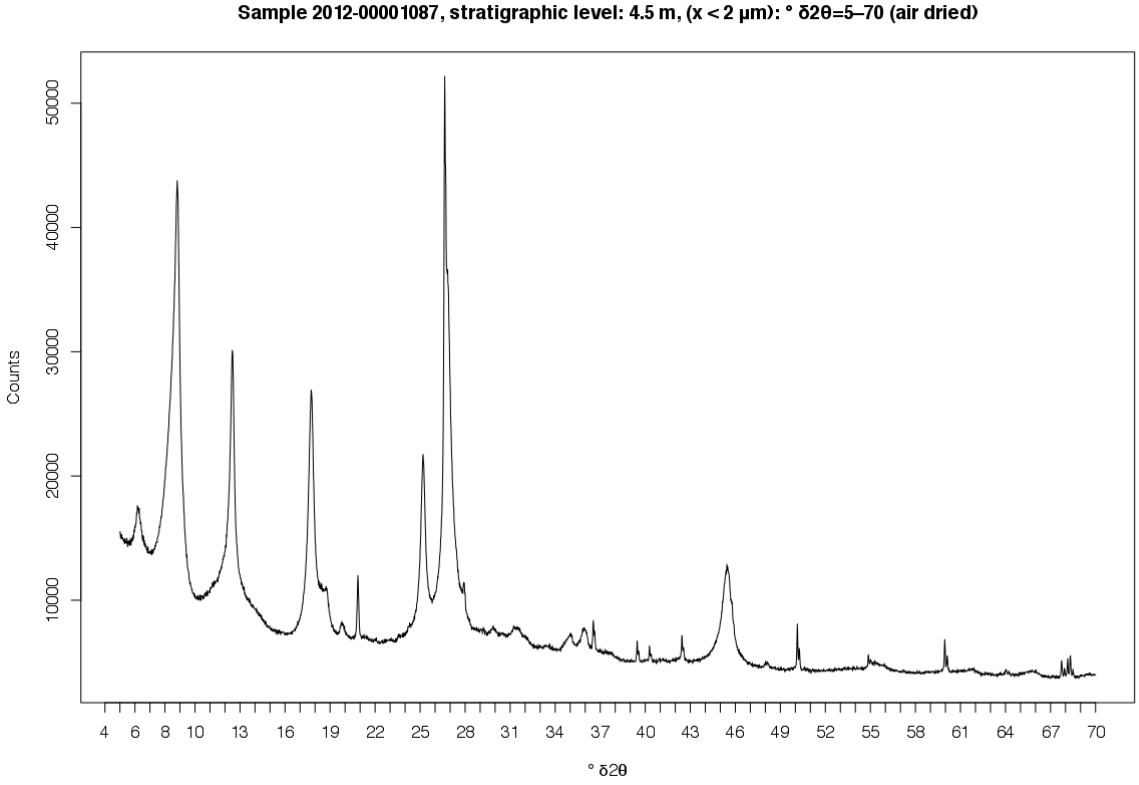
Sample 2012-00001087, stratigraphic level: 4.5 m, (x < 2 µm): ° δ2θ=5–70 (air dried)
Counts
10000
20000
30000
40000
50000
4 6 8 10 13 16 19 22 25 28 31 34 37 40 43 46 49 52 55 58 61 64 67 70
° δ2θ

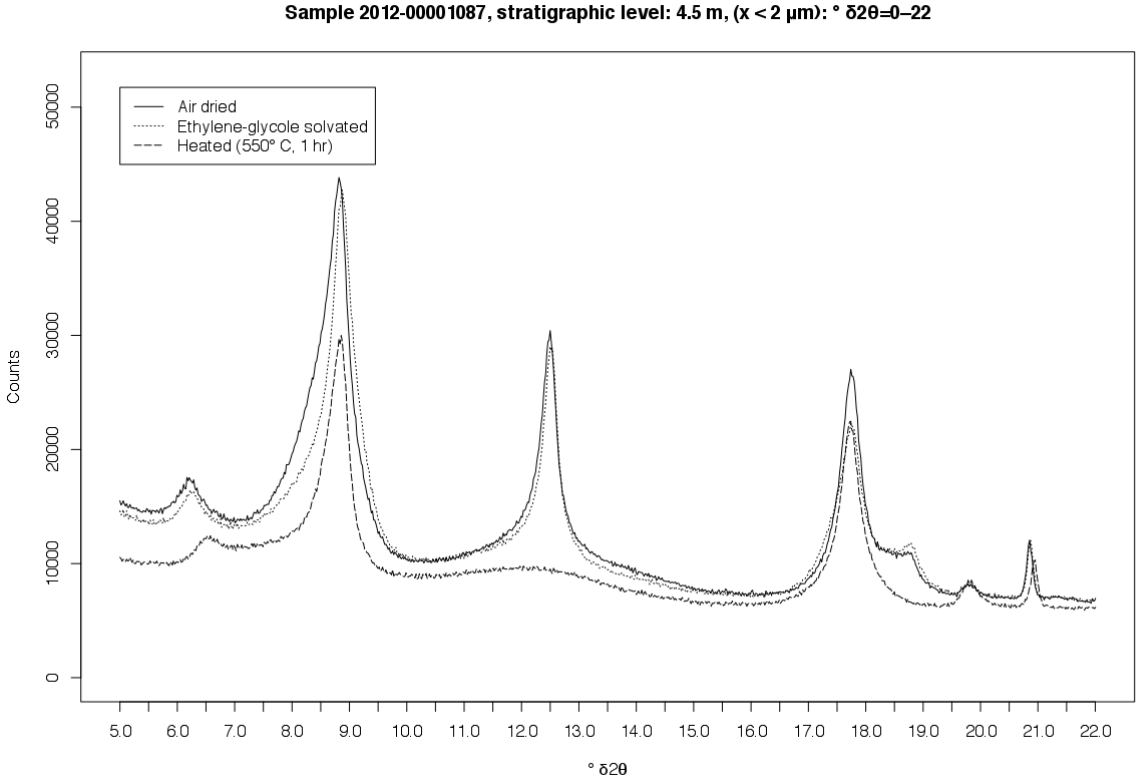
Sample 2012-00001087, stratigraphic level: 4.5 m, (x < 2 µm): ° δ2θ=0–22
Air dried
Ethylene-glycole solvated
Heated (550° C, 1 hr)
Counts
0
10000
20000
30000
40000
50000
5.0 6.0 7.0 8.0 9.0 10.0 11.0 12.0 13.0 14.0 15.0 16.0 17.0 18.0 19.0 20.0 21.0 22.0
° δ2θ

Sample 2012-00001087, stratigraphic level: 4.5 m, (2 µm < x < 16 µm): ° δ2θ=5–70 (air dried)

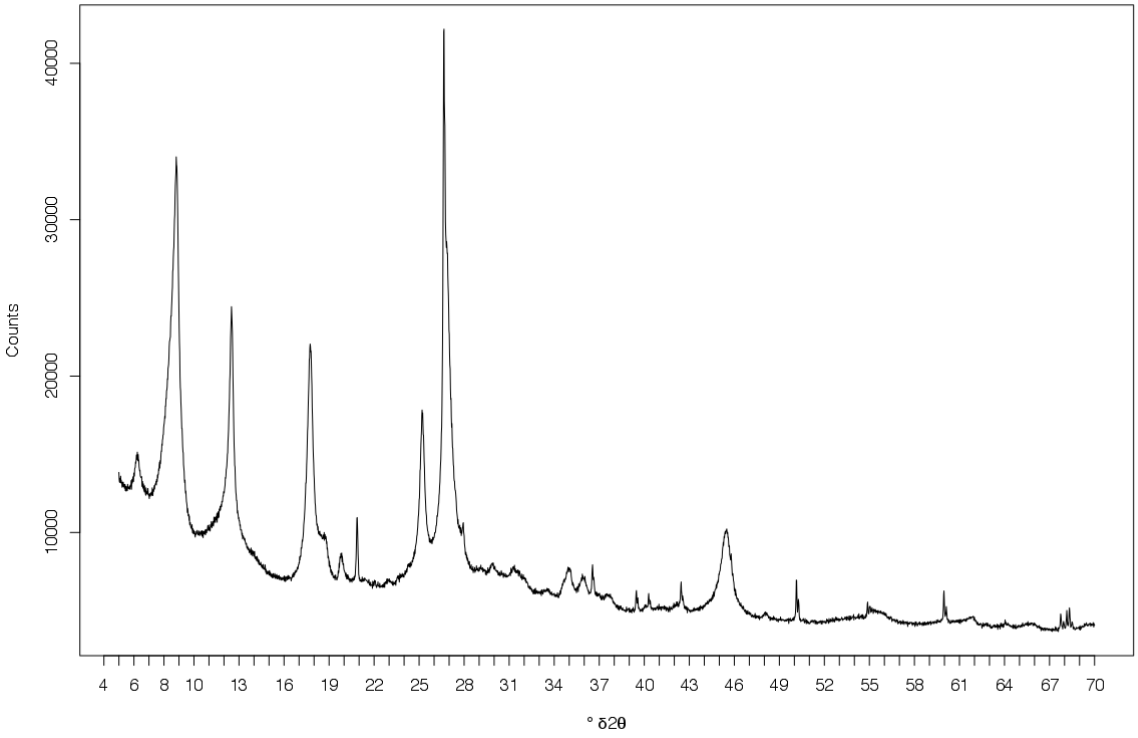

Sample 2012-00001087, stratigraphic level: 4.5 m, (2 µm < x < 16 µm): ° δ2θ=0–22

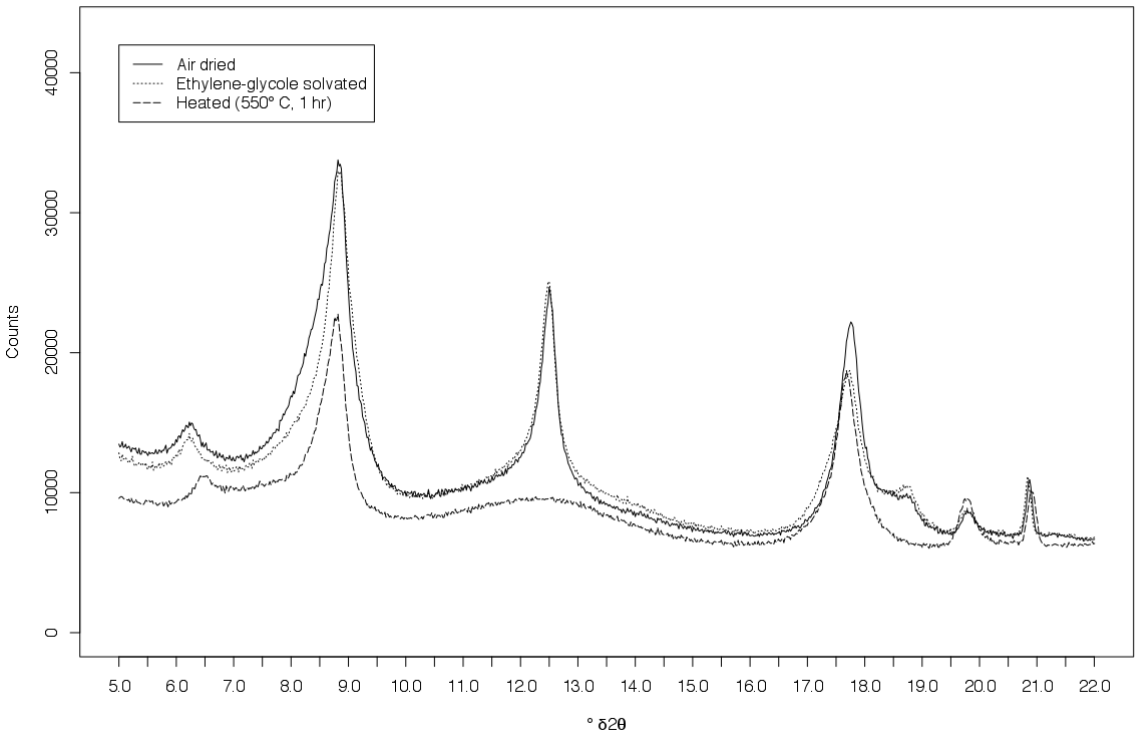

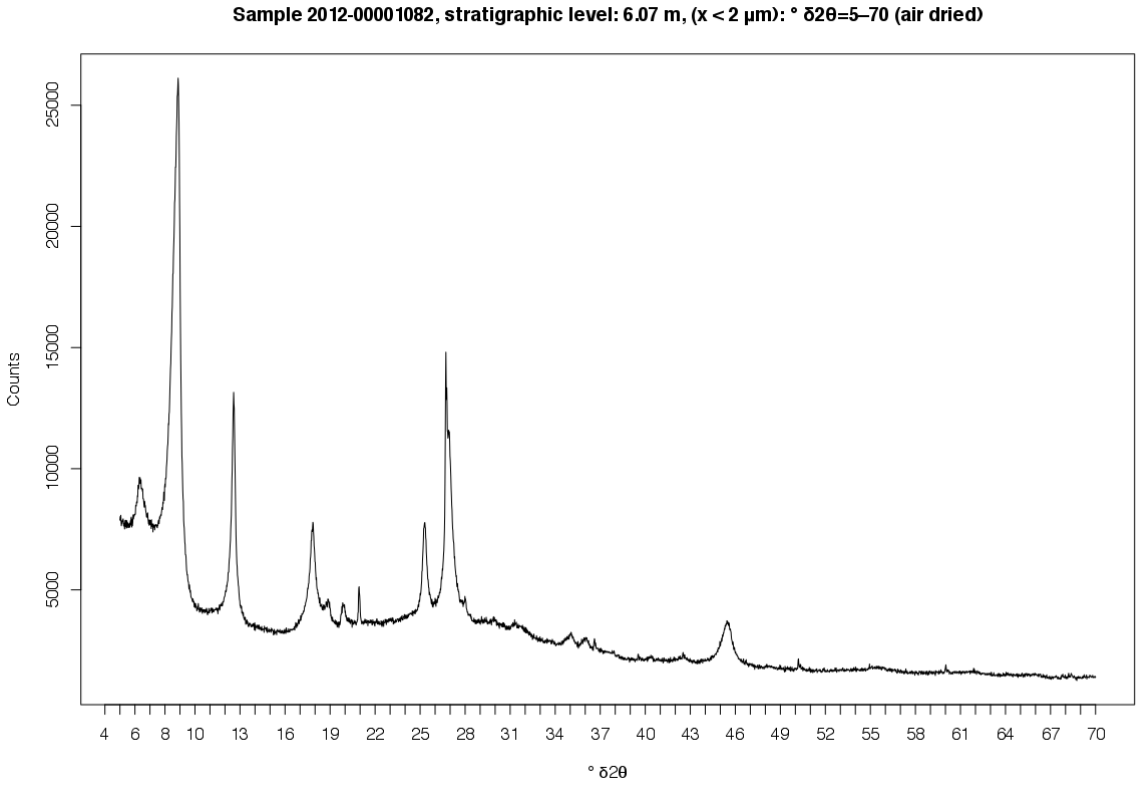
Sample 2012-00001082, stratigraphic level: 6.07 m, (x < 2 µm): ° δ2θ=5–70 (air dried)
Counts
5000
10000
15000
20000
25000
4 6 8 10 13 16 19 22 25 28 31 34 37 40 43 46 49 52 55 58 61 64 67 70
° δ2θ

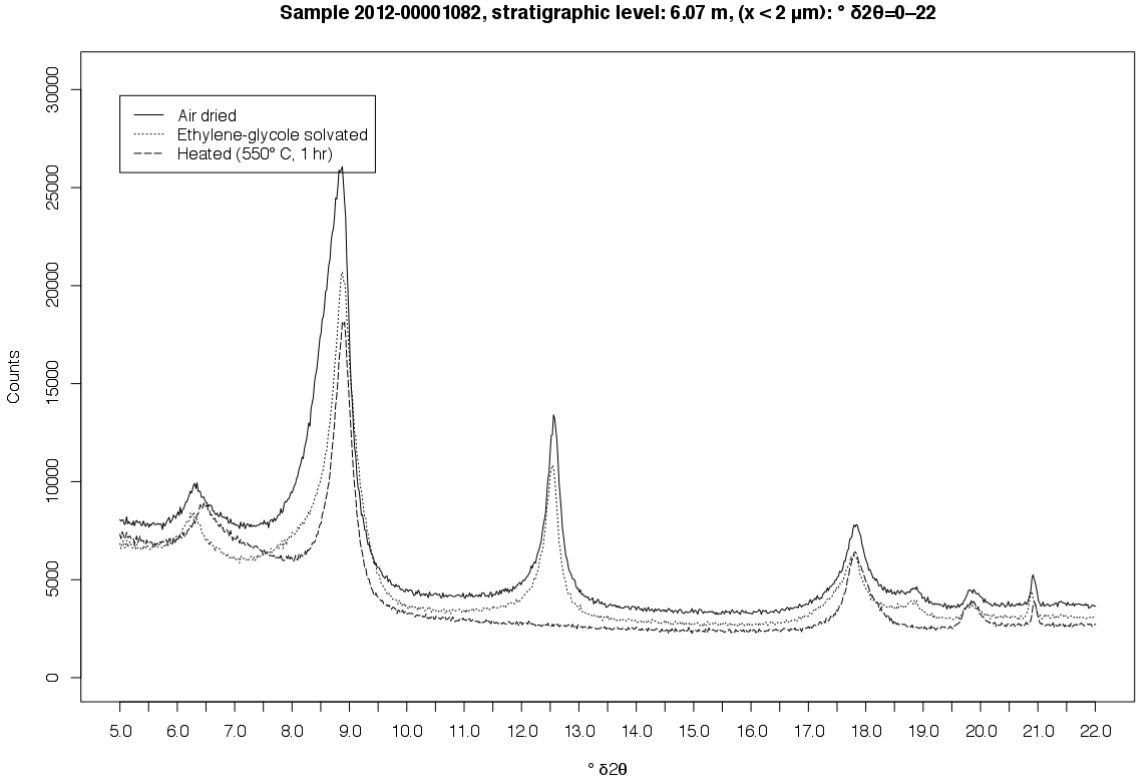
Sample 2012-00001082, stratigraphic level: 6.07 m, (x < 2 µm): ° δ2θ=0–22
Air dried
Ethylene-glycole solvated
Heated (550° C, 1 hr)
Counts
0
5000
10000
15000
20000
25000
30000
5.0 6.0 7.0 8.0 9.0 10.0 11.0 12.0 13.0 14.0 15.0 16.0 17.0 18.0 19.0 20.0 21.0 22.0
° δ2θ

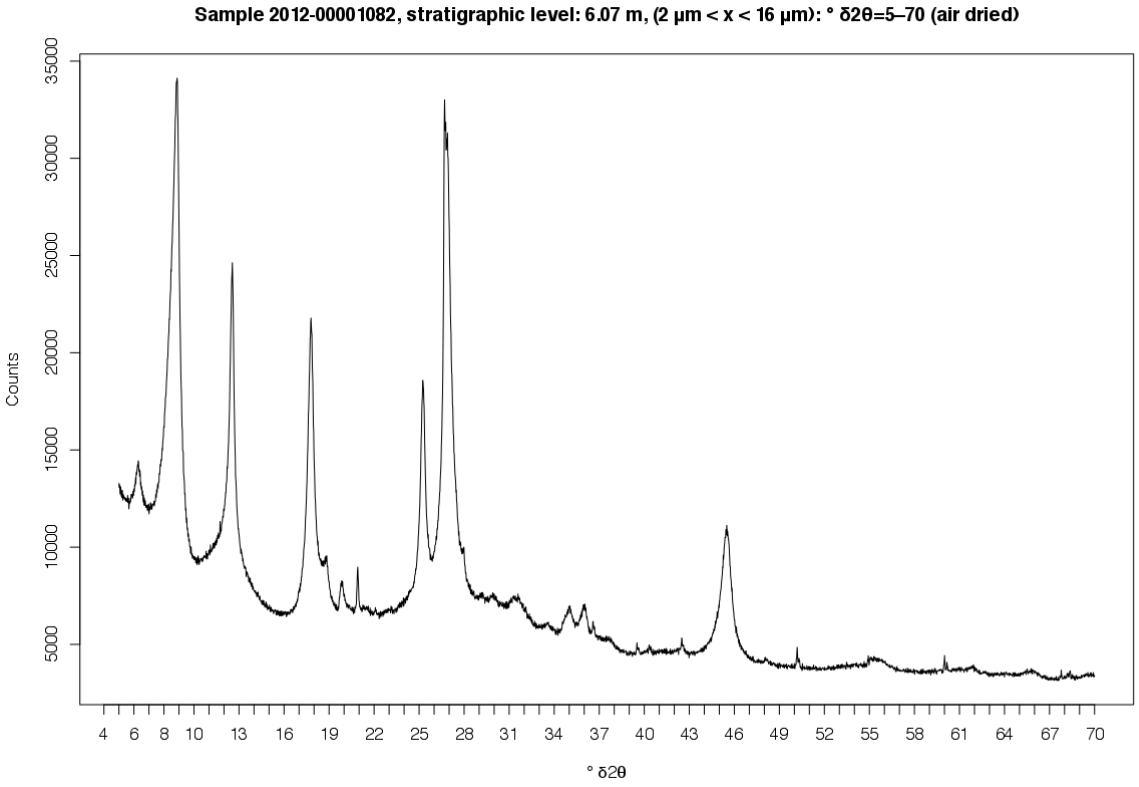
Sample 2012-00001082, stratigraphic level: 6.07 m, (2 µm < x < 16 µm): ° δ2θ=5–70 (air dried)
Counts
5000
10000
15000
20000
25000
30000
35000
4 6 8 10 13 16 19 22 25 28 31 34 37 40 43 46 49 52 55 58 61 64 67 70
° δ2θ

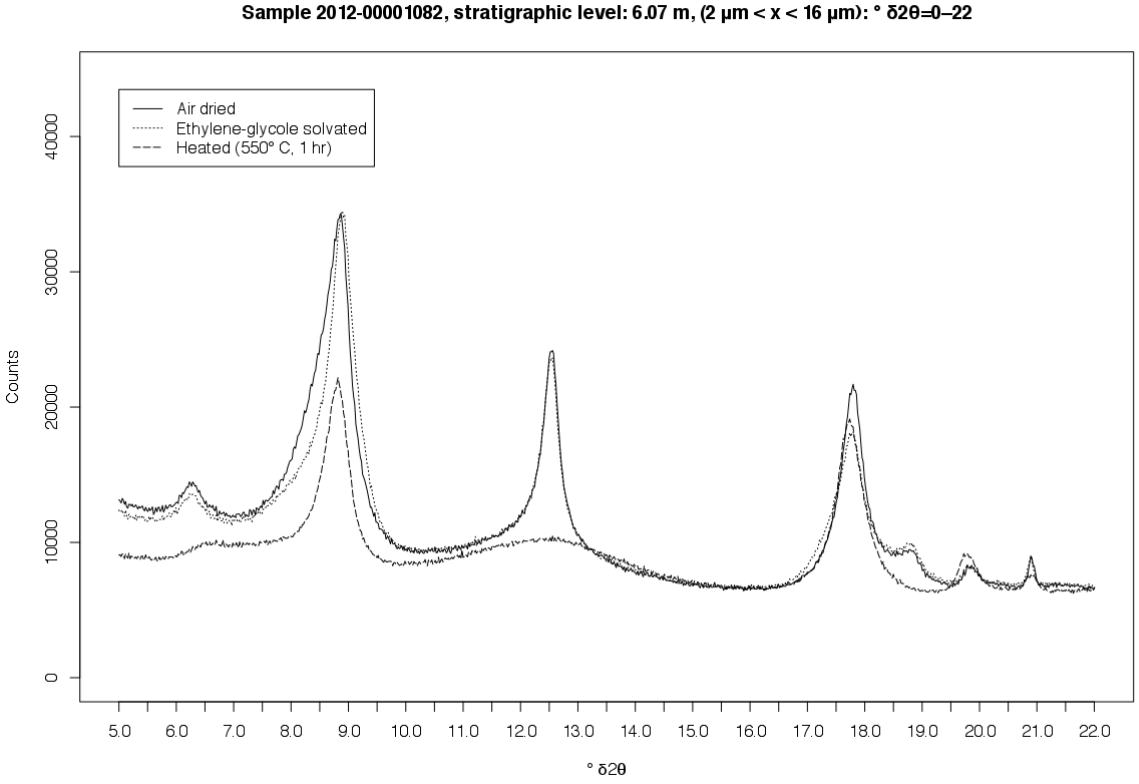
Sample 2012-00001082, stratigraphic level: 6.07 m, (2 µm < x < 16 µm): ° δ2θ=0–22
Air dried
Ethylene-glycole solvated
Heated (550° C, 1 hr)
Counts
0
10000
20000
30000
40000
5.0 6.0 7.0 8.0 9.0 10.0 11.0 12.0 13.0 14.0 15.0 16.0 17.0 18.0 19.0 20.0 21.0 22.0
° δ2θ

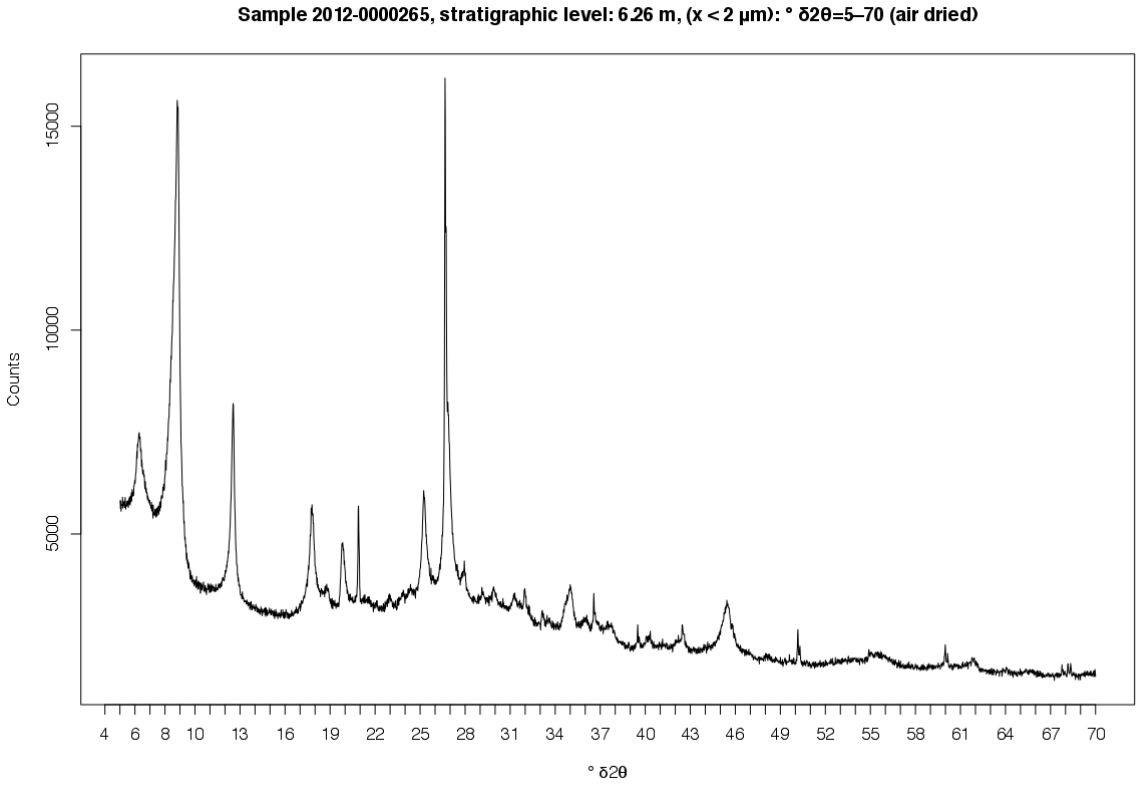
Sample 2012-0000265, stratigraphic level: 6.26 m, (x < 2 µm): ° δ2θ=5–70 (air dried)
Counts
5000
10000
15000
4 6 8 10 13 16 19 22 25 28 31 34 37 40 43 46 49 52 55 58 61 64 67 70
° δ2θ

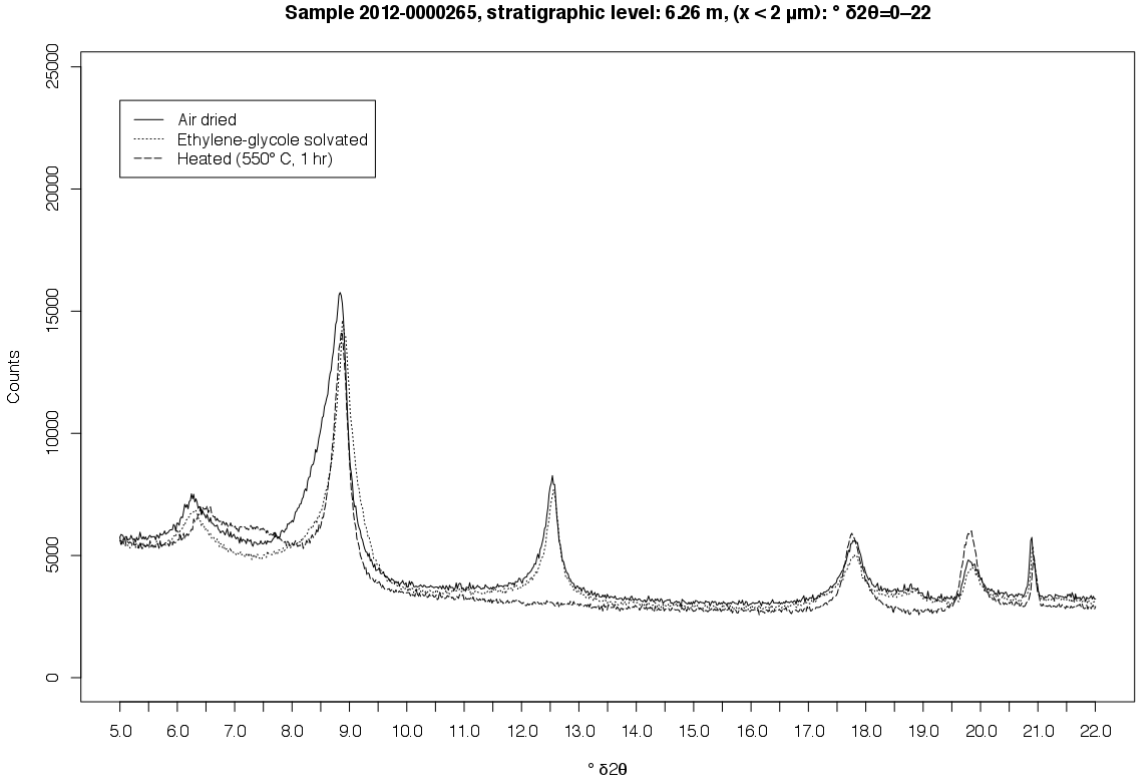
Sample 2012-0000265, stratigraphic level: 6.26 m, (x < 2 µm): ° δ2θ=0–22
Air dried
Ethylene-glycole solvated
Heated (550° C, 1 hr)
Counts
0
5000
10000
15000
20000
25000
5.0 6.0 7.0 8.0 9.0 10.0 11.0 12.0 13.0 14.0 15.0 16.0 17.0 18.0 19.0 20.0 21.0 22.0
° δ2θ

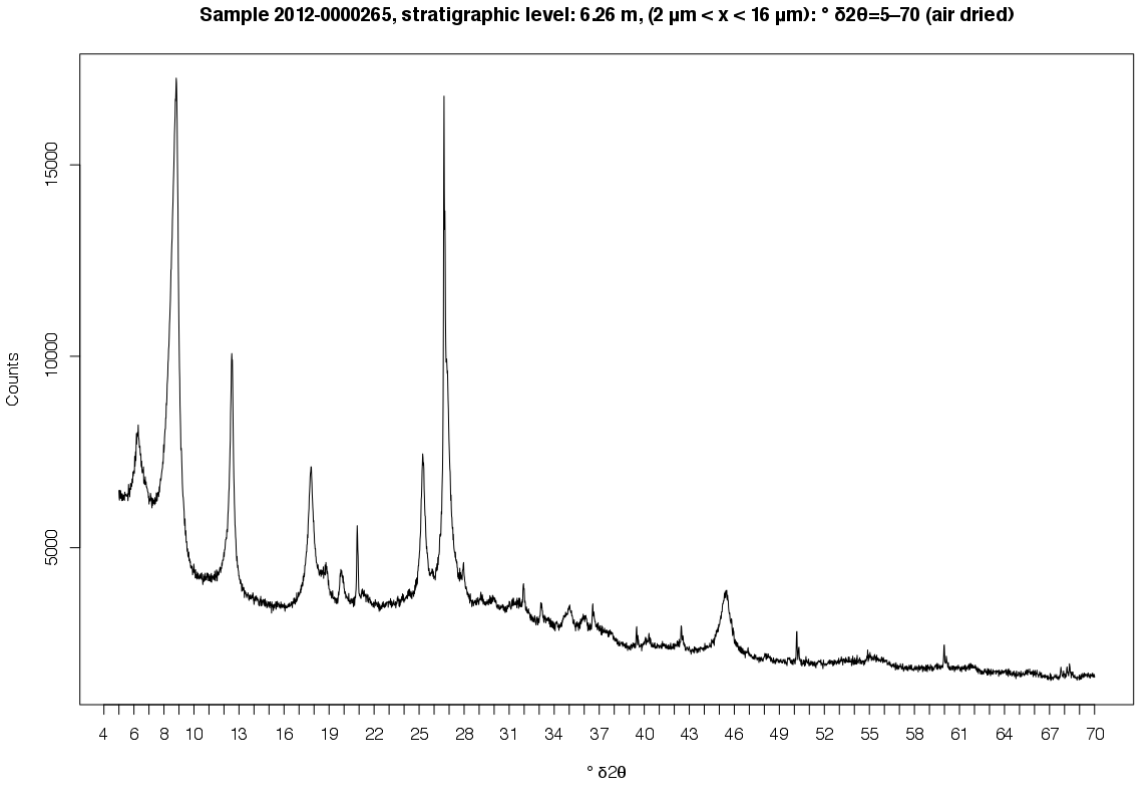
Sample 2012-0000265, stratigraphic level: 6.26 m, (2 µm < x < 16 µm): ° δ2θ=5–70 (air dried)
Counts
5000
10000
15000
4 6 8 10 13 16 19 22 25 28 31 34 37 40 43 46 49 52 55 58 61 64 67 70
° δ2θ

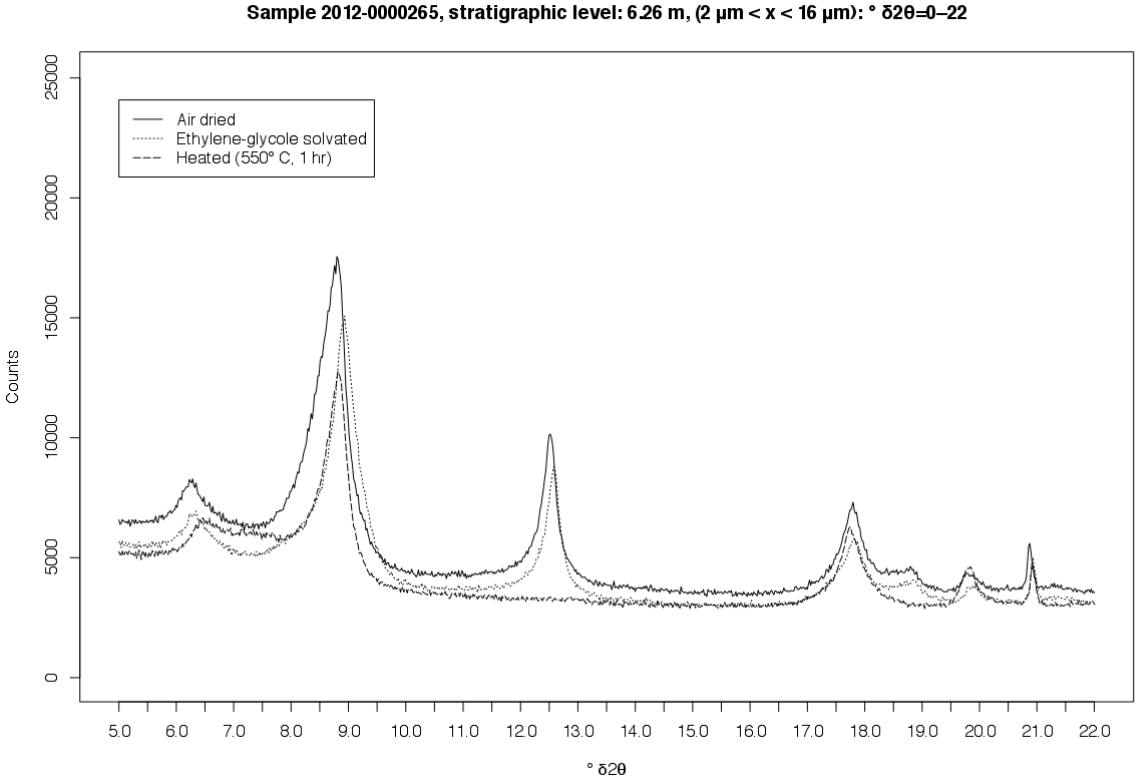
Sample 2012-0000265, stratigraphic level: 6.26 m, (2 µm < x < 16 µm): ° δ2θ=0–22
Air dried
Ethylene-glycole solvated
Heated (550° C, 1 hr)
Counts
0
5000
10000
15000
20000
25000
5.0 6.0 7.0 8.0 9.0 10.0 11.0 12.0 13.0 14.0 15.0 16.0 17.0 18.0 19.0 20.0 21.0 22.0
° δ2θ

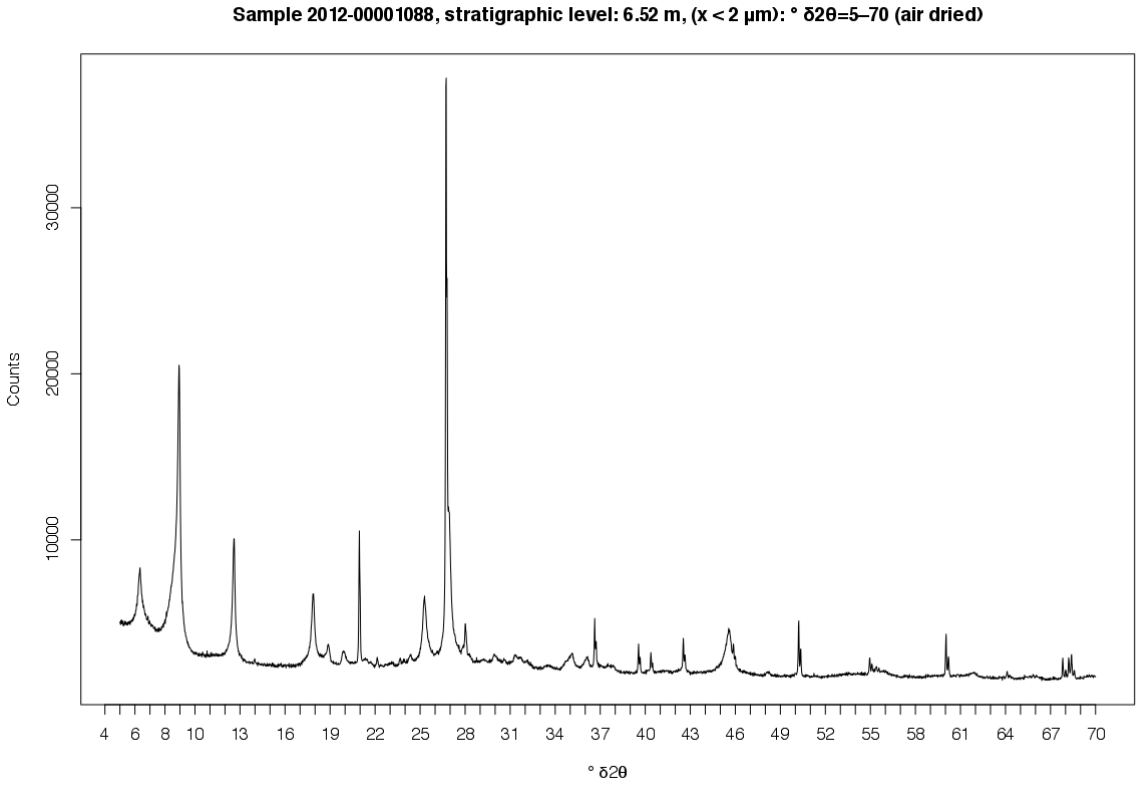
Sample 2012-00001088, stratigraphic level: 6.52 m, (x < 2 µm): ° δ2θ=5–70 (air dried)
Counts
10000
20000
30000
4 6 8 10 13 16 19 22 25 28 31 34 37 40 43 46 49 52 55 58 61 64 67 70
° δ2θ

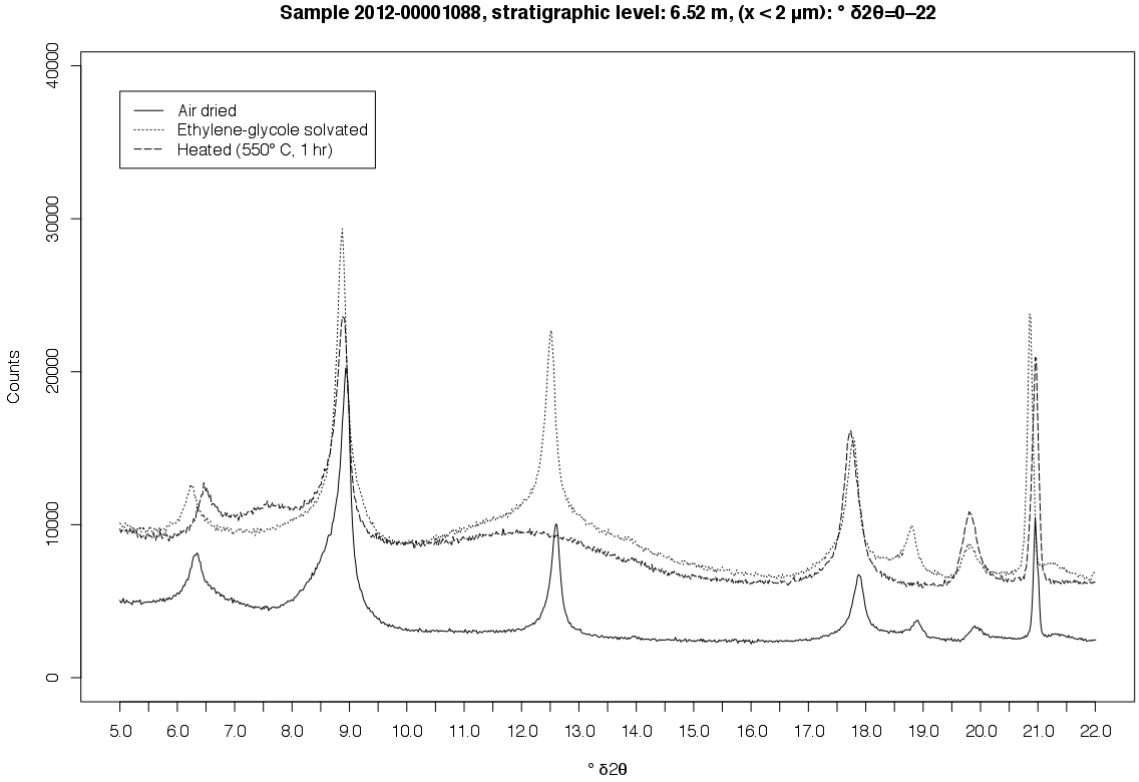
Sample 2012-00001088, stratigraphic level: 6.52 m, (x < 2 µm): ° δ2θ=0–22
Air dried
Ethylene-glycole solvated
Heated (550° C, 1 hr)
Counts
0
10000
20000
30000
40000
5.0 6.0 7.0 8.0 9.0 10.0 11.0 12.0 13.0 14.0 15.0 16.0 17.0 18.0 19.0 20.0 21.0 22.0
° δ2θ

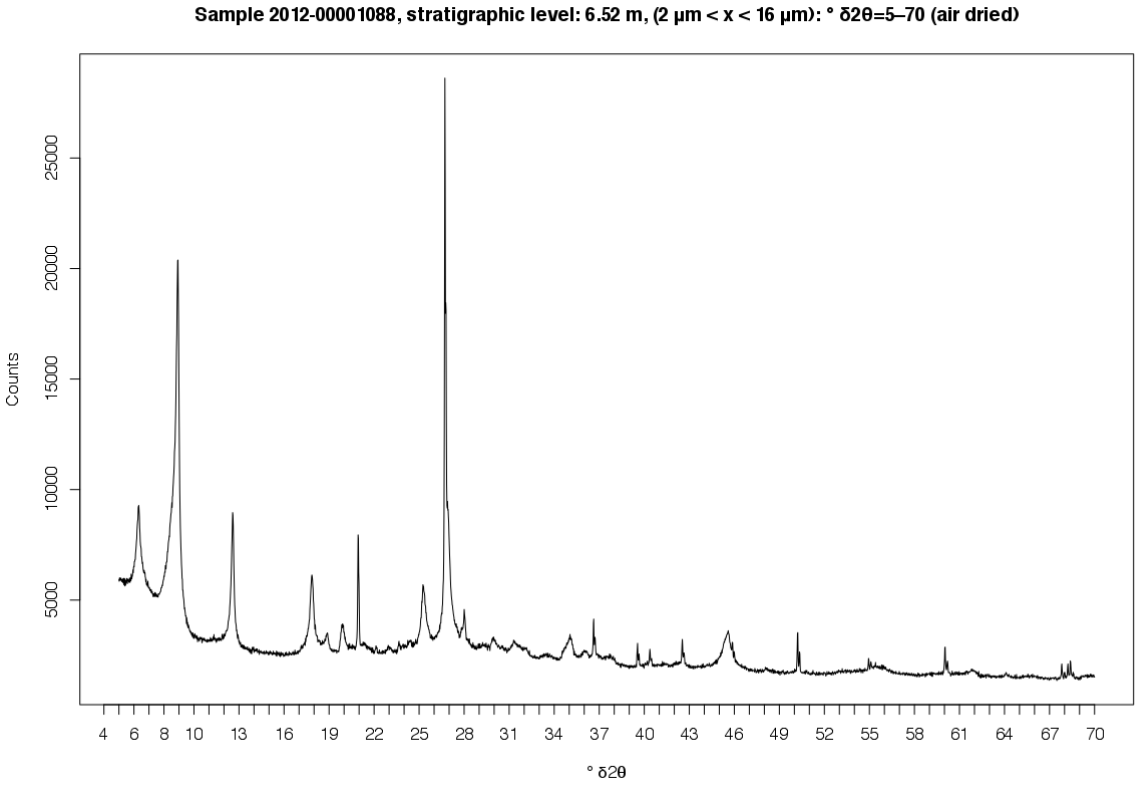
Sample 2012-00001088, stratigraphic level: 6.52 m, (2 µm < x < 16 µm): ° δ2θ=5–70 (air dried)
Counts
5000
10000
15000
20000
25000
4 6 8 10 13 16 19 22 25 28 31 34 37 40 43 46 49 52 55 58 61 64 67 70
° δ2θ

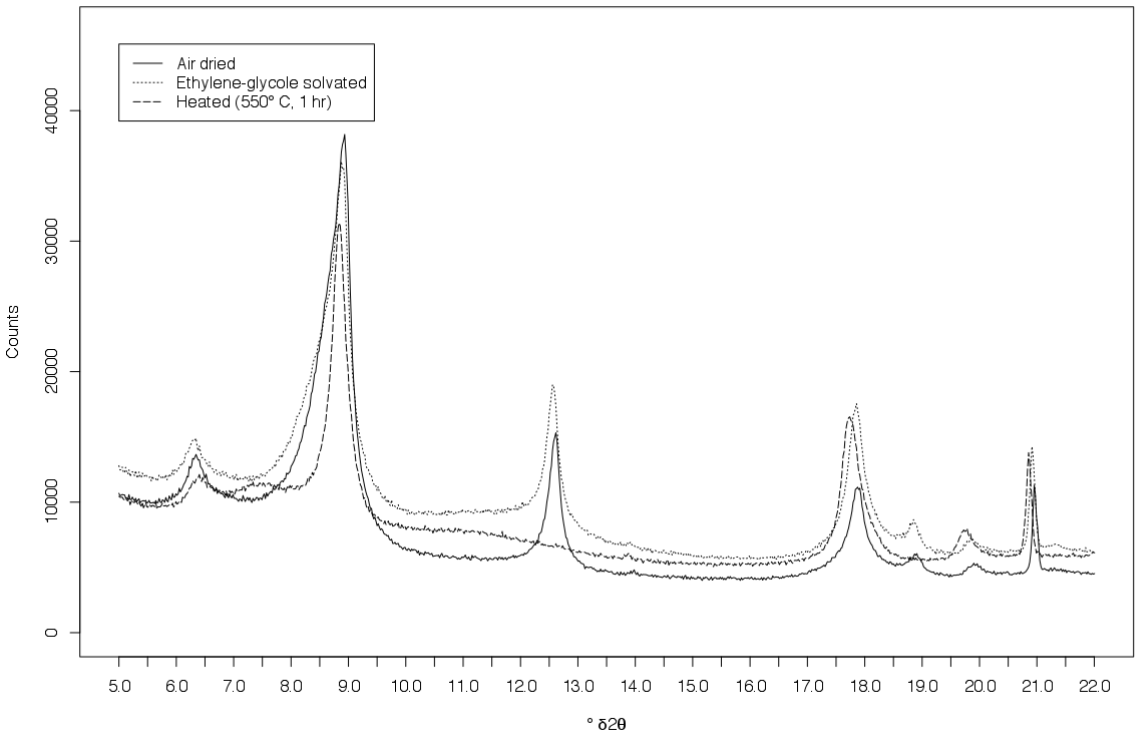
Sample 2012-00001088, stratigraphic level: 6.52 m, (2 µm < x < 16 µm): ° δ2θ=0–22
Air dried
Ethylene-glycole solvated
Heated (550° C, 1 hr)
Counts
0
10000
20000
30000
40000
5.0 6.0 7.0 8.0 9.0 10.0 11.0 12.0 13.0 14.0 15.0 16.0 17.0 18.0 19.0 20.0 21.0 22.0
° δ2θ

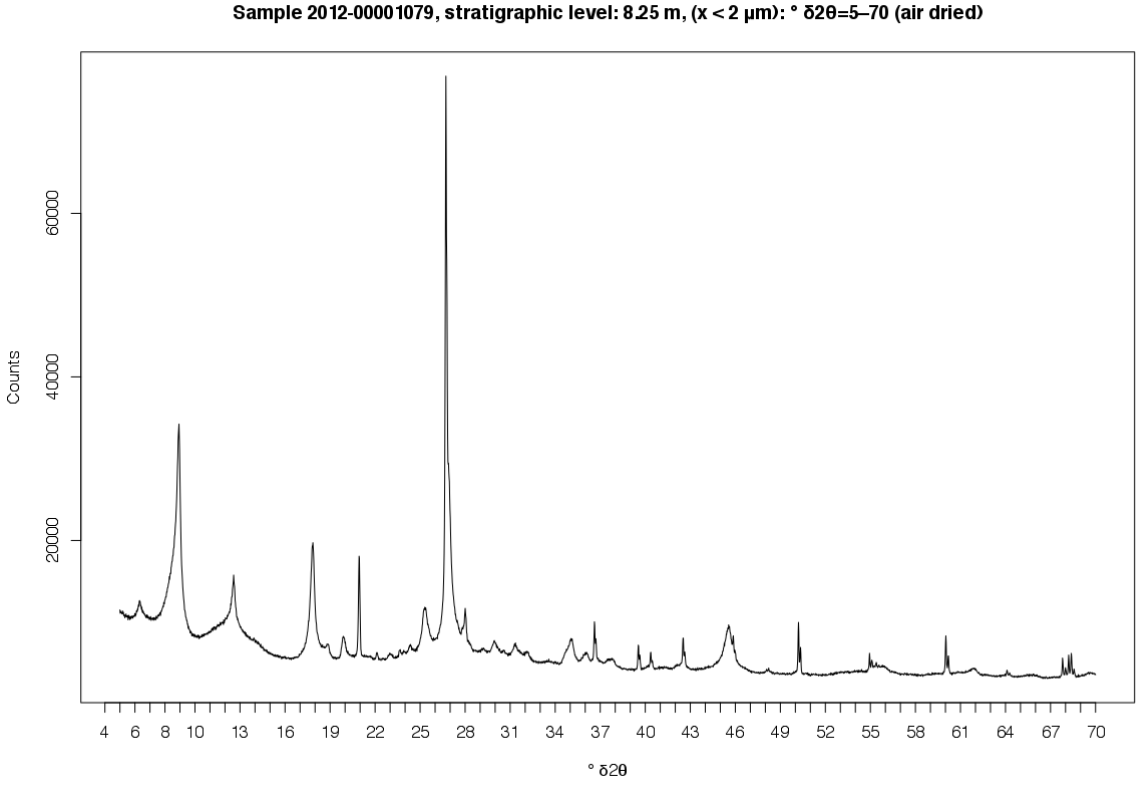
Sample 2012-00001079, stratigraphic level: 8.25 m, (x < 2 µm): ° δ2θ=5–70 (air dried)
Counts
20000
40000
60000
4 6 8 10 13 16 19 22 25 28 31 34 37 40 43 46 49 52 55 58 61 64 67 70
° δ2θ

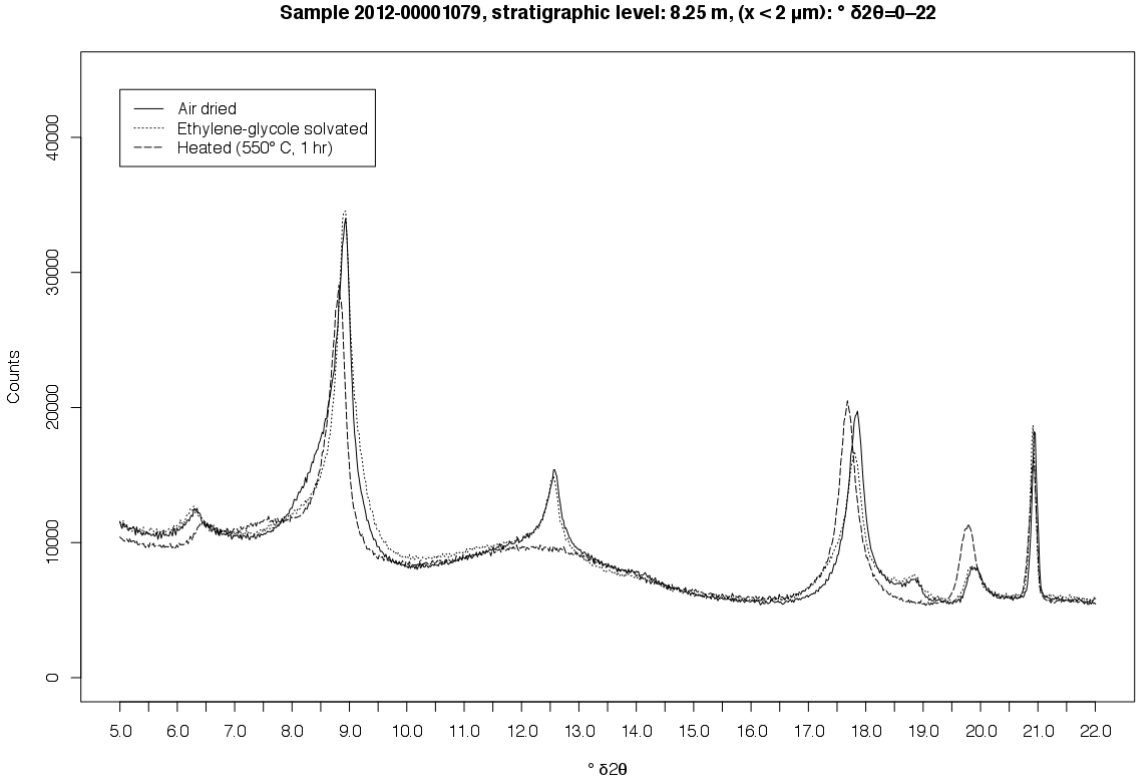
Sample 2012-00001079, stratigraphic level: 8.25 m, (x < 2 µm): ° δ2θ=0–22
Air dried
Ethylene-glycole solvated
Heated (550° C, 1 hr)
Counts
0
10000
20000
30000
40000
5.0 6.0 7.0 8.0 9.0 10.0 11.0 12.0 13.0 14.0 15.0 16.0 17.0 18.0 19.0 20.0 21.0 22.0
° δ2θ

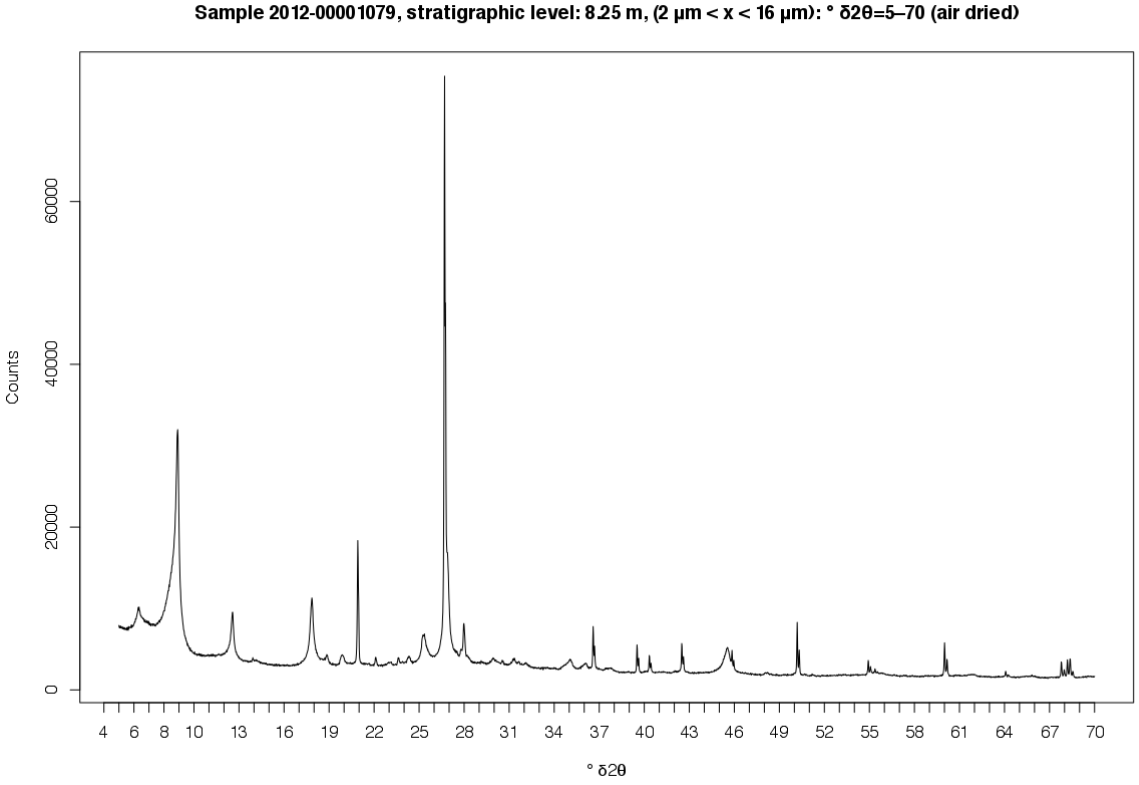
Sample 2012-00001079, stratigraphic level: 8.25 m, (2 µm < x < 16 µm): ° δ2θ=5–70 (air dried)
Counts
0
20000
40000
60000
4 6 8 10 13 16 19 22 25 28 31 34 37 40 43 46 49 52 55 58 61 64 67 70
° δ2θ

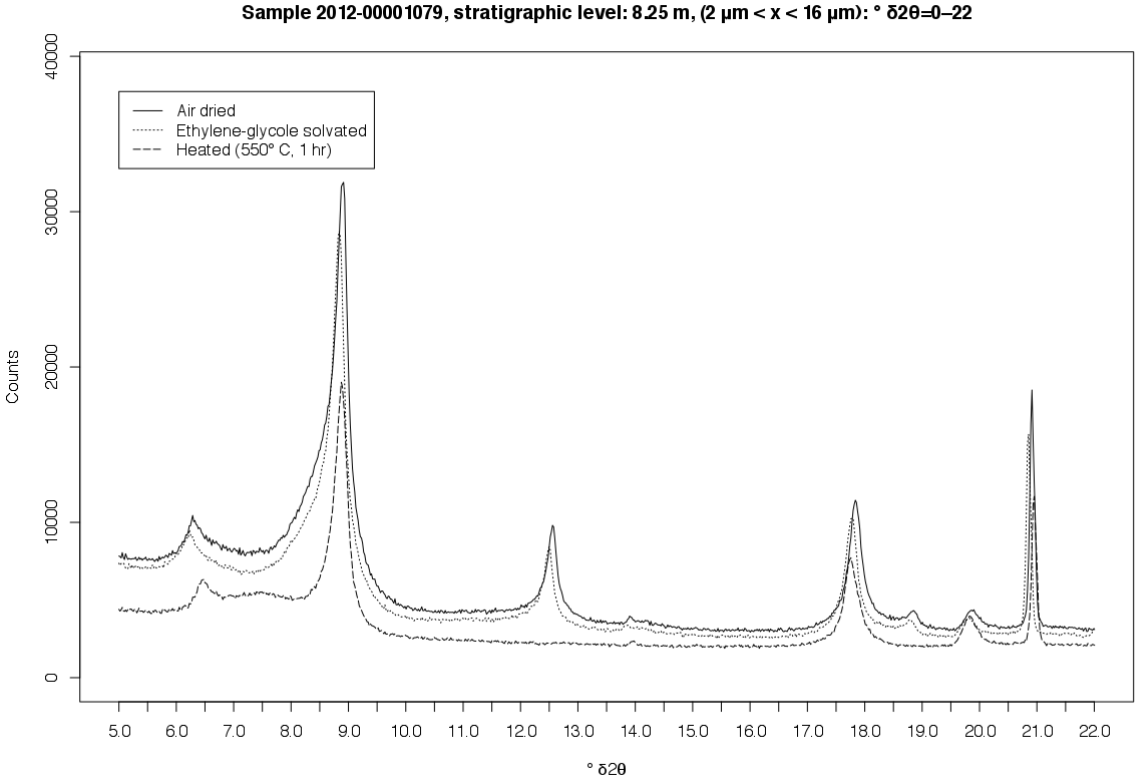
Sample 2012-00001079, stratigraphic level: 8.25 m, (2 µm < x < 16 µm): ° δ2θ=0–22
Air dried
Ethylene-glycole solvated
Heated (550° C, 1 hr)
Counts
0
10000
20000
30000
40000
5.0 6.0 7.0 8.0 9.0 10.0 11.0 12.0 13.0 14.0 15.0 16.0 17.0 18.0 19.0 20.0 21.0 22.0
° δ2θ

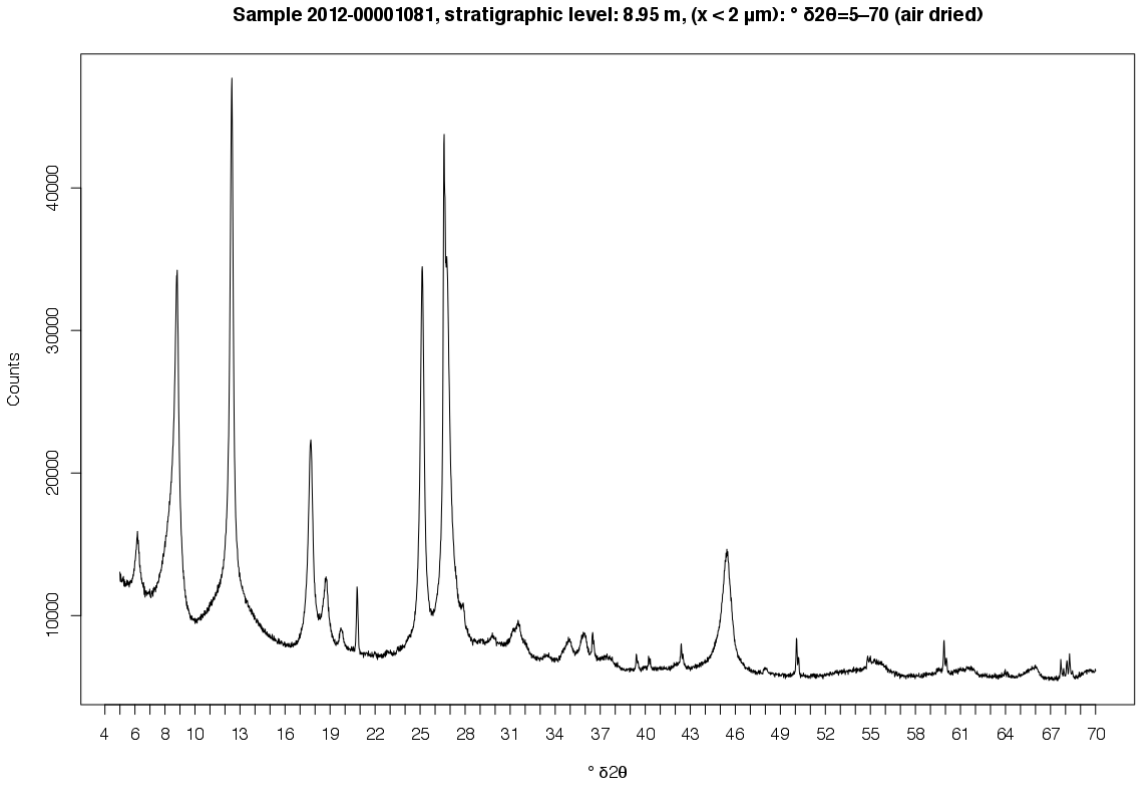
Sample 2012-00001081, stratigraphic level: 8.95 m, (x < 2 µm): ° δ2θ=5–70 (air dried)
Counts
10000
20000
30000
40000
4 6 8 10 13 16 19 22 25 28 31 34 37 40 43 46 49 52 55 58 61 64 67 70
° δ2θ

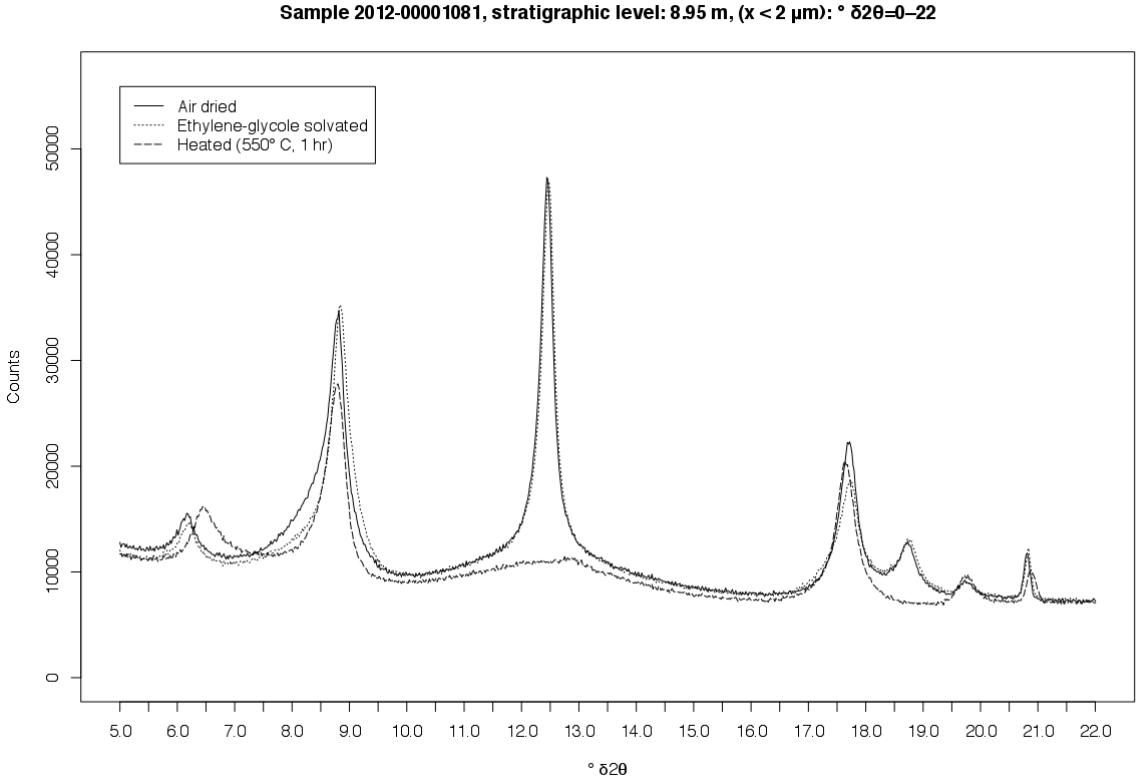
Sample 2012-00001081, stratigraphic level: 8.95 m, (x < 2 µm): ° δ2θ=0–22
Air dried
Ethylene-glycole solvated
Heated (550° C, 1 hr)
Counts
0
10000
20000
30000
40000
50000
5.0 6.0 7.0 8.0 9.0 10.0 11.0 12.0 13.0 14.0 15.0 16.0 17.0 18.0 19.0 20.0 21.0 22.0
° δ2θ

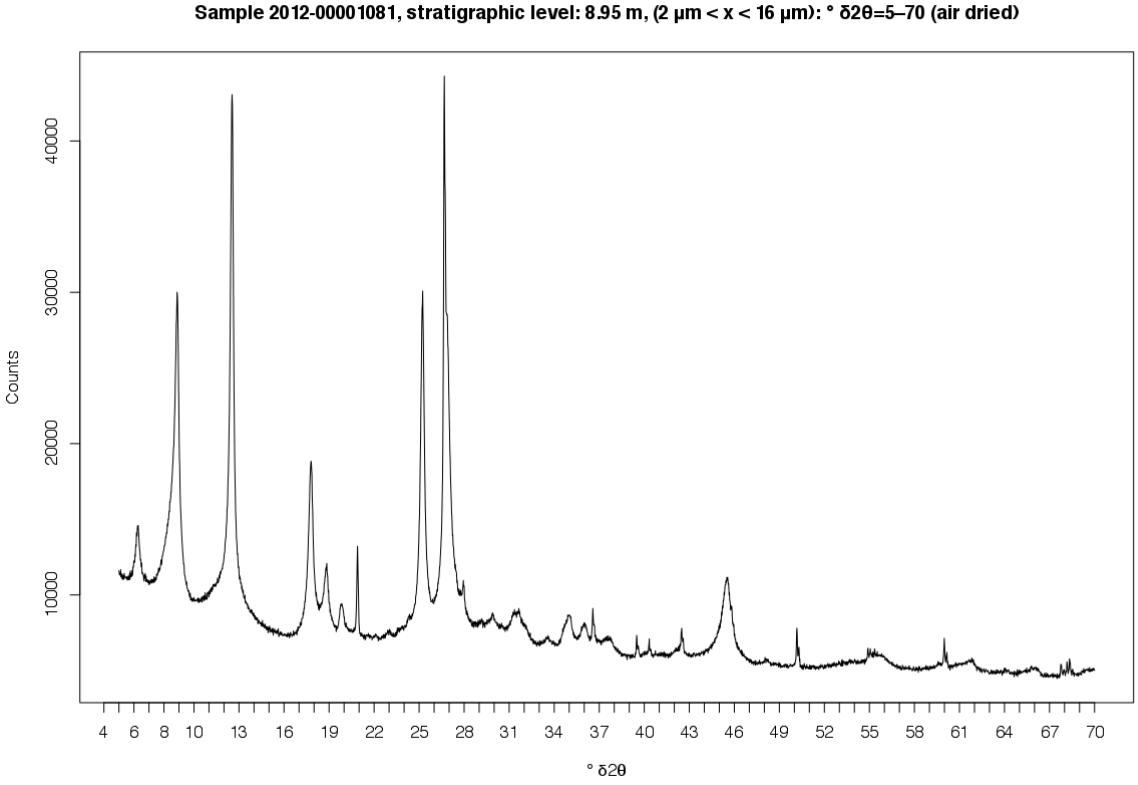
Sample 2012-00001081, stratigraphic level: 8.95 m, (2 µm < x < 16 µm): ° δ2θ=5–70 (air dried)
Counts
10000
20000
30000
40000
4 6 8 10 13 16 19 22 25 28 31 34 37 40 43 46 49 52 55 58 61 64 67 70
° δ2θ

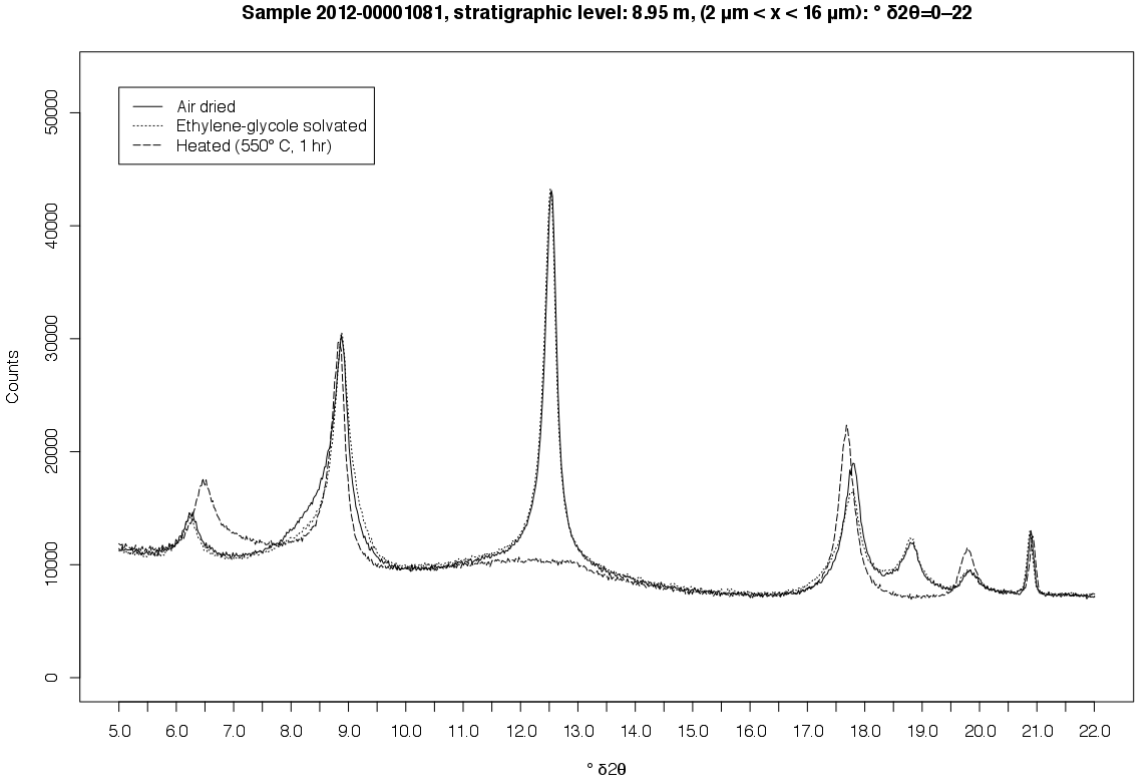
Sample 2012-00001081, stratigraphic level: 8.95 m, (2 µm < x < 16 µm): ° δ2θ=0–22
Air dried
Ethylene-glycole solvated
Heated (550° C, 1 hr)
Counts
0
10000
20000
30000
40000
50000
5.0 6.0 7.0 8.0 9.0 10.0 11.0 12.0 13.0 14.0 15.0 16.0 17.0 18.0 19.0 20.0 21.0 22.0
° δ2θ

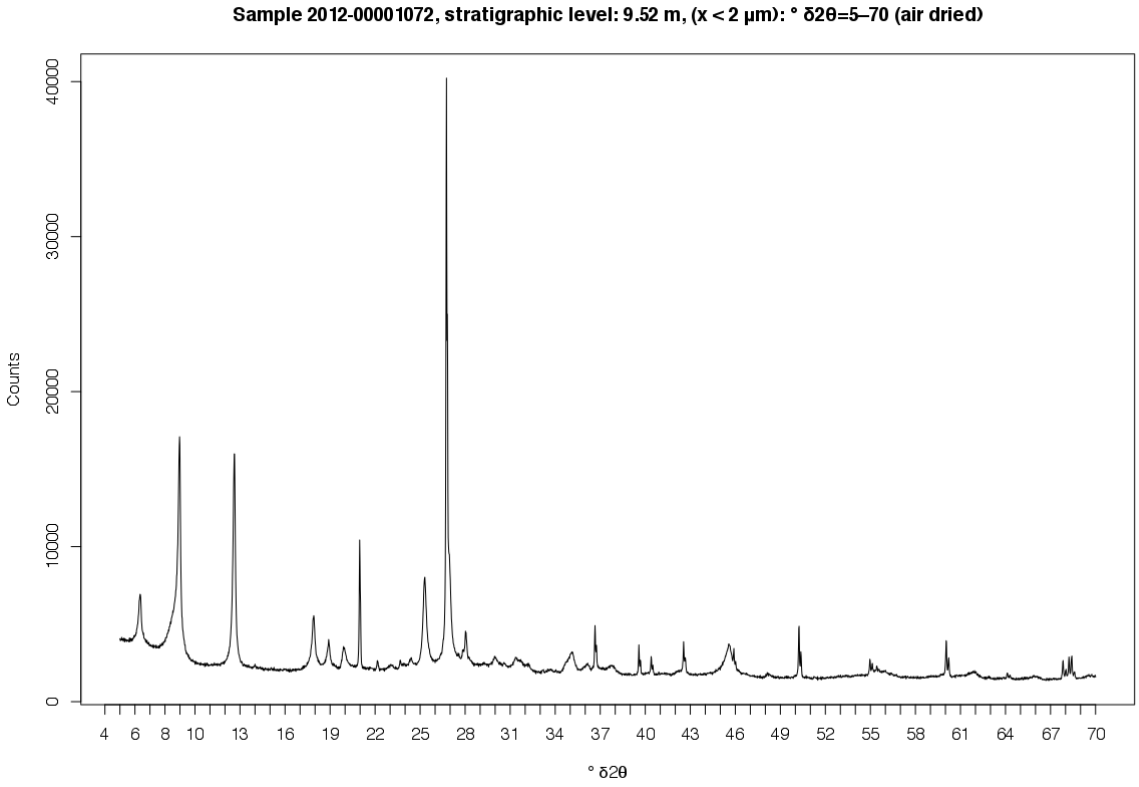
Sample 2012-00001072, stratigraphic level: 9.52 m, (x < 2 µm): ° δ2θ=5–70 (air dried)
Counts
0
10000
20000
30000
40000
4 6 8 10 13 16 19 22 25 28 31 34 37 40 43 46 49 52 55 58 61 64 67 70
° δ2θ

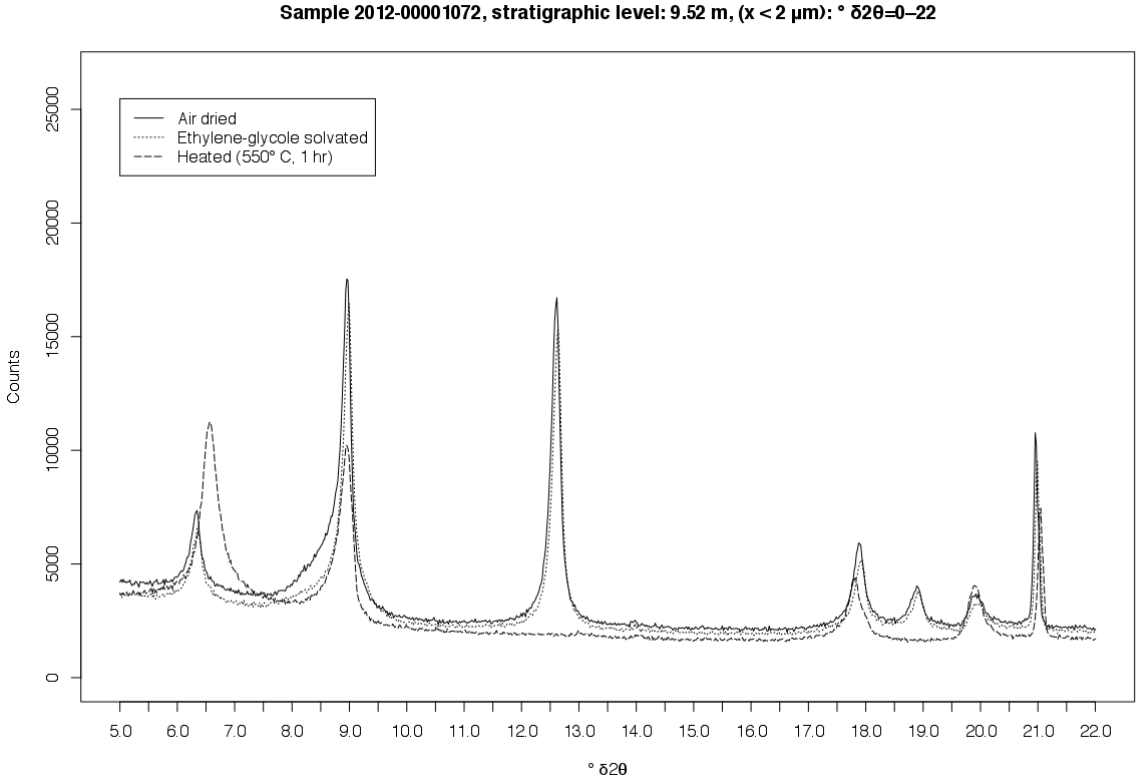
Sample 2012-00001072, stratigraphic level: 9.52 m, (x < 2 µm): ° δ2θ=0–22
Air dried
Ethylene-glycole solvated
Heated (550° C, 1 hr)
Counts
0
5000
10000
15000
20000
25000
5.0 6.0 7.0 8.0 9.0 10.0 11.0 12.0 13.0 14.0 15.0 16.0 17.0 18.0 19.0 20.0 21.0 22.0
° δ2θ

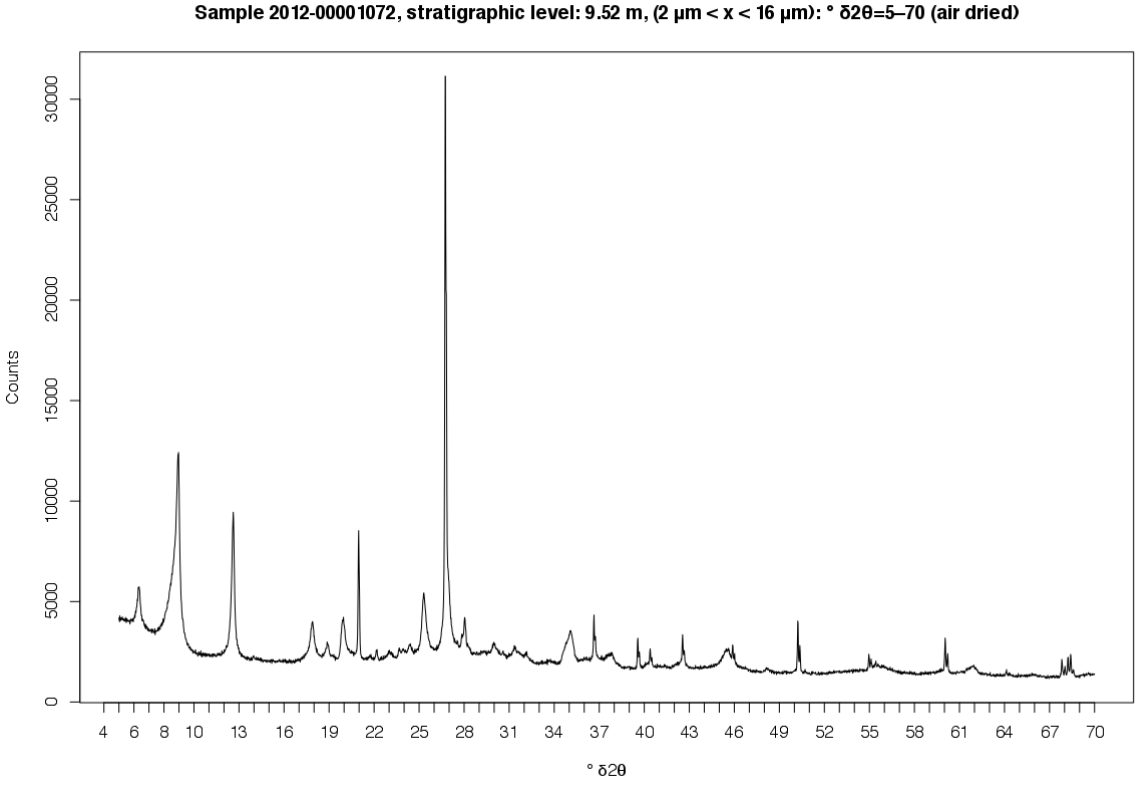
Sample 2012-00001072, stratigraphic level: 9.52 m, (2 µm < x < 16 µm): ° δ2θ=5–70 (air dried)
Counts
0
5000
10000
15000
20000
25000
30000
4 6 8 10 13 16 19 22 25 28 31 34 37 40 43 46 49 52 55 58 61 64 67 70
° δ2θ

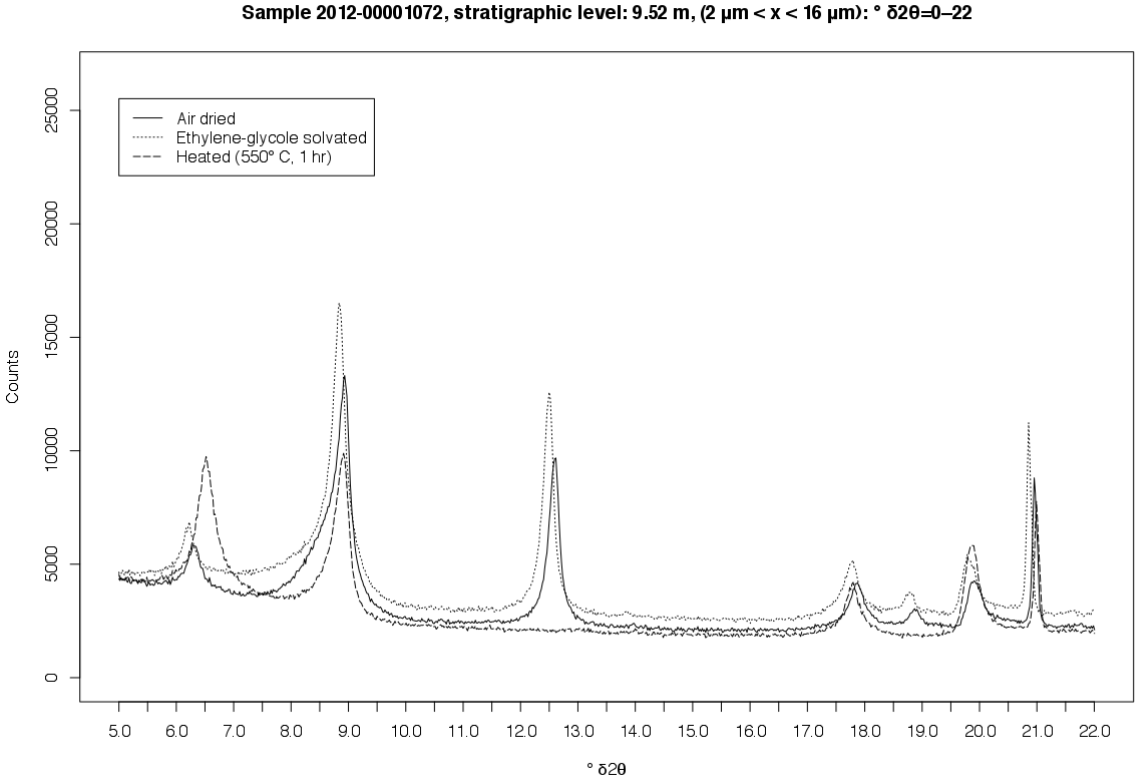
Sample 2012-00001072, stratigraphic level: 9.52 m, (2 µm < x < 16 µm): ° δ2θ=0–22
Air dried
Ethylene-glycole solvated
Heated (550° C, 1 hr)
Counts
0
5000
10000
15000
20000
25000
5.0 6.0 7.0 8.0 9.0 10.0 11.0 12.0 13.0 14.0 15.0 16.0 17.0 18.0 19.0 20.0 21.0 22.0
° δ2θ

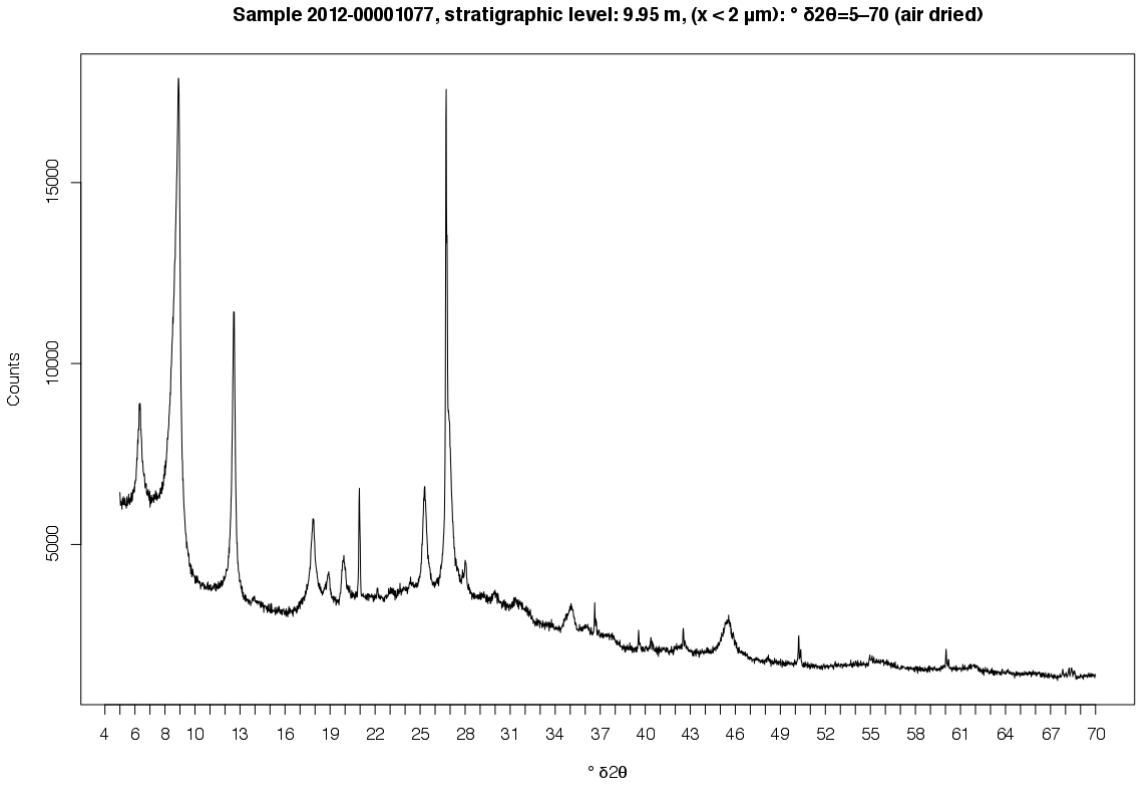
Sample 2012-00001077, stratigraphic level: 9.95 m, (x < 2 µm): ° δ2θ=5–70 (air dried)
Counts
5000
10000
15000
4 6 8 10 13 16 19 22 25 28 31 34 37 40 43 46 49 52 55 58 61 64 67 70
° δ2θ

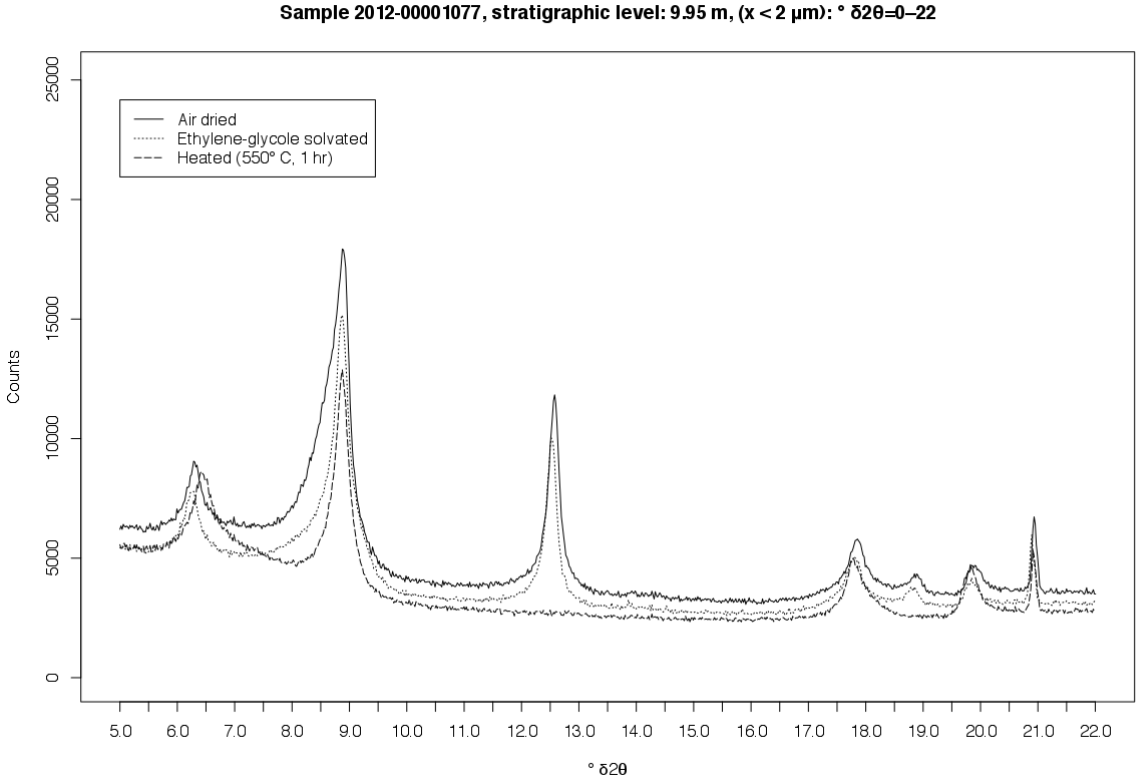
Sample 2012-00001077, stratigraphic level: 9.95 m, (x < 2 µm): ° δ2θ=0–22
Air dried
Ethylene-glycole solvated
Heated (550° C, 1 hr)
Counts
0
5000
10000
15000
20000
25000
5.0 6.0 7.0 8.0 9.0 10.0 11.0 12.0 13.0 14.0 15.0 16.0 17.0 18.0 19.0 20.0 21.0 22.0
° δ2θ

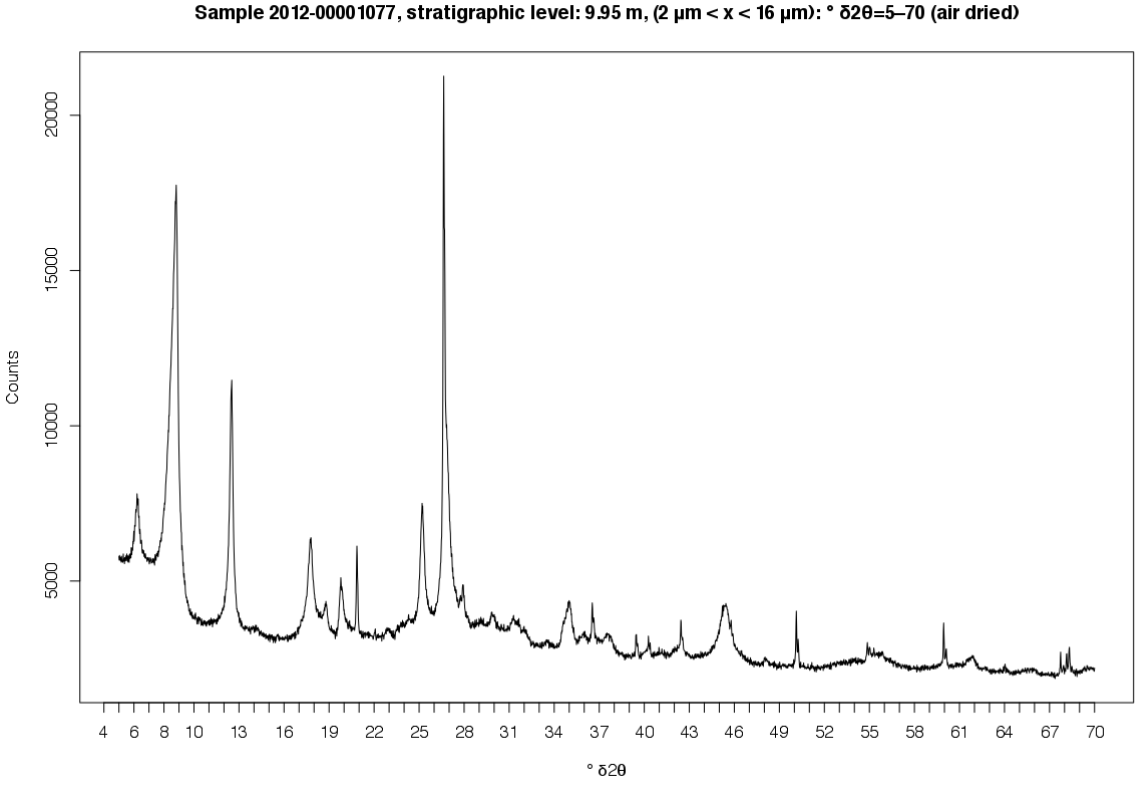
Sample 2012-00001077, stratigraphic level: 9.95 m, (2 µm < x < 16 µm): ° δ2θ=5–70 (air dried)
Counts
5000
10000
15000
20000
4 6 8 10 13 16 19 22 25 28 31 34 37 40 43 46 49 52 55 58 61 64 67 70
° δ2θ

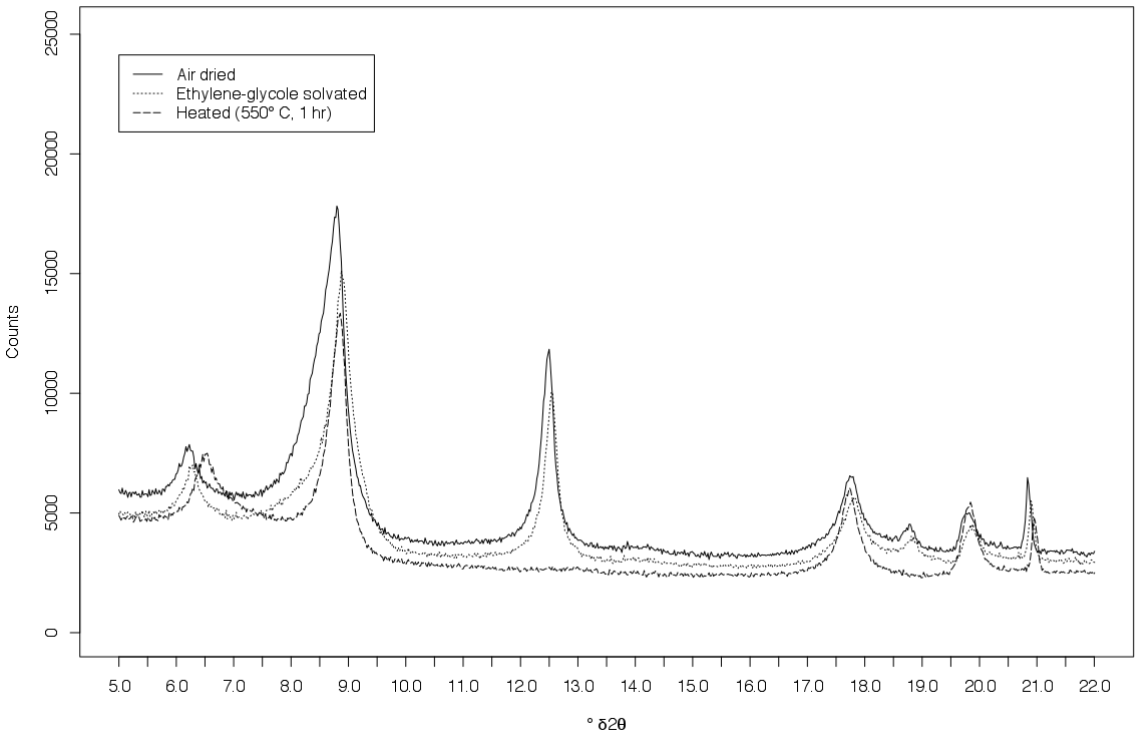
Sample 2012-00001077, stratigraphic level: 9.95 m, (2 µm < x < 16 µm): ° δ2θ=0–22
Air dried
Ethylene-glycole solvated
Heated (550° C, 1 hr)
Counts
0
5000
10000
15000
20000
25000
5.0 6.0 7.0 8.0 9.0 10.0 11.0 12.0 13.0 14.0 15.0 16.0 17.0 18.0 19.0 20.0 21.0 22.0
° δ2θ

Sample 2012-00001073, stratigraphic level: 10.42 m, (x < 2 µm): ° δ2θ=5–70 (air dried)

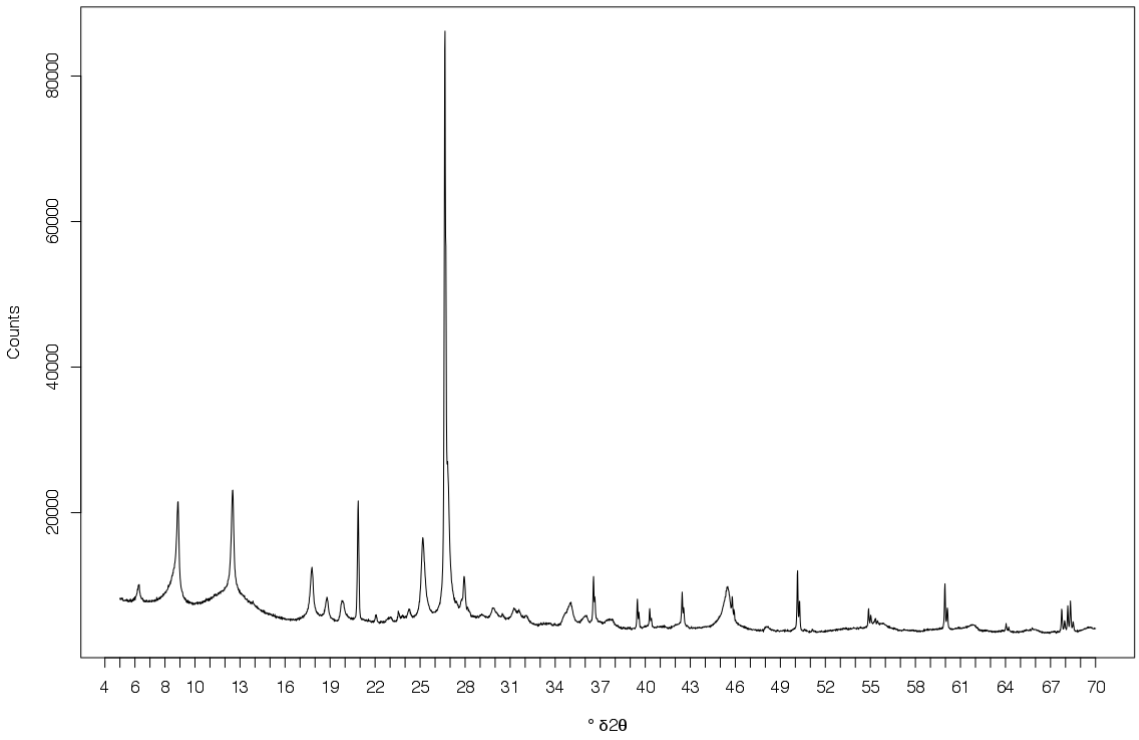

Sample 2012-00001073, stratigraphic level: 10.42 m, (x < 2 µm): ° δ2θ=0–22

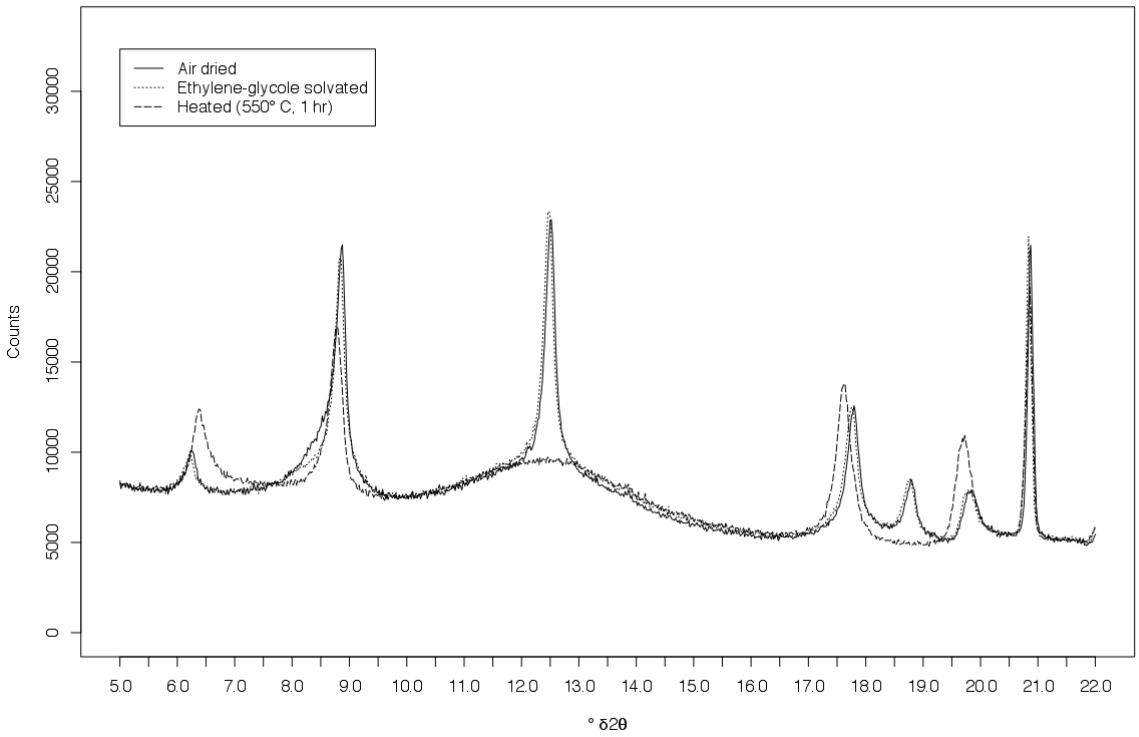

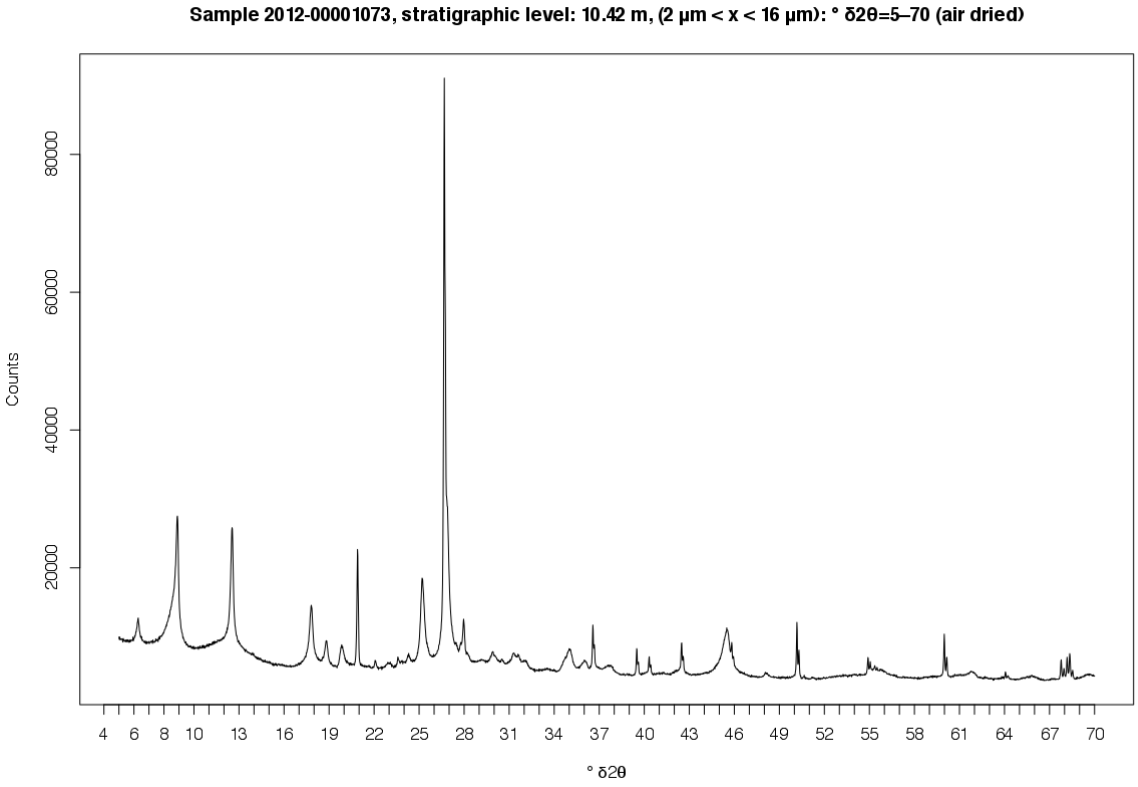
Sample 2012-00001073, stratigraphic level: 10.42 m, (2 µm < x < 16 µm): ° δ2θ=5–70 (air dried)
Counts
20000
40000
60000
80000
4 6 8 10 13 16 19 22 25 28 31 34 37 40 43 46 49 52 55 58 61 64 67 70
° δ2θ

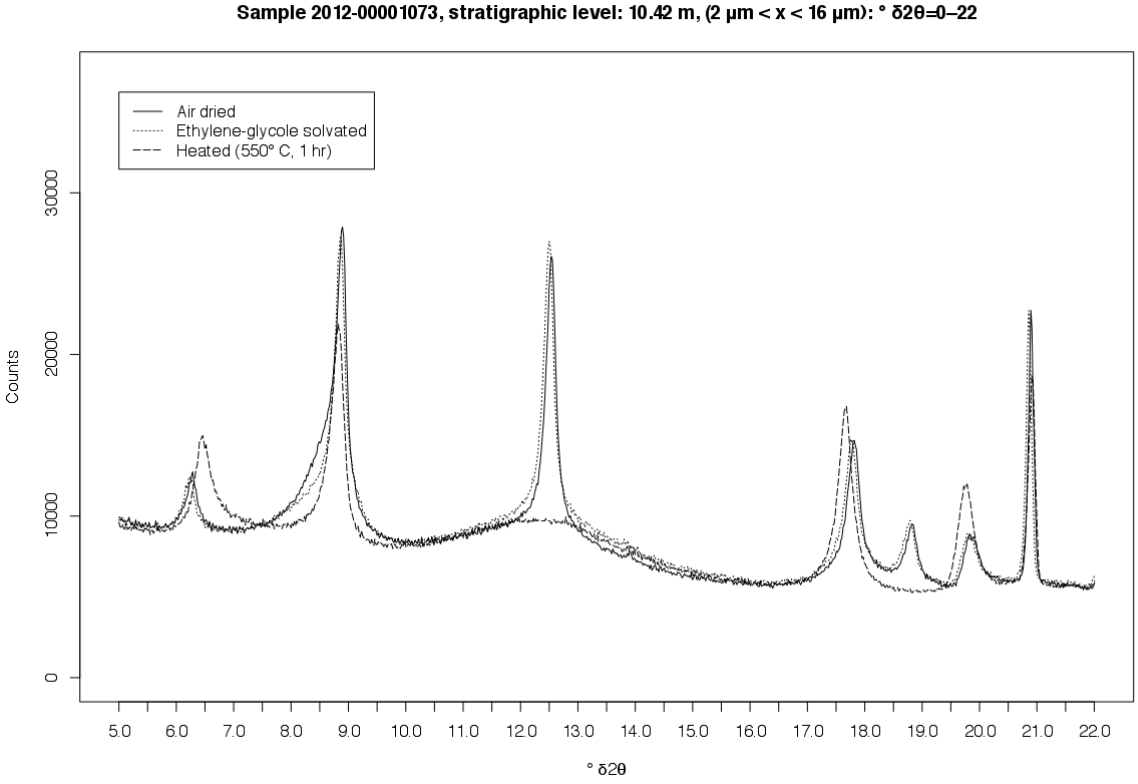
Sample 2012-00001073, stratigraphic level: 10.42 m, (2 µm < x < 16 µm): ° δ2θ=0–22
Air dried
Ethylene-glycole solvated
Heated (550° C, 1 hr)
Counts
0
10000
20000
30000
5.0 6.0 7.0 8.0 9.0 10.0 11.0 12.0 13.0 14.0 15.0 16.0 17.0 18.0 19.0 20.0 21.0 22.0
° δ2θ

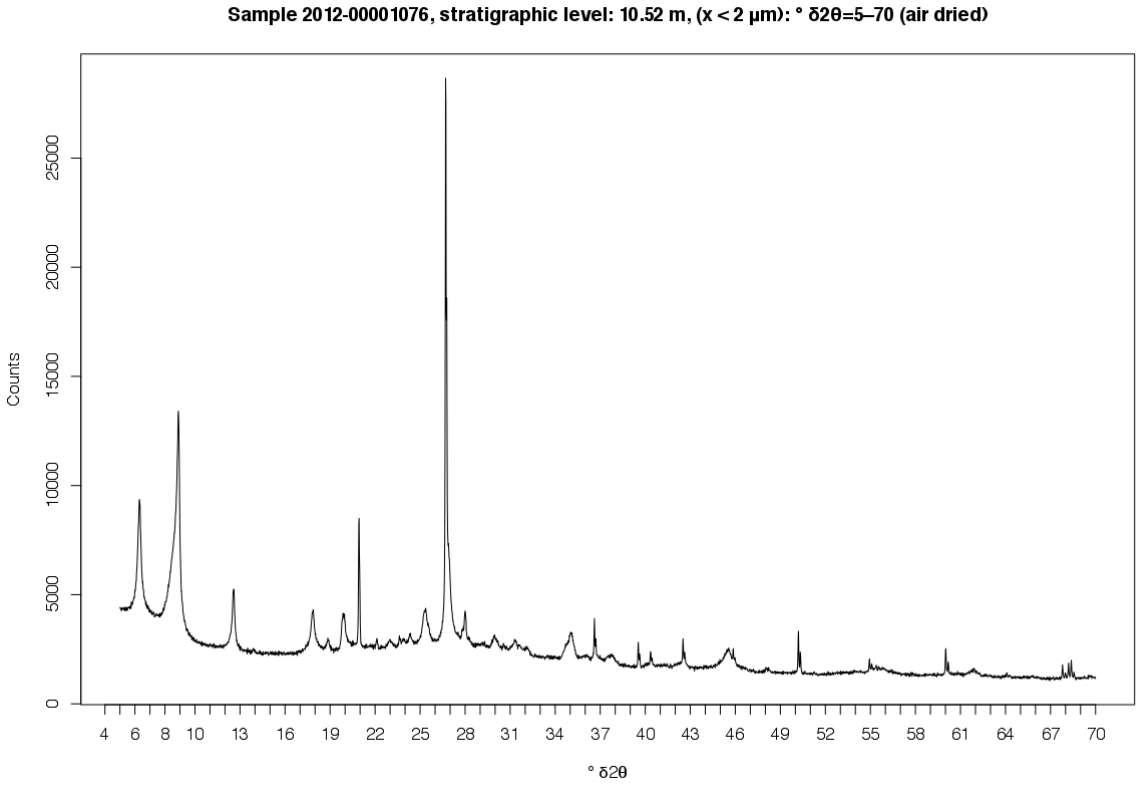
Sample 2012-00001076, stratigraphic level: 10.52 m, (x < 2 µm): ° δ2θ=5–70 (air dried)
Counts
0
5000
10000
15000
20000
25000
4 6 8 10 13 16 19 22 25 28 31 34 37 40 43 46 49 52 55 58 61 64 67 70
° δ2θ

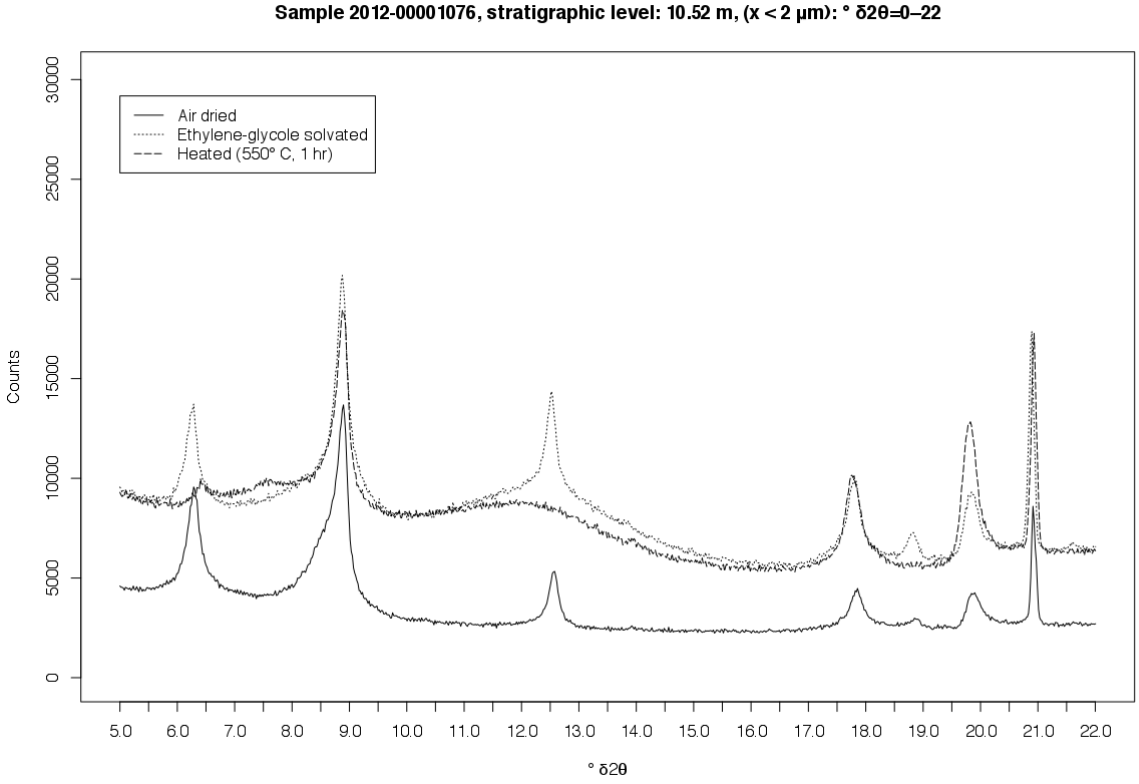
Sample 2012-00001076, stratigraphic level: 10.52 m, (x < 2 µm): ° δ2θ=0–22
Air dried
Ethylene-glycole solvated
Heated (550° C, 1 hr)
Counts
0
5000
10000
15000
20000
25000
30000
5.0 6.0 7.0 8.0 9.0 10.0 11.0 12.0 13.0 14.0 15.0 16.0 17.0 18.0 19.0 20.0 21.0 22.0
° δ2θ

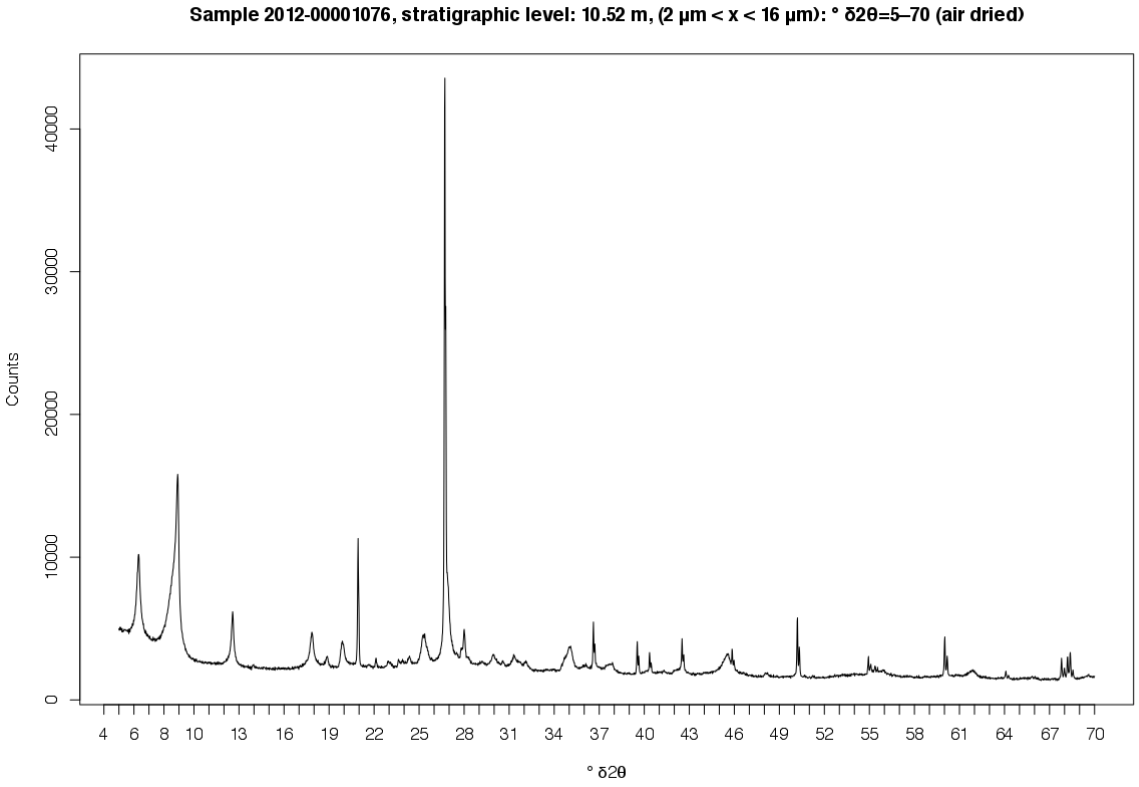
Sample 2012-00001076, stratigraphic level: 10.52 m, (2 µm < x < 16 µm): ° δ2θ=5–70 (air dried)
Counts
0
10000
20000
30000
40000
4 6 8 10 13 16 19 22 25 28 31 34 37 40 43 46 49 52 55 58 61 64 67 70
° δ2θ

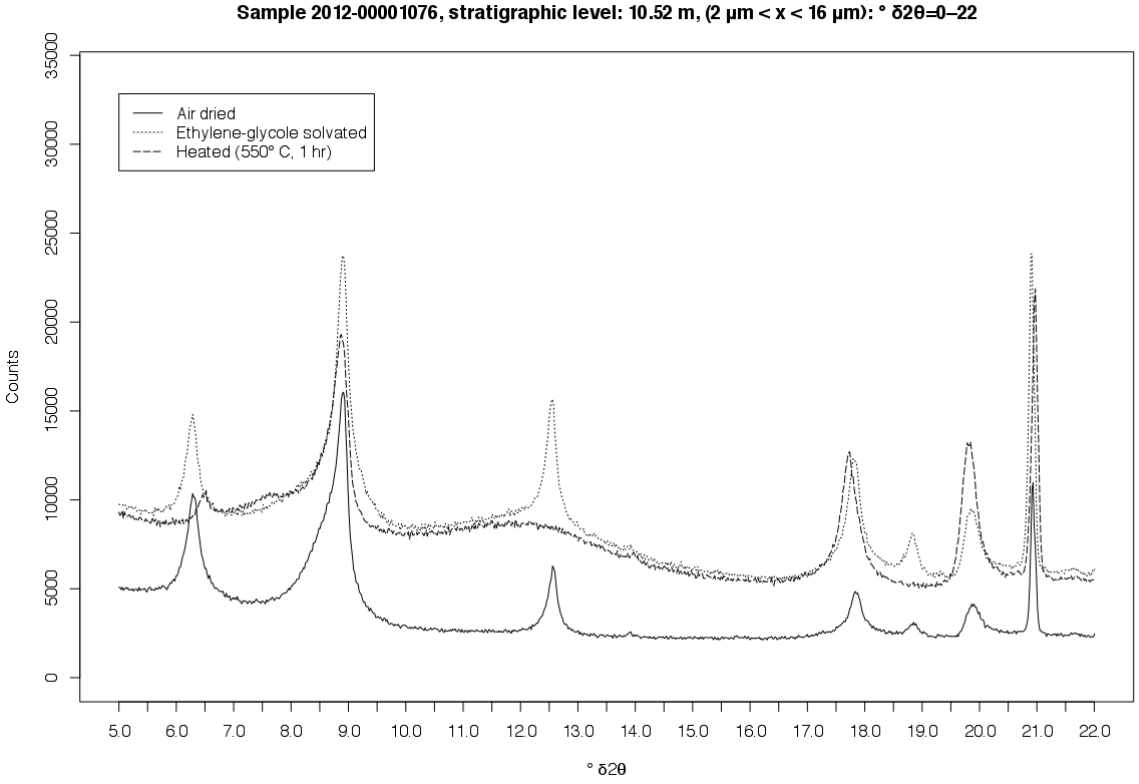
Sample 2012-00001076, stratigraphic level: 10.52 m, (2 µm < x < 16 µm): ° δ2θ=0–22
Air dried
Ethylene-glycole solvated
Heated (550° C, 1 hr)
Counts
0
5000
10000
15000
20000
25000
30000
35000
5.0 6.0 7.0 8.0 9.0 10.0 11.0 12.0 13.0 14.0 15.0 16.0 17.0 18.0 19.0 20.0 21.0 22.0
° δ2θ

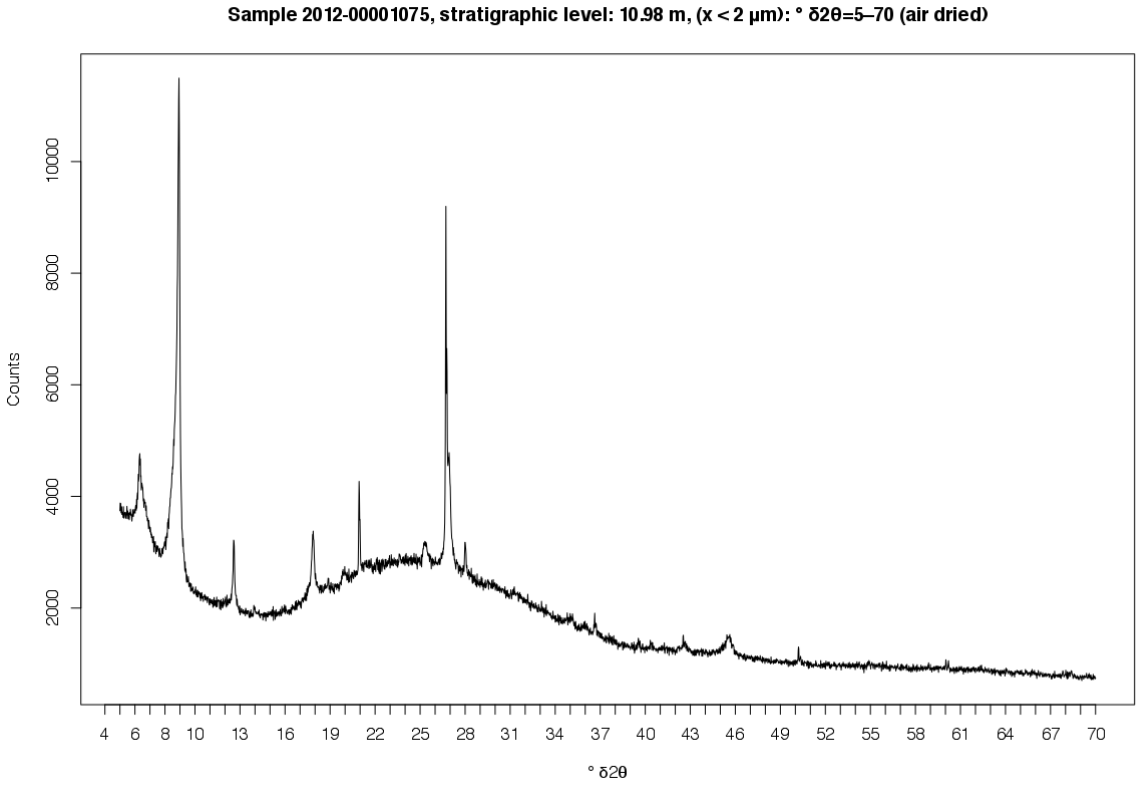
Sample 2012-00001075, stratigraphic level: 10.98 m, (x < 2 µm): ° δ2θ=5–70 (air dried)
Counts
2000
4000
6000
8000
10000
4 6 8 10 13 16 19 22 25 28 31 34 37 40 43 46 49 52 55 58 61 64 67 70
° δ2θ

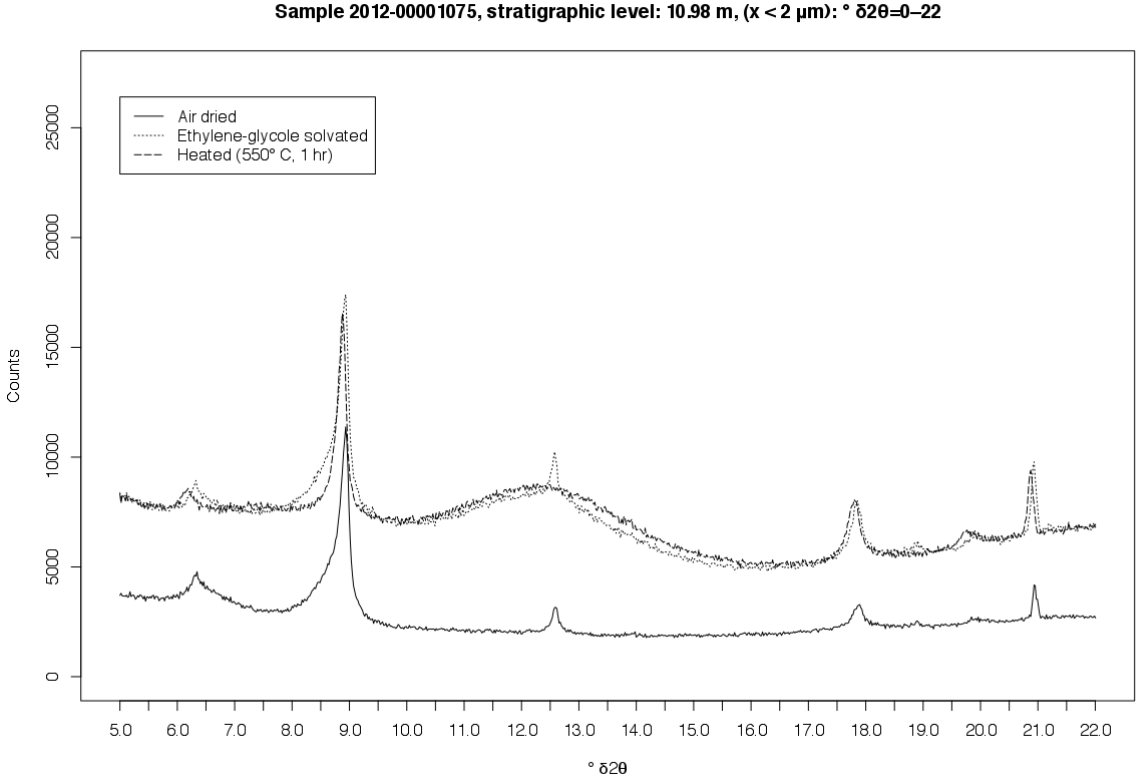
Sample 2012-00001075, stratigraphic level: 10.98 m, (x < 2 µm): ° δ2θ=0–22
Air dried
Ethylene-glycole solvated
Heated (550° C, 1 hr)
Counts
0
5000
10000
15000
20000
25000
5.0 6.0 7.0 8.0 9.0 10.0 11.0 12.0 13.0 14.0 15.0 16.0 17.0 18.0 19.0 20.0 21.0 22.0
° δ2θ

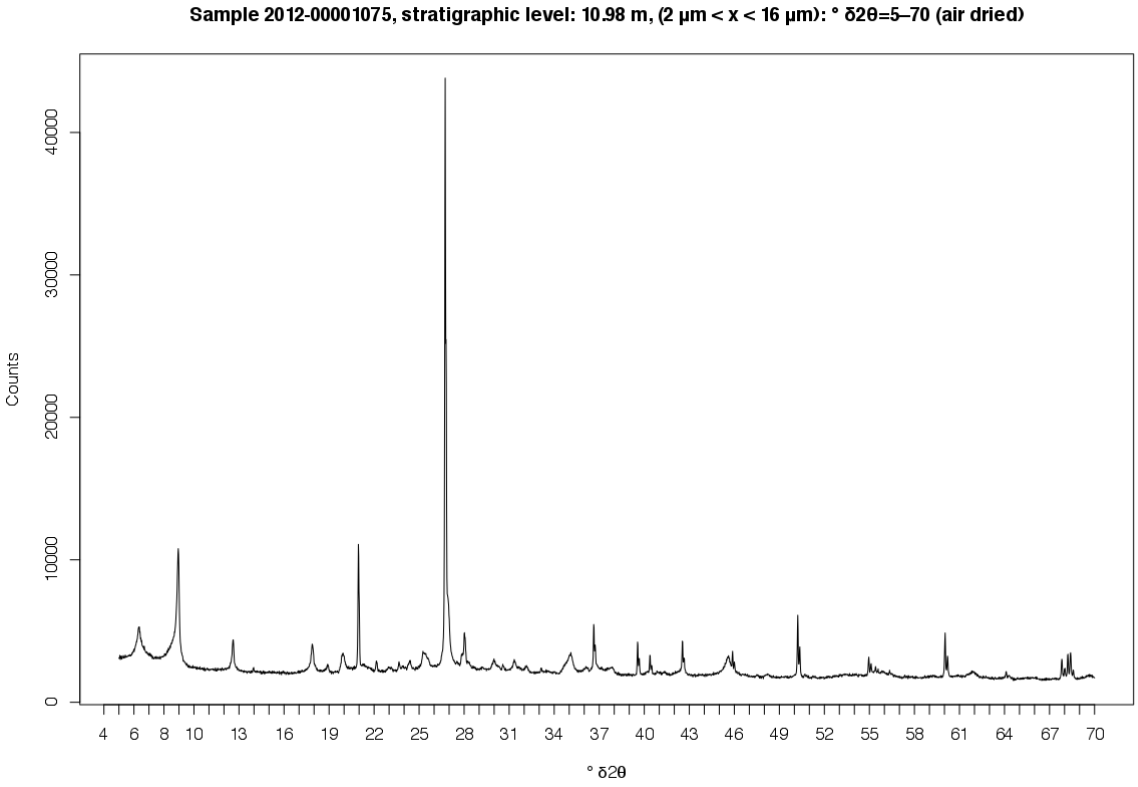
Sample 2012-00001075, stratigraphic level: 10.98 m, (2 µm < x < 16 µm): ° δ2θ=5–70 (air dried)
Counts
0
10000
20000
30000
40000
4 6 8 10 13 16 19 22 25 28 31 34 37 40 43 46 49 52 55 58 61 64 67 70
° δ2θ

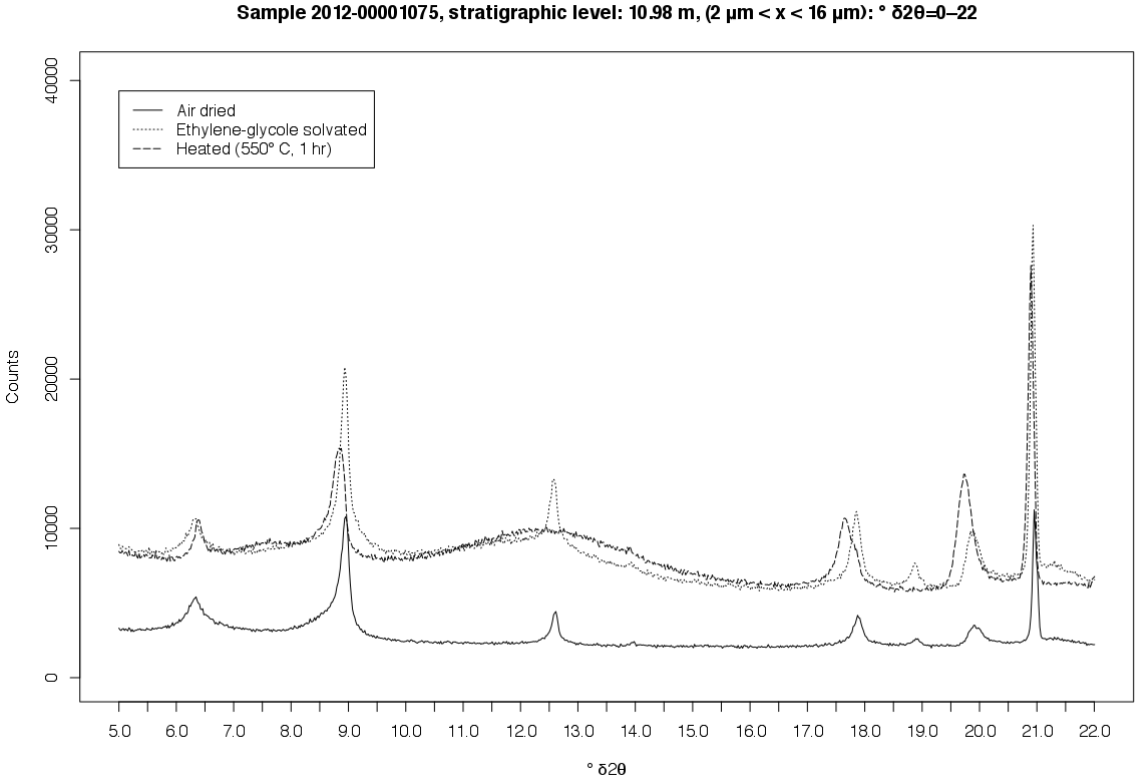
Sample 2012-00001075, stratigraphic level: 10.98 m, (2 µm < x < 16 µm): ° δ2θ=0–22
Air dried
Ethylene-glycole solvated
Heated (550° C, 1 hr)
Counts
0
10000
20000
30000
40000
5.0 6.0 7.0 8.0 9.0 10.0 11.0 12.0 13.0 14.0 15.0 16.0 17.0 18.0 19.0 20.0 21.0 22.0
° δ2θ

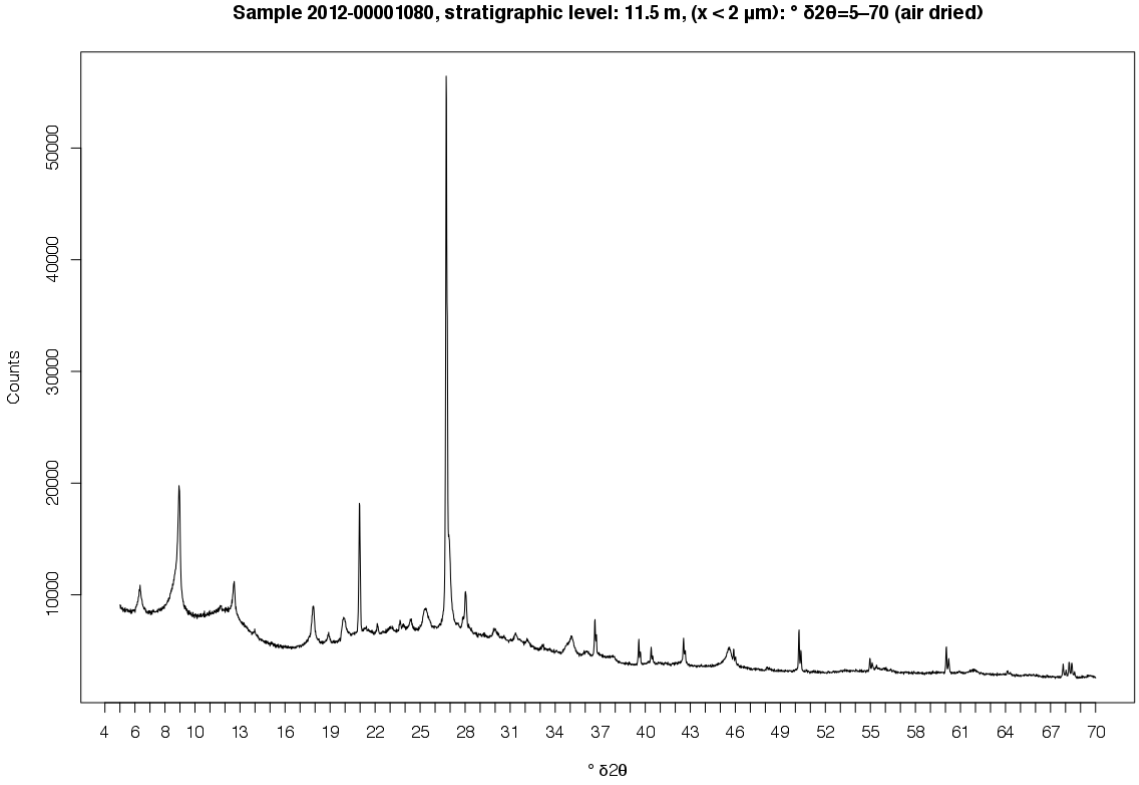
Sample 2012-00001080, stratigraphic level: 11.5 m, (x < 2 µm): ° δ2θ=5–70 (air dried)
Counts
10000
20000
30000
40000
50000
4 6 8 10 13 16 19 22 25 28 31 34 37 40 43 46 49 52 55 58 61 64 67 70
° δ2θ

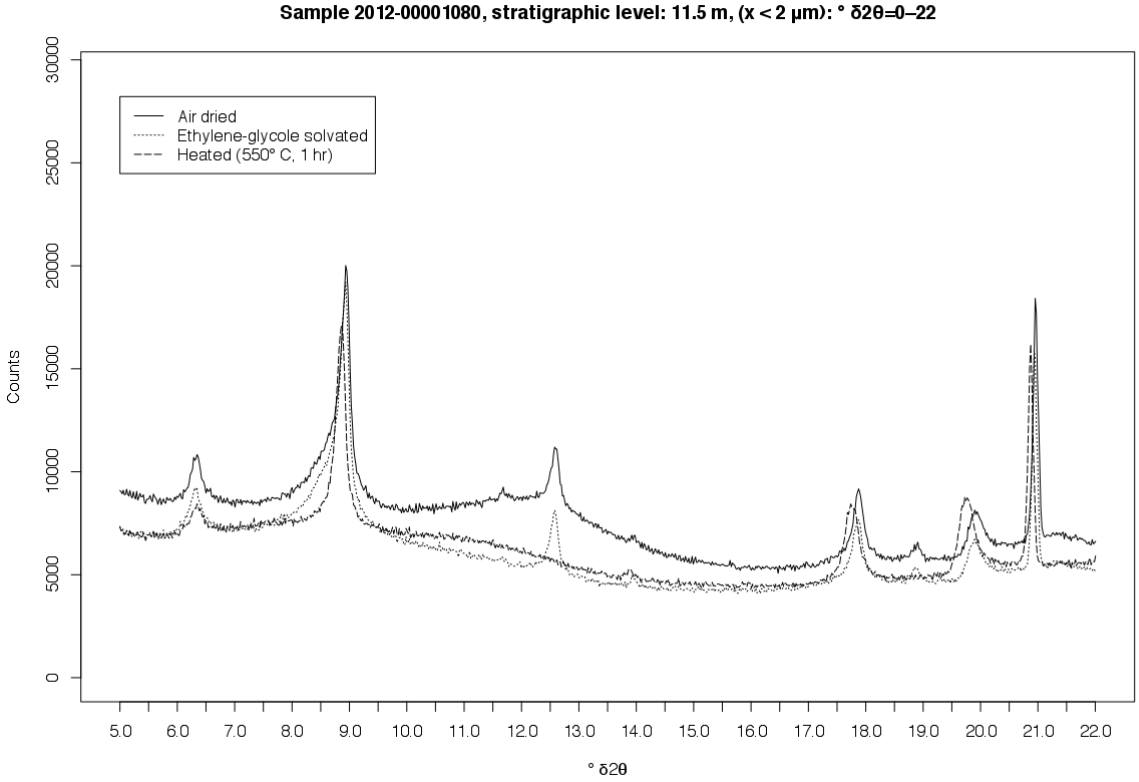
Sample 2012-00001080, stratigraphic level: 11.5 m, (x < 2 µm): ° δ2θ=0–22
Air dried
Ethylene-glycole solvated
Heated (550° C, 1 hr)
Counts
0
5000
10000
15000
20000
25000
30000
5.0 6.0 7.0 8.0 9.0 10.0 11.0 12.0 13.0 14.0 15.0 16.0 17.0 18.0 19.0 20.0 21.0 22.0
° δ2θ

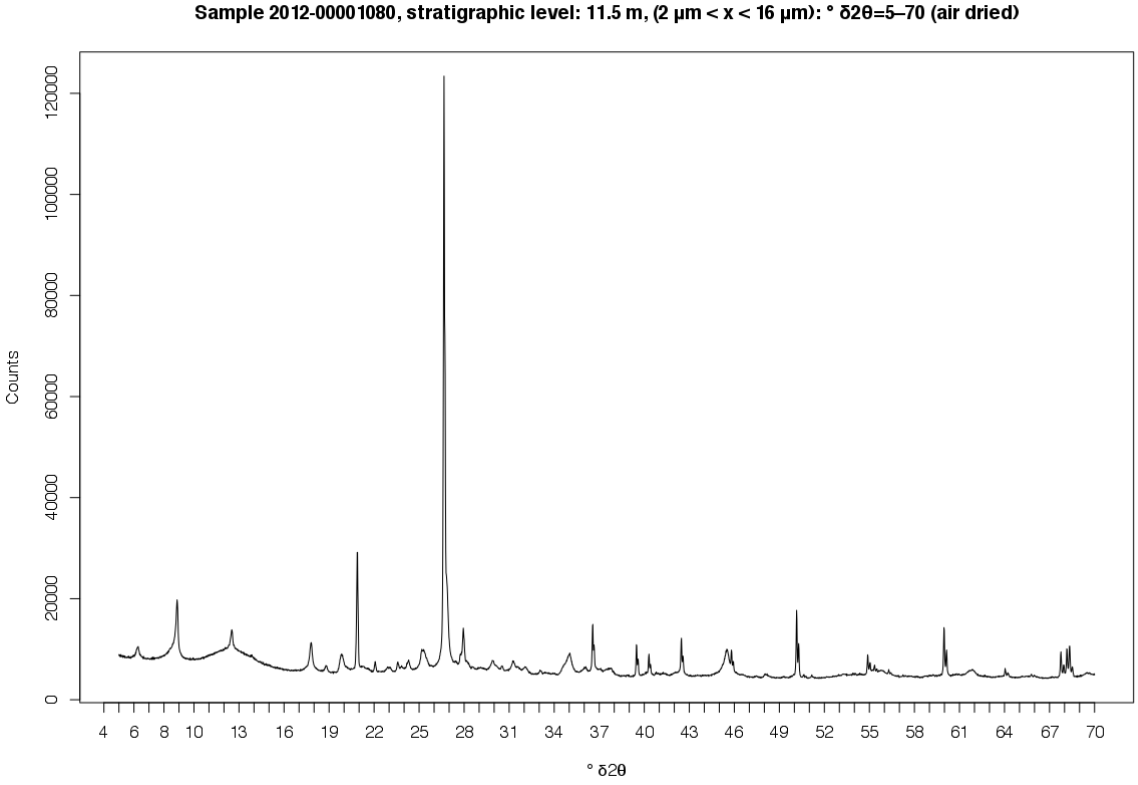
Sample 2012-00001080, stratigraphic level: 11.5 m, (2 µm < x < 16 µm): ° δ2θ=5–70 (air dried)
Counts
0
20000
40000
60000
80000
100000
120000
4 6 8 10 13 16 19 22 25 28 31 34 37 40 43 46 49 52 55 58 61 64 67 70
° δ2θ

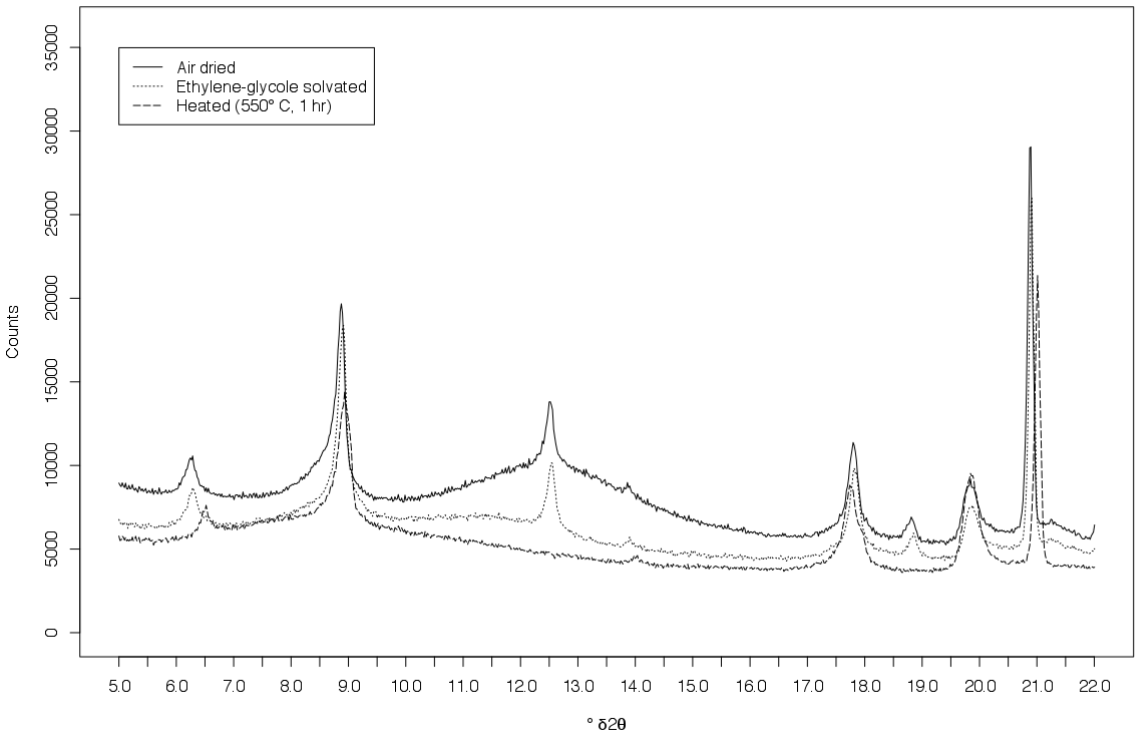
Sample 2012-00001080, stratigraphic level: 11.5 m, (2 µm < x < 16 µm): ° δ2θ=0–22
Air dried
Ethylene-glycole solvated
Heated (550° C, 1 hr)
Counts
0
5000
10000
15000
20000
25000
30000
35000
5.0 6.0 7.0 8.0 9.0 10.0 11.0 12.0 13.0 14.0 15.0 16.0 17.0 18.0 19.0 20.0 21.0 22.0
° δ2θ

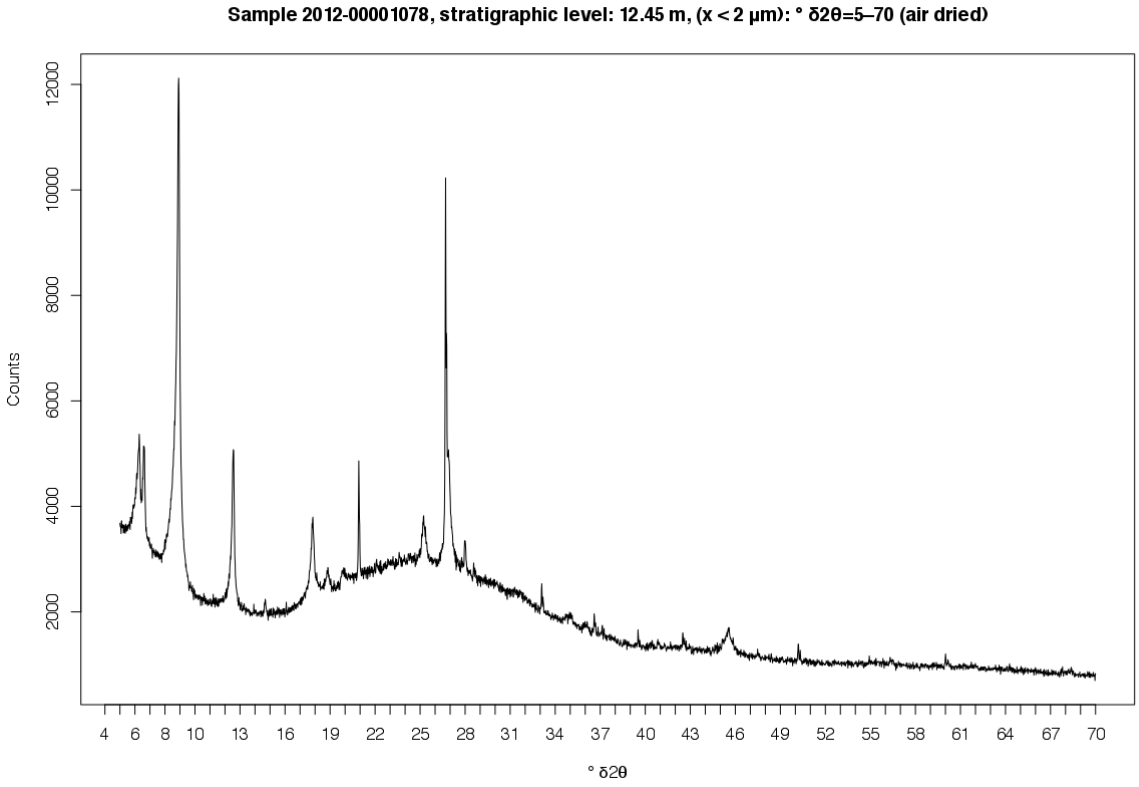
Sample 2012-00001078, stratigraphic level: 12.45 m, (x < 2 µm): ° δ2θ=5–70 (air dried)
Counts
2000
4000
6000
8000
10000
12000
4 6 8 10 13 16 19 22 25 28 31 34 37 40 43 46 49 52 55 58 61 64 67 70
° δ2θ

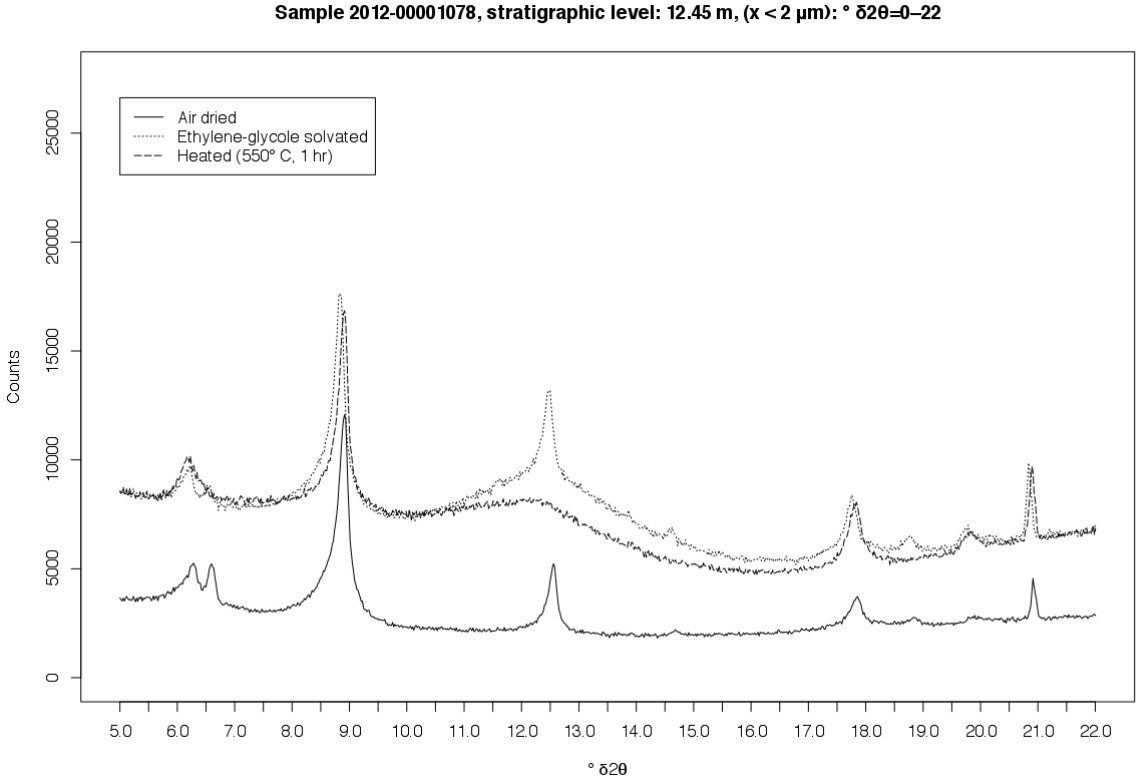
Sample 2012-00001078, stratigraphic level: 12.45 m, (x < 2 µm): ° δ2θ=0–22
Air dried
Ethylene-glycole solvated
Heated (550° C, 1 hr)
Counts
0
5000
10000
15000
20000
25000
5.0 6.0 7.0 8.0 9.0 10.0 11.0 12.0 13.0 14.0 15.0 16.0 17.0 18.0 19.0 20.0 21.0 22.0
° δ2θ

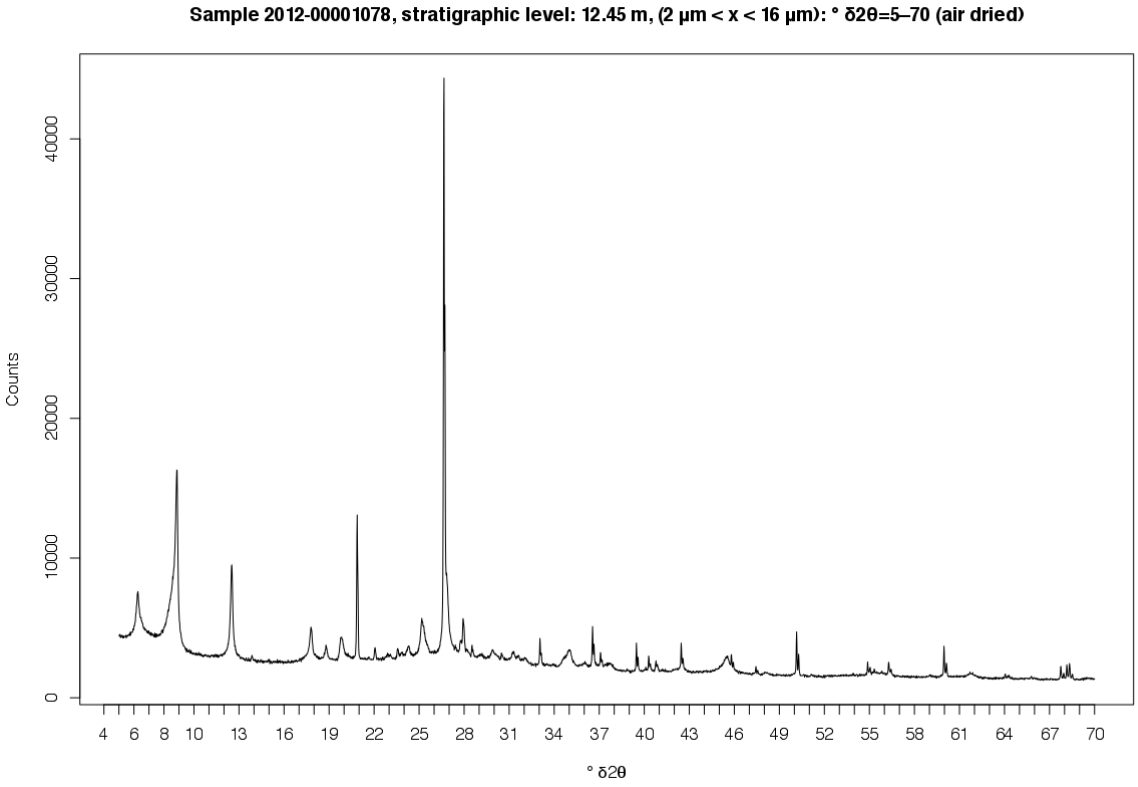
Sample 2012-00001078, stratigraphic level: 12.45 m, (2 µm < x < 16 µm): ° δ2θ=5–70 (air dried)
Counts
0
10000
20000
30000
40000
4 6 8 10 13 16 19 22 25 28 31 34 37 40 43 46 49 52 55 58 61 64 67 70
° δ2θ

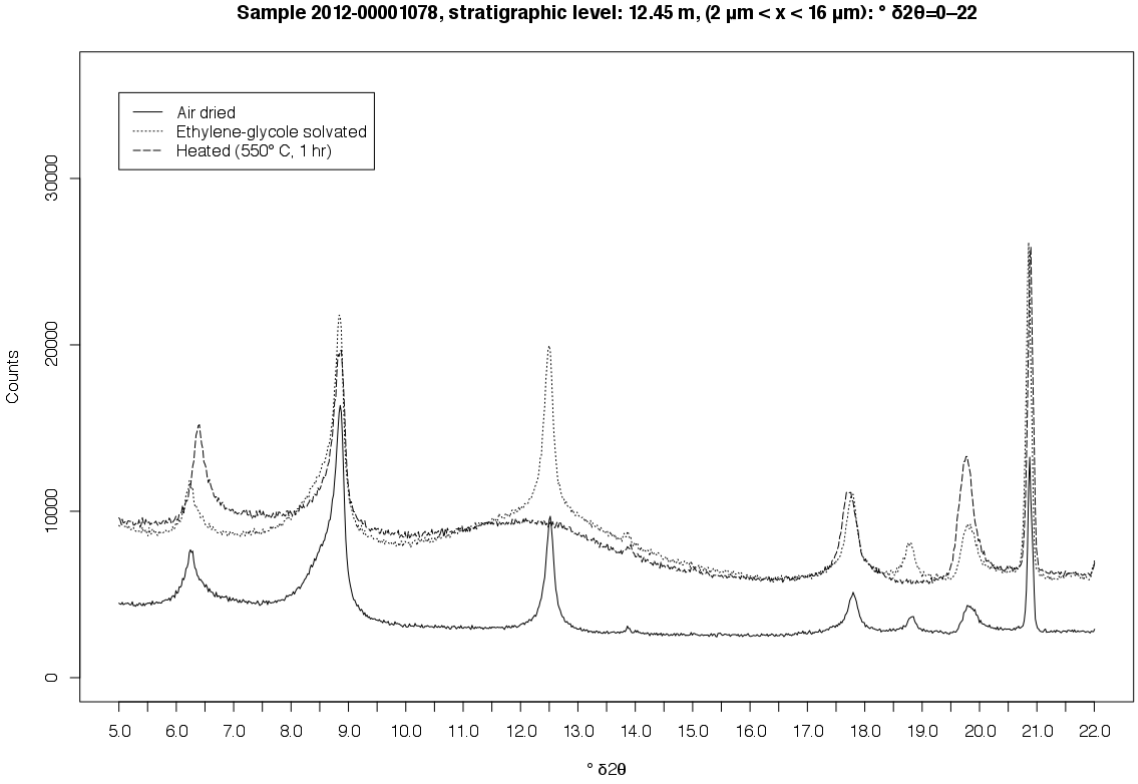
Sample 2012-00001078, stratigraphic level: 12.45 m, (2 µm < x < 16 µm): ° δ2θ=0–22
Air dried
Ethylene-glycole solvated
Heated (550° C, 1 hr)
Counts
0
10000
20000
30000
5.0 6.0 7.0 8.0 9.0 10.0 11.0 12.0 13.0 14.0 15.0 16.0 17.0 18.0 19.0 20.0 21.0 22.0
° δ2θ

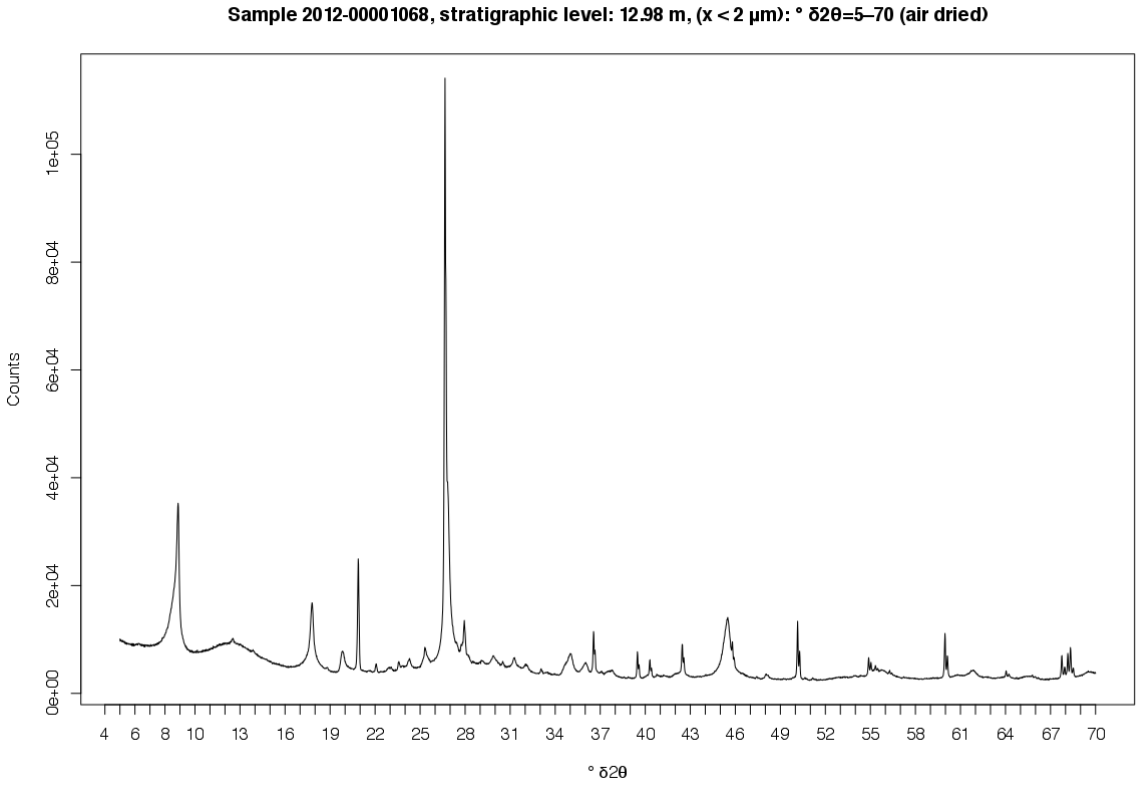
Sample 2012-00001068, stratigraphic level: 12.98 m, (x < 2 µm): ° δ2θ=5–70 (air dried)
Counts
0e+00
2e+04
4e+04
6e+04
8e+04
1e+05
4 6 8 10 13 16 19 22 25 28 31 34 37 40 43 46 49 52 55 58 61 64 67 70
° δ2θ

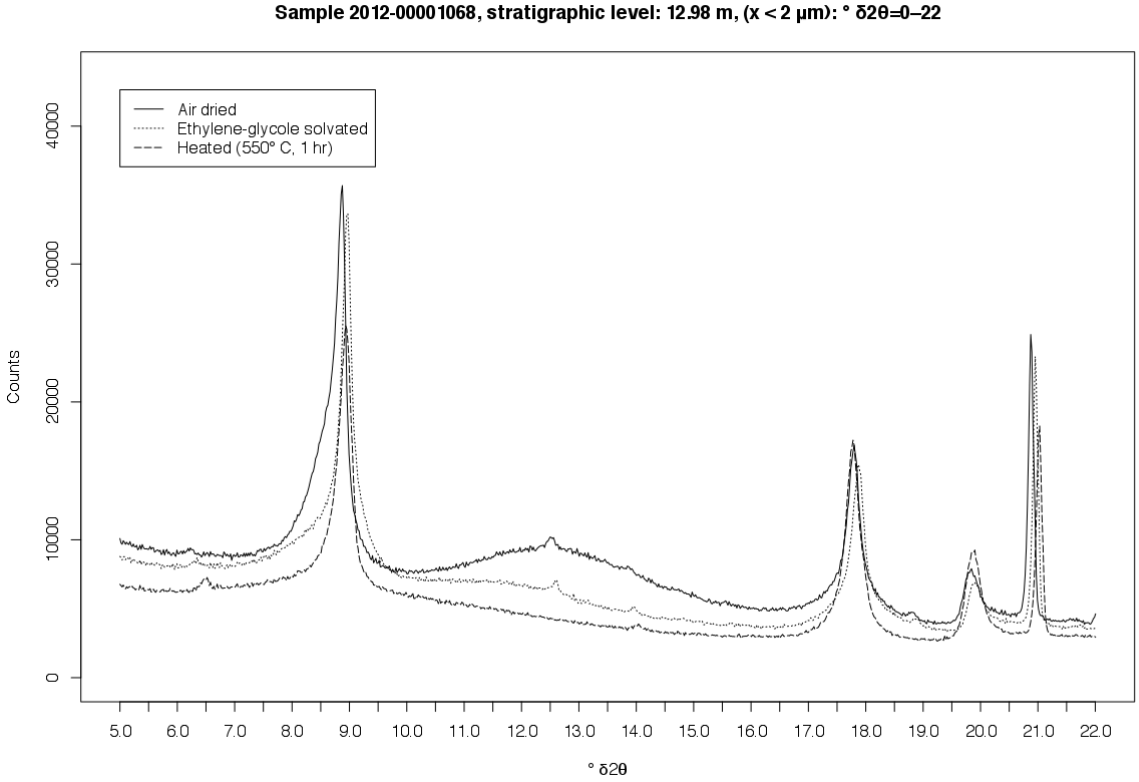
Sample 2012-00001068, stratigraphic level: 12.98 m, (x < 2 µm): ° δ2θ=0–22
Air dried
Ethylene-glycole solvated
Heated (550° C, 1 hr)
Counts
0
10000
20000
30000
40000
5.0 6.0 7.0 8.0 9.0 10.0 11.0 12.0 13.0 14.0 15.0 16.0 17.0 18.0 19.0 20.0 21.0 22.0
° δ2θ

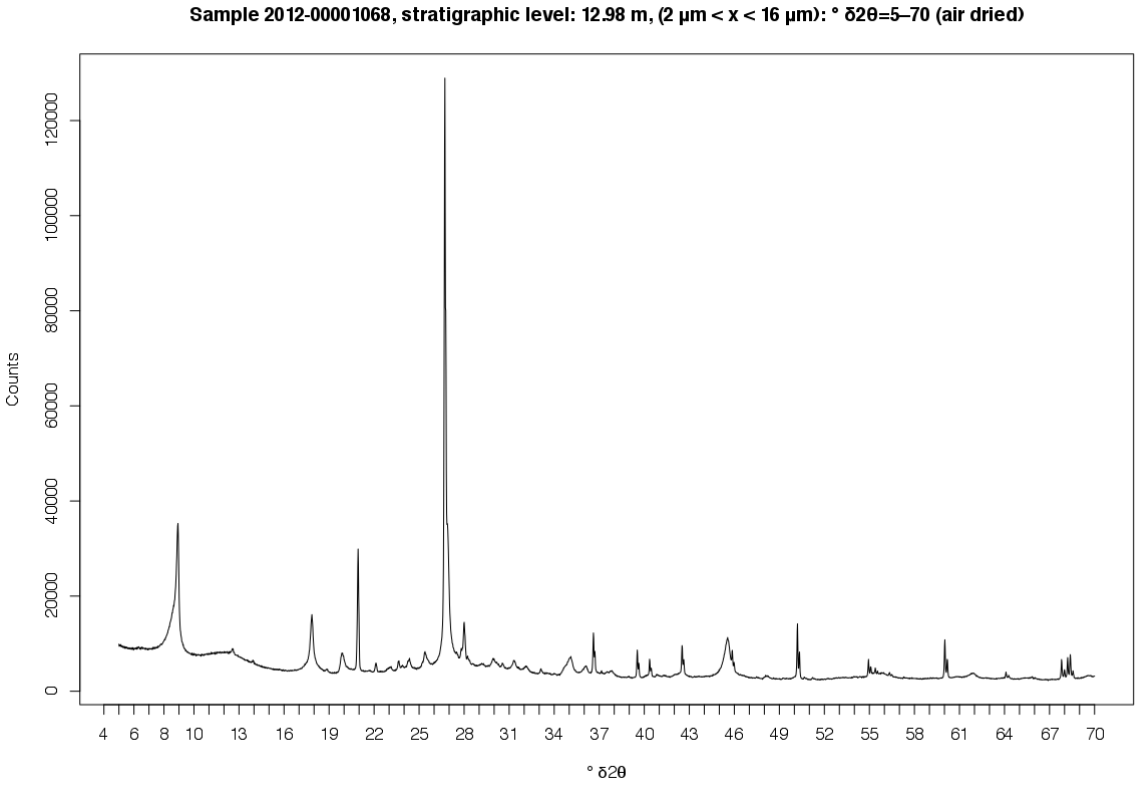
Sample 2012-00001068, stratigraphic level: 12.98 m, (2 µm < x < 16 µm): ° δ2θ=5–70 (air dried)
Counts
0
20000
40000
60000
80000
100000
120000
4 6 8 10 13 16 19 22 25 28 31 34 37 40 43 46 49 52 55 58 61 64 67 70
° δ2θ

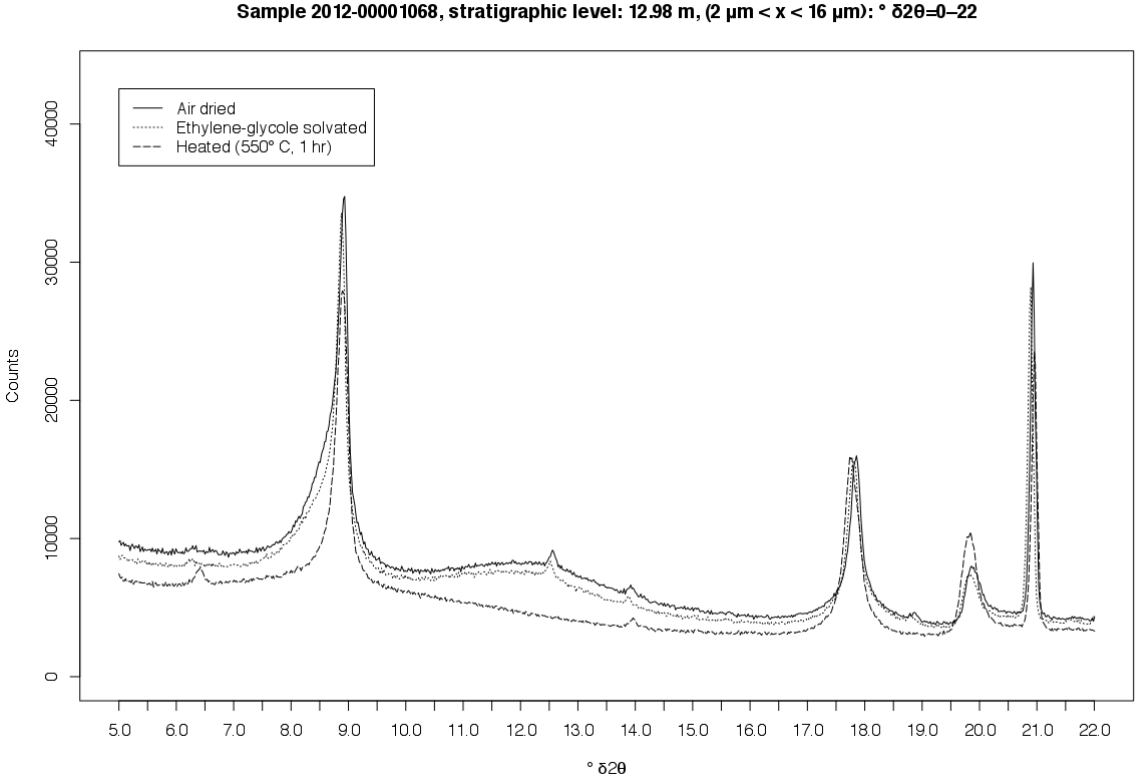
Sample 2012-00001068, stratigraphic level: 12.98 m, (2 µm < x < 16 µm): ° δ2θ=0–22
Air dried
Ethylene-glycole solvated
Heated (550° C, 1 hr)
Counts
0
10000
20000
30000
40000
5.0 6.0 7.0 8.0 9.0 10.0 11.0 12.0 13.0 14.0 15.0 16.0 17.0 18.0 19.0 20.0 21.0 22.0
° δ2θ

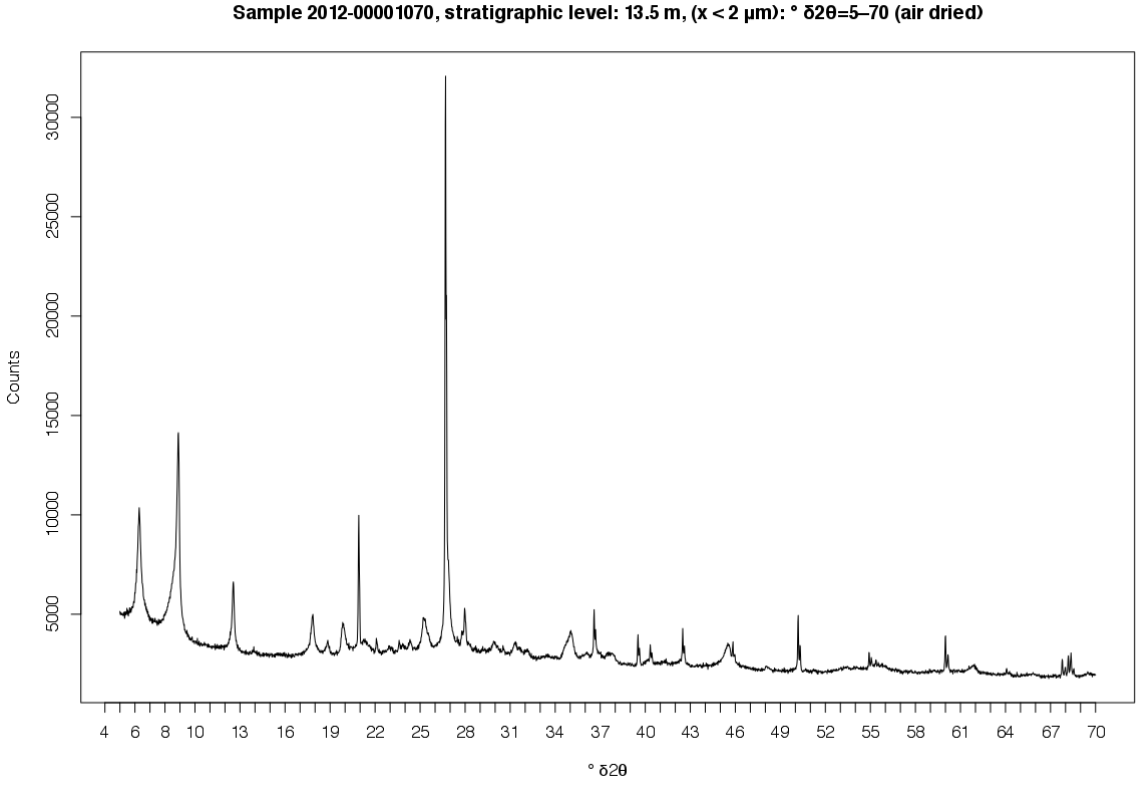
Sample 2012-00001070, stratigraphic level: 13.5 m, (x < 2 µm): ° δ2θ=5–70 (air dried)
Counts
5000
10000
15000
20000
25000
30000
4 6 8 10 13 16 19 22 25 28 31 34 37 40 43 46 49 52 55 58 61 64 67 70
° δ2θ

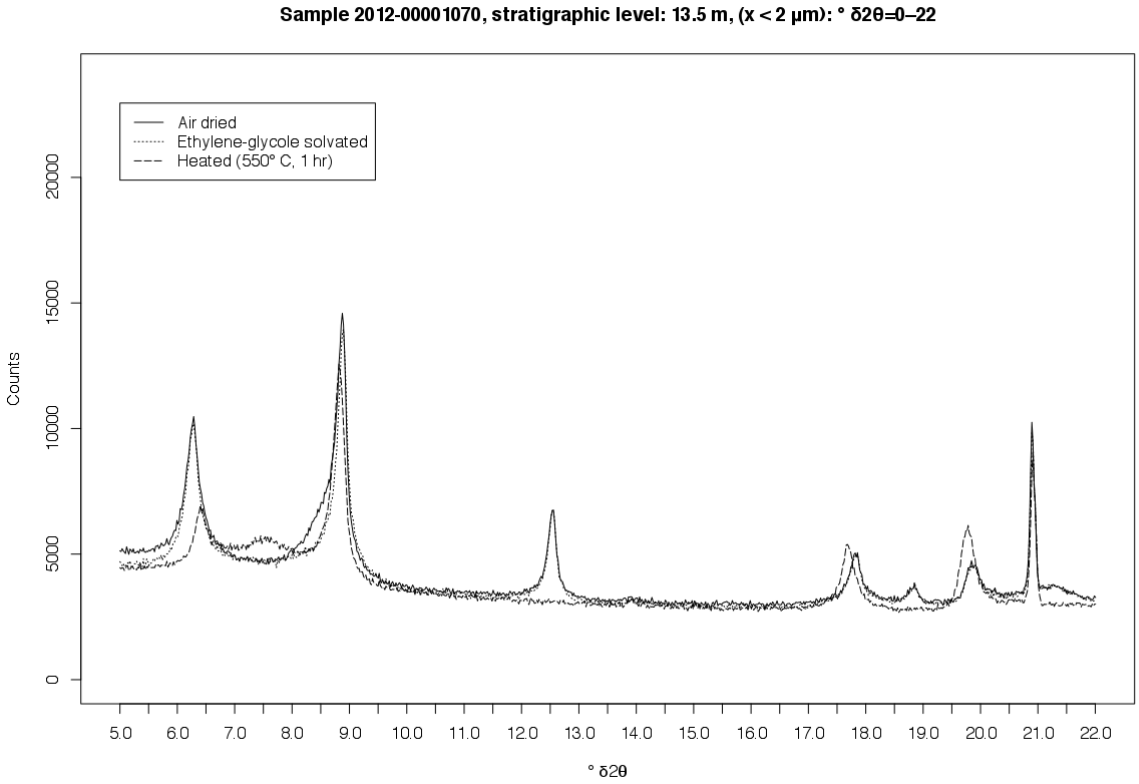
Sample 2012-00001070, stratigraphic level: 13.5 m, (x < 2 µm): ° δ2θ=0–22
Air dried
Ethylene-glycole solvated
Heated (550° C, 1 hr)
Counts
0
5000
10000
15000
20000
5.0 6.0 7.0 8.0 9.0 10.0 11.0 12.0 13.0 14.0 15.0 16.0 17.0 18.0 19.0 20.0 21.0 22.0
° δ2θ

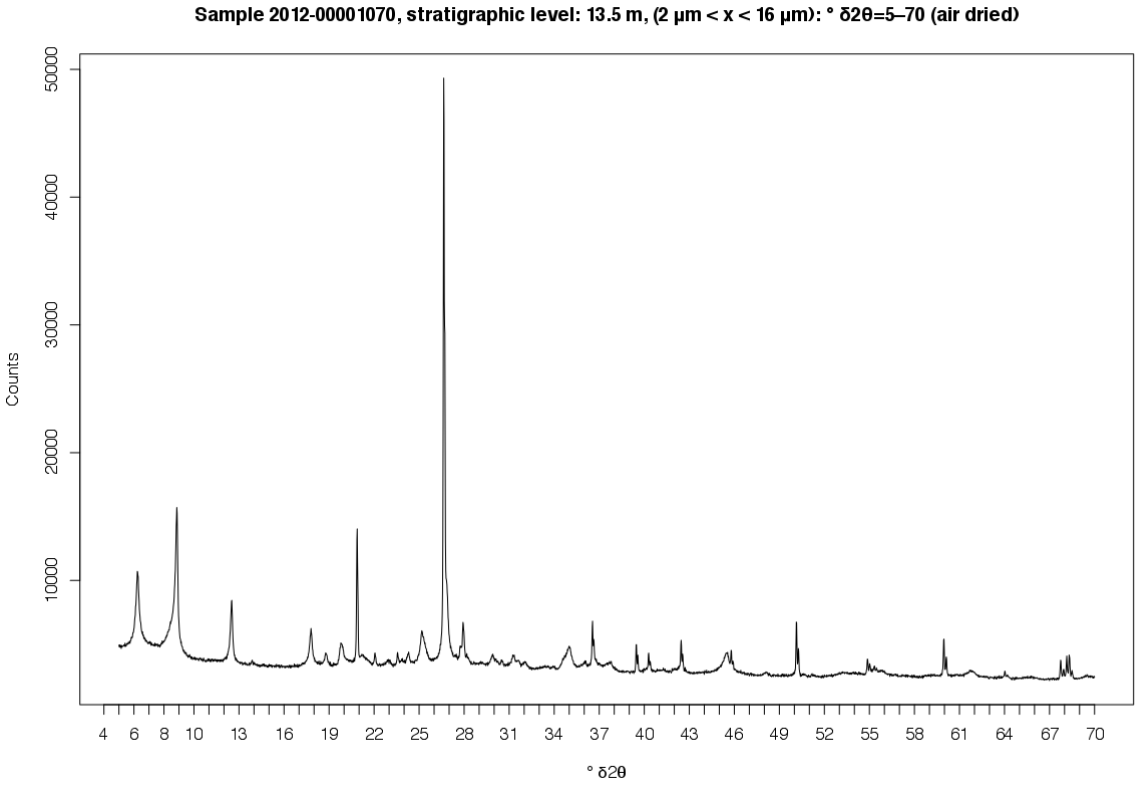
Sample 2012-00001070, stratigraphic level: 13.5 m, (2 µm < x < 16 µm): ° δ2θ=5–70 (air dried)
Counts
10000
20000
30000
40000
50000
4 6 8 10 13 16 19 22 25 28 31 34 37 40 43 46 49 52 55 58 61 64 67 70
° δ2θ

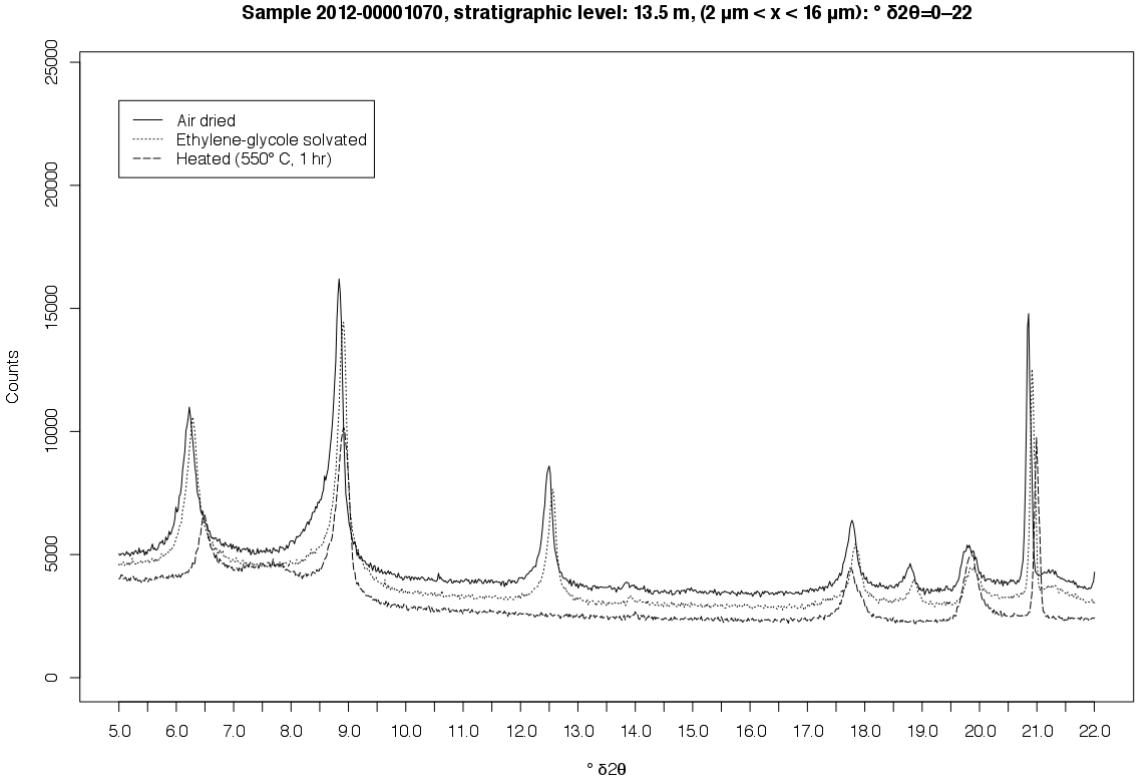
Sample 2012-00001070, stratigraphic level: 13.5 m, (2 µm < x < 16 µm): ° δ2θ=0–22
Air dried
Ethylene-glycole solvated
Heated (550° C, 1 hr)
Counts
0
5000
10000
15000
20000
25000
5.0 6.0 7.0 8.0 9.0 10.0 11.0 12.0 13.0 14.0 15.0 16.0 17.0 18.0 19.0 20.0 21.0 22.0
° δ2θ

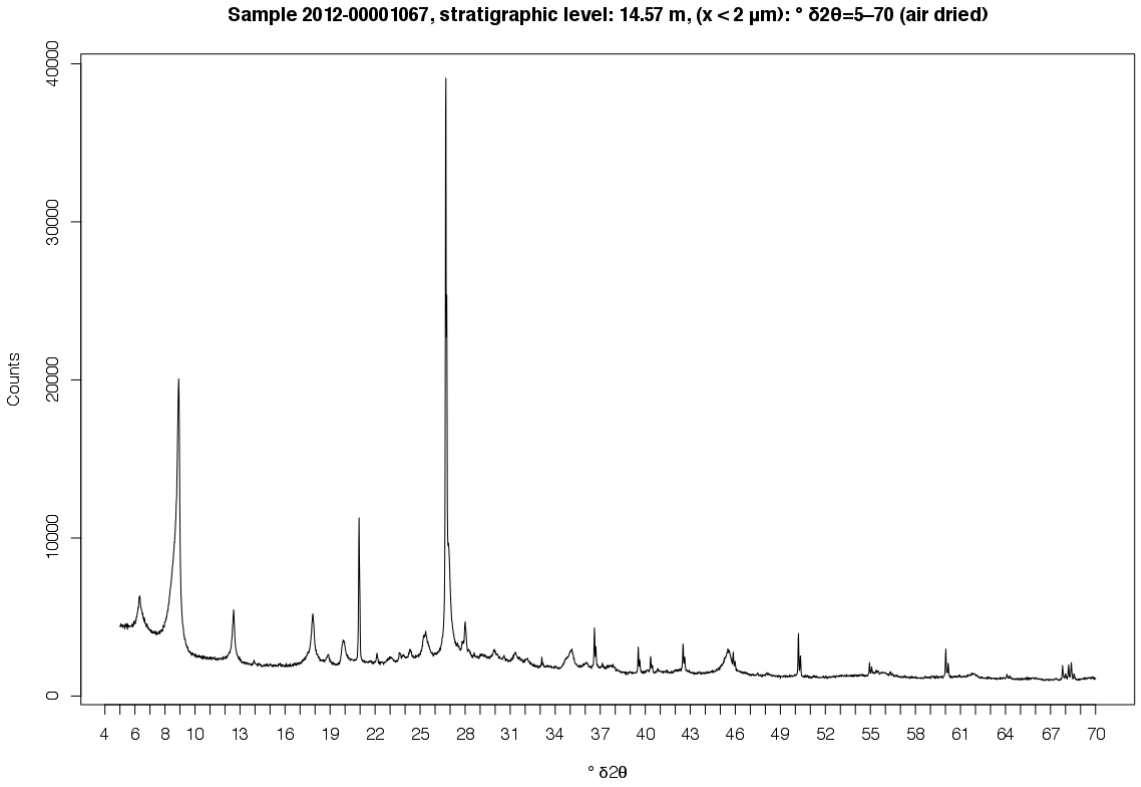
Sample 2012-00001067, stratigraphic level: 14.57 m, (x < 2 µm): ° δ2θ=5–70 (air dried)
Counts
0
10000
20000
30000
40000
4 6 8 10 13 16 19 22 25 28 31 34 37 40 43 46 49 52 55 58 61 64 67 70
° δ2θ

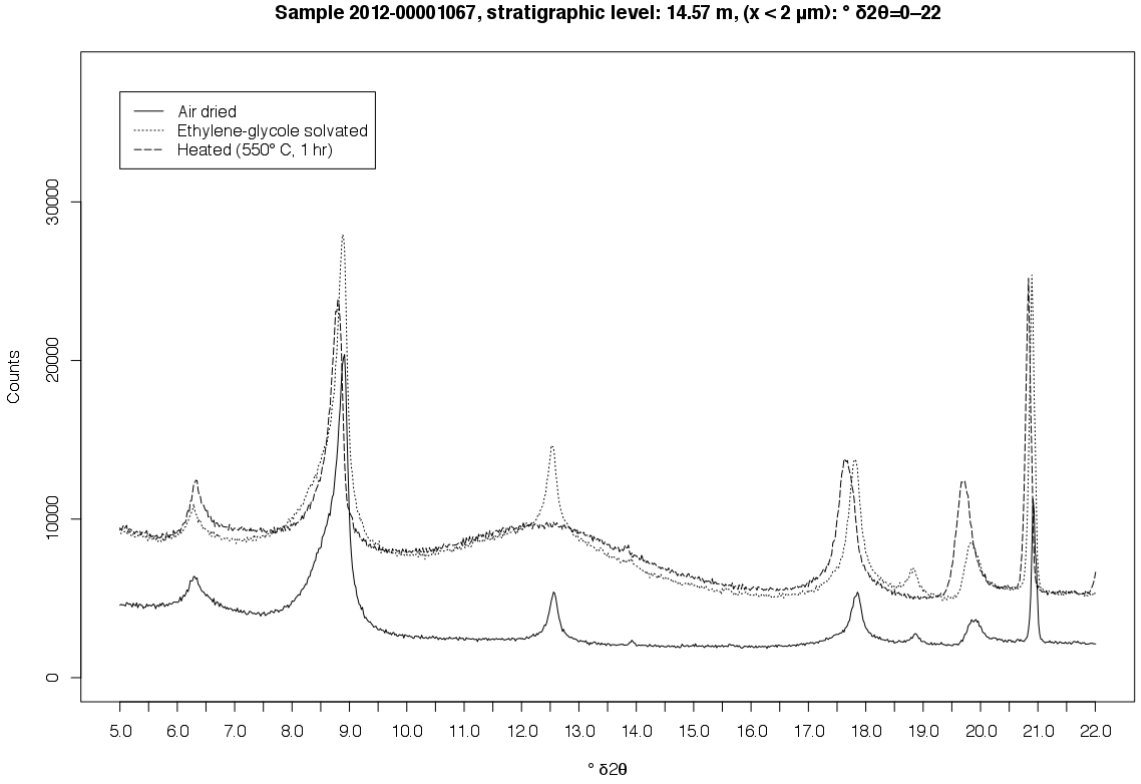
Sample 2012-00001067, stratigraphic level: 14.57 m, (x < 2 µm): ° δ2θ=0–22
Air dried
Ethylene-glycole solvated
Heated (550° C, 1 hr)
Counts
0
10000
20000
30000
5.0 6.0 7.0 8.0 9.0 10.0 11.0 12.0 13.0 14.0 15.0 16.0 17.0 18.0 19.0 20.0 21.0 22.0
° δ2θ

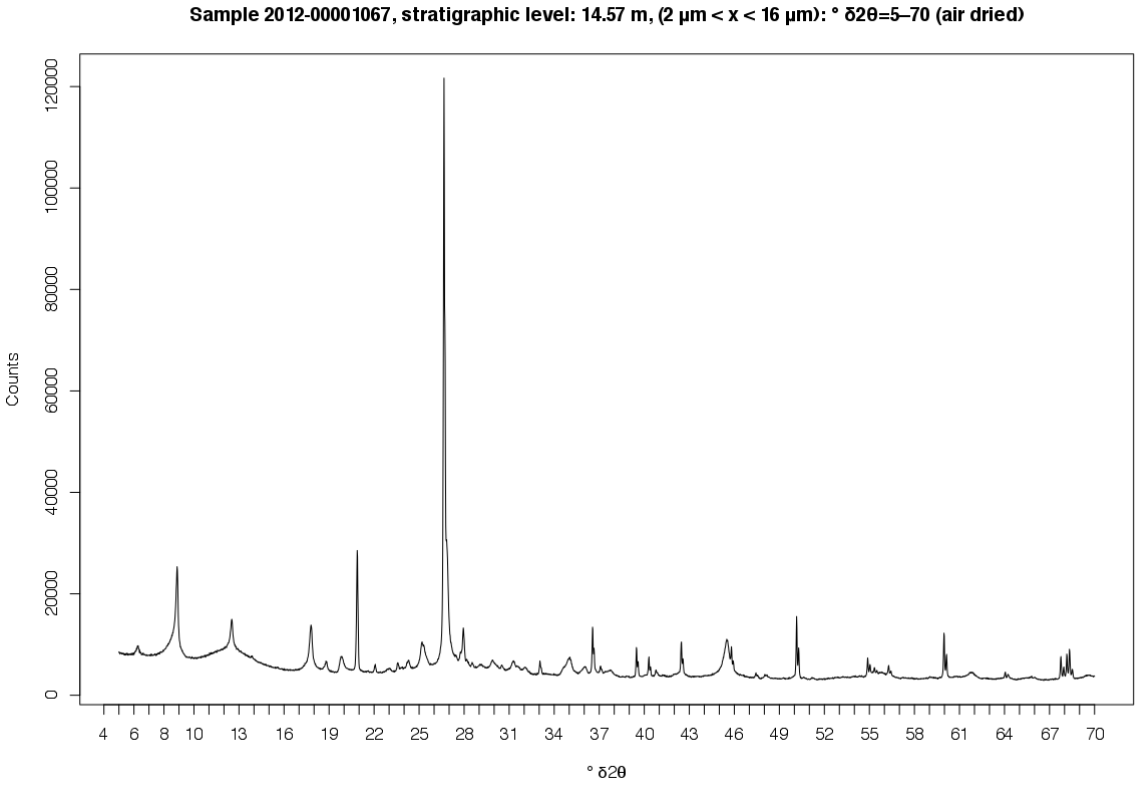
Sample 2012-00001067, stratigraphic level: 14.57 m, (2 µm < x < 16 µm): ° δ2θ=5–70 (air dried)
Counts
0
20000
40000
60000
80000
100000
120000
4 6 8 10 13 16 19 22 25 28 31 34 37 40 43 46 49 52 55 58 61 64 67 70
° δ2θ

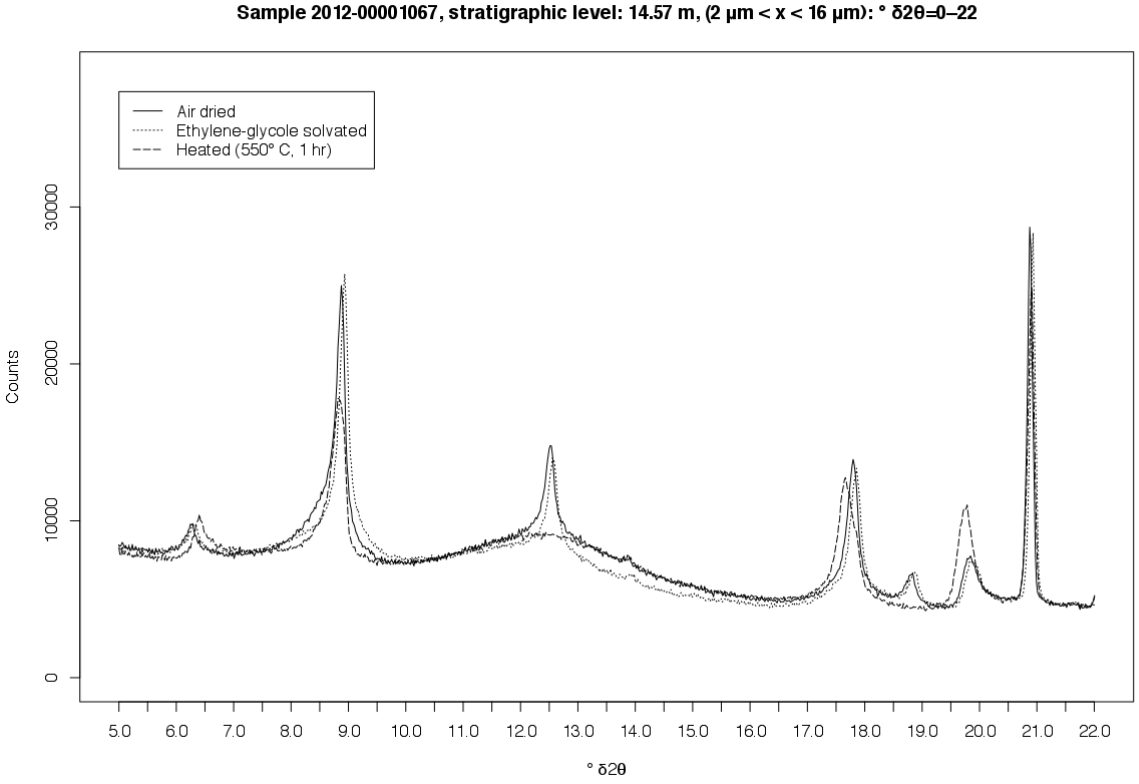
Sample 2012-00001067, stratigraphic level: 14.57 m, (2 µm < x < 16 µm): ° δ2θ=0–22
Air dried
Ethylene-glycole solvated
Heated (550° C, 1 hr)
Counts
0
10000
20000
30000
5.0 6.0 7.0 8.0 9.0 10.0 11.0 12.0 13.0 14.0 15.0 16.0 17.0 18.0 19.0 20.0 21.0 22.0
° δ2θ

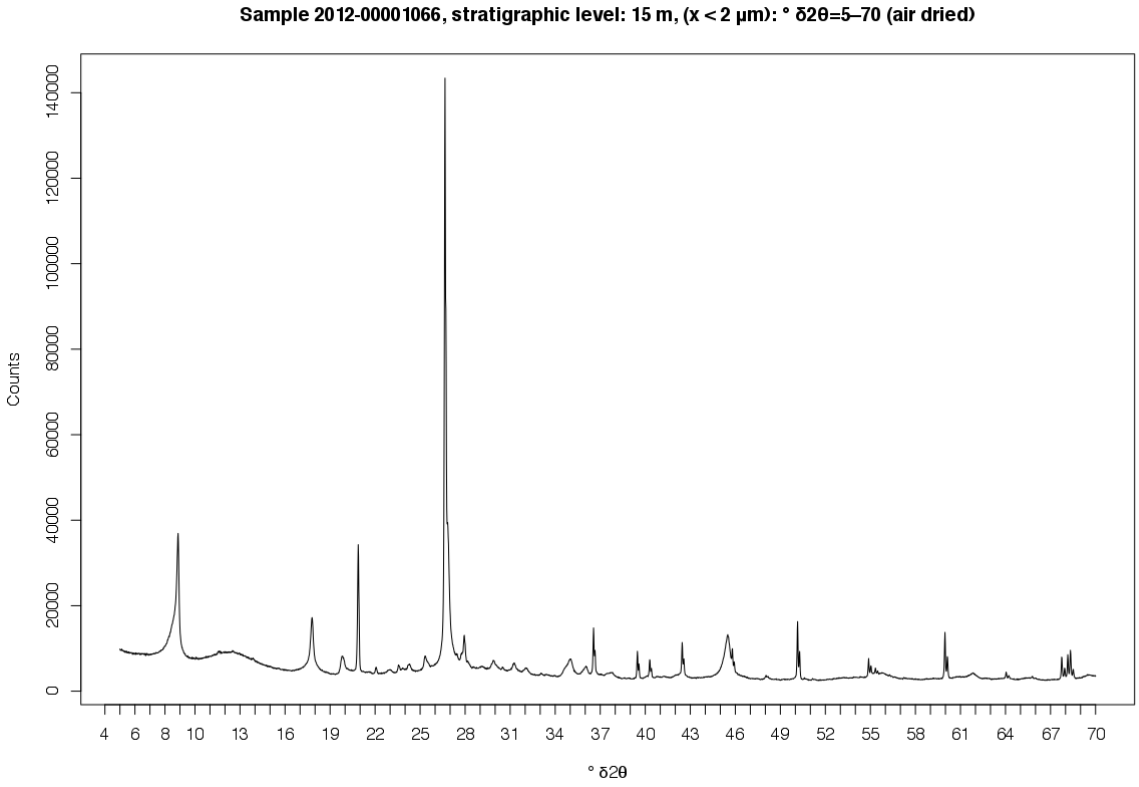
Sample 2012-00001066, stratigraphic level: 15 m, (x < 2 µm): ° δ2θ=5–70 (air dried)
Counts
0
20000
40000
60000
80000
100000
120000
140000
4 6 8 10 13 16 19 22 25 28 31 34 37 40 43 46 49 52 55 58 61 64 67 70
° δ2θ

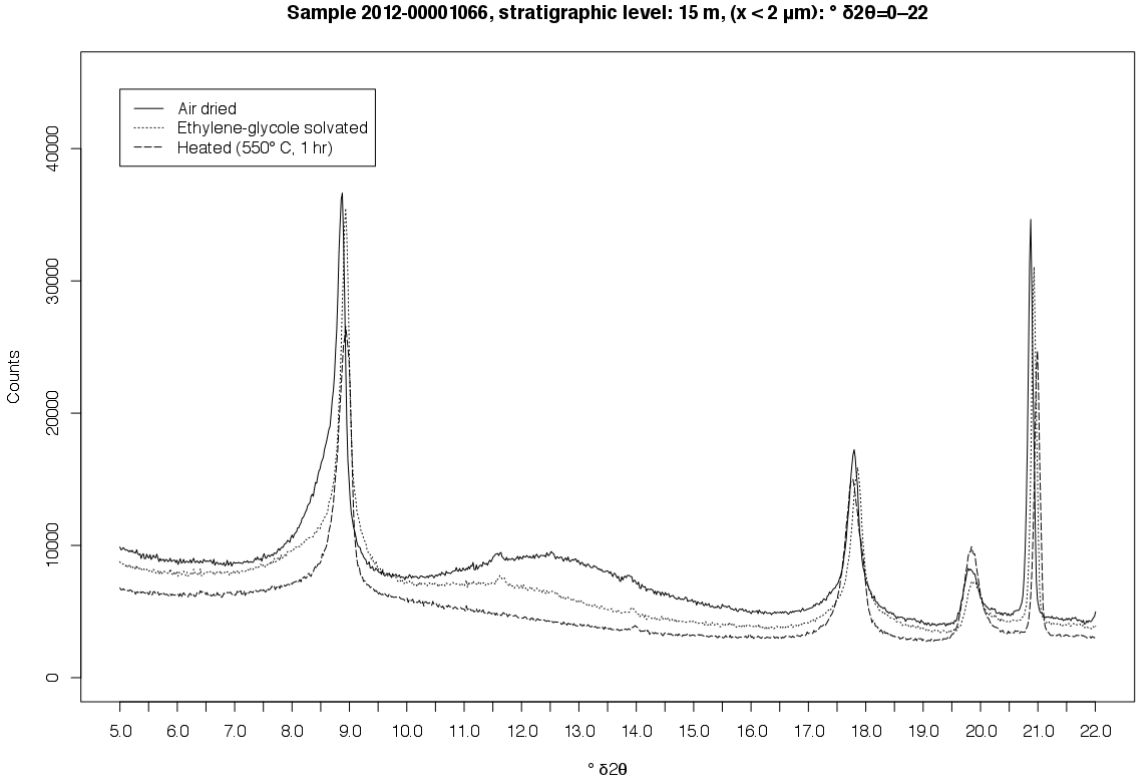
Sample 2012-00001066, stratigraphic level: 15 m, (x < 2 µm): ° δ2θ=0–22
Air dried
Ethylene-glycole solvated
Heated (550° C, 1 hr)
Counts
0
10000
20000
30000
40000
5.0 6.0 7.0 8.0 9.0 10.0 11.0 12.0 13.0 14.0 15.0 16.0 17.0 18.0 19.0 20.0 21.0 22.0
° δ2θ

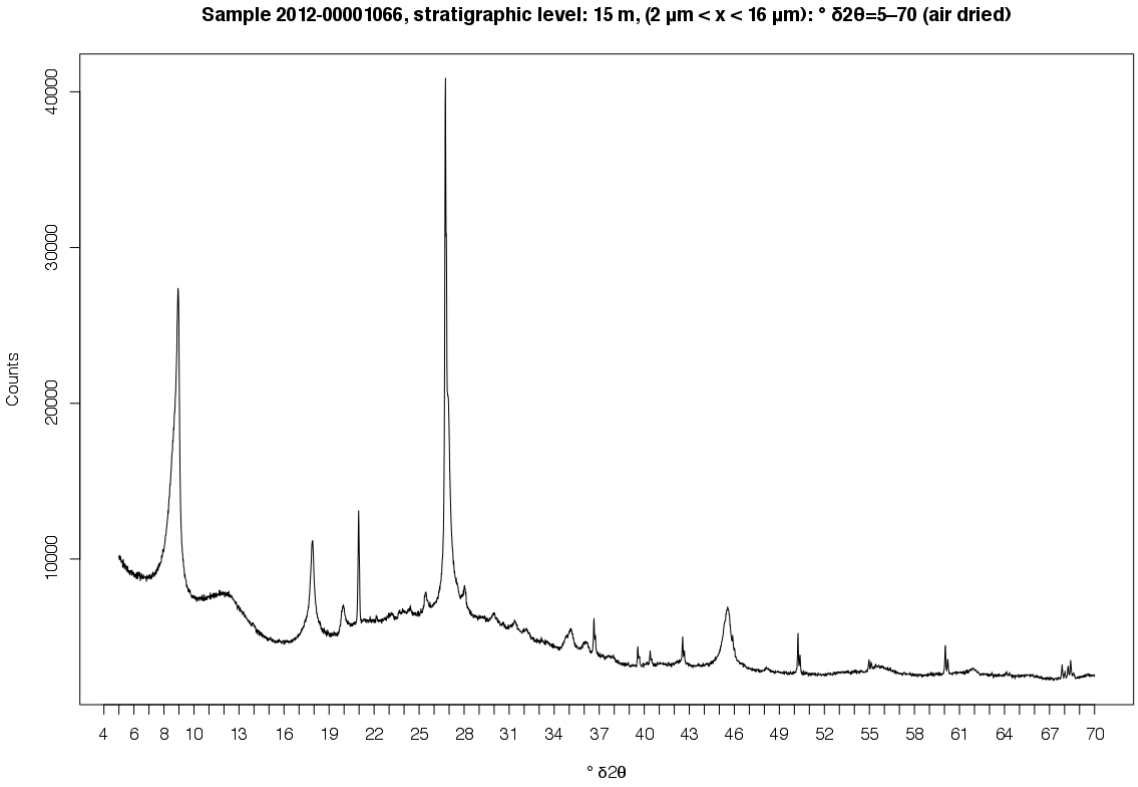
Sample 2012-00001066, stratigraphic level: 15 m, (2 µm < x < 16 µm): ° δ2θ=5–70 (air dried)
Counts
10000
20000
30000
40000
4 6 8 10 13 16 19 22 25 28 31 34 37 40 43 46 49 52 55 58 61 64 67 70
° δ2θ

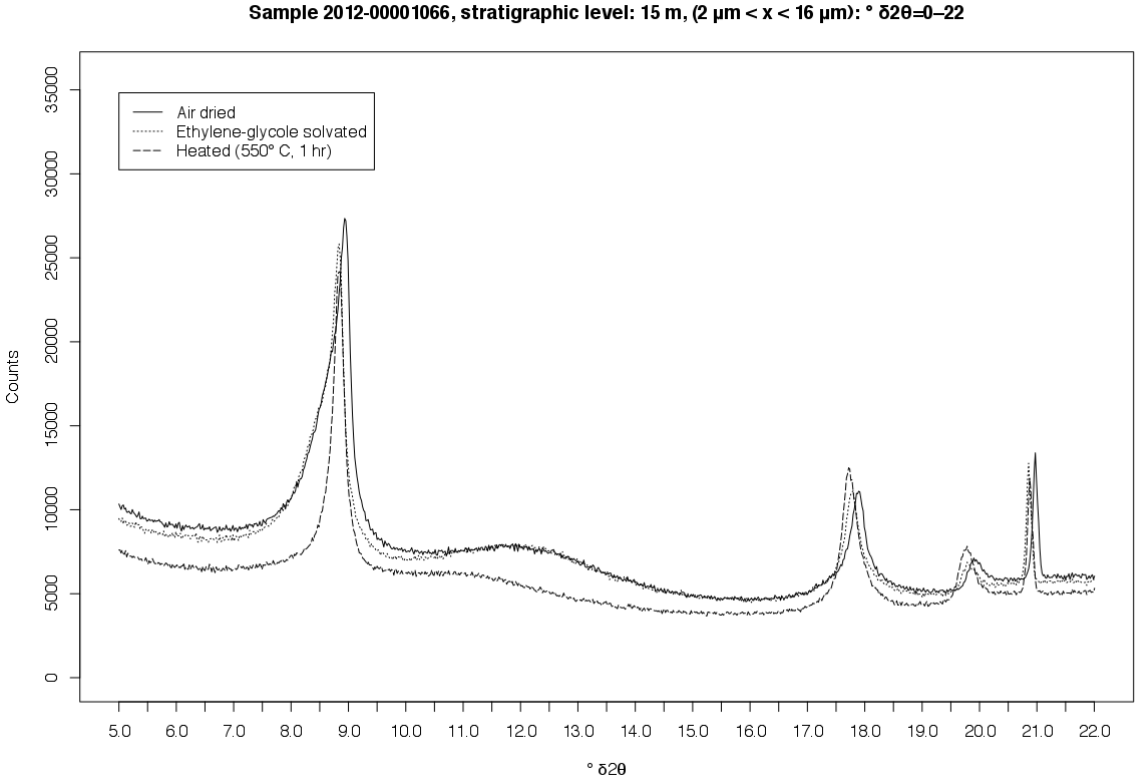
Sample 2012-00001066, stratigraphic level: 15 m, (2 µm < x < 16 µm): ° δ2θ=0–22
Air dried
Ethylene-glycole solvated
Heated (550° C, 1 hr)
Counts
0
5000
10000
15000
20000
25000
30000
35000
5.0 6.0 7.0 8.0 9.0 10.0 11.0 12.0 13.0 14.0 15.0 16.0 17.0 18.0 19.0 20.0 21.0 22.0
° δ2θ

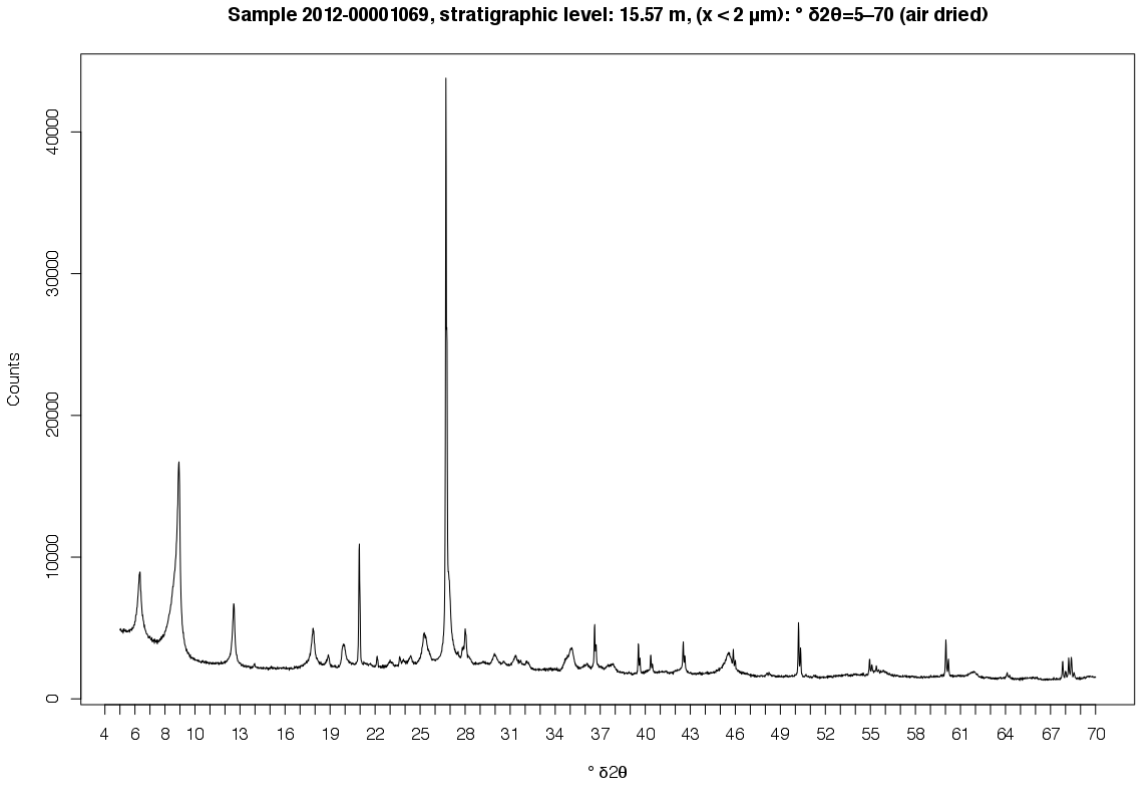
Sample 2012-00001069, stratigraphic level: 15.57 m, (x < 2 µm): ° δ2θ=5–70 (air dried)
Counts
0
10000
20000
30000
40000
4 6 8 10 13 16 19 22 25 28 31 34 37 40 43 46 49 52 55 58 61 64 67 70
° δ2θ

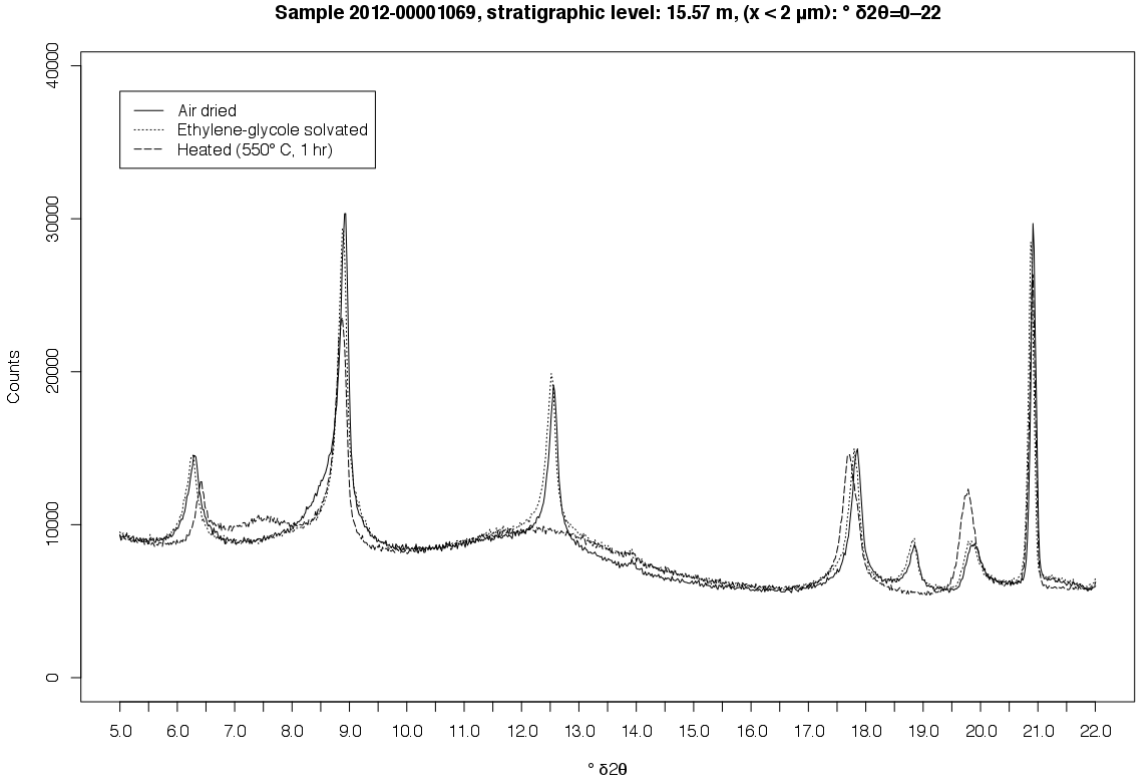
Sample 2012-00001069, stratigraphic level: 15.57 m, (x < 2 µm): ° δ2θ=0–22
Air dried
Ethylene-glycole solvated
Heated (550° C, 1 hr)
Counts
0
10000
20000
30000
40000
5.0 6.0 7.0 8.0 9.0 10.0 11.0 12.0 13.0 14.0 15.0 16.0 17.0 18.0 19.0 20.0 21.0 22.0
° δ2θ

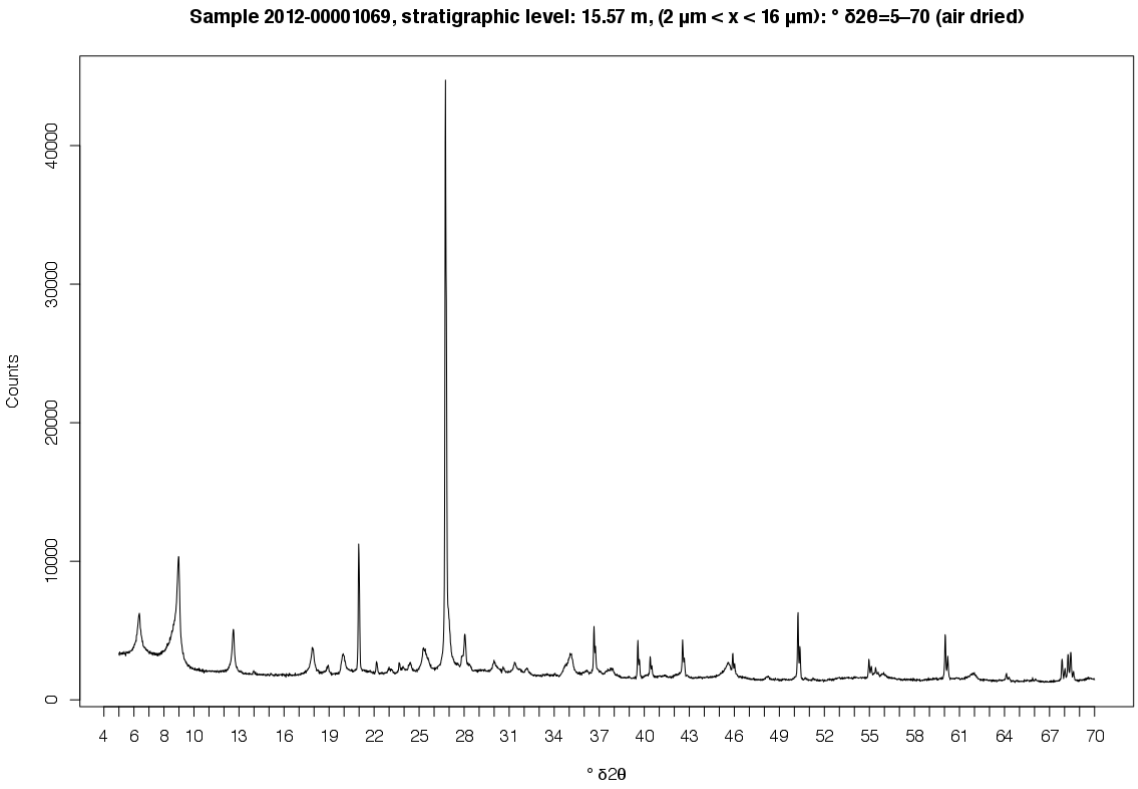
Sample 2012-00001069, stratigraphic level: 15.57 m, (2 µm < x < 16 µm): ° δ2θ=5–70 (air dried)
Counts
0
10000
20000
30000
40000
4 6 8 10 13 16 19 22 25 28 31 34 37 40 43 46 49 52 55 58 61 64 67 70
° δ2θ

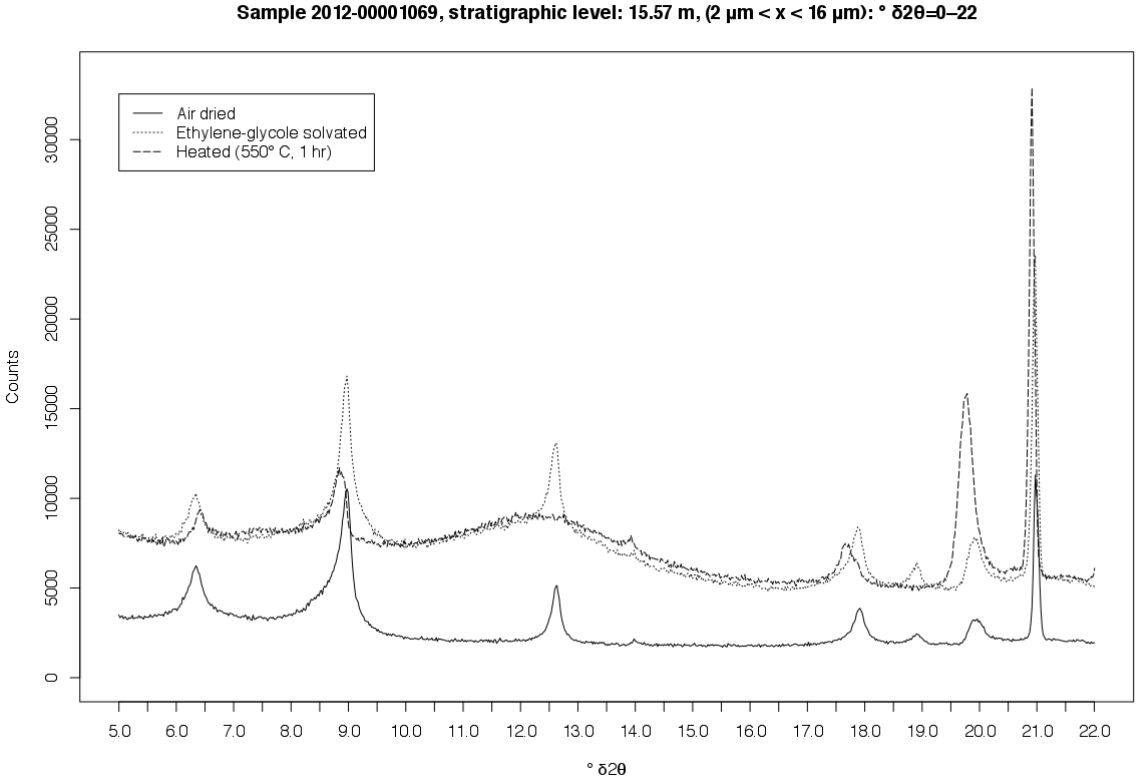
Sample 2012-00001069, stratigraphic level: 15.57 m, (2 µm < x < 16 µm): ° δ2θ=0–22
Air dried
Ethylene-glycole solvated
Heated (550° C, 1 hr)
Counts
0
5000
10000
15000
20000
25000
30000
5.0 6.0 7.0 8.0 9.0 10.0 11.0 12.0 13.0 14.0 15.0 16.0 17.0 18.0 19.0 20.0 21.0 22.0
° δ2θ

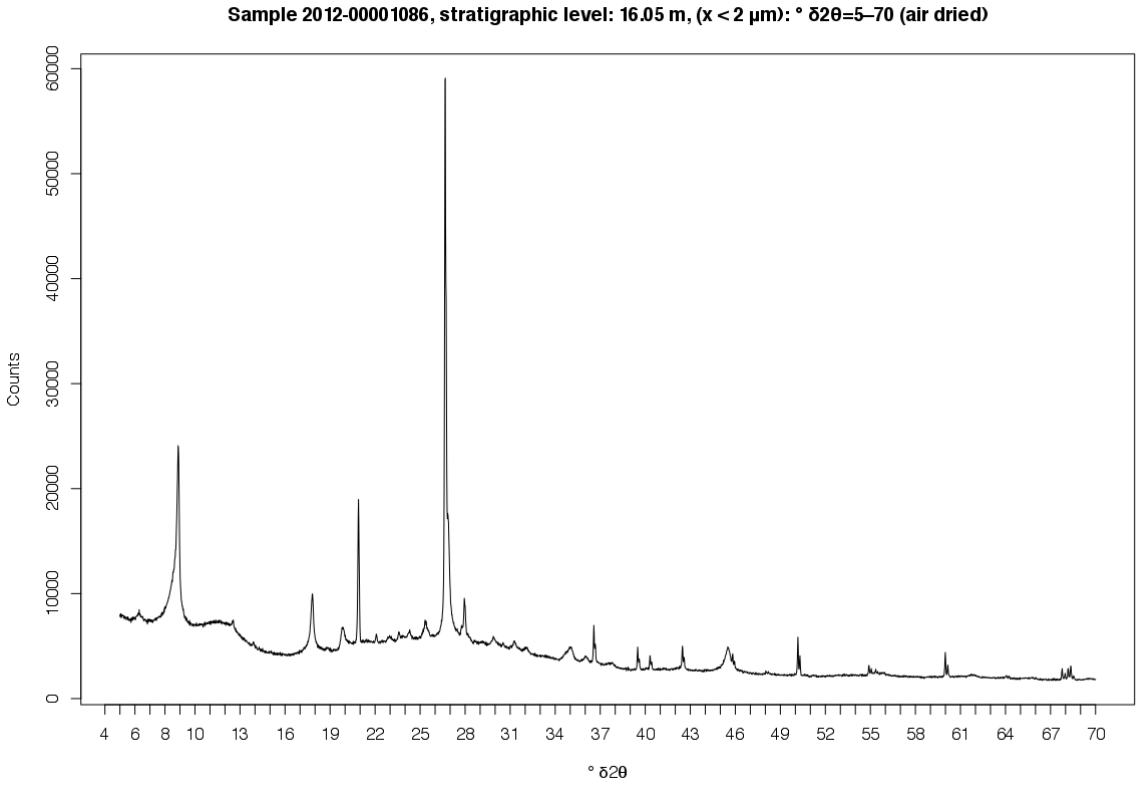
Sample 2012-00001086, stratigraphic level: 16.05 m, (x < 2 µm): ° δ2θ=5–70 (air dried)
Counts
0
10000
20000
30000
40000
50000
60000
4 6 8 10 13 16 19 22 25 28 31 34 37 40 43 46 49 52 55 58 61 64 67 70
° δ2θ

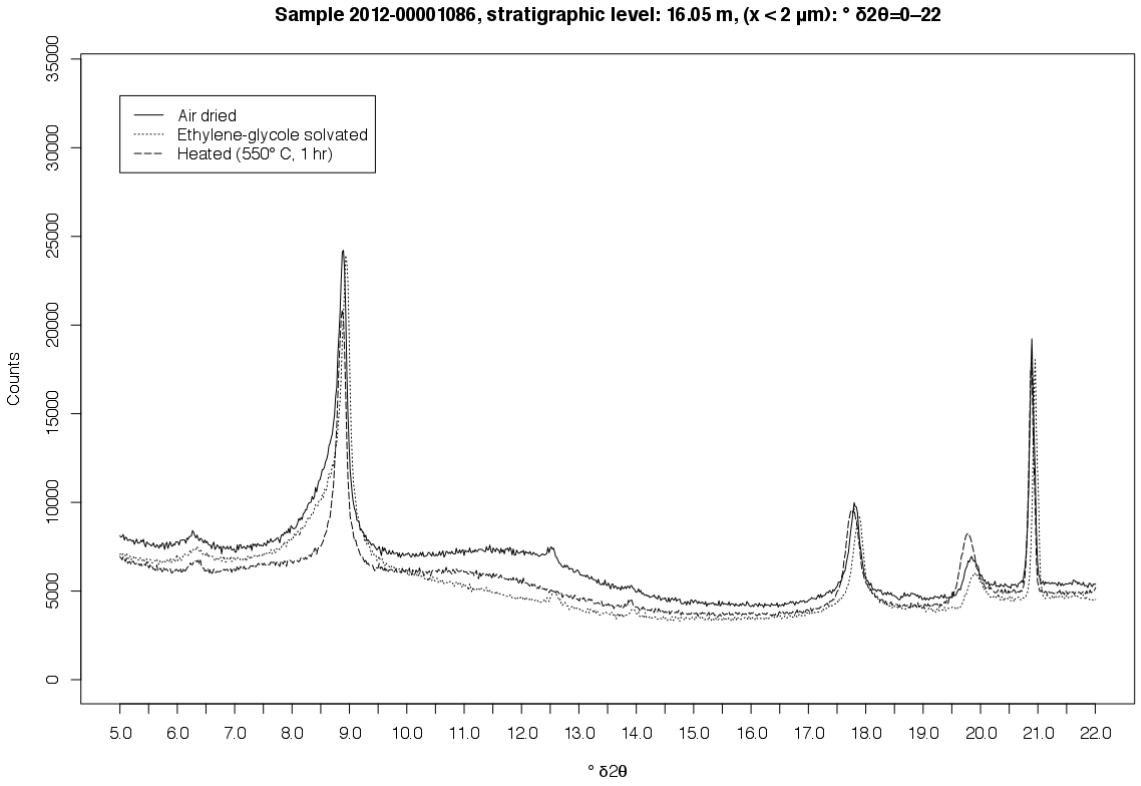
Sample 2012-00001086, stratigraphic level: 16.05 m, (x < 2 µm): ° δ2θ=0–22
Air dried
Ethylene-glycole solvated
Heated (550° C, 1 hr)
Counts
0
5000
10000
15000
20000
25000
30000
35000
5.0 6.0 7.0 8.0 9.0 10.0 11.0 12.0 13.0 14.0 15.0 16.0 17.0 18.0 19.0 20.0 21.0 22.0
° δ2θ

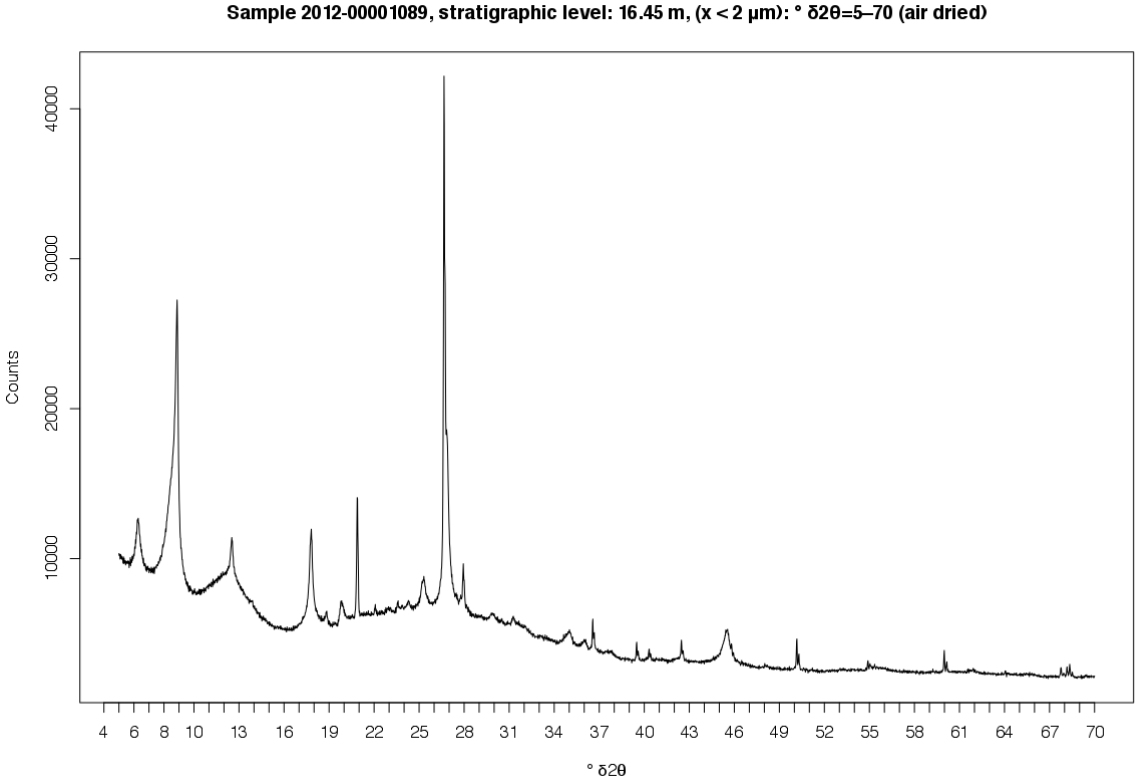
Sample 2012-00001089, stratigraphic level: 16.45 m, (x < 2 µm): ° δ2θ=5–70 (air dried)
Counts
10000
20000
30000
40000
4 6 8 10 13 16 19 22 25 28 31 34 37 40 43 46 49 52 55 58 61 64 67 70
° δ2θ

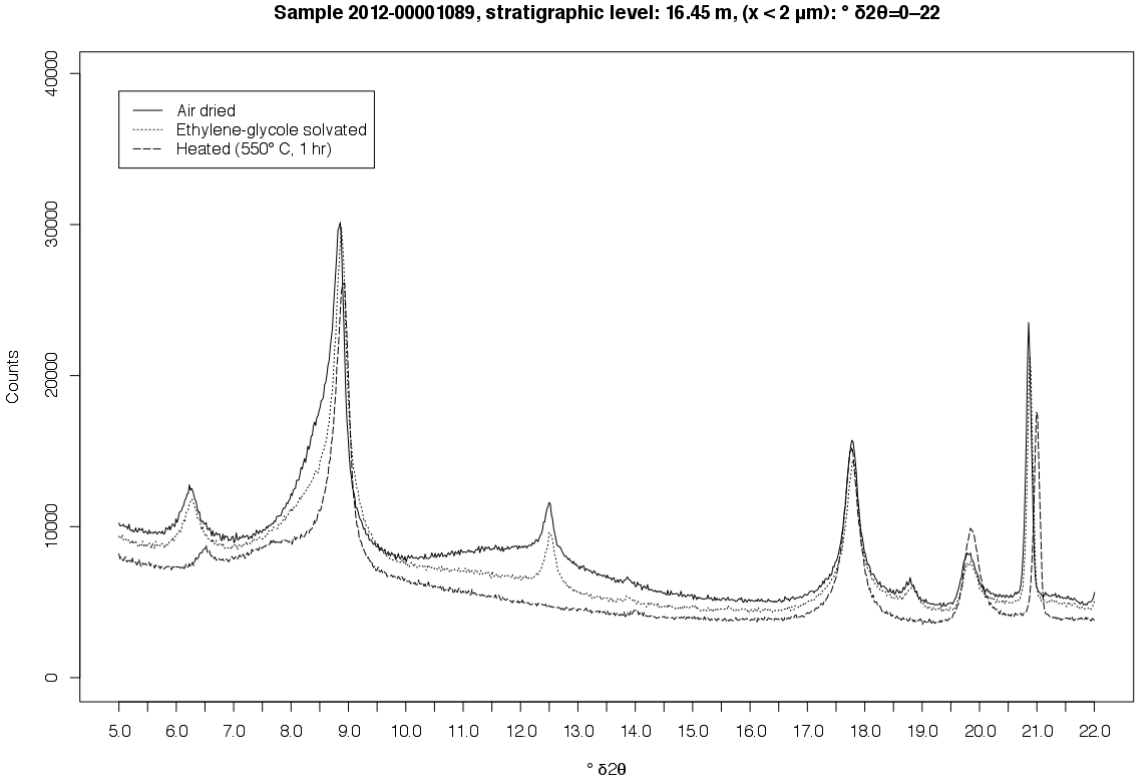
Sample 2012-00001089, stratigraphic level: 16.45 m, (x < 2 µm): ° δ2θ=0–22
Air dried
Ethylene-glycole solvated
Heated (550° C, 1 hr)
Counts
0
10000
20000
30000
40000
5.0 6.0 7.0 8.0 9.0 10.0 11.0 12.0 13.0 14.0 15.0 16.0 17.0 18.0 19.0 20.0 21.0 22.0
° δ2θ

Sample 2012-00001089, stratigraphic level: 16.45 m, (2 µm < x < 16 µm): ° δ2θ=5–70 (air dried)

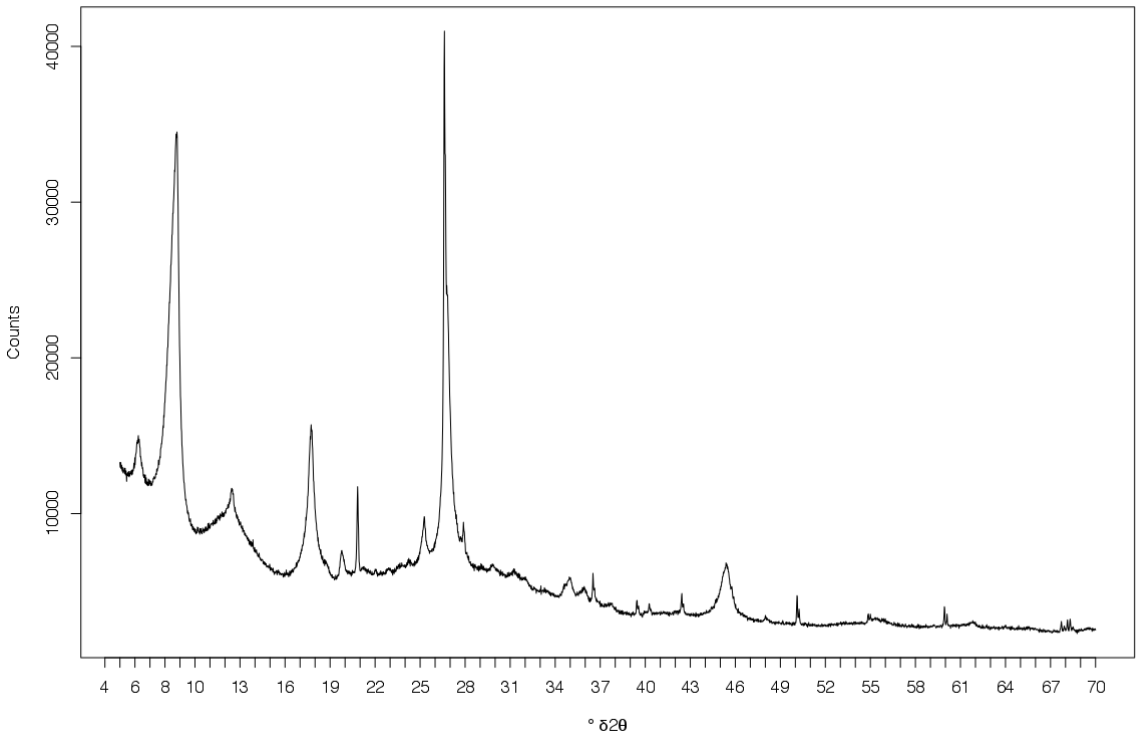

Sample 2012-00001089, stratigraphic level: 16.45 m, (2 µm < x < 16 µm): ° δ2θ=0–22

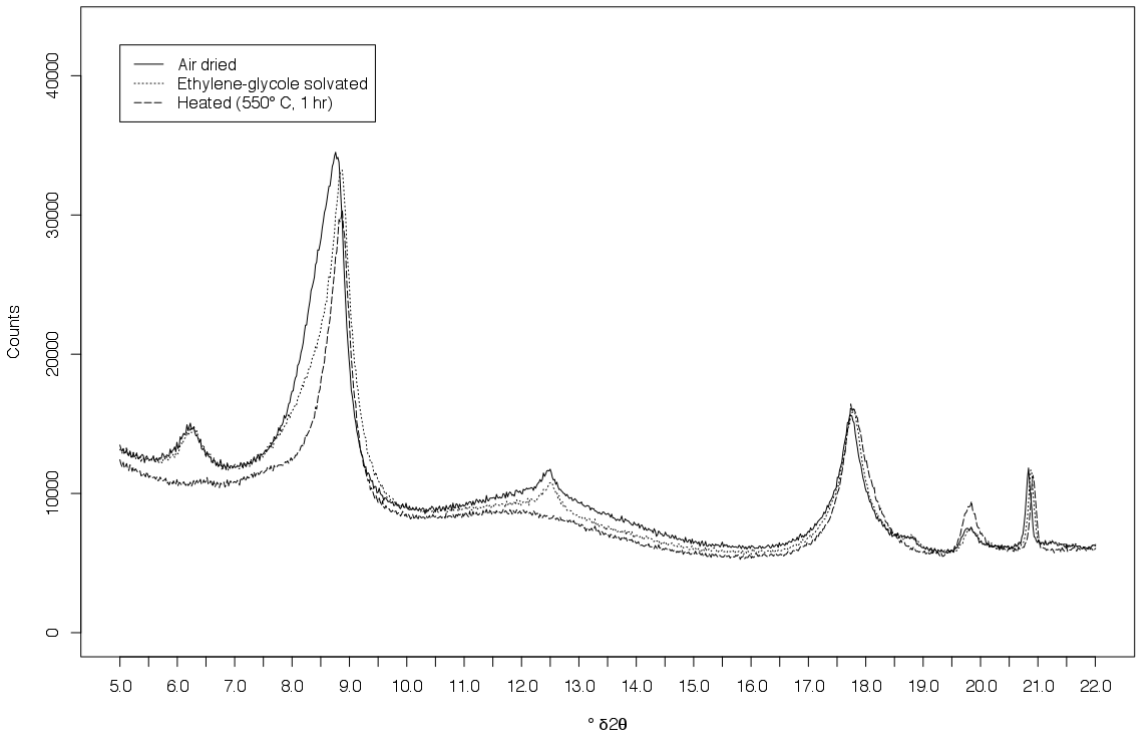

Sample 2012-00001090, stratigraphic level: 17.05 m, (x < 2 µm): ° δ2θ=5–70 (air dried)

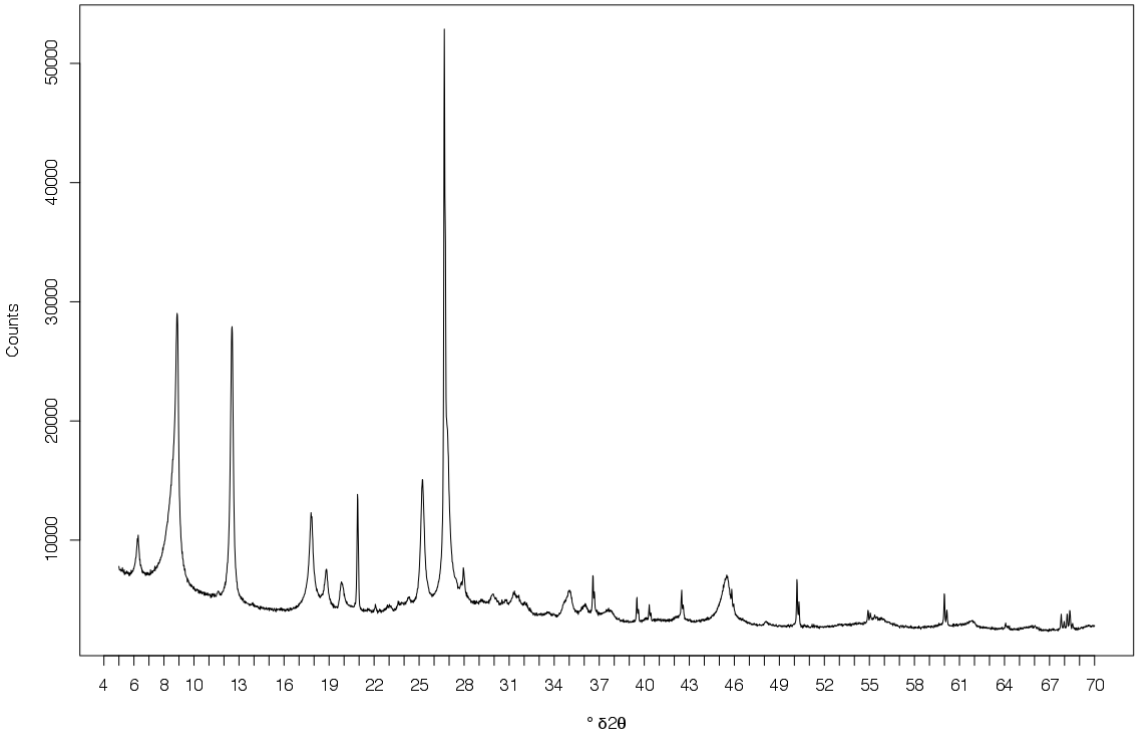

Sample 2012-00001090, stratigraphic level: 17.05 m, (x < 2 µm): ° δ2θ=0–22

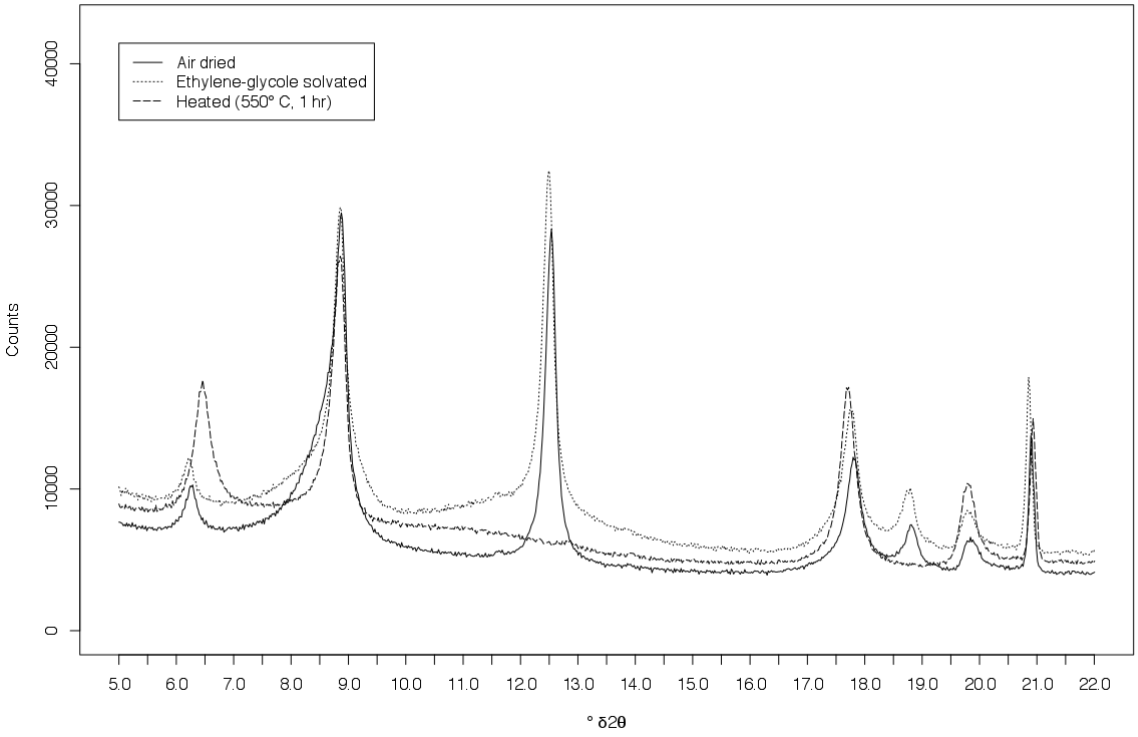

Sample 2012-00001090, stratigraphic level: 17.05 m, (2 µm < x < 16 µm): ° δ2θ=5–70 (air dried)

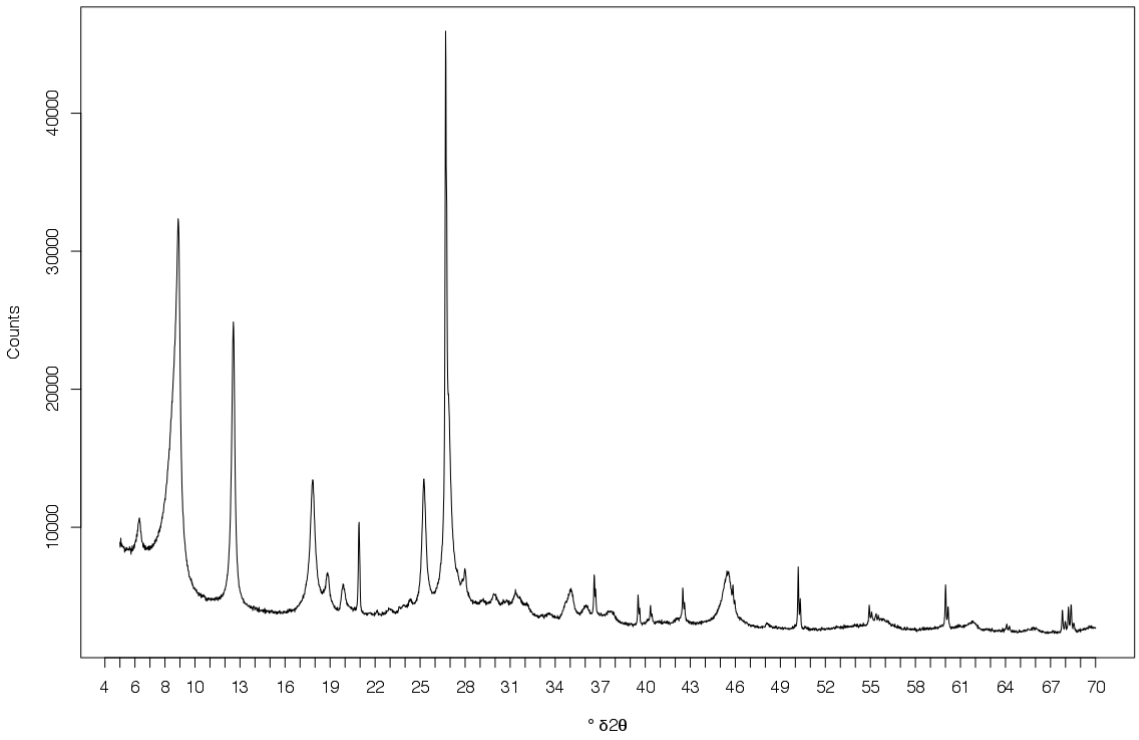

Sample 2012-00001090, stratigraphic level: 17.05 m, (2 µm < x < 16 µm): ° δ2θ=0–22

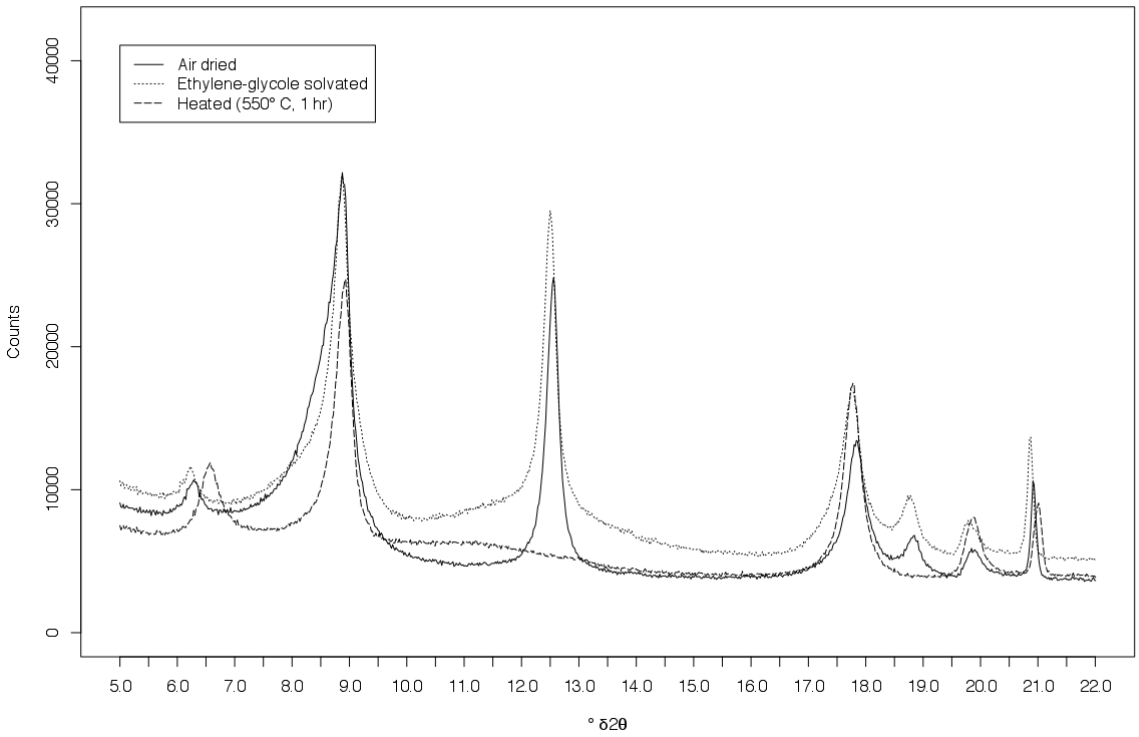

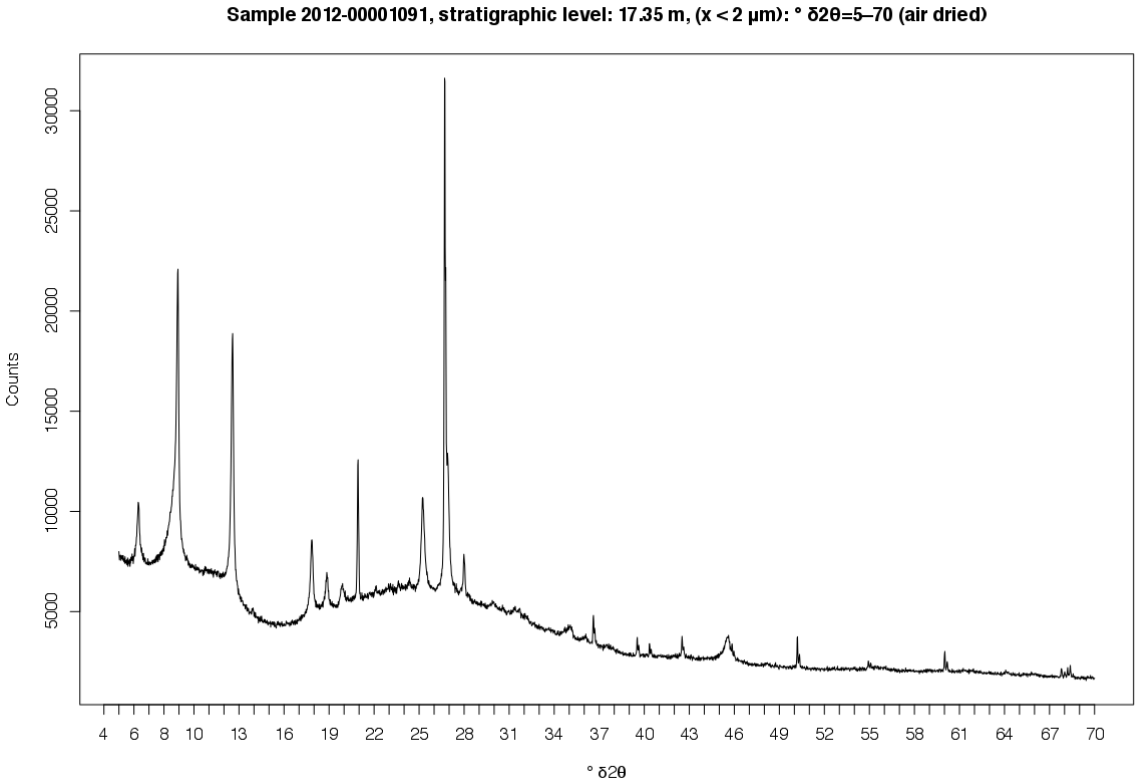
Sample 2012-00001091, stratigraphic level: 17.35 m, (x < 2 µm): ° δ2θ=5–70 (air dried)
Counts
5000
10000
15000
20000
25000
30000
4 6 8 10 13 16 19 22 25 28 31 34 37 40 43 46 49 52 55 58 61 64 67 70
° δ2θ

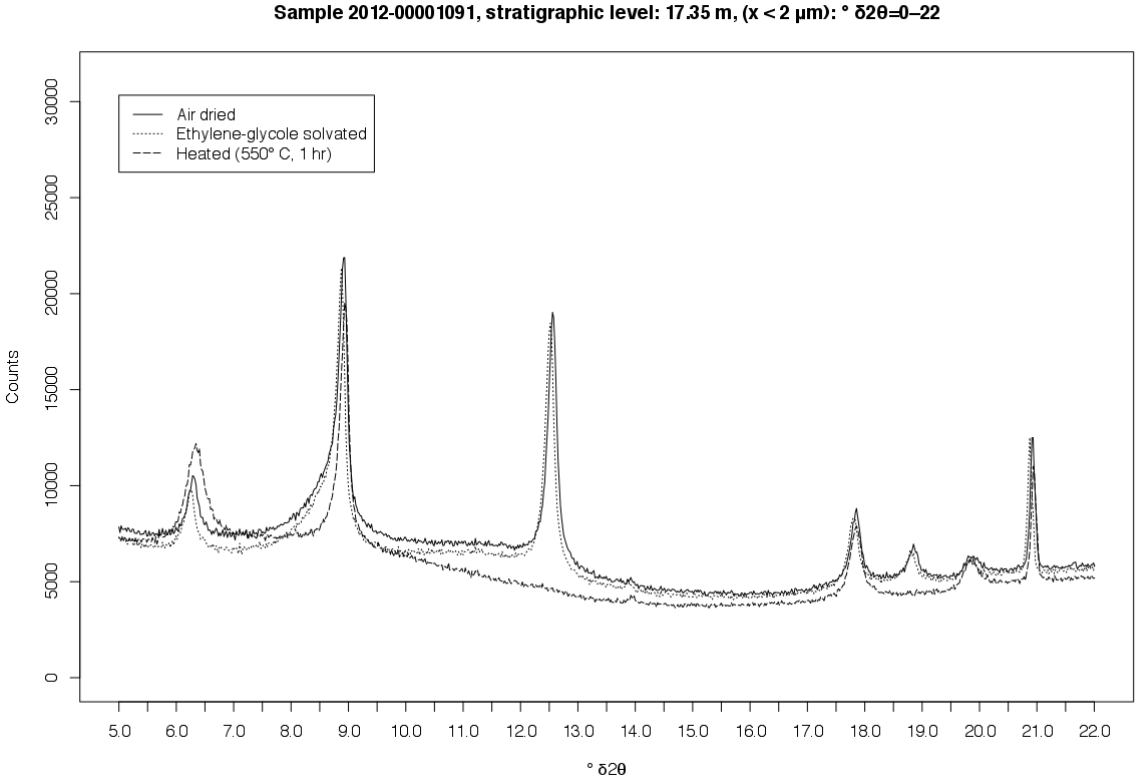
Sample 2012-00001091, stratigraphic level: 17.35 m, (x < 2 µm): ° δ2θ=0–22
Air dried
Ethylene-glycole solvated
Heated (550° C, 1 hr)
Counts
0
5000
10000
15000
20000
25000
30000
5.0 6.0 7.0 8.0 9.0 10.0 11.0 12.0 13.0 14.0 15.0 16.0 17.0 18.0 19.0 20.0 21.0 22.0
° δ2θ

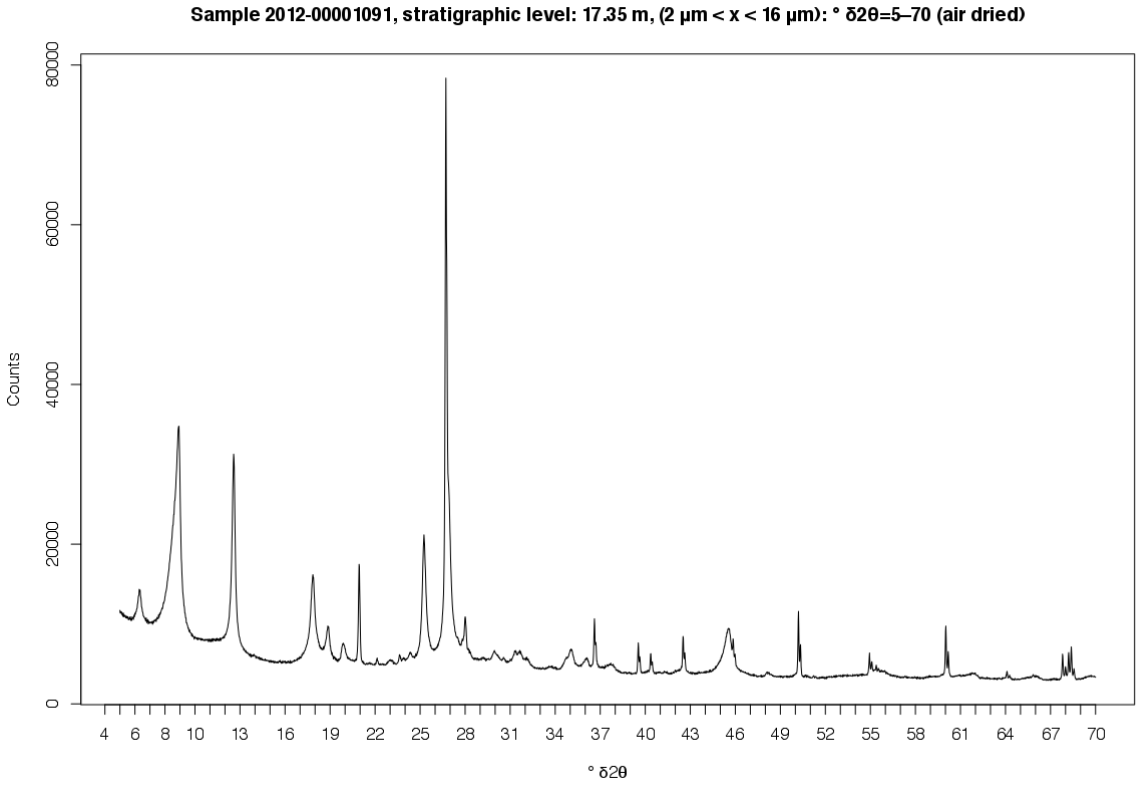
Sample 2012-00001091, stratigraphic level: 17.35 m, (2 µm < x < 16 µm): ° δ2θ=5–70 (air dried)
Counts
0
20000
40000
60000
80000
4 6 8 10 13 16 19 22 25 28 31 34 37 40 43 46 49 52 55 58 61 64 67 70
° δ2θ

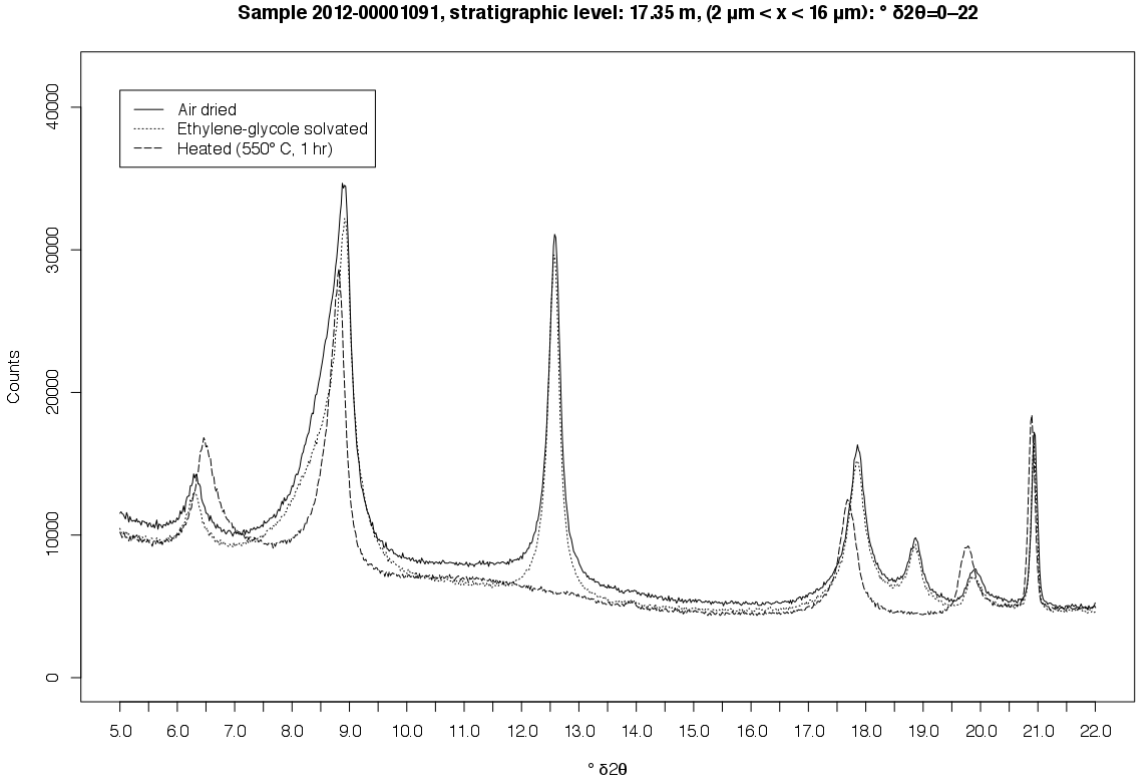
Sample 2012-00001091, stratigraphic level: 17.35 m, (2 µm < x < 16 µm): ° δ2θ=0–22
Air dried
Ethylene-glycole solvated
Heated (550° C, 1 hr)
Counts
0
10000
20000
30000
40000
5.0 6.0 7.0 8.0 9.0 10.0 11.0 12.0 13.0 14.0 15.0 16.0 17.0 18.0 19.0 20.0 21.0 22.0
° δ2θ

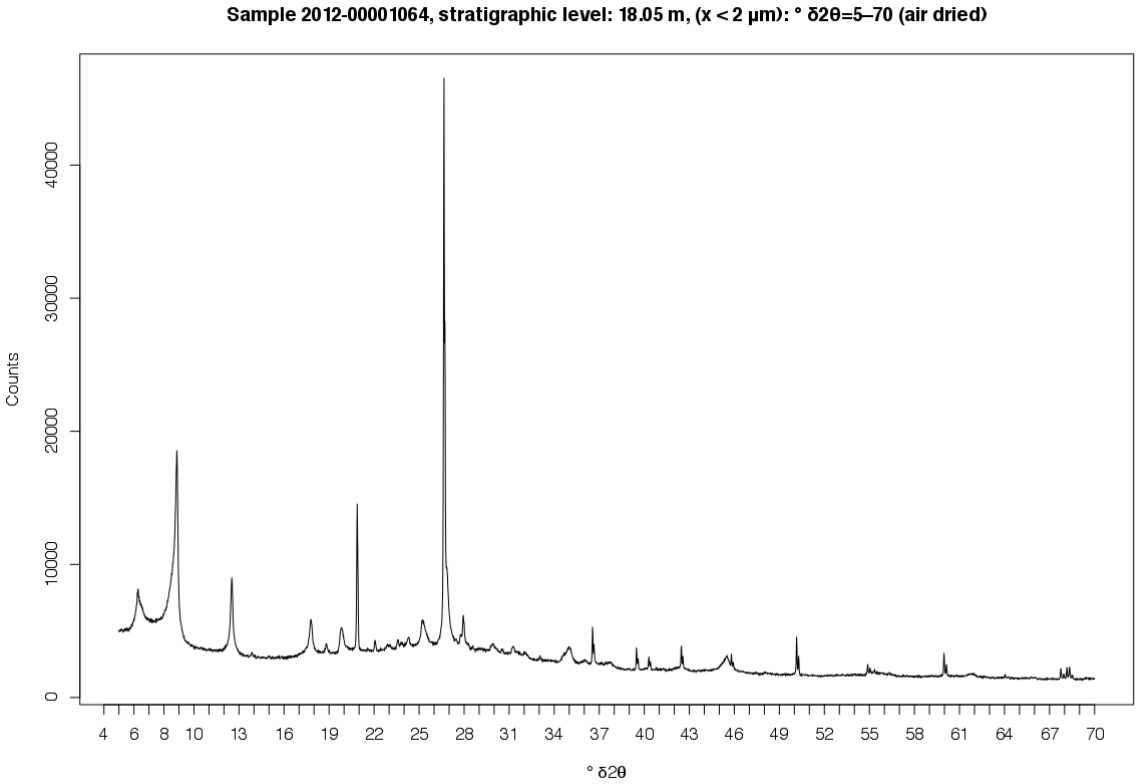
Sample 2012-00001064, stratigraphic level: 18.05 m, (x < 2 µm): ° δ2θ=5–70 (air dried)
Counts
0
10000
20000
30000
40000
4 6 8 10 13 16 19 22 25 28 31 34 37 40 43 46 49 52 55 58 61 64 67 70
° δ2θ

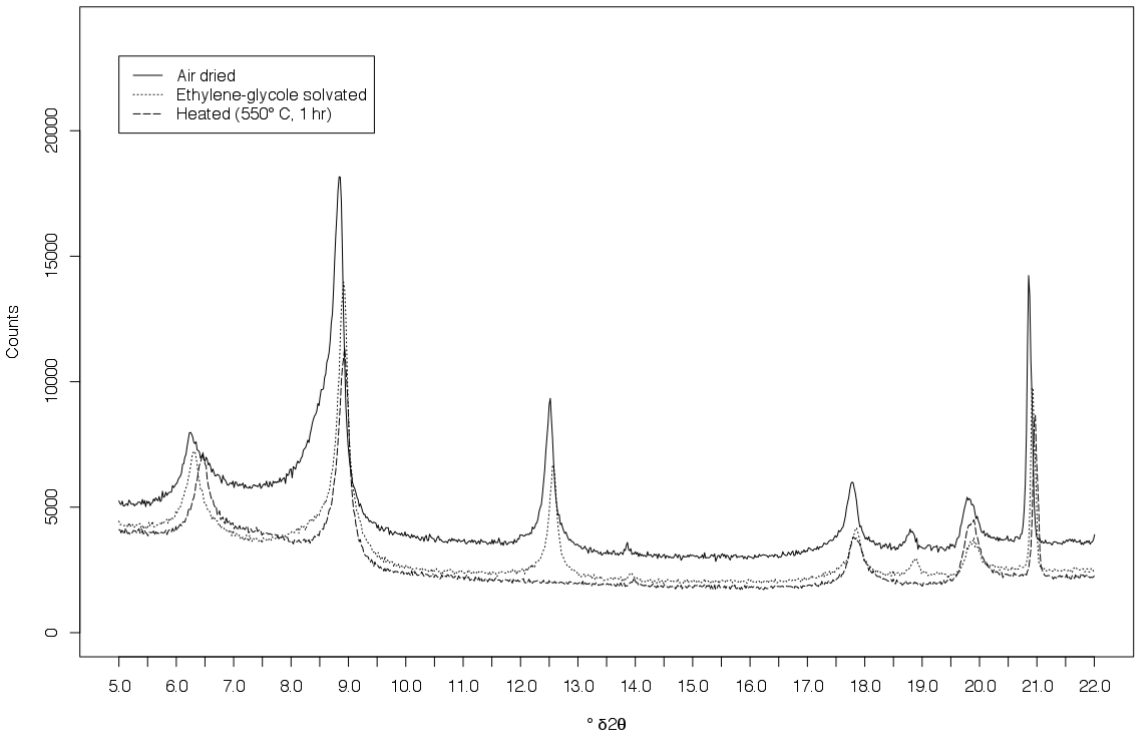
Sample 2012-00001064, stratigraphic level: 18.05 m, (x < 2 µm): ° δ2θ=0–22
Air dried
Ethylene-glycole solvated
Heated (550° C, 1 hr)
Counts
0
5000
10000
15000
20000
5.0 6.0 7.0 8.0 9.0 10.0 11.0 12.0 13.0 14.0 15.0 16.0 17.0 18.0 19.0 20.0 21.0 22.0
° δ2θ

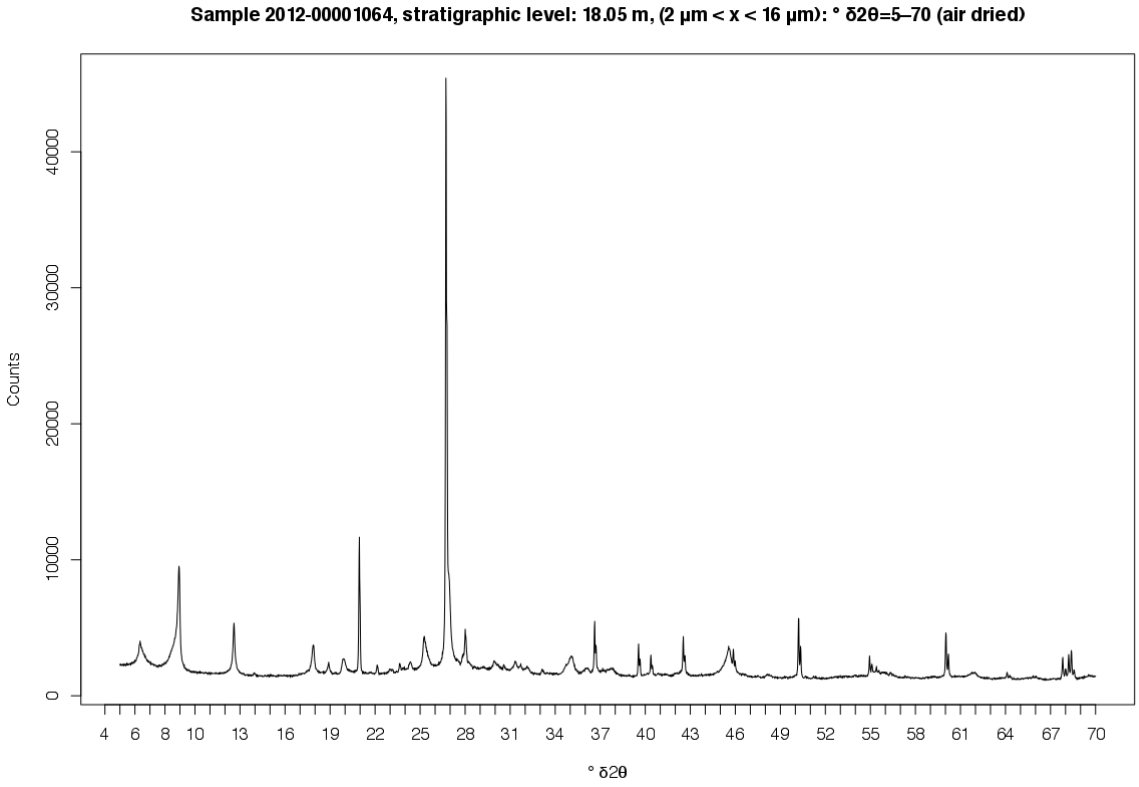
Sample 2012-00001064, stratigraphic level: 18.05 m, (2 µm < x < 16 µm): ° δ2θ=5–70 (air dried)
Counts
0
10000
20000
30000
40000
4 6 8 10 13 16 19 22 25 28 31 34 37 40 43 46 49 52 55 58 61 64 67 70
° δ2θ

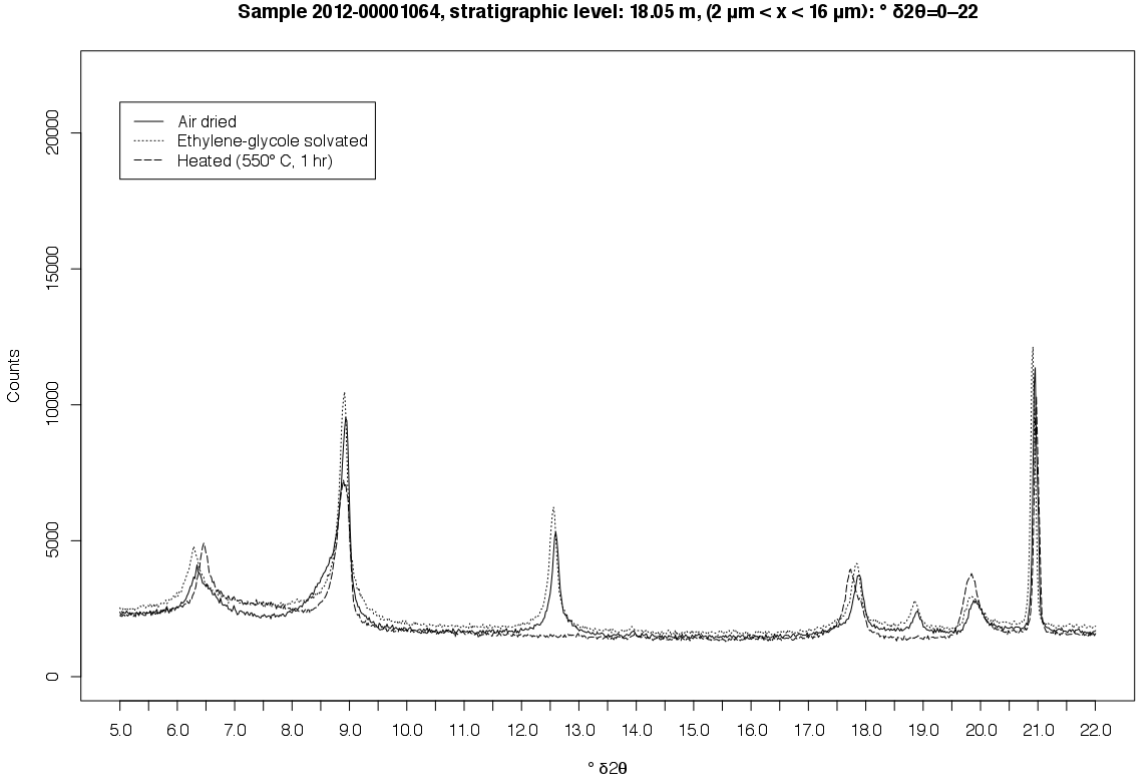
Sample 2012-00001064, stratigraphic level: 18.05 m, (2 µm < x < 16 µm): ° δ2θ=0–22
Air dried
Ethylene-glycole solvated
Heated (550° C, 1 hr)
Counts
0
5000
10000
15000
20000
5.0 6.0 7.0 8.0 9.0 10.0 11.0 12.0 13.0 14.0 15.0 16.0 17.0 18.0 19.0 20.0 21.0 22.0
° δ2θ

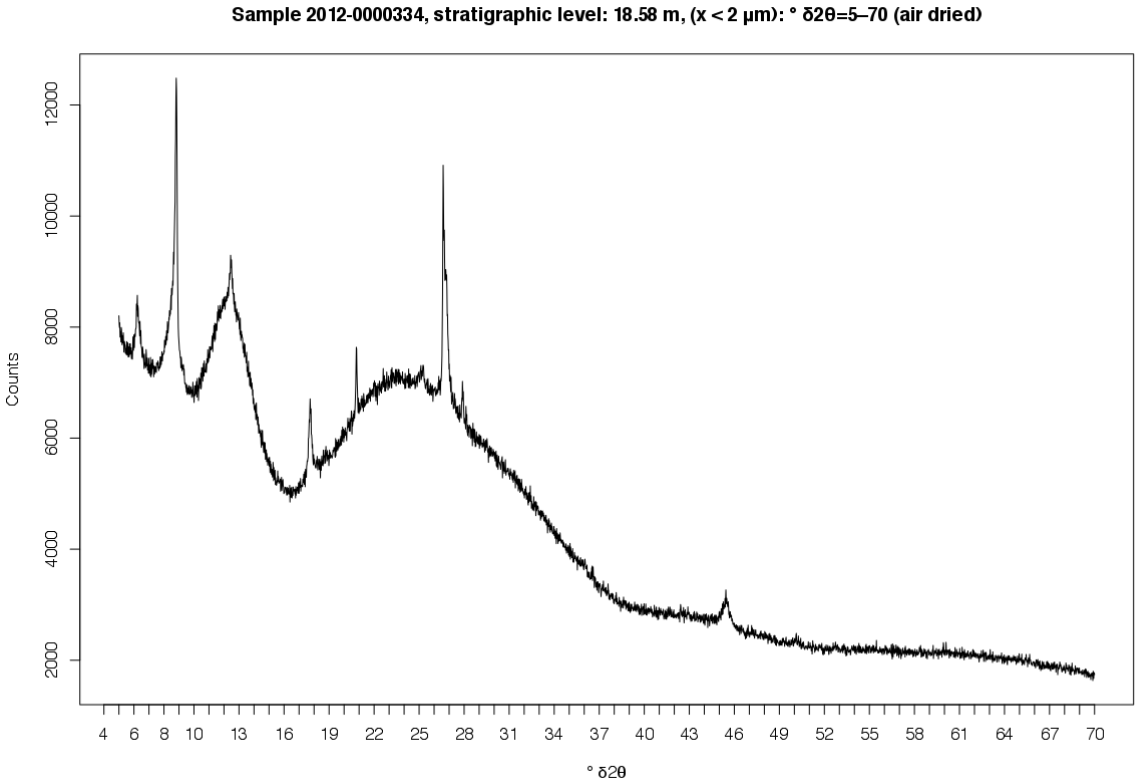
Sample 2012-0000334, stratigraphic level: 18.58 m, (x < 2 µm): ° δ2θ=5–70 (air dried)
Counts
2000
4000
6000
8000
10000
12000
4 6 8 10 13 16 19 22 25 28 31 34 37 40 43 46 49 52 55 58 61 64 67 70
° δ2θ

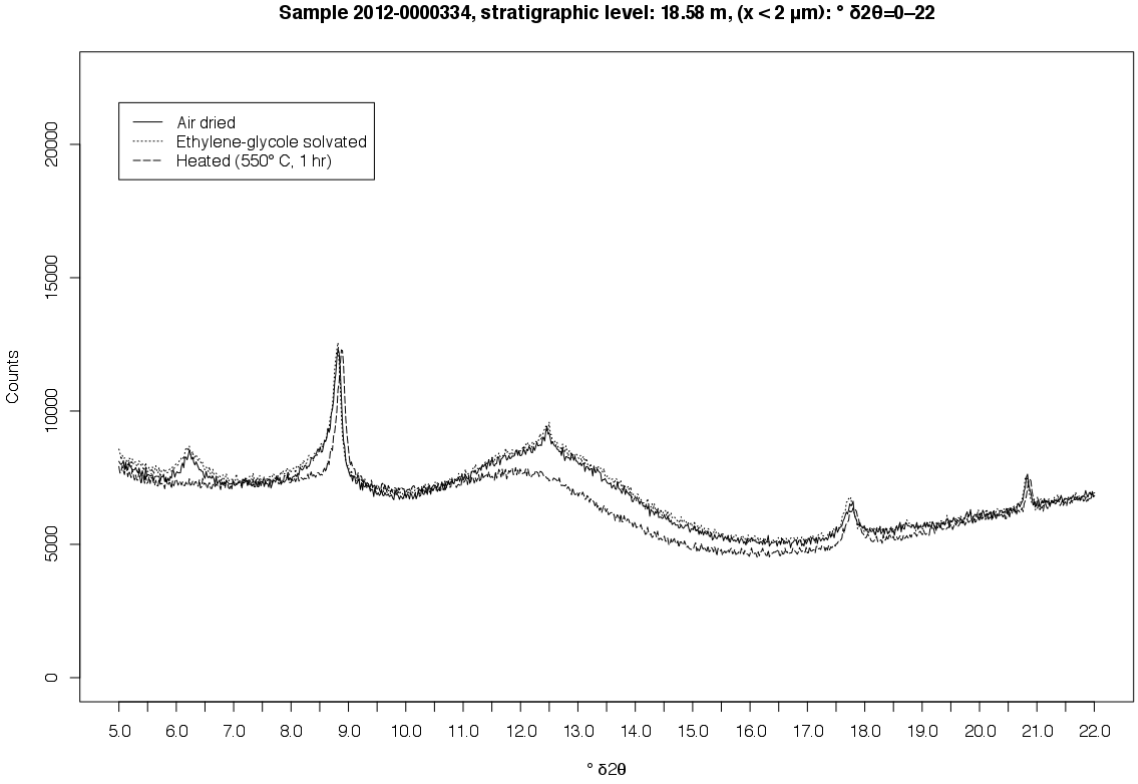
Sample 2012-0000334, stratigraphic level: 18.58 m, (x < 2 µm): ° δ2θ=0–22
Air dried
Ethylene-glycole solvated
Heated (550° C, 1 hr)
Counts
0
5000
10000
15000
20000
5.0 6.0 7.0 8.0 9.0 10.0 11.0 12.0 13.0 14.0 15.0 16.0 17.0 18.0 19.0 20.0 21.0 22.0
° δ2θ

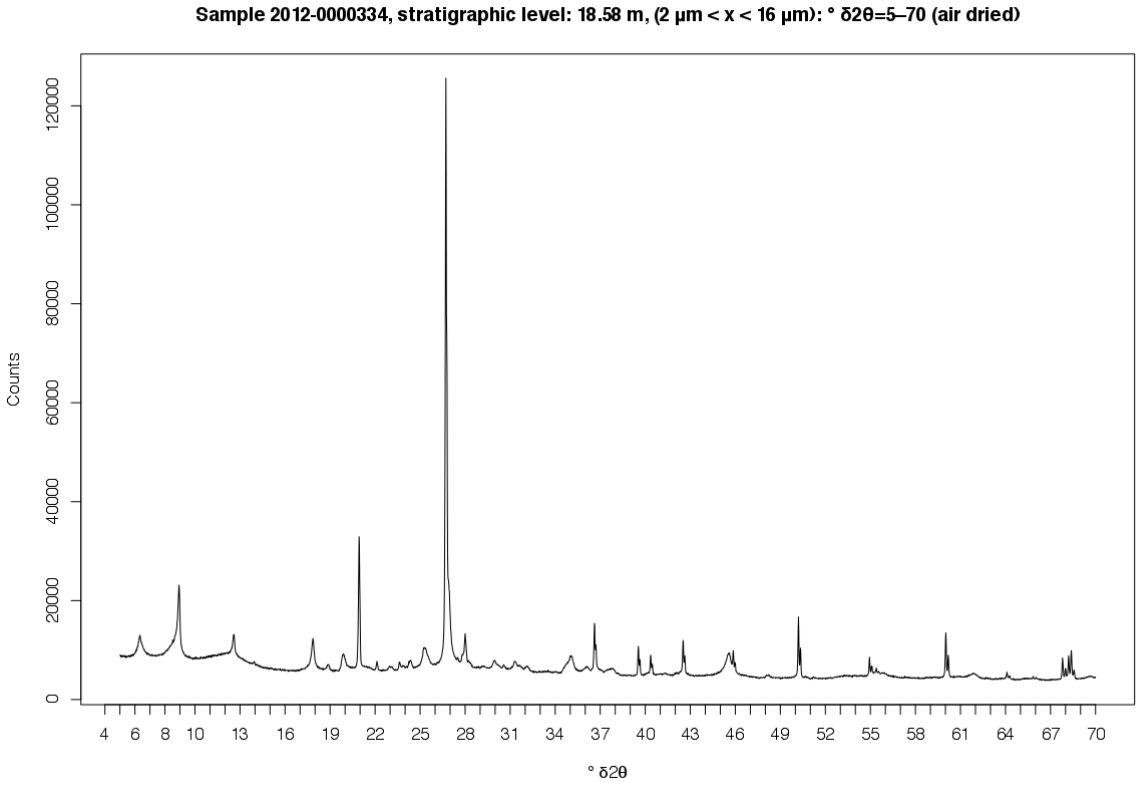
Sample 2012-0000334, stratigraphic level: 18.58 m, (2 µm < x < 16 µm): ° δ2θ=5–70 (air dried)
Counts
0
20000
40000
60000
80000
100000
120000
4 6 8 10 13 16 19 22 25 28 31 34 37 40 43 46 49 52 55 58 61 64 67 70
° δ2θ

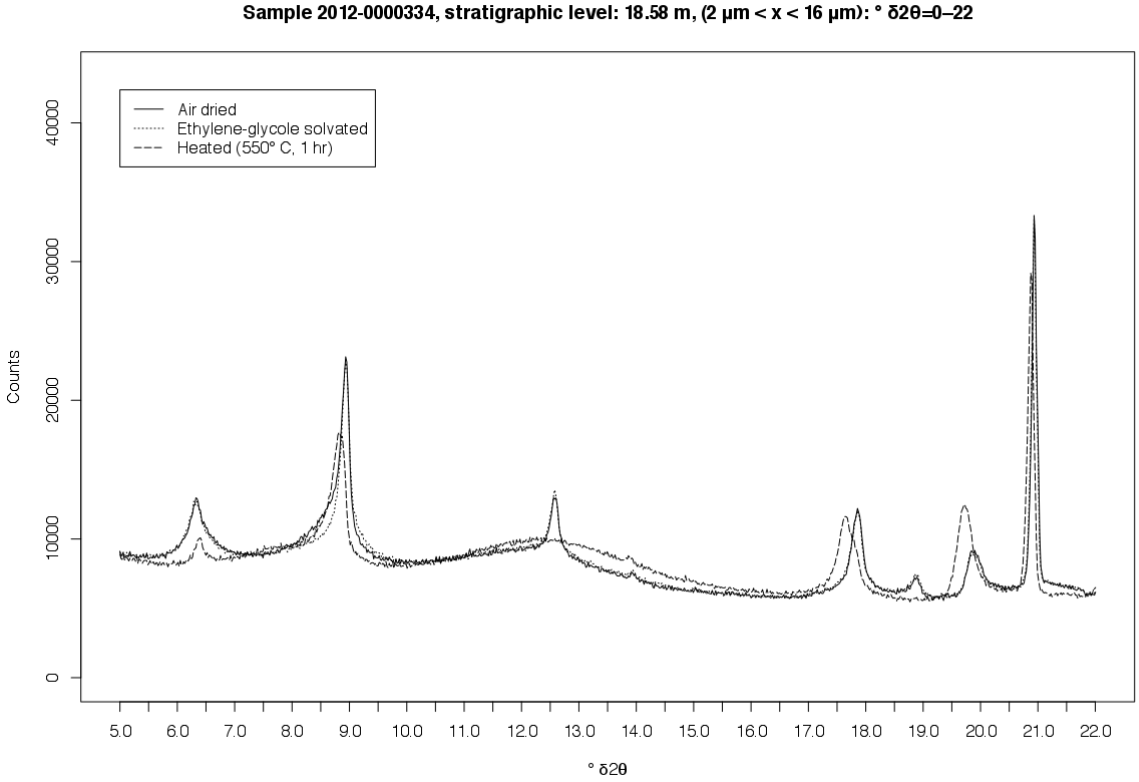
Sample 2012-0000334, stratigraphic level: 18.58 m, (2 µm < x < 16 µm): ° δ2θ=0–22
Air dried
Ethylene-glycole solvated
Heated (550° C, 1 hr)
Counts
0
10000
20000
30000
40000
5.0 6.0 7.0 8.0 9.0 10.0 11.0 12.0 13.0 14.0 15.0 16.0 17.0 18.0 19.0 20.0 21.0 22.0
° δ2θ

9.1.2. Quantitative analyses

9.1.2.1. Sample 2012-0001059, stratigraphic height: 0.06 m

Range Number : 1

R-Values

Rexp : 1.15 Rwp : 8.29 Rp : 6.33 GOF : 7.22
Rexp`: 2.87 Rwp`: 20.71 Rp` : 17.26 DW : 0.08

Quantitative Analysis - Rietveld
Phase 1 : „Quartz low“ 7.746 %
Phase 2 : „Kaolinite 1A II“ 1.916 %
Phase 3 : „Illite 2M1“ 63.101 %
Phase 4 : „Chamosite 1MIIb“ 26.460 %
Phase 5 : „Albite low“ 0.777 %

Background
Chebychev polynomial, Coefficient 0 5039.794
1 -1986.416
2 875.1201
3 -511.3527
4 307.4872
5 -121.491

Instrument
Primary radius (mm) 250
Secondary radius (mm) 250
Linear PSD 2Th angular range (∞) 2.749941
FDS angle (∞) 0.0916
Beam spill, sample length (mm) 9
Intensity not corrected
Full Axial Convolution
Filament length (mm) 8
Sample length (mm) 30
Receiving Slit length (mm) 12
Primary Sollers (∞) 2.5
Secondary Sollers (∞) 2.5

Corrections
Zero error -0.1187046
Specimen displacement -0.2094607
LP Factor 0

Miscellaneous
Excluded Regions
Start/Finish 0 0
Start/Finish 0 0
Start/Finish 0 0
Start/Finish 0 0
Start/Finish 0 0

Structure 1

Phase name	Quartz low
R-Bragg	21.019
Spacegroup	P3221
Scale	0.0183842071
Cell Mass	180.252
Cell Volume (≈^3)	112.86557
Wt% - Rietveld	7.746
Crystal Linear Absorption Coeff. (1/cm)	95.500
Crystal Density (g/cm^3)	2.652
Preferred Orientation (Dir 1 : 0 0 1)	1.113605
PVII peak type	
FWHM = a + b/Cos(Th) + c Tan(Th)	
a	0.03191614
b	0.0001000001
c	0.000100001
Exponent m = 0.6+ma+mb/Cos(Th)+mc/Tan(Th)	
ma	0.0001000095
mb	0.2639853
mc	0.0001000006
Lattice parameters	
a (≈)	4.9115899
c (≈)	5.4023989

Site	Np	x	y	z	Atom	Occ	Beq
Si1	3	0.46900	0.00000	0.66667	Si+4	1	1
O1	6	0.40300	0.25300	0.78900	O-2	1	1

Structure 2

Phase name	Kaolinite 1A II
R-Bragg	22.934
Spacegroup	C1
Scale	0.000658717447
Cell Mass	508.256
Cell Volume (≈^3)	276.30326
Wt% - Rietveld	1.916
Crystal Linear Absorption Coeff. (1/cm)	95.337
Crystal Density (g/cm^3)	3.055
Preferred Orientation (Dir 1 : 0 0 1)	0.226491
PVII peak type	
FWHM = a + b/Cos(Th) + c Tan(Th)	
a	0.6269637
b	1
c	1
Exponent m = 0.6+ma+mb/Cos(Th)+mc/Tan(Th)	
ma	0.0001
mb	0.0001
mc	0.0001
Lattice parameters	
a (≈)	5.5618879
b (≈)	7.0484930
c (≈)	7.3883748
alpha (∞)	96.12869
beta (∞)	104.9248
gamma (∞)	94.97204

Site	Np	x	y	z	Atom	Occ	Beq
O1	2	0.77800	0.18000	-0.14000	O-2	1	1
O2	2	0.27800	0.32000	-0.13800	O-2	1	1
O3	2	0.31600	-0.00800	-0.13600	O-2	1	1
O4	2	0.24800	0.18400	0.15500	O-2	1	1
O5	2	0.75400	0.31500	0.15500	O-2	1	1
O6	2	0.69000	0.00400	0.15700	O-2	1	1
O7	2	0.79100	0.16500	0.48200	O-2	1	1
O8	2	0.61200	-0.12000	0.45500	O-2	1	1
O9	2	0.10800	-0.05800	0.45500	O-2	1	1
Al1	2	0.50200	0.17200	0.00300	Al+3	1	1
Al2	2	0.00200	0.33000	0.00200	Al+3	1	1
Si1	2	0.80000	0.32200	0.38200	Si+4	1	1
Si2	2	0.80000	0.00000	0.38500	Si+4	1	1

Structure 3

Phase name	Illite 2M1
R-Bragg	17.536
Spacegroup	C12/c1
Scale	0.00205853288
Cell Mass	1580.752
Cell Volume (≈^3)	936.37809
Wt% - Rietveld	63.101
Crystallite Size	
Cry size Lorentzian (nm)	20.5
Crystal Linear Absorption Coeff. (1/cm)	119.514
Crystal Density (g/cm^3)	2.803
Preferred Orientation Spherical Harmonics	
Order	4
y00	1
y20	-1.342937
y22m	-1.53108
y22p	-0.700237
y40	0.1970081
y42m	0.219369
y42p	0.2488549
y44m	0.03167524
y44p	-0.3392497
Lattice parameters	
a (≈)	5.2066934
b (≈)	9.0141858
c (≈)	20.0593564
beta (∞)	95.96047

Site	Np	x	y	z	Atom	Occ	Beq
Si1	8	0.48250	0.92970	0.13700	Si+4	1	1.737
Al1	8	0.44320	0.26350	0.13650	Al+3	1	0.8685
Al2	8	0.25860	0.08280	0.00680	Al+3	1	2.132
K1	4	0.00000	0.09010	0.25000	K+1	1	5.922
O1	8	0.46230	0.91940	0.05050	O-2	1	1.184
O2	8	0.38350	0.26650	0.06630	O-2	1	3.711
O3	8	0.42590	0.10390	0.15300	O-2	1	0.9475
O4	8	0.22260	0.83680	0.16850	O-2	1	3.237
O5	8	0.27350	0.37220	0.16780	O-2	1	6.317
O6	8	0.40800	0.56710	0.04540	O-2	1	4.185

Structure 4

Phase name	Chamosite 1MIIb
R-Bragg	35.820
Spacegroup	C-1
Scale	0.00146615701
Cell Mass	1271.241
Cell Volume (≈^3)	685.50678
Wt% - Rietveld	26.460
Crystal Linear Absorption Coeff. (1/cm)	272.126
Crystal Density (g/cm^3)	3.079
Preferred Orientation (Dir 1 : 0 0 1)	0.8270288
PVII peak type	
FWHM = a + b/Cos(Th) + c Tan(Th)	
a	0.000125601
b	0.1233229
c	0.0132041
Exponent m = 0.6+ma+mb/Cos(Th)+mc/Tan(Th)	
ma	0.0001032782
mb	0.000100298
mc	0.000100149
Lattice parameters	
a (≈)	5.4751122
b (≈)	8.8955870
c (≈)	14.3134687
alpha (∞)	89.25534
beta (∞)	99.86613
gamma (∞)	93.53822

Site	Np	x	y	z	Atom	Occ	Beq
Mg1	2	0.00000	0.00000	0.00000	Mg+2	0.538	0.1579
Fe1	2	0.00000	0.00000	0.00000	Fe+2	0.462	0.1579
Mg2	4	0.01410	0.33480	0.00270	Mg+2	0.496	0.1579
Fe2	4	0.01410	0.33480	0.00270	Fe+2	0.504	0.1579
Mg3	4	0.00320	0.16830	0.50040	Mg+2	0.494	0.1579
Fe3	4	0.00320	0.16830	0.50040	Fe+2	0.506	0.1579
Al1	2	0.00000	0.50000	0.50000	Al+3	1.362	0.2369
Si1	4	0.24000	0.17000	0.19410	Si+4	0.7125	0.07896
Al2	4	0.24000	0.17000	0.19410	Al+3	0.2875	0.07896
Si2	4	0.73000	0.99800	0.19450	Si+4	0.7125	0.07896
Al3	4	0.73000	0.99800	0.19450	Al+3	0.2875	0.07896
O1	4	0.19100	0.16350	0.07890	O-2	1	0.8685
O2	4	0.70500	0.99800	0.07560	O-2	1	0.8685
O3	4	0.23100	0.33600	0.23740	O-2	1	0.8685
O4	4	0.52800	0.11800	0.23020	O-2	1	0.8685
O5	4	0.01800	0.06100	0.23060	O-2	1	0.8685
O6	4	0.68900	0.33120	0.07420	O-2	1	0.8685
O7	4	0.14400	0.99900	0.43000	O-2	1	0.8685
O8	4	0.14300	0.33610	0.42860	O-2	1	0.8685
O9	4	0.64300	0.16270	0.43110	O-2	1	0.8685

Structure 5

Phase name	Albite low
R-Bragg	12.873

Spacegroup	C-1
Scale	5.38848678e-005
Cell Mass	1048.846
Cell Volume (≈^3)	664.19438
Wt% - Rietveld	0.777
Crystallite Size	
Cry size Lorentzian (nm)	172.0
Crystal Linear Absorption Coeff. (1/cm)	88.829
Crystal Density (g/cm^3)	2.622
Lattice parameters	
a (≈)	8.1380000
b (≈)	12.7890000
c (≈)	7.1560000
alpha (∞)	94.33
beta (∞)	116.57
gamma (∞)	87.65

Site	Np	x	y	z	Atom	Occ	Beq
O1	4	0.00900	0.13400	0.96700	O-2	1	1
O2	4	0.59500	0.99700	0.27900	O-2	1	1
O3	4	0.81800	0.11200	0.19200	O-2	1	1
O4	4	0.32100	0.35300	0.25900	O-2	1	1
O5	4	0.00600	0.30700	0.26800	O-2	1	1
O6	4	0.52200	0.19600	0.23300	O-2	1	1
O7	4	0.20600	0.11000	0.38900	O-2	1	1
O8	4	0.68300	0.36900	0.43000	O-2	1	1
Si1	4	0.00800	0.17100	0.20900	Si+4	0.28	1
Al1	4	0.00800	0.17100	0.20900	Al+3	0.72	1
Si2	4	0.50800	0.31800	0.24100	Si+4	1	1
Si3	4	0.69200	0.11000	0.31500	Si+4	0.8	1
Al3	4	0.69200	0.11000	0.31500	Al+3	0.2	1
Si4	4	0.18300	0.38200	0.35900	Si+4	0.91	1
Al4	4	0.18300	0.38200	0.35900	Al+3	0.09	1
Na1	4	0.27200	0.99000	0.14500	Na+1	1	1

9.1.2.2. Sample 2012-0001074, stratigraphic height: 0.49 m

Range Number : 1

R-Values

Rexp : 1.61 Rwp : 8.87 Rp : 5.50 GOF : 5.53
Rexp`: 5.19 Rwp`: 28.70 Rp` : 25.64 DW : 0.11

Quantitative Analysis - Rietveld

Phase 1 : „Quartz low“	17.659 %
Phase 2 : „Kaolinite 1A II“	4.049 %
Phase 3 : „Illite 2M1“	76.869 %
Phase 4 : „Chamosite 1MIIb“	0.342 %
Phase 5 : „Albite low“	1.081 %

Background

Chebychev polynomial, Coefficient	0	3214.009
	1	-1310.584
	2	602.2323

3	-435.341
4	336.1708
5	-188.4255
6	54.17637

Instrument

Primary radius (mm)	250
Secondary radius (mm)	250
Linear PSD 2Th angular range (∞)	2.749941
FDS angle (∞)	0.0916
Beam spill, sample length (mm)	9
Intensity not corrected	
Full Axial Convolution	
Filament length (mm)	8
Sample length (mm)	30
Receiving Slit length (mm)	12
Primary Sollers (∞)	2.5
Secondary Sollers (∞)	2.5

Corrections

Zero error	-0.1466467
Specimen displacement	-0.3442226
LP Factor	0

Miscellaneous

Excluded Regions		
Start/Finish	0	0
Start/Finish	0	0
Start/Finish	0	0
Start/Finish	0	0
Start/Finish	0	0

Structure 1

Phase name	Quartz low
R-Bragg	20.827
Spacegroup	P3221
Scale	0.0102471218
Cell Mass	180.252
Cell Volume (≈^3)	112.92727
Wt% - Rietveld	17.659
Crystal Linear Absorption Coeff. (1/cm)	95.448
Crystal Density (g/cm^3)	2.651
Preferred Orientation (Dir 1 : 0 0 1)	1.173227
PVII peak type	
FWHM = a + b/Cos(Th) + c Tan(Th)	
a	0.01902418
b	0.004827596
c	0.0004451322
Exponent m = 0.6+ma+mb/Cos(Th)+mc/Tan(Th)	
ma	0.05011131
mb	0.08229318
mc	0.01039948
Lattice parameters	
a (≈)	4.9123423
c (≈)	5.4036967

Site	Np	x	y	z	Atom	Occ	Beq
Si1	3	0.46900	0.00000	0.66667	Si+4	1	1
O1	6	0.40300	0.25300	0.78900	O-2	1	1

Structure 2

Phase name	Kaolinite 1A II
R-Bragg	34.586
Spacegroup	C1
Scale	0.000289401215
Cell Mass	508.256
Cell Volume (≈^3)	325.10507
Wt% - Rietveld	4.049
Crystal Linear Absorption Coeff. (1/cm)	81.026
Crystal Density (g/cm^3)	2.596
Preferred Orientation (Dir 1 : 0 0 1)	0.5029045
PVII peak type	
FWHM = a + b/Cos(Th) + c Tan(Th)	
a	0.2353891
b	0.281762
c	0.9987278
Exponent m = 0.6+ma+mb/Cos(Th)+mc/Tan(Th)	
ma	0.0004051742
mb	0.0001762924
mc	0.1100684
Lattice parameters	
a (≈)	5.3322134
b (≈)	8.3787153
c (≈)	7.5046934
alpha (∞)	93.05501
beta (∞)	103.7211
gamma (∞)	90.97204

Site	Np	x	y	z	Atom	Occ	Beq
O1	2	0.77800	0.18000	-0.14000	O-2	1	1
O2	2	0.27800	0.32000	-0.13800	O-2	1	1
O3	2	0.31600	-0.00800	-0.13600	O-2	1	1
O4	2	0.24800	0.18400	0.15500	O-2	1	1
O5	2	0.75400	0.31500	0.15500	O-2	1	1
O6	2	0.69000	0.00400	0.15700	O-2	1	1
O7	2	0.79100	0.16500	0.48200	O-2	1	1
O8	2	0.61200	-0.12000	0.45500	O-2	1	1
O9	2	0.10800	-0.05800	0.45500	O-2	1	1
Al1	2	0.50200	0.17200	0.00300	Al+3	1	1
Al2	2	0.00200	0.33000	0.00200	Al+3	1	1
Si1	2	0.80000	0.32200	0.38200	Si+4	1	1
Si2	2	0.80000	0.00000	0.38500	Si+4	1	1

Structure 3

Phase name	Illite 2M1
R-Bragg	35.246
Spacegroup	C12/c1
Scale	0.00061339724
Cell Mass	1580.752

Cell Volume (≈^3)	936.37809
Wt% - Rietveld	76.869
Crystallite Size	
Cry size Lorentzian (nm)	24.7
Crystal Linear Absorption Coeff. (1/cm)	119.514
Crystal Density (g/cm^3)	2.803
Preferred Orientation (Dir 1 : 0 0 1)	0.358663
Preferred Orientation Spherical Harmonics	
Order	8
y00	1
y20	0.5417289
y22m	-0.1366169
y22p	-0.1239812
y40	0.4781226
y42m	-0.2161943
y42p	-0.5260222
y44m	0.804088
y44p	-0.04019087
y60	0.001701531
y62m	0.04363407
y62p	0.4491938
y64m	0.08125991
y64p	-0.2502933
y66m	0.2940051
y66p	0.2940051
y80	0.1538587
y82m	0.6233011
y82p	0.3010364
y84m	-0.6442832
y84p	-0.1320229
y86m	-0.02341102
y86p	0.04773344
y88m	0.2219244
y88p	0.07412482
PVII peak type	
FWHM = a + b/Cos(Th) + c Tan(Th)	
a	0.0001
b	0.0001
c	0.02995076
Exponent m = 0.6+ma+mb/Cos(Th)+mc/Tan(Th)	
ma	0.0004261633
mb	0.02056316
mc	0.02812973
Lattice parameters	
a (≈)	5.2066934
b (≈)	9.0141858
c (≈)	20.0593564
beta (∞)	95.96047

Site	Np	x	y	z	Atom	Occ	Beq
Si1	8	0.48250	0.92970	0.13700	Si+4	1	1.737
Al1	8	0.44320	0.26350	0.13650	Al+3	1	0.8685
Al2	8	0.25860	0.08280	0.00680	Al+3	1	2.132
K1	4	0.00000	0.09010	0.25000	K+1	1	5.922
O1	8	0.46230	0.91940	0.05050	O-2	1	1.184
O2	8	0.38350	0.26650	0.06630	O-2	1	3.711

O3	8	0.42590	0.10390	0.15300	O-2	1 0.9475
O4	8	0.22260	0.83680	0.16850	O-2	1 3.237
O5	8	0.27350	0.37220	0.16780	O-2	1 6.317
O6	8	0.40800	0.56710	0.04540	O-2	1 4.185

Structure 4

Phase name	Chamosite 1MIIb
R-Bragg	63.896
Spacegroup	C-1
Scale	4.62467976e-006
Cell Mass	1271.241
Cell Volume (≈^3)	688.00078
Wt% - Rietveld	0.342
Crystal Linear Absorption Coeff. (1/cm)	271.140
Crystal Density (g/cm^3)	3.068
Preferred Orientation (Dir 1 : 0 0 1)	0.1859567
PVII peak type	
FWHM = a + b/Cos(Th) + c Tan(Th)	
a	0.05062045
b	0.03216827
c	0.2280082
Exponent m = 0.6+ma+mb/Cos(Th)+mc/Tan(Th)	
ma	0.3386788
mb	0.3684399
mc	0.0001128087
Lattice parameters	
a (≈)	5.4083795
b (≈)	9.0044365
c (≈)	14.2985996
alpha (∞)	90.04891
beta (∞)	98.57557
gamma (∞)	92.25189

Site	Np	x	y	z	Atom	Occ	Beq
Mg1	2	0.00000	0.00000	0.00000	Mg+2	0.538	0.1579
Fe1	2	0.00000	0.00000	0.00000	Fe+2	0.462	0.1579
Mg2	4	0.01410	0.33480	0.00270	Mg+2	0.496	0.1579
Fe2	4	0.01410	0.33480	0.00270	Fe+2	0.504	0.1579
Mg3	4	0.00320	0.16830	0.50040	Mg+2	0.494	0.1579
Fe3	4	0.00320	0.16830	0.50040	Fe+2	0.506	0.1579
Al1	2	0.00000	0.50000	0.50000	Al+3	1.362	0.2369
Si1	4	0.24000	0.17000	0.19410	Si+4	0.7125	0.07896
Al2	4	0.24000	0.17000	0.19410	Al+3	0.2875	0.07896
Si2	4	0.73000	0.99800	0.19450	Si+4	0.7125	0.07896
Al3	4	0.73000	0.99800	0.19450	Al+3	0.2875	0.07896
O1	4	0.19100	0.16350	0.07890	O-2	1	0.8685
O2	4	0.70500	0.99800	0.07560	O-2	1	0.8685
O3	4	0.23100	0.33600	0.23740	O-2	1	0.8685
O4	4	0.52800	0.11800	0.23020	O-2	1	0.8685
O5	4	0.01800	0.06100	0.23060	O-2	1	0.8685
O6	4	0.68900	0.33120	0.07420	O-2	1	0.8685
O7	4	0.14400	0.99900	0.43000	O-2	1	0.8685
O8	4	0.14300	0.33610	0.42860	O-2	1	0.8685
O9	4	0.64300	0.16270	0.43110	O-2	1	0.8685

Structure 5
Phase name Albite low
R-Bragg 27.137
Spacegroup C-1
Scale 1.83290645e-005
Cell Mass 1048.846
Cell Volume (≈^3) 664.19438
Wt% - Rietveld 1.081
Crystallite Size
Cry size Lorentzian (nm) 487.8
Crystal Linear Absorption Coeff. (1/cm) 88.829
Crystal Density (g/cm^3) 2.622
Lattice parameters
a (≈) 8.1380000
b (≈) 12.7890000
c (≈) 7.1560000
alpha (∞) 94.33
beta (∞) 116.57
gamma (∞) 87.65

Site	Np	x	y	z	Atom	Occ	Beq
O1	4	0.00900	0.13400	0.96700	O-2	1	1
O2	4	0.59500	0.99700	0.27900	O-2	1	1
O3	4	0.81800	0.11200	0.19200	O-2	1	1
O4	4	0.32100	0.35300	0.25900	O-2	1	1
O5	4	0.00600	0.30700	0.26800	O-2	1	1
O6	4	0.52200	0.19600	0.23300	O-2	1	1
O7	4	0.20600	0.11000	0.38900	O-2	1	1
O8	4	0.68300	0.36900	0.43000	O-2	1	1
Si1	4	0.00800	0.17100	0.20900	Si+4	0.28	1
Al1	4	0.00800	0.17100	0.20900	Al+3	0.72	1
Si2	4	0.50800	0.31800	0.24100	Si+4	1	1
Si3	4	0.69200	0.11000	0.31500	Si+4	0.8	1
Al3	4	0.69200	0.11000	0.31500	Al+3	0.2	1
Si4	4	0.18300	0.38200	0.35900	Si+4	0.91	1
Al4	4	0.18300	0.38200	0.35900	Al+3	0.09	1
Na1	4	0.27200	0.99000	0.14500	Na+1	1	1

9.1.2.3. Sample 2012-0001063, stratigraphic height: 1.07 m

Range Number : 1

R-Values

Rexp : 1.70 Rwp : 8.63 Rp : 5.50 GOF : 5.07
Rexp`: 5.25 Rwp`: 26.60 Rp` : 24.54 DW : 0.13

Quantitative Analysis - Rietveld
Phase 1 : „Quartz low“ 24.183 %
Phase 2 : „Kaolinite 1A II“ 1.684 %
Phase 3 : „Illite 2M1“ 70.779 %
Phase 4 : „Chamosite 1MIIb“ 1.949 %
Phase 5 : „Albite low“ 1.405 %

Background
  Chebychev polynomial, Coefficient 0 2794.864
  1 -988.6767
  2 441.0028
  3 -358.7637
  4 290.2571
  5 -172.4977
  6 44.78085

Instrument
  Primary radius (mm) 250
  Secondary radius (mm) 250
  Linear PSD 2Th angular range (∞) 2.749941
    FDS angle (∞) 0.0916
    Beam spill, sample length (mm) 9
      Intensity not corrected
  Full Axial Convolution
    Filament length (mm) 8
    Sample length (mm) 30
    Receiving Slit length (mm) 12
    Primary Sollers (∞) 2.5
    Secondary Sollers (∞) 2.5

Corrections
  Zero error -0.1029739
  Specimen displacement -0.2929346
  LP Factor 0

Miscellaneous
  Excluded Regions
    Start/Finish 0 0
    Start/Finish 0 0
    Start/Finish 0 0
    Start/Finish 0 0
    Start/Finish 0 0

Structure 1
  Phase name Quartz low
  R-Bragg 13.879
  Spacegroup P3221
  Scale 0.0109169243
  Cell Mass 180.252
  Cell Volume (≈^3) 112.97799
  Wt% - Rietveld 24.183
  Crystal Linear Absorption Coeff. (1/cm) 95.405
  Crystal Density (g/cm^3) 2.649
  Preferred Orientation (Dir 1 : 0 0 1) 1.175971
  PVII peak type
    FWHM = a + b/Cos(Th) + c Tan(Th)
      a 0.02193465
      b 0.003620367
      c 0.0007725955
    Exponent m = 0.6+ma+mb/Cos(Th)+mc/Tan(Th)
      ma 0.02258105
      mb 0.1205058

mc 0.001443192
Lattice parameters
a (≈) 4.9130671
c (≈) 5.4045288

Site	Np	x	y	z	Atom	Occ	Beq
Si1	3	0.46900	0.00000	0.66667	Si+4	1	1
O1	6	0.40300	0.25300	0.78900	O-2	1	1

Structure 2
Phase name Kaolinite 1A II
R-Bragg 29.658
Spacegroup C1
Scale 9.36833344e-005
Cell Mass 508.256
Cell Volume (≈^3) 325.10507
Wt% - Rietveld 1.684
Crystal Linear Absorption Coeff. (1/cm) 81.026
Crystal Density (g/cm^3) 2.596
Preferred Orientation (Dir 1 : 0 0 1) 0.4057058
PVII peak type
FWHM = a + b/Cos(Th) + c Tan(Th)
a 0.5632083
b 0.06475427
c 0.9965475
Exponent m = 0.6+ma+mb/Cos(Th)+mc/Tan(Th)
ma 0.000100297
mb 0.0001269321
mc 4.752498
Lattice parameters
a (≈) 5.3322134
b (≈) 8.3787153
c (≈) 7.5046934
alpha (∞) 93.05501
beta (∞) 103.7211
gamma (∞) 90.97204

Site	Np	x	y	z	Atom	Occ	Beq
O1	2	0.77800	0.18000	-0.14000	O-2	1	1
O2	2	0.27800	0.32000	-0.13800	O-2	1	1
O3	2	0.31600	-0.00800	-0.13600	O-2	1	1
O4	2	0.24800	0.18400	0.15500	O-2	1	1
O5	2	0.75400	0.31500	0.15500	O-2	1	1
O6	2	0.69000	0.00400	0.15700	O-2	1	1
O7	2	0.79100	0.16500	0.48200	O-2	1	1
O8	2	0.61200	-0.12000	0.45500	O-2	1	1
O9	2	0.10800	-0.05800	0.45500	O-2	1	1
Al1	2	0.50200	0.17200	0.00300	Al+3	1	1
Al2	2	0.00200	0.33000	0.00200	Al+3	1	1
Si1	2	0.80000	0.32200	0.38200	Si+4	1	1
Si2	2	0.80000	0.00000	0.38500	Si+4	1	1

Structure 3
Phase name Illite 2M1

R-Bragg	26.387
Spacegroup	C12/c1
Scale	0.000439584765
Cell Mass	1580.752
Cell Volume (≈^3)	936.37809
Wt% - Rietveld	70.779
Crystallite Size	
Cry size Lorentzian (nm)	24.3
Crystal Linear Absorption Coeff. (1/cm)	119.514
Crystal Density (g/cm^3)	2.803
Preferred Orientation (Dir 1 : 0 0 1)	0.3707387
Preferred Orientation Spherical Harmonics	
Order	8
y00	1
y20	0.5664086
y22m	-0.01219096
y22p	-0.1086955
y40	0.4944891
y42m	-0.2021985
y42p	-0.4897818
y44m	0.7504354
y44p	-0.03300458
y60	-0.003201493
y62m	0.4088373
y62p	0.4414064
y64m	-0.2923048
y64p	-0.2428385
y66m	0.3010343
y66p	0.3010343
y80	0.1127249
y82m	1.094195
y82p	0.358576
y84m	-0.9208658
y84p	-0.08104417
y86m	0.1001439
y86p	0.02759526
y88m	0.3689217
y88p	0.09151908
PVII peak type	
FWHM = a + b/Cos(Th) + c Tan(Th)	
a	0.000107908
b	0.0001080154
c	0.04304051
Exponent m = 0.6+ma+mb/Cos(Th)+mc/Tan(Th)	
ma	0.0001005851
mb	0.007320175
mc	0.1013105
Lattice parameters	
a (≈)	5.2066934
b (≈)	9.0141858
c (≈)	20.0593564
beta (∞)	95.96047

Site	Np	x	y	z	Atom	Occ	Beq
Si1	8	0.48250	0.92970	0.13700	Si+4	1	1.737
Al1	8	0.44320	0.26350	0.13650	Al+3	1	0.8685

Al2	8	0.25860	0.08280	0.00680	Al+3 1	2.132
K1	4	0.00000	0.09010	0.25000	K+1 1	5.922
O1	8	0.46230	0.91940	0.05050	O-2 1	1.184
O2	8	0.38350	0.26650	0.06630	O-2 1	3.711
O3	8	0.42590	0.10390	0.15300	O-2 1	0.9475
O4	8	0.22260	0.83680	0.16850	O-2 1	3.237
O5	8	0.27350	0.37220	0.16780	O-2 1	6.317
O6	8	0.40800	0.56710	0.04540	O-2 1	4.185

Structure 4

Phase name	Chamosite 1MIIb
R-Bragg	42.157
Spacegroup	C-1
Scale	2.04874524e-005
Cell Mass	1271.241
Cell Volume (≈^3)	688.00078
Wt% - Rietveld	1.949
Crystal Linear Absorption Coeff. (1/cm)	271.140
Crystal Density (g/cm^3)	3.068
Preferred Orientation (Dir 1 : 0 0 1)	0.3123627
PVII peak type	
FWHM = a + b/Cos(Th) + c Tan(Th)	
a	0.09091952
b	0.01448116
c	0.06951127
Exponent m = 0.6+ma+mb/Cos(Th)+mc/Tan(Th)	
ma	0.5419378
mb	0.5903229
mc	0.000114238
Lattice parameters	
a (≈)	5.4083795
b (≈)	9.0044365
c (≈)	14.2985996
alpha (∞)	90.04891
beta (∞)	98.57557
gamma (∞)	92.25189

Site	Np	x	y	z	Atom	Occ	Beq
Mg1	2	0.00000	0.00000	0.00000	Mg+2	0.538	0.1579
Fe1	2	0.00000	0.00000	0.00000	Fe+2	0.462	0.1579
Mg2	4	0.01410	0.33480	0.00270	Mg+2	0.496	0.1579
Fe2	4	0.01410	0.33480	0.00270	Fe+2	0.504	0.1579
Mg3	4	0.00320	0.16830	0.50040	Mg+2	0.494	0.1579
Fe3	4	0.00320	0.16830	0.50040	Fe+2	0.506	0.1579
Al1	2	0.00000	0.50000	0.50000	Al+3	1.362	0.2369
Si1	4	0.24000	0.17000	0.19410	Si+4	0.7125	0.07896
Al2	4	0.24000	0.17000	0.19410	Al+3	0.2875	0.07896
Si2	4	0.73000	0.99800	0.19450	Si+4	0.7125	0.07896
Al3	4	0.73000	0.99800	0.19450	Al+3	0.2875	0.07896
O1	4	0.19100	0.16350	0.07890	O-2	1	0.8685
O2	4	0.70500	0.99800	0.07560	O-2	1	0.8685
O3	4	0.23100	0.33600	0.23740	O-2	1	0.8685
O4	4	0.52800	0.11800	0.23020	O-2	1	0.8685
O5	4	0.01800	0.06100	0.23060	O-2	1	0.8685
O6	4	0.68900	0.33120	0.07420	O-2	1	0.8685

O7	4	0.14400	0.99900	0.43000	O-2	1	0.8685
O8	4	0.14300	0.33610	0.42860	O-2	1	0.8685
O9	4	0.64300	0.16270	0.43110	O-2	1	0.8685

Structure 5

Phase name	Albite low
R-Bragg	18.014
Spacegroup	C-1
Scale	1.85399542e-005
Cell Mass	1048.846
Cell Volume (≈^3)	664.19438
Wt% - Rietveld	1.405
Crystallite Size	
Cry size Lorentzian (nm)	611.1
Crystal Linear Absorption Coeff. (1/cm)	88.829
Crystal Density (g/cm^3)	2.622
Lattice parameters	
a (≈)	8.1380000
b (≈)	12.7890000
c (≈)	7.1560000
alpha (∞)	94.33
beta (∞)	116.57
gamma (∞)	87.65

Site	Np	x	y	z	Atom	Occ	Beq
O1	4	0.00900	0.13400	0.96700	O-2	1	1
O2	4	0.59500	0.99700	0.27900	O-2	1	1
O3	4	0.81800	0.11200	0.19200	O-2	1	1
O4	4	0.32100	0.35300	0.25900	O-2	1	1
O5	4	0.00600	0.30700	0.26800	O-2	1	1
O6	4	0.52200	0.19600	0.23300	O-2	1	1
O7	4	0.20600	0.11000	0.38900	O-2	1	1
O8	4	0.68300	0.36900	0.43000	O-2	1	1
Si1	4	0.00800	0.17100	0.20900	Si+4	0.28	1
Al1	4	0.00800	0.17100	0.20900	Al+3	0.72	1
Si2	4	0.50800	0.31800	0.24100	Si+4	1	1
Si3	4	0.69200	0.11000	0.31500	Si+4	0.8	1
Al3	4	0.69200	0.11000	0.31500	Al+3	0.2	1
Si4	4	0.18300	0.38200	0.35900	Si+4	0.91	1
Al4	4	0.18300	0.38200	0.35900	Al+3	0.09	1
Na1	4	0.27200	0.99000	0.14500	Na+1	1	1

9.1.2.4. Sample 2012-0001060, stratigraphic height: 1.65 m

Range Number : 1

R-Values

Rexp : 1.75 Rwp : 5.11 Rp : 3.73 GOF : 2.92
Rexp`: 6.80 Rwp`: 19.84 Rp` : 21.98 DW : 0.33

Quantitative Analysis - Rietveld

Phase 1 : „Quartz low“	25.665 %
Phase 2 : „Kaolinite 1A II“	5.597 %

Phase 3 : „Illite 2M1“ 64.064 %
Phase 4 : „Chamosite 1MIIb“ 2.173 %
Phase 5 : „Albite low“ 2.501 %

Background
Chebychev polynomial, Coefficient 0 2759.239
1 -831.6089
2 264.8245
3 -209.2412
4 131.5189
5 -73.74074
6 -29.33008

Instrument
Primary radius (mm) 250
Secondary radius (mm) 250
Linear PSD 2Th angular range (∞) 2.749941
FDS angle (∞) 0.0916
Beam spill, sample length (mm) 9
Intensity not corrected
Full Axial Convolution
Filament length (mm) 8
Sample length (mm) 30
Receiving Slit length (mm) 12
Primary Sollers (∞) 2.5
Secondary Sollers (∞) 2.5

Corrections
Zero error -0.06836235
Specimen displacement -0.3322272
LP Factor 0

Miscellaneous
Excluded Regions
Start/Finish 0 0
Start/Finish 0 0
Start/Finish 0 0
Start/Finish 0 0
Start/Finish 0 0

Structure 1
Phase name Quartz low
R-Bragg 21.989
Spacegroup P3221
Scale 0.0101349608
Cell Mass 180.252
Cell Volume (≈^3) 112.94502
Wt% - Rietveld 25.665
Crystal Linear Absorption Coeff. (1/cm) 95.433
Crystal Density (g/cm^3) 2.650
Preferred Orientation (Dir 1 : 0 0 1) 1.216574
PVII peak type
FWHM = a + b/Cos(Th) + c Tan(Th)
a 0.02081634
b 0.00415091

c 0.0001041435
Exponent m = 0.6+ma+mb/Cos(Th)+mc/Tan(Th)
ma 0.04100619
mb 0.1127128
mc 0.0511175
Lattice parameters
a (≈) 4.9125785
c (≈) 5.4040264

Site	Np	x	y	z	Atom	Occ	Beq
Si1	3	0.46900	0.00000	0.66667	Si+4	1	1
O1	6	0.40300	0.25300	0.78900	O-2	1	1

Structure 2
Phase name Kaolinite 1A II
R-Bragg 21.828
Spacegroup C1
Scale 0.00027231354
Cell Mass 508.256
Cell Volume (≈^3) 325.10507
Wt% - Rietveld 5.597
Crystal Linear Absorption Coeff. (1/cm) 81.026
Crystal Density (g/cm^3) 2.596
Preferred Orientation (Dir 1 : 0 0 1) 0.8073373
PVII peak type
FWHM = a + b/Cos(Th) + c Tan(Th)
a 0.2883872
b 0.001144575
c 0.0001000443
Exponent m = 0.6+ma+mb/Cos(Th)+mc/Tan(Th)
ma 0.009832903
mb 0.002531821
mc 0.1541369
Lattice parameters
a (≈) 5.3322134
b (≈) 8.3787153
c (≈) 7.5046934
alpha (∞) 93.05501
beta (∞) 103.7211
gamma (∞) 90.97204

Site	Np	x	y	z	Atom	Occ	Beq
O1	2	0.77800	0.18000	-0.14000	O-2	1	1
O2	2	0.27800	0.32000	-0.13800	O-2	1	1
O3	2	0.31600	-0.00800	-0.13600	O-2	1	1
O4	2	0.24800	0.18400	0.15500	O-2	1	1
O5	2	0.75400	0.31500	0.15500	O-2	1	1
O6	2	0.69000	0.00400	0.15700	O-2	1	1
O7	2	0.79100	0.16500	0.48200	O-2	1	1
O8	2	0.61200	-0.12000	0.45500	O-2	1	1
O9	2	0.10800	-0.05800	0.45500	O-2	1	1
Al1	2	0.50200	0.17200	0.00300	Al+3	1	1
Al2	2	0.00200	0.33000	0.00200	Al+3	1	1
Si1	2	0.80000	0.32200	0.38200	Si+4	1	1
Si2	2	0.80000	0.00000	0.38500	Si+4	1	1

Structure 3

Phase name	Illite 2M1
R-Bragg	12.929
Spacegroup	C12/c1
Scale	0.000347954165
Cell Mass	1580.752
Cell Volume (≈^3)	936.37809
Wt% - Rietveld	64.064
Crystallite Size	
Cry size Lorentzian (nm)	26.3
Crystal Linear Absorption Coeff. (1/cm)	119.514
Crystal Density (g/cm^3)	2.803
Preferred Orientation (Dir 1 : 0 0 1)	0.3894832
Preferred Orientation Spherical Harmonics	
Order	8
y00	1
y20	0.5868845
y22m	-0.009286364
y22p	-0.08580424
y40	0.5123925
y42m	-0.2511581
y42p	-0.4926561
y44m	1.012194
y44p	-0.02581023
y60	-0.0009505581
y62m	0.266004
y62p	0.4378868
y64m	-0.191239
y64p	-0.2562034
y66m	0.3095274
y66p	0.3095274
y80	0.05820703
y82m	1.044898
y82p	0.3311557
y84m	-0.8172634
y84p	-0.07163539
y86m	0.05599772
y86p	0.02585248
y88m	0.1766893
y88p	0.07095233
PVII peak type	
FWHM = a + b/Cos(Th) + c Tan(Th)	
a	0.0001
b	0.0001
c	0.04309676
Exponent m = 0.6+ma+mb/Cos(Th)+mc/Tan(Th)	
ma	0.01927093
mb	0.08317178
mc	0.06027738
Lattice parameters	
a (≈)	5.2066934
b (≈)	9.0141858
c (≈)	20.0593564
beta (∞)	95.96047

Site	Np	x	y	z	Atom	Occ	Beq
Si1	8	0.48250	0.92970	0.13700	Si+4	1	1.737
Al1	8	0.44320	0.26350	0.13650	Al+3	1	0.8685
Al2	8	0.25860	0.08280	0.00680	Al+3	1	2.132
K1	4	0.00000	0.09010	0.25000	K+1	1	5.922
O1	8	0.46230	0.91940	0.05050	O-2	1	1.184
O2	8	0.38350	0.26650	0.06630	O-2	1	3.711
O3	8	0.42590	0.10390	0.15300	O-2	1	0.9475
O4	8	0.22260	0.83680	0.16850	O-2	1	3.237
O5	8	0.27350	0.37220	0.16780	O-2	1	6.317
O6	8	0.40800	0.56710	0.04540	O-2	1	4.185

Structure 4

Phase name	Chamosite 1MIIb
R-Bragg	32.013
Spacegroup	C-1
Scale	1.99773169e-005
Cell Mass	1271.241
Cell Volume (≈^3)	688.00078
Wt% - Rietveld	2.173
Crystal Linear Absorption Coeff. (1/cm)	271.140
Crystal Density (g/cm^3)	3.068
Preferred Orientation (Dir 1 : 0 0 1)	0.3288249
PVII peak type	
FWHM = a + b/Cos(Th) + c Tan(Th)	
a	0.05657344
b	0.0259586
c	0.1224401
Exponent m = 0.6+ma+mb/Cos(Th)+mc/Tan(Th)	
ma	0.2278584
mb	0.2032876
mc	0.0001021086
Lattice parameters	
a (≈)	5.4083795
b (≈)	9.0044365
c (≈)	14.2985996
alpha (∞)	90.04891
beta (∞)	98.57557
gamma (∞)	92.25189

Site	Np	x	y	z	Atom	Occ	Beq
Mg1	2	0.00000	0.00000	0.00000	Mg+2	0.538	0.1579
Fe1	2	0.00000	0.00000	0.00000	Fe+2	0.462	0.1579
Mg2	4	0.01410	0.33480	0.00270	Mg+2	0.496	0.1579
Fe2	4	0.01410	0.33480	0.00270	Fe+2	0.504	0.1579
Mg3	4	0.00320	0.16830	0.50040	Mg+2	0.494	0.1579
Fe3	4	0.00320	0.16830	0.50040	Fe+2	0.506	0.1579
Al1	2	0.00000	0.50000	0.50000	Al+3	1.362	0.2369
Si1	4	0.24000	0.17000	0.19410	Si+4	0.7125	0.07896
Al2	4	0.24000	0.17000	0.19410	Al+3	0.2875	0.07896
Si2	4	0.73000	0.99800	0.19450	Si+4	0.7125	0.07896
Al3	4	0.73000	0.99800	0.19450	Al+3	0.2875	0.07896
O1	4	0.19100	0.16350	0.07890	O-2	1	0.8685
O2	4	0.70500	0.99800	0.07560	O-2	1	0.8685

O3	4	0.23100	0.33600	0.23740	O-2	1 0.8685
O4	4	0.52800	0.11800	0.23020	O-2	1 0.8685
O5	4	0.01800	0.06100	0.23060	O-2	1 0.8685
O6	4	0.68900	0.33120	0.07420	O-2	1 0.8685
O7	4	0.14400	0.99900	0.43000	O-2	1 0.8685
O8	4	0.14300	0.33610	0.42860	O-2	1 0.8685
O9	4	0.64300	0.16270	0.43110	O-2	1 0.8685

Structure 5

Phase name	Albite low
R-Bragg	15.023
Spacegroup	C-1
Scale	2.88608032e-005
Cell Mass	1048.846
Cell Volume (≈^3)	664.19438
Wt% - Rietveld	2.501
Crystallite Size	
Cry size Lorentzian (nm)	263.7
Crystal Linear Absorption Coeff. (1/cm)	88.829
Crystal Density (g/cm^3)	2.622
Lattice parameters	
a (≈)	8.1380000
b (≈)	12.7890000
c (≈)	7.1560000
alpha (∞)	94.33
beta (∞)	116.57
gamma (∞)	87.65

Site	Np	x	y	z	Atom	Occ	Beq
O1	4	0.00900	0.13400	0.96700	O-2	1	1
O2	4	0.59500	0.99700	0.27900	O-2	1	1
O3	4	0.81800	0.11200	0.19200	O-2	1	1
O4	4	0.32100	0.35300	0.25900	O-2	1	1
O5	4	0.00600	0.30700	0.26800	O-2	1	1
O6	4	0.52200	0.19600	0.23300	O-2	1	1
O7	4	0.20600	0.11000	0.38900	O-2	1	1
O8	4	0.68300	0.36900	0.43000	O-2	1	1
Si1	4	0.00800	0.17100	0.20900	Si+4	0.28	1
Al1	4	0.00800	0.17100	0.20900	Al+3	0.72	1
Si2	4	0.50800	0.31800	0.24100	Si+4	1	1
Si3	4	0.69200	0.11000	0.31500	Si+4	0.8	1
Al3	4	0.69200	0.11000	0.31500	Al+3	0.2	1
Si4	4	0.18300	0.38200	0.35900	Si+4	0.91	1
Al4	4	0.18300	0.38200	0.35900	Al+3	0.09	1
Na1	4	0.27200	0.99000	0.14500	Na+1	1	1

9.1.2.5. Sample 2012-0001062, stratigraphic height: 1.98 m

Range Number : 1

R-Values

Rexp : 1.78 Rwp : 9.81 Rp : 6.55 GOF : 5.51
Rexp`: 4.81 Rwp`: 26.52 Rp` : 24.01 DW : 0.11

Quantitative Analysis - Rietveld
  Phase 1 : „Quartz low“ 13.599 %
  Phase 2 : „Kaolinite 1A II“ 0.269 %
  Phase 3 : „Illite 2M1“ 83.508 %
  Phase 4 : „Chamosite 1MIIb“ 0.071 %
  Phase 5 : „Albite low“ 2.553 %

Background
  Chebychev polynomial, Coefficient 0 2700.887
  1 -1807.765
  2 1171.842
  3 -841.8048
  4 696.918
  5 -447.476
  6 229.1375

Instrument
  Primary radius (mm) 250
  Secondary radius (mm) 250
  Linear PSD 2Th angular range (∞) 2.749941
    FDS angle (∞) 0.0916
    Beam spill, sample length (mm) 9
      Intensity not corrected
  Full Axial Convolution
    Filament length (mm) 8
    Sample length (mm) 30
    Receiving Slit length (mm) 12
    Primary Sollers (∞) 2.5
    Secondary Sollers (∞) 2.5

Corrections
  Zero error -0.1314964
  Specimen displacement -0.3886019
  LP Factor 0

Miscellaneous
  Excluded Regions
    Start/Finish 0 0
    Start/Finish 0 0
    Start/Finish 0 0
    Start/Finish 0 0
    Start/Finish 0 0

Structure 1
  Phase name Quartz low
  R-Bragg 8.617
  Spacegroup P3221
  Scale 0.0077782525
  Cell Mass 180.252
  Cell Volume (≈^3) 112.79771
  Wt% - Rietveld 13.599
  Crystal Linear Absorption Coeff. (1/cm) 95.558
  Crystal Density (g/cm^3) 2.654
  Preferred Orientation (Dir 1 : 0 0 1) 1.213604

PVII peak type
FWHM = a + b/Cos(Th) + c Tan(Th)
a 0.0255433
b 0.005637584
c 0.0001383347
Exponent m = 0.6+ma+mb/Cos(Th)+mc/Tan(Th)
ma 0.03420475
mb 0.4530939
mc 0.01169635
Lattice parameters
a (≈) 4.9107184
c (≈) 5.4010674

Site	Np	x	y	z	Atom	Occ	Beq
Si1	3	0.46900	0.00000	0.66667	Si+4	1	1
O1	6	0.40300	0.25300	0.78900	O-2	1	1

Structure 2
Phase name Kaolinite 1A II
R-Bragg 8.938
Spacegroup C1
Scale 1.89146498e-005
Cell Mass 508.256
Cell Volume (≈^3) 325.10507
Wt% - Rietveld 0.269
Crystal Linear Absorption Coeff. (1/cm) 81.026
Crystal Density (g/cm^3) 2.596
Preferred Orientation (Dir 1 : 0 0 1) 0.6103306
PVII peak type
FWHM = a + b/Cos(Th) + c Tan(Th)
a 0.0131297
b 0.01233619
c 0.5549308
Exponent m = 0.6+ma+mb/Cos(Th)+mc/Tan(Th)
ma 0.000173437
mb 0.0001633907
mc 4.949521
Lattice parameters
a (≈) 5.3322134
b (≈) 8.3787153
c (≈) 7.5046934
alpha (∞) 93.05501
beta (∞) 103.7211
gamma (∞) 90.97204

Site	Np	x	y	z	Atom	Occ	Beq
O1	2	0.77800	0.18000	-0.14000	O-2	1	1
O2	2	0.27800	0.32000	-0.13800	O-2	1	1
O3	2	0.31600	-0.00800	-0.13600	O-2	1	1
O4	2	0.24800	0.18400	0.15500	O-2	1	1
O5	2	0.75400	0.31500	0.15500	O-2	1	1
O6	2	0.69000	0.00400	0.15700	O-2	1	1
O7	2	0.79100	0.16500	0.48200	O-2	1	1
O8	2	0.61200	-0.12000	0.45500	O-2	1	1
O9	2	0.10800	-0.05800	0.45500	O-2	1	1

Al1	2	0.50200	0.17200	0.00300	Al+3 1	1
Al2	2	0.00200	0.33000	0.00200	Al+3 1	1
Si1	2	0.80000	0.32200	0.38200	Si+4 1	1
Si2	2	0.80000	0.00000	0.38500	Si+4 1	1

Structure 3

Phase name	Illite 2M1
R-Bragg	29.306
Spacegroup	C12/c1
Scale	0.000656089944
Cell Mass	1580.752
Cell Volume (≈^3)	936.37809
Wt% - Rietveld	83.508
Crystallite Size	
Cry size Lorentzian (nm)	20.5
Crystal Linear Absorption Coeff. (1/cm)	119.514
Crystal Density (g/cm^3)	2.803
Preferred Orientation (Dir 1 : 0 0 1)	0.3365605
Preferred Orientation Spherical Harmonics	
Order	8
y00	1
y20	0.5140737
y22m	-0.1801719
y22p	-0.1400693
y40	0.4525523
y42m	-0.5686358
y42p	-0.5267385
y44m	0.7252271
y44p	-0.04346279
y60	-0.004113028
y62m	-0.2499176
y62p	0.4701506
y64m	0.08905631
y64p	-0.2559041
y66m	0.2971103
y66p	0.2971103
y80	0.1829712
y82m	0.5668058
y82p	0.3271666
y84m	-0.3715099
y84p	-0.118616
y86m	-0.1562168
y86p	0.04697542
y88m	0.09151262
y88p	0.08137784
PVII peak type	
FWHM = a + b/Cos(Th) + c Tan(Th)	
a	0.0001000116
b	0.0001000116
c	0.0389111
Exponent m = 0.6+ma+mb/Cos(Th)+mc/Tan(Th)	
ma	0.0001005334
mb	0.0005566108
mc	0.03138229
Lattice parameters	

a (≈)	5.2066934
b (≈)	9.0141858
c (≈)	20.0593564
beta (∞)	95.96047

Site	Np	x	y	z	Atom	Occ	Beq
Si1	8	0.48250	0.92970	0.13700	Si+4	1	1.737
Al1	8	0.44320	0.26350	0.13650	Al+3	1	0.8685
Al2	8	0.25860	0.08280	0.00680	Al+3	1	2.132
K1	4	0.00000	0.09010	0.25000	K+1	1	5.922
O1	8	0.46230	0.91940	0.05050	O-2	1	1.184
O2	8	0.38350	0.26650	0.06630	O-2	1	3.711
O3	8	0.42590	0.10390	0.15300	O-2	1	0.9475
O4	8	0.22260	0.83680	0.16850	O-2	1	3.237
O5	8	0.27350	0.37220	0.16780	O-2	1	6.317
O6	8	0.40800	0.56710	0.04540	O-2	1	4.185

Structure 4

Phase name	Chamosite 1MIIb
R-Bragg	46.553
Spacegroup	C-1
Scale	9.50571129e-007
Cell Mass	1271.241
Cell Volume (≈^3)	688.00078
Wt% - Rietveld	0.071
Crystal Linear Absorption Coeff. (1/cm)	271.140
Crystal Density (g/cm^3)	3.068
Preferred Orientation (Dir 1 : 0 0 1)	0.1204959
PVII peak type	
FWHM = a + b/Cos(Th) + c Tan(Th)	
a	0.05951104
b	0.04405392
c	0.1674605
Exponent m = 0.6+ma+mb/Cos(Th)+mc/Tan(Th)	
ma	0.2057566
mb	0.2285163
mc	0.0001560789
Lattice parameters	
a (≈)	5.4083795
b (≈)	9.0044365
c (≈)	14.2985996
alpha (∞)	90.04891
beta (∞)	98.57557
gamma (∞)	92.25189

Site	Np	x	y	z	Atom	Occ	Beq
Mg1	2	0.00000	0.00000	0.00000	Mg+2	0.538	0.1579
Fe1	2	0.00000	0.00000	0.00000	Fe+2	0.462	0.1579
Mg2	4	0.01410	0.33480	0.00270	Mg+2	0.496	0.1579
Fe2	4	0.01410	0.33480	0.00270	Fe+2	0.504	0.1579
Mg3	4	0.00320	0.16830	0.50040	Mg+2	0.494	0.1579
Fe3	4	0.00320	0.16830	0.50040	Fe+2	0.506	0.1579
Al1	2	0.00000	0.50000	0.50000	Al+3	1.362	0.2369
Si1	4	0.24000	0.17000	0.19410	Si+4	0.7125	0.07896
Al2	4	0.24000	0.17000	0.19410	Al+3	0.2875	0.07896

Si2	4	0.73000	0.99800	0.19450	Si+4	0.7125	0.07896
Al3	4	0.73000	0.99800	0.19450	Al+3	0.2875	0.07896
O1	4	0.19100	0.16350	0.07890	O-2	1	0.8685
O2	4	0.70500	0.99800	0.07560	O-2	1	0.8685
O3	4	0.23100	0.33600	0.23740	O-2	1	0.8685
O4	4	0.52800	0.11800	0.23020	O-2	1	0.8685
O5	4	0.01800	0.06100	0.23060	O-2	1	0.8685
O6	4	0.68900	0.33120	0.07420	O-2	1	0.8685
O7	4	0.14400	0.99900	0.43000	O-2	1	0.8685
O8	4	0.14300	0.33610	0.42860	O-2	1	0.8685
O9	4	0.64300	0.16270	0.43110	O-2	1	0.8685

Structure 5

Phase name	Albite low
R-Bragg	6.770
Spacegroup	C-1
Scale	4.26122391e-005
Cell Mass	1048.846
Cell Volume (≈^3)	664.19438
Wt% - Rietveld	2.553
Crystallite Size	
Cry size Lorentzian (nm)	120.6
Crystal Linear Absorption Coeff. (1/cm)	88.829
Crystal Density (g/cm^3)	2.622
Lattice parameters	
a (≈)	8.1380000
b (≈)	12.7890000
c (≈)	7.1560000
alpha (∞)	94.33
beta (∞)	116.57
gamma (∞)	87.65

Site	Np	x	y	z	Atom	Occ	Beq
O1	4	0.00900	0.13400	0.96700	O-2	1	1
O2	4	0.59500	0.99700	0.27900	O-2	1	1
O3	4	0.81800	0.11200	0.19200	O-2	1	1
O4	4	0.32100	0.35300	0.25900	O-2	1	1
O5	4	0.00600	0.30700	0.26800	O-2	1	1
O6	4	0.52200	0.19600	0.23300	O-2	1	1
O7	4	0.20600	0.11000	0.38900	O-2	1	1
O8	4	0.68300	0.36900	0.43000	O-2	1	1
Si1	4	0.00800	0.17100	0.20900	Si+4	0.28	1
Al1	4	0.00800	0.17100	0.20900	Al+3	0.72	1
Si2	4	0.50800	0.31800	0.24100	Si+4	1	1
Si3	4	0.69200	0.11000	0.31500	Si+4	0.8	1
Al3	4	0.69200	0.11000	0.31500	Al+3	0.2	1
Si4	4	0.18300	0.38200	0.35900	Si+4	0.91	1
Al4	4	0.18300	0.38200	0.35900	Al+3	0.09	1
Na1	4	0.27200	0.99000	0.14500	Na+1	1	1

9.1.2.6. Sample 2012-0001061, stratigraphic height: 2.51 m

Range Number : 1

R-Values

Rexp : 1.64 Rwp : 6.25 Rp : 4.28 GOF : 3.81
Rexp`: 5.68 Rwp`: 21.62 Rp` : 21.38 DW : 0.21

Quantitative Analysis - Rietveld
Phase 1 : „Quartz low“ 18.087 %
Phase 2 : „Kaolinite 1A II“ 1.928 %
Phase 3 : „Illite 2M1“ 76.585 %
Phase 4 : „Chamosite 1MIIb“ 1.452 %
Phase 5 : „Albite low“ 1.949 %

Background
Chebychev polynomial, Coefficient 0 3168.331
1 -1429.254
2 691.2926
3 -479.7788
4 365.6793
5 -225.0908
6 79.11545

Instrument
Primary radius (mm) 250
Secondary radius (mm) 250
Linear PSD 2Th angular range (∞) 2.749941
FDS angle (∞) 0.0916
Beam spill, sample length (mm) 9
Intensity not corrected
Full Axial Convolution
Filament length (mm) 8
Sample length (mm) 30
Receiving Slit length (mm) 12
Primary Sollers (∞) 2.5
Secondary Sollers (∞) 2.5

Corrections
Zero error -0.1194582
Specimen displacement -0.3100813
LP Factor 0

Miscellaneous
Excluded Regions
Start/Finish 0 0
Start/Finish 0 0
Start/Finish 0 0
Start/Finish 0 0
Start/Finish 0 0

Structure 1
Phase name Quartz low
R-Bragg 12.265
Spacegroup P3221
Scale 0.00985528551
Cell Mass 180.252

Cell Volume (≈^3) 112.91149
Wt% - Rietveld 18.087
Crystal Linear Absorption Coeff. (1/cm) 95.461
Crystal Density (g/cm^3) 2.651
Preferred Orientation (Dir 1 : 0 0 1) 1.21106
PVII peak type
FWHM = a + b/Cos(Th) + c Tan(Th)
a 0.01186146
b 0.00667953
c 0.001181339
Exponent m = 0.6+ma+mb/Cos(Th)+mc/Tan(Th)
ma 0.040763
mb 0.1094316
mc 0.02587049
Lattice parameters
a (≈) 4.9121498
c (≈) 5.4033651

Site	Np	x	y	z	Atom	Occ	Beq
Si1	3	0.46900	0.00000	0.66667	Si+4	1	1
O1	6	0.40300	0.25300	0.78900	O-2	1	1

Structure 2
Phase name Kaolinite 1A II
R-Bragg 33.877
Spacegroup C1
Scale 0.000129366437
Cell Mass 508.256
Cell Volume (≈^3) 325.10507
Wt% - Rietveld 1.928
Crystal Linear Absorption Coeff. (1/cm) 81.026
Crystal Density (g/cm^3) 2.596
Preferred Orientation (Dir 1 : 0 0 1) 0.536969
PVII peak type
FWHM = a + b/Cos(Th) + c Tan(Th)
a 0.259077
b 0.0001175839
c 0.9999866
Exponent m = 0.6+ma+mb/Cos(Th)+mc/Tan(Th)
ma 0.0001000006
mb 0.0001000526
mc 0.1852889
Lattice parameters
a (≈) 5.3322134
b (≈) 8.3787153
c (≈) 7.5046934
alpha (∞) 93.05501
beta (∞) 103.7211
gamma (∞) 90.97204

Site	Np	x	y	z	Atom	Occ	Beq
O1	2	0.77800	0.18000	-0.14000	O-2	1	1
O2	2	0.27800	0.32000	-0.13800	O-2	1	1
O3	2	0.31600	-0.00800	-0.13600	O-2	1	1
O4	2	0.24800	0.18400	0.15500	O-2	1	1

O5	2	0.75400	0.31500	0.15500	O-2	1	1
O6	2	0.69000	0.00400	0.15700	O-2	1	1
O7	2	0.79100	0.16500	0.48200	O-2	1	1
O8	2	0.61200	-0.12000	0.45500	O-2	1	1
O9	2	0.10800	-0.05800	0.45500	O-2	1	1
Al1	2	0.50200	0.17200	0.00300	Al+3	1	1
Al2	2	0.00200	0.33000	0.00200	Al+3	1	1
Si1	2	0.80000	0.32200	0.38200	Si+4	1	1
Si2	2	0.80000	0.00000	0.38500	Si+4	1	1

Structure 3

Phase name	Illite 2M1
R-Bragg	29.848
Spacegroup	C12/c1
Scale	0.00057378244
Cell Mass	1580.752
Cell Volume (≈^3)	936.37809
Wt% - Rietveld	76.585
Crystallite Size	
Cry size Lorentzian (nm)	23.2
Crystal Linear Absorption Coeff. (1/cm)	119.514
Crystal Density (g/cm^3)	2.803
Preferred Orientation (Dir 1 : 0 0 1)	0.3837712
Preferred Orientation Spherical Harmonics	
Order	8
y00	1
y20	0.5736766
y22m	-0.1772352
y22p	-0.1215529
y40	0.4747414
y42m	-0.4257402
y42p	-0.5056801
y44m	0.7248887
y44p	-0.02576216
y60	-0.006177901
y62m	-0.0007038831
y62p	0.4518133
y64m	-0.0380408
y64p	-0.2362618
y66m	0.2920178
y66p	0.2920178
y80	0.1097039
y82m	0.6662991
y82p	0.3573444
y84m	-0.6274689
y84p	-0.0676547
y86m	-0.01248366
y86p	0.001478773
y88m	0.2020923
y88p	0.07873057
PVII peak type	
FWHM = a + b/Cos(Th) + c Tan(Th)	
a	0.0001004617
b	0.0001005703
c	0.04529979

Exponent m = 0.6+ma+mb/Cos(Th)+mc/Tan(Th)
ma 0.0001000011
mb 0.0001001773
mc 0.038126
Lattice parameters
a (≈) 5.2066934
b (≈) 9.0141858
c (≈) 20.0593564
beta (∞) 95.96047

Site	Np	x	y	z	Atom	Occ	Beq
Si1	8	0.48250	0.92970	0.13700	Si+4	1	1.737
Al1	8	0.44320	0.26350	0.13650	Al+3	1	0.8685
Al2	8	0.25860	0.08280	0.00680	Al+3	1	2.132
K1	4	0.00000	0.09010	0.25000	K+1	1	5.922
O1	8	0.46230	0.91940	0.05050	O-2	1	1.184
O2	8	0.38350	0.26650	0.06630	O-2	1	3.711
O3	8	0.42590	0.10390	0.15300	O-2	1	0.9475
O4	8	0.22260	0.83680	0.16850	O-2	1	3.237
O5	8	0.27350	0.37220	0.16780	O-2	1	6.317
O6	8	0.40800	0.56710	0.04540	O-2	1	4.185

Structure 4
Phase name Chamosite 1MIIb
R-Bragg 39.000
Spacegroup C-1
Scale 1.84069246e-005
Cell Mass 1271.241
Cell Volume (≈^3) 688.00078
Wt% - Rietveld 1.452
Crystal Linear Absorption Coeff. (1/cm) 271.140
Crystal Density (g/cm^3) 3.068
Preferred Orientation (Dir 1 : 0 0 1) 0.3091309
PVII peak type
FWHM = a + b/Cos(Th) + c Tan(Th)
a 0.04706562
b 0.02532563
c 0.1916032
Exponent m = 0.6+ma+mb/Cos(Th)+mc/Tan(Th)
ma 0.2397308
mb 0.2224771
mc 0.0001000278
Lattice parameters
a (≈) 5.4083795
b (≈) 9.0044365
c (≈) 14.2985996
alpha (∞) 90.04891
beta (∞) 98.57557
gamma (∞) 92.25189

Site	Np	x	y	z	Atom	Occ	Beq
Mg1	2	0.00000	0.00000	0.00000	Mg+2	0.538	0.1579
Fe1	2	0.00000	0.00000	0.00000	Fe+2	0.462	0.1579
Mg2	4	0.01410	0.33480	0.00270	Mg+2	0.496	0.1579
Fe2	4	0.01410	0.33480	0.00270	Fe+2	0.504	0.1579

Mg3	4	0.00320	0.16830	0.50040	Mg+2	0.494	0.1579
Fe3	4	0.00320	0.16830	0.50040	Fe+2	0.506	0.1579
Al1	2	0.00000	0.50000	0.50000	Al+3	1.362	0.2369
Si1	4	0.24000	0.17000	0.19410	Si+4	0.7125	0.07896
Al2	4	0.24000	0.17000	0.19410	Al+3	0.2875	0.07896
Si2	4	0.73000	0.99800	0.19450	Si+4	0.7125	0.07896
Al3	4	0.73000	0.99800	0.19450	Al+3	0.2875	0.07896
O1	4	0.19100	0.16350	0.07890	O-2	1	0.8685
O2	4	0.70500	0.99800	0.07560	O-2	1	0.8685
O3	4	0.23100	0.33600	0.23740	O-2	1	0.8685
O4	4	0.52800	0.11800	0.23020	O-2	1	0.8685
O5	4	0.01800	0.06100	0.23060	O-2	1	0.8685
O6	4	0.68900	0.33120	0.07420	O-2	1	0.8685
O7	4	0.14400	0.99900	0.43000	O-2	1	0.8685
O8	4	0.14300	0.33610	0.42860	O-2	1	0.8685
O9	4	0.64300	0.16270	0.43110	O-2	1	0.8685

Structure 5

Phase name	Albite low
R-Bragg	23.569
Spacegroup	C-1
Scale	3.10207979e-005
Cell Mass	1048.846
Cell Volume (≈^3)	664.19438
Wt% - Rietveld	1.949
Crystallite Size	
Cry size Lorentzian (nm)	322.7
Crystal Linear Absorption Coeff. (1/cm)	88.829
Crystal Density (g/cm^3)	2.622
Lattice parameters	
a (≈)	8.1380000
b (≈)	12.7890000
c (≈)	7.1560000
alpha (∞)	94.33
beta (∞)	116.57
gamma (∞)	87.65

Site	Np	x	y	z	Atom	Occ	Beq
O1	4	0.00900	0.13400	0.96700	O-2	1	1
O2	4	0.59500	0.99700	0.27900	O-2	1	1
O3	4	0.81800	0.11200	0.19200	O-2	1	1
O4	4	0.32100	0.35300	0.25900	O-2	1	1
O5	4	0.00600	0.30700	0.26800	O-2	1	1
O6	4	0.52200	0.19600	0.23300	O-2	1	1
O7	4	0.20600	0.11000	0.38900	O-2	1	1
O8	4	0.68300	0.36900	0.43000	O-2	1	1
Si1	4	0.00800	0.17100	0.20900	Si+4	0.28	1
Al1	4	0.00800	0.17100	0.20900	Al+3	0.72	1
Si2	4	0.50800	0.31800	0.24100	Si+4	1	1
Si3	4	0.69200	0.11000	0.31500	Si+4	0.8	1
Al3	4	0.69200	0.11000	0.31500	Al+3	0.2	1
Si4	4	0.18300	0.38200	0.35900	Si+4	0.91	1
Al4	4	0.18300	0.38200	0.35900	Al+3	0.09	1
Na1	4	0.27200	0.99000	0.14500	Na+1	1	1

9.1.2.7. Sample 2012-0001057, stratigraphic height: 3.50 m

Range Number : 1

R-Values

Rexp : 1.23 Rwp : 6.75 Rp : 4.80 GOF : 5.49
Rexp`: 3.66 Rwp`: 20.07 Rp` : 17.45 DW : 0.12

Quantitative Analysis - Rietveld
Phase 1 : „Quartz low“ 26.692 %
Phase 2 : „Kaolinite 1A II“ 2.256 %
Phase 3 : „Illite 2M1“ 67.485 %
Phase 4 : „Chamosite 1MIIb“ 1.886 %
Phase 5 : „Albite low“ 1.681 %

Background
Chebychev polynomial, Coefficient 0 5039.794
1 -1986.416
2 875.1201
3 -511.3527
4 307.4872
5 -121.491

Instrument
Primary radius (mm) 250
Secondary radius (mm) 250
Linear PSD 2Th angular range (∞) 2.749941
FDS angle (∞) 0.0916
Beam spill, sample length (mm) 9
Intensity not corrected
Full Axial Convolution
Filament length (mm) 8
Sample length (mm) 30
Receiving Slit length (mm) 12
Primary Sollers (∞) 2.5
Secondary Sollers (∞) 2.5

Corrections
Zero error -0.004574605
Specimen displacement -0.1607176
LP Factor 0

Miscellaneous
Excluded Regions
Start/Finish 0 0
Start/Finish 0 0
Start/Finish 0 0
Start/Finish 0 0
Start/Finish 0 0

Structure 1
Phase name Quartz low
R-Bragg 1.854

Spacegroup	P3221
Scale	0.0276193354
Cell Mass	180.252
Cell Volume (≈^3)	112.83135
Wt% - Rietveld	26.692
Crystal Linear Absorption Coeff. (1/cm)	95.529
Crystal Density (g/cm^3)	2.653
Preferred Orientation (Dir 1 : 0 0 1)	1.147905
PVII peak type	
FWHM = a + b/Cos(Th) + c Tan(Th)	
a	0.07481043
b	0.0001065798
c	0.0001
Exponent m = 0.6+ma+mb/Cos(Th)+mc/Tan(Th)	
ma	0.3537934
mb	0.2313009
mc	0.0001009291
Lattice parameters	
a (≈)	4.9117177
c (≈)	5.4004799

Site	Np	x	y	z	Atom	Occ	Beq
Si1	3	0.46900	0.00000	0.66667	Si+4	1	1
O1	6	0.40300	0.25300	0.78900	O-2	1	1

Structure 2

Phase name	Kaolinite 1A II
R-Bragg	2.739
Spacegroup	C1
Scale	0.000287269015
Cell Mass	508.256
Cell Volume (≈^3)	325.10507
Wt% - Rietveld	2.256
Crystal Linear Absorption Coeff. (1/cm)	81.026
Crystal Density (g/cm^3)	2.596
Preferred Orientation (Dir 1 : 0 0 1)	0.2504286
PVII peak type	
FWHM = a + b/Cos(Th) + c Tan(Th)	
a	0.4034847
b	0.9999876
c	1
Exponent m = 0.6+ma+mb/Cos(Th)+mc/Tan(Th)	
ma	0.0001
mb	0.0001
mc	0.06117625
Lattice parameters	
a (≈)	5.3322134
b (≈)	8.3787153
c (≈)	7.5046934
alpha (∞)	93.05501
beta (∞)	103.7211
gamma (∞)	90.97204

Site	Np	x	y	z	Atom	Occ	Beq
O1	2	0.77800	0.18000	-0.14000	O-2	1	1
O2	2	0.27800	0.32000	-0.13800	O-2	1	1

O3	2	0.31600	-0.00800	-0.13600	O-2	1	1
O4	2	0.24800	0.18400	0.15500	O-2	1	1
O5	2	0.75400	0.31500	0.15500	O-2	1	1
O6	2	0.69000	0.00400	0.15700	O-2	1	1
O7	2	0.79100	0.16500	0.48200	O-2	1	1
O8	2	0.61200	-0.12000	0.45500	O-2	1	1
O9	2	0.10800	-0.05800	0.45500	O-2	1	1
Al1	2	0.50200	0.17200	0.00300	Al+3	1	1
Al2	2	0.00200	0.33000	0.00200	Al+3	1	1
Si1	2	0.80000	0.32200	0.38200	Si+4	1	1
Si2	2	0.80000	0.00000	0.38500	Si+4	1	1

Structure 3

Phase name	Illite 2M1
R-Bragg	5.425
Spacegroup	C12/c1
Scale	0.000959458882
Cell Mass	1580.752
Cell Volume (≈^3)	936.37809
Wt% - Rietveld	67.485
Crystallite Size	
Cry size Lorentzian (nm)	18.5
Crystal Linear Absorption Coeff. (1/cm)	119.514
Crystal Density (g/cm^3)	2.803
Preferred Orientation (Dir 1 : 0 0 1)	0.6223919
Preferred Orientation Spherical Harmonics	
Order	8
y00	1
y20	-0.04457008
y22m	-0.3200041
y22p	-0.08864784
y40	0.06834813
y42m	-0.2718667
y42p	-0.3148789
y44m	-0.1742468
y44p	0.07440835
y60	-0.004437132
y62m	-0.2239791
y62p	0.1488484
y64m	-0.06738828
y64p	-0.160371
y66m	0.1470609
y66p	0.1470609
y80	-0.2752482
y82m	0.3225778
y82p	0.2211241
y84m	-0.3431424
y84p	-0.02666368
y86m	0.1086417
y86p	-0.2093362
y88m	0.06675995
y88p	0.2531729
PVII peak type	
FWHM = a + b/Cos(Th) + c Tan(Th)	
a	0.0001003005
b	0.0001003773

c 0.2022707
Exponent m = 0.6+ma+mb/Cos(Th)+mc/Tan(Th)
ma 0.0001536704
mb 0.0001281731
mc 0.497609
Lattice parameters
a (≈) 5.2066934
b (≈) 9.0141858
c (≈) 20.0593564
beta (∞) 95.96047

Site	Np	x	y	z	Atom	Occ	Beq
Si1	8	0.48250	0.92970	0.13700	Si+4	1	1.737
Al1	8	0.44320	0.26350	0.13650	Al+3	1	0.8685
Al2	8	0.25860	0.08280	0.00680	Al+3	1	2.132
K1	4	0.00000	0.09010	0.25000	K+1	1	5.922
O1	8	0.46230	0.91940	0.05050	O-2	1	1.184
O2	8	0.38350	0.26650	0.06630	O-2	1	3.711
O3	8	0.42590	0.10390	0.15300	O-2	1	0.9475
O4	8	0.22260	0.83680	0.16850	O-2	1	3.237
O5	8	0.27350	0.37220	0.16780	O-2	1	6.317
O6	8	0.40800	0.56710	0.04540	O-2	1	4.185

Structure 4
Phase name Chamosite 1MIIb
R-Bragg 4.480
Spacegroup C-1
Scale 4.53837433e-005
Cell Mass 1271.241
Cell Volume (≈^3) 688.00078
Wt% - Rietveld 1.886
Crystal Linear Absorption Coeff. (1/cm) 271.140
Crystal Density (g/cm^3) 3.068
Preferred Orientation (Dir 1 : 0 0 1) 0.4046407
PVII peak type
FWHM = a + b/Cos(Th) + c Tan(Th)
a 0.09316921
b 0.03198271
c 0.0001
Exponent m = 0.6+ma+mb/Cos(Th)+mc/Tan(Th)
ma 0.5607558
mb 0.0001002428
mc 0.0001000165
Lattice parameters
a (≈) 5.4083795
b (≈) 9.0044365
c (≈) 14.2985996
alpha (∞) 90.04891
beta (∞) 98.57557
gamma (∞) 92.25189

Site	Np	x	y	z	Atom	Occ	Beq
Mg1	2	0.00000	0.00000	0.00000	Mg+2	0.538	0.1579
Fe1	2	0.00000	0.00000	0.00000	Fe+2	0.462	0.1579
Mg2	4	0.01410	0.33480	0.00270	Mg+2	0.496	0.1579
Fe2	4	0.01410	0.33480	0.00270	Fe+2	0.504	0.1579

Mg3	4	0.00320	0.16830	0.50040	Mg+2	0.494	0.1579
Fe3	4	0.00320	0.16830	0.50040	Fe+2	0.506	0.1579
Al1	2	0.00000	0.50000	0.50000	Al+3	1.362	0.2369
Si1	4	0.24000	0.17000	0.19410	Si+4	0.7125	0.07896
Al2	4	0.24000	0.17000	0.19410	Al+3	0.2875	0.07896
Si2	4	0.73000	0.99800	0.19450	Si+4	0.7125	0.07896
Al3	4	0.73000	0.99800	0.19450	Al+3	0.2875	0.07896
O1	4	0.19100	0.16350	0.07890	O-2	1	0.8685
O2	4	0.70500	0.99800	0.07560	O-2	1	0.8685
O3	4	0.23100	0.33600	0.23740	O-2	1	0.8685
O4	4	0.52800	0.11800	0.23020	O-2	1	0.8685
O5	4	0.01800	0.06100	0.23060	O-2	1	0.8685
O6	4	0.68900	0.33120	0.07420	O-2	1	0.8685
O7	4	0.14400	0.99900	0.43000	O-2	1	0.8685
O8	4	0.14300	0.33610	0.42860	O-2	1	0.8685
O9	4	0.64300	0.16270	0.43110	O-2	1	0.8685

Structure 5

Phase name	Albite low
R-Bragg	10.350
Spacegroup	C-1
Scale	5.07753953e-005
Cell Mass	1048.846
Cell Volume (≈^3)	664.19438
Wt% - Rietveld	1.681
Crystallite Size	
Cry size Lorentzian (nm)	131.7
Crystal Linear Absorption Coeff. (1/cm)	88.829
Crystal Density (g/cm^3)	2.622
Lattice parameters	
a (≈)	8.1380000
b (≈)	12.7890000
c (≈)	7.1560000
alpha (∞)	94.33
beta (∞)	116.57
gamma (∞)	87.65

Site	Np	x	y	z	Atom	Occ	Beq
O1	4	0.00900	0.13400	0.96700	O-2	1	1
O2	4	0.59500	0.99700	0.27900	O-2	1	1
O3	4	0.81800	0.11200	0.19200	O-2	1	1
O4	4	0.32100	0.35300	0.25900	O-2	1	1
O5	4	0.00600	0.30700	0.26800	O-2	1	1
O6	4	0.52200	0.19600	0.23300	O-2	1	1
O7	4	0.20600	0.11000	0.38900	O-2	1	1
O8	4	0.68300	0.36900	0.43000	O-2	1	1
Si1	4	0.00800	0.17100	0.20900	Si+4	0.28	1
Al1	4	0.00800	0.17100	0.20900	Al+3	0.72	1
Si2	4	0.50800	0.31800	0.24100	Si+4	1	1
Si3	4	0.69200	0.11000	0.31500	Si+4	0.8	1
Al3	4	0.69200	0.11000	0.31500	Al+3	0.2	1
Si4	4	0.18300	0.38200	0.35900	Si+4	0.91	1
Al4	4	0.18300	0.38200	0.35900	Al+3	0.09	1
Na1	4	0.27200	0.99000	0.14500	Na+1	1	1

9.1.2.8. Sample 2012-0001083, stratigraphic height: 4.00 m

Range Number : 1

R-Values

Rexp : 1.85 Rwp : 4.88 Rp : 3.65 GOF : 2.64
Rexp`: 7.06 Rwp`: 18.61 Rp` : 19.84 DW : 0.40

Quantitative Analysis - Rietveld
Phase 1 : „Quartz low“ 18.474 %
Phase 2 : „Kaolinite 1A II“ 3.186 %
Phase 3 : „Illite 2M1“ 74.875 %
Phase 4 : „Chamosite 1MIIb“ 1.301 %
Phase 5 : „Albite low“ 2.165 %

Background
Chebychev polynomial, Coefficient 0 2540.304
1 -1104.538
2 533.2816
3 -390.1958
4 322.9378
5 -208.2582
6 82.91017

Instrument
Primary radius (mm) 250
Secondary radius (mm) 250
Linear PSD 2Th angular range (∞) 2.749941
FDS angle (∞) 0.0916
Beam spill, sample length (mm) 9
Intensity not corrected
Full Axial Convolution
Filament length (mm) 8
Sample length (mm) 30
Receiving Slit length (mm) 12
Primary Sollers (∞) 2.5
Secondary Sollers (∞) 2.5

Corrections
Zero error -0.08409145
Specimen displacement -0.4061314
LP Factor 0

Miscellaneous
Excluded Regions
Start/Finish 0 0
Start/Finish 0 0
Start/Finish 0 0
Start/Finish 0 0
Start/Finish 0 0

Structure 1
Phase name Quartz low

R-Bragg 6.327
Spacegroup P3221
Scale 0.00896897302
Cell Mass 180.252
Cell Volume (≈^3) 112.93697
Wt% - Rietveld 18.474
Crystal Linear Absorption Coeff. (1/cm) 95.440
Crystal Density (g/cm^3) 2.650
Preferred Orientation (Dir 1 : 0 0 1) 1.203073
PVII peak type
FWHM = a + b/Cos(Th) + c Tan(Th)
a 0.0106556
b 0.002481208
c 0.01275898
Exponent m = 0.6+ma+mb/Cos(Th)+mc/Tan(Th)
ma 0.003379339
mb 0.05979312
mc 0.09901624
Lattice parameters
a (≈) 4.9125099
c (≈) 5.4037917

Site	Np	x	y	z	Atom	Occ	Beq
Si1	3	0.46900	0.00000	0.66667	Si+4	1	1
O1	6	0.40300	0.25300	0.78900	O-2	1	1

Structure 2
Phase name Kaolinite 1A II
R-Bragg 10.500
Spacegroup C1
Scale 0.000190554172
Cell Mass 508.256
Cell Volume (≈^3) 325.10507
Wt% - Rietveld 3.186
Crystal Linear Absorption Coeff. (1/cm) 81.026
Crystal Density (g/cm^3) 2.596
Preferred Orientation (Dir 1 : 0 0 1) 0.9141041
PVII peak type
FWHM = a + b/Cos(Th) + c Tan(Th)
a 0.1071958
b 0.0007779515
c 0.9682863
Exponent m = 0.6+ma+mb/Cos(Th)+mc/Tan(Th)
ma 0.0001000371
mb 0.0001033665
mc 1.169936
Lattice parameters
a (≈) 5.3322134
b (≈) 8.3787153
c (≈) 7.5046934
alpha (∞) 93.05501
beta (∞) 103.7211
gamma (∞) 90.97204

Site	Np	x	y	z	Atom	Occ	Beq

O1	2	0.77800	0.18000	-0.14000	O-2	1	1
O2	2	0.27800	0.32000	-0.13800	O-2	1	1
O3	2	0.31600	-0.00800	-0.13600	O-2	1	1
O4	2	0.24800	0.18400	0.15500	O-2	1	1
O5	2	0.75400	0.31500	0.15500	O-2	1	1
O6	2	0.69000	0.00400	0.15700	O-2	1	1
O7	2	0.79100	0.16500	0.48200	O-2	1	1
O8	2	0.61200	-0.12000	0.45500	O-2	1	1
O9	2	0.10800	-0.05800	0.45500	O-2	1	1
Al1	2	0.50200	0.17200	0.00300	Al+3	1	1
Al2	2	0.00200	0.33000	0.00200	Al+3	1	1
Si1	2	0.80000	0.32200	0.38200	Si+4	1	1
Si2	2	0.80000	0.00000	0.38500	Si+4	1	1

Structure 3

Phase name	Illite 2M1
R-Bragg	9.689
Spacegroup	C12/c1
Scale	0.000499938101
Cell Mass	1580.752
Cell Volume (≈^3)	936.37809
Wt% - Rietveld	74.875
Crystallite Size	
Cry size Lorentzian (nm)	23.1
Crystal Linear Absorption Coeff. (1/cm)	119.514
Crystal Density (g/cm^3)	2.803
Preferred Orientation (Dir 1 : 0 0 1)	0.3719758
Preferred Orientation Spherical Harmonics	
Order	8
y00	1
y20	0.5647535
y22m	0.02350466
y22p	-0.1336199
y40	0.4565906
y42m	-0.3802709
y42p	-0.5327365
y44m	0.8651269
y44p	-0.03431913
y60	0.002313422
y62m	-0.4899651
y62p	0.4235726
y64m	0.3069255
y64p	-0.23283
y66m	0.2859624
y66p	0.2859624
y80	0.1380342
y82m	0.06365393
y82p	0.3091544
y84m	-0.1838876
y84p	-0.1203985
y86m	-0.2664762
y86p	-0.01144012
y88m	0.04693317
y88p	0.1037255
PVII peak type	

FWHM = a + b/Cos(Th) + c Tan(Th)
a 0.0001001638
b 0.0001001537
c 0.05770809
Exponent m = 0.6+ma+mb/Cos(Th)+mc/Tan(Th)
ma 0.0001000731
mb 0.0001478064
mc 0.04402824
Lattice parameters
a (≈) 5.2066934
b (≈) 9.0141858
c (≈) 20.0593564
beta (∞) 95.96047

Site	Np	x	y	z	Atom	Occ	Beq
Si1	8	0.48250	0.92970	0.13700	Si+4	1	1.737
Al1	8	0.44320	0.26350	0.13650	Al+3	1	0.8685
Al2	8	0.25860	0.08280	0.00680	Al+3	1	2.132
K1	4	0.00000	0.09010	0.25000	K+1	1	5.922
O1	8	0.46230	0.91940	0.05050	O-2	1	1.184
O2	8	0.38350	0.26650	0.06630	O-2	1	3.711
O3	8	0.42590	0.10390	0.15300	O-2	1	0.9475
O4	8	0.22260	0.83680	0.16850	O-2	1	3.237
O5	8	0.27350	0.37220	0.16780	O-2	1	6.317
O6	8	0.40800	0.56710	0.04540	O-2	1	4.185

Structure 4
Phase name Chamosite 1MIIb
R-Bragg 6.724
Spacegroup C-1
Scale 1.46961406e-005
Cell Mass 1271.241
Cell Volume (≈^3) 688.00078
Wt% - Rietveld 1.301
Crystal Linear Absorption Coeff. (1/cm) 271.140
Crystal Density (g/cm^3) 3.068
Preferred Orientation (Dir 1 : 0 0 1) 0.3243504
PVII peak type
FWHM = a + b/Cos(Th) + c Tan(Th)
a 0.0458773
b 0.01300196
c 0.105943
Exponent m = 0.6+ma+mb/Cos(Th)+mc/Tan(Th)
ma 0.0001729739
mb 0.0001594214
mc 0.005621082
Lattice parameters
a (≈) 5.4083795
b (≈) 9.0044365
c (≈) 14.2985996
alpha (∞) 90.04891
beta (∞) 98.57557
gamma (∞) 92.25189

Site	Np	x	y	z	Atom	Occ	Beq

Mg1	2	0.00000	0.00000	0.00000	Mg+2	0.538	0.1579
Fe1	2	0.00000	0.00000	0.00000	Fe+2	0.462	0.1579
Mg2	4	0.01410	0.33480	0.00270	Mg+2	0.496	0.1579
Fe2	4	0.01410	0.33480	0.00270	Fe+2	0.504	0.1579
Mg3	4	0.00320	0.16830	0.50040	Mg+2	0.494	0.1579
Fe3	4	0.00320	0.16830	0.50040	Fe+2	0.506	0.1579
Al1	2	0.00000	0.50000	0.50000	Al+3	1.362	0.2369
Si1	4	0.24000	0.17000	0.19410	Si+4	0.7125	0.07896
Al2	4	0.24000	0.17000	0.19410	Al+3	0.2875	0.07896
Si2	4	0.73000	0.99800	0.19450	Si+4	0.7125	0.07896
Al3	4	0.73000	0.99800	0.19450	Al+3	0.2875	0.07896
O1	4	0.19100	0.16350	0.07890	O-2	1	0.8685
O2	4	0.70500	0.99800	0.07560	O-2	1	0.8685
O3	4	0.23100	0.33600	0.23740	O-2	1	0.8685
O4	4	0.52800	0.11800	0.23020	O-2	1	0.8685
O5	4	0.01800	0.06100	0.23060	O-2	1	0.8685
O6	4	0.68900	0.33120	0.07420	O-2	1	0.8685
O7	4	0.14400	0.99900	0.43000	O-2	1	0.8685
O8	4	0.14300	0.33610	0.42860	O-2	1	0.8685
O9	4	0.64300	0.16270	0.43110	O-2	1	0.8685

Structure 5

Phase name	Albite low
R-Bragg	7.467
Spacegroup	C-1
Scale	3.07101029e-005
Cell Mass	1048.846
Cell Volume (≈^3)	664.19438
Wt% - Rietveld	2.165
Crystallite Size	
Cry size Lorentzian (nm)	372.5
Crystal Linear Absorption Coeff. (1/cm)	88.829
Crystal Density (g/cm^3)	2.622
Lattice parameters	
a (≈)	8.1380000
b (≈)	12.7890000
c (≈)	7.1560000
alpha (∞)	94.33
beta (∞)	116.57
gamma (∞)	87.65

Site	Np	x	y	z	Atom	Occ	Beq
O1	4	0.00900	0.13400	0.96700	O-2	1	1
O2	4	0.59500	0.99700	0.27900	O-2	1	1
O3	4	0.81800	0.11200	0.19200	O-2	1	1
O4	4	0.32100	0.35300	0.25900	O-2	1	1
O5	4	0.00600	0.30700	0.26800	O-2	1	1
O6	4	0.52200	0.19600	0.23300	O-2	1	1
O7	4	0.20600	0.11000	0.38900	O-2	1	1
O8	4	0.68300	0.36900	0.43000	O-2	1	1
Si1	4	0.00800	0.17100	0.20900	Si+4	0.28	1
Al1	4	0.00800	0.17100	0.20900	Al+3	0.72	1
Si2	4	0.50800	0.31800	0.24100	Si+4	1	1
Si3	4	0.69200	0.11000	0.31500	Si+4	0.8	1
Al3	4	0.69200	0.11000	0.31500	Al+3	0.2	1

Si4 4 0.18300 0.38200 0.35900 Si+4 0.91 1
Al4 4 0.18300 0.38200 0.35900 Al+3 0.09 1
Na1 4 0.27200 0.99000 0.14500 Na+1 1 1

9.1.2.9. Sample 2012-0001087, stratigraphic height: 4.50 m

Range Number : 1

R-Values

Rexp : 1.80 Rwp : 8.02 Rp : 5.36 GOF : 4.45
Rexp`: 5.37 Rwp`: 23.87 Rp` : 21.57 DW : 0.15

Quantitative Analysis - Rietveld
Phase 1 : „Quartz low“ 19.705 %
Phase 2 : „Kaolinite 1A II“ 1.864 %
Phase 3 : „Illite 2M1“ 72.678 %
Phase 4 : „Chamosite 1MIIb“ 2.615 %
Phase 5 : „Albite low“ 3.139 %

Background
Chebychev polynomial, Coefficient 0 2613.848
1 -1475.78
2 888.9612
3 -655.1458
4 543.3384
5 -343.1944
6 170.4488

Instrument
Primary radius (mm) 250
Secondary radius (mm) 250
Linear PSD 2Th angular range (∞) 2.749941
FDS angle (∞) 0.0916
Beam spill, sample length (mm) 9
Intensity not corrected
Full Axial Convolution
Filament length (mm) 8
Sample length (mm) 30
Receiving Slit length (mm) 12
Primary Sollers (∞) 2.5
Secondary Sollers (∞) 2.5

Corrections
Zero error -0.04731395
Specimen displacement -0.2762771
LP Factor 0

Miscellaneous
Excluded Regions
Start/Finish 0 0
Start/Finish 0 0
Start/Finish 0 0
Start/Finish 0 0

Start/Finish 0 0

Structure 1
Phase name Quartz low
R-Bragg 141.166
Spacegroup P3221
Scale 0.00800652409
Cell Mass 180.252
Cell Volume (≈^3) 112.92357
Wt% - Rietveld 19.705
Crystal Linear Absorption Coeff. (1/cm) 95.451
Crystal Density (g/cm^3) 2.651
Preferred Orientation (Dir 1 : 0 0 1) 1.201702
PVII peak type
FWHM = a + b/Cos(Th) + c Tan(Th)
a 0.02641727
b 0.0001
c 0.0001
Exponent m = 0.6+ma+mb/Cos(Th)+mc/Tan(Th)
ma 0.1325987
mb 0.3094491
mc 0.0001025467
Lattice parameters
a (≈) 4.9124372
c (≈) 5.4033108

Site	Np	x	y	z	Atom	Occ	Beq
Si1	3	0.46900	0.00000	0.66667	Si+4	1	1
O1	6	0.40300	0.25300	0.78900	O-2	1	1

Structure 2
Phase name Kaolinite 1A II
R-Bragg 131.201
Spacegroup C1
Scale 9.32926805e-005
Cell Mass 508.256
Cell Volume (≈^3) 325.10507
Wt% - Rietveld 1.864
Crystal Linear Absorption Coeff. (1/cm) 81.026
Crystal Density (g/cm^3) 2.596
Preferred Orientation (Dir 1 : 0 0 1) 0.9230551
PVII peak type
FWHM = a + b/Cos(Th) + c Tan(Th)
a 0.003521376
b 0.05165503
c 0.3716033
Exponent m = 0.6+ma+mb/Cos(Th)+mc/Tan(Th)
ma 0.0001
mb 0.0001
mc 0.257317
Lattice parameters
a (≈) 5.3322134
b (≈) 8.3787153
c (≈) 7.5046934

alpha (∞)	93.05501
beta (∞)	103.7211
gamma (∞)	90.97204

Site	Np	x	y	z	Atom	Occ	Beq
O1	2	0.77800	0.18000	-0.14000	O-2	1	1
O2	2	0.27800	0.32000	-0.13800	O-2	1	1
O3	2	0.31600	-0.00800	-0.13600	O-2	1	1
O4	2	0.24800	0.18400	0.15500	O-2	1	1
O5	2	0.75400	0.31500	0.15500	O-2	1	1
O6	2	0.69000	0.00400	0.15700	O-2	1	1
O7	2	0.79100	0.16500	0.48200	O-2	1	1
O8	2	0.61200	-0.12000	0.45500	O-2	1	1
O9	2	0.10800	-0.05800	0.45500	O-2	1	1
Al1	2	0.50200	0.17200	0.00300	Al+3	1	1
Al2	2	0.00200	0.33000	0.00200	Al+3	1	1
Si1	2	0.80000	0.32200	0.38200	Si+4	1	1
Si2	2	0.80000	0.00000	0.38500	Si+4	1	1

Structure 3

Phase name	Illite 2M1
R-Bragg	102.686
Spacegroup	C12/c1
Scale	0.000406092111
Cell Mass	1580.752
Cell Volume (≈^3)	936.37809
Wt% - Rietveld	72.678
Crystallite Size	
Cry size Lorentzian (nm)	19.3
Crystal Linear Absorption Coeff. (1/cm)	119.514
Crystal Density (g/cm^3)	2.803
Preferred Orientation (Dir 1 : 0 0 1)	0.4293475
Preferred Orientation Spherical Harmonics	
Order	8
y00	1
y20	0.3303123
y22m	-0.1392983
y22p	-0.1212126
y40	0.2859888
y42m	-0.496245
y42p	-0.5221785
y44m	0.6876337
y44p	0.03117421
y60	0.004524565
y62m	-0.6228282
y62p	0.4239706
y64m	0.1916913
y64p	-0.295696
y66m	0.2723973
y66p	0.2723973
y80	0.3852252
y82m	0.03424709
y82p	0.4196645
y84m	-0.08933051
y84p	-0.02366692

y86m	-0.2275265
y86p	-0.2272764
y88m	0.1310752
y88p	0.2416618

PVII peak type

FWHM = a + b/Cos(Th) + c Tan(Th)

a	0.0001438022
b	0.0003212593
c	0.0375914

Exponent m = 0.6+ma+mb/Cos(Th)+mc/Tan(Th)

ma	0.0001000001
mb	0.0001
mc	0.04509812

Lattice parameters

a (≈)	5.2066934
b (≈)	9.0141858
c (≈)	20.0593564
beta (∞)	95.96047

Site	Np	x	y	z	Atom	Occ	Beq
Si1	8	0.48250	0.92970	0.13700	Si+4	1	1.737
Al1	8	0.44320	0.26350	0.13650	Al+3	1	0.8685
Al2	8	0.25860	0.08280	0.00680	Al+3	1	2.132
K1	4	0.00000	0.09010	0.25000	K+1	1	5.922
O1	8	0.46230	0.91940	0.05050	O-2	1	1.184
O2	8	0.38350	0.26650	0.06630	O-2	1	3.711
O3	8	0.42590	0.10390	0.15300	O-2	1	0.9475
O4	8	0.22260	0.83680	0.16850	O-2	1	3.237
O5	8	0.27350	0.37220	0.16780	O-2	1	6.317
O6	8	0.40800	0.56710	0.04540	O-2	1	4.185

Structure 4

Phase name	Chamosite 1MIIb
R-Bragg	99.365
Spacegroup	C-1
Scale	2.47276596e-005
Cell Mass	1271.241
Cell Volume (≈^3)	688.00078
Wt% - Rietveld	2.615
Crystal Linear Absorption Coeff. (1/cm)	271.140
Crystal Density (g/cm^3)	3.068
Preferred Orientation (Dir 1 : 0 0 1)	0.3319654

PVII peak type

FWHM = a + b/Cos(Th) + c Tan(Th)

a	0.06556805
b	0.02545984
c	0.09954305

Exponent m = 0.6+ma+mb/Cos(Th)+mc/Tan(Th)

ma	0.1169821
mb	0.001978489
mc	0.002257081

Lattice parameters

a (≈)	5.4083795
b (≈)	9.0044365
c (≈)	14.2985996

alpha (∞) 90.04891
beta (∞) 98.57557
gamma (∞) 92.25189

Site	Np	x	y	z	Atom	Occ	Beq
Mg1	2	0.00000	0.00000	0.00000	Mg+2	0.538	0.1579
Fe1	2	0.00000	0.00000	0.00000	Fe+2	0.462	0.1579
Mg2	4	0.01410	0.33480	0.00270	Mg+2	0.496	0.1579
Fe2	4	0.01410	0.33480	0.00270	Fe+2	0.504	0.1579
Mg3	4	0.00320	0.16830	0.50040	Mg+2	0.494	0.1579
Fe3	4	0.00320	0.16830	0.50040	Fe+2	0.506	0.1579
Al1	2	0.00000	0.50000	0.50000	Al+3	1.362	0.2369
Si1	4	0.24000	0.17000	0.19410	Si+4	0.7125	0.07896
Al2	4	0.24000	0.17000	0.19410	Al+3	0.2875	0.07896
Si2	4	0.73000	0.99800	0.19450	Si+4	0.7125	0.07896
Al3	4	0.73000	0.99800	0.19450	Al+3	0.2875	0.07896
O1	4	0.19100	0.16350	0.07890	O-2	1	0.8685
O2	4	0.70500	0.99800	0.07560	O-2	1	0.8685
O3	4	0.23100	0.33600	0.23740	O-2	1	0.8685
O4	4	0.52800	0.11800	0.23020	O-2	1	0.8685
O5	4	0.01800	0.06100	0.23060	O-2	1	0.8685
O6	4	0.68900	0.33120	0.07420	O-2	1	0.8685
O7	4	0.14400	0.99900	0.43000	O-2	1	0.8685
O8	4	0.14300	0.33610	0.42860	O-2	1	0.8685
O9	4	0.64300	0.16270	0.43110	O-2	1	0.8685

Structure 5
Phase name Albite low
R-Bragg 131.386
Spacegroup C-1
Scale 3.72612182e-005
Cell Mass 1048.846
Cell Volume (≈^3) 664.19438
Wt% - Rietveld 3.139
Crystallite Size
Cry size Lorentzian (nm) 228.5
Crystal Linear Absorption Coeff. (1/cm) 88.829
Crystal Density (g/cm^3) 2.622
Lattice parameters
a (≈) 8.1380000
b (≈) 12.7890000
c (≈) 7.1560000
alpha (∞) 94.33
beta (∞) 116.57
gamma (∞) 87.65

Site	Np	x	y	z	Atom	Occ	Beq
O1	4	0.00900	0.13400	0.96700	O-2	1	1
O2	4	0.59500	0.99700	0.27900	O-2	1	1
O3	4	0.81800	0.11200	0.19200	O-2	1	1
O4	4	0.32100	0.35300	0.25900	O-2	1	1
O5	4	0.00600	0.30700	0.26800	O-2	1	1
O6	4	0.52200	0.19600	0.23300	O-2	1	1
O7	4	0.20600	0.11000	0.38900	O-2	1	1
O8	4	0.68300	0.36900	0.43000	O-2	1	1

Si1	4	0.00800	0.17100	0.20900	Si+4 0.28	1
Al1	4	0.00800	0.17100	0.20900	Al+3 0.72	1
Si2	4	0.50800	0.31800	0.24100	Si+4 1	1
Si3	4	0.69200	0.11000	0.31500	Si+4 0.8	1
Al3	4	0.69200	0.11000	0.31500	Al+3 0.2	1
Si4	4	0.18300	0.38200	0.35900	Si+4 0.91	1
Al4	4	0.18300	0.38200	0.35900	Al+3 0.09	1
Na1	4	0.27200	0.99000	0.14500	Na+1 1	1

9.1.2.10. Sample 2012-0001055, stratigraphic height: 5.02 m

Range Number : 1

R-Values

Rexp : 1.26 Rwp : 5.32 Rp : 4.13 GOF : 4.22
Rexp`: 4.00 Rwp`: 16.91 Rp` : 17.14 DW : 0.22
Quantitative Analysis - Rietveld
Phase 1 : „Quartz low“ 29.420 %
Phase 2 : „Kaolinite 1A II“ 1.445 %
Phase 3 : „Illite 2M1“ 65.434 %
Phase 4 : „Chamosite 1MIIb“ 0.938 %
Phase 5 : „Albite low“ 2.764 %

Background
Chebychev polynomial, Coefficient 0 5039.794
1 -1986.416
2 875.1201
3 -511.3527
4 307.4872
5 -121.491

Instrument
Primary radius (mm) 250
Secondary radius (mm) 250
Linear PSD 2Th angular range (∞) 2.749941
FDS angle (∞) 0.0916
Beam spill, sample length (mm) 9
Intensity not corrected
Full Axial Convolution
Filament length (mm) 8
Sample length (mm) 30
Receiving Slit length (mm) 12
Primary Sollers (∞) 2.5
Secondary Sollers (∞) 2.5

Corrections
Zero error 0.02200627
Specimen displacement -0.1415125
LP Factor 0

Miscellaneous
Excluded Regions
Start/Finish 0 0

Start/Finish	0	0
Start/Finish	0	0
Start/Finish	0	0
Start/Finish	0	0

Structure 1

Phase name	Quartz low
R-Bragg	4.954
Spacegroup	P3221
Scale	0.0333088964
Cell Mass	180.252
Cell Volume (≈^3)	112.99633
Wt% - Rietveld	29.420
Crystal Linear Absorption Coeff. (1/cm)	95.390
Crystal Density (g/cm^3)	2.649
Preferred Orientation (Dir 1 : 0 0 1)	1.184028
PVII peak type	
FWHM = a + b/Cos(Th) + c Tan(Th)	
a	0.04545317
b	0.0001
c	0.0001
Exponent m = 0.6+ma+mb/Cos(Th)+mc/Tan(Th)	
ma	0.1620828
mb	0.0001000034
mc	0.1071058
Lattice parameters	
a (≈)	4.9134567
c (≈)	5.4045488

Site	Np	x	y	z	Atom	Occ	Beq
Si1	3	0.46900	0.00000	0.66667	Si+4	1	1
O1	6	0.40300	0.25300	0.78900	O-2	1	1

Structure 2

Phase name	Kaolinite 1A II
R-Bragg	1.344
Spacegroup	C1
Scale	0.000199660301
Cell Mass	508.256
Cell Volume (≈^3)	328.26941
Wt% - Rietveld	1.445
Crystal Linear Absorption Coeff. (1/cm)	80.245
Crystal Density (g/cm^3)	2.571
Preferred Orientation (Dir 1 : 0 0 1)	0.2590034
PVII peak type	
FWHM = a + b/Cos(Th) + c Tan(Th)	
a	0.1777503
b	0.9420342
c	1
Exponent m = 0.6+ma+mb/Cos(Th)+mc/Tan(Th)	
ma	0.0001
mb	0.0001
mc	0.09578437
Lattice parameters	
a (≈)	5.4085850

b (≈)	8.3781410
c (≈)	7.4945453
alpha (∞)	93.32869
beta (∞)	104.1932
gamma (∞)	91.97204

Site	Np	x	y	z	Atom	Occ	Beq
O1	2	0.77800	0.18000	-0.14000	O-2	1	1
O2	2	0.27800	0.32000	-0.13800	O-2	1	1
O3	2	0.31600	-0.00800	-0.13600	O-2	1	1
O4	2	0.24800	0.18400	0.15500	O-2	1	1
O5	2	0.75400	0.31500	0.15500	O-2	1	1
O6	2	0.69000	0.00400	0.15700	O-2	1	1
O7	2	0.79100	0.16500	0.48200	O-2	1	1
O8	2	0.61200	-0.12000	0.45500	O-2	1	1
O9	2	0.10800	-0.05800	0.45500	O-2	1	1
Al1	2	0.50200	0.17200	0.00300	Al+3	1	1
Al2	2	0.00200	0.33000	0.00200	Al+3	1	1
Si1	2	0.80000	0.32200	0.38200	Si+4	1	1
Si2	2	0.80000	0.00000	0.38500	Si+4	1	1

Structure 3

Phase name	Illite 2M1
R-Bragg	5.757
Spacegroup	C12/c1
Scale	0.00101942081
Cell Mass	1580.752
Cell Volume (≈^3)	936.37809
Wt% - Rietveld	65.434
Crystallite Size	
Cry size Lorentzian (nm)	20.7
Crystal Linear Absorption Coeff. (1/cm)	119.514
Crystal Density (g/cm^3)	2.803
Preferred Orientation Spherical Harmonics	
Order	4
y00	1
y20	-0.6020973
y22m	-0.5529031
y22p	-0.82102
y40	0.1558983
y42m	-0.1400365
y42p	0.1343689
y44m	-0.1771597
y44p	0.09610533
Lattice parameters	
a (≈)	5.2066934
b (≈)	9.0141858
c (≈)	20.0593564
beta (∞)	95.96047

Site	Np	x	y	z	Atom	Occ	Beq
Si1	8	0.48250	0.92970	0.13700	Si+4	1	1.737
Al1	8	0.44320	0.26350	0.13650	Al+3	1	0.8685
Al2	8	0.25860	0.08280	0.00680	Al+3	1	2.132
K1	4	0.00000	0.09010	0.25000	K+1	1	5.922
O1	8	0.46230	0.91940	0.05050	O-2	1	1.184

O2	8	0.38350	0.26650	0.06630	O-2	1 3.711
O3	8	0.42590	0.10390	0.15300	O-2	1 0.9475
O4	8	0.22260	0.83680	0.16850	O-2	1 3.237
O5	8	0.27350	0.37220	0.16780	O-2	1 6.317
O6	8	0.40800	0.56710	0.04540	O-2	1 4.185

Structure 4

Phase name	Chamosite 1MIIb
R-Bragg	5.536
Spacegroup	C-1
Scale	2.46813378e-005
Cell Mass	1271.241
Cell Volume (≈^3)	689.07849
Wt% - Rietveld	0.938
Crystal Linear Absorption Coeff. (1/cm)	270.716
Crystal Density (g/cm^3)	3.063
Preferred Orientation (Dir 1 : 0 0 1)	0.474122
PVII peak type	
FWHM = a + b/Cos(Th) + c Tan(Th)	
a	0.07215188
b	0.04429529
c	0.0001
Exponent m = 0.6+ma+mb/Cos(Th)+mc/Tan(Th)	
ma	20
mb	5
mc	5
Lattice parameters	
a (≈)	5.4262049
b (≈)	8.9865209
c (≈)	14.3147149
alpha (∞)	90.01516
beta (∞)	98.98272
gamma (∞)	91.88837

Site	Np	x	y	z	Atom	Occ	Beq
Mg1	2	0.00000	0.00000	0.00000	Mg+2	0.538	0.1579
Fe1	2	0.00000	0.00000	0.00000	Fe+2	0.462	0.1579
Mg2	4	0.01410	0.33480	0.00270	Mg+2	0.496	0.1579
Fe2	4	0.01410	0.33480	0.00270	Fe+2	0.504	0.1579
Mg3	4	0.00320	0.16830	0.50040	Mg+2	0.494	0.1579
Fe3	4	0.00320	0.16830	0.50040	Fe+2	0.506	0.1579
Al1	2	0.00000	0.50000	0.50000	Al+3	1.362	0.2369
Si1	4	0.24000	0.17000	0.19410	Si+4	0.7125	0.07896
Al2	4	0.24000	0.17000	0.19410	Al+3	0.2875	0.07896
Si2	4	0.73000	0.99800	0.19450	Si+4	0.7125	0.07896
Al3	4	0.73000	0.99800	0.19450	Al+3	0.2875	0.07896
O1	4	0.19100	0.16350	0.07890	O-2	1	0.8685
O2	4	0.70500	0.99800	0.07560	O-2	1	0.8685
O3	4	0.23100	0.33600	0.23740	O-2	1	0.8685
O4	4	0.52800	0.11800	0.23020	O-2	1	0.8685
O5	4	0.01800	0.06100	0.23060	O-2	1	0.8685
O6	4	0.68900	0.33120	0.07420	O-2	1	0.8685
O7	4	0.14400	0.99900	0.43000	O-2	1	0.8685
O8	4	0.14300	0.33610	0.42860	O-2	1	0.8685
O9	4	0.64300	0.16270	0.43110	O-2	1	0.8685

Structure 5

Phase name	Albite low
R-Bragg	4.909
Spacegroup	C-1
Scale	9.14783402e-005
Cell Mass	1048.846
Cell Volume (≈^3)	664.19438
Wt% - Rietveld	2.764
Crystallite Size	
Cry size Lorentzian (nm)	284.4
Crystal Linear Absorption Coeff. (1/cm)	88.829
Crystal Density (g/cm^3)	2.622
Lattice parameters	
a (≈)	8.1380000
b (≈)	12.7890000
c (≈)	7.1560000
alpha (∞)	94.33
beta (∞)	116.57
gamma (∞)	87.65

Site	Np	x	y	z	Atom	Occ	Beq
O1	4	0.00900	0.13400	0.96700	O-2	1	1
O2	4	0.59500	0.99700	0.27900	O-2	1	1
O3	4	0.81800	0.11200	0.19200	O-2	1	1
O4	4	0.32100	0.35300	0.25900	O-2	1	1
O5	4	0.00600	0.30700	0.26800	O-2	1	1
O6	4	0.52200	0.19600	0.23300	O-2	1	1
O7	4	0.20600	0.11000	0.38900	O-2	1	1
O8	4	0.68300	0.36900	0.43000	O-2	1	1
Si1	4	0.00800	0.17100	0.20900	Si+4	0.28	1
Al1	4	0.00800	0.17100	0.20900	Al+3	0.72	1
Si2	4	0.50800	0.31800	0.24100	Si+4	1	1
Si3	4	0.69200	0.11000	0.31500	Si+4	0.8	1
Al3	4	0.69200	0.11000	0.31500	Al+3	0.2	1
Si4	4	0.18300	0.38200	0.35900	Si+4	0.91	1
Al4	4	0.18300	0.38200	0.35900	Al+3	0.09	1
Na1	4	0.27200	0.99000	0.14500	Na+1	1	1

9.1.2.11. Sample 2012-0001085, stratigraphic height: 5.65 m

Range Number : 1

R-Values

Rexp : 1.97 Rwp : 5.03 Rp : 3.74 GOF : 2.55
Rexp`: 6.98 Rwp`: 17.81 Rp` : 19.72 DW : 0.46

Quantitative Analysis - Rietveld

Phase 1 : „Quartz low“	25.486 %
Phase 2 : „Kaolinite 1A II“	1.958 %
Phase 3 : „Illite 2M1“	68.297 %
Phase 4 : „Chamosite 1MIIb“	1.218 %
Phase 5 : „Albite low“	3.041 %

Background
  Chebychev polynomial, Coefficient 0 2166.487
  1 -745.0065
  2 284.424
  3 -229.1358
  4 251.2956
  5 -195.0817
  6 90.94656

Instrument
  Primary radius (mm) 250
  Secondary radius (mm) 250
  Linear PSD 2Th angular range (∞) 2.749941
    FDS angle (∞) 0.0916
    Beam spill, sample length (mm) 9
      Intensity not corrected
  Full Axial Convolution
    Filament length (mm) 8
    Sample length (mm) 30
    Receiving Slit length (mm) 12
    Primary Sollers (∞) 2.5
    Secondary Sollers (∞) 2.5

Corrections
  Zero error -0.08239309
  Specimen displacement -0.4084902
  LP Factor 0

Miscellaneous
  Excluded Regions
    Start/Finish 0 0
    Start/Finish 0 0
    Start/Finish 0 0
    Start/Finish 0 0
    Start/Finish 0 0

Structure 1
  Phase name Quartz low
  R-Bragg 8.284
  Spacegroup P3221
  Scale 0.0124685134
  Cell Mass 180.252
  Cell Volume (≈^3) 112.97647
  Wt% - Rietveld 25.486
  Crystal Linear Absorption Coeff. (1/cm) 95.407
  Crystal Density (g/cm^3) 2.649
  Preferred Orientation (Dir 1 : 0 0 1) 1.186383
  PVII peak type
    FWHM = a + b/Cos(Th) + c Tan(Th)
      a 0.01141942
      b 0.002493677
      c 0.01331231
    Exponent m = 0.6+ma+mb/Cos(Th)+mc/Tan(Th)
      ma 0.0001084636
      mb 0.0008343766

mc 0.1024478
Lattice parameters
a (≈) 4.9130140
c (≈) 5.4045729

Site	Np	x	y	z	Atom	Occ	Beq
Si1	3	0.46900	0.00000	0.66667	Si+4	1	1
O1	6	0.40300	0.25300	0.78900	O-2	1	1

Structure 2
Phase name Kaolinite 1A II
R-Bragg 5.256
Spacegroup C1
Scale 0.000118079805
Cell Mass 508.256
Cell Volume (≈^3) 325.10507
Wt% - Rietveld 1.958
Crystal Linear Absorption Coeff. (1/cm) 81.026
Crystal Density (g/cm^3) 2.596
Preferred Orientation (Dir 1 : 0 0 1) 1.484474
PVII peak type
FWHM = a + b/Cos(Th) + c Tan(Th)
a 0.01699868
b 0.007554514
c 0.5015335
Exponent m = 0.6+ma+mb/Cos(Th)+mc/Tan(Th)
ma 0.0001000743
mb 0.000106733
mc 0.7765462
Lattice parameters
a (≈) 5.3322134
b (≈) 8.3787153
c (≈) 7.5046934
alpha (∞) 93.05501
beta (∞) 103.7211
gamma (∞) 90.97204

Site	Np	x	y	z	Atom	Occ	Beq
O1	2	0.77800	0.18000	-0.14000	O-2	1	1
O2	2	0.27800	0.32000	-0.13800	O-2	1	1
O3	2	0.31600	-0.00800	-0.13600	O-2	1	1
O4	2	0.24800	0.18400	0.15500	O-2	1	1
O5	2	0.75400	0.31500	0.15500	O-2	1	1
O6	2	0.69000	0.00400	0.15700	O-2	1	1
O7	2	0.79100	0.16500	0.48200	O-2	1	1
O8	2	0.61200	-0.12000	0.45500	O-2	1	1
O9	2	0.10800	-0.05800	0.45500	O-2	1	1
Al1	2	0.50200	0.17200	0.00300	Al+3	1	1
Al2	2	0.00200	0.33000	0.00200	Al+3	1	1
Si1	2	0.80000	0.32200	0.38200	Si+4	1	1
Si2	2	0.80000	0.00000	0.38500	Si+4	1	1

Structure 3
Phase name Illite 2M1

R-Bragg	4.428
Spacegroup	C12/c1
Scale	0.000459694938
Cell Mass	1580.752
Cell Volume (≈^3)	936.37809
Wt% - Rietveld	68.297
Crystallite Size	
Cry size Lorentzian (nm)	31.3
Crystal Linear Absorption Coeff. (1/cm)	119.514
Crystal Density (g/cm^3)	2.803
Preferred Orientation (Dir 1 : 0 0 1)	0.3589715
Preferred Orientation Spherical Harmonics	
Order	8
y00	1
y20	0.5603362
y22m	-0.02082519
y22p	-0.1161541
y40	0.4721082
y42m	-0.3253945
y42p	-0.531337
y44m	0.9333777
y44p	-0.02669132
y60	0.00243517
y62m	-0.3134278
y62p	0.4307669
y64m	0.3128475
y64p	-0.240661
y66m	0.3010137
y66p	0.3010137
y80	0.141903
y82m	0.4523326
y82p	0.296914
y84m	-0.3461929
y84p	-0.1154374
y86m	-0.07864152
y86p	0.0009744208
y88m	0.008367675
y88p	0.07590589
PVII peak type	
FWHM = a + b/Cos(Th) + c Tan(Th)	
a	0.0001003851
b	0.0001004014
c	0.07010239
Exponent m = 0.6+ma+mb/Cos(Th)+mc/Tan(Th)	
ma	0.0002487777
mb	0.04754441
mc	0.1079853
Lattice parameters	
a (≈)	5.2066934
b (≈)	9.0141858
c (≈)	20.0593564
beta (∞)	95.96047

Site	Np	x	y	z	Atom	Occ	Beq
Si1	8	0.48250	0.92970	0.13700	Si+4	1	1.737
Al1	8	0.44320	0.26350	0.13650	Al+3	1	0.8685

Al2	8	0.25860	0.08280	0.00680	Al+3 1	2.132
K1	4	0.00000	0.09010	0.25000	K+1 1	5.922
O1	8	0.46230	0.91940	0.05050	O-2 1	1.184
O2	8	0.38350	0.26650	0.06630	O-2 1	3.711
O3	8	0.42590	0.10390	0.15300	O-2 1	0.9475
O4	8	0.22260	0.83680	0.16850	O-2 1	3.237
O5	8	0.27350	0.37220	0.16780	O-2 1	6.317
O6	8	0.40800	0.56710	0.04540	O-2 1	4.185

Structure 4

Phase name	Chamosite 1MIIb
R-Bragg	11.802
Spacegroup	C-1
Scale	1.38688545e-005
Cell Mass	1271.241
Cell Volume (≈^3)	688.00078
Wt% - Rietveld	1.218
Crystal Linear Absorption Coeff. (1/cm)	271.140
Crystal Density (g/cm^3)	3.068
Preferred Orientation (Dir 1 : 0 0 1)	0.3527452
PVII peak type	
FWHM = a + b/Cos(Th) + c Tan(Th)	
a	0.04313395
b	0.008172368
c	0.04809482
Exponent m = 0.6+ma+mb/Cos(Th)+mc/Tan(Th)	
ma	0.0004712666
mb	0.008651755
mc	0.007037625
Lattice parameters	
a (≈)	5.4083795
b (≈)	9.0044365
c (≈)	14.2985996
alpha (∞)	90.04891
beta (∞)	98.57557
gamma (∞)	92.25189

Site	Np	x	y	z	Atom	Occ	Beq
Mg1	2	0.00000	0.00000	0.00000	Mg+2	0.538	0.1579
Fe1	2	0.00000	0.00000	0.00000	Fe+2	0.462	0.1579
Mg2	4	0.01410	0.33480	0.00270	Mg+2	0.496	0.1579
Fe2	4	0.01410	0.33480	0.00270	Fe+2	0.504	0.1579
Mg3	4	0.00320	0.16830	0.50040	Mg+2	0.494	0.1579
Fe3	4	0.00320	0.16830	0.50040	Fe+2	0.506	0.1579
Al1	2	0.00000	0.50000	0.50000	Al+3	1.362	0.2369
Si1	4	0.24000	0.17000	0.19410	Si+4	0.7125	0.07896
Al2	4	0.24000	0.17000	0.19410	Al+3	0.2875	0.07896
Si2	4	0.73000	0.99800	0.19450	Si+4	0.7125	0.07896
Al3	4	0.73000	0.99800	0.19450	Al+3	0.2875	0.07896
O1	4	0.19100	0.16350	0.07890	O-2	1	0.8685
O2	4	0.70500	0.99800	0.07560	O-2	1	0.8685
O3	4	0.23100	0.33600	0.23740	O-2	1	0.8685
O4	4	0.52800	0.11800	0.23020	O-2	1	0.8685
O5	4	0.01800	0.06100	0.23060	O-2	1	0.8685
O6	4	0.68900	0.33120	0.07420	O-2	1	0.8685

O7	4	0.14400	0.99900	0.43000	O-2	1	0.8685
O8	4	0.14300	0.33610	0.42860	O-2	1	0.8685
O9	4	0.64300	0.16270	0.43110	O-2	1	0.8685

Structure 5

Phase name	Albite low
R-Bragg	2.820
Spacegroup	C-1
Scale	4.34854889e-005
Cell Mass	1048.846
Cell Volume (≈^3)	664.19438
Wt% - Rietveld	3.041
Crystallite Size	
Cry size Lorentzian (nm)	275.4
Crystal Linear Absorption Coeff. (1/cm)	88.829
Crystal Density (g/cm^3)	2.622
Lattice parameters	
a (≈)	8.1380000
b (≈)	12.7890000
c (≈)	7.1560000
alpha (∞)	94.33
beta (∞)	116.57
gamma (∞)	87.65

Site	Np	x	y	z	Atom	Occ	Beq
O1	4	0.00900	0.13400	0.96700	O-2	1	1
O2	4	0.59500	0.99700	0.27900	O-2	1	1
O3	4	0.81800	0.11200	0.19200	O-2	1	1
O4	4	0.32100	0.35300	0.25900	O-2	1	1
O5	4	0.00600	0.30700	0.26800	O-2	1	1
O6	4	0.52200	0.19600	0.23300	O-2	1	1
O7	4	0.20600	0.11000	0.38900	O-2	1	1
O8	4	0.68300	0.36900	0.43000	O-2	1	1
Si1	4	0.00800	0.17100	0.20900	Si+4	0.28	1
Al1	4	0.00800	0.17100	0.20900	Al+3	0.72	1
Si2	4	0.50800	0.31800	0.24100	Si+4	1	1
Si3	4	0.69200	0.11000	0.31500	Si+4	0.8	1
Al3	4	0.69200	0.11000	0.31500	Al+3	0.2	1
Si4	4	0.18300	0.38200	0.35900	Si+4	0.91	1
Al4	4	0.18300	0.38200	0.35900	Al+3	0.09	1
Na1	4	0.27200	0.99000	0.14500	Na+1	1	1

9.1.2.12. Sample 2012-0000265, stratigraphic height: 6.26 m

Range Number : 1

R-Values

Rexp : 1.88 Rwp : 5.10 Rp : 3.68 GOF : 2.72
Rexp`: 7.20 Rwp`: 19.56 Rp` : 21.25 DW : 0.36

Quantitative Analysis - Rietveld

Phase 1 : „Quartz low“	25.045 %

Phase 2 : „Kaolinite 1A II“ 2.087 %
Phase 3 : „Illite 2M1“ 68.984 %
Phase 4 : „Chamosite 1MIIb“ 1.655 %
Phase 5 : „Albite low“ 2.229 %

Background
Chebychev polynomial, Coefficient 0 2461.991
1 -909.2904
2 385.812
3 -324.9751
4 296.5846
5 -205.1067
6 78.13007

Instrument
Primary radius (mm) 250
Secondary radius (mm) 250
Linear PSD 2Th angular range (∞) 2.749941
FDS angle (∞) 0.0916
Beam spill, sample length (mm) 9
Intensity not corrected
Full Axial Convolution
Filament length (mm) 8
Sample length (mm) 30
Receiving Slit length (mm) 12
Primary Sollers (∞) 2.5
Secondary Sollers (∞) 2.5

Corrections
Zero error -0.07131354
Specimen displacement -0.361658
LP Factor 0

Miscellaneous
Excluded Regions
Start/Finish 0 0
Start/Finish 0 0
Start/Finish 0 0
Start/Finish 0 0
Start/Finish 0 0

Structure 1
Phase name Quartz low
R-Bragg 5.669
Spacegroup P3221
Scale 0.00992618534
Cell Mass 180.252
Cell Volume (≈^3) 112.99422
Wt% - Rietveld 25.045
Crystal Linear Absorption Coeff. (1/cm) 95.392
Crystal Density (g/cm^3) 2.649
Preferred Orientation (Dir 1 : 0 0 1) 1.183754
PVII peak type
FWHM = a + b/Cos(Th) + c Tan(Th)
a 0.01631944

b 0.006754983
c 0.003535499
Exponent m = 0.6+ma+mb/Cos(Th)+mc/Tan(Th)
ma 0.04618175
mb 0.06390161
mc 0.1055462
Lattice parameters
a (≈) 4.9132208
c (≈) 5.4049671

Site	Np	x	y	z	Atom	Occ	Beq
Si1	3	0.46900	0.00000	0.66667	Si+4	1	1
O1	6	0.40300	0.25300	0.78900	O-2	1	1

Structure 2
Phase name Kaolinite 1A II
R-Bragg 8.113
Spacegroup C1
Scale 0.000101950643
Cell Mass 508.256
Cell Volume (≈^3) 325.10507
Wt% - Rietveld 2.087
Crystal Linear Absorption Coeff. (1/cm) 81.026
Crystal Density (g/cm^3) 2.596
Preferred Orientation (Dir 1 : 0 0 1) 1.067851
PVII peak type
FWHM = a + b/Cos(Th) + c Tan(Th)
a 0.07342233
b 0.0001274797
c 0.2215568
Exponent m = 0.6+ma+mb/Cos(Th)+mc/Tan(Th)
ma 0.0001011881
mb 0.0002077285
mc 0.2316549
Lattice parameters
a (≈) 5.3322134
b (≈) 8.3787153
c (≈) 7.5046934
alpha (∞) 93.05501
beta (∞) 103.7211
gamma (∞) 90.97204

Site	Np	x	y	z	Atom	Occ	Beq
O1	2	0.77800	0.18000	-0.14000	O-2	1	1
O2	2	0.27800	0.32000	-0.13800	O-2	1	1
O3	2	0.31600	-0.00800	-0.13600	O-2	1	1
O4	2	0.24800	0.18400	0.15500	O-2	1	1
O5	2	0.75400	0.31500	0.15500	O-2	1	1
O6	2	0.69000	0.00400	0.15700	O-2	1	1
O7	2	0.79100	0.16500	0.48200	O-2	1	1
O8	2	0.61200	-0.12000	0.45500	O-2	1	1
O9	2	0.10800	-0.05800	0.45500	O-2	1	1
Al1	2	0.50200	0.17200	0.00300	Al+3	1	1
Al2	2	0.00200	0.33000	0.00200	Al+3	1	1
Si1	2	0.80000	0.32200	0.38200	Si+4	1	1

Si2 2 0.80000 0.00000 0.38500 Si+4 1 1

Structure 3

Phase name	Illite 2M1
R-Bragg	7.503
Spacegroup	C12/c1
Scale	0.000376218727
Cell Mass	1580.752
Cell Volume (≈^3)	936.37809
Wt% - Rietveld	68.984
Crystallite Size	
Cry size Lorentzian (nm)	24.3
Crystal Linear Absorption Coeff. (1/cm)	119.514
Crystal Density (g/cm^3)	2.803
Preferred Orientation (Dir 1 : 0 0 1)	0.3672236
Preferred Orientation Spherical Harmonics	
Order	8
y00	1
y20	0.5803734
y22m	-0.07292996
y22p	-0.1017777
y40	0.4998858
y42m	-0.3354587
y42p	-0.5032194
y44m	0.8287199
y44p	-0.02608794
y60	-0.001822579
y62m	-0.05978955
y62p	0.4411845
y64m	0.0007249163
y64p	-0.245715
y66m	0.3073678
y66p	0.3073678
y80	0.07095447
y82m	0.6998456
y82p	0.3298383
y84m	-0.5418439
y84p	-0.07094351
y86m	0.0144792
y86p	0.01749575
y88m	0.04767993
y88p	0.06996294
PVII peak type	
FWHM = a + b/Cos(Th) + c Tan(Th)	
a	0.0001691436
b	0.0001686018
c	0.04402138
Exponent m = 0.6+ma+mb/Cos(Th)+mc/Tan(Th)	
ma	0.01934497
mb	0.06623889
mc	0.07473822
Lattice parameters	
a (≈)	5.2066934
b (≈)	9.0141858
c (≈)	20.0593564

beta (∞) 95.96047

Site	Np	x	y	z	Atom	Occ	Beq
Si1	8	0.48250	0.92970	0.13700	Si+4	1	1.737
Al1	8	0.44320	0.26350	0.13650	Al+3	1	0.8685
Al2	8	0.25860	0.08280	0.00680	Al+3	1	2.132
K1	4	0.00000	0.09010	0.25000	K+1	1	5.922
O1	8	0.46230	0.91940	0.05050	O-2	1	1.184
O2	8	0.38350	0.26650	0.06630	O-2	1	3.711
O3	8	0.42590	0.10390	0.15300	O-2	1	0.9475
O4	8	0.22260	0.83680	0.16850	O-2	1	3.237
O5	8	0.27350	0.37220	0.16780	O-2	1	6.317
O6	8	0.40800	0.56710	0.04540	O-2	1	4.185

Structure 4

Phase name Chamosite 1MIIb
R-Bragg 4.649
Spacegroup C-1
Scale 1.52765288e-005
Cell Mass 1271.241
Cell Volume (≈^3) 688.00078
Wt% - Rietveld 1.655
Crystal Linear Absorption Coeff. (1/cm) 271.140
Crystal Density (g/cm^3) 3.068
Preferred Orientation (Dir 1 : 0 0 1) 0.3464655
PVII peak type
FWHM = a + b/Cos(Th) + c Tan(Th)
a 0.05294775
b 0.02267584
c 0.1100622
Exponent m = 0.6+ma+mb/Cos(Th)+mc/Tan(Th)
ma 0.08268943
mb 0.08134434
mc 0.0005156104
Lattice parameters
a (≈) 5.4083795
b (≈) 9.0044365
c (≈) 14.2985996
alpha (∞) 90.04891
beta (∞) 98.57557
gamma (∞) 92.25189

Site	Np	x	y	z	Atom	Occ	Beq
Mg1	2	0.00000	0.00000	0.00000	Mg+2	0.538	0.1579
Fe1	2	0.00000	0.00000	0.00000	Fe+2	0.462	0.1579
Mg2	4	0.01410	0.33480	0.00270	Mg+2	0.496	0.1579
Fe2	4	0.01410	0.33480	0.00270	Fe+2	0.504	0.1579
Mg3	4	0.00320	0.16830	0.50040	Mg+2	0.494	0.1579
Fe3	4	0.00320	0.16830	0.50040	Fe+2	0.506	0.1579
Al1	2	0.00000	0.50000	0.50000	Al+3	1.362	0.2369
Si1	4	0.24000	0.17000	0.19410	Si+4	0.7125	0.07896
Al2	4	0.24000	0.17000	0.19410	Al+3	0.2875	0.07896
Si2	4	0.73000	0.99800	0.19450	Si+4	0.7125	0.07896
Al3	4	0.73000	0.99800	0.19450	Al+3	0.2875	0.07896
O1	4	0.19100	0.16350	0.07890	O-2	1	0.8685

O2	4	0.70500	0.99800	0.07560	O-2	1	0.8685
O3	4	0.23100	0.33600	0.23740	O-2	1	0.8685
O4	4	0.52800	0.11800	0.23020	O-2	1	0.8685
O5	4	0.01800	0.06100	0.23060	O-2	1	0.8685
O6	4	0.68900	0.33120	0.07420	O-2	1	0.8685
O7	4	0.14400	0.99900	0.43000	O-2	1	0.8685
O8	4	0.14300	0.33610	0.42860	O-2	1	0.8685
O9	4	0.64300	0.16270	0.43110	O-2	1	0.8685

Structure 5

Phase name	Albite low
R-Bragg	6.602
Spacegroup	C-1
Scale	2.58312226e-005
Cell Mass	1048.846
Cell Volume (≈^3)	664.19438
Wt% - Rietveld	2.229
Crystallite Size	
Cry size Lorentzian (nm)	354.7
Crystal Linear Absorption Coeff. (1/cm)	88.829
Crystal Density (g/cm^3)	2.622
Lattice parameters	
a (≈)	8.1380000
b (≈)	12.7890000
c (≈)	7.1560000
alpha (∞)	94.33
beta (∞)	116.57
gamma (∞)	87.65

Site	Np	x	y	z	Atom	Occ	Beq
O1	4	0.00900	0.13400	0.96700	O-2	1	1
O2	4	0.59500	0.99700	0.27900	O-2	1	1
O3	4	0.81800	0.11200	0.19200	O-2	1	1
O4	4	0.32100	0.35300	0.25900	O-2	1	1
O5	4	0.00600	0.30700	0.26800	O-2	1	1
O6	4	0.52200	0.19600	0.23300	O-2	1	1
O7	4	0.20600	0.11000	0.38900	O-2	1	1
O8	4	0.68300	0.36900	0.43000	O-2	1	1
Si1	4	0.00800	0.17100	0.20900	Si+4	0.28	1
Al1	4	0.00800	0.17100	0.20900	Al+3	0.72	1
Si2	4	0.50800	0.31800	0.24100	Si+4	1	1
Si3	4	0.69200	0.11000	0.31500	Si+4	0.8	1
Al3	4	0.69200	0.11000	0.31500	Al+3	0.2	1
Si4	4	0.18300	0.38200	0.35900	Si+4	0.91	1
Al4	4	0.18300	0.38200	0.35900	Al+3	0.09	1
Na1	4	0.27200	0.99000	0.14500	Na+1	1	1

9.1.2.13. Sample 2012-0001088, stratigraphic height: 6.52 m

Range Number : 1

R-Values

Rexp : 1.23 Rwp : 5.87 Rp : 4.61 GOF : 4.79
Rexp`: 3.63 Rwp`: 17.40 Rp` : 16.44 DW : 0.25

Quantitative Analysis - Rietveld
Phase 1 : „Quartz low“ 21.861 %
Phase 2 : „Kaolinite 1A II“ 2.556 %
Phase 3 : „Illite 2M1“ 57.303 %
Phase 4 : „Chamosite 1MIIb“ 16.321 %
Phase 5 : „Albite low“ 1.959 %

Background
Chebychev polynomial, Coefficient 0 5039.794
1 -1986.416
2 875.1201
3 -511.3527
4 307.4872
5 -121.491

Instrument
Primary radius (mm) 250
Secondary radius (mm) 250
Linear PSD 2Th angular range (∞) 2.749941
FDS angle (∞) 0.0916
Beam spill, sample length (mm) 9
Intensity not corrected
Full Axial Convolution
Filament length (mm) 8
Sample length (mm) 30
Receiving Slit length (mm) 12
Primary Sollers (∞) 2.5
Secondary Sollers (∞) 2.5

Corrections
Zero error -0.07227225
Specimen displacement -0.3259741
LP Factor 0

Miscellaneous
Excluded Regions
Start/Finish 0 0
Start/Finish 0 0
Start/Finish 0 0
Start/Finish 0 0
Start/Finish 0 0

Structure 1
Phase name Quartz low
R-Bragg 1.547
Spacegroup P3221
Scale 0.0324453888
Cell Mass 180.252
Cell Volume (≈^3) 112.92521
Wt% - Rietveld 21.861
Crystal Linear Absorption Coeff. (1/cm) 95.450

Crystal Density (g/cm^3) 2.651
Preferred Orientation (Dir 1 : 0 0 1) 1.171499
PVII peak type
FWHM = a + b/Cos(Th) + c Tan(Th)
a 0.02490538
b 0.0001000002
c 0.0001
Exponent m = 0.6+ma+mb/Cos(Th)+mc/Tan(Th)
ma 0.008427318
mb 0.03657377
mc 0.08355387
Lattice parameters
a (≈) 4.9123975
c (≈) 5.4034765

Site	Np	x	y	z	Atom	Occ	Beq
Si1	3	0.46900	0.00000	0.66667	Si+4	1	1
O1	6	0.40300	0.25300	0.78900	O-2	1	1

Structure 2
Phase name Kaolinite 1A II
R-Bragg 0.737
Spacegroup C1
Scale 0.000626565117
Cell Mass 508.256
Cell Volume (≈^3) 242.51636
Wt% - Rietveld 2.556
Crystal Linear Absorption Coeff. (1/cm) 108.620
Crystal Density (g/cm^3) 3.480
Preferred Orientation (Dir 1 : 0 0 1) 0.2810333
PVII peak type
FWHM = a + b/Cos(Th) + c Tan(Th)
a 0.0656984
b 1
c 1
Exponent m = 0.6+ma+mb/Cos(Th)+mc/Tan(Th)
ma 0.0001
mb 0.0001
mc 0.0001
Lattice parameters
a (≈) 5.5087872
b (≈) 6.0410795
c (≈) 7.5466305
alpha (∞) 95.01543
beta (∞) 102.799
gamma (∞) 94.95646

Site	Np	x	y	z	Atom	Occ	Beq
O1	2	0.77800	0.18000	-0.14000	O-2	1	1
O2	2	0.27800	0.32000	-0.13800	O-2	1	1
O3	2	0.31600	-0.00800	-0.13600	O-2	1	1
O4	2	0.24800	0.18400	0.15500	O-2	1	1
O5	2	0.75400	0.31500	0.15500	O-2	1	1
O6	2	0.69000	0.00400	0.15700	O-2	1	1
O7	2	0.79100	0.16500	0.48200	O-2	1	1

O8	2	0.61200	-0.12000	0.45500	O-2	1	1
O9	2	0.10800	-0.05800	0.45500	O-2	1	1
Al1	2	0.50200	0.17200	0.00300	Al+3	1	1
Al2	2	0.00200	0.33000	0.00200	Al+3	1	1
Si1	2	0.80000	0.32200	0.38200	Si+4	1	1
Si2	2	0.80000	0.00000	0.38500	Si+4	1	1

Structure 3

Phase name	Illite 2M1
R-Bragg	1.755
Spacegroup	C12/c1
Scale	0.00116953441
Cell Mass	1580.752
Cell Volume (≈^3)	936.37809
Wt% - Rietveld	57.303
Crystallite Size	
Cry size Lorentzian (nm)	21.7
Crystal Linear Absorption Coeff. (1/cm)	119.514
Crystal Density (g/cm^3)	2.803
Preferred Orientation Spherical Harmonics	
Order	4
y00	1
y20	-0.8637907
y22m	-0.9298683
y22p	-0.6731786
y40	0.137514
y42m	-0.02054978
y42p	0.1063678
y44m	-0.3055844
y44p	-0.119474
Lattice parameters	
a (≈)	5.2066934
b (≈)	9.0141858
c (≈)	20.0593564
beta (∞)	95.96047

Site	Np	x	y	z	Atom	Occ	Beq
Si1	8	0.48250	0.92970	0.13700	Si+4	1	1.737
Al1	8	0.44320	0.26350	0.13650	Al+3	1	0.8685
Al2	8	0.25860	0.08280	0.00680	Al+3	1	2.132
K1	4	0.00000	0.09010	0.25000	K+1	1	5.922
O1	8	0.46230	0.91940	0.05050	O-2	1	1.184
O2	8	0.38350	0.26650	0.06630	O-2	1	3.711
O3	8	0.42590	0.10390	0.15300	O-2	1	0.9475
O4	8	0.22260	0.83680	0.16850	O-2	1	3.237
O5	8	0.27350	0.37220	0.16780	O-2	1	6.317
O6	8	0.40800	0.56710	0.04540	O-2	1	4.185

Structure 4

Phase name	Chamosite 1MIIb
R-Bragg	2.224
Spacegroup	C-1
Scale	0.000565981885
Cell Mass	1271.241

Cell Volume (≈^3) 685.27725
Wt% - Rietveld 16.321
Crystal Linear Absorption Coeff. (1/cm) 272.217
Crystal Density (g/cm^3) 3.080
Preferred Orientation (Dir 1 : 0 0 1) 0.8621986
PVII peak type
FWHM = a + b/Cos(Th) + c Tan(Th)
a 0.0008085271
b 0.0667017
c 0.06501368
Exponent m = 0.6+ma+mb/Cos(Th)+mc/Tan(Th)
ma 0.0001
mb 0.0001
mc 0.0001
Lattice parameters
a (≈) 5.5075645
b (≈) 8.8220486
c (≈) 14.3719365
alpha (∞) 90.19984
beta (∞) 100.4834
gamma (∞) 93.51772

Site	Np	x	y	z	Atom	Occ	Beq
Mg1	2	0.00000	0.00000	0.00000	Mg+2	0.538	0.1579
Fe1	2	0.00000	0.00000	0.00000	Fe+2	0.462	0.1579
Mg2	4	0.01410	0.33480	0.00270	Mg+2	0.496	0.1579
Fe2	4	0.01410	0.33480	0.00270	Fe+2	0.504	0.1579
Mg3	4	0.00320	0.16830	0.50040	Mg+2	0.494	0.1579
Fe3	4	0.00320	0.16830	0.50040	Fe+2	0.506	0.1579
Al1	2	0.00000	0.50000	0.50000	Al+3	1.362	0.2369
Si1	4	0.24000	0.17000	0.19410	Si+4	0.7125	0.07896
Al2	4	0.24000	0.17000	0.19410	Al+3	0.2875	0.07896
Si2	4	0.73000	0.99800	0.19450	Si+4	0.7125	0.07896
Al3	4	0.73000	0.99800	0.19450	Al+3	0.2875	0.07896
O1	4	0.19100	0.16350	0.07890	O-2	1	0.8685
O2	4	0.70500	0.99800	0.07560	O-2	1	0.8685
O3	4	0.23100	0.33600	0.23740	O-2	1	0.8685
O4	4	0.52800	0.11800	0.23020	O-2	1	0.8685
O5	4	0.01800	0.06100	0.23060	O-2	1	0.8685
O6	4	0.68900	0.33120	0.07420	O-2	1	0.8685
O7	4	0.14400	0.99900	0.43000	O-2	1	0.8685
O8	4	0.14300	0.33610	0.42860	O-2	1	0.8685
O9	4	0.64300	0.16270	0.43110	O-2	1	0.8685

Structure 5
Phase name Albite low
R-Bragg 3.560
Spacegroup C-1
Scale 8.49406161e-005
Cell Mass 1048.846
Cell Volume (≈^3) 664.19438
Wt% - Rietveld 1.959
Crystallite Size
Cry size Lorentzian (nm) 413.2
Crystal Linear Absorption Coeff. (1/cm) 88.829

Crystal Density (g/cm^3) 2.622
Lattice parameters
a (≈) 8.1380000
b (≈) 12.7890000
c (≈) 7.1560000
alpha (∞) 94.33
beta (∞) 116.57
gamma (∞) 87.65

Site	Np	x	y	z	Atom	Occ	Beq
O1	4	0.00900	0.13400	0.96700	O-2	1	1
O2	4	0.59500	0.99700	0.27900	O-2	1	1
O3	4	0.81800	0.11200	0.19200	O-2	1	1
O4	4	0.32100	0.35300	0.25900	O-2	1	1
O5	4	0.00600	0.30700	0.26800	O-2	1	1
O6	4	0.52200	0.19600	0.23300	O-2	1	1
O7	4	0.20600	0.11000	0.38900	O-2	1	1
O8	4	0.68300	0.36900	0.43000	O-2	1	1
Si1	4	0.00800	0.17100	0.20900	Si+4	0.28	1
Al1	4	0.00800	0.17100	0.20900	Al+3	0.72	1
Si2	4	0.50800	0.31800	0.24100	Si+4	1	1
Si3	4	0.69200	0.11000	0.31500	Si+4	0.8	1
Al3	4	0.69200	0.11000	0.31500	Al+3	0.2	1
Si4	4	0.18300	0.38200	0.35900	Si+4	0.91	1
Al4	4	0.18300	0.38200	0.35900	Al+3	0.09	1
Na1	4	0.27200	0.99000	0.14500	Na+1	1	1

9.1.2.14. Sample 2012-0001058, stratigraphic height: 7.05 m

Range Number : 1

R-Values

Rexp : 1.16 Rwp : 7.19 Rp : 5.47 GOF : 6.18
Rexp`: 2.96 Rwp`: 18.30 Rp` : 15.70 DW : 0.10

Quantitative Analysis - Rietveld
Phase 1 : „Quartz low“ 7.928 %
Phase 2 : „Kaolinite 1A II“ 0.918 %
Phase 3 : „Illite 2M1“ 76.591 %
Phase 4 : „Chamosite 1MIIb“ 13.561 %
Phase 5 : „Albite low“ 1.002 %

Background
Chebychev polynomial, Coefficient 0 5039.794
1 -1986.416
2 875.1201
3 -511.3527
4 307.4872
5 -121.491

Instrument
Primary radius (mm) 250
Secondary radius (mm) 250

Linear PSD 2Th angular range (∞) 2.749941
FDS angle (∞) 0.0916
Beam spill, sample length (mm) 9
Intensity not corrected
Full Axial Convolution
Filament length (mm) 8
Sample length (mm) 30
Receiving Slit length (mm) 12
Primary Sollers (∞) 2.5
Secondary Sollers (∞) 2.5

Corrections
Zero error -0.08034041
Specimen displacement -0.2917186
LP Factor 0

Miscellaneous
Excluded Regions
Start/Finish 0 0
Start/Finish 0 0
Start/Finish 0 0
Start/Finish 0 0
Start/Finish 0 0

Structure 1
Phase name Quartz low
R-Bragg 31.425
Spacegroup P3221
Scale 0.0198315359
Cell Mass 180.252
Cell Volume (≈^3) 112.89802
Wt% - Rietveld 7.928
Crystal Linear Absorption Coeff. (1/cm) 95.473
Crystal Density (g/cm^3) 2.651
Preferred Orientation (Dir 1 : 0 0 1) 1.166925
PVII peak type
FWHM = a + b/Cos(Th) + c Tan(Th)
a 0.04590324
b 0.0001000001
c 0.0001
Exponent m = 0.6+ma+mb/Cos(Th)+mc/Tan(Th)
ma 0.0001000979
mb 0.6304647
mc 0.0001000001
Lattice parameters
a (≈) 4.9123635
c (≈) 5.4022504

Site	Np	x	y	z	Atom	Occ	Beq
Si1	3	0.46900	0.00000	0.66667	Si+4	1	1
O1	6	0.40300	0.25300	0.78900	O-2	1	1

Structure 2
Phase name Kaolinite 1A II

R-Bragg 12.151
Spacegroup C1
Scale 0.00050087234
Cell Mass 508.256
Cell Volume (≈^3) 183.53187
Wt% - Rietveld 0.918
Crystal Linear Absorption Coeff. (1/cm) 143.528
Crystal Density (g/cm^3) 4.599
Preferred Orientation (Dir 1 : 0 0 1) 0.3101799
PVII peak type
FWHM = a + b/Cos(Th) + c Tan(Th)
a 1
b 1
c 1
Exponent m = 0.6+ma+mb/Cos(Th)+mc/Tan(Th)
ma 0.0001
mb 0.0001
mc 0.009334074
Lattice parameters
a (≈) 3.6297199
b (≈) 6.1753718
c (≈) 8.4043836
alpha (∞) 92.06372
beta (∞) 102.8193
gamma (∞) 90.65771

Site	Np	x	y	z	Atom	Occ	Beq
O1	2	0.77800	0.18000	-0.14000	O-2	1	1
O2	2	0.27800	0.32000	-0.13800	O-2	1	1
O3	2	0.31600	-0.00800	-0.13600	O-2	1	1
O4	2	0.24800	0.18400	0.15500	O-2	1	1
O5	2	0.75400	0.31500	0.15500	O-2	1	1
O6	2	0.69000	0.00400	0.15700	O-2	1	1
O7	2	0.79100	0.16500	0.48200	O-2	1	1
O8	2	0.61200	-0.12000	0.45500	O-2	1	1
O9	2	0.10800	-0.05800	0.45500	O-2	1	1
Al1	2	0.50200	0.17200	0.00300	Al+3	1	1
Al2	2	0.00200	0.33000	0.00200	Al+3	1	1
Si1	2	0.80000	0.32200	0.38200	Si+4	1	1
Si2	2	0.80000	0.00000	0.38500	Si+4	1	1

Structure 3
Phase name Illite 2M1
R-Bragg 14.895
Spacegroup C12/c1
Scale 0.00263408315
Cell Mass 1580.752
Cell Volume (≈^3) 936.37809
Wt% - Rietveld 76.591
Crystallite Size
Cry size Lorentzian (nm) 16.5
Crystal Linear Absorption Coeff. (1/cm) 119.514
Crystal Density (g/cm^3) 2.803
Preferred Orientation Spherical Harmonics
Order 4

y00	1
y20	-1.291161
y22m	-1.598422
y22p	-0.9004444
y40	0.5007511
y42m	0.3423635
y42p	0.1583822
y44m	0.2451632
y44p	-0.4058714

Lattice parameters

a (≈)	5.2066934
b (≈)	9.0141858
c (≈)	20.0593564
beta (∞)	95.96047

Site	Np	x	y	z	Atom	Occ	Beq
Si1	8	0.48250	0.92970	0.13700	Si+4	1	1.737
Al1	8	0.44320	0.26350	0.13650	Al+3	1	0.8685
Al2	8	0.25860	0.08280	0.00680	Al+3	1	2.132
K1	4	0.00000	0.09010	0.25000	K+1	1	5.922
O1	8	0.46230	0.91940	0.05050	O-2	1	1.184
O2	8	0.38350	0.26650	0.06630	O-2	1	3.711
O3	8	0.42590	0.10390	0.15300	O-2	1	0.9475
O4	8	0.22260	0.83680	0.16850	O-2	1	3.237
O5	8	0.27350	0.37220	0.16780	O-2	1	6.317
O6	8	0.40800	0.56710	0.04540	O-2	1	4.185

Structure 4

Phase name	Chamosite 1MIIb
R-Bragg	13.355
Spacegroup	C-1
Scale	0.000797386232
Cell Mass	1271.241
Cell Volume (≈^3)	681.03786
Wt% - Rietveld	13.561
Crystal Linear Absorption Coeff. (1/cm)	273.912
Crystal Density (g/cm^3)	3.100
Preferred Orientation (Dir 1 : 0 0 1)	0.635915

PVII peak type

FWHM = a + b/Cos(Th) + c Tan(Th)

a	0.09516718
b	0.0495164
c	0.0001

Exponent m = 0.6+ma+mb/Cos(Th)+mc/Tan(Th)

ma	0.0001
mb	0.0001
mc	0.0001

Lattice parameters

a (≈)	5.4414099
b (≈)	8.8760224
c (≈)	14.3294826
alpha (∞)	89.21167
beta (∞)	99.44252
gamma (∞)	94.00766

Site	Np	x	y	z	Atom	Occ	Beq
Mg1	2	0.00000	0.00000	0.00000	Mg+2	0.538	0.1579
Fe1	2	0.00000	0.00000	0.00000	Fe+2	0.462	0.1579
Mg2	4	0.01410	0.33480	0.00270	Mg+2	0.496	0.1579
Fe2	4	0.01410	0.33480	0.00270	Fe+2	0.504	0.1579
Mg3	4	0.00320	0.16830	0.50040	Mg+2	0.494	0.1579
Fe3	4	0.00320	0.16830	0.50040	Fe+2	0.506	0.1579
Al1	2	0.00000	0.50000	0.50000	Al+3	1.362	0.2369
Si1	4	0.24000	0.17000	0.19410	Si+4	0.7125	0.07896
Al2	4	0.24000	0.17000	0.19410	Al+3	0.2875	0.07896
Si2	4	0.73000	0.99800	0.19450	Si+4	0.7125	0.07896
Al3	4	0.73000	0.99800	0.19450	Al+3	0.2875	0.07896
O1	4	0.19100	0.16350	0.07890	O-2	1	0.8685
O2	4	0.70500	0.99800	0.07560	O-2	1	0.8685
O3	4	0.23100	0.33600	0.23740	O-2	1	0.8685
O4	4	0.52800	0.11800	0.23020	O-2	1	0.8685
O5	4	0.01800	0.06100	0.23060	O-2	1	0.8685
O6	4	0.68900	0.33120	0.07420	O-2	1	0.8685
O7	4	0.14400	0.99900	0.43000	O-2	1	0.8685
O8	4	0.14300	0.33610	0.42860	O-2	1	0.8685
O9	4	0.64300	0.16270	0.43110	O-2	1	0.8685

Structure 5

Phase name	Albite low
R-Bragg	5.230
Spacegroup	C-1
Scale	7.31898736e-005
Cell Mass	1048.846
Cell Volume (≈^3)	664.19438
Wt% - Rietveld	1.002
Crystallite Size	
Cry size Lorentzian (nm)	186.9
Crystal Linear Absorption Coeff. (1/cm)	88.829
Crystal Density (g/cm^3)	2.622
Lattice parameters	
a (≈)	8.1380000
b (≈)	12.7890000
c (≈)	7.1560000
alpha (∞)	94.33
beta (∞)	116.57
gamma (∞)	87.65

Site	Np	x	y	z	Atom	Occ	Beq
O1	4	0.00900	0.13400	0.96700	O-2	1	1
O2	4	0.59500	0.99700	0.27900	O-2	1	1
O3	4	0.81800	0.11200	0.19200	O-2	1	1
O4	4	0.32100	0.35300	0.25900	O-2	1	1
O5	4	0.00600	0.30700	0.26800	O-2	1	1
O6	4	0.52200	0.19600	0.23300	O-2	1	1
O7	4	0.20600	0.11000	0.38900	O-2	1	1
O8	4	0.68300	0.36900	0.43000	O-2	1	1
Si1	4	0.00800	0.17100	0.20900	Si+4	0.28	1
Al1	4	0.00800	0.17100	0.20900	Al+3	0.72	1
Si2	4	0.50800	0.31800	0.24100	Si+4	1	1
Si3	4	0.69200	0.11000	0.31500	Si+4	0.8	1

Al3 4 0.69200 0.11000 0.31500 Al+3 0.2 1
Si4 4 0.18300 0.38200 0.35900 Si+4 0.91 1
Al4 4 0.18300 0.38200 0.35900 Al+3 0.09 1
Na1 4 0.27200 0.99000 0.14500 Na+1 1 1

9.1.2.15. Sample 2012-0001056, stratigraphic height: 7.53 m

Range Number : 1

R-Values

Rexp : 1.22 Rwp : 5.36 Rp : 4.06 GOF : 4.38
Rexp`: 3.61 Rwp`: 15.79 Rp` : 14.57 DW : 0.21

Quantitative Analysis - Rietveld
Phase 1 : „Quartz low“ 29.465 %
Phase 2 : „Kaolinite 1A II“ 2.602 %
Phase 3 : „Illite 2M1“ 62.259 %
Phase 4 : „Chamosite 1MIIb“ 2.778 %
Phase 5 : „Albite low“ 2.897 %

Background
Chebychev polynomial, Coefficient 0 5039.794
1 -1986.416
2 875.1201
3 -511.3527
4 307.4872
5 -121.491

Instrument
Primary radius (mm) 250
Secondary radius (mm) 250
Linear PSD 2Th angular range (∞) 2.749941
FDS angle (∞) 0.0916
Beam spill, sample length (mm) 9
Intensity not corrected
Full Axial Convolution
Filament length (mm) 8
Sample length (mm) 30
Receiving Slit length (mm) 12
Primary Sollers (∞) 2.5
Secondary Sollers (∞) 2.5

Corrections
Zero error -0.007456441
Specimen displacement -0.1722983
LP Factor 0

Miscellaneous
Excluded Regions
Start/Finish 0 0
Start/Finish 0 0
Start/Finish 0 0
Start/Finish 0 0

Start/Finish 0 0

Structure 1
Phase name Quartz low
R-Bragg 9.588
Spacegroup P3221
Scale 0.0314480631
Cell Mass 180.252
Cell Volume (≈^3) 112.99781
Wt% - Rietveld 29.465
Crystal Linear Absorption Coeff. (1/cm) 95.389
Crystal Density (g/cm^3) 2.649
Preferred Orientation (Dir 1 : 0 0 1) 1.176685
PVII peak type
FWHM = a + b/Cos(Th) + c Tan(Th)
a 0.02919182
b 0.0001001028
c 0.0001
Exponent m = 0.6+ma+mb/Cos(Th)+mc/Tan(Th)
ma 0.0947628
mb 0.03909741
mc 0.0479151
Lattice parameters
a (≈) 4.9134608
c (≈) 5.4046106

Site	Np	x	y	z	Atom	Occ	Beq
Si1	3	0.46900	0.00000	0.66667	Si+4	1	1
O1	6	0.40300	0.25300	0.78900	O-2	1	1

Structure 2
Phase name Kaolinite 1A II
R-Bragg 1.685
Spacegroup C1
Scale 0.000342270599
Cell Mass 508.256
Cell Volume (≈^3) 325.10507
Wt% - Rietveld 2.602
Crystal Linear Absorption Coeff. (1/cm) 81.026
Crystal Density (g/cm^3) 2.596
Preferred Orientation (Dir 1 : 0 0 1) 0.2493358
PVII peak type
FWHM = a + b/Cos(Th) + c Tan(Th)
a 0.2719574
b 0.9999998
c 1
Exponent m = 0.6+ma+mb/Cos(Th)+mc/Tan(Th)
ma 0.0001
mb 0.0001
mc 0.02054317
Lattice parameters
a (≈) 5.3322134
b (≈) 8.3787153
c (≈) 7.5046934

alpha (∞)	93.05501
beta (∞)	103.7211
gamma (∞)	90.97204

Site	Np	x	y	z	Atom	Occ	Beq
O1	2	0.77800	0.18000	-0.14000	O-2	1	1
O2	2	0.27800	0.32000	-0.13800	O-2	1	1
O3	2	0.31600	-0.00800	-0.13600	O-2	1	1
O4	2	0.24800	0.18400	0.15500	O-2	1	1
O5	2	0.75400	0.31500	0.15500	O-2	1	1
O6	2	0.69000	0.00400	0.15700	O-2	1	1
O7	2	0.79100	0.16500	0.48200	O-2	1	1
O8	2	0.61200	-0.12000	0.45500	O-2	1	1
O9	2	0.10800	-0.05800	0.45500	O-2	1	1
Al1	2	0.50200	0.17200	0.00300	Al+3	1	1
Al2	2	0.00200	0.33000	0.00200	Al+3	1	1
Si1	2	0.80000	0.32200	0.38200	Si+4	1	1
Si2	2	0.80000	0.00000	0.38500	Si+4	1	1

Structure 3

Phase name	Illite 2M1
R-Bragg	2.190
Spacegroup	C12/c1
Scale	0.000914386938
Cell Mass	1580.752
Cell Volume (≈^3)	936.37809
Wt% - Rietveld	62.259
Crystallite Size	
Cry size Lorentzian (nm)	19.3
Crystal Linear Absorption Coeff. (1/cm)	119.514
Crystal Density (g/cm^3)	2.803
Preferred Orientation (Dir 1 : 0 0 1)	0.6282947
Preferred Orientation Spherical Harmonics	
Order	8
y00	1
y20	0.01618121
y22m	-0.2938815
y22p	-0.06700253
y40	0.4149418
y42m	-0.2487903
y42p	-0.2599852
y44m	-0.3147809
y44p	0.0243382
y60	0.02316191
y62m	0.2909122
y62p	0.05274468
y64m	-0.5247541
y64p	-0.1533965
y66m	0.06973947
y66p	0.06973947
y80	-0.06140514
y82m	0.6647765
y82p	0.5232965
y84m	-0.3728648
y84p	0.01010179

y86m	0.100129
y86p	-0.430702
y88m	0.1667739
y88p	0.04323866

PVII peak type

FWHM = a + b/Cos(Th) + c Tan(Th)	
a	0.0004548538
b	0.0007778313
c	0.1379862
Exponent m = 0.6+ma+mb/Cos(Th)+mc/Tan(Th)	
ma	0.0001008386
mb	0.0001004402
mc	0.8613694

Lattice parameters

a (≈)	5.2066934
b (≈)	9.0141858
c (≈)	20.0593564
beta (∞)	95.96047

Site	Np	x	y	z	Atom	Occ	Beq
Si1	8	0.48250	0.92970	0.13700	Si+4	1	1.737
Al1	8	0.44320	0.26350	0.13650	Al+3	1	0.8685
Al2	8	0.25860	0.08280	0.00680	Al+3	1	2.132
K1	4	0.00000	0.09010	0.25000	K+1	1	5.922
O1	8	0.46230	0.91940	0.05050	O-2	1	1.184
O2	8	0.38350	0.26650	0.06630	O-2	1	3.711
O3	8	0.42590	0.10390	0.15300	O-2	1	0.9475
O4	8	0.22260	0.83680	0.16850	O-2	1	3.237
O5	8	0.27350	0.37220	0.16780	O-2	1	6.317
O6	8	0.40800	0.56710	0.04540	O-2	1	4.185

Structure 4

Phase name	Chamosite 1MIIb
R-Bragg	9.623
Spacegroup	C-1
Scale	6.90525003e-005
Cell Mass	1271.241
Cell Volume (≈^3)	688.00078
Wt% - Rietveld	2.778
Crystal Linear Absorption Coeff. (1/cm)	271.140
Crystal Density (g/cm^3)	3.068
Preferred Orientation (Dir 1 : 0 0 1)	0.4824924

PVII peak type

FWHM = a + b/Cos(Th) + c Tan(Th)	
a	0.09714325
b	0.004026098
c	0.0001
Exponent m = 0.6+ma+mb/Cos(Th)+mc/Tan(Th)	
ma	0.1740476
mb	0.0001000038
mc	0.0001000003

Lattice parameters

a (≈)	5.4083795
b (≈)	9.0044365
c (≈)	14.2985996

alpha (∞) 90.04891
beta (∞) 98.57557
gamma (∞) 92.25189

Site	Np	x	y	z	Atom	Occ	Beq
Mg1	2	0.00000	0.00000	0.00000	Mg+2	0.538	0.1579
Fe1	2	0.00000	0.00000	0.00000	Fe+2	0.462	0.1579
Mg2	4	0.01410	0.33480	0.00270	Mg+2	0.496	0.1579
Fe2	4	0.01410	0.33480	0.00270	Fe+2	0.504	0.1579
Mg3	4	0.00320	0.16830	0.50040	Mg+2	0.494	0.1579
Fe3	4	0.00320	0.16830	0.50040	Fe+2	0.506	0.1579
Al1	2	0.00000	0.50000	0.50000	Al+3	1.362	0.2369
Si1	4	0.24000	0.17000	0.19410	Si+4	0.7125	0.07896
Al2	4	0.24000	0.17000	0.19410	Al+3	0.2875	0.07896
Si2	4	0.73000	0.99800	0.19450	Si+4	0.7125	0.07896
Al3	4	0.73000	0.99800	0.19450	Al+3	0.2875	0.07896
O1	4	0.19100	0.16350	0.07890	O-2	1	0.8685
O2	4	0.70500	0.99800	0.07560	O-2	1	0.8685
O3	4	0.23100	0.33600	0.23740	O-2	1	0.8685
O4	4	0.52800	0.11800	0.23020	O-2	1	0.8685
O5	4	0.01800	0.06100	0.23060	O-2	1	0.8685
O6	4	0.68900	0.33120	0.07420	O-2	1	0.8685
O7	4	0.14400	0.99900	0.43000	O-2	1	0.8685
O8	4	0.14300	0.33610	0.42860	O-2	1	0.8685
O9	4	0.64300	0.16270	0.43110	O-2	1	0.8685

Structure 5
Phase name Albite low
R-Bragg 4.290
Spacegroup C-1
Scale 9.03988531e-005
Cell Mass 1048.846
Cell Volume (≈^3) 664.19438
Wt% - Rietveld 2.897
Crystallite Size
Cry size Lorentzian (nm) 282.5
Crystal Linear Absorption Coeff. (1/cm) 88.829
Crystal Density (g/cm^3) 2.622
Lattice parameters
a (≈) 8.1380000
b (≈) 12.7890000
c (≈) 7.1560000
alpha (∞) 94.33
beta (∞) 116.57
gamma (∞) 87.65

Site	Np	x	y	z	Atom	Occ	Beq
O1	4	0.00900	0.13400	0.96700	O-2	1	1
O2	4	0.59500	0.99700	0.27900	O-2	1	1
O3	4	0.81800	0.11200	0.19200	O-2	1	1
O4	4	0.32100	0.35300	0.25900	O-2	1	1
O5	4	0.00600	0.30700	0.26800	O-2	1	1
O6	4	0.52200	0.19600	0.23300	O-2	1	1
O7	4	0.20600	0.11000	0.38900	O-2	1	1
O8	4	0.68300	0.36900	0.43000	O-2	1	1

Si1 4 0.00800 0.17100 0.20900 Si+4 0.28 1
Al1 4 0.00800 0.17100 0.20900 Al+3 0.72 1
Si2 4 0.50800 0.31800 0.24100 Si+4 1 1
Si3 4 0.69200 0.11000 0.31500 Si+4 0.8 1
Al3 4 0.69200 0.11000 0.31500 Al+3 0.2 1
Si4 4 0.18300 0.38200 0.35900 Si+4 0.91 1
Al4 4 0.18300 0.38200 0.35900 Al+3 0.09 1
Na1 4 0.27200 0.99000 0.14500 Na+1 1 1

9.1.2.16. Sample 2012-0001081, stratigraphic height: 8.95 m

Range Number : 1

R-Values

Rexp : 1.65 Rwp : 6.93 Rp : 4.67 GOF : 4.19
Rexp`: 5.49 Rwp`: 23.03 Rp` : 22.74 DW : 0.17

Quantitative Analysis - Rietveld
Phase 1 : „Quartz low“ 20.938 %
Phase 2 : „Kaolinite 1A II“ 0.533 %
Phase 3 : „Illite 2M1“ 73.902 %
Phase 4 : „Chamosite 1MIIb“ 1.895 %
Phase 5 : „Albite low“ 2.732 %

Background
Chebychev polynomial, Coefficient 0 3109.337
1 -1449.886
2 668.3359
3 -499.4978
4 389.9553
5 -251.1535
6 93.85811

Instrument
Primary radius (mm) 250
Secondary radius (mm) 250
Linear PSD 2Th angular range (∞) 2.749941
FDS angle (∞) 0.0916
Beam spill, sample length (mm) 9
Intensity not corrected
Full Axial Convolution
Filament length (mm) 8
Sample length (mm) 30
Receiving Slit length (mm) 12
Primary Sollers (∞) 2.5
Secondary Sollers (∞) 2.5

Corrections
Zero error -0.09830758
Specimen displacement -0.3183125
LP Factor 0

Miscellaneous

Excluded Regions
Start/Finish 0 0
Start/Finish 0 0
Start/Finish 0 0
Start/Finish 0 0
Start/Finish 0 0

Structure 1
Phase name Quartz low
R-Bragg 12.929
Spacegroup P3221
Scale 0.00982233137
Cell Mass 180.252
Cell Volume (≈^3) 112.93648
Wt% - Rietveld 20.938
Crystal Linear Absorption Coeff. (1/cm) 95.440
Crystal Density (g/cm^3) 2.650
Preferred Orientation (Dir 1 : 0 0 1) 1.199463
PVII peak type
FWHM = a + b/Cos(Th) + c Tan(Th)
a 0.01669587
b 0.003583779
c 0.0001702951
Exponent m = 0.6+ma+mb/Cos(Th)+mc/Tan(Th)
ma 0.003682962
mb 0.1406514
mc 0.002247315
Lattice parameters
a (≈) 4.9125154
c (≈) 5.4037563

Site	Np	x	y	z	Atom	Occ	Beq
Si1	3	0.46900	0.00000	0.66667	Si+4	1	1
O1	6	0.40300	0.25300	0.78900	O-2	1	1

Structure 2
Phase name Kaolinite 1A II
R-Bragg 33.161
Spacegroup C1
Scale 3.07760545e-005
Cell Mass 508.256
Cell Volume (≈^3) 325.10507
Wt% - Rietveld 0.533
Crystal Linear Absorption Coeff. (1/cm) 81.026
Crystal Density (g/cm^3) 2.596
Preferred Orientation (Dir 1 : 0 0 1) 0.3716098
PVII peak type
FWHM = a + b/Cos(Th) + c Tan(Th)
a 0.09521499
b 0.186387
c 0.9984379
Exponent m = 0.6+ma+mb/Cos(Th)+mc/Tan(Th)
ma 0.009865613
mb 0.002544724

mc	2.496998
Lattice parameters	
a (≈)	5.3322134
b (≈)	8.3787153
c (≈)	7.5046934
alpha (∞)	93.05501
beta (∞)	103.7211
gamma (∞)	90.97204

Site	Np	x	y	z	Atom	Occ	Beq
O1	2	0.77800	0.18000	-0.14000	O-2	1	1
O2	2	0.27800	0.32000	-0.13800	O-2	1	1
O3	2	0.31600	-0.00800	-0.13600	O-2	1	1
O4	2	0.24800	0.18400	0.15500	O-2	1	1
O5	2	0.75400	0.31500	0.15500	O-2	1	1
O6	2	0.69000	0.00400	0.15700	O-2	1	1
O7	2	0.79100	0.16500	0.48200	O-2	1	1
O8	2	0.61200	-0.12000	0.45500	O-2	1	1
O9	2	0.10800	-0.05800	0.45500	O-2	1	1
Al1	2	0.50200	0.17200	0.00300	Al+3	1	1
Al2	2	0.00200	0.33000	0.00200	Al+3	1	1
Si1	2	0.80000	0.32200	0.38200	Si+4	1	1
Si2	2	0.80000	0.00000	0.38500	Si+4	1	1

Structure 3

Phase name	Illite 2M1
R-Bragg	28.434
Spacegroup	C12/c1
Scale	0.00047679115
Cell Mass	1580.752
Cell Volume (≈^3)	936.37809
Wt% - Rietveld	73.902
Crystallite Size	
Cry size Lorentzian (nm)	24.4
Crystal Linear Absorption Coeff. (1/cm)	119.514
Crystal Density (g/cm^3)	2.803
Preferred Orientation (Dir 1 : 0 0 1)	0.3742873
Preferred Orientation Spherical Harmonics	
Order	8
y00	1
y20	0.5691349
y22m	-0.2219263
y22p	-0.1130727
y40	0.4859238
y42m	-0.4906254
y42p	-0.4975798
y44m	0.734528
y44p	-0.02849539
y60	-0.007743161
y62m	-0.05331248
y62p	0.4526019
y64m	-0.01669457
y64p	-0.2465838
y66m	0.2985994
y66p	0.2985994

y80	0.07977866
y82m	0.746457
y82p	0.3501084
y84m	-0.5499607
y84p	-0.0669519
y86m	-0.08062666
y86p	0.002722092
y88m	0.2612454
y88p	0.08406434

PVII peak type

FWHM = a + b/Cos(Th) + c Tan(Th)

a	0.0001009188
b	0.00010091
c	0.03753449

Exponent m = 0.6+ma+mb/Cos(Th)+mc/Tan(Th)

ma	0.0001000731
mb	0.0001113453
mc	0.04880457

Lattice parameters

a (≈)	5.2066934
b (≈)	9.0141858
c (≈)	20.0593564
beta (∞)	95.96047

Site	Np	x	y	z	Atom	Occ	Beq
Si1	8	0.48250	0.92970	0.13700	Si+4	1	1.737
Al1	8	0.44320	0.26350	0.13650	Al+3	1	0.8685
Al2	8	0.25860	0.08280	0.00680	Al+3	1	2.132
K1	4	0.00000	0.09010	0.25000	K+1	1	5.922
O1	8	0.46230	0.91940	0.05050	O-2	1	1.184
O2	8	0.38350	0.26650	0.06630	O-2	1	3.711
O3	8	0.42590	0.10390	0.15300	O-2	1	0.9475
O4	8	0.22260	0.83680	0.16850	O-2	1	3.237
O5	8	0.27350	0.37220	0.16780	O-2	1	6.317
O6	8	0.40800	0.56710	0.04540	O-2	1	4.185

Structure 4

Phase name	Chamosite 1MIIb
R-Bragg	46.131
Spacegroup	C-1
Scale	2.06953574e-005
Cell Mass	1271.241
Cell Volume (≈^3)	688.00078
Wt% - Rietveld	1.895
Crystal Linear Absorption Coeff. (1/cm)	271.140
Crystal Density (g/cm^3)	3.068
Preferred Orientation (Dir 1 : 0 0 1)	0.2900993

PVII peak type

FWHM = a + b/Cos(Th) + c Tan(Th)

a	0.0676327
b	0.01961481
c	0.1257375

Exponent m = 0.6+ma+mb/Cos(Th)+mc/Tan(Th)

ma	0.2300825
mb	0.2087701

mc	0.0001017798
Lattice parameters	
a (≈)	5.4083795
b (≈)	9.0044365
c (≈)	14.2985996
alpha (∞)	90.04891
beta (∞)	98.57557
gamma (∞)	92.25189

Site	Np	x	y	z	Atom	Occ	Beq
Mg1	2	0.00000	0.00000	0.00000	Mg+2	0.538	0.1579
Fe1	2	0.00000	0.00000	0.00000	Fe+2	0.462	0.1579
Mg2	4	0.01410	0.33480	0.00270	Mg+2	0.496	0.1579
Fe2	4	0.01410	0.33480	0.00270	Fe+2	0.504	0.1579
Mg3	4	0.00320	0.16830	0.50040	Mg+2	0.494	0.1579
Fe3	4	0.00320	0.16830	0.50040	Fe+2	0.506	0.1579
Al1	2	0.00000	0.50000	0.50000	Al+3	1.362	0.2369
Si1	4	0.24000	0.17000	0.19410	Si+4	0.7125	0.07896
Al2	4	0.24000	0.17000	0.19410	Al+3	0.2875	0.07896
Si2	4	0.73000	0.99800	0.19450	Si+4	0.7125	0.07896
Al3	4	0.73000	0.99800	0.19450	Al+3	0.2875	0.07896
O1	4	0.19100	0.16350	0.07890	O-2	1	0.8685
O2	4	0.70500	0.99800	0.07560	O-2	1	0.8685
O3	4	0.23100	0.33600	0.23740	O-2	1	0.8685
O4	4	0.52800	0.11800	0.23020	O-2	1	0.8685
O5	4	0.01800	0.06100	0.23060	O-2	1	0.8685
O6	4	0.68900	0.33120	0.07420	O-2	1	0.8685
O7	4	0.14400	0.99900	0.43000	O-2	1	0.8685
O8	4	0.14300	0.33610	0.42860	O-2	1	0.8685
O9	4	0.64300	0.16270	0.43110	O-2	1	0.8685

Structure 5

Phase name	Albite low
R-Bragg	21.480
Spacegroup	C-1
Scale	3.74548478e-005
Cell Mass	1048.846
Cell Volume (≈^3)	664.19438
Wt% - Rietveld	2.732
Crystallite Size	
Cry size Lorentzian (nm)	158.5
Crystal Linear Absorption Coeff. (1/cm)	88.829
Crystal Density (g/cm^3)	2.622
Lattice parameters	
a (≈)	8.1380000
b (≈)	12.7890000
c (≈)	7.1560000
alpha (∞)	94.33
beta (∞)	116.57
gamma (∞)	87.65

Site	Np	x	y	z	Atom	Occ	Beq
O1	4	0.00900	0.13400	0.96700	O-2	1	1
O2	4	0.59500	0.99700	0.27900	O-2	1	1
O3	4	0.81800	0.11200	0.19200	O-2	1	1

O4	4	0.32100	0.35300	0.25900	O-2	1	1
O5	4	0.00600	0.30700	0.26800	O-2	1	1
O6	4	0.52200	0.19600	0.23300	O-2	1	1
O7	4	0.20600	0.11000	0.38900	O-2	1	1
O8	4	0.68300	0.36900	0.43000	O-2	1	1
Si1	4	0.00800	0.17100	0.20900	Si+4	0.28	1
Al1	4	0.00800	0.17100	0.20900	Al+3	0.72	1
Si2	4	0.50800	0.31800	0.24100	Si+4	1	1
Si3	4	0.69200	0.11000	0.31500	Si+4	0.8	1
Al3	4	0.69200	0.11000	0.31500	Al+3	0.2	1
Si4	4	0.18300	0.38200	0.35900	Si+4	0.91	1
Al4	4	0.18300	0.38200	0.35900	Al+3	0.09	1
Na1	4	0.27200	0.99000	0.14500	Na+1	1	1

9.1.2.17. Sample 2012-0001072, stratigraphic height: 9.52 m

Range Number : 1

R-Values

Rexp : 1.84 Rwp : 7.25 Rp : 5.18 GOF : 3.93
Rexp`: 5.30 Rwp`: 20.86 Rp` : 20.30 DW : 0.22

Quantitative Analysis - Rietveld
Phase 1 : „Quartz low“ 22.484 %
Phase 2 : „Kaolinite 1A II“ 0.533 %
Phase 3 : „Illite 2M1“ 71.954 %
Phase 4 : „Chamosite 1MIIb“ 1.285 %
Phase 5 : „Albite low“ 3.743 %

Background
Chebychev polynomial, Coefficient 0 2381.811
1 -1191.827
2 597.2652
3 -414.0848
4 350.8274
5 -234.7003
6 96.9742

Instrument
Primary radius (mm) 250
Secondary radius (mm) 250
Linear PSD 2Th angular range (∞) 2.749941
FDS angle (∞) 0.0916
Beam spill, sample length (mm) 9
Intensity not corrected
Full Axial Convolution
Filament length (mm) 8
Sample length (mm) 30
Receiving Slit length (mm) 12
Primary Sollers (∞) 2.5
Secondary Sollers (∞) 2.5

Corrections

Zero error -0.1213085
Specimen displacement -0.3237722
LP Factor 0

Miscellaneous
Excluded Regions
Start/Finish 0 0
Start/Finish 0 0
Start/Finish 0 0
Start/Finish 0 0
Start/Finish 0 0

Structure 1
Phase name Quartz low
R-Bragg 7.837
Spacegroup P3221
Scale 0.0135516518
Cell Mass 180.252
Cell Volume (≈^3) 112.89355
Wt% - Rietveld 22.484
Crystal Linear Absorption Coeff. (1/cm) 95.477
Crystal Density (g/cm^3) 2.651
Preferred Orientation (Dir 1 : 0 0 1) 1.180753
PVII peak type
FWHM = a + b/Cos(Th) + c Tan(Th)
a 0.01205876
b 0.004484725
c 0.007003702
Exponent m = 0.6+ma+mb/Cos(Th)+mc/Tan(Th)
ma 0.004083112
mb 0.02838747
mc 0.09737176
Lattice parameters
a (≈) 4.9118525
c (≈) 5.4031603

Site	Np	x	y	z	Atom	Occ	Beq
Si1	3	0.46900	0.00000	0.66667	Si+4	1	1
O1	6	0.40300	0.25300	0.78900	O-2	1	1

Structure 2
Phase name Kaolinite 1A II
R-Bragg 14.070
Spacegroup C1
Scale 3.95746349e-005
Cell Mass 508.256
Cell Volume (≈^3) 325.10507
Wt% - Rietveld 0.533
Crystal Linear Absorption Coeff. (1/cm) 81.026
Crystal Density (g/cm^3) 2.596
Preferred Orientation (Dir 1 : 0 0 1) 0.5705598
PVII peak type
FWHM = a + b/Cos(Th) + c Tan(Th)
a 0.2961534

b	0.0001019327
c	0.03517714
Exponent m = 0.6+ma+mb/Cos(Th)+mc/Tan(Th)	
ma	17.50001
mb	4.68752
mc	4.798647
Lattice parameters	
a (≈)	5.3322134
b (≈)	8.3787153
c (≈)	7.5046934
alpha (∞)	93.05501
beta (∞)	103.7211
gamma (∞)	90.97204

Site	Np	x	y	z	Atom	Occ	Beq
O1	2	0.77800	0.18000	-0.14000	O-2	1	1
O2	2	0.27800	0.32000	-0.13800	O-2	1	1
O3	2	0.31600	-0.00800	-0.13600	O-2	1	1
O4	2	0.24800	0.18400	0.15500	O-2	1	1
O5	2	0.75400	0.31500	0.15500	O-2	1	1
O6	2	0.69000	0.00400	0.15700	O-2	1	1
O7	2	0.79100	0.16500	0.48200	O-2	1	1
O8	2	0.61200	-0.12000	0.45500	O-2	1	1
O9	2	0.10800	-0.05800	0.45500	O-2	1	1
Al1	2	0.50200	0.17200	0.00300	Al+3	1	1
Al2	2	0.00200	0.33000	0.00200	Al+3	1	1
Si1	2	0.80000	0.32200	0.38200	Si+4	1	1
Si2	2	0.80000	0.00000	0.38500	Si+4	1	1

Structure 3

Phase name	Illite 2M1
R-Bragg	15.558
Spacegroup	C12/c1
Scale	0.000596210391
Cell Mass	1580.752
Cell Volume (≈^3)	936.37809
Wt% - Rietveld	71.954
Crystallite Size	
Cry size Lorentzian (nm)	25.8
Crystal Linear Absorption Coeff. (1/cm)	119.514
Crystal Density (g/cm^3)	2.803
Preferred Orientation (Dir 1 : 0 0 1)	0.4062896
Preferred Orientation Spherical Harmonics	
Order	8
y00	1
y20	0.582488
y22m	0.0221562
y22p	-0.1063945
y40	0.511616
y42m	-0.3449061
y42p	-0.4958864
y44m	0.9620393
y44p	-0.03191576
y60	-0.001594853
y62m	-0.04759863

y62p	0.4372295
y64m	0.1195223
y64p	-0.241864
y66m	0.3032321
y66p	0.3032321
y80	0.09347208
y82m	0.6254208
y82p	0.3421345
y84m	-0.4053654
y84p	-0.07088552
y86m	0.01401891
y86p	0.0247658
y88m	-0.02145674
y88p	0.08113176

PVII peak type

FWHM = a + b/Cos(Th) + c Tan(Th)

a	0.0001184045
b	0.0001187272
c	0.04700173

Exponent m = 0.6+ma+mb/Cos(Th)+mc/Tan(Th)

ma	0.0001002925
mb	0.0001453812
mc	0.07449981

Lattice parameters

a (≈)	5.2066934
b (≈)	9.0141858
c (≈)	20.0593564
beta (∞)	95.96047

Site	Np	x	y	z	Atom	Occ	Beq
Si1	8	0.48250	0.92970	0.13700	Si+4	1	1.737
Al1	8	0.44320	0.26350	0.13650	Al+3	1	0.8685
Al2	8	0.25860	0.08280	0.00680	Al+3	1	2.132
K1	4	0.00000	0.09010	0.25000	K+1	1	5.922
O1	8	0.46230	0.91940	0.05050	O-2	1	1.184
O2	8	0.38350	0.26650	0.06630	O-2	1	3.711
O3	8	0.42590	0.10390	0.15300	O-2	1	0.9475
O4	8	0.22260	0.83680	0.16850	O-2	1	3.237
O5	8	0.27350	0.37220	0.16780	O-2	1	6.317
O6	8	0.40800	0.56710	0.04540	O-2	1	4.185

Structure 4

Phase name	Chamosite 1MIIb
R-Bragg	20.500
Spacegroup	C-1
Scale	1.80245003e-005
Cell Mass	1271.241
Cell Volume (≈^3)	688.00078
Wt% - Rietveld	1.285
Crystal Linear Absorption Coeff. (1/cm)	271.140
Crystal Density (g/cm^3)	3.068
Preferred Orientation (Dir 1 : 0 0 1)	0.3250058

PVII peak type

FWHM = a + b/Cos(Th) + c Tan(Th)

a	0.04702191

b	0.01879255
c	0.1045436
Exponent m = 0.6+ma+mb/Cos(Th)+mc/Tan(Th)	
ma	0.1444381
mb	0.1289761
mc	0.000107119
Lattice parameters	
a (≈)	5.4083795
b (≈)	9.0044365
c (≈)	14.2985996
alpha (∞)	90.04891
beta (∞)	98.57557
gamma (∞)	92.25189

Site	Np	x	y	z	Atom	Occ	Beq
Mg1	2	0.00000	0.00000	0.00000	Mg+2	0.538	0.1579
Fe1	2	0.00000	0.00000	0.00000	Fe+2	0.462	0.1579
Mg2	4	0.01410	0.33480	0.00270	Mg+2	0.496	0.1579
Fe2	4	0.01410	0.33480	0.00270	Fe+2	0.504	0.1579
Mg3	4	0.00320	0.16830	0.50040	Mg+2	0.494	0.1579
Fe3	4	0.00320	0.16830	0.50040	Fe+2	0.506	0.1579
Al1	2	0.00000	0.50000	0.50000	Al+3	1.362	0.2369
Si1	4	0.24000	0.17000	0.19410	Si+4	0.7125	0.07896
Al2	4	0.24000	0.17000	0.19410	Al+3	0.2875	0.07896
Si2	4	0.73000	0.99800	0.19450	Si+4	0.7125	0.07896
Al3	4	0.73000	0.99800	0.19450	Al+3	0.2875	0.07896
O1	4	0.19100	0.16350	0.07890	O-2	1	0.8685
O2	4	0.70500	0.99800	0.07560	O-2	1	0.8685
O3	4	0.23100	0.33600	0.23740	O-2	1	0.8685
O4	4	0.52800	0.11800	0.23020	O-2	1	0.8685
O5	4	0.01800	0.06100	0.23060	O-2	1	0.8685
O6	4	0.68900	0.33120	0.07420	O-2	1	0.8685
O7	4	0.14400	0.99900	0.43000	O-2	1	0.8685
O8	4	0.14300	0.33610	0.42860	O-2	1	0.8685
O9	4	0.64300	0.16270	0.43110	O-2	1	0.8685

Structure 5

Phase name	Albite low
R-Bragg	8.937
Spacegroup	C-1
Scale	6.59021813e-005
Cell Mass	1048.846
Cell Volume (≈^3)	664.19438
Wt% - Rietveld	3.743
Crystallite Size	
Cry size Lorentzian (nm)	219.2
Crystal Linear Absorption Coeff. (1/cm)	88.829
Crystal Density (g/cm^3)	2.622
Lattice parameters	
a (≈)	8.1380000
b (≈)	12.7890000
c (≈)	7.1560000
alpha (∞)	94.33
beta (∞)	116.57
gamma (∞)	87.65

Site	Np	x	y	z	Atom	Occ	Beq
O1	4	0.00900	0.13400	0.96700	O-2	1	1
O2	4	0.59500	0.99700	0.27900	O-2	1	1
O3	4	0.81800	0.11200	0.19200	O-2	1	1
O4	4	0.32100	0.35300	0.25900	O-2	1	1
O5	4	0.00600	0.30700	0.26800	O-2	1	1
O6	4	0.52200	0.19600	0.23300	O-2	1	1
O7	4	0.20600	0.11000	0.38900	O-2	1	1
O8	4	0.68300	0.36900	0.43000	O-2	1	1
Si1	4	0.00800	0.17100	0.20900	Si+4	0.28	1
Al1	4	0.00800	0.17100	0.20900	Al+3	0.72	1
Si2	4	0.50800	0.31800	0.24100	Si+4	1	1
Si3	4	0.69200	0.11000	0.31500	Si+4	0.8	1
Al3	4	0.69200	0.11000	0.31500	Al+3	0.2	1
Si4	4	0.18300	0.38200	0.35900	Si+4	0.91	1
Al4	4	0.18300	0.38200	0.35900	Al+3	0.09	1
Na1	4	0.27200	0.99000	0.14500	Na+1	1	1

9.1.2.18. Sample 2012-0001077, stratigraphic height: 9.95 m

Range Number : 1

R-Values

Rexp : 1.95 Rwp : 5.29 Rp : 3.77 GOF : 2.71
Rexp`: 6.95 Rwp`: 18.85 Rp` : 19.76 DW : 0.42

Quantitative Analysis - Rietveld
Phase 1 : „Quartz low“ 24.291 %
Phase 2 : „Kaolinite 1A II“ 1.603 %
Phase 3 : „Illite 2M1“ 68.570 %
Phase 4 : „Chamosite 1MIIb“ 1.471 %
Phase 5 : „Albite low“ 4.066 %

Background
Chebychev polynomial, Coefficient 0 2252.291
1 -947.949
2 427.4707
3 -309.5919
4 274.7751
5 -189.0696
6 75.80405

Instrument
Primary radius (mm) 250
Secondary radius (mm) 250
Linear PSD 2Th angular range (∞) 2.749941
FDS angle (∞) 0.0916
Beam spill, sample length (mm) 9
Intensity not corrected
Full Axial Convolution
Filament length (mm) 8
Sample length (mm) 30

Receiving Slit length (mm) 12
Primary Sollers (∞) 2.5
Secondary Sollers (∞) 2.5

Corrections
Zero error -0.06323051
Specimen displacement -0.3771659
LP Factor 0

Miscellaneous
Excluded Regions
Start/Finish 0 0
Start/Finish 0 0
Start/Finish 0 0
Start/Finish 0 0
Start/Finish 0 0

Structure 1
Phase name Quartz low
R-Bragg 10.824
Spacegroup P3221
Scale 0.0108255658
Cell Mass 180.252
Cell Volume (≈^3) 112.96782
Wt% - Rietveld 24.291
Crystal Linear Absorption Coeff. (1/cm) 95.414
Crystal Density (g/cm^3) 2.650
Preferred Orientation (Dir 1 : 0 0 1) 1.178052
PVII peak type
FWHM = a + b/Cos(Th) + c Tan(Th)
a 0.01018318
b 0.001819878
c 0.009090429
Exponent m = 0.6+ma+mb/Cos(Th)+mc/Tan(Th)
ma 0.001317194
mb 0.00725877
mc 0.07763798
Lattice parameters
a (≈) 4.9129316
c (≈) 5.4043401

Site	Np	x	y	z	Atom	Occ	Beq
Si1	3	0.46900	0.00000	0.66667	Si+4	1	1
O1	6	0.40300	0.25300	0.78900	O-2	1	1

Structure 2
Phase name Kaolinite 1A II
R-Bragg 30.401
Spacegroup C1
Scale 8.80572312e-005
Cell Mass 508.256
Cell Volume (≈^3) 325.10507
Wt% - Rietveld 1.603
Crystal Linear Absorption Coeff. (1/cm) 81.026

Crystal Density (g/cm^3) 2.596
Preferred Orientation (Dir 1 : 0 0 1) 0.8669155
PVII peak type
FWHM = a + b/Cos(Th) + c Tan(Th)
a 0.1817443
b 0.001089558
c 0.1161617
Exponent m = 0.6+ma+mb/Cos(Th)+mc/Tan(Th)
ma 0.0001760383
mb 0.006994623
mc 4.54781
Lattice parameters
a (≈) 5.3322134
b (≈) 8.3787153
c (≈) 7.5046934
alpha (∞) 93.05501
beta (∞) 103.7211
gamma (∞) 90.97204

Site	Np	x	y	z	Atom	Occ	Beq
O1	2	0.77800	0.18000	-0.14000	O-2	1	1
O2	2	0.27800	0.32000	-0.13800	O-2	1	1
O3	2	0.31600	-0.00800	-0.13600	O-2	1	1
O4	2	0.24800	0.18400	0.15500	O-2	1	1
O5	2	0.75400	0.31500	0.15500	O-2	1	1
O6	2	0.69000	0.00400	0.15700	O-2	1	1
O7	2	0.79100	0.16500	0.48200	O-2	1	1
O8	2	0.61200	-0.12000	0.45500	O-2	1	1
O9	2	0.10800	-0.05800	0.45500	O-2	1	1
Al1	2	0.50200	0.17200	0.00300	Al+3	1	1
Al2	2	0.00200	0.33000	0.00200	Al+3	1	1
Si1	2	0.80000	0.32200	0.38200	Si+4	1	1
Si2	2	0.80000	0.00000	0.38500	Si+4	1	1

Structure 3
Phase name Illite 2M1
R-Bragg 16.848
Spacegroup C12/c1
Scale 0.000420402058
Cell Mass 1580.752
Cell Volume (≈^3) 936.37809
Wt% - Rietveld 68.570
Crystallite Size
Cry size Lorentzian (nm) 28.5
Crystal Linear Absorption Coeff. (1/cm) 119.514
Crystal Density (g/cm^3) 2.803
Preferred Orientation (Dir 1 : 0 0 1) 0.3831019
Preferred Orientation Spherical Harmonics
Order 8
y00 1
y20 0.5836252
y22m 0.009546697
y22p -0.09781043
y40 0.5022931
y42m -0.311914

y42p	-0.4992556
y44m	0.9619757
y44p	-0.0308008
y60	-0.0009775204
y62m	0.01349139
y62p	0.4428643
y64m	0.1074016
y64p	-0.2443379
y66m	0.3097314
y66p	0.3097314
y80	0.06336704
y82m	0.7981638
y82p	0.3322329
y84m	-0.5050269
y84p	-0.07323739
y86m	0.01540325
y86p	0.02323557
y88m	-0.05892438
y88p	0.07106017

PVII peak type

FWHM = a + b/Cos(Th) + c Tan(Th)

a	0.0001049707
b	0.0001053046
c	0.04955242

Exponent m = 0.6+ma+mb/Cos(Th)+mc/Tan(Th)

ma	0.0002497729
mb	0.02333518
mc	0.07689906

Lattice parameters

a (≈)	5.2066934
b (≈)	9.0141858
c (≈)	20.0593564
beta (∞)	95.96047

Site	Np	x	y	z	Atom	Occ	Beq
Si1	8	0.48250	0.92970	0.13700	Si+4	1	1.737
Al1	8	0.44320	0.26350	0.13650	Al+3	1	0.8685
Al2	8	0.25860	0.08280	0.00680	Al+3	1	2.132
K1	4	0.00000	0.09010	0.25000	K+1	1	5.922
O1	8	0.46230	0.91940	0.05050	O-2	1	1.184
O2	8	0.38350	0.26650	0.06630	O-2	1	3.711
O3	8	0.42590	0.10390	0.15300	O-2	1	0.9475
O4	8	0.22260	0.83680	0.16850	O-2	1	3.237
O5	8	0.27350	0.37220	0.16780	O-2	1	6.317
O6	8	0.40800	0.56710	0.04540	O-2	1	4.185

Structure 4

Phase name	Chamosite 1MIIb
R-Bragg	44.821
Spacegroup	C-1
Scale	1.52587059e-005
Cell Mass	1271.241
Cell Volume (≈^3)	688.00078
Wt% - Rietveld	1.471
Crystal Linear Absorption Coeff. (1/cm)	271.140

Crystal Density (g/cm^3) 3.068
Preferred Orientation (Dir 1 : 0 0 1) 0.348955
PVII peak type
FWHM = a + b/Cos(Th) + c Tan(Th)
a 0.03738521
b 0.007080663
c 0.1694393
Exponent m = 0.6+ma+mb/Cos(Th)+mc/Tan(Th)
ma 0.05348769
mb 0.04416829
mc 0.003744929
Lattice parameters
a (≈) 5.4083795
b (≈) 9.0044365
c (≈) 14.2985996
alpha (∞) 90.04891
beta (∞) 98.57557
gamma (∞) 92.25189

Site	Np	x	y	z	Atom	Occ	Beq
Mg1	2	0.00000	0.00000	0.00000	Mg+2	0.538	0.1579
Fe1	2	0.00000	0.00000	0.00000	Fe+2	0.462	0.1579
Mg2	4	0.01410	0.33480	0.00270	Mg+2	0.496	0.1579
Fe2	4	0.01410	0.33480	0.00270	Fe+2	0.504	0.1579
Mg3	4	0.00320	0.16830	0.50040	Mg+2	0.494	0.1579
Fe3	4	0.00320	0.16830	0.50040	Fe+2	0.506	0.1579
Al1	2	0.00000	0.50000	0.50000	Al+3	1.362	0.2369
Si1	4	0.24000	0.17000	0.19410	Si+4	0.7125	0.07896
Al2	4	0.24000	0.17000	0.19410	Al+3	0.2875	0.07896
Si2	4	0.73000	0.99800	0.19450	Si+4	0.7125	0.07896
Al3	4	0.73000	0.99800	0.19450	Al+3	0.2875	0.07896
O1	4	0.19100	0.16350	0.07890	O-2	1	0.8685
O2	4	0.70500	0.99800	0.07560	O-2	1	0.8685
O3	4	0.23100	0.33600	0.23740	O-2	1	0.8685
O4	4	0.52800	0.11800	0.23020	O-2	1	0.8685
O5	4	0.01800	0.06100	0.23060	O-2	1	0.8685
O6	4	0.68900	0.33120	0.07420	O-2	1	0.8685
O7	4	0.14400	0.99900	0.43000	O-2	1	0.8685
O8	4	0.14300	0.33610	0.42860	O-2	1	0.8685
O9	4	0.64300	0.16270	0.43110	O-2	1	0.8685

Structure 5
Phase name Albite low
R-Bragg 18.760
Spacegroup C-1
Scale 5.29626814e-005
Cell Mass 1048.846
Cell Volume (≈^3) 664.19438
Wt% - Rietveld 4.066
Crystallite Size
Cry size Lorentzian (nm) 221.0
Crystal Linear Absorption Coeff. (1/cm) 88.829
Crystal Density (g/cm^3) 2.622
Lattice parameters
a (≈) 8.1380000

b (≈) 12.7890000
c (≈) 7.1560000
alpha (∞) 94.33
beta (∞) 116.57
gamma (∞) 87.65

Site	Np	x	y	z	Atom	Occ	Beq
O1	4	0.00900	0.13400	0.96700	O-2	1	1
O2	4	0.59500	0.99700	0.27900	O-2	1	1
O3	4	0.81800	0.11200	0.19200	O-2	1	1
O4	4	0.32100	0.35300	0.25900	O-2	1	1
O5	4	0.00600	0.30700	0.26800	O-2	1	1
O6	4	0.52200	0.19600	0.23300	O-2	1	1
O7	4	0.20600	0.11000	0.38900	O-2	1	1
O8	4	0.68300	0.36900	0.43000	O-2	1	1
Si1	4	0.00800	0.17100	0.20900	Si+4	0.28	1
Al1	4	0.00800	0.17100	0.20900	Al+3	0.72	1
Si2	4	0.50800	0.31800	0.24100	Si+4	1	1
Si3	4	0.69200	0.11000	0.31500	Si+4	0.8	1
Al3	4	0.69200	0.11000	0.31500	Al+3	0.2	1
Si4	4	0.18300	0.38200	0.35900	Si+4	0.91	1
Al4	4	0.18300	0.38200	0.35900	Al+3	0.09	1
Na1	4	0.27200	0.99000	0.14500	Na+1	1	1

9.1.2.19. Sample 2012-0001073, stratigraphic height: 10.42 m

Range Number : 1

R-Values

Rexp : 1.91 Rwp : 7.32 Rp : 5.15 GOF : 3.83
Rexp`: 5.71 Rwp`: 21.86 Rp` : 21.08 DW : 0.25

Quantitative Analysis - Rietveld
Phase 1 : „Quartz low“ 25.074 %
Phase 2 : „Kaolinite 1A II“ 0.722 %
Phase 3 : „Illite 2M1“ 68.174 %
Phase 4 : „Chamosite 1MIIb“ 1.269 %
Phase 5 : „Albite low“ 4.761 %

Background
Chebychev polynomial, Coefficient 0 2258.956
1 -1147.034
2 575.853
3 -407.0489
4 390.0555
5 -273.666
6 133.839

Instrument
Primary radius (mm) 250
Secondary radius (mm) 250
Linear PSD 2Th angular range (∞) 2.749941
FDS angle (∞) 0.0916

Beam spill, sample length (mm) 9
Intensity not corrected
Full Axial Convolution
Filament length (mm) 8
Sample length (mm) 30
Receiving Slit length (mm) 12
Primary Sollers (∞) 2.5
Secondary Sollers (∞) 2.5

Corrections
Zero error -0.115238
Specimen displacement -0.3363683
LP Factor 0

Miscellaneous
Excluded Regions
Start/Finish 0 0
Start/Finish 0 0
Start/Finish 0 0
Start/Finish 0 0
Start/Finish 0 0

Structure 1
Phase name Quartz low
R-Bragg 11.159
Spacegroup P3221
Scale 0.0150532026
Cell Mass 180.252
Cell Volume (≈^3) 112.89935
Wt% - Rietveld 25.074
Crystal Linear Absorption Coeff. (1/cm) 95.472
Crystal Density (g/cm^3) 2.651
Preferred Orientation (Dir 1 : 0 0 1) 1.18668
PVII peak type
FWHM = a + b/Cos(Th) + c Tan(Th)
a 0.01025479
b 0.003821816
c 0.01109589
Exponent m = 0.6+ma+mb/Cos(Th)+mc/Tan(Th)
ma 0.008312819
mb 0.02796789
mc 0.08804857
Lattice parameters
a (≈) 4.9120226
c (≈) 5.4030640

Site	Np	x	y	z	Atom	Occ	Beq
Si1	3	0.46900	0.00000	0.66667	Si+4	1	1
O1	6	0.40300	0.25300	0.78900	O-2	1	1

Structure 2
Phase name Kaolinite 1A II
R-Bragg 6.191
Spacegroup C1

Scale	5.33578854e-005
Cell Mass	508.256
Cell Volume (≈^3)	325.10507
Wt% - Rietveld	0.722
Crystal Linear Absorption Coeff. (1/cm)	81.026
Crystal Density (g/cm^3)	2.596
Preferred Orientation (Dir 1 : 0 0 1)	1.003365
PVII peak type	
FWHM = a + b/Cos(Th) + c Tan(Th)	
a	0.1222224
b	0.0001019327
c	0.001845334
Exponent m = 0.6+ma+mb/Cos(Th)+mc/Tan(Th)	
ma	19.96094
mb	4.990248
mc	4.999117
Lattice parameters	
a (≈)	5.3322134
b (≈)	8.3787153
c (≈)	7.5046934
alpha (∞)	93.05501
beta (∞)	103.7211
gamma (∞)	90.97204

Site	Np	x	y	z	Atom	Occ	Beq
O1	2	0.77800	0.18000	-0.14000	O-2	1	1
O2	2	0.27800	0.32000	-0.13800	O-2	1	1
O3	2	0.31600	-0.00800	-0.13600	O-2	1	1
O4	2	0.24800	0.18400	0.15500	O-2	1	1
O5	2	0.75400	0.31500	0.15500	O-2	1	1
O6	2	0.69000	0.00400	0.15700	O-2	1	1
O7	2	0.79100	0.16500	0.48200	O-2	1	1
O8	2	0.61200	-0.12000	0.45500	O-2	1	1
O9	2	0.10800	-0.05800	0.45500	O-2	1	1
Al1	2	0.50200	0.17200	0.00300	Al+3	1	1
Al2	2	0.00200	0.33000	0.00200	Al+3	1	1
Si1	2	0.80000	0.32200	0.38200	Si+4	1	1
Si2	2	0.80000	0.00000	0.38500	Si+4	1	1

Structure 3

Phase name	Illite 2M1
R-Bragg	7.961
Spacegroup	C12/c1
Scale	0.000562700327
Cell Mass	1580.752
Cell Volume (≈^3)	936.37809
Wt% - Rietveld	68.174
Crystallite Size	
Cry size Lorentzian (nm)	34.9
Crystal Linear Absorption Coeff. (1/cm)	119.514
Crystal Density (g/cm^3)	2.803
Preferred Orientation (Dir 1 : 0 0 1)	0.4029344
Preferred Orientation Spherical Harmonics	
Order	8
y00	1

y20	0.5812209
y22m	0.09744082
y22p	-0.1028738
y40	0.5142496
y42m	-0.2518127
y42p	-0.4961862
y44m	0.9885107
y44p	-0.032143
y60	0.00111743
y62m	-0.1394815
y62p	0.4380129
y64m	0.3162413
y64p	-0.2454828
y66m	0.3080466
y66p	0.3080466
y80	0.08483007
y82m	0.5872221
y82p	0.3270583
y84m	-0.3257774
y84p	-0.08096972
y86m	-0.004261854
y86p	0.02554855
y88m	-0.1044255
y88p	0.07745006
PVII peak type	
FWHM = a + b/Cos(Th) + c Tan(Th)	
a	0.0001000097
b	0.0001000104
c	0.07144096
Exponent m = 0.6+ma+mb/Cos(Th)+mc/Tan(Th)	
ma	0.00514857
mb	0.01380986
mc	0.05592893
Lattice parameters	
a (≈)	5.2066934
b (≈)	9.0141858
c (≈)	20.0593564
beta (∞)	95.96047

Site	Np	x	y	z	Atom	Occ	Beq
Si1	8	0.48250	0.92970	0.13700	Si+4	1	1.737
Al1	8	0.44320	0.26350	0.13650	Al+3	1	0.8685
Al2	8	0.25860	0.08280	0.00680	Al+3	1	2.132
K1	4	0.00000	0.09010	0.25000	K+1	1	5.922
O1	8	0.46230	0.91940	0.05050	O-2	1	1.184
O2	8	0.38350	0.26650	0.06630	O-2	1	3.711
O3	8	0.42590	0.10390	0.15300	O-2	1	0.9475
O4	8	0.22260	0.83680	0.16850	O-2	1	3.237
O5	8	0.27350	0.37220	0.16780	O-2	1	6.317
O6	8	0.40800	0.56710	0.04540	O-2	1	4.185

Structure 4

Phase name	Chamosite 1MIIb
R-Bragg	7.496
Spacegroup	C-1

Scale	1.77296953e-005
Cell Mass	1271.241
Cell Volume (≈^3)	688.00078
Wt% - Rietveld	1.269
Crystal Linear Absorption Coeff. (1/cm)	271.140
Crystal Density (g/cm^3)	3.068
Preferred Orientation (Dir 1 : 0 0 1)	0.3309375
PVII peak type	
FWHM = a + b/Cos(Th) + c Tan(Th)	
a	0.0369953
b	0.005954549
c	0.1167237
Exponent m = 0.6+ma+mb/Cos(Th)+mc/Tan(Th)	
ma	0.0007135779
mb	0.0006699811
mc	0.006279956
Lattice parameters	
a (≈)	5.4083795
b (≈)	9.0044365
c (≈)	14.2985996
alpha (∞)	90.04891
beta (∞)	98.57557
gamma (∞)	92.25189

Site	Np	x	y	z	Atom	Occ	Beq
Mg1	2	0.00000	0.00000	0.00000	Mg+2	0.538	0.1579
Fe1	2	0.00000	0.00000	0.00000	Fe+2	0.462	0.1579
Mg2	4	0.01410	0.33480	0.00270	Mg+2	0.496	0.1579
Fe2	4	0.01410	0.33480	0.00270	Fe+2	0.504	0.1579
Mg3	4	0.00320	0.16830	0.50040	Mg+2	0.494	0.1579
Fe3	4	0.00320	0.16830	0.50040	Fe+2	0.506	0.1579
Al1	2	0.00000	0.50000	0.50000	Al+3	1.362	0.2369
Si1	4	0.24000	0.17000	0.19410	Si+4	0.7125	0.07896
Al2	4	0.24000	0.17000	0.19410	Al+3	0.2875	0.07896
Si2	4	0.73000	0.99800	0.19450	Si+4	0.7125	0.07896
Al3	4	0.73000	0.99800	0.19450	Al+3	0.2875	0.07896
O1	4	0.19100	0.16350	0.07890	O-2	1	0.8685
O2	4	0.70500	0.99800	0.07560	O-2	1	0.8685
O3	4	0.23100	0.33600	0.23740	O-2	1	0.8685
O4	4	0.52800	0.11800	0.23020	O-2	1	0.8685
O5	4	0.01800	0.06100	0.23060	O-2	1	0.8685
O6	4	0.68900	0.33120	0.07420	O-2	1	0.8685
O7	4	0.14400	0.99900	0.43000	O-2	1	0.8685
O8	4	0.14300	0.33610	0.42860	O-2	1	0.8685
O9	4	0.64300	0.16270	0.43110	O-2	1	0.8685

Structure 5

Phase name	Albite low
R-Bragg	7.903
Spacegroup	C-1
Scale	8.3491675e-005
Cell Mass	1048.846
Cell Volume (≈^3)	664.19438
Wt% - Rietveld	4.761
Crystallite Size	

Cry size Lorentzian (nm) 216.2
Crystal Linear Absorption Coeff. (1/cm) 88.829
Crystal Density (g/cm^3) 2.622
Lattice parameters
a (≈) 8.1380000
b (≈) 12.7890000
c (≈) 7.1560000
alpha (∞) 94.33
beta (∞) 116.57
gamma (∞) 87.65

Site	Np	x	y	z	Atom	Occ	Beq
O1	4	0.00900	0.13400	0.96700	O-2	1	1
O2	4	0.59500	0.99700	0.27900	O-2	1	1
O3	4	0.81800	0.11200	0.19200	O-2	1	1
O4	4	0.32100	0.35300	0.25900	O-2	1	1
O5	4	0.00600	0.30700	0.26800	O-2	1	1
O6	4	0.52200	0.19600	0.23300	O-2	1	1
O7	4	0.20600	0.11000	0.38900	O-2	1	1
O8	4	0.68300	0.36900	0.43000	O-2	1	1
Si1	4	0.00800	0.17100	0.20900	Si+4	0.28	1
Al1	4	0.00800	0.17100	0.20900	Al+3	0.72	1
Si2	4	0.50800	0.31800	0.24100	Si+4	1	1
Si3	4	0.69200	0.11000	0.31500	Si+4	0.8	1
Al3	4	0.69200	0.11000	0.31500	Al+3	0.2	1
Si4	4	0.18300	0.38200	0.35900	Si+4	0.91	1
Al4	4	0.18300	0.38200	0.35900	Al+3	0.09	1
Na1	4	0.27200	0.99000	0.14500	Na+1	1	1

9.1.2.20. Sample 2012-0001076, stratigraphic height: 10.52 m

Range Number : 1

R-Values

Rexp : 2.01 Rwp : 7.93 Rp : 5.44 GOF : 3.95
Rexp`: 6.13 Rwp`: 24.20 Rp` : 22.76 DW : 0.20

Quantitative Analysis - Rietveld
Phase 1 : „Quartz low“ 21.934 %
Phase 2 : „Kaolinite 1A II“ 0.604 %
Phase 3 : „Illite 2M1“ 73.098 %
Phase 4 : „Chamosite 1MIIb“ 0.892 %
Phase 5 : „Albite low“ 3.472 %

Background
Chebychev polynomial, Coefficient 0 2077.205
1 -1067.929
2 555.8273
3 -392.8871
4 373.8363
5 -257.6574
6 115.3684

Instrument
  Primary radius (mm) 250
  Secondary radius (mm) 250
  Linear PSD 2Th angular range (∞) 2.749941
    FDS angle (∞) 0.0916
    Beam spill, sample length (mm) 9
      Intensity not corrected
  Full Axial Convolution
    Filament length (mm) 8
    Sample length (mm) 30
    Receiving Slit length (mm) 12
    Primary Sollers (∞) 2.5
    Secondary Sollers (∞) 2.5

Corrections
  Zero error -0.1035101
  Specimen displacement -0.4137339
  LP Factor 0

Miscellaneous
  Excluded Regions
    Start/Finish 0 0
    Start/Finish 0 0
    Start/Finish 0 0
    Start/Finish 0 0
    Start/Finish 0 0

Structure 1
  Phase name Quartz low
  R-Bragg 8.497
  Spacegroup P3221
  Scale 0.0127194569
  Cell Mass 180.252
  Cell Volume (≈^3) 112.94030
  Wt% - Rietveld 21.934
  Crystal Linear Absorption Coeff. (1/cm) 95.437
  Crystal Density (g/cm^3) 2.650
  Preferred Orientation (Dir 1 : 0 0 1) 1.175833
  PVII peak type
    FWHM = a + b/Cos(Th) + c Tan(Th)
      a 0.01336051
      b 0.002230149
      c 0.006535316
    Exponent m = 0.6+ma+mb/Cos(Th)+mc/Tan(Th)
      ma 0.0001002215
      mb 0.0001002535
      mc 0.1174331
  Lattice parameters
    a (≈) 4.9125020
    c (≈) 5.4039688

Site	Np	x	y	z	Atom	Occ	Beq
Si1	3	0.46900	0.00000	0.66667	Si+4	1	1
O1	6	0.40300	0.25300	0.78900	O-2	1	1

Structure 2

Phase name	Kaolinite 1A II
R-Bragg	17.065
Spacegroup	C1
Scale	4.31594885e-005
Cell Mass	508.256
Cell Volume (≈^3)	325.10507
Wt% - Rietveld	0.604
Crystal Linear Absorption Coeff. (1/cm)	81.026
Crystal Density (g/cm^3)	2.596
Preferred Orientation (Dir 1 : 0 0 1)	1.170121
PVII peak type	
FWHM = a + b/Cos(Th) + c Tan(Th)	
a	0.00405099
b	0.0001133756
c	0.5376188
Exponent m = 0.6+ma+mb/Cos(Th)+mc/Tan(Th)	
ma	19.99986
mb	4.999905
mc	4.999972
Lattice parameters	
a (≈)	5.3322134
b (≈)	8.3787153
c (≈)	7.5046934
alpha (∞)	93.05501
beta (∞)	103.7211
gamma (∞)	90.97204

Site	Np	x	y	z	Atom	Occ	Beq
O1	2	0.77800	0.18000	-0.14000	O-2	1	1
O2	2	0.27800	0.32000	-0.13800	O-2	1	1
O3	2	0.31600	-0.00800	-0.13600	O-2	1	1
O4	2	0.24800	0.18400	0.15500	O-2	1	1
O5	2	0.75400	0.31500	0.15500	O-2	1	1
O6	2	0.69000	0.00400	0.15700	O-2	1	1
O7	2	0.79100	0.16500	0.48200	O-2	1	1
O8	2	0.61200	-0.12000	0.45500	O-2	1	1
O9	2	0.10800	-0.05800	0.45500	O-2	1	1
Al1	2	0.50200	0.17200	0.00300	Al+3	1	1
Al2	2	0.00200	0.33000	0.00200	Al+3	1	1
Si1	2	0.80000	0.32200	0.38200	Si+4	1	1
Si2	2	0.80000	0.00000	0.38500	Si+4	1	1

Structure 3

Phase name	Illite 2M1
R-Bragg	14.627
Spacegroup	C12/c1
Scale	0.000582994233
Cell Mass	1580.752
Cell Volume (≈^3)	936.37809
Wt% - Rietveld	73.098
Crystallite Size	
Cry size Lorentzian (nm)	28.9
Crystal Linear Absorption Coeff. (1/cm)	119.514

Crystal Density (g/cm^3)	2.803
Preferred Orientation (Dir 1 : 0 0 1)	0.3695877
Preferred Orientation Spherical Harmonics	
Order	8
y00	1
y20	0.5730494
y22m	0.09219519
y22p	-0.1156302
y40	0.4915524
y42m	-0.2821655
y42p	-0.5149286
y44m	0.9493087
y44p	-0.03790752
y60	-0.004584998
y62m	0.2442328
y62p	0.4488578
y64m	-0.0420709
y64p	-0.2511103
y66m	0.300415
y66p	0.300415
y80	0.05396127
y82m	0.9942556
y82p	0.3005904
y84m	-0.6060609
y84p	-0.1045874
y86m	0.00318762
y86p	0.02929148
y88m	-0.1560954
y88p	0.05971394
PVII peak type	
FWHM = a + b/Cos(Th) + c Tan(Th)	
a	0.0001
b	0.0001
c	0.06275187
Exponent m = 0.6+ma+mb/Cos(Th)+mc/Tan(Th)	
ma	0.002633259
mb	0.03006185
mc	0.08432644
Lattice parameters	
a (≈)	5.2066934
b (≈)	9.0141858
c (≈)	20.0593564
beta (∞)	95.96047

Site	Np	x	y	z	Atom	Occ	Beq
Si1	8	0.48250	0.92970	0.13700	Si+4	1	1.737
Al1	8	0.44320	0.26350	0.13650	Al+3	1	0.8685
Al2	8	0.25860	0.08280	0.00680	Al+3	1	2.132
K1	4	0.00000	0.09010	0.25000	K+1	1	5.922
O1	8	0.46230	0.91940	0.05050	O-2	1	1.184
O2	8	0.38350	0.26650	0.06630	O-2	1	3.711
O3	8	0.42590	0.10390	0.15300	O-2	1	0.9475
O4	8	0.22260	0.83680	0.16850	O-2	1	3.237
O5	8	0.27350	0.37220	0.16780	O-2	1	6.317
O6	8	0.40800	0.56710	0.04540	O-2	1	4.185

Structure 4

Phase name	Chamosite 1MIIb
R-Bragg	20.154
Spacegroup	C-1
Scale	1.20454453e-005
Cell Mass	1271.241
Cell Volume (≈^3)	688.00078
Wt% - Rietveld	0.892
Crystal Linear Absorption Coeff. (1/cm)	271.140
Crystal Density (g/cm^3)	3.068
Preferred Orientation (Dir 1 : 0 0 1)	0.3490831
PVII peak type	
FWHM = a + b/Cos(Th) + c Tan(Th)	
a	0.03098219
b	0.001189032
c	0.2129377
Exponent m = 0.6+ma+mb/Cos(Th)+mc/Tan(Th)	
ma	0.0001001909
mb	0.0001002191
mc	0.006862954
Lattice parameters	
a (≈)	5.4083795
b (≈)	9.0044365
c (≈)	14.2985996
alpha (∞)	90.04891
beta (∞)	98.57557
gamma (∞)	92.25189

Site	Np	x	y	z	Atom	Occ	Beq
Mg1	2	0.00000	0.00000	0.00000	Mg+2	0.538	0.1579
Fe1	2	0.00000	0.00000	0.00000	Fe+2	0.462	0.1579
Mg2	4	0.01410	0.33480	0.00270	Mg+2	0.496	0.1579
Fe2	4	0.01410	0.33480	0.00270	Fe+2	0.504	0.1579
Mg3	4	0.00320	0.16830	0.50040	Mg+2	0.494	0.1579
Fe3	4	0.00320	0.16830	0.50040	Fe+2	0.506	0.1579
Al1	2	0.00000	0.50000	0.50000	Al+3	1.362	0.2369
Si1	4	0.24000	0.17000	0.19410	Si+4	0.7125	0.07896
Al2	4	0.24000	0.17000	0.19410	Al+3	0.2875	0.07896
Si2	4	0.73000	0.99800	0.19450	Si+4	0.7125	0.07896
Al3	4	0.73000	0.99800	0.19450	Al+3	0.2875	0.07896
O1	4	0.19100	0.16350	0.07890	O-2	1	0.8685
O2	4	0.70500	0.99800	0.07560	O-2	1	0.8685
O3	4	0.23100	0.33600	0.23740	O-2	1	0.8685
O4	4	0.52800	0.11800	0.23020	O-2	1	0.8685
O5	4	0.01800	0.06100	0.23060	O-2	1	0.8685
O6	4	0.68900	0.33120	0.07420	O-2	1	0.8685
O7	4	0.14400	0.99900	0.43000	O-2	1	0.8685
O8	4	0.14300	0.33610	0.42860	O-2	1	0.8685
O9	4	0.64300	0.16270	0.43110	O-2	1	0.8685

Structure 5

Phase name	Albite low
R-Bragg	14.733
Spacegroup	C-1

Scale 5.88321206e-005
Cell Mass 1048.846
Cell Volume (≈^3) 664.19438
Wt% - Rietveld 3.472
Crystallite Size
Cry size Lorentzian (nm) 273.7
Crystal Linear Absorption Coeff. (1/cm) 88.829
Crystal Density (g/cm^3) 2.622
Lattice parameters
a (≈) 8.1380000
b (≈) 12.7890000
c (≈) 7.1560000
alpha (∞) 94.33
beta (∞) 116.57
gamma (∞) 87.65

Site	Np	x	y	z	Atom	Occ	Beq
O1	4	0.00900	0.13400	0.96700	O-2	1	1
O2	4	0.59500	0.99700	0.27900	O-2	1	1
O3	4	0.81800	0.11200	0.19200	O-2	1	1
O4	4	0.32100	0.35300	0.25900	O-2	1	1
O5	4	0.00600	0.30700	0.26800	O-2	1	1
O6	4	0.52200	0.19600	0.23300	O-2	1	1
O7	4	0.20600	0.11000	0.38900	O-2	1	1
O8	4	0.68300	0.36900	0.43000	O-2	1	1
Si1	4	0.00800	0.17100	0.20900	Si+4	0.28	1
Al1	4	0.00800	0.17100	0.20900	Al+3	0.72	1
Si2	4	0.50800	0.31800	0.24100	Si+4	1	1
Si3	4	0.69200	0.11000	0.31500	Si+4	0.8	1
Al3	4	0.69200	0.11000	0.31500	Al+3	0.2	1
Si4	4	0.18300	0.38200	0.35900	Si+4	0.91	1
Al4	4	0.18300	0.38200	0.35900	Al+3	0.09	1
Na1	4	0.27200	0.99000	0.14500	Na+1	1	1

9.1.2.21. Sample 2012-0001075, stratigraphic height: 10.98 m

Range Number : 1

R-Values

Rexp : 1.99 Rwp : 5.38 Rp : 3.98 GOF : 2.70
Rexp`: 7.43 Rwp`: 20.07 Rp` : 22.05 DW : 0.38

Quantitative Analysis - Rietveld
Phase 1 : „Quartz low“ 20.387 %
Phase 2 : „Kaolinite 1A II“ 2.271 %
Phase 3 : „Illite 2M1“ 73.346 %
Phase 4 : „Chamosite 1MIIb“ 0.145 %
Phase 5 : „Albite low“ 3.850 %

Background
Chebychev polynomial, Coefficient 0 2153.214
1 -798.3837
2 303.5858

3	-228.2466
4	243.7709
5	-187.128
6	86.11894

Instrument

Primary radius (mm)	250
Secondary radius (mm)	250
Linear PSD 2Th angular range (∞)	2.749941
FDS angle (∞)	0.0916
Beam spill, sample length (mm)	9
Intensity not corrected	
Full Axial Convolution	
Filament length (mm)	8
Sample length (mm)	30
Receiving Slit length (mm)	12
Primary Sollers (∞)	2.5
Secondary Sollers (∞)	2.5

Corrections

Zero error	-0.09582335
Specimen displacement	-0.4565121
LP Factor	0

Miscellaneous

Excluded Regions		
Start/Finish	0	0
Start/Finish	0	0
Start/Finish	0	0
Start/Finish	0	0
Start/Finish	0	0

Structure 1

Phase name	Quartz low
R-Bragg	36.857
Spacegroup	P3221
Scale	0.011251603
Cell Mass	180.252
Cell Volume (≈^3)	112.96096
Wt% - Rietveld	20.387
Crystal Linear Absorption Coeff. (1/cm)	95.420
Crystal Density (g/cm^3)	2.650
Preferred Orientation (Dir 1 : 0 0 1)	1.199317
PVII peak type	
FWHM = a + b/Cos(Th) + c Tan(Th)	
a	0.0157597
b	0.006696181
c	0.005006848
Exponent m = 0.6+ma+mb/Cos(Th)+mc/Tan(Th)	
ma	0.01446586
mb	0.01304993
mc	0.1158388
Lattice parameters	
a (≈)	4.9127418
c (≈)	5.4044294

Site	Np	x	y	z	Atom	Occ	Beq
Si1	3	0.46900	0.00000	0.66667	Si+4	1	1
O1	6	0.40300	0.25300	0.78900	O-2	1	1

Structure 2

Phase name	Kaolinite 1A II
R-Bragg	72.429
Spacegroup	C1
Scale	0.000154466431
Cell Mass	508.256
Cell Volume (≈^3)	325.10507
Wt% - Rietveld	2.271
Crystal Linear Absorption Coeff. (1/cm)	81.026
Crystal Density (g/cm^3)	2.596
Preferred Orientation (Dir 1 : 0 0 1)	1.598784
PVII peak type	
FWHM = a + b/Cos(Th) + c Tan(Th)	
a	0.0004106811
b	0.0006793172
c	0.6066664
Exponent m = 0.6+ma+mb/Cos(Th)+mc/Tan(Th)	
ma	0.009499937
mb	0.008214012
mc	0.413674
Lattice parameters	
a (≈)	5.3322134
b (≈)	8.3787153
c (≈)	7.5046934
alpha (∞)	93.05501
beta (∞)	103.7211
gamma (∞)	90.97204

Site	Np	x	y	z	Atom	Occ	Beq
O1	2	0.77800	0.18000	-0.14000	O-2	1	1
O2	2	0.27800	0.32000	-0.13800	O-2	1	1
O3	2	0.31600	-0.00800	-0.13600	O-2	1	1
O4	2	0.24800	0.18400	0.15500	O-2	1	1
O5	2	0.75400	0.31500	0.15500	O-2	1	1
O6	2	0.69000	0.00400	0.15700	O-2	1	1
O7	2	0.79100	0.16500	0.48200	O-2	1	1
O8	2	0.61200	-0.12000	0.45500	O-2	1	1
O9	2	0.10800	-0.05800	0.45500	O-2	1	1
Al1	2	0.50200	0.17200	0.00300	Al+3	1	1
Al2	2	0.00200	0.33000	0.00200	Al+3	1	1
Si1	2	0.80000	0.32200	0.38200	Si+4	1	1
Si2	2	0.80000	0.00000	0.38500	Si+4	1	1

Structure 3

Phase name	Illite 2M1
R-Bragg	45.392
Spacegroup	C12/c1
Scale	0.000556826727
Cell Mass	1580.752

Cell Volume (≈^3)	936.37809
Wt% - Rietveld	73.346
Crystallite Size	
Cry size Lorentzian (nm)	37.6
Crystal Linear Absorption Coeff. (1/cm)	119.514
Crystal Density (g/cm^3)	2.803
Preferred Orientation (Dir 1 : 0 0 1)	0.3508764
Preferred Orientation Spherical Harmonics	
Order	8
y00	1
y20	0.5397501
y22m	-0.09648858
y22p	-0.122519
y40	0.4523772
y42m	-0.4154884
y42p	-0.5368765
y44m	0.9047056
y44p	-0.04504551
y60	0.004316091
y62m	-0.1645614
y62p	0.4588269
y64m	0.1829594
y64p	-0.2463006
y66m	0.298921
y66p	0.298921
y80	0.1663918
y82m	0.6799827
y82p	0.294552
y84m	-0.4952991
y84p	-0.1471362
y86m	-0.09043419
y86p	0.04868289
y88m	-0.04092967
y88p	0.06754531
PVII peak type	
FWHM = a + b/Cos(Th) + c Tan(Th)	
a	0.0001014835
b	0.0001014874
c	0.09033583
Exponent m = 0.6+ma+mb/Cos(Th)+mc/Tan(Th)	
ma	0.0001682805
mb	0.05854618
mc	0.0394308
Lattice parameters	
a (≈)	5.2066934
b (≈)	9.0141858
c (≈)	20.0593564
beta (∞)	95.96047

Site	Np	x	y	z	Atom	Occ	Beq
Si1	8	0.48250	0.92970	0.13700	Si+4	1	1.737
Al1	8	0.44320	0.26350	0.13650	Al+3	1	0.8685
Al2	8	0.25860	0.08280	0.00680	Al+3	1	2.132
K1	4	0.00000	0.09010	0.25000	K+1	1	5.922
O1	8	0.46230	0.91940	0.05050	O-2	1	1.184
O2	8	0.38350	0.26650	0.06630	O-2	1	3.711

O3	8	0.42590	0.10390	0.15300	O-2	1 0.9475
O4	8	0.22260	0.83680	0.16850	O-2	1 3.237
O5	8	0.27350	0.37220	0.16780	O-2	1 6.317
O6	8	0.40800	0.56710	0.04540	O-2	1 4.185

Structure 4

Phase name	Chamosite 1MIIb
R-Bragg	160.170
Spacegroup	C-1
Scale	1.86886899e-006
Cell Mass	1271.241
Cell Volume (≈^3)	688.00078
Wt% - Rietveld	0.145
Crystal Linear Absorption Coeff. (1/cm)	271.140
Crystal Density (g/cm^3)	3.068
Preferred Orientation (Dir 1 : 0 0 1)	0.2324963
PVII peak type	
FWHM = a + b/Cos(Th) + c Tan(Th)	
a	0.03530064
b	0.01479362
c	0.193505
Exponent m = 0.6+ma+mb/Cos(Th)+mc/Tan(Th)	
ma	0.0002240094
mb	0.002199564
mc	0.007278099
Lattice parameters	
a (≈)	5.4083795
b (≈)	9.0044365
c (≈)	14.2985996
alpha (∞)	90.04891
beta (∞)	98.57557
gamma (∞)	92.25189

Site	Np	x	y	z	Atom	Occ	Beq
Mg1	2	0.00000	0.00000	0.00000	Mg+2	0.538	0.1579
Fe1	2	0.00000	0.00000	0.00000	Fe+2	0.462	0.1579
Mg2	4	0.01410	0.33480	0.00270	Mg+2	0.496	0.1579
Fe2	4	0.01410	0.33480	0.00270	Fe+2	0.504	0.1579
Mg3	4	0.00320	0.16830	0.50040	Mg+2	0.494	0.1579
Fe3	4	0.00320	0.16830	0.50040	Fe+2	0.506	0.1579
Al1	2	0.00000	0.50000	0.50000	Al+3	1.362	0.2369
Si1	4	0.24000	0.17000	0.19410	Si+4	0.7125	0.07896
Al2	4	0.24000	0.17000	0.19410	Al+3	0.2875	0.07896
Si2	4	0.73000	0.99800	0.19450	Si+4	0.7125	0.07896
Al3	4	0.73000	0.99800	0.19450	Al+3	0.2875	0.07896
O1	4	0.19100	0.16350	0.07890	O-2	1	0.8685
O2	4	0.70500	0.99800	0.07560	O-2	1	0.8685
O3	4	0.23100	0.33600	0.23740	O-2	1	0.8685
O4	4	0.52800	0.11800	0.23020	O-2	1	0.8685
O5	4	0.01800	0.06100	0.23060	O-2	1	0.8685
O6	4	0.68900	0.33120	0.07420	O-2	1	0.8685
O7	4	0.14400	0.99900	0.43000	O-2	1	0.8685
O8	4	0.14300	0.33610	0.42860	O-2	1	0.8685
O9	4	0.64300	0.16270	0.43110	O-2	1	0.8685

Structure 5

Phase name	Albite low
R-Bragg	37.199
Spacegroup	C-1
Scale	6.21048929e-005
Cell Mass	1048.846
Cell Volume (≈^3)	664.19438
Wt% - Rietveld	3.850
Crystallite Size	
Cry size Lorentzian (nm)	210.9
Crystal Linear Absorption Coeff. (1/cm)	88.829
Crystal Density (g/cm^3)	2.622
Lattice parameters	
a (≈)	8.1380000
b (≈)	12.7890000
c (≈)	7.1560000
alpha (∞)	94.33
beta (∞)	116.57
gamma (∞)	87.65

Site	Np	x	y	z	Atom	Occ	Beq
O1	4	0.00900	0.13400	0.96700	O-2	1	1
O2	4	0.59500	0.99700	0.27900	O-2	1	1
O3	4	0.81800	0.11200	0.19200	O-2	1	1
O4	4	0.32100	0.35300	0.25900	O-2	1	1
O5	4	0.00600	0.30700	0.26800	O-2	1	1
O6	4	0.52200	0.19600	0.23300	O-2	1	1
O7	4	0.20600	0.11000	0.38900	O-2	1	1
O8	4	0.68300	0.36900	0.43000	O-2	1	1
Si1	4	0.00800	0.17100	0.20900	Si+4	0.28	1
Al1	4	0.00800	0.17100	0.20900	Al+3	0.72	1
Si2	4	0.50800	0.31800	0.24100	Si+4	1	1
Si3	4	0.69200	0.11000	0.31500	Si+4	0.8	1
Al3	4	0.69200	0.11000	0.31500	Al+3	0.2	1
Si4	4	0.18300	0.38200	0.35900	Si+4	0.91	1
Al4	4	0.18300	0.38200	0.35900	Al+3	0.09	1
Na1	4	0.27200	0.99000	0.14500	Na+1	1	1

9.1.2.22. Sample 2012-0001080, stratigraphic height: 11.50 m

Range Number : 1

R-Values

Rexp : 2.01 Rwp : 6.45 Rp : 4.73 GOF : 3.22
Rexp`: 6.60 Rwp`: 21.22 Rp` : 22.09 DW : 0.30

Quantitative Analysis - Rietveld

Phase 1 : „Quartz low“	21.703 %
Phase 2 : „Kaolinite 1A II“	1.750 %
Phase 3 : „Illite 2M1“	71.994 %
Phase 4 : „Chamosite 1MIIb“	0.504 %
Phase 5 : „Albite low“	4.049 %

Background
  Chebychev polynomial, Coefficient 0 2086.4
  1 -920.4057
  2 411.1471
  3 -292.4025
  4 277.1486
  5 -201.2813
  6 84.60114

Instrument
  Primary radius (mm) 250
  Secondary radius (mm) 250
  Linear PSD 2Th angular range (∞) 2.749941
    FDS angle (∞) 0.0916
    Beam spill, sample length (mm) 9
      Intensity not corrected
  Full Axial Convolution
    Filament length (mm) 8
    Sample length (mm) 30
    Receiving Slit length (mm) 12
    Primary Sollers (∞) 2.5
    Secondary Sollers (∞) 2.5

Corrections
  Zero error -0.1100719
  Specimen displacement -0.4224292
  LP Factor 0

Miscellaneous
  Excluded Regions
    Start/Finish 0 0
    Start/Finish 0 0
    Start/Finish 0 0
    Start/Finish 0 0
    Start/Finish 0 0

Structure 1
  Phase name Quartz low
  R-Bragg 10.803
  Spacegroup P3221
  Scale 0.013361117
  Cell Mass 180.252
  Cell Volume (≈^3) 112.92625
  Wt% - Rietveld 21.703
  Crystal Linear Absorption Coeff. (1/cm) 95.449
  Crystal Density (g/cm^3) 2.651
  Preferred Orientation (Dir 1 : 0 0 1) 1.19376
  PVII peak type
    FWHM = a + b/Cos(Th) + c Tan(Th)
      a 0.01445349
      b 0.004280997
      c 0.004268285
    Exponent m = 0.6+ma+mb/Cos(Th)+mc/Tan(Th)
      ma 0.0001

mb	0.0001
mc	0.1106887
Lattice parameters	
a (≈)	4.9123916
c (≈)	5.4035394

Site	Np	x	y	z	Atom	Occ	Beq
Si1	3	0.46900	0.00000	0.66667	Si+4	1	1
O1	6	0.40300	0.25300	0.78900	O-2	1	1

Structure 2

Phase name	Kaolinite 1A II
R-Bragg	11.364
Spacegroup	C1
Scale	0.000132732716
Cell Mass	508.256
Cell Volume (≈^3)	325.10507
Wt% - Rietveld	1.750
Crystal Linear Absorption Coeff. (1/cm)	81.026
Crystal Density (g/cm^3)	2.596
Preferred Orientation (Dir 1 : 0 0 1)	1.42542
PVII peak type	
FWHM = a + b/Cos(Th) + c Tan(Th)	
a	0.003186079
b	0.01413051
c	0.4924493
Exponent m = 0.6+ma+mb/Cos(Th)+mc/Tan(Th)	
ma	0.1563492
mb	0.03916171
mc	1.013019
Lattice parameters	
a (≈)	5.3322134
b (≈)	8.3787153
c (≈)	7.5046934
alpha (∞)	93.05501
beta (∞)	103.7211
gamma (∞)	90.97204

Site	Np	x	y	z	Atom	Occ	Beq
O1	2	0.77800	0.18000	-0.14000	O-2	1	1
O2	2	0.27800	0.32000	-0.13800	O-2	1	1
O3	2	0.31600	-0.00800	-0.13600	O-2	1	1
O4	2	0.24800	0.18400	0.15500	O-2	1	1
O5	2	0.75400	0.31500	0.15500	O-2	1	1
O6	2	0.69000	0.00400	0.15700	O-2	1	1
O7	2	0.79100	0.16500	0.48200	O-2	1	1
O8	2	0.61200	-0.12000	0.45500	O-2	1	1
O9	2	0.10800	-0.05800	0.45500	O-2	1	1
Al1	2	0.50200	0.17200	0.00300	Al+3	1	1
Al2	2	0.00200	0.33000	0.00200	Al+3	1	1
Si1	2	0.80000	0.32200	0.38200	Si+4	1	1
Si2	2	0.80000	0.00000	0.38500	Si+4	1	1

Structure 3

Phase name	Illite 2M1
R-Bragg	8.030
Spacegroup	C12/c1
Scale	0.000609505683
Cell Mass	1580.752
Cell Volume (≈^3)	936.37809
Wt% - Rietveld	71.994
Crystallite Size	
Cry size Lorentzian (nm)	36.2
Crystal Linear Absorption Coeff. (1/cm)	119.514
Crystal Density (g/cm^3)	2.803
Preferred Orientation (Dir 1 : 0 0 1)	0.3683155
Preferred Orientation Spherical Harmonics	
Order	8
y00	1
y20	0.5679712
y22m	0.03157224
y22p	-0.1158727
y40	0.4858035
y42m	-0.4010256
y42p	-0.5183621
y44m	0.9363813
y44p	-0.0396859
y60	-0.002352415
y62m	-0.2287521
y62p	0.4592876
y64m	0.1699642
y64p	-0.2507414
y66m	0.3018527
y66p	0.3018527
y80	0.09439929
y82m	0.5208457
y82p	0.2999884
y84m	-0.3776462
y84p	-0.1202494
y86m	-0.1373133
y86p	0.02833367
y88m	-0.07780559
y88p	0.06312174
PVII peak type	
FWHM = a + b/Cos(Th) + c Tan(Th)	
a	0.0001
b	0.0001
c	0.07789675
Exponent m = 0.6+ma+mb/Cos(Th)+mc/Tan(Th)	
ma	0.0001003092
mb	0.05825363
mc	0.03241579
Lattice parameters	
a (≈)	5.2066934
b (≈)	9.0141858
c (≈)	20.0593564
beta (∞)	95.96047

Site	Np	x	y	z	Atom	Occ	Beq
Si1	8	0.48250	0.92970	0.13700	Si+4	1	1.737

Al1	8	0.44320	0.26350	0.13650	Al+3 1	0.8685
Al2	8	0.25860	0.08280	0.00680	Al+3 1	2.132
K1	4	0.00000	0.09010	0.25000	K+1 1	5.922
O1	8	0.46230	0.91940	0.05050	O-2 1	1.184
O2	8	0.38350	0.26650	0.06630	O-2 1	3.711
O3	8	0.42590	0.10390	0.15300	O-2 1	0.9475
O4	8	0.22260	0.83680	0.16850	O-2 1	3.237
O5	8	0.27350	0.37220	0.16780	O-2 1	6.317
O6	8	0.40800	0.56710	0.04540	O-2 1	4.185

Structure 4

Phase name	Chamosite 1MIIb
R-Bragg	15.943
Spacegroup	C-1
Scale	7.21914333e-006
Cell Mass	1271.241
Cell Volume (≈^3)	688.00078
Wt% - Rietveld	0.504
Crystal Linear Absorption Coeff. (1/cm)	271.140
Crystal Density (g/cm^3)	3.068
Preferred Orientation (Dir 1 : 0 0 1)	0.3731178
PVII peak type	
FWHM = a + b/Cos(Th) + c Tan(Th)	
a	0.03904886
b	0.002401771
c	0.1373763
Exponent m = 0.6+ma+mb/Cos(Th)+mc/Tan(Th)	
ma	0.0001
mb	0.0001
mc	0.006658038
Lattice parameters	
a (≈)	5.4083795
b (≈)	9.0044365
c (≈)	14.2985996
alpha (∞)	90.04891
beta (∞)	98.57557
gamma (∞)	92.25189

Site	Np	x	y	z	Atom	Occ	Beq
Mg1	2	0.00000	0.00000	0.00000	Mg+2	0.538	0.1579
Fe1	2	0.00000	0.00000	0.00000	Fe+2	0.462	0.1579
Mg2	4	0.01410	0.33480	0.00270	Mg+2	0.496	0.1579
Fe2	4	0.01410	0.33480	0.00270	Fe+2	0.504	0.1579
Mg3	4	0.00320	0.16830	0.50040	Mg+2	0.494	0.1579
Fe3	4	0.00320	0.16830	0.50040	Fe+2	0.506	0.1579
Al1	2	0.00000	0.50000	0.50000	Al+3	1.362	0.2369
Si1	4	0.24000	0.17000	0.19410	Si+4	0.7125	0.07896
Al2	4	0.24000	0.17000	0.19410	Al+3	0.2875	0.07896
Si2	4	0.73000	0.99800	0.19450	Si+4	0.7125	0.07896
Al3	4	0.73000	0.99800	0.19450	Al+3	0.2875	0.07896
O1	4	0.19100	0.16350	0.07890	O-2	1	0.8685
O2	4	0.70500	0.99800	0.07560	O-2	1	0.8685
O3	4	0.23100	0.33600	0.23740	O-2	1	0.8685
O4	4	0.52800	0.11800	0.23020	O-2	1	0.8685
O5	4	0.01800	0.06100	0.23060	O-2	1	0.8685

O6	4	0.68900	0.33120	0.07420	O-2	1 0.8685
O7	4	0.14400	0.99900	0.43000	O-2	1 0.8685
O8	4	0.14300	0.33610	0.42860	O-2	1 0.8685
O9	4	0.64300	0.16270	0.43110	O-2	1 0.8685

Structure 5

Phase name	Albite low
R-Bragg	7.922
Spacegroup	C-1
Scale	7.28383806e-005
Cell Mass	1048.846
Cell Volume (≈^3)	664.19438
Wt% - Rietveld	4.049
Crystallite Size	
Cry size Lorentzian (nm)	250.1
Crystal Linear Absorption Coeff. (1/cm)	88.829
Crystal Density (g/cm^3)	2.622
Lattice parameters	
a (≈)	8.1380000
b (≈)	12.7890000
c (≈)	7.1560000
alpha (∞)	94.33
beta (∞)	116.57
gamma (∞)	87.65

Site	Np	x	y	z	Atom	Occ	Beq
O1	4	0.00900	0.13400	0.96700	O-2	1	1
O2	4	0.59500	0.99700	0.27900	O-2	1	1
O3	4	0.81800	0.11200	0.19200	O-2	1	1
O4	4	0.32100	0.35300	0.25900	O-2	1	1
O5	4	0.00600	0.30700	0.26800	O-2	1	1
O6	4	0.52200	0.19600	0.23300	O-2	1	1
O7	4	0.20600	0.11000	0.38900	O-2	1	1
O8	4	0.68300	0.36900	0.43000	O-2	1	1
Si1	4	0.00800	0.17100	0.20900	Si+4	0.28	1
Al1	4	0.00800	0.17100	0.20900	Al+3	0.72	1
Si2	4	0.50800	0.31800	0.24100	Si+4	1	1
Si3	4	0.69200	0.11000	0.31500	Si+4	0.8	1
Al3	4	0.69200	0.11000	0.31500	Al+3	0.2	1
Si4	4	0.18300	0.38200	0.35900	Si+4	0.91	1
Al4	4	0.18300	0.38200	0.35900	Al+3	0.09	1
Na1	4	0.27200	0.99000	0.14500	Na+1	1	1

9.1.2.23. Sample 2012-0001084, stratigraphic height: 12.05 m

Range Number : 1

R-Values

Rexp : 1.90 Rwp : 8.70 Rp : 5.39 GOF : 4.58
Rexp`: 6.66 Rwp`: 30.50 Rp` : 26.94 DW : 0.18

Quantitative Analysis - Rietveld

Phase 1 : „Quartz low“ 18.189 %
Phase 2 : „Kaolinite 1A II“ 0.955 %
Phase 3 : „Illite 2M1“ 77.015 %
Phase 4 : „Chamosite 1MIIb“ 0.991 %
Phase 5 : „Albite low“ 2.850 %

Background
Chebychev polynomial, Coefficient 0 2297.047
1 -803.7546
2 285.9437
3 -234.6113
4 229.4759
5 -160.4626
6 38.56043

Instrument
Primary radius (mm) 250
Secondary radius (mm) 250
Linear PSD 2Th angular range (∞) 2.749941
FDS angle (∞) 0.0916
Beam spill, sample length (mm) 9
Intensity not corrected
Full Axial Convolution
Filament length (mm) 8
Sample length (mm) 30
Receiving Slit length (mm) 12
Primary Sollers (∞) 2.5
Secondary Sollers (∞) 2.5

Corrections
Zero error -0.1141093
Specimen displacement -0.3701611
LP Factor 0

Miscellaneous
Excluded Regions
Start/Finish 0 0
Start/Finish 0 0
Start/Finish 0 0
Start/Finish 0 0
Start/Finish 0 0

Structure 1
Phase name Quartz low
R-Bragg 7.562
Spacegroup P3221
Scale 0.0110193661
Cell Mass 180.252
Cell Volume (≈^3) 112.90989
Wt% - Rietveld 18.189
Crystal Linear Absorption Coeff. (1/cm) 95.463
Crystal Density (g/cm^3) 2.651
Preferred Orientation (Dir 1 : 0 0 1) 1.195715
PVII peak type
FWHM = a + b/Cos(Th) + c Tan(Th)

a	0.0158357
b	0.005157868
c	0.0001498225
Exponent m = 0.6+ma+mb/Cos(Th)+mc/Tan(Th)	
ma	0.0001567048
mb	0.0001648964
mc	0.1387423
Lattice parameters	
a (≈)	4.9121650
c (≈)	5.4032549

Site	Np	x	y	z	Atom	Occ	Beq
Si1	3	0.46900	0.00000	0.66667	Si+4	1	1
O1	6	0.40300	0.25300	0.78900	O-2	1	1

Structure 2

Phase name	Kaolinite 1A II
R-Bragg	7.292
Spacegroup	C1
Scale	7.12263459e-005
Cell Mass	508.256
Cell Volume (≈^3)	325.10507
Wt% - Rietveld	0.955
Crystal Linear Absorption Coeff. (1/cm)	81.026
Crystal Density (g/cm^3)	2.596
Preferred Orientation (Dir 1 : 0 0 1)	0.8573304
PVII peak type	
FWHM = a + b/Cos(Th) + c Tan(Th)	
a	0.1994766
b	0.003524157
c	0.000740687
Exponent m = 0.6+ma+mb/Cos(Th)+mc/Tan(Th)	
ma	19.96308
mb	4.975586
mc	4.992893
Lattice parameters	
a (≈)	5.3322134
b (≈)	8.3787153
c (≈)	7.5046934
alpha (∞)	93.05501
beta (∞)	103.7211
gamma (∞)	90.97204

Site	Np	x	y	z	Atom	Occ	Beq
O1	2	0.77800	0.18000	-0.14000	O-2	1	1
O2	2	0.27800	0.32000	-0.13800	O-2	1	1
O3	2	0.31600	-0.00800	-0.13600	O-2	1	1
O4	2	0.24800	0.18400	0.15500	O-2	1	1
O5	2	0.75400	0.31500	0.15500	O-2	1	1
O6	2	0.69000	0.00400	0.15700	O-2	1	1
O7	2	0.79100	0.16500	0.48200	O-2	1	1
O8	2	0.61200	-0.12000	0.45500	O-2	1	1
O9	2	0.10800	-0.05800	0.45500	O-2	1	1
Al1	2	0.50200	0.17200	0.00300	Al+3	1	1
Al2	2	0.00200	0.33000	0.00200	Al+3	1	1

Si1	2	0.80000	0.32200	0.38200	Si+4	1	1
Si2	2	0.80000	0.00000	0.38500	Si+4	1	1

Structure 3

Phase name	Illite 2M1
R-Bragg	7.521
Spacegroup	C12/c1
Scale	0.000641540525
Cell Mass	1580.752
Cell Volume (≈^3)	936.37809
Wt% - Rietveld	77.015
Crystallite Size	
Cry size Lorentzian (nm)	31.7
Crystal Linear Absorption Coeff. (1/cm)	119.514
Crystal Density (g/cm^3)	2.803
Preferred Orientation (Dir 1 : 0 0 1)	0.3824991
Preferred Orientation Spherical Harmonics	
Order	8
y00	1
y20	0.5847138
y22m	-0.1492532
y22p	-0.1127209
y40	0.4972762
y42m	-0.5807056
y42p	-0.5202339
y44m	0.5758423
y44p	-0.03240301
y60	-0.005153381
y62m	0.8200458
y62p	0.4469674
y64m	-0.7068426
y64p	-0.2465084
y66m	0.3030159
y66p	0.3030159
y80	0.04432052
y82m	1.631108
y82p	0.2998072
y84m	-1.123327
y84p	-0.09133206
y86m	-0.1797046
y86p	0.02866055
y88m	-0.03214993
y88p	0.06002627
PVII peak type	
FWHM = a + b/Cos(Th) + c Tan(Th)	
a	0.0001000004
b	0.0001000004
c	0.09658914
Exponent m = 0.6+ma+mb/Cos(Th)+mc/Tan(Th)	
ma	0.0001001453
mb	0.008134506
mc	0.04787938
Lattice parameters	
a (≈)	5.2066934
b (≈)	9.0141858

c (≈) 20.0593564
beta (∞) 95.96047

Site	Np	x	y	z	Atom	Occ	Beq
Si1	8	0.48250	0.92970	0.13700	Si+4	1	1.737
Al1	8	0.44320	0.26350	0.13650	Al+3	1	0.8685
Al2	8	0.25860	0.08280	0.00680	Al+3	1	2.132
K1	4	0.00000	0.09010	0.25000	K+1	1	5.922
O1	8	0.46230	0.91940	0.05050	O-2	1	1.184
O2	8	0.38350	0.26650	0.06630	O-2	1	3.711
O3	8	0.42590	0.10390	0.15300	O-2	1	0.9475
O4	8	0.22260	0.83680	0.16850	O-2	1	3.237
O5	8	0.27350	0.37220	0.16780	O-2	1	6.317
O6	8	0.40800	0.56710	0.04540	O-2	1	4.185

Structure 4
Phase name Chamosite 1MIIb
R-Bragg 5.682
Spacegroup C-1
Scale 1.39685455e-005
Cell Mass 1271.241
Cell Volume (≈^3) 688.00078
Wt% - Rietveld 0.991
Crystal Linear Absorption Coeff. (1/cm) 271.140
Crystal Density (g/cm^3) 3.068
Preferred Orientation (Dir 1 : 0 0 1) 0.3415739
PVII peak type
FWHM = a + b/Cos(Th) + c Tan(Th)
a 0.04110703
b 0.009161461
c 0.0001764029
Exponent m = 0.6+ma+mb/Cos(Th)+mc/Tan(Th)
ma 0.0001488645
mb 0.0001560889
mc 0.003463315
Lattice parameters
a (≈) 5.4083795
b (≈) 9.0044365
c (≈) 14.2985996
alpha (∞) 90.04891
beta (∞) 98.57557
gamma (∞) 92.25189

Site	Np	x	y	z	Atom	Occ	Beq
Mg1	2	0.00000	0.00000	0.00000	Mg+2	0.538	0.1579
Fe1	2	0.00000	0.00000	0.00000	Fe+2	0.462	0.1579
Mg2	4	0.01410	0.33480	0.00270	Mg+2	0.496	0.1579
Fe2	4	0.01410	0.33480	0.00270	Fe+2	0.504	0.1579
Mg3	4	0.00320	0.16830	0.50040	Mg+2	0.494	0.1579
Fe3	4	0.00320	0.16830	0.50040	Fe+2	0.506	0.1579
Al1	2	0.00000	0.50000	0.50000	Al+3	1.362	0.2369
Si1	4	0.24000	0.17000	0.19410	Si+4	0.7125	0.07896
Al2	4	0.24000	0.17000	0.19410	Al+3	0.2875	0.07896
Si2	4	0.73000	0.99800	0.19450	Si+4	0.7125	0.07896
Al3	4	0.73000	0.99800	0.19450	Al+3	0.2875	0.07896

O1	4	0.19100	0.16350	0.07890	O-2	1 0.8685
O2	4	0.70500	0.99800	0.07560	O-2	1 0.8685
O3	4	0.23100	0.33600	0.23740	O-2	1 0.8685
O4	4	0.52800	0.11800	0.23020	O-2	1 0.8685
O5	4	0.01800	0.06100	0.23060	O-2	1 0.8685
O6	4	0.68900	0.33120	0.07420	O-2	1 0.8685
O7	4	0.14400	0.99900	0.43000	O-2	1 0.8685
O8	4	0.14300	0.33610	0.42860	O-2	1 0.8685
O9	4	0.64300	0.16270	0.43110	O-2	1 0.8685

Structure 5

Phase name	Albite low
R-Bragg	8.909
Spacegroup	C-1
Scale	5.04456157e-005
Cell Mass	1048.846
Cell Volume (≈^3)	664.19438
Wt% - Rietveld	2.850
Crystallite Size	
Cry size Lorentzian (nm)	343.0
Crystal Linear Absorption Coeff. (1/cm)	88.829
Crystal Density (g/cm^3)	2.622
Lattice parameters	
a (≈)	8.1380000
b (≈)	12.7890000
c (≈)	7.1560000
alpha (∞)	94.33
beta (∞)	116.57
gamma (∞)	87.65

Site	Np	x	y	z	Atom	Occ	Beq
O1	4	0.00900	0.13400	0.96700	O-2	1	1
O2	4	0.59500	0.99700	0.27900	O-2	1	1
O3	4	0.81800	0.11200	0.19200	O-2	1	1
O4	4	0.32100	0.35300	0.25900	O-2	1	1
O5	4	0.00600	0.30700	0.26800	O-2	1	1
O6	4	0.52200	0.19600	0.23300	O-2	1	1
O7	4	0.20600	0.11000	0.38900	O-2	1	1
O8	4	0.68300	0.36900	0.43000	O-2	1	1
Si1	4	0.00800	0.17100	0.20900	Si+4	0.28	1
Al1	4	0.00800	0.17100	0.20900	Al+3	0.72	1
Si2	4	0.50800	0.31800	0.24100	Si+4	1	1
Si3	4	0.69200	0.11000	0.31500	Si+4	0.8	1
Al3	4	0.69200	0.11000	0.31500	Al+3	0.2	1
Si4	4	0.18300	0.38200	0.35900	Si+4	0.91	1
Al4	4	0.18300	0.38200	0.35900	Al+3	0.09	1
Na1	4	0.27200	0.99000	0.14500	Na+1	1	1

9.1.2.24. Sample 2012-0001078, stratigraphic height: 12.45 m

Range Number : 1

R-Values

Rexp : 1.91 Rwp : 7.93 Rp : 5.32 GOF : 4.14
Rexp`: 6.25 Rwp`: 25.89 Rp` : 24.39 DW : 0.23

Quantitative Analysis - Rietveld
Phase 1 : „Quartz low“ 23.837 %
Phase 2 : „Kaolinite 1A II“ 0.896 %
Phase 3 : „Illite 2M1“ 69.929 %
Phase 4 : „Chamosite 1MIIb“ 1.406 %
Phase 5 : „Albite low“ 3.932 %

Background
Chebychev polynomial, Coefficient 0 2283.377
1 -1002.748
2 463.2028
3 -345.7387
4 318.1269
5 -218.7015
6 91.67016

Instrument
Primary radius (mm) 250
Secondary radius (mm) 250
Linear PSD 2Th angular range (∞) 2.749941
FDS angle (∞) 0.0916
Beam spill, sample length (mm) 9
Intensity not corrected
Full Axial Convolution
Filament length (mm) 8
Sample length (mm) 30
Receiving Slit length (mm) 12
Primary Sollers (∞) 2.5
Secondary Sollers (∞) 2.5

Corrections
Zero error -0.08539127
Specimen displacement -0.2902799
LP Factor 0

Miscellaneous
Excluded Regions
Start/Finish 0 0
Start/Finish 0 0
Start/Finish 0 0
Start/Finish 0 0
Start/Finish 0 0

Structure 1
Phase name Quartz low
R-Bragg 16.425
Spacegroup P3221
Scale 0.0122941923
Cell Mass 180.252
Cell Volume (≈^3) 112.92827
Wt% - Rietveld 23.837

Crystal Linear Absorption Coeff. (1/cm) 95.447
Crystal Density (g/cm^3) 2.650
Preferred Orientation (Dir 1 : 0 0 1) 1.191932
PVII peak type
FWHM = a + b/Cos(Th) + c Tan(Th)
a 0.01053542
b 0.0001
c 0.01679029
Exponent m = 0.6+ma+mb/Cos(Th)+mc/Tan(Th)
ma 0.0003093573
mb 0.03496153
mc 0.0889197
Lattice parameters
a (≈) 4.9123642
c (≈) 5.4036964

Site	Np	x	y	z	Atom	Occ	Beq
Si1	3	0.46900	0.00000	0.66667	Si+4	1	1
O1	6	0.40300	0.25300	0.78900	O-2	1	1

Structure 2
Phase name Kaolinite 1A II
R-Bragg 10.025
Spacegroup C1
Scale 5.69369131e-005
Cell Mass 508.256
Cell Volume (≈^3) 325.10507
Wt% - Rietveld 0.896
Crystal Linear Absorption Coeff. (1/cm) 81.026
Crystal Density (g/cm^3) 2.596
Preferred Orientation (Dir 1 : 0 0 1) 0.8574237
PVII peak type
FWHM = a + b/Cos(Th) + c Tan(Th)
a 0.1443693
b 0.01600712
c 0.0002813981
Exponent m = 0.6+ma+mb/Cos(Th)+mc/Tan(Th)
ma 19.86617
mb 4.960938
mc 4.985806
Lattice parameters
a (≈) 5.3322134
b (≈) 8.3787153
c (≈) 7.5046934
alpha (∞) 93.05501
beta (∞) 103.7211
gamma (∞) 90.97204

Site	Np	x	y	z	Atom	Occ	Beq
O1	2	0.77800	0.18000	-0.14000	O-2	1	1
O2	2	0.27800	0.32000	-0.13800	O-2	1	1
O3	2	0.31600	-0.00800	-0.13600	O-2	1	1
O4	2	0.24800	0.18400	0.15500	O-2	1	1
O5	2	0.75400	0.31500	0.15500	O-2	1	1
O6	2	0.69000	0.00400	0.15700	O-2	1	1

O7	2	0.79100	0.16500	0.48200	O-2	1 1
O8	2	0.61200	-0.12000	0.45500	O-2	1 1
O9	2	0.10800	-0.05800	0.45500	O-2	1 1
Al1	2	0.50200	0.17200	0.00300	Al+3	1 1
Al2	2	0.00200	0.33000	0.00200	Al+3	1 1
Si1	2	0.80000	0.32200	0.38200	Si+4	1 1
Si2	2	0.80000	0.00000	0.38500	Si+4	1 1

Structure 3

Phase name	Illite 2M1
R-Bragg	19.619
Spacegroup	C12/c1
Scale	0.000495994293
Cell Mass	1580.752
Cell Volume (≈^3)	936.37809
Wt% - Rietveld	69.929
Crystallite Size	
Cry size Lorentzian (nm)	33.5
Crystal Linear Absorption Coeff. (1/cm)	119.514
Crystal Density (g/cm^3)	2.803
Preferred Orientation (Dir 1 : 0 0 1)	0.4456081
Preferred Orientation Spherical Harmonics	
Order	8
y00	1
y20	0.6262524
y22m	0.07223169
y22p	-0.06247018
y40	0.571124
y42m	-0.4543452
y42p	-0.4535179
y44m	0.7018353
y44p	-0.03653704
y60	-0.007345261
y62m	0.1186663
y62p	0.4654941
y64m	-0.1633433
y64p	-0.2846237
y66m	0.324083
y66p	0.324083
y80	-0.07566961
y82m	0.7806679
y82p	0.3706545
y84m	-0.7555963
y84p	0.03358068
y86m	-0.07386968
y86p	0.04284892
y88m	-0.1746651
y88p	0.0867026
PVII peak type	
FWHM = a + b/Cos(Th) + c Tan(Th)	
a	0.0001000214
b	0.000100108
c	0.07984661
Exponent m = 0.6+ma+mb/Cos(Th)+mc/Tan(Th)	
ma	0.0001

mb 0.04531132
mc 0.02843972
Lattice parameters
a (≈) 5.2066934
b (≈) 9.0141858
c (≈) 20.0593564
beta (∞) 95.96047

Site	Np	x	y	z	Atom	Occ	Beq
Si1	8	0.48250	0.92970	0.13700	Si+4	1	1.737
Al1	8	0.44320	0.26350	0.13650	Al+3	1	0.8685
Al2	8	0.25860	0.08280	0.00680	Al+3	1	2.132
K1	4	0.00000	0.09010	0.25000	K+1	1	5.922
O1	8	0.46230	0.91940	0.05050	O-2	1	1.184
O2	8	0.38350	0.26650	0.06630	O-2	1	3.711
O3	8	0.42590	0.10390	0.15300	O-2	1	0.9475
O4	8	0.22260	0.83680	0.16850	O-2	1	3.237
O5	8	0.27350	0.37220	0.16780	O-2	1	6.317
O6	8	0.40800	0.56710	0.04540	O-2	1	4.185

Structure 4
Phase name Chamosite 1MIIb
R-Bragg 31.367
Spacegroup C-1
Scale 1.6878828e-005
Cell Mass 1271.241
Cell Volume (≈^3) 688.00078
Wt% - Rietveld 1.406
Crystal Linear Absorption Coeff. (1/cm) 271.140
Crystal Density (g/cm^3) 3.068
Preferred Orientation (Dir 1 : 0 0 1) 0.3568792
PVII peak type
FWHM = a + b/Cos(Th) + c Tan(Th)
a 0.04168071
b 0.007559126
c 0.01272784
Exponent m = 0.6+ma+mb/Cos(Th)+mc/Tan(Th)
ma 0.001581845
mb 0.0001009172
mc 0.004932297
Lattice parameters
a (≈) 5.4083795
b (≈) 9.0044365
c (≈) 14.2985996
alpha (∞) 90.04891
beta (∞) 98.57557
gamma (∞) 92.25189

Site	Np	x	y	z	Atom	Occ	Beq
Mg1	2	0.00000	0.00000	0.00000	Mg+2	0.538	0.1579
Fe1	2	0.00000	0.00000	0.00000	Fe+2	0.462	0.1579
Mg2	4	0.01410	0.33480	0.00270	Mg+2	0.496	0.1579
Fe2	4	0.01410	0.33480	0.00270	Fe+2	0.504	0.1579
Mg3	4	0.00320	0.16830	0.50040	Mg+2	0.494	0.1579
Fe3	4	0.00320	0.16830	0.50040	Fe+2	0.506	0.1579

Al1	2	0.00000	0.50000	0.50000	Al+3 1.362	0.2369
Si1	4	0.24000	0.17000	0.19410	Si+4 0.7125	0.07896
Al2	4	0.24000	0.17000	0.19410	Al+3 0.2875	0.07896
Si2	4	0.73000	0.99800	0.19450	Si+4 0.7125	0.07896
Al3	4	0.73000	0.99800	0.19450	Al+3 0.2875	0.07896
O1	4	0.19100	0.16350	0.07890	O-2 1	0.8685
O2	4	0.70500	0.99800	0.07560	O-2 1	0.8685
O3	4	0.23100	0.33600	0.23740	O-2 1	0.8685
O4	4	0.52800	0.11800	0.23020	O-2 1	0.8685
O5	4	0.01800	0.06100	0.23060	O-2 1	0.8685
O6	4	0.68900	0.33120	0.07420	O-2 1	0.8685
O7	4	0.14400	0.99900	0.43000	O-2 1	0.8685
O8	4	0.14300	0.33610	0.42860	O-2 1	0.8685
O9	4	0.64300	0.16270	0.43110	O-2 1	0.8685

Structure 5

Phase name	Albite low
R-Bragg	6.199
Spacegroup	C-1
Scale	5.92531402e-005
Cell Mass	1048.846
Cell Volume (≈^3)	664.19438
Wt% - Rietveld	3.932
Crystallite Size	
Cry size Lorentzian (nm)	351.1
Crystal Linear Absorption Coeff. (1/cm)	88.829
Crystal Density (g/cm^3)	2.622
Lattice parameters	
a (≈)	8.1380000
b (≈)	12.7890000
c (≈)	7.1560000
alpha (∞)	94.33
beta (∞)	116.57
gamma (∞)	87.65

Site	Np	x	y	z	Atom	Occ	Beq
O1	4	0.00900	0.13400	0.96700	O-2	1	1
O2	4	0.59500	0.99700	0.27900	O-2	1	1
O3	4	0.81800	0.11200	0.19200	O-2	1	1
O4	4	0.32100	0.35300	0.25900	O-2	1	1
O5	4	0.00600	0.30700	0.26800	O-2	1	1
O6	4	0.52200	0.19600	0.23300	O-2	1	1
O7	4	0.20600	0.11000	0.38900	O-2	1	1
O8	4	0.68300	0.36900	0.43000	O-2	1	1
Si1	4	0.00800	0.17100	0.20900	Si+4	0.28	1
Al1	4	0.00800	0.17100	0.20900	Al+3	0.72	1
Si2	4	0.50800	0.31800	0.24100	Si+4	1	1
Si3	4	0.69200	0.11000	0.31500	Si+4	0.8	1
Al3	4	0.69200	0.11000	0.31500	Al+3	0.2	1
Si4	4	0.18300	0.38200	0.35900	Si+4	0.91	1
Al4	4	0.18300	0.38200	0.35900	Al+3	0.09	1
Na1	4	0.27200	0.99000	0.14500	Na+1	1	1

9.1.2.25. Sample 2012-0001068, stratigraphic height: 12.98 m

Range Number : 1

R-Values

Rexp : 1.40 Rwp : 13.48 Rp : 9.69 GOF : 9.63
Rexp`: 2.27 Rwp`: 21.84 Rp` : 16.78 DW : 0.17

Quantitative Analysis - Rietveld
Phase 1 : „Quartz low“ 17.726 %
Phase 2 : „Kaolinite 1A II“ 0.308 %
Phase 3 : „Illite 2M1“ 76.732 %
Phase 4 : „Chamosite 1MIIb“ 2.895 %
Phase 5 : „Albite low“ 2.339 %

Background
Chebychev polynomial, Coefficient 0 2738.004
1 -2096.938
2 1740.877
3 -1098.442
4 529.775
5 -88.06979

Instrument
Primary radius (mm) 250
Secondary radius (mm) 250
Linear PSD 2Th angular range (∞) 2.749941
FDS angle (∞) 0.0916
Beam spill, sample length (mm) 9
Intensity not corrected
Full Axial Convolution
Filament length (mm) 8
Sample length (mm) 30
Receiving Slit length (mm) 12
Primary Sollers (∞) 2.5
Secondary Sollers (∞) 2.5

Corrections
Zero error -0
Specimen displacement -0.1606575
LP Factor 0

Miscellaneous
Excluded Regions
Start/Finish 0 0
Start/Finish 0 0
Start/Finish 0 0
Start/Finish 0 0
Start/Finish 0 0

Structure 1
Phase name Quartz low
R-Bragg 11.769

Spacegroup	P3221
Scale	0.0391481492
Cell Mass	180.252
Cell Volume (≈^3)	113.58879
Wt% - Rietveld	17.726
Crystal Linear Absorption Coeff. (1/cm)	94.892
Crystal Density (g/cm^3)	2.635
Preferred Orientation (Dir 1 : 0 0 1)	1.114293
PVII peak type	
FWHM = a + b/Cos(Th) + c Tan(Th)	
a	0.0001008248
b	0.0001011309
c	0.1108076
Exponent m = 0.6+ma+mb/Cos(Th)+mc/Tan(Th)	
ma	0.0001
mb	0.0001
mc	0.08971709
Lattice parameters	
a (≈)	4.9227981
c (≈)	5.4122865

Site	Np	x	y	z	Atom	Occ	Beq
Si1	3	0.46900	0.00000	0.66667	Si+4	1	1
O1	6	0.40300	0.25300	0.78900	O-2	1	1

Structure 2

Phase name	Kaolinite 1A II
R-Bragg	5.542
Spacegroup	C1
Scale	8.43040293e-005
Cell Mass	508.256
Cell Volume (≈^3)	325.10507
Wt% - Rietveld	0.308
Crystal Linear Absorption Coeff. (1/cm)	81.026
Crystal Density (g/cm^3)	2.596
Preferred Orientation (Dir 1 : 0 0 1)	0.1296098
PVII peak type	
FWHM = a + b/Cos(Th) + c Tan(Th)	
a	1
b	1
c	1
Exponent m = 0.6+ma+mb/Cos(Th)+mc/Tan(Th)	
ma	0.0001
mb	0.0001
mc	0.02702153
Lattice parameters	
a (≈)	5.3322134
b (≈)	8.3787153
c (≈)	7.5046934
alpha (∞)	93.05501
beta (∞)	103.7211
gamma (∞)	90.97204

Site	Np	x	y	z	Atom	Occ	Beq
O1	2	0.77800	0.18000	-0.14000	O-2	1	1

O2	2	0.27800	0.32000	-0.13800	O-2	1	1
O3	2	0.31600	-0.00800	-0.13600	O-2	1	1
O4	2	0.24800	0.18400	0.15500	O-2	1	1
O5	2	0.75400	0.31500	0.15500	O-2	1	1
O6	2	0.69000	0.00400	0.15700	O-2	1	1
O7	2	0.79100	0.16500	0.48200	O-2	1	1
O8	2	0.61200	-0.12000	0.45500	O-2	1	1
O9	2	0.10800	-0.05800	0.45500	O-2	1	1
Al1	2	0.50200	0.17200	0.00300	Al+3	1	1
Al2	2	0.00200	0.33000	0.00200	Al+3	1	1
Si1	2	0.80000	0.32200	0.38200	Si+4	1	1
Si2	2	0.80000	0.00000	0.38500	Si+4	1	1

Structure 3

Phase name	Illite 2M1
R-Bragg	7.413
Spacegroup	C12/c1
Scale	0.00225537422
Cell Mass	1580.752
Cell Volume (≈^3)	940.14454
Wt% - Rietveld	76.732
Crystal Linear Absorption Coeff. (1/cm)	119.036
Crystal Density (g/cm^3)	2.792
Preferred Orientation (Dir 1 : 0 0 1)	0.6657763
PVII peak type	
FWHM = a + b/Cos(Th) + c Tan(Th)	
a	0.1371083
b	0.0001
c	0.03363249
Exponent m = 0.6+ma+mb/Cos(Th)+mc/Tan(Th)	
ma	0.0001
mb	0.0001
mc	0.0001
Lattice parameters	
a (≈)	5.2191537
b (≈)	9.0178312
c (≈)	20.0811433
beta (∞)	95.88638

Site	Np	x	y	z	Atom	Occ	Beq
Si1	8	0.48250	0.92970	0.13700	Si+4	1	1.737
Al1	8	0.44320	0.26350	0.13650	Al+3	1	0.8685
Al2	8	0.25860	0.08280	0.00680	Al+3	1	2.132
K1	4	0.00000	0.09010	0.25000	K+1	1	5.922
O1	8	0.46230	0.91940	0.05050	O-2	1	1.184
O2	8	0.38350	0.26650	0.06630	O-2	1	3.711
O3	8	0.42590	0.10390	0.15300	O-2	1	0.9475
O4	8	0.22260	0.83680	0.16850	O-2	1	3.237
O5	8	0.27350	0.37220	0.16780	O-2	1	6.317
O6	8	0.40800	0.56710	0.04540	O-2	1	4.185

Structure 4

Phase name	Chamosite 1MIIb
R-Bragg	10.127

Spacegroup	C-1
Scale	0.000149682487
Cell Mass	1271.241
Cell Volume (≈^3)	688.00078
Wt% - Rietveld	2.895
Crystal Linear Absorption Coeff. (1/cm)	271.140
Crystal Density (g/cm^3)	3.068
Preferred Orientation (Dir 1 : 0 0 1)	7.06046
PVII peak type	
FWHM = a + b/Cos(Th) + c Tan(Th)	
a	1
b	1
c	1
Exponent m = 0.6+ma+mb/Cos(Th)+mc/Tan(Th)	
ma	0.0001
mb	0.0001
mc	0.0001
Lattice parameters	
a (≈)	5.4083795
b (≈)	9.0044365
c (≈)	14.2985996
alpha (∞)	90.04891
beta (∞)	98.57557
gamma (∞)	92.25189

Site	Np	x	y	z	Atom	Occ	Beq
Mg1	2	0.00000	0.00000	0.00000	Mg+2	0.538	0.1579
Fe1	2	0.00000	0.00000	0.00000	Fe+2	0.462	0.1579
Mg2	4	0.01410	0.33480	0.00270	Mg+2	0.496	0.1579
Fe2	4	0.01410	0.33480	0.00270	Fe+2	0.504	0.1579
Mg3	4	0.00320	0.16830	0.50040	Mg+2	0.494	0.1579
Fe3	4	0.00320	0.16830	0.50040	Fe+2	0.506	0.1579
Al1	2	0.00000	0.50000	0.50000	Al+3	1.362	0.2369
Si1	4	0.24000	0.17000	0.19410	Si+4	0.7125	0.07896
Al2	4	0.24000	0.17000	0.19410	Al+3	0.2875	0.07896
Si2	4	0.73000	0.99800	0.19450	Si+4	0.7125	0.07896
Al3	4	0.73000	0.99800	0.19450	Al+3	0.2875	0.07896
O1	4	0.19100	0.16350	0.07890	O-2	1	0.8685
O2	4	0.70500	0.99800	0.07560	O-2	1	0.8685
O3	4	0.23100	0.33600	0.23740	O-2	1	0.8685
O4	4	0.52800	0.11800	0.23020	O-2	1	0.8685
O5	4	0.01800	0.06100	0.23060	O-2	1	0.8685
O6	4	0.68900	0.33120	0.07420	O-2	1	0.8685
O7	4	0.14400	0.99900	0.43000	O-2	1	0.8685
O8	4	0.14300	0.33610	0.42860	O-2	1	0.8685
O9	4	0.64300	0.16270	0.43110	O-2	1	0.8685

Structure 5

Phase name	Albite low
R-Bragg	12.798
Spacegroup	C-1
Scale	0.000151812602
Cell Mass	1048.846
Cell Volume (≈^3)	664.19438
Wt% - Rietveld	2.339

Crystallite Size
Cry size Lorentzian (nm) 108.9
Crystal Linear Absorption Coeff. (1/cm) 88.829
Crystal Density (g/cm^3) 2.622
Lattice parameters
a (≈) 8.1380000
b (≈) 12.7890000
c (≈) 7.1560000
alpha (∞) 94.33
beta (∞) 116.57
gamma (∞) 87.65

Site	Np	x	y	z	Atom	Occ	Beq
O1	4	0.00900	0.13400	0.96700	O-2	1	1
O2	4	0.59500	0.99700	0.27900	O-2	1	1
O3	4	0.81800	0.11200	0.19200	O-2	1	1
O4	4	0.32100	0.35300	0.25900	O-2	1	1
O5	4	0.00600	0.30700	0.26800	O-2	1	1
O6	4	0.52200	0.19600	0.23300	O-2	1	1
O7	4	0.20600	0.11000	0.38900	O-2	1	1
O8	4	0.68300	0.36900	0.43000	O-2	1	1
Si1	4	0.00800	0.17100	0.20900	Si+4	0.28	1
Al1	4	0.00800	0.17100	0.20900	Al+3	0.72	1
Si2	4	0.50800	0.31800	0.24100	Si+4	1	1
Si3	4	0.69200	0.11000	0.31500	Si+4	0.8	1
Al3	4	0.69200	0.11000	0.31500	Al+3	0.2	1
Si4	4	0.18300	0.38200	0.35900	Si+4	0.91	1
Al4	4	0.18300	0.38200	0.35900	Al+3	0.09	1
Na1	4	0.27200	0.99000	0.14500	Na+1	1	1

9.1.2.26. Sample 2012-0001070, stratigraphic height: 13.50 m

Range Number : 1

R-Values

Rexp : 1.80 Rwp : 5.53 Rp : 3.74 GOF : 3.07
Rexp`: 7.42 Rwp`: 22.77 Rp` : 23.43 DW : 0.32

Quantitative Analysis - Rietveld
Phase 1 : „Quartz low“ 22.829 %
Phase 2 : „Kaolinite 1A II“ 4.544 %
Phase 3 : „Illite 2M1“ 66.762 %
Phase 4 : „Chamosite 1MIIb“ 1.062 %
Phase 5 : „Albite low“ 4.802 %

Background
Chebychev polynomial, Coefficient 0 2731.365
1 -1072.418
2 450.6373
3 -336.8821
4 327.8496
5 -250.9813
6 122.4386

Instrument
  Primary radius (mm) 250
  Secondary radius (mm) 250
  Linear PSD 2Th angular range (∞) 2.749941
    FDS angle (∞) 0.0916
    Beam spill, sample length (mm) 9
      Intensity not corrected
  Full Axial Convolution
    Filament length (mm) 8
    Sample length (mm) 30
    Receiving Slit length (mm) 12
    Primary Sollers (∞) 2.5
    Secondary Sollers (∞) 2.5

Corrections
  Zero error -0.08942821
  Specimen displacement -0.3552682
  LP Factor 0

Miscellaneous
  Excluded Regions
    Start/Finish 0 0
    Start/Finish 0 0
    Start/Finish 0 0
    Start/Finish 0 0
    Start/Finish 0 0

Structure 1
  Phase name Quartz low
  R-Bragg 7.603
  Spacegroup P3221
  Scale 0.0115242519
  Cell Mass 180.252
  Cell Volume (≈^3) 112.94569
  Wt% - Rietveld 22.829
  Crystal Linear Absorption Coeff. (1/cm) 95.433
  Crystal Density (g/cm^3) 2.650
  Preferred Orientation (Dir 1 : 0 0 1) 1.211958
  PVII peak type
    FWHM = a + b/Cos(Th) + c Tan(Th)
      a 0.009959663
      b 0.002850403
      c 0.01146737
    Exponent m = 0.6+ma+mb/Cos(Th)+mc/Tan(Th)
      ma 0.0001002972
      mb 0.0001017477
      mc 0.09358226
  Lattice parameters
    a (≈) 4.9124840
    c (≈) 5.4042662

Site	Np	x	y	z	Atom	Occ	Beq
Si1	3	0.46900	0.00000	0.66667	Si+4	1	1
O1	6	0.40300	0.25300	0.78900	O-2	1	1

Structure 2

Phase name	Kaolinite 1A II
R-Bragg	15.958
Spacegroup	C1
Scale	0.000282653565
Cell Mass	508.256
Cell Volume (≈^3)	325.10507
Wt% - Rietveld	4.544
Crystal Linear Absorption Coeff. (1/cm)	81.026
Crystal Density (g/cm^3)	2.596
Preferred Orientation (Dir 1 : 0 0 1)	1.672236
PVII peak type	
FWHM = a + b/Cos(Th) + c Tan(Th)	
a	0.000686177
b	0.0001020569
c	0.6515075
Exponent m = 0.6+ma+mb/Cos(Th)+mc/Tan(Th)	
ma	0.01295341
mb	0.001831551
mc	0.09608643
Lattice parameters	
a (≈)	5.3322134
b (≈)	8.3787153
c (≈)	7.5046934
alpha (∞)	93.05501
beta (∞)	103.7211
gamma (∞)	90.97204

Site	Np	x	y	z	Atom	Occ	Beq
O1	2	0.77800	0.18000	-0.14000	O-2	1	1
O2	2	0.27800	0.32000	-0.13800	O-2	1	1
O3	2	0.31600	-0.00800	-0.13600	O-2	1	1
O4	2	0.24800	0.18400	0.15500	O-2	1	1
O5	2	0.75400	0.31500	0.15500	O-2	1	1
O6	2	0.69000	0.00400	0.15700	O-2	1	1
O7	2	0.79100	0.16500	0.48200	O-2	1	1
O8	2	0.61200	-0.12000	0.45500	O-2	1	1
O9	2	0.10800	-0.05800	0.45500	O-2	1	1
Al1	2	0.50200	0.17200	0.00300	Al+3	1	1
Al2	2	0.00200	0.33000	0.00200	Al+3	1	1
Si1	2	0.80000	0.32200	0.38200	Si+4	1	1
Si2	2	0.80000	0.00000	0.38500	Si+4	1	1

Structure 3

Phase name	Illite 2M1
R-Bragg	13.901
Spacegroup	C12/c1
Scale	0.000463551829
Cell Mass	1580.752
Cell Volume (≈^3)	936.37809
Wt% - Rietveld	66.762
Crystallite Size	
Cry size Lorentzian (nm)	35.6

Crystal Linear Absorption Coeff. (1/cm) 119.514
Crystal Density (g/cm^3) 2.803
Preferred Orientation (Dir 1 : 0 0 1) 0.3833195
Preferred Orientation Spherical Harmonics
Order 8
y00 1
y20 0.5724132
y22m -0.03227184
y22p -0.101487
y40 0.5114479
y42m -0.3001489
y42p -0.5100887
y44m 0.9647151
y44p -0.01940657
y60 0.00656471
y62m -0.5208047
y62p 0.4241697
y64m 0.4878394
y64p -0.2458747
y66m 0.3094761
y66p 0.3094761
y80 0.1435163
y82m 0.2377616
y82p 0.3109277
y84m -0.2328292
y84p -0.102184
y86m -0.06074441
y86p 0.01736013
y88m -0.05288691
y88p 0.06137513
PVII peak type
FWHM = a + b/Cos(Th) + c Tan(Th)
a 0.0001000012
b 0.0001000013
c 0.06266752
Exponent m = 0.6+ma+mb/Cos(Th)+mc/Tan(Th)
ma 0.0001217227
mb 0.05609438
mc 0.04561495
Lattice parameters
a (≈) 5.2066934
b (≈) 9.0141858
c (≈) 20.0593564
beta (∞) 95.96047

Site	Np	x	y	z	Atom	Occ	Beq
Si1	8	0.48250	0.92970	0.13700	Si+4	1	1.737
Al1	8	0.44320	0.26350	0.13650	Al+3	1	0.8685
Al2	8	0.25860	0.08280	0.00680	Al+3	1	2.132
K1	4	0.00000	0.09010	0.25000	K+1	1	5.922
O1	8	0.46230	0.91940	0.05050	O-2	1	1.184
O2	8	0.38350	0.26650	0.06630	O-2	1	3.711
O3	8	0.42590	0.10390	0.15300	O-2	1	0.9475
O4	8	0.22260	0.83680	0.16850	O-2	1	3.237
O5	8	0.27350	0.37220	0.16780	O-2	1	6.317
O6	8	0.40800	0.56710	0.04540	O-2	1	4.185

Structure 4

Phase name	Chamosite 1MIIb
R-Bragg	15.545
Spacegroup	C-1
Scale	1.24840644e-005
Cell Mass	1271.241
Cell Volume (≈^3)	688.00078
Wt% - Rietveld	1.062
Crystal Linear Absorption Coeff. (1/cm)	271.140
Crystal Density (g/cm^3)	3.068
Preferred Orientation (Dir 1 : 0 0 1)	0.3715853
PVII peak type	
FWHM = a + b/Cos(Th) + c Tan(Th)	
a	0.002042086
b	0.0001047826
c	0.4961426
Exponent m = 0.6+ma+mb/Cos(Th)+mc/Tan(Th)	
ma	0.0001188917
mb	0.0001155018
mc	0.006138661
Lattice parameters	
a (≈)	5.4083795
b (≈)	9.0044365
c (≈)	14.2985996
alpha (∞)	90.04891
beta (∞)	98.57557
gamma (∞)	92.25189

Site	Np	x	y	z	Atom	Occ	Beq
Mg1	2	0.00000	0.00000	0.00000	Mg+2	0.538	0.1579
Fe1	2	0.00000	0.00000	0.00000	Fe+2	0.462	0.1579
Mg2	4	0.01410	0.33480	0.00270	Mg+2	0.496	0.1579
Fe2	4	0.01410	0.33480	0.00270	Fe+2	0.504	0.1579
Mg3	4	0.00320	0.16830	0.50040	Mg+2	0.494	0.1579
Fe3	4	0.00320	0.16830	0.50040	Fe+2	0.506	0.1579
Al1	2	0.00000	0.50000	0.50000	Al+3	1.362	0.2369
Si1	4	0.24000	0.17000	0.19410	Si+4	0.7125	0.07896
Al2	4	0.24000	0.17000	0.19410	Al+3	0.2875	0.07896
Si2	4	0.73000	0.99800	0.19450	Si+4	0.7125	0.07896
Al3	4	0.73000	0.99800	0.19450	Al+3	0.2875	0.07896
O1	4	0.19100	0.16350	0.07890	O-2	1	0.8685
O2	4	0.70500	0.99800	0.07560	O-2	1	0.8685
O3	4	0.23100	0.33600	0.23740	O-2	1	0.8685
O4	4	0.52800	0.11800	0.23020	O-2	1	0.8685
O5	4	0.01800	0.06100	0.23060	O-2	1	0.8685
O6	4	0.68900	0.33120	0.07420	O-2	1	0.8685
O7	4	0.14400	0.99900	0.43000	O-2	1	0.8685
O8	4	0.14300	0.33610	0.42860	O-2	1	0.8685
O9	4	0.64300	0.16270	0.43110	O-2	1	0.8685

Structure 5

Phase name	Albite low
R-Bragg	17.948

Spacegroup	C-1
Scale	7.08481539e-005
Cell Mass	1048.846
Cell Volume (≈^3)	664.19438
Wt% - Rietveld	4.802
Crystallite Size	
Cry size Lorentzian (nm)	254.4
Crystal Linear Absorption Coeff. (1/cm)	88.829
Crystal Density (g/cm^3)	2.622
Lattice parameters	
a (≈)	8.1380000
b (≈)	12.7890000
c (≈)	7.1560000
alpha (∞)	94.33
beta (∞)	116.57
gamma (∞)	87.65

Site	Np	x	y	z	Atom	Occ	Beq
O1	4	0.00900	0.13400	0.96700	O-2	1	1
O2	4	0.59500	0.99700	0.27900	O-2	1	1
O3	4	0.81800	0.11200	0.19200	O-2	1	1
O4	4	0.32100	0.35300	0.25900	O-2	1	1
O5	4	0.00600	0.30700	0.26800	O-2	1	1
O6	4	0.52200	0.19600	0.23300	O-2	1	1
O7	4	0.20600	0.11000	0.38900	O-2	1	1
O8	4	0.68300	0.36900	0.43000	O-2	1	1
Si1	4	0.00800	0.17100	0.20900	Si+4	0.28	1
Al1	4	0.00800	0.17100	0.20900	Al+3	0.72	1
Si2	4	0.50800	0.31800	0.24100	Si+4	1	1
Si3	4	0.69200	0.11000	0.31500	Si+4	0.8	1
Al3	4	0.69200	0.11000	0.31500	Al+3	0.2	1
Si4	4	0.18300	0.38200	0.35900	Si+4	0.91	1
Al4	4	0.18300	0.38200	0.35900	Al+3	0.09	1
Na1	4	0.27200	0.99000	0.14500	Na+1	1	1

9.1.2.27. Sample 2012-0000666, stratigraphic height: 14.04 m

Range Number : 1

R-Values

Rexp : 1.30 Rwp : 12.50 Rp : 9.91 GOF : 9.61
Rexp`: 1.97 Rwp`: 18.92 Rp` : 15.58 DW : 0.05

Quantitative Analysis - Rietveld

Phase 1 : „Quartz low“	12.083 %
Phase 2 : „Kaolinite 1A II“	0.347 %
Phase 3 : „Illite 2M1“	80.444 %
Phase 4 : „Chamosite 1MIIb“	5.892 %
Phase 5 : „Albite low“	1.235 %

Background

Chebychev polynomial, Coefficient	0	2738.004
	1	-2096.938

2 1740.877
3 -1098.442
4 529.775
5 -88.06979

Instrument
Primary radius (mm) 250
Secondary radius (mm) 250
Linear PSD 2Th angular range (∞) 2.749941
FDS angle (∞) 0.0916
Beam spill, sample length (mm) 9
Intensity not corrected
Full Axial Convolution
Filament length (mm) 8
Sample length (mm) 30
Receiving Slit length (mm) 12
Primary Sollers (∞) 2.5
Secondary Sollers (∞) 2.5

Corrections
Zero error -0
Specimen displacement -0.1606575
LP Factor 0

Miscellaneous
Excluded Regions
Start/Finish 0 0
Start/Finish 0 0
Start/Finish 0 0
Start/Finish 0 0
Start/Finish 0 0

Structure 1
Phase name Quartz low
R-Bragg 3.281
Spacegroup P3221
Scale 0.0307746688
Cell Mass 180.252
Cell Volume (≈^3) 113.01588
Wt% - Rietveld 12.083
Crystal Linear Absorption Coeff. (1/cm) 95.373
Crystal Density (g/cm^3) 2.648
Preferred Orientation (Dir 1 : 0 0 1) 1.127039
PVII peak type
FWHM = a + b/Cos(Th) + c Tan(Th)
a 0.0178809
b 0.03175862
c 0.0001
Exponent m = 0.6+ma+mb/Cos(Th)+mc/Tan(Th)
ma 0.0902881
mb 0.1477258
mc 0.01637787
Lattice parameters
a (≈) 4.9140302
c (≈) 5.4042221

Site	Np	x	y	z	Atom	Occ	Beq
Si1	3	0.46900	0.00000	0.66667	Si+4	1	1
O1	6	0.40300	0.25300	0.78900	O-2	1	1

Structure 2

Phase name	Kaolinite 1A II
R-Bragg	2.501
Spacegroup	C1
Scale	0.000108846777
Cell Mass	508.256
Cell Volume (≈^3)	325.10507
Wt% - Rietveld	0.347
Crystal Linear Absorption Coeff. (1/cm)	81.026
Crystal Density (g/cm^3)	2.596
Preferred Orientation (Dir 1 : 0 0 1)	0.1318136
PVII peak type	
FWHM = a + b/Cos(Th) + c Tan(Th)	
a	1
b	1
c	1
Exponent m = 0.6+ma+mb/Cos(Th)+mc/Tan(Th)	
ma	0.0001
mb	0.0001
mc	0.008151831
Lattice parameters	
a (≈)	5.3322134
b (≈)	8.3787153
c (≈)	7.5046934
alpha (∞)	93.05501
beta (∞)	103.7211
gamma (∞)	90.97204

Site	Np	x	y	z	Atom	Occ	Beq
O1	2	0.77800	0.18000	-0.14000	O-2	1	1
O2	2	0.27800	0.32000	-0.13800	O-2	1	1
O3	2	0.31600	-0.00800	-0.13600	O-2	1	1
O4	2	0.24800	0.18400	0.15500	O-2	1	1
O5	2	0.75400	0.31500	0.15500	O-2	1	1
O6	2	0.69000	0.00400	0.15700	O-2	1	1
O7	2	0.79100	0.16500	0.48200	O-2	1	1
O8	2	0.61200	-0.12000	0.45500	O-2	1	1
O9	2	0.10800	-0.05800	0.45500	O-2	1	1
Al1	2	0.50200	0.17200	0.00300	Al+3	1	1
Al2	2	0.00200	0.33000	0.00200	Al+3	1	1
Si1	2	0.80000	0.32200	0.38200	Si+4	1	1
Si2	2	0.80000	0.00000	0.38500	Si+4	1	1

Structure 3

Phase name	Illite 2M1
R-Bragg	3.744
Spacegroup	C12/c1
Scale	0.00278960477
Cell Mass	1580.752

Cell Volume (≈^3) 936.05169
Wt% - Rietveld 80.444
Crystal Linear Absorption Coeff. (1/cm) 119.556
Crystal Density (g/cm^3) 2.804
Preferred Orientation (Dir 1 : 0 0 1) 0.5108904
PVII peak type
FWHM = a + b/Cos(Th) + c Tan(Th)
a 0.1786855
b 0.0001000736
c 0.05906942
Exponent m = 0.6+ma+mb/Cos(Th)+mc/Tan(Th)
ma 0.0001
mb 0.0001
mc 0.0001
Lattice parameters
a (≈) 5.2217036
b (≈) 8.9826274
c (≈) 20.0637957
beta (∞) 95.92829

Site	Np	x	y	z	Atom	Occ	Beq
Si1	8	0.48250	0.92970	0.13700	Si+4	1	1.737
Al1	8	0.44320	0.26350	0.13650	Al+3	1	0.8685
Al2	8	0.25860	0.08280	0.00680	Al+3	1	2.132
K1	4	0.00000	0.09010	0.25000	K+1	1	5.922
O1	8	0.46230	0.91940	0.05050	O-2	1	1.184
O2	8	0.38350	0.26650	0.06630	O-2	1	3.711
O3	8	0.42590	0.10390	0.15300	O-2	1	0.9475
O4	8	0.22260	0.83680	0.16850	O-2	1	3.237
O5	8	0.27350	0.37220	0.16780	O-2	1	6.317
O6	8	0.40800	0.56710	0.04540	O-2	1	4.185

Structure 4
Phase name Chamosite 1MIIb
R-Bragg 4.815
Spacegroup C-1
Scale 0.000349524175
Cell Mass 1271.241
Cell Volume (≈^3) 688.00078
Wt% - Rietveld 5.892
Crystal Linear Absorption Coeff. (1/cm) 271.140
Crystal Density (g/cm^3) 3.068
Preferred Orientation (Dir 1 : 0 0 1) 34.51428
PVII peak type
FWHM = a + b/Cos(Th) + c Tan(Th)
a 0.9999866
b 0.9999786
c 0.9999985
Exponent m = 0.6+ma+mb/Cos(Th)+mc/Tan(Th)
ma 0.006881613
mb 0.01101536
mc 0.0001007838
Lattice parameters
a (≈) 5.4083795
b (≈) 9.0044365

c (≈)	14.2985996
alpha (∞)	90.04891
beta (∞)	98.57557
gamma (∞)	92.25189

Site	Np	x	y	z	Atom	Occ	Beq
Mg1	2	0.00000	0.00000	0.00000	Mg+2	0.538	0.1579
Fe1	2	0.00000	0.00000	0.00000	Fe+2	0.462	0.1579
Mg2	4	0.01410	0.33480	0.00270	Mg+2	0.496	0.1579
Fe2	4	0.01410	0.33480	0.00270	Fe+2	0.504	0.1579
Mg3	4	0.00320	0.16830	0.50040	Mg+2	0.494	0.1579
Fe3	4	0.00320	0.16830	0.50040	Fe+2	0.506	0.1579
Al1	2	0.00000	0.50000	0.50000	Al+3	1.362	0.2369
Si1	4	0.24000	0.17000	0.19410	Si+4	0.7125	0.07896
Al2	4	0.24000	0.17000	0.19410	Al+3	0.2875	0.07896
Si2	4	0.73000	0.99800	0.19450	Si+4	0.7125	0.07896
Al3	4	0.73000	0.99800	0.19450	Al+3	0.2875	0.07896
O1	4	0.19100	0.16350	0.07890	O-2	1	0.8685
O2	4	0.70500	0.99800	0.07560	O-2	1	0.8685
O3	4	0.23100	0.33600	0.23740	O-2	1	0.8685
O4	4	0.52800	0.11800	0.23020	O-2	1	0.8685
O5	4	0.01800	0.06100	0.23060	O-2	1	0.8685
O6	4	0.68900	0.33120	0.07420	O-2	1	0.8685
O7	4	0.14400	0.99900	0.43000	O-2	1	0.8685
O8	4	0.14300	0.33610	0.42860	O-2	1	0.8685
O9	4	0.64300	0.16270	0.43110	O-2	1	0.8685

Structure 5

Phase name	Albite low
R-Bragg	7.290
Spacegroup	C-1
Scale	9.19526958e-005
Cell Mass	1048.846
Cell Volume (≈^3)	664.19438
Wt% - Rietveld	1.235
Crystallite Size	
Cry size Lorentzian (nm)	256.5
Crystal Linear Absorption Coeff. (1/cm)	88.829
Crystal Density (g/cm^3)	2.622
Lattice parameters	
a (≈)	8.1380000
b (≈)	12.7890000
c (≈)	7.1560000
alpha (∞)	94.33
beta (∞)	116.57
gamma (∞)	87.65

Site	Np	x	y	z	Atom	Occ	Beq
O1	4	0.00900	0.13400	0.96700	O-2	1	1
O2	4	0.59500	0.99700	0.27900	O-2	1	1
O3	4	0.81800	0.11200	0.19200	O-2	1	1
O4	4	0.32100	0.35300	0.25900	O-2	1	1
O5	4	0.00600	0.30700	0.26800	O-2	1	1
O6	4	0.52200	0.19600	0.23300	O-2	1	1
O7	4	0.20600	0.11000	0.38900	O-2	1	1

O8 4 0.68300 0.36900 0.43000 O-2 1 1
Si1 4 0.00800 0.17100 0.20900 Si+4 0.28 1
Al1 4 0.00800 0.17100 0.20900 Al+3 0.72 1
Si2 4 0.50800 0.31800 0.24100 Si+4 1 1
Si3 4 0.69200 0.11000 0.31500 Si+4 0.8 1
Al3 4 0.69200 0.11000 0.31500 Al+3 0.2 1
Si4 4 0.18300 0.38200 0.35900 Si+4 0.91 1
Al4 4 0.18300 0.38200 0.35900 Al+3 0.09 1
Na1 4 0.27200 0.99000 0.14500 Na+1 1 1

9.1.2.28. Sample 2012-0001067, stratigraphic height: 14.57 m

Range Number : 1

R-Values

Rexp : 1.39 Rwp : 10.18 Rp : 7.69 GOF : 7.34
Rexp`: 2.08 Rwp`: 15.26 Rp` : 11.84 DW : 0.19

Quantitative Analysis - Rietveld
Phase 1 : „Quartz low“ 9.904 %
Phase 2 : „Kaolinite 1A II“ 0.229 %
Phase 3 : „Illite 2M1“ 68.878 %
Phase 4 : „Chamosite 1MIIb“ 19.435 %
Phase 5 : „Albite low“ 1.553 %

Background
Chebychev polynomial, Coefficient 0 2738.004
1 -2096.938
2 1740.877
3 -1098.442
4 529.775
5 -88.06979

Instrument
Primary radius (mm) 250
Secondary radius (mm) 250
Linear PSD 2Th angular range (∞) 2.749941
FDS angle (∞) 0.0916
Beam spill, sample length (mm) 9
Intensity not corrected
Full Axial Convolution
Filament length (mm) 8
Sample length (mm) 30
Receiving Slit length (mm) 12
Primary Sollers (∞) 2.5
Secondary Sollers (∞) 2.5

Corrections
Zero error -0
Specimen displacement -0.1606575
LP Factor 0

Miscellaneous

Excluded Regions
Start/Finish 0 9.5
Start/Finish 0 0
Start/Finish 0 0
Start/Finish 0 0
Start/Finish 0 0

Structure 1
Phase name Quartz low
R-Bragg 16.187
Spacegroup P3221
Scale 0.0321352898
Cell Mass 180.252
Cell Volume (≈^3) 112.80144
Wt% - Rietveld 9.904
Crystal Linear Absorption Coeff. (1/cm) 95.555
Crystal Density (g/cm^3) 2.653
Preferred Orientation (Dir 1 : 0 0 1) 1.164537
PVII peak type
FWHM = a + b/Cos(Th) + c Tan(Th)
a 0.01223212
b 0.02000065
c 0.0001008588
Exponent m = 0.6+ma+mb/Cos(Th)+mc/Tan(Th)
ma 0.0001092241
mb 0.000113476
mc 0.233073
Lattice parameters
a (≈) 4.9109187
c (≈) 5.4008053

Site	Np	x	y	z	Atom	Occ	Beq
Si1	3	0.46900	0.00000	0.66667	Si+4	1	1
O1	6	0.40300	0.25300	0.78900	O-2	1	1

Structure 2
Phase name Kaolinite 1A II
R-Bragg 7.020
Spacegroup C1
Scale 9.1564335e-005
Cell Mass 508.256
Cell Volume (≈^3) 325.10507
Wt% - Rietveld 0.229
Crystal Linear Absorption Coeff. (1/cm) 81.026
Crystal Density (g/cm^3) 2.596
Preferred Orientation (Dir 1 : 0 0 1) 0.1385586
PVII peak type
FWHM = a + b/Cos(Th) + c Tan(Th)
a 0.6131351
b 0.9776202
c 1
Exponent m = 0.6+ma+mb/Cos(Th)+mc/Tan(Th)
ma 0.0001
mb 0.0001

mc	0.01624893
Lattice parameters	
a (≈)	5.3322134
b (≈)	8.3787153
c (≈)	7.5046934
alpha (∞)	93.05501
beta (∞)	103.7211
gamma (∞)	90.97204

Site	Np	x	y	z	Atom	Occ	Beq
O1	2	0.77800	0.18000	-0.14000	O-2	1	1
O2	2	0.27800	0.32000	-0.13800	O-2	1	1
O3	2	0.31600	-0.00800	-0.13600	O-2	1	1
O4	2	0.24800	0.18400	0.15500	O-2	1	1
O5	2	0.75400	0.31500	0.15500	O-2	1	1
O6	2	0.69000	0.00400	0.15700	O-2	1	1
O7	2	0.79100	0.16500	0.48200	O-2	1	1
O8	2	0.61200	-0.12000	0.45500	O-2	1	1
O9	2	0.10800	-0.05800	0.45500	O-2	1	1
Al1	2	0.50200	0.17200	0.00300	Al+3	1	1
Al2	2	0.00200	0.33000	0.00200	Al+3	1	1
Si1	2	0.80000	0.32200	0.38200	Si+4	1	1
Si2	2	0.80000	0.00000	0.38500	Si+4	1	1

Structure 3

Phase name	Illite 2M1
R-Bragg	19.587
Spacegroup	C12/c1
Scale	0.0030182382
Cell Mass	1580.752
Cell Volume (≈^3)	933.02594
Wt% - Rietveld	68.878
Crystal Linear Absorption Coeff. (1/cm)	119.944
Crystal Density (g/cm^3)	2.813
Preferred Orientation (Dir 1 : 0 0 1)	0.7040459
PVII peak type	
FWHM = a + b/Cos(Th) + c Tan(Th)	
a	0.381322
b	0.001530395
c	0.0001000206
Exponent m = 0.6+ma+mb/Cos(Th)+mc/Tan(Th)	
ma	0.0001
mb	0.0001
mc	0.0001
Lattice parameters	
a (≈)	5.1982136
b (≈)	9.0029484
c (≈)	20.0452292
beta (∞)	95.9629

Site	Np	x	y	z	Atom	Occ	Beq
Si1	8	0.48250	0.92970	0.13700	Si+4	1	1.737
Al1	8	0.44320	0.26350	0.13650	Al+3	1	0.8685
Al2	8	0.25860	0.08280	0.00680	Al+3	1	2.132
K1	4	0.00000	0.09010	0.25000	K+1	1	5.922

O1	8	0.46230	0.91940	0.05050	O-2	1	1.184
O2	8	0.38350	0.26650	0.06630	O-2	1	3.711
O3	8	0.42590	0.10390	0.15300	O-2	1	0.9475
O4	8	0.22260	0.83680	0.16850	O-2	1	3.237
O5	8	0.27350	0.37220	0.16780	O-2	1	6.317
O6	8	0.40800	0.56710	0.04540	O-2	1	4.185

Structure 4

Phase name	Chamosite 1MIIb
R-Bragg	15.720
Spacegroup	C-1
Scale	0.00146606036
Cell Mass	1271.241
Cell Volume (≈^3)	688.00078
Wt% - Rietveld	19.435
Crystal Linear Absorption Coeff. (1/cm)	271.140
Crystal Density (g/cm^3)	3.068
Preferred Orientation (Dir 1 : 0 0 1)	3.072105
PVII peak type	
FWHM = a + b/Cos(Th) + c Tan(Th)	
a	0.9992204
b	0.9992659
c	0.9999546
Exponent m = 0.6+ma+mb/Cos(Th)+mc/Tan(Th)	
ma	0.0001000148
mb	0.0001000023
mc	0.0001107906
Lattice parameters	
a (≈)	5.4083795
b (≈)	9.0044365
c (≈)	14.2985996
alpha (∞)	90.04891
beta (∞)	98.57557
gamma (∞)	92.25189

Site	Np	x	y	z	Atom	Occ	Beq
Mg1	2	0.00000	0.00000	0.00000	Mg+2	0.538	0.1579
Fe1	2	0.00000	0.00000	0.00000	Fe+2	0.462	0.1579
Mg2	4	0.01410	0.33480	0.00270	Mg+2	0.496	0.1579
Fe2	4	0.01410	0.33480	0.00270	Fe+2	0.504	0.1579
Mg3	4	0.00320	0.16830	0.50040	Mg+2	0.494	0.1579
Fe3	4	0.00320	0.16830	0.50040	Fe+2	0.506	0.1579
Al1	2	0.00000	0.50000	0.50000	Al+3	1.362	0.2369
Si1	4	0.24000	0.17000	0.19410	Si+4	0.7125	0.07896
Al2	4	0.24000	0.17000	0.19410	Al+3	0.2875	0.07896
Si2	4	0.73000	0.99800	0.19450	Si+4	0.7125	0.07896
Al3	4	0.73000	0.99800	0.19450	Al+3	0.2875	0.07896
O1	4	0.19100	0.16350	0.07890	O-2	1	0.8685
O2	4	0.70500	0.99800	0.07560	O-2	1	0.8685
O3	4	0.23100	0.33600	0.23740	O-2	1	0.8685
O4	4	0.52800	0.11800	0.23020	O-2	1	0.8685
O5	4	0.01800	0.06100	0.23060	O-2	1	0.8685
O6	4	0.68900	0.33120	0.07420	O-2	1	0.8685
O7	4	0.14400	0.99900	0.43000	O-2	1	0.8685
O8	4	0.14300	0.33610	0.42860	O-2	1	0.8685

O9 4 0.64300 0.16270 0.43110 O-2 1 0.8685

Structure 5
Phase name Albite low
R-Bragg 13.919
Spacegroup C-1
Scale 0.000147057869
Cell Mass 1048.846
Cell Volume (≈^3) 664.19438
Wt% - Rietveld 1.553
Crystallite Size
Cry size Lorentzian (nm) 237.7
Crystal Linear Absorption Coeff. (1/cm) 88.829
Crystal Density (g/cm^3) 2.622
Lattice parameters
a (≈) 8.1380000
b (≈) 12.7890000
c (≈) 7.1560000
alpha (∞) 94.33
beta (∞) 116.57
gamma (∞) 87.65

Site	Np	x	y	z	Atom	Occ	Beq
O1	4	0.00900	0.13400	0.96700	O-2	1	1
O2	4	0.59500	0.99700	0.27900	O-2	1	1
O3	4	0.81800	0.11200	0.19200	O-2	1	1
O4	4	0.32100	0.35300	0.25900	O-2	1	1
O5	4	0.00600	0.30700	0.26800	O-2	1	1
O6	4	0.52200	0.19600	0.23300	O-2	1	1
O7	4	0.20600	0.11000	0.38900	O-2	1	1
O8	4	0.68300	0.36900	0.43000	O-2	1	1
Si1	4	0.00800	0.17100	0.20900	Si+4	0.28	1
Al1	4	0.00800	0.17100	0.20900	Al+3	0.72	1
Si2	4	0.50800	0.31800	0.24100	Si+4	1	1
Si3	4	0.69200	0.11000	0.31500	Si+4	0.8	1
Al3	4	0.69200	0.11000	0.31500	Al+3	0.2	1
Si4	4	0.18300	0.38200	0.35900	Si+4	0.91	1
Al4	4	0.18300	0.38200	0.35900	Al+3	0.09	1
Na1	4	0.27200	0.99000	0.14500	Na+1	1	1

9.1.2.29. Sample 2012-0001066, stratigraphic height: 15.00 m

Range Number : 1

R-Values

Rexp : 1.42 Rwp : 8.28 Rp : 6.44 GOF : 5.82
Rexp`: 2.34 Rwp`: 13.59 Rp` : 11.41 DW : 0.18

Quantitative Analysis - Rietveld
Phase 1 : „Quartz low“ 19.280 %
Phase 2 : „Kaolinite 1A II“ 0.295 %
Phase 3 : „Illite 2M1“ 78.293 %

Phase 4 : „Albite low“ 2.132 %

Background
Chebychev polynomial, Coefficient 0 2738.004
1 -2096.938
2 1740.877
3 -1098.442
4 529.775
5 -88.06979

Instrument
Primary radius (mm) 250
Secondary radius (mm) 250
Linear PSD 2Th angular range (∞) 2.749941
FDS angle (∞) 0.0916
Beam spill, sample length (mm) 9
Intensity not corrected
Full Axial Convolution
Filament length (mm) 8
Sample length (mm) 30
Receiving Slit length (mm) 12
Primary Sollers (∞) 2.5
Secondary Sollers (∞) 2.5

Corrections
Zero error -0
Specimen displacement -0.1606575
LP Factor 0

Miscellaneous
Excluded Regions
Start/Finish 0 0
Start/Finish 0 0
Start/Finish 0 0
Start/Finish 0 0
Start/Finish 0 0

Structure 1
Phase name Quartz low
R-Bragg 3.502
Spacegroup P3221
Scale 0.0440065153
Cell Mass 180.252
Cell Volume (≈^3) 113.00472
Wt% - Rietveld 19.280
Crystal Linear Absorption Coeff. (1/cm) 95.383
Crystal Density (g/cm^3) 2.649
Preferred Orientation (Dir 1 : 0 0 1) 1.175911
PVII peak type
FWHM = a + b/Cos(Th) + c Tan(Th)
a 0.000244772
b 0.02492544
c 0.0001000016
Exponent m = 0.6+ma+mb/Cos(Th)+mc/Tan(Th)
ma 0.02118833

mb 0.03952983
mc 0.1134199
Lattice parameters
a (≈) 4.9135701
b (≈) 0.0000000
c (≈) 5.4047004
gamma (∞) 120

Site	Np	x	y	z	Atom	Occ	Beq
Si1	3	0.46900	0.00000	0.66667	Si+4	1	1
O1	6	0.40300	0.25300	0.78900	O-2	1	1

Structure 2
Phase name Kaolinite 1A II
R-Bragg 1.645
Spacegroup C1
Scale 8.28812581e-005
Cell Mass 508.256
Cell Volume (≈^3) 325.10507
Wt% - Rietveld 0.295
Crystal Linear Absorption Coeff. (1/cm) 81.026
Crystal Density (g/cm^3) 2.596
Preferred Orientation (Dir 1 : 0 0 1) 0.144634
PVII peak type
FWHM = a + b/Cos(Th) + c Tan(Th)
a 1
b 1
c 1
Exponent m = 0.6+ma+mb/Cos(Th)+mc/Tan(Th)
ma 0.0001
mb 0.0001
mc 0.03700695
Lattice parameters
a (≈) 5.3322134
b (≈) 8.3787153
c (≈) 7.5046934
alpha (∞) 93.05501
beta (∞) 103.7211
gamma (∞) 90.97204

Site	Np	x	y	z	Atom	Occ	Beq
O1	2	0.77800	0.18000	-0.14000	O-2	1	1
O2	2	0.27800	0.32000	-0.13800	O-2	1	1
O3	2	0.31600	-0.00800	-0.13600	O-2	1	1
O4	2	0.24800	0.18400	0.15500	O-2	1	1
O5	2	0.75400	0.31500	0.15500	O-2	1	1
O6	2	0.69000	0.00400	0.15700	O-2	1	1
O7	2	0.79100	0.16500	0.48200	O-2	1	1
O8	2	0.61200	-0.12000	0.45500	O-2	1	1
O9	2	0.10800	-0.05800	0.45500	O-2	1	1
Al1	2	0.50200	0.17200	0.00300	Al+3	1	1
Al2	2	0.00200	0.33000	0.00200	Al+3	1	1
Si1	2	0.80000	0.32200	0.38200	Si+4	1	1
Si2	2	0.80000	0.00000	0.38500	Si+4	1	1

Structure 3

Phase name	Illite 2M1
R-Bragg	2.181
Spacegroup	C12/c1
Scale	0.00241295617
Cell Mass	1580.752
Cell Volume (≈^3)	935.05903
Wt% - Rietveld	78.293
Crystal Linear Absorption Coeff. (1/cm)	119.683
Crystal Density (g/cm^3)	2.807
Preferred Orientation (Dir 1 : 0 0 1)	0.6716731
PVII peak type	
FWHM = a + b/Cos(Th) + c Tan(Th)	
a	0.1770243
b	0.00214328
c	0.001842908
Exponent m = 0.6+ma+mb/Cos(Th)+mc/Tan(Th)	
ma	0.0001
mb	0.0001
mc	0.0001
Lattice parameters	
a (≈)	5.2022411
b (≈)	9.0032366
c (≈)	20.0667107
beta (∞)	95.79651

Site	Np	x	y	z	Atom	Occ	Beq
Si1	8	0.48250	0.92970	0.13700	Si+4	1	1.737
Al1	8	0.44320	0.26350	0.13650	Al+3	1	0.8685
Al2	8	0.25860	0.08280	0.00680	Al+3	1	2.132
K1	4	0.00000	0.09010	0.25000	K+1	1	5.922
O1	8	0.46230	0.91940	0.05050	O-2	1	1.184
O2	8	0.38350	0.26650	0.06630	O-2	1	3.711
O3	8	0.42590	0.10390	0.15300	O-2	1	0.9475
O4	8	0.22260	0.83680	0.16850	O-2	1	3.237
O5	8	0.27350	0.37220	0.16780	O-2	1	6.317
O6	8	0.40800	0.56710	0.04540	O-2	1	4.185

Site	Np	x	y	z	Atom	Occ	Beq
Si1	8	0.48250	0.92970	0.13700	Si+4	1	1.737
Al1	8	0.44320	0.26350	0.13650	Al+3	1	0.8685
Al2	8	0.25860	0.08280	0.00680	Al+3	1	2.132
K1	4	0.00000	0.09010	0.25000	K+1	1	5.922
O1	8	0.46230	0.91940	0.05050	O-2	1	1.184
O2	8	0.38350	0.26650	0.06630	O-2	1	3.711
O3	8	0.42590	0.10390	0.15300	O-2	1	0.9475
O4	8	0.22260	0.83680	0.16850	O-2	1	3.237
O5	8	0.27350	0.37220	0.16780	O-2	1	6.317
O6	8	0.40800	0.56710	0.04540	O-2	1	4.185

Structure 4

Phase name	Albite low
R-Bragg	5.437
Spacegroup	C-1

Scale 0.000142299802
Cell Mass 1048.846
Cell Volume (≈^3) 664.19438
Wt% - Rietveld 2.132
Crystallite Size
Cry size Lorentzian (nm) 287.1
Crystal Linear Absorption Coeff. (1/cm) 88.829
Crystal Density (g/cm^3) 2.622
Lattice parameters
a (≈) 8.1380000
b (≈) 12.7890000
c (≈) 7.1560000
alpha (∞) 94.33
beta (∞) 116.57
gamma (∞) 87.65

Site	Np	x	y	z	Atom	Occ	Beq
O1	4	0.00900	0.13400	0.96700	O-2	1	1
O2	4	0.59500	0.99700	0.27900	O-2	1	1
O3	4	0.81800	0.11200	0.19200	O-2	1	1
O4	4	0.32100	0.35300	0.25900	O-2	1	1
O5	4	0.00600	0.30700	0.26800	O-2	1	1
O6	4	0.52200	0.19600	0.23300	O-2	1	1
O7	4	0.20600	0.11000	0.38900	O-2	1	1
O8	4	0.68300	0.36900	0.43000	O-2	1	1
Si1	4	0.00800	0.17100	0.20900	Si+4	0.28	1
Al1	4	0.00800	0.17100	0.20900	Al+3	0.72	1
Si2	4	0.50800	0.31800	0.24100	Si+4	1	1
Si3	4	0.69200	0.11000	0.31500	Si+4	0.8	1
Al3	4	0.69200	0.11000	0.31500	Al+3	0.2	1
Si4	4	0.18300	0.38200	0.35900	Si+4	0.91	1
Al4	4	0.18300	0.38200	0.35900	Al+3	0.09	1
Na1	4	0.27200	0.99000	0.14500	Na+1	1	1

9.1.2.30. Sample 2012-0001069, stratigraphic height: 15.57 m

Range Number : 1

R-Values

Rexp : 1.26 Rwp : 6.10 Rp : 4.89 GOF : 4.83
Rexp`: 3.86 Rwp`: 18.66 Rp` : 20.52 DW : 0.27

Quantitative Analysis - Rietveld
Phase 1 : „Quartz low“ 34.652 %
Phase 2 : „Kaolinite 1A II“ 1.613 %
Phase 3 : „Illite 2M1“ 58.316 %
Phase 4 : „Chamosite 1MIIb“ 0.698 %
Phase 5 : „Albite low“ 4.721 %

Background
Chebychev polynomial, Coefficient 0 5039.794
1 -1986.416
2 875.1201

3	-511.3527
4	307.4872
5	-121.491

Instrument

Primary radius (mm)	250
Secondary radius (mm)	250
Linear PSD 2Th angular range (∞)	2.749941
FDS angle (∞)	0.0916
Beam spill, sample length (mm)	9
Intensity not corrected	
Full Axial Convolution	
Filament length (mm)	8
Sample length (mm)	30
Receiving Slit length (mm)	12
Primary Sollers (∞)	2.5
Secondary Sollers (∞)	2.5

Corrections

Zero error	0.007178269
Specimen displacement	-0.1009369
LP Factor	0

Miscellaneous

Excluded Regions

Start/Finish	0	0
Start/Finish	0	0
Start/Finish	0	0
Start/Finish	0	0
Start/Finish	0	0

Structure 1

Phase name	Quartz low
R-Bragg	9.798
Spacegroup	P3221
Scale	0.037455411
Cell Mass	180.252
Cell Volume (≈^3)	112.99795
Wt% - Rietveld	34.652
Crystal Linear Absorption Coeff. (1/cm)	95.388
Crystal Density (g/cm^3)	2.649
Preferred Orientation (Dir 1 : 0 0 1)	1.180913
PVII peak type	
FWHM = a + b/Cos(Th) + c Tan(Th)	
a	0.02745399
b	0.0001
c	0.0001
Exponent m = 0.6+ma+mb/Cos(Th)+mc/Tan(Th)	
ma	0.02908919
mb	0.01029364
mc	0.1287203
Lattice parameters	
a (≈)	4.9134470
c (≈)	5.4046473

Site	Np	x	y	z	Atom	Occ	Beq
Si1	3	0.46900	0.00000	0.66667	Si+4	1	1
O1	6	0.40300	0.25300	0.78900	O-2	1	1

Structure 2

Phase name	Kaolinite 1A II
R-Bragg	3.437
Spacegroup	C1
Scale	0.000207038231
Cell Mass	508.256
Cell Volume (≈^3)	337.44918
Wt% - Rietveld	1.613
Crystal Linear Absorption Coeff. (1/cm)	78.062
Crystal Density (g/cm^3)	2.501
Preferred Orientation (Dir 1 : 0 0 1)	0.2461171
PVII peak type	
FWHM = a + b/Cos(Th) + c Tan(Th)	
a	0.2114355
b	0.9696645
c	1
Exponent m = 0.6+ma+mb/Cos(Th)+mc/Tan(Th)	
ma	0.0001
mb	0.0001
mc	0.1281846
Lattice parameters	
a (≈)	5.2164628
b (≈)	9.0795136
c (≈)	7.3998899
alpha (∞)	94.17556
beta (∞)	104.6806
gamma (∞)	92.47204

Site	Np	x	y	z	Atom	Occ	Beq
O1	2	0.77800	0.18000	-0.14000	O-2	1	1
O2	2	0.27800	0.32000	-0.13800	O-2	1	1
O3	2	0.31600	-0.00800	-0.13600	O-2	1	1
O4	2	0.24800	0.18400	0.15500	O-2	1	1
O5	2	0.75400	0.31500	0.15500	O-2	1	1
O6	2	0.69000	0.00400	0.15700	O-2	1	1
O7	2	0.79100	0.16500	0.48200	O-2	1	1
O8	2	0.61200	-0.12000	0.45500	O-2	1	1
O9	2	0.10800	-0.05800	0.45500	O-2	1	1
Al1	2	0.50200	0.17200	0.00300	Al+3	1	1
Al2	2	0.00200	0.33000	0.00200	Al+3	1	1
Si1	2	0.80000	0.32200	0.38200	Si+4	1	1
Si2	2	0.80000	0.00000	0.38500	Si+4	1	1

Structure 3

Phase name	Illite 2M1
R-Bragg	2.351
Spacegroup	C12/c1
Scale	0.00086739265
Cell Mass	1580.752
Cell Volume (≈^3)	936.37809

Wt% - Rietveld 58.316
Crystallite Size
Cry size Lorentzian (nm) 28.2
Crystal Linear Absorption Coeff. (1/cm) 119.514
Crystal Density (g/cm^3) 2.803
Preferred Orientation Spherical Harmonics
Order 4
y00 1
y20 -0.5924551
y22m -0.612672
y22p -0.8134916
y40 0.168078
y42m -0.1683192
y42p 0.2537269
y44m -0.0978486
y44p 0.1118889
Lattice parameters
a (≈) 5.2066934
b (≈) 9.0141858
c (≈) 20.0593564
beta (∞) 95.96047

Site	Np	x	y	z	Atom	Occ	Beq
Si1	8	0.48250	0.92970	0.13700	Si+4	1	1.737
Al1	8	0.44320	0.26350	0.13650	Al+3	1	0.8685
Al2	8	0.25860	0.08280	0.00680	Al+3	1	2.132
K1	4	0.00000	0.09010	0.25000	K+1	1	5.922
O1	8	0.46230	0.91940	0.05050	O-2	1	1.184
O2	8	0.38350	0.26650	0.06630	O-2	1	3.711
O3	8	0.42590	0.10390	0.15300	O-2	1	0.9475
O4	8	0.22260	0.83680	0.16850	O-2	1	3.237
O5	8	0.27350	0.37220	0.16780	O-2	1	6.317
O6	8	0.40800	0.56710	0.04540	O-2	1	4.185

Structure 4
Phase name Chamosite 1MIIb
R-Bragg 4.552
Spacegroup C-1
Scale 1.75805005e-005
Cell Mass 1271.241
Cell Volume (≈^3) 687.94862
Wt% - Rietveld 0.698
Crystal Linear Absorption Coeff. (1/cm) 271.160
Crystal Density (g/cm^3) 3.068
Preferred Orientation (Dir 1 : 0 0 1) 0.453475
PVII peak type
FWHM = a + b/Cos(Th) + c Tan(Th)
a 0.06444694
b 0.03189836
c 0.0001
Exponent m = 0.6+ma+mb/Cos(Th)+mc/Tan(Th)
ma 20
mb 5
mc 0.6250875
Lattice parameters

a (≈)	5.4223558
b (≈)	8.9799140
c (≈)	14.3209756
alpha (∞)	89.8823
beta (∞)	99.19879
gamma (∞)	91.95477

Site	Np	x	y	z	Atom	Occ	Beq
Mg1	2	0.00000	0.00000	0.00000	Mg+2	0.538	0.1579
Fe1	2	0.00000	0.00000	0.00000	Fe+2	0.462	0.1579
Mg2	4	0.01410	0.33480	0.00270	Mg+2	0.496	0.1579
Fe2	4	0.01410	0.33480	0.00270	Fe+2	0.504	0.1579
Mg3	4	0.00320	0.16830	0.50040	Mg+2	0.494	0.1579
Fe3	4	0.00320	0.16830	0.50040	Fe+2	0.506	0.1579
Al1	2	0.00000	0.50000	0.50000	Al+3	1.362	0.2369
Si1	4	0.24000	0.17000	0.19410	Si+4	0.7125	0.07896
Al2	4	0.24000	0.17000	0.19410	Al+3	0.2875	0.07896
Si2	4	0.73000	0.99800	0.19450	Si+4	0.7125	0.07896
Al3	4	0.73000	0.99800	0.19450	Al+3	0.2875	0.07896
O1	4	0.19100	0.16350	0.07890	O-2	1	0.8685
O2	4	0.70500	0.99800	0.07560	O-2	1	0.8685
O3	4	0.23100	0.33600	0.23740	O-2	1	0.8685
O4	4	0.52800	0.11800	0.23020	O-2	1	0.8685
O5	4	0.01800	0.06100	0.23060	O-2	1	0.8685
O6	4	0.68900	0.33120	0.07420	O-2	1	0.8685
O7	4	0.14400	0.99900	0.43000	O-2	1	0.8685
O8	4	0.14300	0.33610	0.42860	O-2	1	0.8685
O9	4	0.64300	0.16270	0.43110	O-2	1	0.8685

Structure 5

Phase name	Albite low
R-Bragg	5.408
Spacegroup	C-1
Scale	0.000149187685
Cell Mass	1048.846
Cell Volume (≈^3)	664.19438
Wt% - Rietveld	4.721
Crystallite Size	
Cry size Lorentzian (nm)	282.2
Crystal Linear Absorption Coeff. (1/cm)	88.829
Crystal Density (g/cm^3)	2.622
Lattice parameters	
a (≈)	8.1380000
b (≈)	12.7890000
c (≈)	7.1560000
alpha (∞)	94.33
beta (∞)	116.57
gamma (∞)	87.65

Site	Np	x	y	z	Atom	Occ	Beq
O1	4	0.00900	0.13400	0.96700	O-2	1	1
O2	4	0.59500	0.99700	0.27900	O-2	1	1
O3	4	0.81800	0.11200	0.19200	O-2	1	1
O4	4	0.32100	0.35300	0.25900	O-2	1	1
O5	4	0.00600	0.30700	0.26800	O-2	1	1

O6 4 0.52200 0.19600 0.23300 O-2 1 1
O7 4 0.20600 0.11000 0.38900 O-2 1 1
O8 4 0.68300 0.36900 0.43000 O-2 1 1
Si1 4 0.00800 0.17100 0.20900 Si+4 0.28 1
Al1 4 0.00800 0.17100 0.20900 Al+3 0.72 1
Si2 4 0.50800 0.31800 0.24100 Si+4 1 1
Si3 4 0.69200 0.11000 0.31500 Si+4 0.8 1
Al3 4 0.69200 0.11000 0.31500 Al+3 0.2 1
Si4 4 0.18300 0.38200 0.35900 Si+4 0.91 1
Al4 4 0.18300 0.38200 0.35900 Al+3 0.09 1
Na1 4 0.27200 0.99000 0.14500 Na+1 1 1

9.1.2.31. Sample 2012-0001086, stratigraphic height: 16.05 m

Range Number : 1

R-Values

Rexp : 1.39 Rwp : 10.48 Rp : 7.87 GOF : 7.53
Rexp`: 2.23 Rwp`: 16.80 Rp` : 13.49 DW : 0.21

Quantitative Analysis - Rietveld
Phase 1 : „Quartz low“ 18.640 %
Phase 2 : „Kaolinite 1A II“ 0.335 %
Phase 3 : „Illite 2M1“ 78.794 %
Phase 4 : „Albite low“ 2.232 %

Background
Chebychev polynomial, Coefficient 0 2738.004
1 -2096.938
2 1740.877
3 -1098.442
4 529.775
5 -88.06979

Instrument
Primary radius (mm) 250
Secondary radius (mm) 250
Linear PSD 2Th angular range (∞) 2.749941
FDS angle (∞) 0.0916
Beam spill, sample length (mm) 9
Intensity not corrected
Full Axial Convolution
Filament length (mm) 8
Sample length (mm) 30
Receiving Slit length (mm) 12
Primary Sollers (∞) 2.5
Secondary Sollers (∞) 2.5

Corrections
Zero error -0
Specimen displacement -0.1606575
LP Factor 0

Miscellaneous
  Excluded Regions
    Start/Finish 0 0
    Start/Finish 0 0
    Start/Finish 0 0
    Start/Finish 0 0
    Start/Finish 0 0

Structure 1
  Phase name Quartz low
  R-Bragg 4.351
  Spacegroup P3221
  Scale 0.0449714381
  Cell Mass 180.252
  Cell Volume (≈^3) 113.25530
  Wt% - Rietveld 18.640
  Crystal Linear Absorption Coeff. (1/cm) 95.172
  Crystal Density (g/cm^3) 2.643
  Preferred Orientation (Dir 1 : 0 0 1) 1.152399
  PVII peak type
    FWHM = a + b/Cos(Th) + c Tan(Th)
      a 0.0001000044
      b 0.007794955
      c 0.03687639
    Exponent m = 0.6+ma+mb/Cos(Th)+mc/Tan(Th)
      ma 0.0197347
      mb 0.02276238
      mc 0.07574705
  Lattice parameters
    a (≈) 4.9168908
    c (≈) 5.4093712

Site	Np	x	y	z	Atom	Occ	Beq
Si1	3	0.46900	0.00000	0.66667	Si+4	1	1
O1	6	0.40300	0.25300	0.78900	O-2	1	1

Structure 2
  Phase name Kaolinite 1A II
  R-Bragg 5.661
  Spacegroup C1
  Scale 9.97134021e-005
  Cell Mass 508.256
  Cell Volume (≈^3) 325.10507
  Wt% - Rietveld 0.335
  Crystal Linear Absorption Coeff. (1/cm) 81.026
  Crystal Density (g/cm^3) 2.596
  Preferred Orientation (Dir 1 : 0 0 1) 0.134796
  PVII peak type
    FWHM = a + b/Cos(Th) + c Tan(Th)
      a 1
      b 1
      c 1
    Exponent m = 0.6+ma+mb/Cos(Th)+mc/Tan(Th)
      ma 0.0001

mb	0.0001
mc	0.01683795
Lattice parameters	
a (≈)	5.3322134
b (≈)	8.3787153
c (≈)	7.5046934
alpha (∞)	93.05501
beta (∞)	103.7211
gamma (∞)	90.97204

Site	Np	x	y	z	Atom	Occ	Beq
O1	2	0.77800	0.18000	-0.14000	O-2	1	1
O2	2	0.27800	0.32000	-0.13800	O-2	1	1
O3	2	0.31600	-0.00800	-0.13600	O-2	1	1
O4	2	0.24800	0.18400	0.15500	O-2	1	1
O5	2	0.75400	0.31500	0.15500	O-2	1	1
O6	2	0.69000	0.00400	0.15700	O-2	1	1
O7	2	0.79100	0.16500	0.48200	O-2	1	1
O8	2	0.61200	-0.12000	0.45500	O-2	1	1
O9	2	0.10800	-0.05800	0.45500	O-2	1	1
Al1	2	0.50200	0.17200	0.00300	Al+3	1	1
Al2	2	0.00200	0.33000	0.00200	Al+3	1	1
Si1	2	0.80000	0.32200	0.38200	Si+4	1	1
Si2	2	0.80000	0.00000	0.38500	Si+4	1	1

Structure 3

Phase name	Illite 2M1
R-Bragg	5.276
Spacegroup	C12/c1
Scale	0.00258017324
Cell Mass	1580.752
Cell Volume (≈^3)	938.46967
Wt% - Rietveld	78.794
Crystal Linear Absorption Coeff. (1/cm)	119.248
Crystal Density (g/cm^3)	2.797
Preferred Orientation (Dir 1 : 0 0 1)	0.7396503
PVII peak type	
FWHM = a + b/Cos(Th) + c Tan(Th)	
a	0.2012262
b	0.01036414
c	0.002141309
Exponent m = 0.6+ma+mb/Cos(Th)+mc/Tan(Th)	
ma	0.0001
mb	0.0001
mc	0.0001
Lattice parameters	
a (≈)	5.2071562
b (≈)	9.0107917
c (≈)	20.1040837
beta (∞)	95.79819

Site	Np	x	y	z	Atom	Occ	Beq
Si1	8	0.48250	0.92970	0.13700	Si+4	1	1.737
Al1	8	0.44320	0.26350	0.13650	Al+3	1	0.8685
Al2	8	0.25860	0.08280	0.00680	Al+3	1	2.132

K1	4	0.00000	0.09010	0.25000	K+1	1	5.922
O1	8	0.46230	0.91940	0.05050	O-2	1	1.184
O2	8	0.38350	0.26650	0.06630	O-2	1	3.711
O3	8	0.42590	0.10390	0.15300	O-2	1	0.9475
O4	8	0.22260	0.83680	0.16850	O-2	1	3.237
O5	8	0.27350	0.37220	0.16780	O-2	1	6.317
O6	8	0.40800	0.56710	0.04540	O-2	1	4.185

Structure 4

Phase name	Albite low
R-Bragg	7.571
Spacegroup	C-1
Scale	0.000157781953
Cell Mass	1048.846
Cell Volume (≈^3)	664.19438
Wt% - Rietveld	2.232
Crystallite Size	
Cry size Lorentzian (nm)	222.6
Crystal Linear Absorption Coeff. (1/cm)	88.829
Crystal Density (g/cm^3)	2.622
Lattice parameters	
a (≈)	8.1380000
b (≈)	12.7890000
c (≈)	7.1560000
alpha (∞)	94.33
beta (∞)	116.57
gamma (∞)	87.65

Site	Np	x	y	z	Atom	Occ	Beq
O1	4	0.00900	0.13400	0.96700	O-2	1	1
O2	4	0.59500	0.99700	0.27900	O-2	1	1
O3	4	0.81800	0.11200	0.19200	O-2	1	1
O4	4	0.32100	0.35300	0.25900	O-2	1	1
O5	4	0.00600	0.30700	0.26800	O-2	1	1
O6	4	0.52200	0.19600	0.23300	O-2	1	1
O7	4	0.20600	0.11000	0.38900	O-2	1	1
O8	4	0.68300	0.36900	0.43000	O-2	1	1
Si1	4	0.00800	0.17100	0.20900	Si+4	0.28	1
Al1	4	0.00800	0.17100	0.20900	Al+3	0.72	1
Si2	4	0.50800	0.31800	0.24100	Si+4	1	1
Si3	4	0.69200	0.11000	0.31500	Si+4	0.8	1
Al3	4	0.69200	0.11000	0.31500	Al+3	0.2	1
Si4	4	0.18300	0.38200	0.35900	Si+4	0.91	1
Al4	4	0.18300	0.38200	0.35900	Al+3	0.09	1
Na1	4	0.27200	0.99000	0.14500	Na+1	1	1

9.1.2.32. Sample 2012-0001089, stratigraphic height: 16.45 m

Range Number : 1

R-Values

Rexp : 1.35 Rwp : 8.79 Rp : 6.79 GOF : 6.50

Rexp`: 2.13  Rwp`: 13.84 Rp` : 11.20 DW : 0.13

Quantitative Analysis - Rietveld
  Phase 1 : „Quartz low“ 11.350 %
  Phase 2 : „Kaolinite 1A II“ 0.316 %
  Phase 3 : „Illite 2M1“ 67.089 %
  Phase 4 : „Chamosite 1MIIb“ 19.802 %
  Phase 5 : „Albite low“ 1.443 %

Background
  Chebychev polynomial, Coefficient 0 2738.004
  1 -2096.938
  2 1740.877
  3 -1098.442
  4 529.775
  5 -88.06979

Instrument
  Primary radius (mm) 250
  Secondary radius (mm) 250
  Linear PSD 2Th angular range (∞) 2.749941
    FDS angle (∞) 0.0916
    Beam spill, sample length (mm) 9
      Intensity not corrected
  Full Axial Convolution
    Filament length (mm) 8
    Sample length (mm) 30
    Receiving Slit length (mm) 12
    Primary Sollers (∞) 2.5
    Secondary Sollers (∞) 2.5

Corrections
  Zero error -0
  Specimen displacement -0.1606575
  LP Factor 0

Miscellaneous
  Excluded Regions
    Start/Finish 0 0
    Start/Finish 0 0
    Start/Finish 0 0
    Start/Finish 0 0
    Start/Finish 0 0

Structure 1
  Phase name Quartz low
  R-Bragg 2.920
  Spacegroup P3221
  Scale 0.0318160434
  Cell Mass 180.252
  Cell Volume (≈^3) 112.53024
  Wt% - Rietveld 11.350
  Crystal Linear Absorption Coeff. (1/cm) 95.785
  Crystal Density (g/cm^3) 2.660
  Preferred Orientation (Dir 1 : 0 0 1) 1.152451

PVII peak type
FWHM = a + b/Cos(Th) + c Tan(Th)
a 0.03055148
b 0.03550146
c 0.0001003148
Exponent m = 0.6+ma+mb/Cos(Th)+mc/Tan(Th)
ma 0.0001021598
mb 0.00010164
mc 0.5654388
Lattice parameters
a (≈) 4.9077427
c (≈) 5.3947961

Site	Np	x	y	z	Atom	Occ	Beq
Si1	3	0.46900	0.00000	0.66667	Si+4	1	1
O1	6	0.40300	0.25300	0.78900	O-2	1	1

Structure 2
Phase name Kaolinite 1A II
R-Bragg 1.187
Spacegroup C1
Scale 0.000108912801
Cell Mass 508.256
Cell Volume (≈^3) 325.10507
Wt% - Rietveld 0.316
Crystal Linear Absorption Coeff. (1/cm) 81.026
Crystal Density (g/cm^3) 2.596
Preferred Orientation (Dir 1 : 0 0 1) 0.1308694
PVII peak type
FWHM = a + b/Cos(Th) + c Tan(Th)
a 1
b 1
c 1
Exponent m = 0.6+ma+mb/Cos(Th)+mc/Tan(Th)
ma 0.0001
mb 0.0001
mc 0.008170444
Lattice parameters
a (≈) 5.3322134
b (≈) 8.3787153
c (≈) 7.5046934
alpha (∞) 93.05501
beta (∞) 103.7211
gamma (∞) 90.97204

Site	Np	x	y	z	Atom	Occ	Beq
O1	2	0.77800	0.18000	-0.14000	O-2	1	1
O2	2	0.27800	0.32000	-0.13800	O-2	1	1
O3	2	0.31600	-0.00800	-0.13600	O-2	1	1
O4	2	0.24800	0.18400	0.15500	O-2	1	1
O5	2	0.75400	0.31500	0.15500	O-2	1	1
O6	2	0.69000	0.00400	0.15700	O-2	1	1
O7	2	0.79100	0.16500	0.48200	O-2	1	1
O8	2	0.61200	-0.12000	0.45500	O-2	1	1
O9	2	0.10800	-0.05800	0.45500	O-2	1	1

Al1	2	0.50200	0.17200	0.00300	Al+3	1 1
Al2	2	0.00200	0.33000	0.00200	Al+3	1 1
Si1	2	0.80000	0.32200	0.38200	Si+4	1 1
Si2	2	0.80000	0.00000	0.38500	Si+4	1 1

Structure 3

Phase name	Illite 2M1
R-Bragg	1.797
Spacegroup	C12/c1
Scale	0.00256005321
Cell Mass	1580.752
Cell Volume (≈^3)	931.54634
Wt% - Rietveld	67.089
Crystal Linear Absorption Coeff. (1/cm)	120.134
Crystal Density (g/cm^3)	2.818
Preferred Orientation (Dir 1 : 0 0 1)	0.6243965
PVII peak type	
FWHM = a + b/Cos(Th) + c Tan(Th)	
a	0.1815702
b	0.0001001784
c	0.1247749
Exponent m = 0.6+ma+mb/Cos(Th)+mc/Tan(Th)	
ma	0.0001
mb	0.0001
mc	0.0001
Lattice parameters	
a (≈)	5.1965404
b (≈)	8.9944443
c (≈)	20.0381731
beta (∞)	95.94533

Site	Np	x	y	z	Atom	Occ	Beq
Si1	8	0.48250	0.92970	0.13700	Si+4	1	1.737
Al1	8	0.44320	0.26350	0.13650	Al+3	1	0.8685
Al2	8	0.25860	0.08280	0.00680	Al+3	1	2.132
K1	4	0.00000	0.09010	0.25000	K+1	1	5.922
O1	8	0.46230	0.91940	0.05050	O-2	1	1.184
O2	8	0.38350	0.26650	0.06630	O-2	1	3.711
O3	8	0.42590	0.10390	0.15300	O-2	1	0.9475
O4	8	0.22260	0.83680	0.16850	O-2	1	3.237
O5	8	0.27350	0.37220	0.16780	O-2	1	6.317
O6	8	0.40800	0.56710	0.04540	O-2	1	4.185

Structure 4

Phase name	Chamosite 1MIIb
R-Bragg	0.567
Spacegroup	C-1
Scale	0.00128734981
Cell Mass	1271.241
Cell Volume (≈^3)	688.00078
Wt% - Rietveld	19.802
Crystal Linear Absorption Coeff. (1/cm)	271.140
Crystal Density (g/cm^3)	3.068
Preferred Orientation (Dir 1 : 0 0 1)	2.679889

PVII peak type
FWHM = a + b/Cos(Th) + c Tan(Th)

a	1
b	1
c	1

Exponent m = 0.6+ma+mb/Cos(Th)+mc/Tan(Th)

ma	0.0001006854
mb	0.0001008959
mc	0.0001

Lattice parameters

a (≈)	5.4083795
b (≈)	9.0044365
c (≈)	14.2985996
alpha (∞)	90.04891
beta (∞)	98.57557
gamma (∞)	92.25189

Site	Np	x	y	z	Atom	Occ	Beq
Mg1	2	0.00000	0.00000	0.00000	Mg+2	0.538	0.1579
Fe1	2	0.00000	0.00000	0.00000	Fe+2	0.462	0.1579
Mg2	4	0.01410	0.33480	0.00270	Mg+2	0.496	0.1579
Fe2	4	0.01410	0.33480	0.00270	Fe+2	0.504	0.1579
Mg3	4	0.00320	0.16830	0.50040	Mg+2	0.494	0.1579
Fe3	4	0.00320	0.16830	0.50040	Fe+2	0.506	0.1579
Al1	2	0.00000	0.50000	0.50000	Al+3	1.362	0.2369
Si1	4	0.24000	0.17000	0.19410	Si+4	0.7125	0.07896
Al2	4	0.24000	0.17000	0.19410	Al+3	0.2875	0.07896
Si2	4	0.73000	0.99800	0.19450	Si+4	0.7125	0.07896
Al3	4	0.73000	0.99800	0.19450	Al+3	0.2875	0.07896
O1	4	0.19100	0.16350	0.07890	O-2	1	0.8685
O2	4	0.70500	0.99800	0.07560	O-2	1	0.8685
O3	4	0.23100	0.33600	0.23740	O-2	1	0.8685
O4	4	0.52800	0.11800	0.23020	O-2	1	0.8685
O5	4	0.01800	0.06100	0.23060	O-2	1	0.8685
O6	4	0.68900	0.33120	0.07420	O-2	1	0.8685
O7	4	0.14400	0.99900	0.43000	O-2	1	0.8685
O8	4	0.14300	0.33610	0.42860	O-2	1	0.8685
O9	4	0.64300	0.16270	0.43110	O-2	1	0.8685

Structure 5

Phase name	Albite low
R-Bragg	5.021
Spacegroup	C-1
Scale	0.0001178089
Cell Mass	1048.846
Cell Volume (≈^3)	664.19438
Wt% - Rietveld	1.443
Crystallite Size	
Cry size Lorentzian (nm)	146.7
Crystal Linear Absorption Coeff. (1/cm)	88.829
Crystal Density (g/cm^3)	2.622
Lattice parameters	
a (≈)	8.1380000
b (≈)	12.7890000
c (≈)	7.1560000

alpha (∞) 94.33
beta (∞) 116.57
gamma (∞) 87.65

Site	Np	x	y	z	Atom	Occ	Beq
O1	4	0.00900	0.13400	0.96700	O-2	1	1
O2	4	0.59500	0.99700	0.27900	O-2	1	1
O3	4	0.81800	0.11200	0.19200	O-2	1	1
O4	4	0.32100	0.35300	0.25900	O-2	1	1
O5	4	0.00600	0.30700	0.26800	O-2	1	1
O6	4	0.52200	0.19600	0.23300	O-2	1	1
O7	4	0.20600	0.11000	0.38900	O-2	1	1
O8	4	0.68300	0.36900	0.43000	O-2	1	1
Si1	4	0.00800	0.17100	0.20900	Si+4	0.28	1
Al1	4	0.00800	0.17100	0.20900	Al+3	0.72	1
Si2	4	0.50800	0.31800	0.24100	Si+4	1	1
Si3	4	0.69200	0.11000	0.31500	Si+4	0.8	1
Al3	4	0.69200	0.11000	0.31500	Al+3	0.2	1
Si4	4	0.18300	0.38200	0.35900	Si+4	0.91	1
Al4	4	0.18300	0.38200	0.35900	Al+3	0.09	1
Na1	4	0.27200	0.99000	0.14500	Na+1	1	1

9.1.2.33. Sample 2012-0001090, stratigraphic height: 17.05 m

Range Number : 1

R-Values

Rexp : 2.00 Rwp : 8.76 Rp : 5.98 GOF : 4.38
Rexp`: 5.47 Rwp`: 23.97 Rp` : 22.40 DW : 0.15

Quantitative Analysis - Rietveld
Phase 1 : „Quartz low“ 20.867 %
Phase 2 : „Kaolinite 1A II“ 0.014 %
Phase 3 : „Illite 2M1“ 74.781 %
Phase 4 : „Chamosite 1MIIb“ 1.274 %
Phase 5 : „Albite low“ 3.065 %

Background
Chebychev polynomial, Coefficient 0 2020.941
1 -1064.89
2 572.3558
3 -413.562
4 374.2067
5 -247.2492
6 108.188
7 32.0702
8 -38.70741

Instrument
Primary radius (mm) 250
Secondary radius (mm) 250
Linear PSD 2Th angular range (∞) 2.749941
FDS angle (∞) 0.0916

Beam spill, sample length (mm) 9
Intensity not corrected
Full Axial Convolution
Filament length (mm) 8
Sample length (mm) 30
Receiving Slit length (mm) 12
Primary Sollers (∞) 2.5
Secondary Sollers (∞) 2.5

Corrections
Zero error -0.1065212
Specimen displacement -0.4488958
LP Factor 0

Miscellaneous
Excluded Regions
Start/Finish 0 0
Start/Finish 0 0
Start/Finish 0 0
Start/Finish 0 0
Start/Finish 0 0

Structure 1
Phase name Quartz low
R-Bragg 2.157
Spacegroup P3221
Scale 0.0106890052
Cell Mass 180.252
Cell Volume (≈^3) 112.91255
Wt% - Rietveld 20.867
Crystal Linear Absorption Coeff. (1/cm) 95.461
Crystal Density (g/cm^3) 2.651
Preferred Orientation (Dir 1 : 0 0 1) 1.185624
PVII peak type
FWHM = a + b/Cos(Th) + c Tan(Th)
a 0.02240383
b 0.0026361
c 0.0001000722
Exponent m = 0.6+ma+mb/Cos(Th)+mc/Tan(Th)
ma 0.1583478
mb 0.07722966
mc 0.0805745
Lattice parameters
a (≈) 4.9121355
c (≈) 5.4034473

Site	Np	x	y	z	Atom	Occ	Beq
Si1	3	0.46900	0.00000	0.66667	Si+4	1	1
O1	6	0.40300	0.25300	0.78900	O-2	1	1

Structure 2
Phase name Kaolinite 1A II
R-Bragg 0.902
Spacegroup C1

Scale	8.836903e-007
Cell Mass	508.256
Cell Volume (≈^3)	325.10507
Wt% - Rietveld	0.014
Crystal Linear Absorption Coeff. (1/cm)	81.026
Crystal Density (g/cm^3)	2.596
Preferred Orientation (Dir 1 : 0 0 1)	0.2250224
PVII peak type	
FWHM = a + b/Cos(Th) + c Tan(Th)	
a	0.2558337
b	0.0001006185
c	0.0001002214
Exponent m = 0.6+ma+mb/Cos(Th)+mc/Tan(Th)	
ma	19.99992
mb	4.999981
mc	4.99999
Lattice parameters	
a (≈)	5.3322134
b (≈)	8.3787153
c (≈)	7.5046934
alpha (∞)	93.05501
beta (∞)	103.7211
gamma (∞)	90.97204

Site	Np	x	y	z	Atom	Occ	Beq
O1	2	0.77800	0.18000	-0.14000	O-2	1	1
O2	2	0.27800	0.32000	-0.13800	O-2	1	1
O3	2	0.31600	-0.00800	-0.13600	O-2	1	1
O4	2	0.24800	0.18400	0.15500	O-2	1	1
O5	2	0.75400	0.31500	0.15500	O-2	1	1
O6	2	0.69000	0.00400	0.15700	O-2	1	1
O7	2	0.79100	0.16500	0.48200	O-2	1	1
O8	2	0.61200	-0.12000	0.45500	O-2	1	1
O9	2	0.10800	-0.05800	0.45500	O-2	1	1
Al1	2	0.50200	0.17200	0.00300	Al+3	1	1
Al2	2	0.00200	0.33000	0.00200	Al+3	1	1
Si1	2	0.80000	0.32200	0.38200	Si+4	1	1
Si2	2	0.80000	0.00000	0.38500	Si+4	1	1

Structure 3

Phase name	Illite 2M1
R-Bragg	1.976
Spacegroup	C12/c1
Scale	0.000526724273
Cell Mass	1580.752
Cell Volume (≈^3)	936.37809
Wt% - Rietveld	74.781
Crystallite Size	
Cry size Lorentzian (nm)	25.0
Crystal Linear Absorption Coeff. (1/cm)	119.514
Crystal Density (g/cm^3)	2.803
Preferred Orientation (Dir 1 : 0 0 1)	0.3782863
Preferred Orientation Spherical Harmonics	
Order	8
y00	1

y20	0.6074423
y22m	-0.1305005
y22p	-0.1174089
y40	0.4975718
y42m	-0.6327532
y42p	-0.5067326
y44m	0.750217
y44p	-0.07063892
y60	-0.02679416
y62m	-0.3552182
y62p	0.4979665
y64m	0.0965896
y64p	-0.2612493
y66m	0.2987792
y66p	0.2987792
y80	0.009613396
y82m	0.7338415
y82p	0.3474851
y84m	-0.54655
y84p	0.004862456
y86m	0.02167287
y86p	-0.04179841
y88m	-0.087286
y88p	0.1001954
PVII peak type	
FWHM = a + b/Cos(Th) + c Tan(Th)	
a	0.0001000045
b	0.0001000046
c	0.04219752
Exponent m = 0.6+ma+mb/Cos(Th)+mc/Tan(Th)	
ma	0.0001000003
mb	0.0001002444
mc	0.04442719
Lattice parameters	
a (≈)	5.2066934
b (≈)	9.0141858
c (≈)	20.0593564
beta (∞)	95.96047

Site	Np	x	y	z	Atom	Occ	Beq
Si1	8	0.48250	0.92970	0.13700	Si+4	1	1.737
Al1	8	0.44320	0.26350	0.13650	Al+3	1	0.8685
Al2	8	0.25860	0.08280	0.00680	Al+3	1	2.132
K1	4	0.00000	0.09010	0.25000	K+1	1	5.922
O1	8	0.46230	0.91940	0.05050	O-2	1	1.184
O2	8	0.38350	0.26650	0.06630	O-2	1	3.711
O3	8	0.42590	0.10390	0.15300	O-2	1	0.9475
O4	8	0.22260	0.83680	0.16850	O-2	1	3.237
O5	8	0.27350	0.37220	0.16780	O-2	1	6.317
O6	8	0.40800	0.56710	0.04540	O-2	1	4.185

Structure 4

Phase name	Chamosite 1MIIb
R-Bragg	3.875
Spacegroup	C-1

Scale 1.51813836e-005
Cell Mass 1271.241
Cell Volume (≈^3) 688.00078
Wt% - Rietveld 1.274
Crystal Linear Absorption Coeff. (1/cm) 271.140
Crystal Density (g/cm^3) 3.068
Preferred Orientation (Dir 1 : 0 0 1) 0.3125861
PVII peak type
FWHM = a + b/Cos(Th) + c Tan(Th)
a 0.05921984
b 0.01796058
c 0.1072758
Exponent m = 0.6+ma+mb/Cos(Th)+mc/Tan(Th)
ma 0.207784
mb 0.1140952
mc 0.000100007
Lattice parameters
a (≈) 5.4083795
b (≈) 9.0044365
c (≈) 14.2985996
alpha (∞) 90.04891
beta (∞) 98.57557
gamma (∞) 92.25189

Site	Np	x	y	z	Atom	Occ	Beq
Mg1	2	0.00000	0.00000	0.00000	Mg+2	0.538	0.1579
Fe1	2	0.00000	0.00000	0.00000	Fe+2	0.462	0.1579
Mg2	4	0.01410	0.33480	0.00270	Mg+2	0.496	0.1579
Fe2	4	0.01410	0.33480	0.00270	Fe+2	0.504	0.1579
Mg3	4	0.00320	0.16830	0.50040	Mg+2	0.494	0.1579
Fe3	4	0.00320	0.16830	0.50040	Fe+2	0.506	0.1579
Al1	2	0.00000	0.50000	0.50000	Al+3	1.362	0.2369
Si1	4	0.24000	0.17000	0.19410	Si+4	0.7125	0.07896
Al2	4	0.24000	0.17000	0.19410	Al+3	0.2875	0.07896
Si2	4	0.73000	0.99800	0.19450	Si+4	0.7125	0.07896
Al3	4	0.73000	0.99800	0.19450	Al+3	0.2875	0.07896
O1	4	0.19100	0.16350	0.07890	O-2	1	0.8685
O2	4	0.70500	0.99800	0.07560	O-2	1	0.8685
O3	4	0.23100	0.33600	0.23740	O-2	1	0.8685
O4	4	0.52800	0.11800	0.23020	O-2	1	0.8685
O5	4	0.01800	0.06100	0.23060	O-2	1	0.8685
O6	4	0.68900	0.33120	0.07420	O-2	1	0.8685
O7	4	0.14400	0.99900	0.43000	O-2	1	0.8685
O8	4	0.14300	0.33610	0.42860	O-2	1	0.8685
O9	4	0.64300	0.16270	0.43110	O-2	1	0.8685

Structure 5
Phase name Albite low
R-Bragg 3.182
Spacegroup C-1
Scale 4.58724413e-005
Cell Mass 1048.846
Cell Volume (≈^3) 664.19438
Wt% - Rietveld 3.065
Crystallite Size

Cry size Lorentzian (nm) 191.6
Crystal Linear Absorption Coeff. (1/cm) 88.829
Crystal Density (g/cm^3) 2.622
Lattice parameters
a (≈) 8.1380000
b (≈) 12.7890000
c (≈) 7.1560000
alpha (∞) 94.33
beta (∞) 116.57
gamma (∞) 87.65

Site	Np	x	y	z	Atom	Occ	Beq
O1	4	0.00900	0.13400	0.96700	O-2	1	1
O2	4	0.59500	0.99700	0.27900	O-2	1	1
O3	4	0.81800	0.11200	0.19200	O-2	1	1
O4	4	0.32100	0.35300	0.25900	O-2	1	1
O5	4	0.00600	0.30700	0.26800	O-2	1	1
O6	4	0.52200	0.19600	0.23300	O-2	1	1
O7	4	0.20600	0.11000	0.38900	O-2	1	1
O8	4	0.68300	0.36900	0.43000	O-2	1	1
Si1	4	0.00800	0.17100	0.20900	Si+4	0.28	1
Al1	4	0.00800	0.17100	0.20900	Al+3	0.72	1
Si2	4	0.50800	0.31800	0.24100	Si+4	1	1
Si3	4	0.69200	0.11000	0.31500	Si+4	0.8	1
Al3	4	0.69200	0.11000	0.31500	Al+3	0.2	1
Si4	4	0.18300	0.38200	0.35900	Si+4	0.91	1
Al4	4	0.18300	0.38200	0.35900	Al+3	0.09	1
Na1	4	0.27200	0.99000	0.14500	Na+1	1	1

9.1.2.34. Sample 2012-0001091, stratigraphic height: 17.35 m

Range Number : 1

R-Values

Rexp : 1.92 Rwp : 7.16 Rp : 5.09 GOF : 3.72
Rexp`: 5.39 Rwp`: 20.05 Rp` : 19.25 DW : 0.24

Quantitative Analysis - Rietveld
Phase 1 : „Quartz low“ 25.057 %
Phase 2 : „Kaolinite 1A II“ 0.617 %
Phase 3 : „Illite 2M1“ 68.580 %
Phase 4 : „Chamosite 1MIIb“ 1.294 %
Phase 5 : „Albite low“ 4.451 %

Background
Chebychev polynomial, Coefficient 0 2165.733
1 -1115.315
2 550.8925
3 -383.6138
4 335.0555
5 -229.6226
6 97.6036

Instrument
  Primary radius (mm) 250
  Secondary radius (mm) 250
  Linear PSD 2Th angular range (∞) 2.749941
    FDS angle (∞) 0.0916
    Beam spill, sample length (mm) 9
      Intensity not corrected
  Full Axial Convolution
    Filament length (mm) 8
    Sample length (mm) 30
    Receiving Slit length (mm) 12
    Primary Sollers (∞) 2.5
    Secondary Sollers (∞) 2.5

Corrections
  Zero error -0.1150364
  Specimen displacement -0.3633268
  LP Factor 0

Miscellaneous
  Excluded Regions
    Start/Finish 0 0
    Start/Finish 0 0
    Start/Finish 0 0
    Start/Finish 0 0
    Start/Finish 0 0

Structure 1
  Phase name Quartz low
  R-Bragg 13.056
  Spacegroup P3221
  Scale 0.0148783186
  Cell Mass 180.252
  Cell Volume (≈^3) 112.89409
  Wt% - Rietveld 25.057
  Crystal Linear Absorption Coeff. (1/cm) 95.476
  Crystal Density (g/cm^3) 2.651
  Preferred Orientation (Dir 1 : 0 0 1) 1.189324
  PVII peak type
    FWHM = a + b/Cos(Th) + c Tan(Th)
      a 0.01606273
      b 0.005841149
      c 0.0001582811
    Exponent m = 0.6+ma+mb/Cos(Th)+mc/Tan(Th)
      ma 0.0004464698
      mb 0.0031941
      mc 0.1261057
  Lattice parameters
    a (≈) 4.9118882
    c (≈) 5.4031078

Site	Np	x	y	z	Atom	Occ	Beq
Si1	3	0.46900	0.00000	0.66667	Si+4	1	1
O1	6	0.40300	0.25300	0.78900	O-2	1	1

Structure 2

Phase name	Kaolinite 1A II
R-Bragg	8.677
Spacegroup	C1
Scale	4.51534177e-005
Cell Mass	508.256
Cell Volume (≈^3)	325.10507
Wt% - Rietveld	0.617
Crystal Linear Absorption Coeff. (1/cm)	81.026
Crystal Density (g/cm^3)	2.596
Preferred Orientation (Dir 1 : 0 0 1)	0.7380254
PVII peak type	
FWHM = a + b/Cos(Th) + c Tan(Th)	
a	0.2270986
b	0.0005831452
c	0.001088364
Exponent m = 0.6+ma+mb/Cos(Th)+mc/Tan(Th)	
ma	19.96094
mb	4.990248
mc	4.999117
Lattice parameters	
a (≈)	5.3322134
b (≈)	8.3787153
c (≈)	7.5046934
alpha (∞)	93.05501
beta (∞)	103.7211
gamma (∞)	90.97204

Site	Np	x	y	z	Atom	Occ	Beq
O1	2	0.77800	0.18000	-0.14000	O-2	1	1
O2	2	0.27800	0.32000	-0.13800	O-2	1	1
O3	2	0.31600	-0.00800	-0.13600	O-2	1	1
O4	2	0.24800	0.18400	0.15500	O-2	1	1
O5	2	0.75400	0.31500	0.15500	O-2	1	1
O6	2	0.69000	0.00400	0.15700	O-2	1	1
O7	2	0.79100	0.16500	0.48200	O-2	1	1
O8	2	0.61200	-0.12000	0.45500	O-2	1	1
O9	2	0.10800	-0.05800	0.45500	O-2	1	1
Al1	2	0.50200	0.17200	0.00300	Al+3	1	1
Al2	2	0.00200	0.33000	0.00200	Al+3	1	1
Si1	2	0.80000	0.32200	0.38200	Si+4	1	1
Si2	2	0.80000	0.00000	0.38500	Si+4	1	1

Structure 3

Phase name	Illite 2M1
R-Bragg	9.495
Spacegroup	C12/c1
Scale	0.000559827479
Cell Mass	1580.752
Cell Volume (≈^3)	936.37809
Wt% - Rietveld	68.580
Crystallite Size	
Cry size Lorentzian (nm)	27.8
Crystal Linear Absorption Coeff. (1/cm)	119.514

Crystal Density (g/cm^3)	2.803
Preferred Orientation (Dir 1 : 0 0 1)	0.3946479
Preferred Orientation Spherical Harmonics	
Order	8
y00	1
y20	0.5752464
y22m	0.1377535
y22p	-0.1070796
y40	0.4989479
y42m	-0.2616841
y42p	-0.5029987
y44m	0.9653226
y44p	-0.03432992
y60	-0.001710406
y62m	-0.07329117
y62p	0.4388553
y64m	0.242388
y64p	-0.2442176
y66m	0.3026884
y66p	0.3026884
y80	0.08645961
y82m	0.6127966
y82p	0.3278279
y84m	-0.3354817
y84p	-0.08029759
y86m	0.01303923
y86p	0.02108891
y88m	-0.1168662
y88p	0.07776377
PVII peak type	
FWHM = a + b/Cos(Th) + c Tan(Th)	
a	0.0001000097
b	0.0001000104
c	0.05480943
Exponent m = 0.6+ma+mb/Cos(Th)+mc/Tan(Th)	
ma	0.0001002925
mb	0.0001453812
mc	0.08305757
Lattice parameters	
a (≈)	5.2066934
b (≈)	9.0141858
c (≈)	20.0593564
beta (∞)	95.96047

Site	Np	x	y	z	Atom	Occ	Beq
Si1	8	0.48250	0.92970	0.13700	Si+4	1	1.737
Al1	8	0.44320	0.26350	0.13650	Al+3	1	0.8685
Al2	8	0.25860	0.08280	0.00680	Al+3	1	2.132
K1	4	0.00000	0.09010	0.25000	K+1	1	5.922
O1	8	0.46230	0.91940	0.05050	O-2	1	1.184
O2	8	0.38350	0.26650	0.06630	O-2	1	3.711
O3	8	0.42590	0.10390	0.15300	O-2	1	0.9475
O4	8	0.22260	0.83680	0.16850	O-2	1	3.237
O5	8	0.27350	0.37220	0.16780	O-2	1	6.317
O6	8	0.40800	0.56710	0.04540	O-2	1	4.185

Structure 4

Phase name	Chamosite 1MIIb
R-Bragg	13.125
Spacegroup	C-1
Scale	1.78705552e-005
Cell Mass	1271.241
Cell Volume (≈^3)	688.00078
Wt% - Rietveld	1.294
Crystal Linear Absorption Coeff. (1/cm)	271.140
Crystal Density (g/cm^3)	3.068
Preferred Orientation (Dir 1 : 0 0 1)	0.3286681
PVII peak type	
FWHM = a + b/Cos(Th) + c Tan(Th)	
a	0.05914309
b	0.0001136341
c	0.106912
Exponent m = 0.6+ma+mb/Cos(Th)+mc/Tan(Th)	
ma	0.09616972
mb	0.08936759
mc	0.000107119
Lattice parameters	
a (≈)	5.4083795
b (≈)	9.0044365
c (≈)	14.2985996
alpha (∞)	90.04891
beta (∞)	98.57557
gamma (∞)	92.25189

Site	Np	x	y	z	Atom	Occ	Beq
Mg1	2	0.00000	0.00000	0.00000	Mg+2	0.538	0.1579
Fe1	2	0.00000	0.00000	0.00000	Fe+2	0.462	0.1579
Mg2	4	0.01410	0.33480	0.00270	Mg+2	0.496	0.1579
Fe2	4	0.01410	0.33480	0.00270	Fe+2	0.504	0.1579
Mg3	4	0.00320	0.16830	0.50040	Mg+2	0.494	0.1579
Fe3	4	0.00320	0.16830	0.50040	Fe+2	0.506	0.1579
Al1	2	0.00000	0.50000	0.50000	Al+3	1.362	0.2369
Si1	4	0.24000	0.17000	0.19410	Si+4	0.7125	0.07896
Al2	4	0.24000	0.17000	0.19410	Al+3	0.2875	0.07896
Si2	4	0.73000	0.99800	0.19450	Si+4	0.7125	0.07896
Al3	4	0.73000	0.99800	0.19450	Al+3	0.2875	0.07896
O1	4	0.19100	0.16350	0.07890	O-2	1	0.8685
O2	4	0.70500	0.99800	0.07560	O-2	1	0.8685
O3	4	0.23100	0.33600	0.23740	O-2	1	0.8685
O4	4	0.52800	0.11800	0.23020	O-2	1	0.8685
O5	4	0.01800	0.06100	0.23060	O-2	1	0.8685
O6	4	0.68900	0.33120	0.07420	O-2	1	0.8685
O7	4	0.14400	0.99900	0.43000	O-2	1	0.8685
O8	4	0.14300	0.33610	0.42860	O-2	1	0.8685
O9	4	0.64300	0.16270	0.43110	O-2	1	0.8685

Structure 5

Phase name	Albite low
R-Bragg	7.932
Spacegroup	C-1

Scale 7.72066328e-005
Cell Mass 1048.846
Cell Volume (≈^3) 664.19438
Wt% - Rietveld 4.451
Crystallite Size
Cry size Lorentzian (nm) 210.9
Crystal Linear Absorption Coeff. (1/cm) 88.829
Crystal Density (g/cm^3) 2.622
Lattice parameters
a (≈) 8.1380000
b (≈) 12.7890000
c (≈) 7.1560000
alpha (∞) 94.33
beta (∞) 116.57
gamma (∞) 87.65

Site	Np	x	y	z	Atom	Occ	Beq
O1	4	0.00900	0.13400	0.96700	O-2	1	1
O2	4	0.59500	0.99700	0.27900	O-2	1	1
O3	4	0.81800	0.11200	0.19200	O-2	1	1
O4	4	0.32100	0.35300	0.25900	O-2	1	1
O5	4	0.00600	0.30700	0.26800	O-2	1	1
O6	4	0.52200	0.19600	0.23300	O-2	1	1
O7	4	0.20600	0.11000	0.38900	O-2	1	1
O8	4	0.68300	0.36900	0.43000	O-2	1	1
Si1	4	0.00800	0.17100	0.20900	Si+4	0.28	1
Al1	4	0.00800	0.17100	0.20900	Al+3	0.72	1
Si2	4	0.50800	0.31800	0.24100	Si+4	1	1
Si3	4	0.69200	0.11000	0.31500	Si+4	0.8	1
Al3	4	0.69200	0.11000	0.31500	Al+3	0.2	1
Si4	4	0.18300	0.38200	0.35900	Si+4	0.91	1
Al4	4	0.18300	0.38200	0.35900	Al+3	0.09	1
Na1	4	0.27200	0.99000	0.14500	Na+1	1	1

9.1.2.35. Sample 2012-0001064, stratigraphic height: 18.05 m

Range Number : 1

R-Values

Rexp : 2.05 Rwp : 7.69 Rp : 5.61 GOF : 3.76
Rexp`: 5.67 Rwp`: 21.31 Rp` : 20.94 DW : 0.26

Quantitative Analysis - Rietveld
Phase 1 : „Quartz low“ 23.786 %
Phase 2 : „Kaolinite 1A II“ 0.493 %
Phase 3 : „Illite 2M1“ 70.703 %
Phase 4 : „Chamosite 1MIIb“ 0.872 %
Phase 5 : „Albite low“ 4.145 %

Background
Chebychev polynomial, Coefficient 0 1944.237
1 -1107.692
2 568.2017

3 -399.4009
4 372.3488
5 -260.0845
6 125.2865

Instrument
Primary radius (mm) 250
Secondary radius (mm) 250
Linear PSD 2Th angular range (∞) 2.749941
FDS angle (∞) 0.0916
Beam spill, sample length (mm) 9
Intensity not corrected
Full Axial Convolution
Filament length (mm) 8
Sample length (mm) 30
Receiving Slit length (mm) 12
Primary Sollers (∞) 2.5
Secondary Sollers (∞) 2.5

Corrections
Zero error -0.1095567
Specimen displacement -0.4088909
LP Factor 0

Miscellaneous
Excluded Regions
Start/Finish 0 0
Start/Finish 0 0
Start/Finish 0 0
Start/Finish 0 0
Start/Finish 0 0

Structure 1
Phase name Quartz low
R-Bragg 9.952
Spacegroup P3221
Scale 0.0153028837
Cell Mass 180.252
Cell Volume (≈^3) 112.91238
Wt% - Rietveld 23.786
Crystal Linear Absorption Coeff. (1/cm) 95.461
Crystal Density (g/cm^3) 2.651
Preferred Orientation (Dir 1 : 0 0 1) 1.204454
PVII peak type
FWHM = a + b/Cos(Th) + c Tan(Th)
a 0.01081208
b 0.001861185
c 0.01214313
Exponent m = 0.6+ma+mb/Cos(Th)+mc/Tan(Th)
ma 0.0001000069
mb 0.0001000079
mc 0.1067931
Lattice parameters
a (≈) 4.9120680
c (≈) 5.4035873

Site	Np	x	y	z	Atom	Occ	Beq
Si1	3	0.46900	0.00000	0.66667	Si+4	1	1
O1	6	0.40300	0.25300	0.78900	O-2	1	1

Structure 2

Phase name	Kaolinite 1A II
R-Bragg	6.035
Spacegroup	C1
Scale	3.908827e-005
Cell Mass	508.256
Cell Volume (≈^3)	325.10507
Wt% - Rietveld	0.493
Crystal Linear Absorption Coeff. (1/cm)	81.026
Crystal Density (g/cm^3)	2.596
Preferred Orientation (Dir 1 : 0 0 1)	1.148209
PVII peak type	
FWHM = a + b/Cos(Th) + c Tan(Th)	
a	0.02898246
b	0.03137047
c	0.07619753
Exponent m = 0.6+ma+mb/Cos(Th)+mc/Tan(Th)	
ma	20
mb	4.999997
mc	4.999999
Lattice parameters	
a (≈)	5.3322134
b (≈)	8.3787153
c (≈)	7.5046934
alpha (∞)	93.05501
beta (∞)	103.7211
gamma (∞)	90.97204

Site	Np	x	y	z	Atom	Occ	Beq
O1	2	0.77800	0.18000	-0.14000	O-2	1	1
O2	2	0.27800	0.32000	-0.13800	O-2	1	1
O3	2	0.31600	-0.00800	-0.13600	O-2	1	1
O4	2	0.24800	0.18400	0.15500	O-2	1	1
O5	2	0.75400	0.31500	0.15500	O-2	1	1
O6	2	0.69000	0.00400	0.15700	O-2	1	1
O7	2	0.79100	0.16500	0.48200	O-2	1	1
O8	2	0.61200	-0.12000	0.45500	O-2	1	1
O9	2	0.10800	-0.05800	0.45500	O-2	1	1
Al1	2	0.50200	0.17200	0.00300	Al+3	1	1
Al2	2	0.00200	0.33000	0.00200	Al+3	1	1
Si1	2	0.80000	0.32200	0.38200	Si+4	1	1
Si2	2	0.80000	0.00000	0.38500	Si+4	1	1

Structure 3

Phase name	Illite 2M1
R-Bragg	5.026
Spacegroup	C12/c1
Scale	0.000625441254
Cell Mass	1580.752

Cell Volume (≈^3)	936.37809
Wt% - Rietveld	70.703
Crystallite Size	
Cry size Lorentzian (nm)	36.8
Crystal Linear Absorption Coeff. (1/cm)	119.514
Crystal Density (g/cm^3)	2.803
Preferred Orientation (Dir 1 : 0 0 1)	0.3744997
Preferred Orientation Spherical Harmonics	
Order	8
y00	1
y20	0.5751676
y22m	0.09986375
y22p	-0.1158719
y40	0.4918022
y42m	-0.3458878
y42p	-0.5119418
y44m	0.9196595
y44p	-0.04090031
y60	-0.005759745
y62m	0.0347474
y62p	0.4581667
y64m	0.0727419
y64p	-0.2515575
y66m	0.3004144
y66p	0.3004144
y80	0.05625636
y82m	0.749578
y82p	0.3067469
y84m	-0.485687
y84p	-0.1016342
y86m	-0.07332852
y86p	0.02931886
y88m	-0.1644559
y88p	0.06413023
PVII peak type	
FWHM = a + b/Cos(Th) + c Tan(Th)	
a	0.0001
b	0.0001
c	0.0738111
Exponent m = 0.6+ma+mb/Cos(Th)+mc/Tan(Th)	
ma	0.0001791644
mb	0.04321426
mc	0.02906168
Lattice parameters	
a (≈)	5.2066934
b (≈)	9.0141858
c (≈)	20.0593564
beta (∞)	95.96047

Site	Np	x	y	z	Atom	Occ	Beq
Si1	8	0.48250	0.92970	0.13700	Si+4	1	1.737
Al1	8	0.44320	0.26350	0.13650	Al+3	1	0.8685
Al2	8	0.25860	0.08280	0.00680	Al+3	1	2.132
K1	4	0.00000	0.09010	0.25000	K+1	1	5.922
O1	8	0.46230	0.91940	0.05050	O-2	1	1.184
O2	8	0.38350	0.26650	0.06630	O-2	1	3.711

O3	8	0.42590	0.10390	0.15300	O-2	1 0.9475
O4	8	0.22260	0.83680	0.16850	O-2	1 3.237
O5	8	0.27350	0.37220	0.16780	O-2	1 6.317
O6	8	0.40800	0.56710	0.04540	O-2	1 4.185

Structure 4

Phase name	Chamosite 1MIIb
R-Bragg	4.915
Spacegroup	C-1
Scale	1.30557433e-005
Cell Mass	1271.241
Cell Volume (≈^3)	688.00078
Wt% - Rietveld	0.872
Crystal Linear Absorption Coeff. (1/cm)	271.140
Crystal Density (g/cm^3)	3.068
Preferred Orientation (Dir 1 : 0 0 1)	0.3326499
PVII peak type	
FWHM = a + b/Cos(Th) + c Tan(Th)	
a	0.0412065
b	0.002601903
c	0.1285808
Exponent m = 0.6+ma+mb/Cos(Th)+mc/Tan(Th)	
ma	0.000100006
mb	0.0001000068
mc	0.006194428
Lattice parameters	
a (≈)	5.4083795
b (≈)	9.0044365
c (≈)	14.2985996
alpha (∞)	90.04891
beta (∞)	98.57557
gamma (∞)	92.25189

Site	Np	x	y	z	Atom	Occ	Beq
Mg1	2	0.00000	0.00000	0.00000	Mg+2	0.538	0.1579
Fe1	2	0.00000	0.00000	0.00000	Fe+2	0.462	0.1579
Mg2	4	0.01410	0.33480	0.00270	Mg+2	0.496	0.1579
Fe2	4	0.01410	0.33480	0.00270	Fe+2	0.504	0.1579
Mg3	4	0.00320	0.16830	0.50040	Mg+2	0.494	0.1579
Fe3	4	0.00320	0.16830	0.50040	Fe+2	0.506	0.1579
Al1	2	0.00000	0.50000	0.50000	Al+3	1.362	0.2369
Si1	4	0.24000	0.17000	0.19410	Si+4	0.7125	0.07896
Al2	4	0.24000	0.17000	0.19410	Al+3	0.2875	0.07896
Si2	4	0.73000	0.99800	0.19450	Si+4	0.7125	0.07896
Al3	4	0.73000	0.99800	0.19450	Al+3	0.2875	0.07896
O1	4	0.19100	0.16350	0.07890	O-2	1	0.8685
O2	4	0.70500	0.99800	0.07560	O-2	1	0.8685
O3	4	0.23100	0.33600	0.23740	O-2	1	0.8685
O4	4	0.52800	0.11800	0.23020	O-2	1	0.8685
O5	4	0.01800	0.06100	0.23060	O-2	1	0.8685
O6	4	0.68900	0.33120	0.07420	O-2	1	0.8685
O7	4	0.14400	0.99900	0.43000	O-2	1	0.8685
O8	4	0.14300	0.33610	0.42860	O-2	1	0.8685
O9	4	0.64300	0.16270	0.43110	O-2	1	0.8685

Structure 5
Phase name Albite low
R-Bragg 6.175
Spacegroup C-1
Scale 7.79167097e-005
Cell Mass 1048.846
Cell Volume (≈^3) 664.19438
Wt% - Rietveld 4.145
Crystallite Size
Cry size Lorentzian (nm) 246.9
Crystal Linear Absorption Coeff. (1/cm) 88.829
Crystal Density (g/cm^3) 2.622
Lattice parameters
a (≈) 8.1380000
b (≈) 12.7890000
c (≈) 7.1560000
alpha (∞) 94.33
beta (∞) 116.57
gamma (∞) 87.65

Site	Np	x	y	z	Atom	Occ	Beq
O1	4	0.00900	0.13400	0.96700	O-2	1	1
O2	4	0.59500	0.99700	0.27900	O-2	1	1
O3	4	0.81800	0.11200	0.19200	O-2	1	1
O4	4	0.32100	0.35300	0.25900	O-2	1	1
O5	4	0.00600	0.30700	0.26800	O-2	1	1
O6	4	0.52200	0.19600	0.23300	O-2	1	1
O7	4	0.20600	0.11000	0.38900	O-2	1	1
O8	4	0.68300	0.36900	0.43000	O-2	1	1
Si1	4	0.00800	0.17100	0.20900	Si+4	0.28	1
Al1	4	0.00800	0.17100	0.20900	Al+3	0.72	1
Si2	4	0.50800	0.31800	0.24100	Si+4	1	1
Si3	4	0.69200	0.11000	0.31500	Si+4	0.8	1
Al3	4	0.69200	0.11000	0.31500	Al+3	0.2	1
Si4	4	0.18300	0.38200	0.35900	Si+4	0.91	1
Al4	4	0.18300	0.38200	0.35900	Al+3	0.09	1
Na1	4	0.27200	0.99000	0.14500	Na+1	1	1

9.1.2.36. Sample 2012-0000334, stratigraphic height: 18.58 m

Range Number : 1

R-Values

Rexp : 1.21 Rwp : 5.63 Rp : 4.48 GOF : 4.64
Rexp`: 3.48 Rwp`: 16.14 Rp` : 15.28 DW : 0.24

Quantitative Analysis - Rietveld
Phase 1 : „Quartz low“ 29.360 %
Phase 2 : „Kaolinite 1A II“ 2.108 %
Phase 3 : „Illite 2M1“ 49.183 %
Phase 4 : „Chamosite 1MIIb“ 15.593 %
Phase 5 : „Albite low“ 3.757 %

Background
  Chebychev polynomial, Coefficient 0 5039.794
  1 -1986.416
  2 875.1201
  3 -511.3527
  4 307.4872
  5 -121.491

Instrument
  Primary radius (mm) 250
  Secondary radius (mm) 250
  Linear PSD 2Th angular range (∞) 2.749941
    FDS angle (∞) 0.0916
    Beam spill, sample length (mm) 9
      Intensity not corrected
  Full Axial Convolution
    Filament length (mm) 8
    Sample length (mm) 30
    Receiving Slit length (mm) 12
    Primary Sollers (∞) 2.5
    Secondary Sollers (∞) 2.5

Corrections
  Zero error -0.05272271
  Specimen displacement -0.1300733
  LP Factor 0

Miscellaneous
  Excluded Regions
    Start/Finish 0 0
    Start/Finish 0 0
    Start/Finish 0 0
    Start/Finish 0 0
    Start/Finish 0 0

Structure 1
  Phase name Quartz low
  R-Bragg 4.855
  Spacegroup P3221
  Scale 0.0373340888
  Cell Mass 180.252
  Cell Volume (≈^3) 112.96876
  Wt% - Rietveld 29.360
  Crystal Linear Absorption Coeff. (1/cm) 95.413
  Crystal Density (g/cm^3) 2.650
  Preferred Orientation (Dir 1 : 0 0 1) 1.222227
  PVII peak type
    FWHM = a + b/Cos(Th) + c Tan(Th)
      a 0.02502061
      b 0.000113189
      c 0.000100037
    Exponent m = 0.6+ma+mb/Cos(Th)+mc/Tan(Th)
      ma 0.0001007712
      mb 0.007588502

mc 0.1036808
Lattice parameters
a (≈) 4.9130295
c (≈) 5.4041699

Site	Np	x	y	z	Atom	Occ	Beq
Si1	3	0.46900	0.00000	0.66667	Si+4	1	1
O1	6	0.40300	0.25300	0.78900	O-2	1	1

Structure 2
Phase name Kaolinite 1A II
R-Bragg 7.444
Spacegroup C1
Scale 0.000413186265
Cell Mass 508.256
Cell Volume (≈^3) 259.90965
Wt% - Rietveld 2.108
Crystal Linear Absorption Coeff. (1/cm) 101.351
Crystal Density (g/cm^3) 3.247
Preferred Orientation (Dir 1 : 0 0 1) 0.2334345
PVII peak type
FWHM = a + b/Cos(Th) + c Tan(Th)
a 0.6513494
b 1
c 1
Exponent m = 0.6+ma+mb/Cos(Th)+mc/Tan(Th)
ma 0.0001
mb 0.0001
mc 0.01170048
Lattice parameters
a (≈) 4.8404880
b (≈) 7.6122777
c (≈) 7.3913356
alpha (∞) 94.86372
beta (∞) 105.7643
gamma (∞) 94.05771

Site	Np	x	y	z	Atom	Occ	Beq
O1	2	0.77800	0.18000	-0.14000	O-2	1	1
O2	2	0.27800	0.32000	-0.13800	O-2	1	1
O3	2	0.31600	-0.00800	-0.13600	O-2	1	1
O4	2	0.24800	0.18400	0.15500	O-2	1	1
O5	2	0.75400	0.31500	0.15500	O-2	1	1
O6	2	0.69000	0.00400	0.15700	O-2	1	1
O7	2	0.79100	0.16500	0.48200	O-2	1	1
O8	2	0.61200	-0.12000	0.45500	O-2	1	1
O9	2	0.10800	-0.05800	0.45500	O-2	1	1
Al1	2	0.50200	0.17200	0.00300	Al+3	1	1
Al2	2	0.00200	0.33000	0.00200	Al+3	1	1
Si1	2	0.80000	0.32200	0.38200	Si+4	1	1
Si2	2	0.80000	0.00000	0.38500	Si+4	1	1

Structure 3
Phase name Illite 2M1

R-Bragg	6.381
Spacegroup	C12/c1
Scale	0.000860380402
Cell Mass	1580.752
Cell Volume (≈^3)	936.37809
Wt% - Rietveld	49.183
Crystallite Size	
Cry size Lorentzian (nm)	24.4
Crystal Linear Absorption Coeff. (1/cm)	119.514
Crystal Density (g/cm^3)	2.803
Preferred Orientation Spherical Harmonics	
Order	4
y00	1
y20	-0.4870632
y22m	-0.2431478
y22p	-0.8906265
y40	-0.2528347
y42m	-0.5468344
y42p	0.2271998
y44m	-0.1085868
y44p	0.39003
Lattice parameters	
a (≈)	5.2066934
b (≈)	9.0141858
c (≈)	20.0593564
beta (∞)	95.96047

Site	Np	x	y	z	Atom	Occ	Beq
Si1	8	0.48250	0.92970	0.13700	Si+4	1	1.737
Al1	8	0.44320	0.26350	0.13650	Al+3	1	0.8685
Al2	8	0.25860	0.08280	0.00680	Al+3	1	2.132
K1	4	0.00000	0.09010	0.25000	K+1	1	5.922
O1	8	0.46230	0.91940	0.05050	O-2	1	1.184
O2	8	0.38350	0.26650	0.06630	O-2	1	3.711
O3	8	0.42590	0.10390	0.15300	O-2	1	0.9475
O4	8	0.22260	0.83680	0.16850	O-2	1	3.237
O5	8	0.27350	0.37220	0.16780	O-2	1	6.317
O6	8	0.40800	0.56710	0.04540	O-2	1	4.185

Structure 4

Phase name	Chamosite 1MIIb
R-Bragg	8.559
Spacegroup	C-1
Scale	0.000459895946
Cell Mass	1271.241
Cell Volume (≈^3)	690.59349
Wt% - Rietveld	15.593
Crystal Linear Absorption Coeff. (1/cm)	270.122
Crystal Density (g/cm^3)	3.057
Preferred Orientation (Dir 1 : 0 0 1)	0.9470364
PVII peak type	
FWHM = a + b/Cos(Th) + c Tan(Th)	
a	0.0741174
b	0.03062913
c	0.1738338

Exponent m = 0.6+ma+mb/Cos(Th)+mc/Tan(Th)
ma 0.0001202453
mb 0.0001099718
mc 0.004151582
Lattice parameters
a (≈) 5.4545664
b (≈) 8.9674186
c (≈) 14.3304255
alpha (∞) 89.77319
beta (∞) 99.52923
gamma (∞) 92.54116

Site	Np	x	y	z	Atom	Occ	Beq
Mg1	2	0.00000	0.00000	0.00000	Mg+2	0.538	0.1579
Fe1	2	0.00000	0.00000	0.00000	Fe+2	0.462	0.1579
Mg2	4	0.01410	0.33480	0.00270	Mg+2	0.496	0.1579
Fe2	4	0.01410	0.33480	0.00270	Fe+2	0.504	0.1579
Mg3	4	0.00320	0.16830	0.50040	Mg+2	0.494	0.1579
Fe3	4	0.00320	0.16830	0.50040	Fe+2	0.506	0.1579
Al1	2	0.00000	0.50000	0.50000	Al+3	1.362	0.2369
Si1	4	0.24000	0.17000	0.19410	Si+4	0.7125	0.07896
Al2	4	0.24000	0.17000	0.19410	Al+3	0.2875	0.07896
Si2	4	0.73000	0.99800	0.19450	Si+4	0.7125	0.07896
Al3	4	0.73000	0.99800	0.19450	Al+3	0.2875	0.07896
O1	4	0.19100	0.16350	0.07890	O-2	1	0.8685
O2	4	0.70500	0.99800	0.07560	O-2	1	0.8685
O3	4	0.23100	0.33600	0.23740	O-2	1	0.8685
O4	4	0.52800	0.11800	0.23020	O-2	1	0.8685
O5	4	0.01800	0.06100	0.23060	O-2	1	0.8685
O6	4	0.68900	0.33120	0.07420	O-2	1	0.8685
O7	4	0.14400	0.99900	0.43000	O-2	1	0.8685
O8	4	0.14300	0.33610	0.42860	O-2	1	0.8685
O9	4	0.64300	0.16270	0.43110	O-2	1	0.8685

Structure 5
Phase name Albite low
R-Bragg 7.356
Spacegroup C-1
Scale 0.00013965206
Cell Mass 1048.846
Cell Volume (≈^3) 664.19438
Wt% - Rietveld 3.757
Crystallite Size
Cry size Lorentzian (nm) 210.1
Crystal Linear Absorption Coeff. (1/cm) 88.829
Crystal Density (g/cm^3) 2.622
Lattice parameters
a (≈) 8.1380000
b (≈) 12.7890000
c (≈) 7.1560000
alpha (∞) 94.33
beta (∞) 116.57
gamma (∞) 87.65

Site	Np	x	y	z	Atom	Occ	Beq

O1 4 0.00900 0.13400 0.96700 O-2 1 1
O2 4 0.59500 0.99700 0.27900 O-2 1 1
O3 4 0.81800 0.11200 0.19200 O-2 1 1
O4 4 0.32100 0.35300 0.25900 O-2 1 1
O5 4 0.00600 0.30700 0.26800 O-2 1 1
O6 4 0.52200 0.19600 0.23300 O-2 1 1
O7 4 0.20600 0.11000 0.38900 O-2 1 1
O8 4 0.68300 0.36900 0.43000 O-2 1 1
Si1 4 0.00800 0.17100 0.20900 Si+4 0.28 1
Al1 4 0.00800 0.17100 0.20900 Al+3 0.72 1
Si2 4 0.50800 0.31800 0.24100 Si+4 1 1
Si3 4 0.69200 0.11000 0.31500 Si+4 0.8 1
Al3 4 0.69200 0.11000 0.31500 Al+3 0.2 1
Si4 4 0.18300 0.38200 0.35900 Si+4 0.91 1
Al4 4 0.18300 0.38200 0.35900 Al+3 0.09 1
Na1 4 0.27200 0.99000 0.14500 Na+1 1 1